Zekai Şen

Spatial Modeling Principles in Earth Sciences

Springer

Spatial Modeling Principles in Earth Sciences

Zekai Şen

Spatial Modeling Principles in Earth Sciences

Springer

Prof. Zekai Şen
İstanbul Technical University
Civil Engineering Faculty
Campus Maslak
34469 Istanbul
Turkey
zsen@itu.edu.tr

ISBN 978-1-4020-9671-6 e-ISBN 978-1-4020-9672-3
DOI 10.1007/978-1-4020-9672-3
Springer Dordrecht Heidelberg London New York

Library of Congress Control Number: 2009920941

This work is dedicated to my students all over the world with the hope that they will produce more advanced scientific works in different aspects of earth sciences

Preface

Earth sciences phenomena have evolved in time and space jointly, but in practical applications their records are available as temporal records, spatial measurements, or both. If the records are available only spatially, then they are one realization from the regionalized variable (ReV), which has geometrical locations as longitudes (or easting) or latitudes (or northing), with a record of the earth sciences phenomena at the same location, Hence, in practical applications a set of triplicate values (longitude, latitude, record) provides the realization out of many realizations from the ReV concerned. The worth of data in earth sciences and geology is very high since most of the interpretations and decisions are based on their qualitative and quantitative information content. This information is hidden in representative field samples, which are analyzed for the extraction of numerical or descriptive characteristics. These characteristics are referred to as data. Data collection in earth sciences is difficult, expensive, and requires special care for accurately representing the geological phenomenon. After all various parameters necessary for the description and modeling of the geological event, such as bearing capacity, effective strength, porosity, hydraulic conductivity, chemical contents, are hidden within each sample, they individually represent a specific point in space and time. Change of locations leads to another realization, which is different than the others, but they are statistically indistinguishable from each other. This property provides a common basis for the development of convenient prediction models for the ReVs. In general, the collection of methodologies for modeling such a set of triplicates falls within the geostatistical domain, which has been in practical use for the past four decades. Kriging is the methodology that is used invariably in earth sciences for the regional (spatial) prediction of spatial variability. Prior to its application, a descriptive function of spatial variability as the change of square-differenced spatial variation at two sides with the distance is constructed under the name of semivariogram (SV), which describes the spatial variation in a quantitative manner. This is rather similar to covariance in the classical time series analysis of stochastic processes. Since its origin in the 1960s, few other alternatives as the cumulative SV (CSV), point CSV (PCSV), and spatial dependence function based on these conceptions are developed and applied in different aspects of earth sciences. Each one of these techniques is explained in this book, and their various uses in modeling several earth sciences events, such as earthquake, meteorology, hydrology, are presented. Various alternatives of

the Kriging methodology are presented and the necessary steps in their applications are exposed in a rather simple manner. Simple spatial variation prediction methodologies are also revised with up-to-date literature, and their connections to the most advanced spatial modeling methodologies are explained with basic conceptions.

Spatial simulation methodologies in earth sciences are necessary to explore inherent variabilities such as those in fracture frequencies, spacing, rock quality designation, grain size distribution, and many similar random behaviors of the rock and porous medium. Innovative methodologies are presented for simulation purpose with convenient applications.

The purpose of the book is to provide a comprehensive presentation of up-to-date models for utilization in earth sciences and their applications. Some portions of the textbook will deal with the material already covered in different books and in recent literature like the top journals related to various topics of earth sciences. However, a significant part of the book will consist of the original techniques developed and presented into open literature by the author. Additionally, many unique physical approaches, field cases, and sample interpretations will be presented prior to the application of different models.

I could not have completed this work without the love, patience, support, and assistance of my wife, Fatma Şen. I also extend my appreciation to my stay at the Faculty of Earth Sciences, Hydrogeology Department, and field experience for many years at this university and later on to my stay with the Saudi Geological Survey (SGS), where every facility was provided at my disposal for scientific achievements within different aspects of earth sciences, so that many parts of this book have been materialized. In the mean time, I am also grateful to the Istanbul Technical University for giving me every opportunity to work in different aspects of earth sciences, including meteorology, atmospheric sciences, hydrology, and alike topics.

İstanbul, Turkey Zekai Şen

Contents

Chapter 1
Introduction

Abstract Earth sciences events have spatial, temporal, and spatio-temporal variabilities depending on the scale and purpose of the assessments. For instance, in geology, geophysics, rock mechanicals, and alike aspects the spatial variability is dominant, whereas in hydrology, meteorology, etc., aspects the temporal variability has preference; but in general, irrespective of time scale, all of the earth sciences events have spatio-temporal variability. Plate tectonics has temporal variations during millions of years whereas spatial variability exists at any time instant. Hence, variability is one of the major factors in the modeling of earth sciences events for their future behavior predictions or estimations at any given location where there is no sampling information. Variability implies similarity at some instances and therefore similar representative patterns play significant role in earth sciences modeling.

Keywords Atmosphere · Geometry · Dynamism · Kinematic · Model · Randomness · Random field · Regionalization · Regionalized variable · Similarity · Variability

1.1 General

Mathematical, statistical, probabilistic, stochastic, and alike procedures are applicable only in the case of spatial or temporal variability in natural or artificial phenomena. It is not possible to consider any approach of earth sciences phenomena without the variability property, which is encountered everywhere almost explicitly but also implicitly at times and places. Explicit variability is the main source of reasoning, but implicit variability leads to thousands of imagination with different geometrical shapes on which one is then able to ponder and generate ideas and conclusions. It is possible to sum up that variability is one of the fundamental ingredients of philosophical thinking, which can be separated into different rational components by mental restrictions based on the logic. Almost all social, physical, economical, and natural events in small scales and phenomena in large scales include variability at different levels (micro, meso, or macro) and types (geometry, kinematics, and dynamics). Hence, the very word "variability" deserves detailed qualitative understanding for the construction of our future quantitative models.

Z. Şen, *Spatial Modeling Principles in Earth Sciences*,
DOI 10.1007/978-1-4020-9672-3_1,

Proper understanding of earth sciences phenomenon is itself incomplete, rather vague, and cannot provide a unique or precise answer. However, in the case of data availability the statistical methods support the understanding of the phenomenon and deducing meaningful and rational results. These methods suggest the way to weight the available data so as to compute the best estimates and predictions with acceptable error limits. Unfortunately, statistics and use of its methods are taken as cookbook procedures without fundamental rational background in problem solving. There are many software programs available to use, but the results cannot be interpreted in a meaningful, plausible, and rational manner for the service of practical applications or further researches.

It is, therefore, the purpose of this book to provide fundamentals, logical basis, and insights into spatial statistical techniques that are frequently used in engineering applications and scientific research works. In this manner, prior to cookbook procedure applications and software use, the professional can give his/her expert view about the phenomenon concerned and the treatment alternatives of the available data. The major problems in the spatial analysis are the point estimation from a set of data sampling points where the measurements are not found, areal average calculations, and contour mapping of the regionalized variables. The main purpose of this chapter is to layout the basic spatial variability ingredients, their simple conceptual grasp and models.

1.2 Earth Sciences Phenomena

Geology, hydrology, and meteorology are the sciences of lithosphere, hydrosphere, and atmosphere, which consist of different rock, water, and air layers, their occurrences, distribution, physical and chemical genesis, mechanical properties, and structural constitutions and interrelationships. It is also one of the significant subjects of these phenomena to deal with the historical evolution of rock, water, and atmosphere types and masses concerning their positions, movement, and internal contents. These features indicate the wide content of earth sciences studies. Unfortunately, these phenomena cannot be simulated under laboratory conditions and, therefore, field observations and measurements are the basic information sources of information.

In large scales geological, hydrological, and meteorological compositions are very anisotropic and heterogeneous; in small scales their homogeneity and isotropy increase, but the practical representativity decreases. It is therefore necessary to study them in rather medium scales that can be assumable as homogeneous and isotropic. In any phenomenon study, the general procedure is to have its behavioral features and properties at small locations and by correlation to generalize to larger scales. Unfortunately, most often the description of earth sciences phenomena provides linguistic and verbal qualitative interpretations that are most often subjective and depend on the common consensus. The more the contribution to such consensus of experts the better the conclusions and interpretations, but even then it is not

possible to estimate or derive general conclusions on objective basis. It is, therefore, necessary to try and increase the effect of quantitative approaches and methodologies in earth sciences, especially by the use of personal computers, which help to minimize the calculation procedures and time requirements by software. However, software programs are attractive in appearance and usage, but without fundamental handling of procedures and methodologies, the results from these programs cannot be done properly with useful interpretations and satisfactory calculations that are acceptable by common expertise. This is one of the very sensitive issues that are mostly missing in software program training or ready software uses.

It is advised in this book that without knowing the fundamentals of earth sciences procedure, methodology, or data processing, one must refrain the use of software programs. Otherwise, mechanical learning of software from colleagues, friends, or during tutorials with missing fundamentals does not lead the user to write proper reports or even to discuss the results of software with somebody who is an expert in the area but may not know software use.

Phenomena in earth sciences are of multitude types and each needs at times special interpretation, but whatever the differences there is one common basis, which is data processing. Hence, any earth science equipped with proper data-processing technique with fundamentals can help others and makes significant contributions to open literature, which is of great need for such interpretations. Besides, whatever the techniques and technological levels reached, these phenomena show especially spatial (length, area, volume) differences at many scales, areas, locations, and depths and, consequently, development of any technique cannot cover the whole of these variations simultaneously, and there is always an empty space for further interpretations and researches. It is possible to consider the earth sciences all over the world in two categories, namely conventionalists that are more descriptive working groups with linguistic and verbal interpretations and conclusions with very basic and simple calculations. The second group includes those who are well equipped with advanced quantitative techniques starting with simple probabilistic, statistics, stochastic, and deterministic mathematical models and calculation principles. The latter group might be very addicted to the quantitative approaches with little linguistic, verbal, i.e., qualitative interpretations. The view taken in this book remains in between where the earth scientist should not ignore the verbal and linguistic descriptive information or conclusions, but he/she also looks for quantitative interpretation techniques to support the views and arrive at general conclusions. Unfortunately, most often earth scientists are within these two extremes and sometimes cannot understand each other although the same phenomena are considered. Both views are necessary but not exclusive. The best conclusions are possible with a good combination of two views. However, the priority is always with the linguistic and verbal descriptions, because in scientific training these are the first stones of learning and their logical combinations rationalistically constitute quantitative descriptions. Even during the quantitative studies, the interpretations are based on descriptive, qualitative, linguistic, and verbal statements. It is well known in scientific arena that the basic information is in the forms of logical sentences, postulates, definitions, or theorems, and in earth sciences even speculations might be proposed prior to

quantitative studies and the objectivity increases with shifting toward quantitative interpretations.

Any geological phenomenon can be viewed initially without detailed information to have the following general characteristics:

1. It does not change with time or at least within the lifetime of human, and therefore geological variations have spatial characters and these variations can be presented in the best possible way by convenient maps. For example, geological description leads to lithological variation of different rock types. The simplest of such descriptions is the spatial variation of three basic rock types in any study area. For instance, in Fig. 1.1 the sedimentary, igneous, and metamorphic rock lithology is shown. In this simplest classification of rocks, the researcher is not able to look for different possibilities or ore reserves, water sources, oil field possibilities, etc. Oil reserves cannot be in igneous or metamorphic rock units and, therefore, he/she has to restrict the attention on the areas of sedimentary rocks.

On the other hand, a more detailed geological map can be obtained for different rock types as shown in Fig. 1.2 for the Arabian Peninsula where the subunits of three basic rock types are shown. Now, it is possible to look for regions of groundwater, which is in connection with atmosphere, i.e., the rainfall leads to direct infiltration. This information implies shallow groundwater possibilities and consequently quaternary sediments (wadi alluviums of present epoch geological activity) can be delimited from such a map. Each of the above mentioned maps shows spatial variation of geological phenomena.

2. Geological units are neither uniform nor isotropic nor heterogeneous in horizontal and vertical extends. It is obvious from the maps in Figs. 1.1 and 1.2 that in any direction (NS, EW, etc.) the geological variation is not constant. Of course, the vertical direction will include succession of different rock types and subunits, which are referred to as stratigraphic variation. Such a stratigraphic section is shown in Fig. 1.3, where neither the thickness of each unit nor their slopes are constant.

It is possible to conclude from these two points that the spatial geometry of geological phenomena is not definite and, furthermore, its description is not possible with Euclidean geometry, which is based on lines, planes, and volumes of regular shapes. However, in practical calculations, the geometric dimensions are simplified

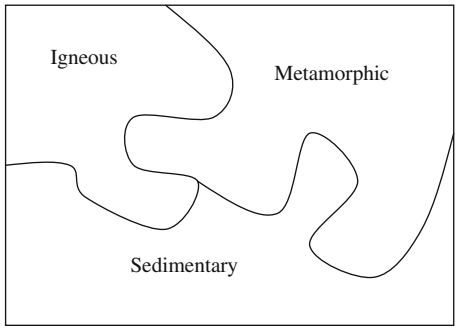

Fig. 1.1 Three rock type map

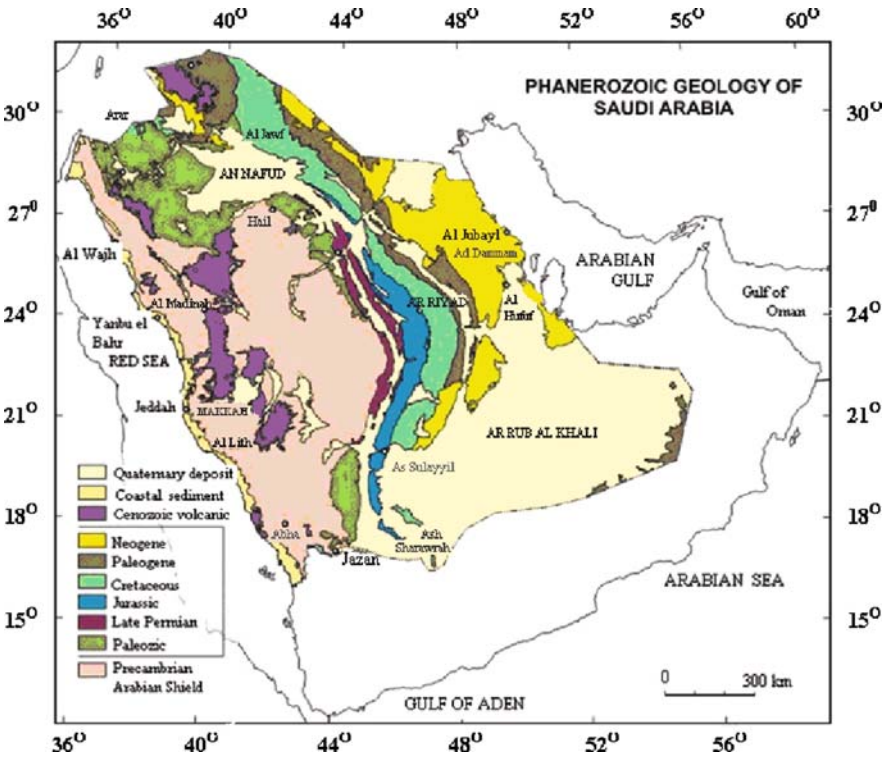

Fig. 1.2 Rock subunit map

so as to use Euclidean representations and make simple calculations. Otherwise, just the geometry can be intangible, hindering calculations. This indicates that in calculations besides other earth sciences quantities that will be mentioned later in this book, initially geometry causes approximations in the calculations, and in any calculation geometry is involved. One can conclude from this statement that even if the other spatial variations are constant, approximation in geometry gives rise to approximate results. It is very convenient to mention here that the only definite Euclidean geometry exists at rock crystalline elements. However, their accumulation leads to irregular geometry that is not expressible by classical geometry.

3. Rock materials are not isotropic and heterogeneous even at small scales of few centimeters, except at crystalline or atomic levels. Hence, the compositional variation within the geometrical boundaries appears from a point to another, which makes the quantitative appreciation almost impossible. In order to alleviate the situation mentally, researchers enter an idealistic world by simplifications for grasping the features as isotropic and homogeneous. If one views the thin section of any rock as shown in Fig. 1.4, he/she will appreciate detailed minute variations from point to point and conclude that the rock cannot be considered as isotropic and homogeneous.

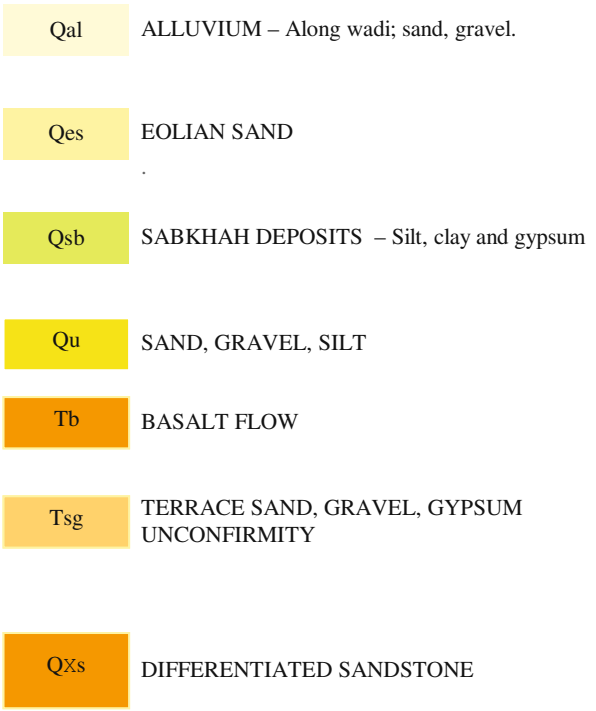

Fig. 1.3 Stratigraphic sequence

Fig. 1.4 Thin-section spatial variability

4. Isotropy implies uniformity along any direction, i.e., directional property constancy. The homogeneity means constancy of any property at each point. These properties can be satisfied in the artificial material produced by man, but natural material such as rocks and any natural phenomenon in hydrology and meteorology

cannot have these properties in the absolute sense. However, provided that the directional or point-wise variations are not very appreciably different from each other, then the geological medium can be considered as homogeneous and isotropic on the average. In this last sentence, the word "average" is the most widely used parameter in quantitative descriptions, but there are many other averages that are used in the earth sciences evaluations. If there is not any specification with this world, then it will imply arithmetic average. Arithmetic average does not attach any weight or priority to any point or direction, i.e., it is an equal weight average.

5. It can be concluded from the previous points that spatial variations cannot be deterministic in the sense of isotropy and homogeneity, and therefore they can be considered as non-deterministic, which implies uncertainty and in turn it means that the spatial assessments and calculations cannot be adopted as the final crisp value. At this stage, rather than well-founded deterministic mathematical rules of calculation and evaluation, it is possible to deal with spatial assessments and evaluations by uncertainty calculations, which are probability, statistics, and stochastic processes.

6. Apart from the geometry and material features, the earth sciences event media also includes in a non-deterministic way the tectonic effects such as fissures, fractures, faults, folds, or chemical solution cavities, which appear rather randomly. Figure 1.5 indicates the appearance of these features in some of the geological media.

From these explanations, it is a scientific truth that the earth sciences phenomena cannot be studied with deterministic methodologies for meaningful and useful interpretations or applications. The non-deterministic, i.e., uncertainty techniques such as probability, statistics, and stochastic, methodologies are more suitable for the reflection of any spatial behavior.

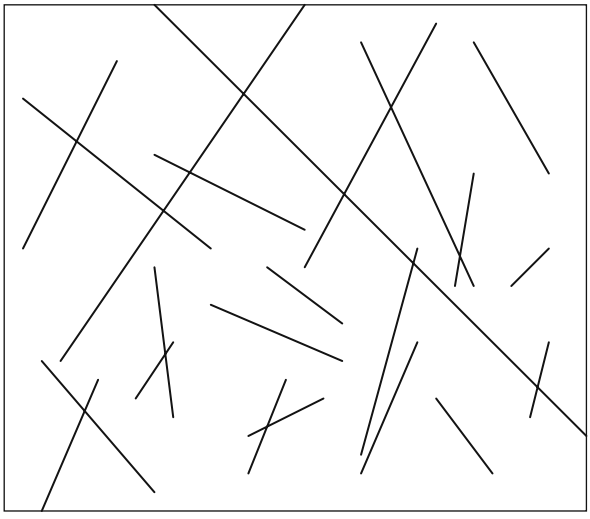

Fig. 1.5 Structural non-determinacy

1.3 Variability

Spatial and temporal variability are the common occurrences in nature. The patterns caused by the spatial variability of a phenomenon occur at many scales, ranging from simple chemical reactions between activator and inhibitor reagents to the large-scale structure of the universe. For example, spiral wave patterns are well known in chemical reactions, hurricanes, galaxies, and simulated predator–prey systems. Because common mechanisms may be responsible for generating patterns among diverse physical, chemical, and biological systems, new pattern formation phenomena are potentially of great scientific interest. The mechanisms that cause patterns to evolve, however, are not well understood. An understanding of the causes and consequences of pattern formation in nature will increase our understanding of processes in nature such as succession, spread, and persistence of species and management. With the ability to detect and describe different patterns comes the power to discover the determinants of patterns and the mechanisms that generate, maintain, modify, and destroy those patterns.

Spatial variability from one site to another leads to the concept of regional variability within the area. This variability determines the regional behavior as well as the predictability of the precipitation amounts on the basis of which the interpretations are derived, provided that suitable techniques and models are identified. For spatial variability the classical time series techniques yield useful interpretations, but for equal-distance sampling only. However, a great deal of progress has been made in the adaptation of statistical techniques to unevenly sampled data (North et al., 1982). These techniques do indeed yield useful information, which is significantly different from the information obtained by the use of semivariogram technique in geostatistics (Chapter 4). Regular scatter of sites might not provide enough regional information as irregular sites since earth sciences agents and surface features are almost always heterogeneous and anisotropic. Consequently, the following significant questions remain unanswered so far in the literature on spatial (regional) earth sciences assessments:

1) How to quantify from irregular site measurements whether the regional distribution is homogeneous, continuous, dependent, etc.?
2) How to model the heterogeneity so as to represent continuous variability within the area concerned?
3) How to construct maps concerning the regional variability such that the estimates are unbiased?

Earth sciences variability amounts in any area show considerable spatial and temporal variations. The variation is brought about by differences in the type and scale of development in event-producing processes and also influenced strongly by local or regional factors such as topographic elevations and atmospheric conditions (Wilson and Atwater, 1972). In practice, however, the variation of event is considered to be significantly site- or, at the very least, area-dependent. In addition,

for most areas in the world each individual measurement site is assumed to be representative of a very considerable area around it. Logically, measurement at any individual site will have an area of influence around it, but there is no physical or data-based objective criterion for the definition of such an area (Chapters 2 and 4). The assumption of very considerable spatial variation is a very dangerous one, especially at short distances and for severe conditions. For instance, there is no guarantee that point rainfall will in any way produce a reliable guide to the rainfall of immediate surrounding areas (Summer, 1988).

The spatial distribution of any event has always been a factor important in many earth sciences analyses. Reliable estimations of average values are essential for adequate planning. The same is true for water balance calculations, groundwater recharge boundaries, urban drainage purposes, and for climatic conditions. Hence, in practice the basic problem is that of point representativeness and, subsequently, further problem is how to derive pictures of spatial relationships, which are reasonably close to reality. In overcoming this problem, it is important to determine the spatial pattern based on a sparse and uneven network of measuring stations.

Variability is a general term used for a fundamental property of all events, which is boiled down in a more quantitative term "difference." The equivalence of these two words at least in the implications provides a bridge between the philosophical thinking and the rational quantitative modeling of social, economical, and natural events. The word difference as an expression for variability gives rise to various algorithms that are currently in use in many disciplines. For instance, the global numerical values cannot explain the internal or external features of the concerned event except its scale, but the comparison of any two leads to additional and detailed information such as the difference (with dimension of the numerical values) and unit difference (slope). There are many categories of variability such as geometric, kinematics, and dynamic types. In addition, the variability may be in regular (certain) or irregular (uncertain) domains.

The geometrical similarity can be split into two types, namely size corresponding to scale and shape.

In Fig. 1.6a, three shapes are exactly the same but their scales are different. However, they cannot be considered as having different variability from each other. Especially, if the last shape in Fig. 1.6a is further downscaled, it approaches a point. Downscaling or upscaling each one of these shapes helps to convert each to others easily, and therefore there is no real variability between them. The only variability is within each shape, because each point on the figure has different coordinates or slopes (tangents). The variability in shape is different than scale type, because the overall appearance of different objects may look like almost the same with local differences as in Fig. 1.6b. Since these shapes are not exactly the same, there are relative deviations between the two. For the relative difference either of the shapes may be taken as the basis and the other is considered as deviating from the first one. Hence, it is possible that the differences are relative not absolute. This implies the significance of relative variability. The geometric difference is referred to as the spatial variability in this book.

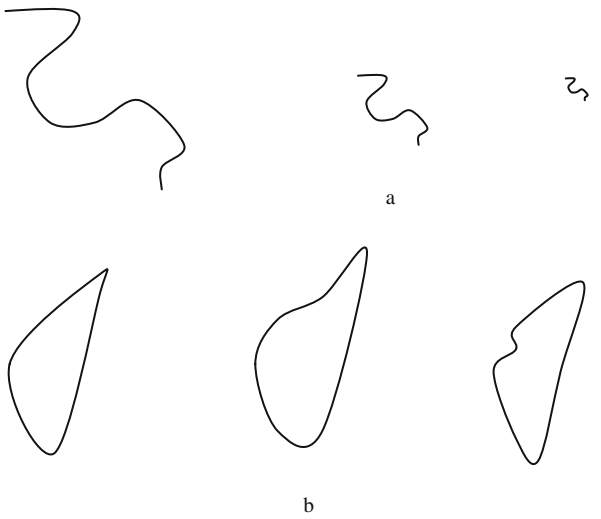

Fig. 1.6 Geometric similarities: (**a**) size (**b**) shape

Kinematics variability is concerned with the similarity in the time variations, especially concerning the physical definition of the velocity. In a more general term, any similarity not concerning the force is referred to as the kinematics variability. Such a variability and consequent similarity or geometry is very significant in physical modeling of natural or man-made events. For instance, the laboratory modeling of runoff variability in the drainage basin should be similar to each other.

The most significant value of the variability in natural events is the velocity variations after the geometrical variability. Figure 1.7 indicates the kinematics variability and its correspondence between the natural and the laboratory units. In this figure, in addition to the geometrical similarity there is also kinematics similarity, because at each subsection the ratio of velocities is constant, that is $v_1/V_1 = v_2/V_2 = v_3/V_3 = v_4/V_4 = v_5/V_5 = c$ where c is a constant, less than 1. This constant is the guarantee for the temporal variability at spatially distributed points.

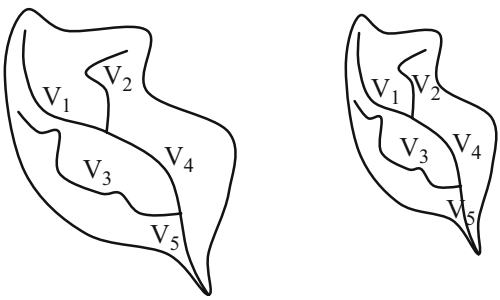

Fig. 1.7 Kinematics variability and similarity

Finally, the dynamic similarity is similar to the kinematics similarity where instead of velocities forces are taken into consideration. After all, in any spatial variability, depending on the type of program the variability must be considered from geometric, kinematics, and dynamics points of view.

During the discussion of the variability, in addition to the basic word "difference" another one "similarity" emerged rather unintentionally. Similarity is a type of difference and consequent variability measure between two events. Depending on the quantitative calculations as will be mentioned in the following chapters, it is possible to conclude that two events are different or similar. Difference or similarity implies the difference or similarity in the variability. Variability is a general term that is used for the comparison of multitude of points, but the difference can be quantified between two points only.

The variability may have not only very regular forms like waves, functions, static maps but also irregular behaviors that cannot be described by the mathematical or classical physical rules where uncertainty techniques such as statistics, probability, and stochastic become helpful (see Fig. 1.8). Uncertain variations are referred to as the random variables, RV, or regionalized variables, ReV, which assume any value randomly at any time or space. Whatever the degree of uncertainty, each RV or ReV may include regular variations, and in general the regional variability may be considered as the summation of deterministic and stochastic (statistical or probability) components. Although mathematical concepts, operations, and functions are sufficient for the depiction of deterministic part, they fail to emulate the stochastic part, which is the subject of this book.

The following points are significant in the quantitative consideration of the variability in any modeling study:

1) Quantitative variability is possible by pair-wise consideration of two events, objects, points, numbers, etc.
2) The subtraction operation is the only one among the four arithmetical operations that represent the variability.
3) It is preferable to use dimensionless values between two different events, say, groundwater levels and transmissivity map in order to compare their variability. It is not possible to compare soil moisture content with runoff directly because they are different in dimensions. In order to bring various events into equal dimensional footing, it is necessary to use division operator, which cancels the dimension.

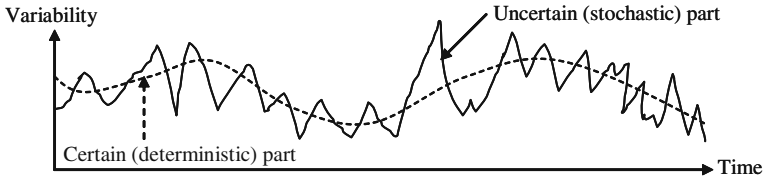

Fig. 1.8 Deterministic and stochastic variations

After the foregoing logical explanations the two most significant explanations for the variability measurement appear as difference and division. Furthermore, these operations can be applied between two points for a given ReV or between two ReVs at a single point. Hence, if there are n measurements or sampling points, there are then n(n–1)/2 different ways of distance variability samplings. The variability of ReVs is represented most often by the arithmetic or preferably weighted-average procedure. This indicates for a multitude of point variability, the summation operation provides a general representative value for the regional variability of ReVs.

1.4 Determinism Versus Uncertainty

In general, any field, office, or theoretical study relating to natural phenomena that occur within the lithosphere, hydrosphere, or atmosphere is referred to as the earth sciences event. For instance, the lithological compositions in terms of stratigraphy, historical evolutions, structural and tectonic dynamism are under continuous spatial and temporal changes, and therefore their analysis, control, and predictions are quite difficult. The difficulty arises not only from the insufficiency of the techniques only, but inherently from the random behavior of the earth sciences elements in an area. In earth sciences concerning lithology, there are no significant changes temporally within the average human life, but the lithological characteristics change even after, say, 1 cm apart. For instance, occurrence of fracture systems including fracture number, direction, dip, length, aperture, frequency, etc., are all very complicated and sophisticated for measurement; and, consequently, right from the field studies, there arise uncertainties either due to the human ignorance or due to a significant extent as a result of inherent randomness that exists in nature. Another example is the rate, time, and direction of individual pebble movement along a river, and this phenomenon cannot be predicted with any reasonable degree of determinism. It is possible to state different premises and then conclusions deduced logically from a set of premises, but all these are in terms of linguistic variables and statements. It is the role of quantification methods to translate these verbal statements into mathematical equations or inequalities so as to come closer to final conclusions or decisions. Idealization, assumption, and simplification in earth sciences are more difficult than the atmospheric sciences where the sky does not have, say, any fracture or discontinuity as in the subsurface. Hence, in earth sciences more than any other physical or atmospheric sciences, the element of randomness is embedded in the field, office, and theoretical studies. Unfortunately, geologists have worked so many years in a descriptive manner and did not care about the uncertainty techniques such as probability and statistics in their quantitative studies until 1960. However, then onward many statistical and specifically developed statistics in geology as geostatistics started to be used in many ore reserve, groundwater, petroleum, etc., studies. The movement of the pebbles, sand, silt, and clay particles may be described as random within the limits of environmental parameters. This randomness of movement is interpreted as a result of chance events inherent in the transporting medium and the transported material.

Deterministic phenomena are those in which outcomes of the individual events are predictable with complete certainty under any given set of circumstances, if the required initial conditions are known. In all the physical and astronomical sciences, traditionally deterministic nature of the phenomena is assumed. It is, therefore, necessary in the use of such approaches the validity of the assumption sets and initial conditions. In a way, with idealization concepts, assumptions, and simplifications, deterministic scientific researches yield conclusions in the forms of algorithms, procedures, or mathematical formulations, which should be used with caution for restrictive circumstances. The very essence of determinism is the idealization and assumptions so that uncertain phenomenon becomes graspable and conceivable to work with the available physical concepts and mathematical procedures. In a way, idealization and assumption sets render uncertain phenomenon into conceptually certain situation by trashing out the uncertainty components. A significant question that may be asked at this point is whether there is any benefit from the deterministic approaches in the earth and atmospheric studies if the general behavior of the events is uncertain? The answer to this question is affirmative because in spite of the simplifying assumptions and idealizations the skeleton (trend, seasonality) of the uncertain phenomenon is captured by the deterministic methods. For instance, the diurnal temperature change at any location has more or less a sinusoidal fluctuation as shown in Fig. 1.9, and the idealization of temporal temperature changes within a day as a sinusoidal regular curve provides a skeleton on which the uncertain parts appear as deviations in a random manner.

At the very core of scientific theories lies the notion of "cause" and "effect" relationship as an absolute certainty in scientific studies. One of the modern philosopher of science, Popper (2002) stated that "to give a causal explanation of a certain specific event means deducing a statement describing this event from two kinds of premises: from some universal laws, and from some singular or specific statements which we may call the specific initial conditions." According to him, there must be a very special kind of connection between the premises and the conclusions in a causal explanation and it must be deductive. In this manner, the conclusion follows necessarily from the premises. Prior to any mathematical formulation, the premises and theconclusion consist of verbal (linguistic) statements. It is necessary to justify at every step of deductive argument by citing a logical rule that is concerned with the relationship among statements. On the other hand, the concept of "law" lies at the heart of deductive explanation, and therefore at the heart of the certainty of our knowledge about specific events.

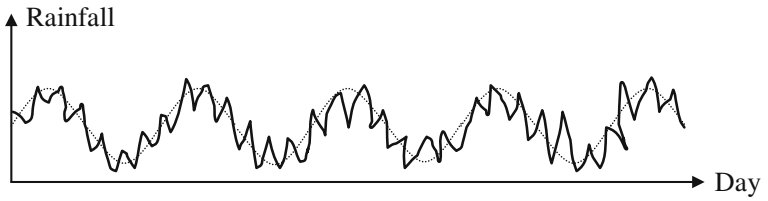

Fig. 1.9 Diurnal temperature variation

ReV phenomena evolve with time and space, and their appreciation as to the occurrence, magnitude, and location is possible by observations and still better by measurements along the time and/or space reference systems. The basic information about the phenomenon is obtained from the measurements. Any measurement can be considered as the trace of the phenomenon at a given time and location. Hence, it should be specified by time and location, but its magnitude is not at the hand of researcher. Initial observance of the phenomenon leads to non-numerical form of descriptive data that cannot be evaluated with certainty.

The use of uncertainty techniques such as the probability, statistics, and stochastic methods in earth, environmental, and atmospheric sciences has increased rapidly since 1960s and most of the researchers as students and teachers seek more training in these disciplines for dealing with uncertainty in a better quantitative way. Many professional journals, books, and technical reports in the earth, environment, and atmospheric science studies include significant parts on the uncertainty techniques in dealing with uncertain natural phenomena. Yet, relatively few scientists and engineers in these disciplines have a strong background in school mathematics and the question is then how can they obtain sufficient knowledge of uncertainty methods including probability, statistics, and stochastic processes in describing natural phenomena appreciating the arguments, which they must read and then digest for successful applications in making predictions and interpretations.

The inability to predict specific events might stem from the fact that nature is intrinsically random and randomness is used in a statistical sense to describe any phenomenon that is unpredictable with any degree of uncertainty for a specific event; and deterministic phenomena, on the contrary, are those in which outcomes of the individual events are predictable with complete certainty under any given set of circumstances, if the required initial conditions are known. In general, the nature is considered as random. Consequently, randomness has been suggested as the ultimate and most profound physical concept of nature.

Moreover, it is almost true to claim that classical approaches (analytical, empirical, etc.) are not deterministic theory if the claim simply means that actual measurements confirm the predictions of the theory only approximately or only within certain statistically expressed limits. Any theory formulated in terms of magnitudes capable of mathematically continuous variation must, in the nature of the case, be statistical and not quite deterministic in this sense, for the numerical values of physical magnitudes (such a permeability) obtained by laboratory or field measurement never form a mathematically continuous series; any set of values so obtained will show some dispersion around the values calculated from theory. Nevertheless, a theory is labeled properly as a deterministic one if analysis of its internal structure shows that the theoretical state of a system at one instant logically determines a unique state of that system for any other instant. In this sense, and with respect to the theoretically defined mechanical states of systems, mechanics is unquestionably a deterministic theory. Consequently, when a predictor is introduced into a philosophical discussion of determinism, it is not a human being but a "superhuman intelligence." Human predictors cannot settle the issue of determinism because they are unable to predict physical events no matter what the world is really like.

The uncertainty in the earth and atmospheric knowledge arises out of the conviction that earth and atmospheric generalizations are immensely complicated instantiations of abstract, and often universal, physical laws. Earth and atmospheric generalizations always contain the assumptions of boundary and initial conditions. In a way, the uncertainty in the predictions arises from the ignorance of the researcher to know the initial and boundary conditions in exactness. They cannot control these conditions with certainty. On the assumptions of physical theory, earth and atmospherically significant configurations are regarded as highly complex. This is true whether or not the "world" is deterministic. Physical laws, which are not formulated as universal statements, may impose uncertainty directly upon earth and atmospheric events as in the case of inferences based on the principles of radioactive disintegration.

Earth and atmospheric sciences deal with spatial and temporal behaviors of natural phenomena at every scale for the purpose of predicting the future replicas of the similar phenomena, which help to make significant decisions in planning, management, operation, and maintenance of natural occurrences related to social, environmental, and engineering activities. Since any of these phenomena cannot be accounted by measurements, which involve uncertain behaviors, their analysis, control, and prediction need to use uncertainty techniques for significant achievements for future characteristic estimations. Many natural phenomena cannot be monitored at desired instances of time and locations in space and such restrictive time and location limitations bring additional irregularity in the measurements. Consequently, the analysis, in addition to uncertain temporal and spatial occurrences, has the problem of sampling the natural phenomenon at irregular sites and times. For instance, floods, earthquakes, car accidents, fracture occurrences are all among the irregularly distributed temporal and spatial events. Uncertainty and irregularity are the common properties of natural phenomena measurements in earth and atmospheric researches, but the analytical solutions through numerical approximations all require regularly available initial and boundary conditions that cannot be obtained by lying regular measurement sites or time instances. In an uncertain environment any cause will be associated with different effects, each with different level of possibilities. Herein possibility means some preference index for the occurrence of each effect. The greater the possibility index the more frequent the event occurrence. Figure 1.10 indicates the deterministic and uncertain cause–environment–effect system in a simplified manner. In the deterministic case any single cause will lead to a certain single effect, whereas in the uncertain domain single cause (effect) might be associated

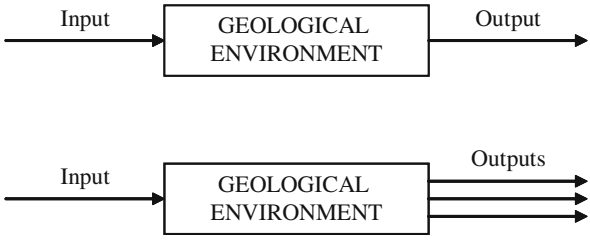

Fig. 1.10 Cause, environment, and effect triplicate

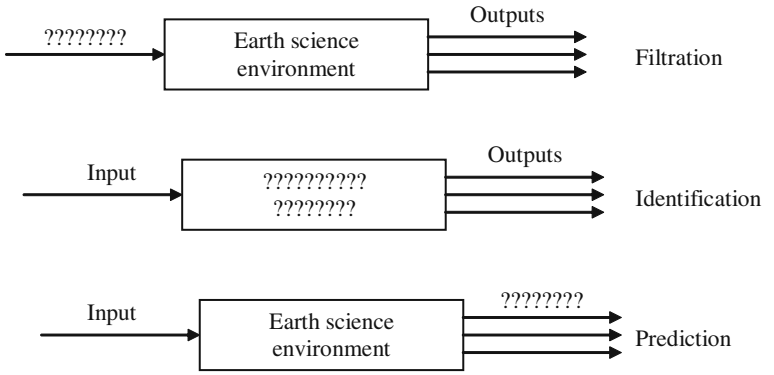

Fig. 1.11 Estimation, identification, and prediction

with a multitude of effect (cause). In practice, however, the case of single-input multiple-output situations is most valid and the prediction is, in fact, deciding on which one of the effects will occur under a certain cause.

In this figure any one of the triplicate components might be uncertain. Furthermore, any two or collectively all three components may be uncertain. In all these cases, the uncertainty plays significant role in the evolution and prediction of the phenomenon concerned. In the practical studies, given any two of these components the third one might be estimated, identified, or predicted. These three cases are shown in Fig. 1.11. In the case of unknown causal effects, the problem is referred to as the estimation or filtration; given the cause and effect knowledge, the search for the functioning environmental system is identification; and, finally, given the cause as input and the functional duty of the environment, the search for knowledge on the effect is known as prediction.

Uncertainty is introduced into any problem through the variation inherent in nature, through man's lack of understanding of all the causes and effects in physical systems, and through insufficient data in practice. Even with long history of data, one cannot predict the natural phenomenon except within an error band. As a result of uncertainties, the future can never be predicted entirely by the researchers. Consequently, the researcher must consider the uncertainty methods for the assessment of the occurrences and amounts of particular events and then try to determine their likelihood of occurrences.

1.5 Earth, Environment, and Atmospheric Researches

Recently, the scientific evolution of methodologies has shown that the more the researchers try to clarify the boundaries of their domain of interest the more they become blurred with other domains of research. For instance, a hydrogeologist tries to model the groundwater pollution as one of the modern nuisances of humanity so

far as the water resources are concerned; he/she needs information about the geological environment of the aquifers, meteorological and atmospheric conditions for the groundwater recharge, in addition to social and human settlement environmental issues for the pollution sources. Hence, many common philosophies, logical basic deductions, methodologies, and approaches become common to different disciplines and the data processing is among the most important common topics, which include the same methodologies applicable to diversity of disciplines. The way that earth, environmental, and atmospheric scientists frame their questions varies enormously, but the solution algorithms may include the same or at least similar procedures.

Any natural phenomenon or its similitude occurs extensively over a region, and therefore its recordings or observations at different locations pose some questions as, for instance, are there relationships between phenomena in various locations? In such a question, the time appears as if it is frozen and the phenomenon concerned is investigated over the area with its behavioral occurrences between the locations. Answer to this question may be provided descriptively in linguistic, subjective, and vague terms, which may be understood even by non-specialists in the discipline. However, their quantification necessitates objective, regionally applicable methodologies to ReV, which is one of the purposes of this book.

Another question that may be stated right at the beginning of the research in the earth, environment, and atmospheric sciences are places different in terms of the phenomena present there? Such questions are the source of many researches' interest in the subject. Scientific treatment and interpretation of even error-laden data lead to significant practical knowledge concerning the oceans and atmosphere. It is the prime duty of the earth scientists to filter out the meaningful portions of the data and to model randomly the error part.

1.6 Random Field (RF)

Precipitation evolves temporally as well as spatially. Under given specific circumstances, precipitation has only a single value at each instant of time. Such a space–time distribution is referred to as a field quantity. Since meteorological quantities cannot be predicted with certainty, they are assumed to be random and hence it is necessary to study a new class of fields, i.e., random fields. Quantitatively, a random field is characterized, $\xi(s,t)$, called a random function at a point, s, and time, t. It is obvious that random field concept is the generalization of a stochastic process for which time is the scale variable. The expression "the random function of the coordinate (s,t)" must be understood in the sense that at each point (s,t) of four-dimensional space–time, the value $\xi(s,t)$ is a random variable and, consequently, cannot be predicted exactly. In addition, the values $\xi(s,t)$ are subject to a certain law of probability. A complete description of a random field can be achieved by constructing all the finite-dimensional probability distribution functions (pdf) of the field at different points in space. A random field $\xi(s)$ at a fixed time instant with the given finite dimensional pdf is called homogeneous, if this function is invariant

with respect to a shift of the system of points (Chapter 4). The same random field is called statistically homogeneous and isotropic (if it is homogeneous in the sense indicated above), while the pdfs are invariant with respect to an arbitrary rotation of the system of points such as of a solid body and to a mirror reflection of this system with respect to the arbitrary plane passing through the origin of the coordinate system. In other words, statistical moments depend upon the configuration of the system of points for which they are formed, but not upon the position of the system in space.

1.7 Regionalized Variable (ReV)

When the variable is distributed in space, it is regionalized. An ReV has the characteristics of a certain phenomena. For example, ore grade, rainfall, transmissivity, and water level data are regionalized variables. This theory was first applied in mining, rapidly widening its range in the earth sciences. The procedure of the theory of regionalized variables follows two main steps. The first step establishes the theoretical ground for expressing the structural properties of the phenomenon (experimental semivariogram, SV, covariance, or cumulative SV, CSV, see Chapter 5). The second step provides a model that uses a combination of functions, which guarantee a solution to the estimation problem (Kriging), and deals with the ReV by using the probabilistic theory of random functions. The ReV is denoted by Z(x) and interpreted as a realization of RF denoted by z(x); the random function being an infinite collection of random variables z(x)s. A well-defined unique numerical value is rendered into a realization of random process. From the field of observations or measurements one can have only a single realization of that random function. The problem consists of finding the characteristics of random function, z(x), to make the estimation of the unknown point possible, and statistical inference will require further hypothesis of stationarity (David, 1977; Delhomme, 1979; Isaaks and Srivastava, 1989).

As a result of spatial variability in the regionalized variable, it is not possible to obtain exact and error-free estimates of unknowns. However, spatial analysis procedures weight the available evidence so as to make the best estimates in an unbiased manner. Sample of any ReV at distinct sites is considered to be a single realization of a random function. Let $P_i(X)$ and $H_i(X)$ denote the average areal amount and elevation, respectively, at station i. Many methods have been proposed for interpretation and mapping. Most of them are quite empirical and many are intuitively reasonable, but they lack intellectual rigor. However, in order to provide interpretations on a sound theoretical basis, the spatial attributes are treated as mathematical variables that are the functions of their positions on or above the earth's surface. This is tantamount to saying that their values are treated as functions of the spatial coordinates. Similar problems of estimating and mapping properties arose in meteorology (Cressman, 1959; Gandin, 1965) and in mining (Matheron, 1963), where the ore concentrations vary in space. Although Gandin (1965) described the application of optimum interpolation developed by Kolmogorov (1941) for estimating the

values of atmospheric pressure and rainfall at sites between the recording stations, he did not propose a definite procedure for the distance, i.e., radius of influence. However, in mining geology rapid and effective solutions are needed because of the enormous costs incurred, and therefore it was in mining geology that the advances in spatial analysis were made.

References

Cressman, G. P., 1959. An operational objective analysis system. Mon. Wea. Rev. 87(10), 367–374.
David, M., 1977. Geostatistical Ore Reserve Estimation. Elsevier Scientific Publishing Company, Amsterdam, 364 pp.
Delhomme J. P., 1979. Kriging in the hydrosciences. Adv. Water Resour. 1, 251.
Gandin, L. S., 1965. Objective Analysis, Lectures on Numerical Short-range Weather Prediction, WMO, Regional Training Seminar, pp. 633–677.
Isaaks, E. H., and Srivastava, R. M., 1989. An Introduction to Applied Geostatistics. Oxford University Press, Oxford, 561 pp.
Kolmogorov, A. N., 1941. Interpolation and extrapolation von stationaren zufalligen folgen. Bull. Acad. Sci. USSR, Ser. Math. 5, 3–14.
Matheron, G., 1963. Principles of geostatistics. Econ. Geology 58, 1246–1266.
North, G. R., Bell, T.L., and Cahalan, F., 1982. Sampling errors in the estimation of Empirical orthogonal functions. Monthly Weather Rev. 110, 699–706.
Popper, K., 2002. The Logic of Scientific Discovery. Routledge Publishing Company, London and New York, 479 pp.
Summer, G., 1988. Precipitation Process and Analysis. John Wiley and Sons, New York, 455 pp.
Wilson, J. W., and Atwater, M. A., 1972. Storm rainfall variability over Connecticut. J. Geophys. Res. 77(21), 3950–3956.

Chapter 2
Data Types and Logical Processing Methods

Abstract Not only numerical but also linguistic data are necessary in the modeling of earth sciences events. Measurements are sources of numerical data whereas observations lead to linguistic data. Numerical data include randomness and errors but linguistic data are rather fuzzy, which means that there are uncertainties in both data types. Accordingly, the final model results as predictions or estimations include errors that must be confined within $\pm 5\%$ limits in practical applications. Spatial estimations can be obtained either on point basis or on sub-areal basis depending on the refinement of the problem at hand and purpose. In general, longitude (easting), latitude (northing), and regionalized variable (ReV) value at this location are necessary for a complete description and establishment of a point-wise spatial model, where these three values are referred to as triplicate; but in the case of pixel location its size is also necessary, which leads to four variables (quadruple) for the description of ReV. Simple classical triangularization, polygonalization techniques are used in addition to innovative percentage polygon methodology. Droughts are a kind of spatial earth sciences with coverage area that can be modeled by probabilistic approaches.

Keywords Droughts · Observation · Measurement · Linguistic data · Numerical data · Sampling · Small sample · Triangularization · Polygonalization · Percentage polygon

2.1 General

Scientific and engineering solutions can be given about any earth sciences phenomena through relevant spatial modeling techniques, provided that representative data are available. However, in many cases it is difficult and expensive to collect the field data, and therefore it is necessary to make the best use of available linguistic information, knowledge, and numerical data to estimate the spatial (regional) behavior of the event with relevant parameter estimations and suitable models. Available data provide numerical information at a set of finite points, but

Z. Şen, *Spatial Modeling Principles in Earth Sciences*,
DOI 10.1007/978-1-4020-9672-3_2,

the professional must fill in the gaps using information, knowledge, and understanding about the phenomena with expert views. Data are the treasure of knowledge and information leading to meaningful interpretations. Observations are also potential source of information, which provides linguistic rational and logical expressions in the form of premises. Data imply numerical measurements using different instruments either in the field or in the laboratory. Observations are not numerical but rather verbal data that assist to describe and identify the phenomenon concerned.

The development of data estimation methods can be traced back to Gauss (1809), who suggested the technique of deterministic least-squares approach and employed it in a relatively simple orbit measurement problem. The next significant contribution to the extensive subject of estimation theory occurred more than 100 years later when Fisher (1912), working with pdf, introduced the approach of maximum likelihood estimation. However, Wiener (1942, 1949) set forth a procedure for the frequency domain design of statistically optimal filters. The technique addressed the continuous-time problem in terms of correlation functions and the continuous filter impulse response. Moreover, the Wiener solution does not lend itself very well to the corresponding discrete-data problem, nor it is easily extended to more complicated time-variable, multiple-input/output problems. It was limited to statistically stationary processes and provided optimal estimates only in the steady-state regime. In the same time period, Kolmogorov (1941) treated the discrete-time problem.

In this chapter, observation and data types are explained and their preliminary simple logical treatments for useful spatial information deductions are presented and applied through examples.

2.2 Observations

They provide information on the phenomenon through sense organs, which cannot provide numerical measurements but their expressions are linguistic (verbal) descriptions. In any study, the collection of such information is unavoidable and they are very precious in the construction of conceptions and models for the control of the phenomenon concerned. Observations may be expressed rather subjectively by different persons, but experts may deduce the best set of verbal information. Depending on the personal experience and background, an observation may instigate different conceptualization and impression on each person. In a way observations provide subjective information about the behavior of the phenomenon concerned. In some branches of scientific applications, observational descriptions are the only source of data that help for future predictions. Even though observations may be achieved through some instruments as long as their description remains in verbal terms, they are not numerical data. Observations were very significant in the early developments of the scientific and technological developments especially before the

17th century, but they became more important in modern times including linguistic implications and logical deductions explaining the fundamentals of any natural or man-made event (Zadeh, 1965). For instance, in general, geological description of rocks can be made by field observations and concise linguistic categorizations are then planned for others to understand again linguistically. It is important to stress at this point that linguistic expressions of observations help to categorize the event. Although such a categorization set forward crisp and mutually exclusive classes according to classical Aristotelian logic, recently, fuzzy logic classification including mutually inclusive classes is suggested by Zadeh (1973) and it is most frequently used in every discipline in an increasing rate. In many disciplines observations are extremely important such as in geological sciences, medicine, social studies, physiology, military movements, economics, social sciences, meteorology, engineering, etc. At times they are more valuable than numerical data, but unfortunately, their role is almost forgotten due to recent mechanical and software programs that work with numerical data.

Example 2.1
What type of observational information can be obtained when one takes hand specimen from a rock? Even a non-specialist in geology try to deduce the following basic linguistic information based on his/her observation and inspection of the specimen through a combined use of his/her sense organs.

1) Shape: Regular, irregular, round, spiky, elongated, flat, etc. This information can be supported for detailed knowledge, with the addition of adjectives such as "rather," "quite," "extremely," "moderately." Note that these words imply fuzzy information.
2) Color: Any color can be attached to whole specimen or different colors for different parts. Detailed information can be provided again by fuzzy adjectives such as "open," "dark," "gray."
3) Texture: The words for the expression of this feature are "porous," "fissured," "fractured," "sandy," "gravelly," "silty," etc.
4) Taste: The previous descriptions are through the eye but the tongue can also provide information as "saline," "sour," "sweet," "brackish," and so on.
5) Weight: It is possible to judge approximate weight of the specimen and have description feelings as "light," "heavy," "medium," "very heavy," "floatable," and likewise other descriptions can also be specified.
6) Hardness: The relative hardness of two minerals is defined by scratching each with the other and seeing which one is gouged. It is defined by an arbitrary scale of ten standard minerals, arranged in Mohr's scale hardness and subjectively numbered in scale based on degrees of increasing hardness from 1 to 10. The hardness scale provides guidance for the classification of hand specimen according to Table 2.1, where the verbal information is converted to a scale through numbers.

Table 2.1 Mohr's scale of hardness

Hardness scale	Mineral	Example
1	Talc	Hydrated magnesium silicate
2	Gypsum	Hydrated calcium sulfate
3	Calcite	Calcium carbonate
4	Fluorspar	Calcium fluoride
5	Apatite	Calcium phosphate
6	Feldspar	Alkali silicate
7	Quartz	Silicate
8	Topaz	Aluminum silicate
9	Corundum	Alumina
10	Diamond	Carbon

Example 2.2
Earthquake effect on structures can be described according to Table 2.2 guidance, which is referred to Mercalli scale. The following is an abbreviated description of the 12 scales of Modified Mercalli intensity.

Table 2.2 Mercalli earthquake intensity scales

Scales	Description
I	Not felt except by a very few under especially favorable conditions.
II	Felt only by a few persons at rest, especially on upper floors of buildings. Delicately suspended objects may swing.
III	Felt quite noticeably by persons indoors, especially on upper floors of buildings. Many people do not recognize it as an earthquake. Standing motor cars may rock slightly. Vibration similar to the passing of a truck. Duration estimated.
IV	I. Felt indoors by many, outdoors by few during the day. At night, some awakened. Dishes, windows, doors disturbed; walls make cracking sound. Sensation like heavy truck striking building. Standing motor cars rocked noticeably.
V	Felt by nearly everyone; many awakened. Some dishes, windows broken. Unstable objects overturned. Pendulum clocks may stop.
VI	Felt by all, many frightened. Some heavy furniture moved; a few instances of fallen plaster. Damage slight.
VII	Damage negligible in buildings of good design and construction; slight to moderate in well-built ordinary structures; considerable damage in poorly built or badly designed structures; some chimneys broken.
VIII	Damage slight in specially designed structures; considerable damage in ordinary substantial buildings with partial collapse. Damage great in poorly built structures. Fall of chimneys, factory stacks, columns, monuments, walls. Heavy furniture overturned.
IX	Damage considerable in specially designed structures; well-designed frame structures thrown out of plumb. Damage great in substantial buildings, with partial collapse. Buildings shifted off foundations.
X	Some well-built wooden structures destroyed; most masonry and frame structures destroyed with foundations. Rail bent.
XI	Few, if any (masonry), structures remain standing. Bridges destroyed. Rails bent greatly.
XII	Damage total. Lines of sight and level are distorted. Objects thrown into the air.

It is important to notice that the linguistic descriptions and scales are neither time- nor space-dependent, but they have event basis. The reference to any system is not required apart from logical rules.

2.3 Numerical Data Types

Evolution of any event takes place both in time and in space, but depending on the practical purposes they can be viewed either temporally or spatially or spatio-temporally. Accordingly, instruments yield numerical data based on either time or space reference system. In this book, only spatial data interpretations and treatment processes are presented. It is assumed herein that the spatial phenomena continuously cover the whole study area. Since the most elemental part of space is a point in earth sciences, the basic sampling locations are points that may be scattered in the study area either regularly or irregularly. Theoretically, there is infinite number of points, but the sampling of all points is not conceivable practically. There are two ways of sampling for conceivable studies. These are as follows:

1) Point sampling: The size of points is considered as dimensionless or infinitesimally small, with no practically considerable influence area. This is referred to as sink or source in classical analytical solutions (see Fig. 2.1).
2) Pixel sampling: The size of each point is appreciable and, therefore, the whole study area is covered with a mesh of very small squares (see Fig. 2.2).

In general, any point or pixel has a system of longitudes and latitudes. Hence, the whole earth surface is covered by quadrangles, which may be regarded as large-scale pixels. In practice, for Cartesian distance, area, and volume calculation purposes, longitudes and latitudes are converted to "northing" and "southing" values with respect to an initial reference point (see Figs. 2.1 and 2.2). This means that the elements of spatial point data include triple variables, namely, easting, e, northing, n, and the spatial variable measured at this location, say, z. In short, we can show

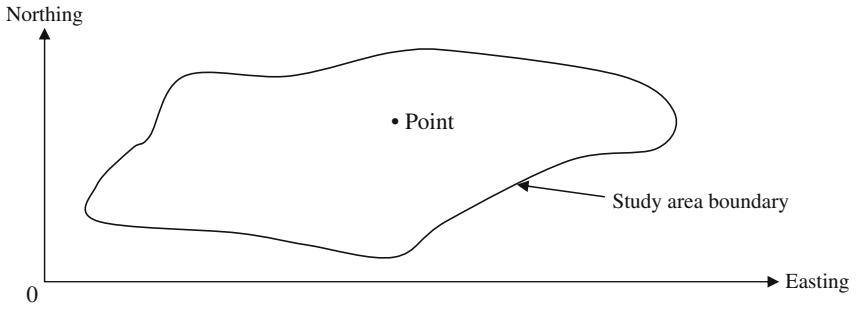

Fig. 2.1 Point sampling in an area

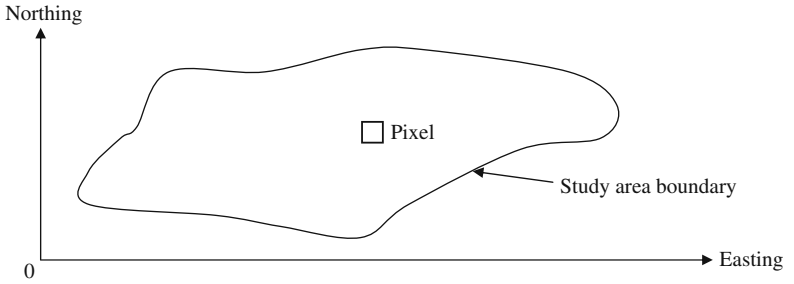

Fig. 2.2 Pixel sampling in an area

the point data as a triple, {e, n, z}. Likewise, in addition to these triple values any pixel includes its resolution size, r, which can be represented by a quadruple, {e, n, z, r}. Even though the pixel size is small, one can practically calculate the number of pixels that is necessary to cover a given area.

Example 2.3
If a study region has an area of 45 km^2 and pixel dimension is 100×100 m^2, what is the number of pixels for the representation of the whole region? The number can be calculated as $45 \times 10^6/10^4 = 4{,}500$ pixels. This simple calculation indicates that each pixel has an area of influence defined by its square area. However, it is not possible to make the same calculation for point data, since a point does not have an area of influence by itself. However, it is possible to define the area of influence for each point based on a set of neighboring points, as will be explained later in this chapter.

Irregularity is not necessarily related to randomness and has its own connotation in earth and atmospheric sciences. A very brief distinction between these two terms is that although randomness is inherent in the behavior of natural events out of human control, irregularity implies human implications in the measurement and description or definition of natural events. For instance, the locations of meteorological stations or groundwater wells are irregularly scattered in the area or space, and consequently they do not comply by any regular or random pattern. Once the irregularity is established, then it does not change with time and space easily until there are other additional inferences by human. Another good distinction in the earth and atmospheric sciences between regularity and irregularity can be considered in the solution of differential equations by numerical techniques. Finite element method requires a definite and regular mesh to be laid over the solution domain of interest (study area) with regular mesh. Boundary and initial conditions must be defined at regular set of nodes. Various types of regularity are shown in Fig. 2.3. In practical studies, measurements as initial conditions are available at a set of irregularly scattered station locations and hence there is not a desirable match between these locations and consequent regular nodes.

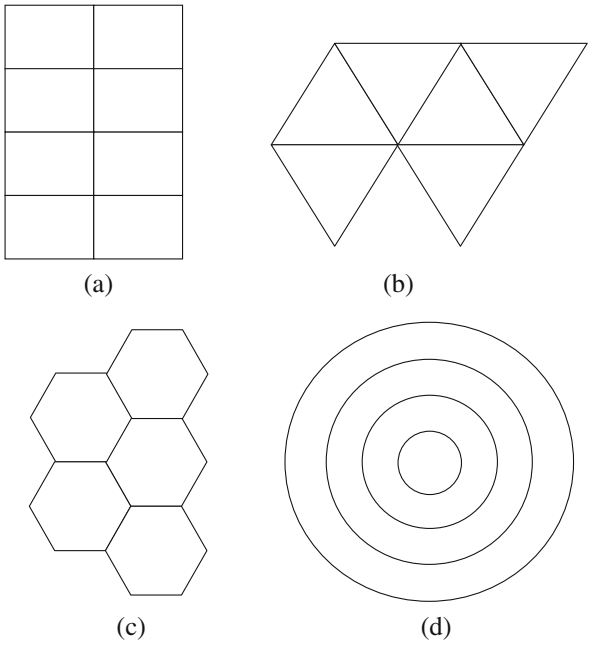

Fig. 2.3 Different regularities (**a**) rectangular; (**b**) triangular; (**c**) pentagonal; (**d**) radial

Many irregularities appear in practical applications and there is beauty even in the irregularity of the measurement points. Random sampling may be regarded as another type of irregular sampling procedure. All the meteorology station locations, water or oil well sites, soil-sampling points, etc., have irregular patterns in character. The transfer of knowledge from irregular points to regular nodes will be dealt with in detail later in this chapter and other chapters. Without such a knowledge and information transfer, none of the numerical solution models such as Kriging in earth sciences and especially General Circulation Models (GCM) in atmospheric sciences and others alike can be successfully applicable for practical solutions.

In theoretical and practical studies, randomness is accounted by the statistical and especially probabilistic methods whereas irregularity does not need uncertainty methodology for their treatment, but for the treatment of random events measured at these irregular points.

2.4 Sampling

The very significant prospect of sampling is the distribution of measurement sites within the study area. Depending on the prevailing conditions, sometimes the scatter of sampling points is already set up due to previous human activities such as water well locations, oil drillings, settlement areas, roads, etc. However, in detailed studies

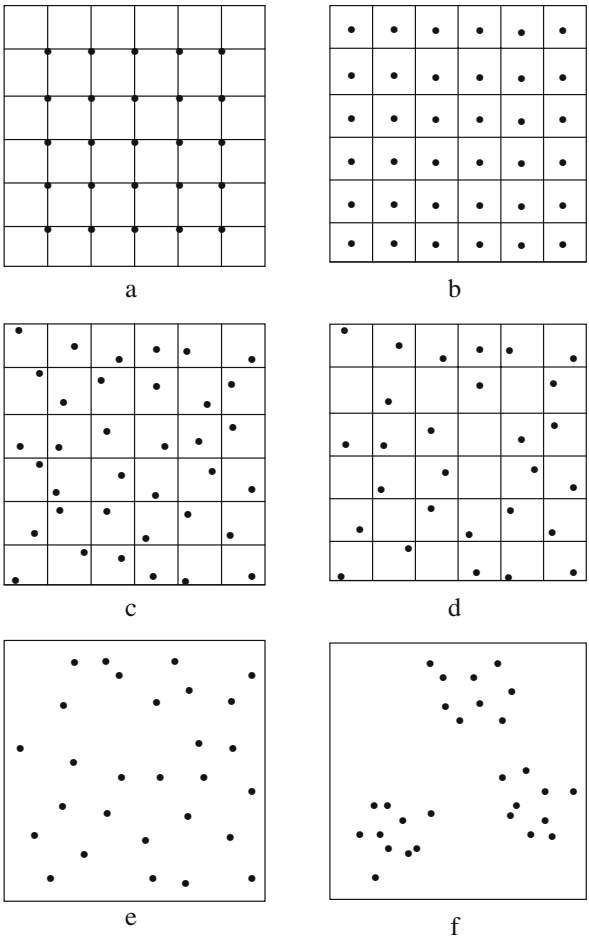

Fig. 2.4 Areal sampling patterns

at smaller scales the researches have to lay down the set of points so as to sample the concerned phenomenon in a representative manner. There are different techniques in deciding about the position of the sampling points. If nothing is known before hand, then it may seem logical to select the sampling points at nodes or centers of a suitable mesh over the study area. This is the most uniform sampling procedure as shown in Fig. 2.4.

These sampling patterns can be divided into three different categories as the regular, random, and aggregated or clustered. Figure 2.4a and b are of regular sampling procedures. In Fig. 2.4c and d, the randomness is in small scales and the random pattern remains within the sub-areal regular grids. In Fig. 2.4b although each sub-area is sampled, in Fig. 2.4d only randomly chosen sub-areas are sampled. In Fig. 2.4a the maximum distance between the two neighboring points cannot be greater than twice of the sub-area diagonal length. In Fig. 2.4c the distance is of several times

the main diagonal length of the sub-area. Large-scale random sampling patters are given in Fig. 2.4e, where there is no restriction on the distance between the sampling points. In Fig. 2.4f there are three clusters of the spatial sampling, each with random sampling patterns. Such categorized samplings are possible depending on the areal occurrence of the phenomenon studied. For instance, if ore, water, or oil deposits are intact from each other at three neighboring areas, then the cluster sampling patterns arise.

Another feature of spatial sampling points is its uniformity concerning the frequency of occurrence per area. If the density defined in this manner is equal in each sub-area, then the spatial sampling is uniform; otherwise, it is non-uniform. This definition implies that the regular sampling points in Fig. 2.4a and b, in addition to small-scale random pattern in Fig. 2.4c, are all uniform because there is one point per sub-area.

Uniformity gains significance if there are many sampling points within each sub-area. In geological or meteorological studies, sub-areas are quadrangles between two successive longitudes and latitudes. For instance, such a situation is shown in Fig. 2.5 where each quadrangle has random number of random sampling points. Hence, the question is whether the sampling point distribution is uniform or not?

The pixels present a regular mesh over a region, which is conceptually similar to numerical solution of analytical models. The difference is that in the case of pixels the measurements (brightness values) are known, but this is not the case in numerical analysis where the values either at the center of each cell or at each node are necessary for calculation.

A set of point data from a region on interested event such as the elevations at 25 different sites can be presented in three columns, two of which are location descriptions and the third column includes the regional variable, which is elevation in this case (see Table 2.3). This table is an example for triple values as mentioned before.

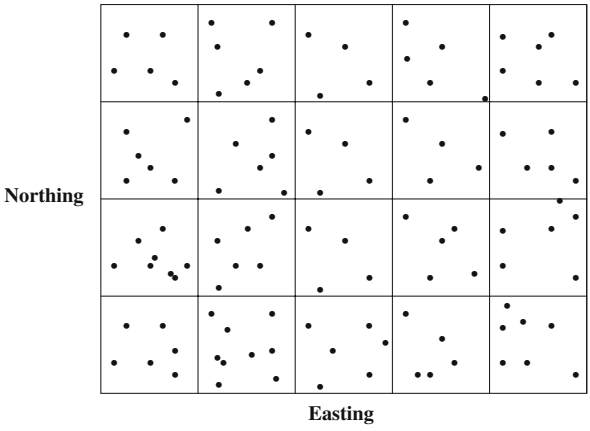

Fig. 2.5 Quadrangle sampling

Table 2.3 Elevation data

Points	Easting	Northing	Elevation (m)	Points	Easting	Northing	Elevation (m)
1	534371.3	2449324	60	14	569732.8	2353515	750
2	589853.8	2362837	116	15	620966.6	2362115	570
3	539568.8	2432734	570	16	612983.4	2391577	110
4	605430.4	2359240	228	17	596556.5	2397926	700
5	626244	2350163	710	18	619828.7	2399006	60
6	619177.6	2370404	60	19	527607.4	2385670	710
7	570437.2	2454979	520	20	658855.3	2376279	1240
8	560157.4	2447557	280	21	520716.1	2377359	540
9	563857.7	2453414	11	22	655595.2	2355951	280
10	615788.4	2361155	660	23	646632.6	2390925	125
11	543309.8	2427824	720	24	650305.8	2366972	90
12	572452.4	2389806	910	25	641826.4	2348446	350
13	604572	2358312	11				

In this table, the scatter of sample points can be obtained from the second and third columns, which appear as in Fig. 2.6. The first appearance indicates that the sampling points are irregularly distributed in the study area. However, it is not possible to say whether their distribution is random or there is a systematic correlation. This question will be answered in Chapter 3.

This may not be a representative sampling set for the study area because there are no sampling points in the upper right and lower left parts of the area.

Although the spatial data are understood as the sampling of a variable with respect to longitudes and latitudes, it is also possible to consider another two variables instead of longitude and latitude. For instance, similar to Table 2.3 in Table 2.4 calcium, magnesium, and chloride variables are given in three columns. These values are taken at a single point in space at a set of time instances.

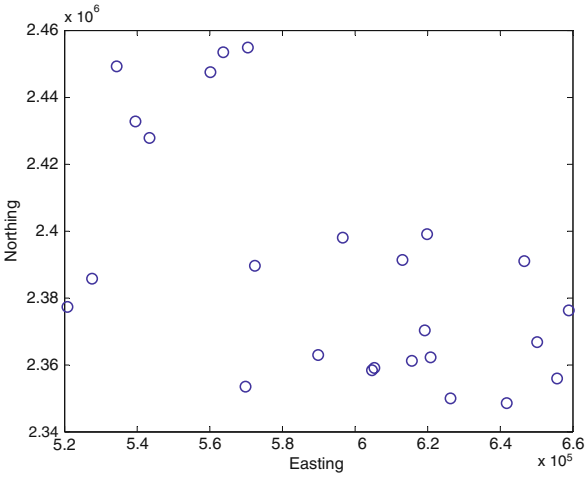

Fig. 2.6 Irregular sample points scatter

Table 2.4 Calcium, sodium, and chloride measurements

Point	Calcium (ppm)	Sodium (ppm)	Chloride (ppm)	Point	Calcium (ppm)	Sodium (ppm)	Chloride (ppm)
1	135.01	20.76	134.48	16	80.57	45.14	165.41
2	63.11	57.34	194.97	17	133.55	55.47	141.99
3	100.68	42.25	183.24	18	131.69	41.44	126.73
4	88.60	66.59	156.74	19	81.03	35.23	164.19
5	129.13	43.30	182.70	20	129.37	29.48	153.20
6	116.21	40.93	159.03	21	45.79	29.67	179.22
7	85.65	62.31	111.30	22	75.29	54.11	203.53
8	41.85	46.26	103.46	23	121.32	35.14	138.39
9	122.14	30.13	111.18	24	40.99	47.08	192.02
10	84.47	53.61	140.11	25	53.89	27.54	85.94
11	101.54	61.91	169.07	26	60.28	54.89	206.96
12	119.19	20.98	106.39	27	59.87	38.92	100.72
13	132.18	54.06	185.77	28	100.38	63.00	97.85
14	113.82	38.97	145.21	29	67.22	62.68	191.36
15	57.63	61.59	115.56	30	59.88	49.68	170.60

In this case there are three alternatives for data treatment purposes. The following similar questions can be asked:

1) Does one want the change of chloride with respect to calcium and sodium? or
2) Does one want the change of calcium with respect to chloride and sodium? or
3) Does one want the change of sodium with respect to calcium and chloride?

Of course, each one of these cases presents different scatter diagrams as presented in Fig. 2.7. In each case, the third variable plays the role of elevation as in the preparation of topographic maps.

In each case, the triplicate {e, n, z} has {e, n}, {e, z}, and (n, z} alternatives, which are referred to as scatter diagrams.

2.5 Number of Data

In this book spatial data will imply at the minimum the existence of three points within the study area, because they represent a spatial form as the simplest plain trend. However, it must not be understood that only triplets are necessary for spatial modeling. The practical question is how many data are necessary for spatial data modeling. There is not an easy answer to such a question. The ready answers as appearing in open literature such as 12 or 30 data points are not logical, but they may provide vague and practical solutions depending on the circumstances. If the purpose is to check whether the data confirms with the normal probability distribution, then 12 data are enough. On the other hand, 30 is a number which is based on empirical observations that in the representation of average meteorological

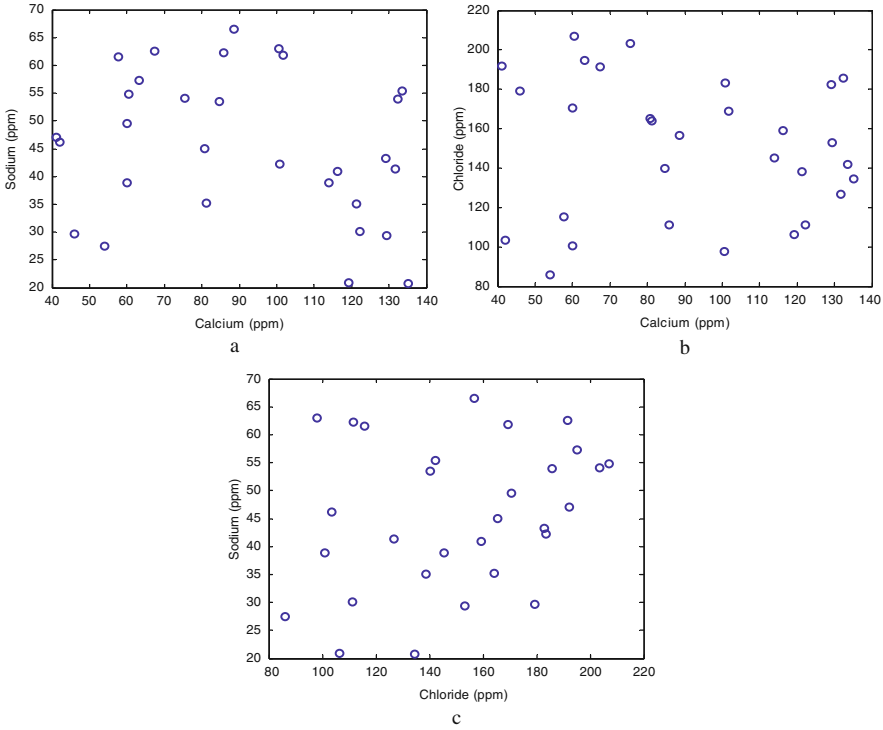

Fig. 2.7 Sample points scatter diagrams (**a**) Calcium-sodium; (**b**) Calcium-chloride; (**c**) Chloride-sodium

phenomenon it is adopted by the World Meteorological Organization (WMO) as a normal period. Unfortunately, neither of these numbers can be adopted in practical applications without looking at the behavior of the concerned phenomenon features, properties, and environmental conditions. In order to have answer in a more realistic manner, the following points must be taken into consideration:

1) If the phenomenon is spatially homogeneous in a deterministic manner, then the number of sample will be as small as possible. In fact, in the case of perfectly homogeneous spatial distribution only one sample point is enough. This is a very theoretical situation and difficult to come across in earth sciences studies. Logically, in such a case there is no spatial variation and therefore the variance of the spatial variation is equal to zero. This implies that the smaller the standard deviation the smaller is the representative sample size. Numerical expression of this situation can be achieved by standard deviation, similarity, or correlation coefficients (Şen, 2002). The more the correlation coefficient (close to either +1, i.e., completely positively proportional or –1 as the negatively inverse), the smaller will be the data number. Finally, the more the similarity coefficient (equal to 1) the smaller will be the data number.

2) If the regional phenomenon is randomly homogeneous (heterogeneous), it is then necessary to take as much data sample (measurement) as possible. However, there must be an upper limit for the data number, which may be decided not only on the basis of statistical criterion but also at times more significantly on the cost of samples and on sampling occasions such as in rare events (floods, droughts, etc.).
3) Areal coverage of the samples must also be decided by taking into consideration the effective area of influence of each sample, which will be explained in Chapter 3 in detail.

2.5.1 Small Sample Length of Independent Models

In general, statistical parameters from finite length records are biased estimations of population (very long samples) counterparts. Estimates whose population values (expectations) are not equal to the parameter they estimate are said to be biased. This is due to the lack of complete information concerning the phenomenon and, consequently, the parameter will be under- or over-estimated with respect to its true population value. In practice, the true population parameters, which are independent of sample length, are not known, but it is possible to estimate them from the available finite length records. As mentioned before, as a rule of thumb it is necessary to have at least 30 values in order to have normal parameter estimations. However, 30-year period cannot be equally valid for all random or regionalized variables (ReV). It is very much a function of the correlation structure. In short, the more the persistence, (correlation) the smaller the necessary data. In practical applications, it is of great interest to know the number of data that is necessary to have a stable value on the average. This is equivalent to saying that the variance of the average parameter estimation must be constant. From this point, Cramer (1946) showed theoretically for the normal independent ReVs that the variance, $V_I(\overline{x})$, of the arithmetic averages for sample length n is

$$V_I(\overline{x}) = \frac{\sigma^2}{n}, \tag{2.1}$$

where σ^2 is the unknown population variance and n is the number of data. This is also due to the central limit theorem that the average of random samples accords in normal pdf with mean equal to the average of the data, $\overline{x}$, and the variance of the averages is given as in Eq. (2.1). The square root of this expression is referred to as the standard error, e, of estimate of arithmetic mean. If the original data come from an independent ReV process with population mean, μ, and standard deviation, σ, then the finite sample averages will have the same arithmetic mean with variance as in Eq. (2.1). This means that the sample average is an unbiased estimate of the arithmetic mean with a standard error as

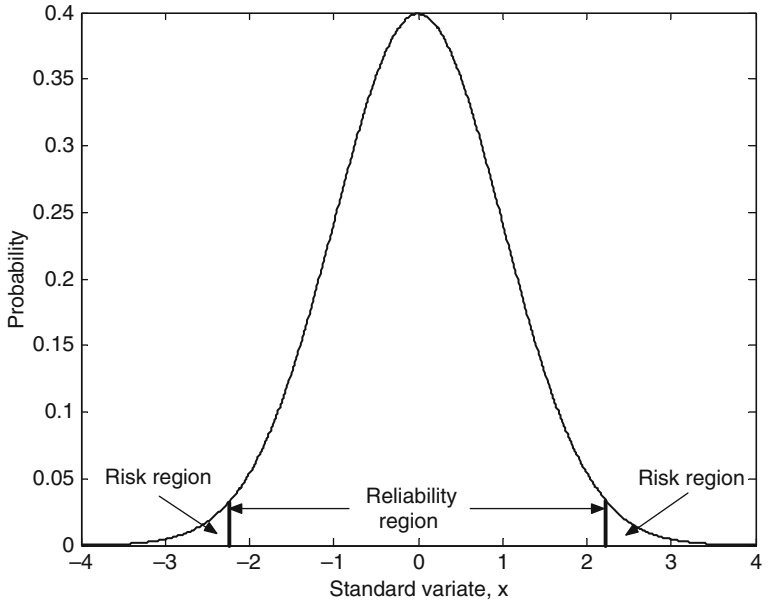

Fig. 2.8 Standard Gaussian pdf

$$e = \frac{\sigma}{\sqrt{n}}, \tag{2.2}$$

which decreases with the square root of the sample length. ReVs are sampled over various space (or time) intervals. It is necessary to take 10 (90)% standard error (reliability, significance) level corresponding to standard deviate, x_{90} value from a standard Gaussian distribution as shown in Fig. 2.8. This level separates the whole area under the standard normal pdf into two parts as reliability and risk regions (Şen, 1998a).

It is possible to obtain a practical chart between the three variables in Eq. (2.2), which gives the relationship between the data number depending on the reliability level as in Fig. 2.9.

Example 2.4

In an extensive area there is an unconfined groundwater aquifer in rather homogenous sandstone. The field tests indicated that the radius of influence of each well is 650 m. So how many samples must be drilled such that there will not be interference between the adjacent wells in a total region of 5 km^2? For the numerical answer, it is necessary to first calculate the area of influence for each well as $3.14(650)^2 = 1{,}326{,}650\ m^2 = 1.3266\ km^2$. Now the number of wells can be found as $5/1.3266 = 3.769 \sim 4$ wells.

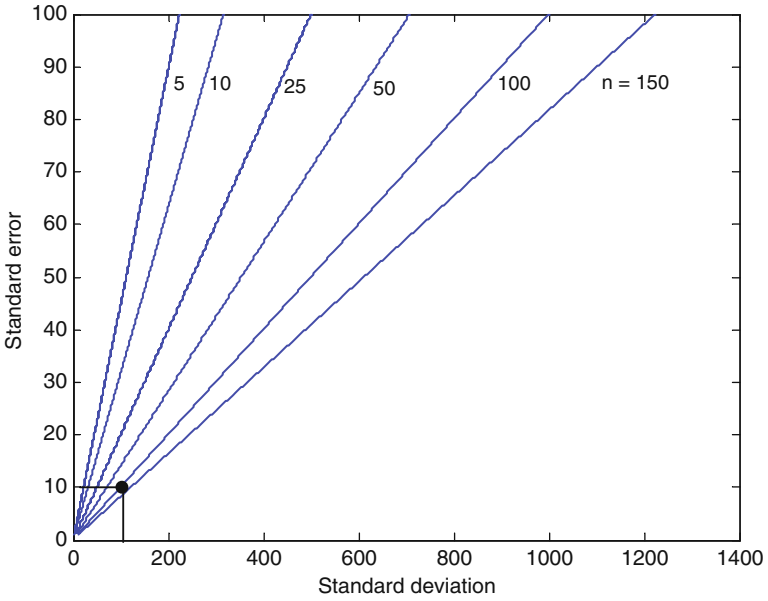

Fig. 2.9 Sample number with the standard deviation and reliability level

Example 2.5
In a region n = 10 well samples of electric conductivity (EC) in micromhos per centimeter are recorded as given in Table 2.5. What is the representative number of data?

Table 2.5 EC samples

Data number	1	2	3	4	5	6	7	8	9	10
EC	770	1020	997	790	750	760	765	850	1029	900

The arithmetic average and the standard deviation of the data values are 863.1 μmhos/cm and 114.82 μmhos/cm, respectively. The samples are assumed to have spatial independence. Find the number of data for e = 10%.

Since the standard deviation for the given example is 114.82 ppm then at 10% standard error level one can find the number of representative data from Fig. 2.9 as 100.

2.5.2 Small Sample Length of Dependent Models

The smaller the sampling interval (distance) the more is the correlation between nearby observations, and consequently the simple result in Eq. (2.2) cannot be

applied directly to the averages of dependent series. The physical phenomena within the earth sciences (as atmosphere) that give rise to such features are non-linear dynamic systems with limited predictabilities. Therefore, it is not convenient to have a very persistent process in their systematic modeling, but rather lower-order processes seem more convenient without any mathematical complications. For instance, Schubert et al. (1992) proposed a first-order Markov process to provide a general picture of the persistence-based model behaviors compared to the General Circulation Model (GCM) in atmospheric sciences. First-order Markov processes have short memory of the correlation function and therefore they are not sufficient in the GCM. The same authors then attempted to improve the situation upon the statistical model by fitting low-order univariate Auto-Regressive Integrated Moving Average (ARIMA) models to the control run of the GCM. Detailed information concerning these models is available from Box and Jenkins (1976) as a natural extension of the first-order Markov model, and they are useful in modeling atmospheric behaviors (Chu and Karz, 1985). In addition to finite sample length, the autocorrelation structure of the process causes further source of bias (Kendall, 1954; Quenouille, 1956).

In order to model persistence within earth sciences ReVs, herein, the ARIMA (1,0,1) model is considered. It is the mixture of separate stochastic processes including autoregressive and moving average models. The numbers in the argument as (1,0,1) imply that this type of ARIMA model is composed of first-order autoregressive (Markov) and first-order moving average processes with zero order difference between successive values. Generally, the model is written mathematically as follows:

$$x_i = \phi x_{i-1} - \theta \varepsilon_{i-1} + \varepsilon_i, \tag{2.3}$$

where ϕ and θ are the autoregressive and moving average parameters, respectively, and ε_i is a zero-mean independent (white noise) random variable. The autocorrelation structure of the same process is presented in terms of the model parameters as (Box and Jenkins, 1976)

$$\begin{aligned} \rho &= 0, \\ \rho_1 &= \frac{(\phi - \theta)(1 - \phi\theta)}{(1 + \theta^2 - 2\phi\theta)}, \\ \rho_i &= \phi\, \rho_{i-1} \quad (i \geq 2). \end{aligned} \tag{2.4}$$

These expressions reduce to the white noise case when ϕ and θ are equal to zero; to first-order Markov process case if $\theta = 0$ and $\phi = \rho$; and finally, to the moving average process for $\phi = 0$. For this model, the variance of time averages can be calculated by using model parameters, which are the fundamental quantities related to some statistical parameters that can be estimated from available data. In order to illustrate this point, let us consider the data smoothened using a simple arithmetic average of length m less than record length n. Hence, the arithmetic average for such a subsample length n is

$$\overline{X}_n = \frac{1}{n}\sum_{i=1}^{n} X_i. \tag{2.5}$$

By taking first the square and then the expectation operator on both sides leads after some algebra to

$$V(\overline{X}_n) = \frac{1}{n^2}\left[\sum_{i=1}^{n} E(X_i^2) + \sum_{i=1}^{n}\sum_{j=1}^{n} E(X_i X_j)\right] - \mu^2. \tag{2.6}$$

Of course, it is assumed $E(X_i) = \mu$. It is well known from mathematical statistics that for identically distributed random variables $E(X_i^2) = E(S^2) + \mu^2$ and $E(X_i X_j) = E(S^2)\rho^{|i-j|} + \mu^2$ and their substitution into the last expression yields

$$V_A(\overline{X}_n) = \frac{E(S^2)}{n^2}\left[n + 2\sum_{i=1}^{n}(n-i)\,\rho_i\right]. \tag{2.7}$$

The substitution of ARIMA (1,0,1) autocorrelation structure from Eq. (2.4) leads to

$$V_A(\overline{X}_n) = \frac{E(S^2)}{n^2}\left\{n + \frac{2\,\rho_1}{(1-\phi)^2}\left[(1-\phi) - (1-\phi^n)\right]\right\}. \tag{2.8}$$

This expression provides a common basis for the change calculations by giving the variance of the pdf of the ReV means for finite lengths, i.e., sub-samples, from a complete data set. For large samples ($n > 30$) the distribution of means converge to a normal pdf due to the well-known central limit theorem in statistics. Square root of Eq. (2.8) is equal to the standard deviation of such a normal pdf. Consequently, it can be used for determining whether the small sample mean value in a given REV is significantly different from its long-term mean value, μ, supposedly calculated from the whole record. For this purpose, the executions of the following steps are necessary:

1) Identify the underlying stochastic or ReV model for the given earth sciences phenomenon.
2) Find the theoretical variance of the averages by substituting the necessary model parameters into Eq. (2.8).
3) Consider the population pdf of the given data averages as a normal pdf with mean, μ, and standard deviation $\sigma_A = \sqrt{V_A(\overline{X}_n)}$
4) Find the standard deviate, t, for the means calculated from a given length, m, as

$$t = \frac{\overline{X}_n - \mu}{\sigma_A}. \tag{2.9}$$

5) Accept a certain level of significance, α_s, and find the corresponding confidence limit, $\pm t_c$, from the standard normal pdf table given in any statistics book (Davis, 2002).
6) If $t \leq |t_c|$, then the conclusion is that only sampling errors cause random variability and there is no long-term persistence variability (change); otherwise, the earth sciences data are effected from systematic changes due to some atmospheric and/or environmental reasons.

For the first-order Markov process, similar expressions to Eq. (2.8) can be obtained provided that ϕ is substituted by ρ_1, which leads to

$$V_A(\overline{X}_n) = \frac{E(S^2)}{n^2}\left\{n + \frac{2\,\rho_1}{(1-\rho_1)^2}\left[(1-\rho_1) - (1-\rho_1^n)\right]\right\}. \tag{2.10}$$

This expression reduces to Eq. (2.1) for $\rho_1 = 0$, which corresponds to the case of independent model as explained in the previous section.

Generally, even for very small samples ($n < 30$) one can use Chebyshev inequality, which states that the probability of single value, say σ_A, selected at random to deviate from μ of the pdf more than $\pm\sqrt{V_A(\overline{X}_n)}$ is less than or equal to $1/K^2$, and it can be expressed in mathematical form as

$$P\left[|\sigma_A - \mu| \geq K\sqrt{V_A(\overline{X}_n)}\right] \leq 1/K^2. \tag{2.11}$$

This inequality yields upper and lower limits on the probability of deviation of a given magnitude from the mean value. Hence, it is possible to find confidence intervals on either sides of the average value.

Example 2.6
Let us calculate 95% confidence (reliability) limits for an ARIMA (1, 0, 1) model with model parameters $\phi = 0.6$ and for a finite length data, $n = 15$. First of all, from Eq. (2.4) one can find that $\rho_1 = 0.34$, the substitution of which with other relevant values into Eq. (2.8) gives $\sqrt{V_A(\overline{X}_n)} = 0.40\,\sigma$. Confidence level of 95% implies that $1/K^2 = 0.95$ or $K = 1.026$ and accordingly $K\sqrt{V_A(\overline{X}_n)} = 0.41\,\sigma$. Consequently, the confidence interval limits are. Finally, if the calculated square root of variance of a finite data averages with $n = 15$ lies outside of these limits, then there is a trend with the possibility of ReV change. Of course, for any desired small sample size confidence interval limits can be calculated easily according to the aforementioned procedure.

On the other hand, for the moving average case $\phi = 0$, and hence from Eq. (2.4) $\rho_1 = -\theta/(1+\theta^2)$ and its substitution into Eq. (2.8) leads to

$$V_A\left(\overline{X}_n\right) = \frac{\sigma^2}{n^2}\left[n - \frac{2\,(n-1)\,\theta}{1+\theta^2}\right]. \tag{2.12}$$

It is important to notice that when $\theta = 0$ this expression becomes identical to Eq. (2.1). On the other hand, the well-known statistical estimate of small sample variance, S^2, is given as

$$S^2 = \frac{1}{n-1}\sum_{i=1}^{n}(X_i - \overline{X})^2. \tag{2.13}$$

The existence of n–1 rather than n in the denominator of Eq. (2.13) is because of obtaining unbiased variance estimate for independent processes. Indeed, taking the expectation of both sides leads to $E(S^2) = \sigma^2$. This indicates with no hesitation that it is possible to substitute σ^2 in Eq. (2.1) by its sample estimate for independent ReVs. However, as will be shown in the following sequel this is not true for dependent processes. It has already been shown by Şen (1974) that for dependent processes

$$E(S^2) = \sigma^2\left[1 - \frac{2}{n(n-1)}\sum_{i=1}^{n}(n-i)\rho_i\right], \tag{2.14}$$

where ρ_i represents lag-i autocorrelation coefficient. This last expression shows that there is bias effect not only due to the finite sample length, n, but also more significantly due to autocorrelation structure of the ReV. Substitution of Eq. (2.4) into Eq. (2.14) leads, after some algebraic manipulations, to

$$E(S^2) = \sigma^2\left\{1 - \frac{2\,\rho_1}{n(n-1)}\left[\frac{n(1-\phi) - (1-\phi^n)}{(1-\phi)^2}\right]\right\}. \tag{2.15}$$

This expression proves that there is always an under-estimation of the population variance from a given finite data set; the amount of bias depends on the finite sample length and the model parameters that govern the dependence structure. In order to obtain an unbiased estimate of the population variance, the sample estimate of the variance must be divided by the curly bracket term in Eq. (2.15) as explained in detail by Şen (1974).

A common point of the equations derived above is their asymptotic convergence to a common value (σ^2/n) as the finite size of data n increases. In order to objectively define a characteristic sample length for convergence, a certain level of relative error percentage α_r will be adopted and it is defined generally as

$$\alpha_r = 100\,\frac{\sigma^2 - E(S^2)}{\sigma^2}.$$

Hence, substitution of Eq. (2.15) into this expression leads to the most general form of the relative error for the ARIMA (1,0,1) model as

$$\alpha_r = \frac{2\,\rho_1}{n(n-1)}\left[\frac{n(1-\phi) - (1-\phi^n)}{(1-\phi)^2}\right]\text{x}100. \tag{2.16}$$

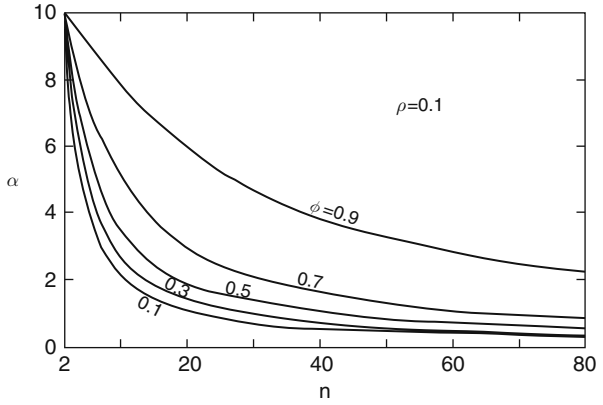

Fig. 2.10 Variance of average estimate relative error change with sample length ($\rho_1 = 0.1$)

Based on this expression the change of relative error, α_r, with the sample length n for a set of ρ_1 values are presented as charts in terms of ϕ values in Fig. 2.10.

A close inspection shows an exponential decrease in all the charts with sample length. Increase in ρ_1 implies increase in the relative error percentage for a given sample length. In these figures the Markov model case corresponds to the curves where $\rho_1 = \phi$. These charts are useful tools in finding equivalent independent model length for a given dependent model length, provided that the relative error percentage is given. For instance, when 10% error level is acceptable in the first-order Markov model small data mean variance estimation with $\rho_1 = 0.3$, then it is possible to find from chart in Fig. 2.10 that after at least eight samples the ReV will not have dependence structure. However, for the same error level and dependence coefficient, an ARIMA (1,0,1) model requires at least 11, 16, and 48 samples for $\phi = 0.5$, 0.7, and 0.9, respectively.

These charts can also be used as indicators whether there is a trend in a given ReV. For example, if the underlying generating mechanism is identified using the procedures of Box and Jenkins (1976) as an ARIMA (1, 0, 1) model with $\rho_1 = 0.5$ and $\phi = 0.7$, then the error percentage is calculated from Eq. (2.16). If this error percentage is greater than the theoretically calculated counterpart, then there is a possibility of trend.

Another relative error for measuring any deviation from the independent model with no long-term systematic features can be defined by considering Eqs. (2.1) and (2.8) as

$$\beta = 100\frac{V_A(\overline{X}n) - V_I(\overline{X}_n)}{V_A(\overline{X}_n)}.$$

This expression provides information about the necessary sample length concerning the variance of climatic sub-sample averages. It is possible to write this expression explicitly in terms of model parameters from Eqs. (2.1) and (2.8) as

$$\beta = 100\left\{1 - \frac{1}{n + \frac{2\rho_1}{(1-\theta)^2}\left[(1-\theta) - (1-\theta^n)\right]}\right\}. \tag{2.17}$$

Finally, if the variance of short data and the variance of sub-sample averages are calculated for the same sample length, then the relationship between these two types of relative errors can be found from Eqs. (2.16) and (2.17) as

$$\beta = 100\left[1 - \frac{1}{1 + \frac{n-1}{100}\alpha_r}\right], \tag{2.18}$$

which implies that β is equal to zero only when α_r approaches to zero. Otherwise, for any given α_r, there is an implied β-type error. The graphical representation of Eq. (2.18) is given in Fig. 2.11. If any pair of α_r, β, and n values are known, then the third one can be determined from this chart easily.

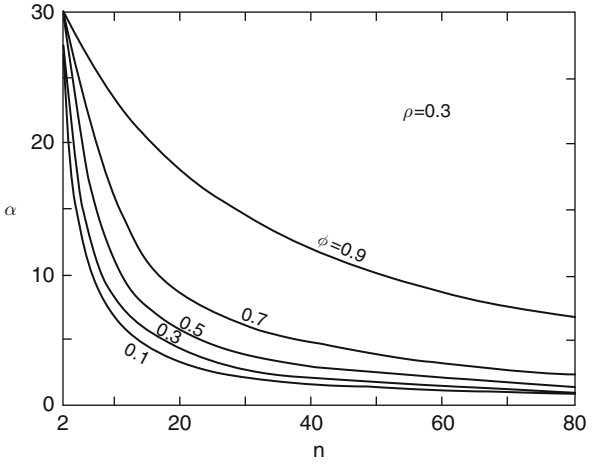

Fig. 2.11 Variance of climatic series average estimate relative error change with sample length ($\rho_1 = 0.3$)

2.6 Regional Representation

Decision-making about which model to use for spatial estimation should be based on some simple criteria as the number of data points, variability range, arithmetic average, standard deviation, geometrical configuration of sampling points, distances, and in general distance-regional variability. Classical parameters such as the arithmetic average, standard deviation, skewness coefficient in terms of summary statistics can be readily known by the reader, and therefore they will not be elaborated in this book (see Davis, 2002).

2.6.1 Variability Range

In spatial analysis, the purpose is to estimate ReV at any desired point within the study area using the measurements at a set of sampling points. Such a task will depend not only on the internal variability at a fixed site of the variable but also more significantly on the regional scatter of sampling points and the number of points. Provided that the internal variability range does not differ more than 5% between the maximum and the minimum data values, then one can depend on either the arithmetic average or more specifically on the mode (the most frequently appearing data value) as the sole representative for whole region. This method depends on any number of data without data number specification. If the maximum and the minimum ReV values are Z_M and Z_m, respectively, then the range of data variability is defined as

$$R_Z = Z_M - Z_m. \tag{2.19}$$

The maximum percentage error can be defined as follows:

$$e_m = 100\,\frac{R_Z}{Z_M}. \tag{2.20}$$

If $e_m \leq 5$, then the regional representative value can be taken as the arithmetic average, $\overline{Z}$, at any point. This needs no detailed spatial modeling and it shows that the phenomenon is not complex within the area and its behavior is more or less homogeneous.

In order to be on a better side instead of arithmetic value, the mode, M_Z, value can be adopted. The mode is the most frequently occurring data vale within the whole record.

Whatever the case may be, the regionalized variable is represented by a constant value and, therefore, there will be deviations from this constant level, which are the errors that could not be accounted by the constant value. Mathematically, it is possible to suggest a procedure where the sum of square deviations (SSD) is the minimum. Hence, if the constant level of n data values Z_i (i = 1, 2, …, n) is indicated by Z_C, then the SSD becomes

$$SSD = \sum_{i=1}^{n} (Z_i - Z_C)^2, \tag{2.21}$$

which on expansion becomes

$$SSD = \sum_{i=1}^{n} Z_i^2 - 2Z_C \sum_{i=1}^{n} Z_i + n\,Z_C^2. \tag{2.22}$$

Since the minimum value is sought, the derivative of this last expression with respect to Z_C leads to

$$\frac{\partial\,(\mathrm{SSD})}{\partial\,Z_C} = -2\sum_{i=1}^{n} Z_i + 2\,n\,Z_C. \tag{2.23}$$

If this is set equal to zero, then the result becomes

$$Z_C = \frac{1}{n}\sum_{i=1}^{n} Z_i, \tag{2.24}$$

which is equal to the arithmetic average, $\overline{Z}$. This proves that irrespective of any practical requirement, the use of arithmetic average as a representative value for the regionalized variable is a mathematical necessity. Further interpretation of Eq. (2.24) can be given after its explicit form as

$$Z_C = \frac{1}{n}Z_1 + \frac{1}{n}Z_2 + \frac{1}{n}Z_3 + \ldots + \frac{1}{n}Z_{n1}, \tag{2.25}$$

which means that the arithmetic average is the summation of point data value multiplied by a factor (1/n as weighting factor), which may have different interpretations.

1) The factors may be considered as weights for each data point, and therefore they may represent some specific feature of the data point apart from the data point value. For instance, weight may be the influence area of the point or some important coefficient such as the relationship of this data value with the available points. In this latter case, the factors may be the function of correlation between data point pairs in addition to distances. In Eq. (2.25) the factors are the same, which implies the isotropic behavior of the regionalized phenomenon, which is not the case in natural events, and therefore each factor is expected to be different than others.
2) In Eq. (2.25) equivalence of factors as 1/n reminds one that if there are n data points, provided that they have equally likely future occurrence chances, the probability of occurrence for each data value is $p = 1/n$. This corresponds to random field case where the occurrences are completely independent from each other, i.e., there is no regional correlation within the regionalized variable. However, in actual situations these probability of occurrences are not equal.
3) Another significant point from Eq. (2.25) is that the summation of the factors or probabilities is always equal to 1. Furthermore, the factors are in percentages.
4) Finally, each factor is distance-independent whereas in any natural phenomenon there are regional dependences, which may be simply expressed as inverse distance or inverse distance square weightings without natural consideration (see Section 2.6.2).

If the word "weight" is used instead of the aforementioned factor or probability, then the arithmetic average expression in Eq. (2.25) can be written for more general uses as the weighted average as

$$Z_C = \sum_{i=1}^{n} \alpha_i Z_i, \tag{2.26}$$

where α_i's are the weightings. Consideration of percentage property of the weightings, this last expression can be written in its most explicit form as

$$Z_C = \sum_{i=1}^{n} \left(\frac{W_i}{W_T} \right) Z_i, \tag{2.27}$$

where W_i is the weight attached to i-th data point and W_T represents the total weight as the summation of all weights

$$W_T = W_1 + W_2 + \ldots + W_n, \tag{2.28}$$

with n number of data points. The weights that are assigned to the estimation points according to the weighting function are adjusted to sum to 1.0. Therefore, the weighting function actually assigns proportional weights and expresses the relative influence of each estimation point. A widely used version of the weighting process assigns a function whose exact form depends upon the distance from the location being estimated and the most distant point used in the estimation procedure. This inverse distance-squared weighting function is then scaled so that it extends from 1 to 0 over this distance. Equation (2.26) is in the form of linear multiple regression and it furnishes the basis of all the linear estimation models in spatial analysis as will be explained in this book.

Logically, the use of mode value is preferable because it is the most frequently occurring data value within the given set of data points. The basis of mode is probabilistic rather than mathematical, and it has the most likely probability of occurrence. A decision is to be made between the arithmetic average and the mode value in practical applications. If the pdf of the regionalized variable is symmetric, then the two concepts fall on each other. Otherwise, the use of mode must be preferable, but mathematically its calculation is not easy and therefore in any statistical or mathematical modeling arithmetic average is used invariably. The reader should keep in mind that although it yields the minimum error, it does not abide with the most frequently occurring data value. The arithmetic average value renders the mathematical procedures into a tractable form.

2.6.2 Inverse Distance Models

As mentioned in the previous section, the general regional estimation procedure is given in Eqs. (2.26) or (2.27). In these expressions the most important part is the attachment of weights. Once the weights are known, the remaining is simple calculation of the desired value at the point of estimation. Rational and logical procedures are straightforward and one can conclude that as the distance, d, between two sites increases, their effect on each other becomes meager; and hence, if only the distance is considered without the regional variability feature of the phenomenon concerned, then the first rational approach suggests that the weights can be taken as inverse distances, 1/d. However, in such an approach very small distances yield big weights and at zero distance it is not defined. Another path of thought is the gravitational force between two heavenly bodies where the attraction force is inversely proportional with the square of distance, $1/d^2$. It is even possible to generalize the inverse distance methodology as $1/d^{\alpha}$, where α is a power parameter assuming values greater than 1. The explicit expression used for the estimation, $\hat{Z}_j$ at point j according to IDP is given as

$$\hat{Z}_j = \frac{\sum_{i=1}^{n} \frac{1}{d_{ij}^{\alpha}} Z_i}{\sum_{i=1}^{n} \frac{1}{d_{ij}^{\alpha}}}, \tag{2.29}$$

where d_{ij} is the effective separation distance between grid node "j" and the neighboring points "i," Z_i's are the neighboring point ReV values and α is the weighting (smoothing) power. It is possible to derive special features from this general expression, which are well known in the literature. The last equation becomes equal to inverse distance and inverse square distance for $\alpha = 1$ and $\alpha = 2$, respectively. The slopes at the points used in the estimation procedure are weighted according to the distances between the estimation node and the other points. Various inverse distance functions are presented in Fig. 2.12.

Weighting is assigned to data through the use of a weighting power that controls how the weighting factors drop off as distance from a grid node increases. The greater the weighting power the less effect points far from the grid node has during interpolation. As the power increases, the grid node value approaches the value of the nearest point. For a smaller power, the weights are more evenly distributed among the neighboring data points. Normally, inverse distance function behaves as an exact interpolator, but still does not take into consideration the inherent ReV variability in the phenomenon concerned. In calculating a grid node, the weights assigned to the data points are fractions and the sum of all the weights is equal to 1.0 (Eq. 2.28). When a particular observation is coincident with a grid node, the distance between that observation and the grid node is 0.0, and that observation is given a weight of 1.0 while all other observations are given weights of 0.0. Thus, the

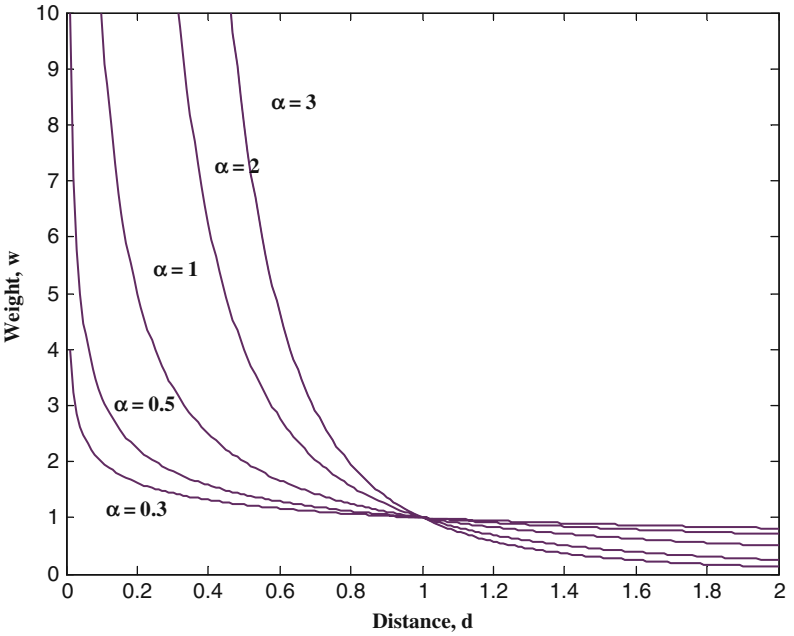

Fig. 2.12 Various inverse distance models

grid node is assigned the value of the coincident observation. Here α is a mechanism for buffering this behavior. When one assigns a non-zero smoothing parameter, no point is given an overwhelming weight so that no point is given a weighting factor equal to 1.0.

One of the characteristics of inverse distance function is the generation of "bull's-eyes" surrounding the position of observations within the gridded area. One can assign a smoothing parameter during inverse distance function to reduce the "bull's-eye" effect by smoothing the interpolated grid. Inverse distance function is a very fast method for gridding. With less than 500 points, one can use all data search types and gridding proceeds rapidly.

2.7 Sub-areal Partition

The whole study area may be partitioned into regular or irregular sub-areas each with the same feature, hence the regional changes are considered as partially homogeneous within each sub-area. For instance, in Figs. 2.3 and 2.4 although the sub-areas are in the form of regular quadrangles, sample points are located within these sub-areas in a systematic or random manner. In this section, instead of points, sub-areas are considered in the modeling of ReV variability.

2.7.1 Triangularization

The number of data points is also important in deciding which spatial prediction model must be adopted. No need to say that spatial variability is describable by at least three data points, which give the shape of a triangle; and, therefore, in the early approaches before the advent of computers, triangularization method was preferred due to its simplicity. If there are n data points, it is possible to obtain n–2 adjacent triangles. For instance, five sampling points (A, B, C, D, and E) in Fig. 2.13 yield to three triangles. Each corner is a measurement station. The ReV within each triangle may be represented as the arithmetic average of the data values at three apices. In this manner, rather than the use of arithmetic average over all the study area, it is partitioned into triangular sub-areas where the arithmetic averages are used. In this manner, the amount of the error in the global arithmetic average usage is reduced significantly.

The problem in triangularization is that one point record enters more than one sub-area. The question is, is it not better to define an influence area for each sub-area separately? So that the whole study region is divided into a set of sub-areas with influence of the data point.

In practice, given the scarcity of gauges and the spatial variability of ReV, for instance, in the case of precipitation many storms completely miss several gauges within a drainage area. Therefore, two basic tasks must be performed, namely the assessment of the representativeness of point rainfall and picture derivations of spatial patterns that reflect reality. Summer (1988) states, "In the ideal world, it should be possible to track and then model, mathematically or statistically the passage of a storm across an area with a great degree of accuracy and precision. In reality, this is very difficult, and one must be content with generalized spatial models of storm structure relating intensity or depth to storm area." Kriging and stochastic methods for the areal average estimation (AAE) based on the spatial correlation coefficient are summarized by Bras and Rodriguez-Iturbe (1985). However, the use of these methods needs recordings at many stations for the results to be reliable. Tabios and Salas (1985) compared several AAE methods with rainfall variability and concluded that a geostatistical method, ordinary and universal (Kriging, Chapter 4), with spatial correlation structure is superior to Thiessen polygons, polynomial interpretation, and inverse-distance weighting. Hevesi et al. (1992) suggested the use of multivariate geostatistical techniques for areal precipitation estimation in mountainous

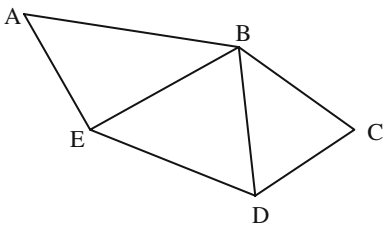

Fig. 2.13 Triangularization

terrain. Reliable estimates by these techniques are particularly difficult when the areal coverage of stations is sparse or when precipitation characteristics vary greatly with locations. Such situations frequently occur in arid regions due to sporadic and haphazard meteorological occurrences. On the other hand, Kedem et al. (1990) have shown, by considering satellite images and simple probability models, that the higher the rainfall the smaller the affected area over large regions. All these methods require high-speed computers and they are not as practical as conventional procedures such as the arithmetic average, Thiessen polygons, or isohyetal map techniques, which do not require much data (Chow, 1964).

An alternative AAE calculation method is presented by Akin (1971). It is assumed that the precipitation over the sub-area varies linearly between the three-corner (triangular) gauge points. Thus, at any point (x, y) interior to the n-th sub-area the precipitation height $H_n(x,y)$ is expressed as

$$H_n(x,y) = \alpha_n + \beta_n x + \gamma_n y, \tag{2.30}$$

where α_n, β_n, and γ_n are constants related to the gauge measurements at the corners. It is possible to write three simultaneous equations one for each apex (i, j, k) as

$$\begin{aligned} H_i(x,y) &= \alpha_n + \beta_n x_i + \gamma_n y_i. \\ H_j(x,y) &= \alpha_n + \beta_n x_j + \gamma_n y_j. \\ H_k(x,y) &= \alpha_n + \beta_n x_k + \gamma_n y_k. \end{aligned} \tag{2.31}$$

The solution of constants from these equations in terms of known quantities leads to

$$\begin{aligned} \alpha_n &= \left[a_i H_i + a_j H_j + a_k H_k\right]/2A_n, \\ \beta_n &= \left[b_i H_i + b_j H_j + b_k H_k\right]/2A_n, \\ \gamma_n &= \left[c_i H_i + c_j H_j + c_k H_k\right]/2A_n \end{aligned} \tag{2.32}$$

where

$$\begin{aligned} a_i &= x_j y_k - x_k y_j. \\ b_i &= y_j - y_k. \\ c_i &= x_k - x_j. \end{aligned} \tag{2.33}$$

Following a cyclic permutation of (i, j, k) the sub-area A_n can be calculated as follows:

$$A_n = \left[a_i + a_j + a_k\right]/2. \tag{2.34}$$

The differential volume of rainfall at any point within the sub-area is defined as

$$dQ = H(x,y)dA. \tag{2.35}$$

So that the total volume of rainfall associated with the sub-area becomes theoretically as

$$Q_n = \int\int \left[\alpha_n + \beta_n x_n + \gamma_n y_n\right] dxdy, \tag{2.36}$$

where the substitution of the above relevant expressions leads after some algebra, finally, to the volume of rainfall for the n-th sub-areas as

$$Q_n = A_n \left[\alpha_n + \beta_n(x_i + x_j + x_k)/3 + \gamma_n(y_i + y_j + y_k)/3\right]. \tag{2.37}$$

In the case of m triangular sub-areas, the total rainfall volume becomes

$$Q = \sum_{n=1}^{m} Q_n, \tag{2.38}$$

and, corresponding total area is

$$A = \sum_{n=1}^{m} A_n. \tag{2.39}$$

Finally, the ratio of Eq. (2.38) to Eq. (2.39) gives the AAE height over m sub-areas as

$$\overline{H} = \frac{Q}{A}.$$

By means of this procedure, the AAE area and volume are easily calculated if the gauge locations and rainfall amounts are known.

The development is analogous to some elementary concepts used in finite element analysis techniques. Consider a region of interest with station locations and amounts that are plotted on a map, then a series of straight lines are drawn arbitrarily to connect every gauge points with the adjacent gauges. Straight lines are drawn in anti-clockwise direction as shown in Fig. 2.14. These straight lines should produce a series of triangles "not necessary to have the same shape."

Each triangle area is known as sub-area and the corners of the triangles are shown by [i, j, k]. Precipitation values at the corners are denoted as H_i, H_j, H_k (i, j, k = 1, 2, . . . , n), where n is the number of sub-areas. Triangularization of all the stations for the northern part of Libya is shown in Fig. 2.15. On the other hand, Table 2.6 shows sub-areas for this study.

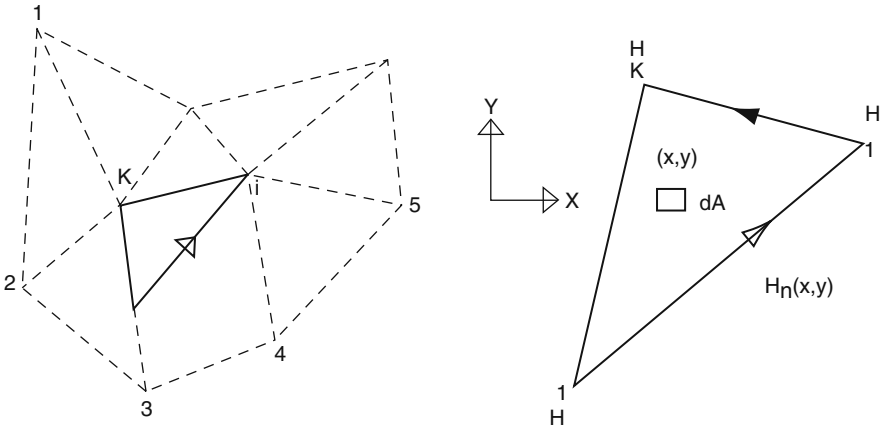

Fig. 2.14 Notations used for a triangular sub-area

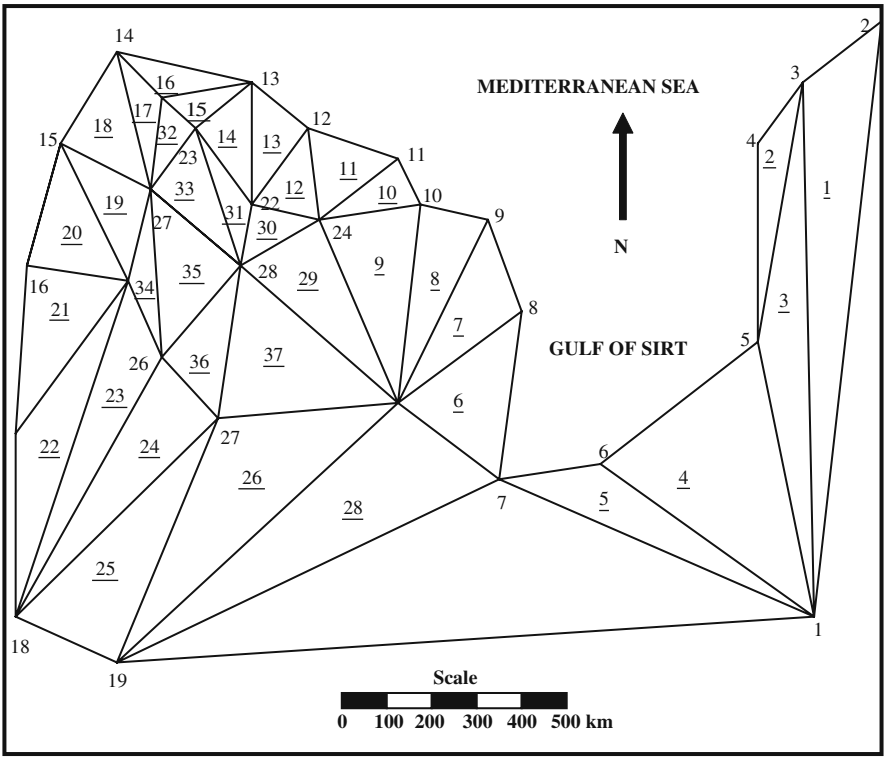

29 - point number

37 - area number

Fig. 2.15 Triangular mesh for northern Libya

Table 2.6 Values of i, j, k for each sub-area

Sub-area number	i	j	k	Sub-area number	i	j	k
1	1	2	3	20	15	16	29
2	3	4	5	21	16	17	29
3	3	5	1	22	17	18	29
4	5	6	1	23	18	26	29
5	6	7	1	24	18	27	26
6	7	8	20	25	18	18	27
7	7	8	20	26	19	20	27
8	9	10	20	27	19	1	7
9	10	21	20	28	19	7	20
10	20	11	21	29	20	21	25
11	11	12	21	30	21	22	28
12	12	22	21	31	22	23	28
13	12	13	22	32	15	25	24
14	13	23	22	33	28	23	25
15	13	24	23	34	26	25	29
16	13	14	24	35	26	28	25
17	14	25	24	36	27	28	26
18	14	15	25	37	20	28	27
19	15	29	25				

Convenient software is developed to calculate the sub-areas, associated AAR depths, and volumes falling on each sub-area as well as the total area of interest. The results are shown for monthly AARs in Table 2.7, while the seasonal AAR depths and volumes are presented in Table 2.8.

These values are computed by developed software over the study area as a summation of 37 sub-areas already shown in Fig. 2.15 and Table 2.8.

Table 2.7 Monthly averages of rainfall depths and volumes

Months	Average depth (mm)	Average volume ($\times 10^6 m^3$)
Jan	28.2	97.400
Feb	12.7	64.889
Mar	16.2	47.684
Apr	4.4	16.564
May	5.5	19.980
Jun	0.41	1.600
Jul	0.03	0.160
Aug	0.17	0.800
Sep	2.9	9.060
Oct	7.13	23.230
Nov	15.7	39.600
Dec	28.9	112.10

Table 2.8 Seasonal averages of rainfall depths and volumes

Season	Average depth (mm)	Average volume ($\times 10^6 m^3$)
Winter	72.800	274.389
Spring	26.100	84.228
Summer	0.613	2.560
Autumn	25.700	71.890

2.8 Polygonizations

The idea is to surround each data point with a polygonal area of influence so that the number of points will be equal to the number of sub-areas. In the case of n data points, there will be n area of influence.

2.8.1 Delaney, Varoni, and Thiessen Polygons

These polygonal methods are all related to each other with simple differences but the basic logic is the same. Different names are used in different disciplines for the same method. According to these polygon methods, the study area can be partitioned into a set of convex polygons, each containing only one measurement point such that every point within a given polygon is closer to the measurement point than any other measurement points. Each polygon defines the area of influence around the measurement point (Fig. 2.16). Each one of these polygons is also called as Thiessen polygon whose boundaries define the area that is closer to each point relative to all other points.

They are geometrically defined by the perpendicular bisectors of the lines between all points. A Voronoi diagram is sometimes also known as a Dirichlet (1850) tessellation, with cells that are Dirichlet regions, Thiessen or Voronoi polygons (Dirichlet, 1850; Voronoi, 1907; Thiessen, 1912). On the other hand, the Delaunay triangulation and Voronoi diagram in 2D space are dual to each other in the graph theoretical sense. Voronoi diagrams are named after Russian mathematician who defined and studied the general n-dimensional case in 1908. Voronoi diagrams that are used in geophysics and meteorology to analyze spatially distributed data (such as rainfall measurements) are called Thiessen polygons. In climatology, Voronoi diagrams are used to calculate the rainfall of an area, based on a series of point measurements. In this usage, they are generally referred to as Thiessen polygons.

Thiessen method is quick to apply because once the sub-polygons are fixed with a set of observation points, they remain the same all the time. The only change occurs artificially when additional observation points are added to the available set of measurement points. It is based on the hypothesis that for each point in the area,

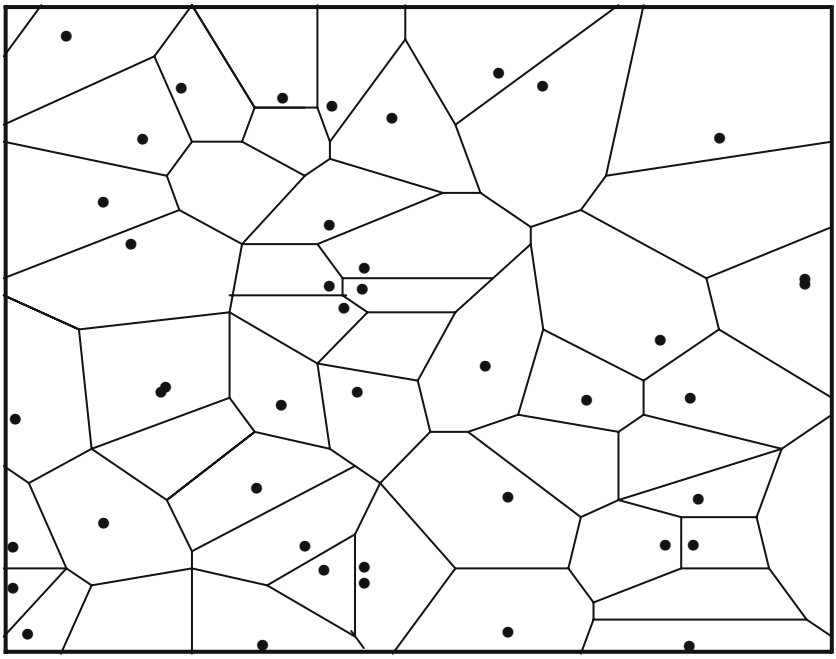

Fig. 2.16 Polygonalization

the best estimate of ReV is the measurement physically closest to that point. This concept is implemented by drawing perpendicular bisectors to the straight lines connecting each two-measurement stations, which yields with the consideration of the watershed boundary a set of closed areas known as Thiessen polygons. Based on the given measurement stations, the sub-polygons are obtained according to the following steps:

1) Connect each station to each nearby station with a straight line. These lines cannot cross and should connect only the nearest stations. The end product is several triangles.
2) Each side of the triangles is then bisected with a perpendicular line, thus forming polygons around each station.
3) Using an appropriate method calculate the total area, A, and sub-areas represented by each polygon (A_1, A_2, …, A_n). The number of sub-areas is equal to the number of measurement locations (Eq. 2.28).
4) Calculate the areal average estimation (AAE) of ReV as Z_C according to the weighted average formulation in Eq. (2.27). In this equation, W_i's correspond to the sub-area at measurement location i with measurement Z_i and W_T is the total area.

Example 2.7
Consider the measurement locations A, B, C, and D as shown in Fig. 2.17. Let the precipitation values be as 3.5, 2.9, 5.8, and 4.2 mm, respectively. Draw the Theissen sub-polygons and calculate the areal average ReV value. The total area is given as $A = 50\,km^2$, and after the polygon partitioning each sub-polygon area are calculated as $A_A = 12\,km^2$, $B_A = 17\,km^2$, $C_A = 13\,km^2$ and $D_A = 8\,km^2$.

Using Eq. (2.27) the Thiessen areal average of ReV estimation for the entire area becomes

$$Z_C = \frac{12\times3.5 + 17\times2.9 + 13\times5.8 + 8\times4.2}{50} = 4.174\,mm\,.$$

In contrast, the simple arithmetic average of precipitations is 4.1 inches. Differences between arithmetic and Thiessen averages increase for non-uniform ReVs when the Thiessen areas differ widely. In the above given example since the ReV measurements are close to each other, the AAE of ReV is close to the arithmetic average. However, if the ReV values at the same measurement locations are 2.5, 15.3, 8.5, and 22.9 mm, then the AAE ReV value becomes

$$Z_C = \frac{12\times2.5 + 17\times15.3 + 13\times8.5 + 8\times22.9}{50} = 11.675\,mm,$$

which indicates significant difference from the arithmetic average.

Unfortunately, the most commonly used Thiessen (1912) polygon method for AAE calculations do not consider the areal precipitation amounts recorded at individual stations in the partition of the whole catchment area into smaller polygonal sub-areas. Therefore, once the polygons are obtained on the basis station

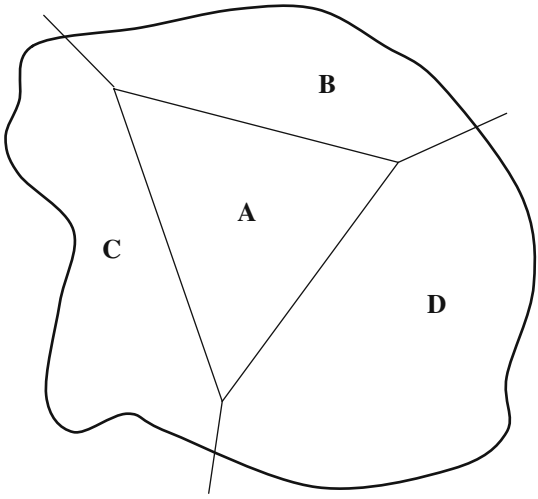

Fig. 2.17 Thiessen polygons

location configuration, they remain the same as long as the measurement locations do not change or there are no additional stations. However, it is logically plausible to expect that the sub-areas should change in response to the spatial variation of the phenomenon concerned. In other words, the partition should be based not only on the measurement location network configuration but also on the ReV measurements at each location.

2.8.2 Percentage-Weighted Polygon (PWP) Method

It is a new, simple, practical, and objective AAE method for determining the areal average of the spatial event based on a sparse and/or irregular network of measurement locations (Şen, 1998b). This method takes into account ReV measurement percentage weightings for each station and also has geometrical advantages, i.e., a better representation of the ReV on the study area compared to the conventional Thiessen polygon method. For instance, ReV data such as precipitation show a considerable spatial variation over any region, as explained by Huff and Neill (1957), Stout (1960), Jackson (1972), and Summer (1988). Wilson and Atwater (1972) suggested that this variation is due to differences in the type and scale of precipitation-producing models, which are strongly influenced by local or regional factors such as topography and wind direction. The AAE of the ReV over an area is most conveniently determined from a well-sited network of measurement locations, which show the local variations of ReV. For most areas, each measurement station is assumed to represent a very considerable area around it. However, this is a restrictive and frequently invalid assumption because of the spatial variation of ReV, especially for short distances (durations), such as during severe storms (Summer, 1988). There is no guarantee that point measurements provide reliable estimation for immediate surrounding areas. Relief often leads to large variations in ReV over relatively short distances. In the case of, say, precipitation if upward motion of air occurs uniformly over thousands of square kilometers, the associated precipitation has usually light or moderate intensity and may continue for a long time. On the other hand, convective storms accompanied by compensating downdrafts (as best illustrated by the thunderstorm) may be extremely intense, but their areal extent and local duration are comparatively limited. In practice, given the scarcity of gauges and the spatial variability of ReV, many stations may miss complete measurement. Therefore, two basic tasks must be performed:

1) Assess the representativeness of point measurement.
2) Derive pictures of spatial patterns, which reflect reality.

After deciding on the triangles, the following procedure is necessary for dividing the study area into polygons, leading to the percentage weighting method. If the precipitation values at three apices of a triangle are A, B, and C, then their respective percentages are

$$PA = 100A/(A + B + C), \tag{2.40}$$

$$PB = 100B/(A + B + C), \tag{2.41}$$

and

$$PC = 100C/(A + B + C), \tag{2.42}$$

respectively. Hence, it is possible to find the three-variable percentage data of constant sums for each triangle. A two-dimensional plot of three variables can be shown on a triangular graph paper as one point (see Fig. 2.18). Such papers are very common tools in earth sciences (Koch and Link, 1971).

In order to demonstrate the method more explicitly, the following step-by-step algorithm is provided, which can be computerized:

1) Draw lines between each adjacent pair of precipitation stations. Hence, a set of triangles is obtained, which cover the study area.
2) For each triangle calculate the precipitation percentage at its apices according to Eqs. (2.40, 2.41, and 2.42). Consider in each station that each apex has the value of 100% with 0% on the opposite side.
3) Consider bi-sector, which connects an apex to the midpoint of the opposite side, and graduate it into 100 equal pieces.
4) By making use of one precipitation percentage calculated in step 2, mark it along the convenient bi-sector starting from the opposite side toward the apex.
5) Draw a parallel line from this marked point in step 4 to the side opposite to the apex considered with its precipitation percentage.
6) Repeat steps 4 and 5 for the next precipitation percentage and find similar parallel line this time to another opposite side.
7) The intersection of these two lines defines the key point for the triangle considered.
8) In order to check the correctness of this key point, repeat steps 4 and 5 for the remaining third precipitation percentage value. If the parallel line to the side

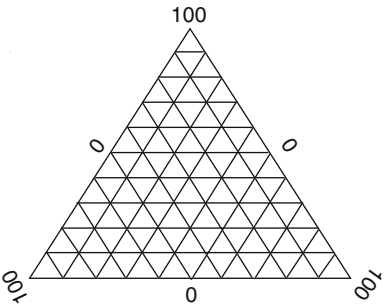

Fig. 2.18 The triangular coordinate paper

crosses through the aforementioned key point, then the procedure of finding the key point for the triangle is complete. Otherwise, there is a mistake either in the precipitation percentage calculations or in the location of marked points along the bi-sectors in steps 3 through 6 inclusive.

9) Return to step 2 and repeat the process for the triangles constructed in step 1. In this manner each triangle will have its key point. The location of this point within the triangle depends on the percentages of recorded precipitation amounts at the three adjacent apices. The greater the precipitation percentage for an apex the closer the point will lie to this apex. It is not necessary that the triangles resulting from a given set of stations in a network should be exactly equilateral. However, in the Thiessen method, for an obtuse-angle triangle the intersection of the three perpendicular bi-sectors occurs outside the triangular area.
10) Key points at adjacent triangles are connected with each other to form polygons, each including a single precipitation station.
11) The boundaries of polygons around the basin perimeter are defined by drawing a perpendicular to the sides of triangles from the key points. Now, the division of the whole basin area into sub areas is complete.

The triangular or polygon methods are preferred in practice when there are several data points about eight to ten.

Example 2.8

A simple example of plotting on a triangular coordinate paper is presented in Fig. 2.19 for an obtuse-angle triangle.

If the precipitation amounts at three apices are A = 12.5 cm, B = 20.1 cm, and C = 7.4 cm, then the corresponding percentages from Eqs. (2.40, 2.41, and 2.42) are $p_A = 31$, $p_B = 50$, and $p_C = 19$. In Fig. 2.19, point D on the A–A′ bi-sector corresponds to 31% of the A–A′ length starting from A′, which lies on the B–C side of the triangle representing 0%. A parallel line to side B–C is drawn from point D. Likewise, the next percentage is considered for the precipitation amount at apex B. The bi-sector B–B′ is drawn starting from point B′ on the side A–C toward B. On the bi-sector, point E corresponding to 50% is depicted. A parallel line from this point to the side A–C is drawn. Finally, the intersection of these two parallels at point F defines the "key point'' for triangle ABC. The following steps are necessary for the implementation of the PWP:

1) Three adjacent stations are considered such as in Fig. 2.19, where each apex is coded by its longitude (X_A, X_B, and X_C), latitude (Y_A, Y_B, and Y_C) and precipitation value (Z_A, Z_B, and Z_C).
2) The slopes (m_{AB}, m_{BC}, and m_{CA}) of triangle sides are calculated by making use of the apices coordinates.

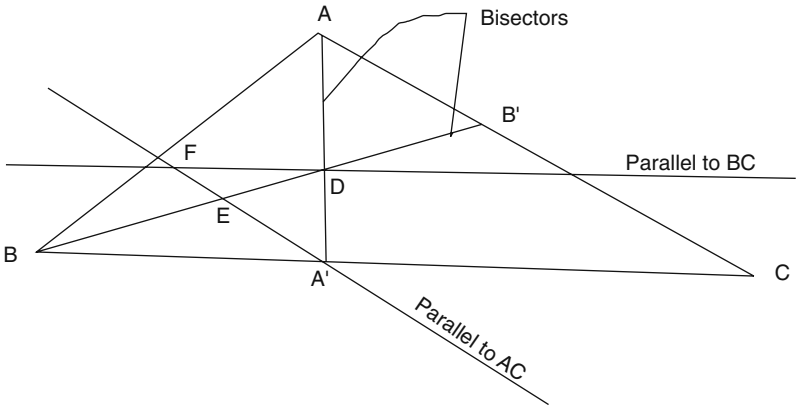

Fig. 2.19 Subdivision of triangular area

3) Determine the straight line equations perpendicular to each of the sides, but crossing from the opposite apex by analytical formulations. First of all, the coordinates of the projection point such as A′ and B′ of each apex on the opposite side must be calculated. For instance, the coordinates $X_{A'}$ and $Y_{A'}$ of point A′ can be expressed in terms of known quantities as

$$X'_A = \frac{1}{m_{BC}^2 + 1}\left[m_{BC}^2(X_B) + m_{BC}\ (Y_A - Y_B) + X_A\right], \tag{2.43}$$

$$Y'_A = \frac{1}{m_{BC}}\left(X_A - X'_A\right) + Y_A, \tag{2.44}$$

where

$$m_{BC} = \frac{Y_B - Y_C}{X_B - X_C}. \tag{2.45}$$

Similarly, the coordinates $X_{B'}$ and $Y_{B'}$ of point B′ on A–C side are

$$X'_B = \frac{1}{m_{CA}^2 + 1}\left[m_{CA}^2(X_C) + m_{CA}\ (Y_B - Y_C) + X_B\right], \tag{2.46}$$

$$Y'_B = \frac{1}{m_{CA}}\left(X_B - X'_B\right) + Y_B, \tag{2.47}$$

where

$$m_{CA} = \frac{Y_C - Y_A}{X_C - X_A}. \tag{2.48}$$

4) The precipitation amounts (Z_A, Z_B, and Z_C) are used in order to find points along the perpendiculars starting from the side toward the apex, which divide each one in proportions λ_1, λ_2, and λ_3. By use of these ratios and the previous known quantities, the coordinates of points A″, B″, and C″ are determined. For instance, the coordinates $X_{A''}$ and $Y_{A''}$ are defined as

$$X''_A = x'_A + \lambda_1 (X_A - x'_A). \tag{2.49}$$

$$Y''_A = Y'_A + \lambda_2 (Y_A - Y'_A). \tag{2.50}$$

5) On the other hand, from the precipitation measurements at the three apices of any triangle, the total precipitation T value becomes

$$T = Z_A + Z_B + Z_C,$$

which can be written in terms of percentages as

$$Z_A/T + Z_B/T + Z_C/T = 1.0,$$

or

$$\lambda_1 + \lambda_2 + \lambda_3 = 1.0$$

Hence, lambda values are defined as the percentage of precipitation amounts at the three apices of a triangle. Similarly, the coordinates of point B' can be written with the relevant notations as

$$X''_B = x'_B + \lambda_2 (X_B - x'_B), \tag{2.51}$$

$$Y''_B = Y'_B + \lambda_2 (Y_B - Y'_B), \tag{2.52}$$

where

$$\lambda_2 = \frac{Z_B}{Z_A + Z_B + Z_C}. \tag{2.53}$$

6) The straight lines are drawn, which pass through point A″ and parallel to the B–C side of the triangle and similarly parallel to A–C crossing through B″. Let these parallel lines be D_1 and D_2. The equations of these lines are given as follows:

$$D_1 = m_{BC}\,X + (Y''_{A''} - m_{BC}X''_{A''}). \tag{2.54}$$

$$D_2 = m_{CA}\,X + (Y''_{B''} - m_{CA}X''_{B''}). \tag{2.55}$$

7) The intersection point of lines D_1 and D_2 is referred to as the "key point," M_K, for triangle ABC. The coordinates of this key point (X_K, Y_K) can be found by simultaneous solution of Eqs. (2.54) and (2.55).
8) Previous steps are repeated for each triangle, representing sub-area within the whole catchment.
9) Adjacent key points are connected with each other, hence constituting polygons each enclosing a single meteorology station. The key point coordinates become

$$X_k = \frac{1}{m_{CA} - m_{BC}}\left[\left(m_{CA}X''_B - m_{BC}X''_A\right) - \left(Y''_B - Y''_A\right)\right]. \tag{2.56}$$

$$Y_k = m_{BC}\left(X_k - X''_A\right) + Y''_A \tag{2.57}$$

10) The area of each polygon is calculated by one of the available convenient mathematical methods.
11) Multiplication of each polygon area by its representative station precipitation value gives the volume of water that is gathered over this polygonal sub-area.
12) Summation of these volumes for all the relevant polygons that cover the whole catchment area gives the total water volume which falls over the catchment area.
13) Division of this total water volume by the total catchment area yields the AAE value for the catchment.

In general, the comparison of the Thiessen and PWP methods indicates the following significant points:

1) If triangulation of stations produces obtuse triangles, then the Thiessen method gives bi-sector intersections that fall outside the triangle area. However, in the PWP method all the key points lie within the triangle itself. In this way the common effect of precipitation amounts at triangle apices falls within the triangle domain.
2) In the Thiessen method the station lies within the sub-areal polygon at almost equal distances from the sides. This implies that almost equal weights are given to precipitation amounts in the separation of polygons. On the contrary, the PWP method produces polygon sides closer to the station, depending on the relative magnitude of precipitation amounts between adjacent stations. This implies that in the PWP method the center of recorded precipitation amounts at three neighboring stations (not the geometrical center of station locations) plays the most significant role in the areal partition calculations.

3) The size of any closed polygon for a station in the PWP method is always smaller than the corresponding Thiessen method. Hence, more refined partition of the catchment area into sub-areas is obtained. This implies that more refined AAE values result by use of the PWP method. In fact, in the PWP method the biggest precipitation record station results in the smallest sub-area.
4) Variations in the precipitation amounts, due to some different storms, change the polygonal partition in the PWP method, whereas Thiessen polygons remain the same.

Example 2.9

The implementation of PWP method was applied first to spatial precipitation data given by Wiesner (1970) and Bruce and Clark (1966) as in Fig. 2.20, where the geometric configuration of precipitation stations are given for the same data according to the Thiessen and PWP methods. In order to assess the reliability of these methods, the average sum of square deviations (ASSD) from the AAE value is calculated for each method as

$$\mathrm{ASSD} = \frac{1}{n}\sum_{i=1}^{n}\left(P_i - \mathrm{AAE}\right)^2, \tag{2.58}$$

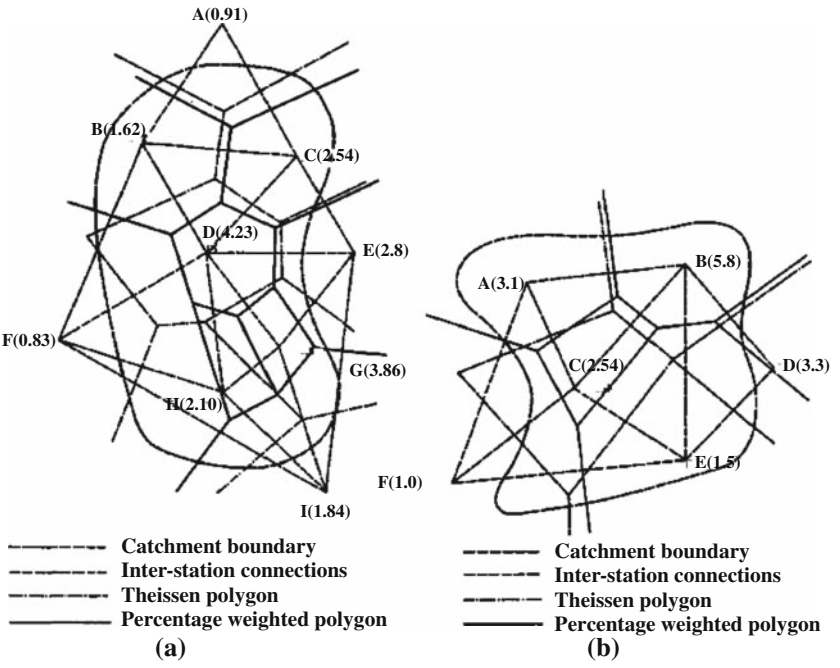

Fig. 2.20 Precipitation data (**a**) Wiesner, (**b**) Bruce, and Clark

Table 2.9 AAE of precipitation

	Wiesner data		Bruce and Clark data	
Method	AAE (inches)	ASSD (inches^2)	AAE (inches)	ASSD (inches^2)
Thiessen	2.67	1.34	3.10	2.54
PWP	2.45	1.15	2.50	2.37

where n is the number of stations. The results for various methods are shown in Table 2.9.

The PWP method yields smaller AAE and ASSD values than the Thiessen method.

As mentioned earlier, with the Thiessen method, in the obtuse triangle BDF a perpendicular bi-sector's intersection appears to the left of BF line (see Fig. 2.20a). By considering precipitation amounts at stations B and F, it is not possible to expect a value of about 4 inches. On the other hand, in the PWP method there is no such confusion. Wiesner (1970) has shown, after completion of an isohyetal map for the same precipitation data, that the storm peak occurs within a small area around station D in Fig. 2.20a. This is also confirmed by the PWP method as shown in Fig. 2.20a. Again, in the same figure Thiessen method yields only one closed polygon, whereas PWP provides three such polygons. Extensions of Thiessen boundary polygons between the pairs of stations F and I and E and I suffer from the same drawbacks in that it is not possible to have precipitation values greater than 1.8 inches between F and I, and more than 2.83 inches between E and I. Similar general interpretations are valid also for Fig. 2.20b where there are two odd bi-sectors' intersection points that lie outside the triangles, resulting from the application of Thiessen method. These lie to the left of line A–F and below line F–E. Comparatively, even in this figure, the closed polygon from the PWP method is smaller in size than the Thiessen case. The PWP method can be applied to local or regional scales due to the following reasons:

1) The assumption that convective, intense precipitation is comparatively limited in areal extent and duration is valid for small or regional scales. Thinking in larger space and time scales (e.g., global and monthly), there are also broader areas with intense precipitation, such as the large-scale convergence zones (ITCZ and SPCZ) and the monsoon regions.
2) The limited areal extent and duration of intense convective precipitation compared to stratiform, light precipitation is generally compensated by the fact that many storms might be missed by the rain gauge network (see the "Introduction" section). So if the rain gauge network is nearly equally distributed, there is not any reason to compensate for this a second time by reducing the areal weight of heavier precipitation, unless there is not really an indication that intense precipitation is over-represented due to the spatial distribution of the rain gauges in the network. This might be the case in arid regions, because there are almost no stations in desert regions. However, in mountainous areas precipitation is often

underestimated, because most rain gauge stations are located in valleys and do not catch very well the heavy precipitation on the slopes or mountain peaks.

3) The proposed PWP method is very convenient in areas where the precipitation stations are irregularly located.

Example 2.10

In order to determine the AAE of rainfall from ten different meteorological stations, the PWP method is applied together with the other conventional methods (arithmetic mean, Thiessen polygon, isohyetal map technique) to the Southeastern Anatolia Region of Turkey (Bayraktar et al., 2005). Total monthly rainfall values of these stations in 1993 are used and presented in Table 2.10.

About 1/500,000 scaled maps are used to draw the sub-areas, which are measured with a planimetry. For each method, AAR values are calculated with the help of Eq. (2.27).

Application map of Thiessen method and areal values of Thiessen polygons are merely given in Fig. 2.21, because the key points remain the same as long as the meteorological stations do not change. Monthly isohyetal maps are prepared for January, April, July, and October as in Fig. 2.22.

For the same months rainfall values and sub-areas are given in Fig. 2.23a,b,c,d. In PWP method, which is the main purpose of this study, values of rainfall and percentage weightings are calculated for each of the three adjacent stations constituting sub-triangles.

During the application, PWP rainfall values are calculated by considering Eqs. (2.40, 2.41, and 2.42) used for the determination of sub-areas. PWP method calculations and sub-areal values are given in Fig. 2.23a,b,c,d. For the comparison of different methods all results are presented collectively in Table 2.11.

As can be seen from this application, the PWP method yields more reliable results and smaller AAE values depending on the regional variability of the rainfall amounts over the catchment area. For instance, in July, rainfall values have many regional variations. This is due to the semi-arid characteristics of the study area and

Table 2.10 Total monthly rainfall values of stations (mm)

Stations	Jan	Feb	Mar	Apr	May	Jun	Jul	Aug	Sept	Oct	Nov	Dec
Silvan	104	116	116	84	61	6	0	1	1	19	69	116
Siirt	115	107	111	106	66	9	1	0	5	48	86	102
Ahlat	64	67	79	84	62	23	9	4	15	50	68	53
Bitlis	180	156	141	107	65	19	5	3	14	58	97	130
Van	42	35	46	58	41	17	6	3	12	44	49	83
Şırnak	136	121	143	141	64	5	2	1	6	33	83	123
Başkale	47	43	69	102	100	42	20	9	16	39	43	38
Nusaybin	92	62	63	63	40	1	1	0	1	16	43	79
Şemdinli	106	155	151	195	56	9	3	4	5	77	119	97
Hakkari	102	105	125	146	57	15	3	1	10	26	76	91

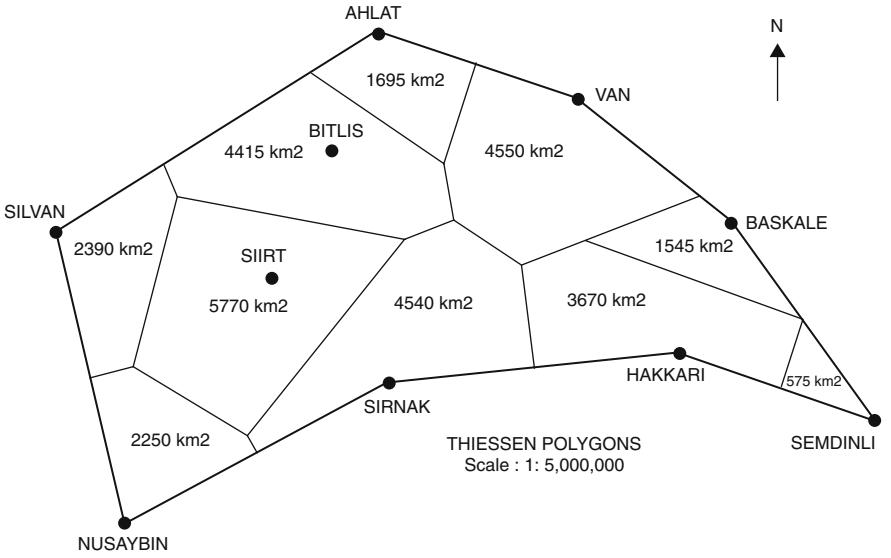

Fig. 2.21 Application map of Thiessen method (January, April, July, October 1993)

frequent occurrence of convective rainfalls, which are not expected to cover large areas. It is noted that in July, Başkale station surrounding appears as the most rainfall reception area, which is represented by a sub-area of 1,545 km^2 in the Thiessen method, whereas by the sub-areas of 3,140 km^2 and 519 km^2 in the arithmetic mean and the isohyetal map technique, respectively. On the other hand, it is represented by a sub-area of 153 km^2 when PWP method is considered. Hence, the representation of the most rainfall intercepting meteorology station with the smallest subarea gives rise to a smaller value of AAE for the catchment area during convective storms. The monthly AAEs of the catchment area in this month according to isohyetal map, Thiessen Polygon, and arithmetic mean techniques are estimated as 44, 41, and 54%, respectively. They are smaller than the PWP method AAE value. The areal rainfall variability in October is comparatively less than July because of the north polar maritime air mass penetration into the study area, which gives rise to frontal rainfall occurrences. It is well known that the frontal rainfalls have more extensive areal coverage than the convective rainfall types and consequently the percentages are smaller in the PWP method calculations. This is tantamount to saying that percentage calculations from the three adjacent stations are not very different as they are in the convective rainfall events. It is timely to state that similar effects can be expected from the orographic rainfall occurrences to the convective rainfall types in mountainous areas. Such distinctions cannot be considered in the Thiessen approach, where the sub-areas are determined according to the geometric configuration of the station locations, without the consideration of actually recorded rainfall amounts at these stations. For example, in October, the AAE calculations by using the PWP method yielded 13, 15, and 18% smaller values than other three

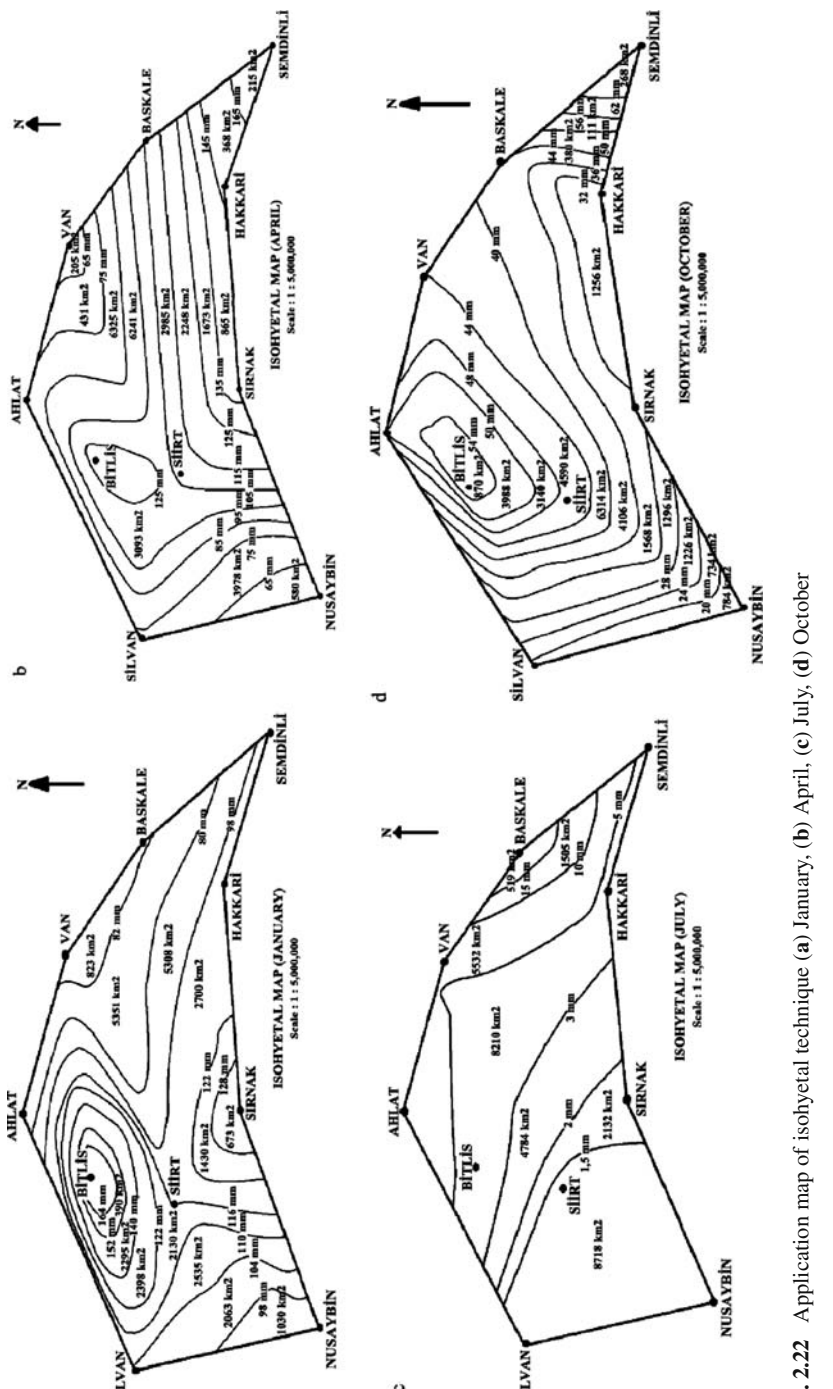

Fig. 2.22 Application map of isohyetal technique (**a**) January, (**b**) April, (**c**) July, (**d**) October

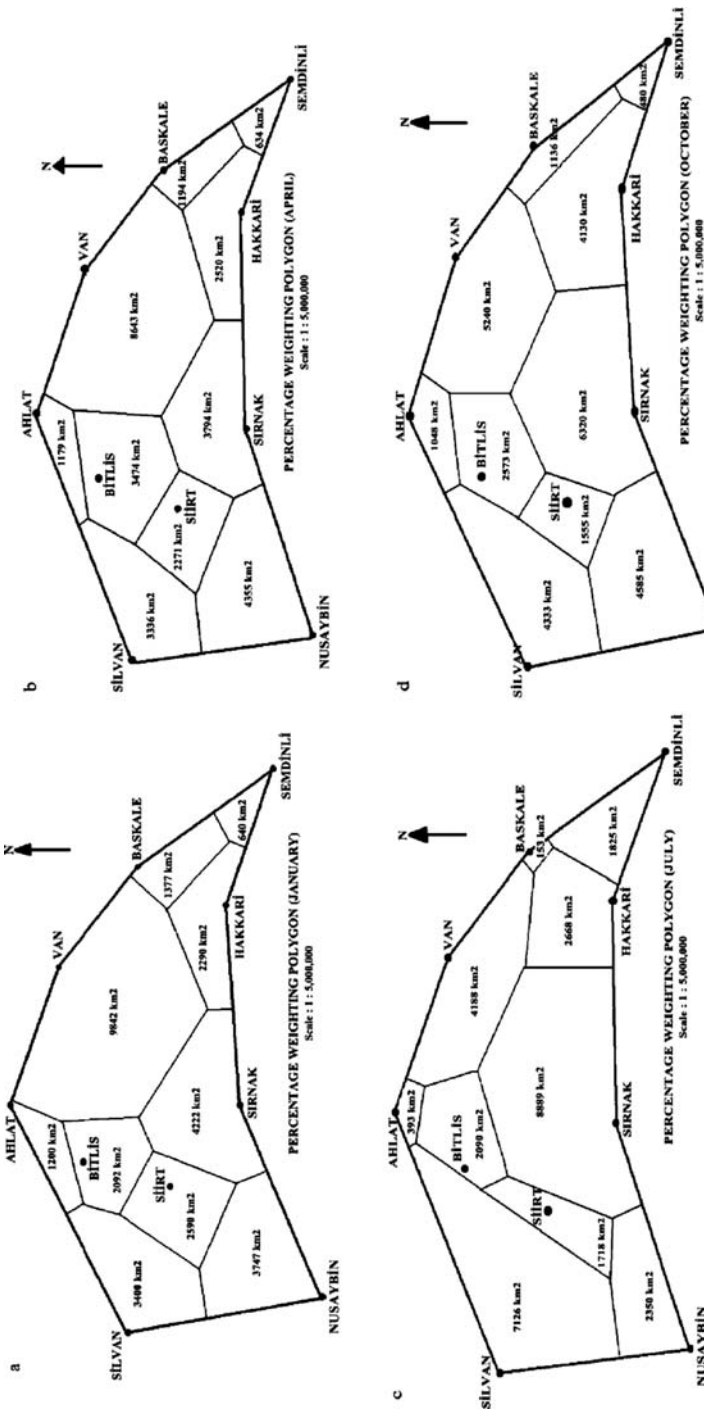

Fig. 2.23 Application map of PWP technique (**a**) January, (**b**) April, (**c**) July, (**d**) October

Table 2.11 AAE value for each method (mm)

Method	January	April	July	October	Annual
Percentage weighting polygon	89.22	92.70	2.32	33.75	54.49
Isohyetal map	102.72	102.72	4.12	38.96	62.13
Thiessen polygon	106.30	104.30	3.94	39.74	63.57
The arithmetic average	98.76	108.49	5.00	40.97	63.31

conventional methods. This is due to the lesser areal variability of rainfall in this month than in July. Furthermore, the AAE amounts by use of the PWP method and the annual average rainfall amounts are found 12, 14, 14% and on the average 13.5% lesser than the isohyetal map, Thiessen polygon, and arithmetic average methods, respectively. Arithmetic average method yields in January smaller AAE than all other methods because this is the month where the effect of frontal rainfall is the most dominant with high rainfalls in the area except low rainfalls at few stations, such as at Van and Başkale stations as 42 and 47 mm, respectively. Last but not the least, the arithmetic average method is affected from extreme rainfall values more than any other method.

As the frontal and more homogeneous type of rainfalls are recorded during a specific period, then it is expected that the results of the PWP and Thiessen polygon methodologies will approach to each other, provided that there are approximate rainfall records at each meteorological station. However, in practice the use of PWP method is recommended. In fact, whatever the circumstances are, it is preferable to adopt PWP method since it yields almost the same result as the Thiessen method if the conditions are satisfied as the homogeneous type of rainfalls.

2.9 Areal Coverage Probability

A rigorous probabilistic methodology is developed on the basis of random field concept for determining various probability of precipitation (PoP) areal coverage probability (ACP) over a region. The necessary analytical formulations are derived with the restrictive assumption that the precipitation occurrences at different sites and times are independent from each other. However, the regional heterogeneity in precipitation occurrence is exemplified by either non-identical probability of precipitation values or non-uniform threshold levels. Finally, extreme value probabilities of precipitation coverage area are formulated in their most general forms. The probability statements derived are helpful in predicting the regional probable potential future precipitation or drought coverage areas. The drought basic time unit can be adopted as hour, day, week, month, or year in addition to unit area for spatial analysis. If the basic unit is day, then each day can be labeled as “rainy” and “non-rainy” and the calculations are performed accordingly (Şen, 2008). Similarly, in the case of regular division of an area into a set of sub-areas as in Fig. 2.24b, each sub-unit may have either a “dry” or a “wet” spell. For instance, in Fig. 2.24a and b there are six and nine time and sub-area units, respectively.

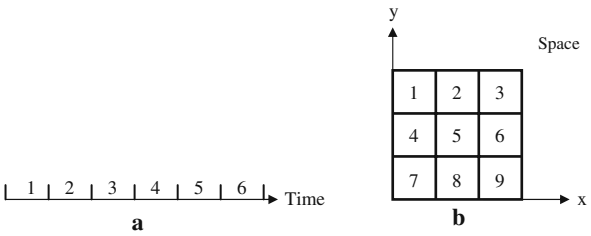

Fig. 2.24 Time and spatial units

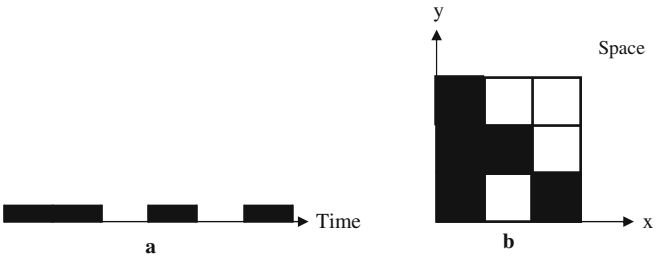

Fig. 2.25 Dry time and sub-area units

If "dry" units are shown by black and "wet" units by white colors, then in Fig. 2.25 there are four and five time and sub-areal dry units, respectively,

As the number of basic unit increases, then the "dry," D, and "wet," W, time and spatial features start to become clearer as in Fig. 2.26.

In this section precipitation phenomenon is modeled as a random field where time-wise probabilities at a fixed site are referred to as PoP, and spatial probabilities for a fixed time instant are ACP. The areal probability is, in fact, the fraction of the area hit by rainfall. It does not provide a means for depicting which of the sub-areas is going to be hit with precipitation event. However, it simply represents the estimate of what the fractional coverage will be. Furthermore, it is clearly a conditional probability being conditioned by whether at least one precipitation event actually occurs in the sub-area during a certain time interval.

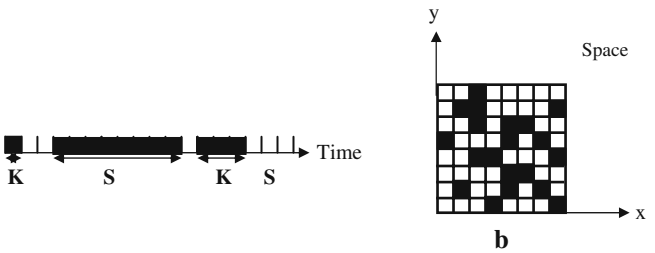

Fig. 2.26 Dry durations and areas

The PoP at any desired threshold value, x_0, such as standard 0.01 inches is equivalent to the exceedence probability of this value. If the pdf of precipitation at site i is denoted by $f_i(X)$, then the PoP, p_i, at this site is

$$p_i = \int_{x_0}^{\infty} f_i\,(X)\,dX.$$

If the forecast area is thought in terms of n sample sites, then the average areal probability p can be defined formally as

$$p = \frac{1}{n}\sum_{i=1}^{n} p_i. \tag{2.59}$$

In the special case where the point probability is uniform over the forecast area, p is equal to the common value of PoP. Note that since p is a lumped value it does not, in general, contain detailed information provided by the set of individual point probabilities. However, if for some reason some of the sub-areas vary in size, then each probability value must be percentage area weighted. It should be noted that the areas associated with sub-areas need to be small enough that a single probability value can be applied to each one.

2.9.1 Theoretical Treatment

In the most general case, none of the sites have equal PoPs, which implies that the random field is heterogeneous. It is quite likely that probabilities might vary from place to place even within a single area. In practice, in addition to the spatial correlation variations, the following three situations give rise to heterogeneous and anisotropic random fields. These are:

1) Identical pdfs of precipitation at different sites, but non-uniform threshold levels.
2) Non-identical pdf of precipitation at sites, but uniform threshold level.
3) Non-identical pdfs at sites and non-uniform threshold levels.

Let the PoP and its complementary probability at j-th site within a region of n sites be given by p_j and q_j ($j = 1, 2, \ldots, n$), respectively. They are point-wise mutually exclusive and complementary, i.e., $p_j + q_j = 1$. The ACP, $P(A = i)$ including i sites can be evaluated through enumeration technique after the application of summation and multiplication rules of probability theory. Hence

$$P(A = i) = \tfrac{1}{i!}\sum_{j1=1}^{n} p_{j1}\sum_{\substack{j2=1\\ j_2 \neq j_1}}^{n} p_{j2}\cdot\cdot\sum_{\substack{j_i\\ j_i \neq j_{i-1}}}^{n} p_{ji}\prod_{\substack{k=1\\ k \neq j_1,}}^{n} q_k \tag{2.60}$$

or succinctly

$$P(A = i) = \frac{1}{i!} \sum_{j_1=1}^{n} p_{j1} \sum_{\substack{j_2=j_1 \\ j_2 \neq j_1}}^{n} p_{j2} \cdots \sum_{\substack{j_i \\ j_i \neq j_{i-1}}}^{n} p_{ji} \prod_{\substack{k=1 \\ k \neq j_i,}}^{n} q_k \tag{2.61}$$

$$P(A = i) = \frac{1}{i!} \left(\prod_{k_1=1}^{n} \sum_{\substack{j_{k_1}=1 \\ j_{k_1} \neq j_m}}^{n} p_{jk_1} \right) \prod_{\substack{k_2=1 \\ k_2 \neq j_m \\ m = 1,2,\ldots j_{k_{m-1}},}}^{n} q_{k_2} \tag{2.62}$$

where the multiplication of i summations in the brackets includes all the possible combinations of i precipitation occurrences at n sites, whereas the last multiplication term corresponds to possible no-precipitation combinations. For identical PoPs the term in brackets simplifies to $n(n–1)\ldots(n–i+1)p^i$ and the last multiplication to $q^{n—I}$, hence Eq. (2.62) reduces to

$$P(A = i) = \binom{n}{i} p^i q^{n-i}, \tag{2.63}$$

which is actually the Binomial distribution with two-stage Bernoulli trials (Feller, 1967).

This is the well-known Binomial distribution with mean np and variance npq. The probability, p_A, that all the sites, hence area, are covered by precipitation at an instant can be found from Eq. (2.62) as

$$p_A = \prod_{i=1}^{n} p_i. \tag{2.64}$$

Comparison of Eqs. (2.59) and (2.64) yields

$$p > p_A, \tag{2.65}$$

and accordingly

$$\min(p_1, p_2, \ldots, p_n) < p < \max(p_1, p_2, \ldots, p_n). \tag{2.66}$$

The conditional probability of partial area, given a group of randomly or systematically selected k precipitation occurrences or non-occurrences, is of great interest in practical applications. The joint probability that any k_1 of n sites have significant precipitation occurrences can be defined by virtue of independence and hence multiplication rule of the probability theory as

$$P(X_1 > x_0, X_2 > x_0, \ldots, X_{k_1} > x_0) = p^{k_1}. \tag{2.67}$$

Assuming that any one of the sites is equally likely to experience a precipitation, the conditional probability that only a certain group of i sites has precipitation can be written as

$$P(X_1 > x_0, X_2 > x_0, \ldots, X_{k_1} > x_0 / A = i) = \left(\frac{i}{n}\right)^{k_1}.$$

By definition the joint probability becomes

$$P(X_1 > x_0, X_2 > x_0, \ldots, X_{k_1} > x_0, A = i) = \left(\frac{i}{n}\right)^{k_1} P(A = i).$$

The conditional ACP of precipitation can then be obtained after dividing this last expression by Eq. (2.67), which leads to

$$P(A = i / X_1 > x_0, X_2 > x_0, \ldots, X_{k_1} > x_0) = \left(\frac{i}{np}\right)^{k_1} P(A = i). \tag{2.68}$$

Hence, in order to obtain the most general case of heterogeneous PoP's conditional areal coverage, it is necessary to substitute Eq. (2.62) into Eq. (2.68). On the other hand, for homogeneously distributed PoPs, Eq. (2.68) takes its explicit form by the substitution of Eq. (2.63)

$$P\big(A = i / X_1 > x_0, X_2 > x_0, \ldots, X_{k_1} > x_0\big) = \left(\frac{i}{np}\right)^{k_1} \binom{n}{i} p^i q^{n-1}. \tag{2.69}$$

Since some initial information is given with certainty, the conditional probability in Eq. (2.69) has more information content than the original unconditional distribution in Eq. (2.63). This fact can be objectively shown by considering the variances of pdfs in Eqs. (2.63) and (2.69), which are npq and (n–1)pq, respectively. Hence, the conditional variance is smaller, and therefore conditional ACP is more certain. However, the unconditional areal precipitation coverage expectation from Eq. (2.63) is equal to np, whereas the conditional coverage area expectation is greater and can be obtained from Eq. (2.68) as np + q.

Similarly, the conditional ACP of precipitation, given that a group of k_2 sites have no-precipitation, can be found for homogeneous PoPs as

$$P(A = i / X_1 < x_0, X_2 < x_0, \ldots, X_{k_2} < x_0,) = \left(\frac{n - i}{nq}\right) \binom{n}{i} q^i p^{n-1}. \tag{2.70}$$

Finally, the conditional ACP of precipitation, given that a group of k_1 sites has precipitation and another group of k_2 sites has no-precipitation, is obtained as

$$P(A = i/X_1 > x_0, X_2 > x_0, \ldots, X_{k_1} > x_0, X_{k_1+1} > x_0, X_{k_1+2} < x_0, \ldots X_{k_2} < x_0,) = \left(\frac{i}{nq}\right)\left(\frac{n-i}{np}\right)\binom{n}{i} q^i p^{n-1}. \tag{2.71}$$

The probability expressions in Eqs. (2.68, 2.69, 2.70, and 2.71) can be effectively employed to study regional precipitation occurrence patterns.

2.9.2 Extreme Value Probabilities

In practice, it is also important to know the probability of maximum and minimum areal coverage of precipitation. The probability of maximum areal coverage, A_M, of precipitation can be found provided that the precipitation coverage area evolution along the time axis is assumed to be independent from each other. In general, for m time instances the probability of maximum areal coverage of precipitation to be less than or equal to an integer value, i, can be written as

$$P(A_M \leq i) = [P(A \leq i)]^m, \tag{2.72}$$

where $P(A \leq i)$ can be evaluated, in general, from Eq. (2.62) for heterogeneous PoPs by employing

$$P(A \leq i) = \sum_{j=0}^{i} P(A = j).$$

The substitution of which into Eq. (2.72) leads to

$$P(A_M \leq i) = \left[\sum_{j=1}^{i} P(A = j)\right]^m.$$

However, it is a well-known fact that $P(A_M = i) = P(A_M \leq i) - P(A_M \leq i-1)$, and therefore one can obtain consequently that

$$P(A_M = i) = \left[\sum_{j=0}^{i} \binom{n}{j} p^j q^{n-j}\right]^m - \left[\sum_{j=0}^{i-1} \binom{n}{j} p^j q^{n-j}\right]^m. \tag{2.73}$$

It is then possible to rewrite Eq. (2.73) for homogeneous PoPs from Eq. (2.63) explicitly as

$$P(A_M = i) = \left[\sum_{j=0}^{i} \binom{n}{j} p^j q^{n-j}\right]^m - \left[\sum_{j=0}^{i-1} \binom{n}{j} p^j q^{n-j}\right]^m.$$

Hence, the probability $P(A_M = n)$ that the whole area is covered by precipitation can be obtained from Eq. (2.70) as

$$P(A_M = n) = 1 - (1 - p^n)^m. \tag{2.74}$$

One can interpret from this expression that for small regions the number of sites is also small, in which case the probability in Eq. (2.74) is not zero and there is a chance for the whole area to be covered by precipitation. Similarly, the probability of minimum areal coverage, A_m, of precipitation can be written for homogeneous PoPs as

$$P(A_m = i) = \left[\sum_{j=i}^{n} \binom{n}{j} p^j q^{n-j}\right]^m - \left[\sum_{j=i+1}^{n} \binom{n}{j} p^j q^{n-j}\right]^m. \tag{2.75}$$

2.10 Spatio-Temporal Drought Theory and Analysis

Let an agricultural land be divided into m mutually exclusive sub-areas, each with the same spatial and temporal drought chance. The Bernoulli distribution theory can be employed to find the extent of drought area, A_d, during a time interval, Δt. The probability of n_1 sub-areas stricken by drought can be written according to Bernoulli distribution as (Feller, 1967)

$$P_{\Delta t}(A_d = n_1) = \binom{m}{n_1} p_r^{n_1} q_r^{m-n_1} \qquad p_r + q_r = 1.0. \tag{2.76}$$

This implies that out of m possible drought-prone sub-areas, n_1 have deficit and hence the areal coverage of drought is equal to n_1 or in percentages n_1/m. For the subsequent time interval Δt, there are $(m–n_1)$ drought-prone sub-areas. Assuming that the evolution of possible deficit and surplus spells along time axis is independent over mutually exclusive sub-areas, similar to the concept in Eq. (2.76), it is possible to write for the second time interval that

$$P_{2\Delta t}(A_d = n_2) = \sum_{n_1=0}^{n_2} \binom{m}{n_1} \binom{m - n_1}{n_2 - n_1} p_r^{n_1} p_r^{n_2 - n_1} q_r^{m-n_1} q_r^{m-n_2}, \tag{2.77}$$

where n_2 is the total number of drought-affected sub-areas during the second time interval. By considering Eq. (2.76), this expression can be rewritten succinctly in the form of recurrence relationship as

$$P_{2\Delta t}(A_d = n_2) = \sum_{n_1=0}^{n_2} P_{\Delta t}(A_d = n_1)\, P(A_d = n_2 - n_1), \tag{2.78}$$

where $P(A_d = n_2 - n_1)$ is the probability of additional $(n_2 - n_1)$ sub-areas to be effected by deficit during the second time interval out of the remaining $(m–n_1)$ potential sub-areas from the previous time interval. With the same logic, extension of Eq. (2.78) for any successive time interval, i, furnishes all the required drought-area probabilities as

$$P_{i\Delta t}(A_d = n_i) = \sum_{n_{i-1}=0}^{n_i} P_{(i-1)\Delta t}(A_d = n_{i-1})\, P(A_d = n_i - n_{i-1}). \tag{2.79}$$

For $i = 1$ this expression reduces to its simplest case, which does not consider time variability of drought occurrences as presented by Şen (1980) and experimentally on digital computers by Tase (1976). Furthermore, the probability of agricultural drought area to be equal to or less than a specific number of sub-areas j can be evaluated from Eq. (2.79) according to

$$P_{i\Delta t}(A_d \le j) = \sum_{k=0}^{j} P_{i\Delta t}(A_d = k). \tag{2.80}$$

The probability of having, n_1', deficit sub-areas, given that there are n_1 deficit sub-areas at the beginning of the same time interval within the whole region, can be expressed as

$$P_{\Delta t}\left(A_d = n_1' \,|A_d = n_1\right) = \binom{m}{n_1} \binom{n_1}{n_1 - n_1'} p_r^{n_1} p_t^{n_1 - n_1'} q_r^{m-n} q_t^{n_1'},$$

or shortly,

$$P_{\Delta t}\left(A_d = n_1' \,|A_d = n_1\right) = P_{\Delta t}(A_d = n_1) \binom{n_1}{n_1 - n_1'} p_t^{n_1 - n_1'} q_t^{n_1'}. \tag{2.81}$$

It should be noted that always $n_1 \ge n_1'$ and the difference $j = n_1 - n_1'$ gives the number of transitions. On the basis of Eq. (2.81), a general equation for the marginal probability of observing n_1' deficit spells at the end of the same time interval, after simple algebra, becomes

$$P_{\Delta t}\left(A_d = n_1'\right) = \sum_{k=0}^{m=n_i'} P_{i\Delta t}\left(A_d = k + n_i'\right) \binom{k = n_i'}{k} p_t^k q_t^{n_i'}. \tag{2.82}$$

Hence, the regional agricultural drought occurrences during the second time interval follow similarly to this last expression, and generally, for the i-th step, it takes the following form:

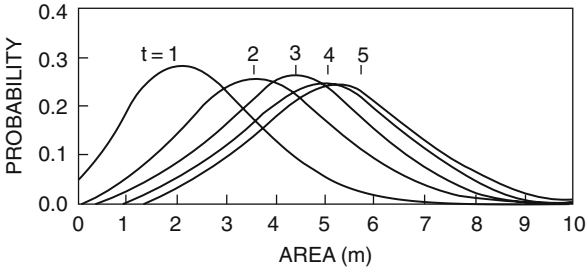

Fig. 2.27 Probability of drought area for multi-seasonal model m=10; p_r=0.3; p_t=0.2)

$$P_{i\Delta t}\left(A_d = n_i'\right) = \sum_{k=0}^{m=n_i'} P_{i\Delta t}\left(A_d = k + n_i'\right) \binom{k + n_i'}{k} p_t^k q_t^{n_i'}. \tag{2.83}$$

Its validity has been verified using digital computers. The pdfs of areal agricultural droughts for this model are shown in Fig. 2.27, with parameters $m = 10, p_r = 0.3, p_t = 0.2$ and $i = 1, 2, 3, 4$, and 5.

The probability functions exhibit almost symmetrical forms irrespective of time intervals although they have very small positive skewness.

Another version of the multi-seasonal model is interesting when the number of continuously deficit sub-areas appear along the whole observation period. In such a case, the probability of drought area in the first time interval can be calculated from Eq. (2.76). At the end of the second time interval, the probability of j sub-areas with two successive deficits, given that already n_1 sub-areas had SMC deficit in the previous interval, can be expressed as

$$P_{2\Delta t}\left(A_d = j \,|A_d = n_1\right) = P\Delta t\left(A_d = n_1\right) \binom{n_1}{j} p_t^j q_t^{n_1 - j}. \tag{2.84}$$

This expression yields the probability of having n_1 sub-areas to have deficit out of which j sub-areas are hit by two deficits, i.e., there are $(n_1 - j)$ sub-areas with one deficit. Hence, the marginal probability of continuous deficit sub-area numbers is

$$P_{2\Delta t}\left(A_d = j\right) = \sum_{k=0}^{m-j} P_{\Delta t}\left(A_d = k + j\right) \binom{k + j}{j} p_t^j q_t^k.$$

In general, for the i-th time interval it is possible to write

$$P_{i\Delta t}\left(A_d = j\right) = \sum_{k=0}^{m-j} P_{(i-1)\Delta t}\left(A_d = k + j\right) \binom{k + j}{j} p_t^j q_t^k. \tag{2.85}$$

The numerical solutions of this expression are presented in Fig. 2.28 for $m = 10$, $p_r = 0.3$ and $p_t = 0.5$. The probability distribution function is positively skewed.

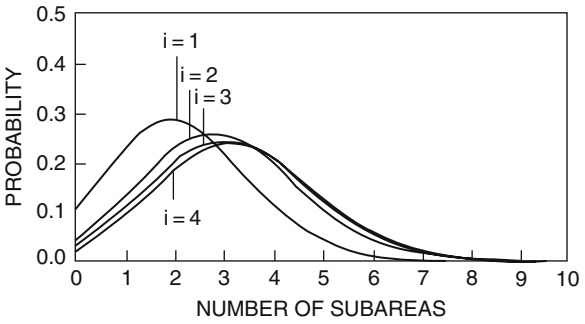

Fig. 2.28 Drought area probability for multi-seasonal model (m=10; p_r=0.3; p_t=0.2)

2.10.1 Drought Parameters

The global assessment of model performances can be achieved on the basis of drought parameters such as averages, i.e., expectations and variances, but for drought predictions the pdf expressions as derived above are significant. The expected, i.e., average number of deficits, $E_i\,(A_d)$, over a region of m sub-areas during time interval, $i\Delta t$ is defined as

$$E_i\,(A_d) = \sum_{k=0}^{m} kP_{i\Delta t}\,(A_d = k). \tag{2.86}$$

Similarly, the variance, $V_i\,(A_d)$, of drought-affected area is given by definition as

$$V_i\,(A_d) = \sum_{k=0}^{m} k^2 P_{i\Delta t}\,(A_d = k) - E_i^2\,(A_d). \tag{2.87}$$

Substitution of Eq. (2.79) into Eq. (2.86) leads to drought-stricken average area within the whole region as

$$E_i\,(A_d) = mp_r \sum_{k=0}^{i-1} q_r^k, \tag{2.88}$$

or succinctly

$$E_i\,(A_d) = m\left(1 - q_r^i\right). \tag{2.89}$$

Furthermore, the percentage of agricultural drought-stricken area, $P^i{}_A$, can be calculated by dividing both sides by the total number of sub-areas, m, leading to

$$P_A^i = (1 - q_r^i). \tag{2.90}$$

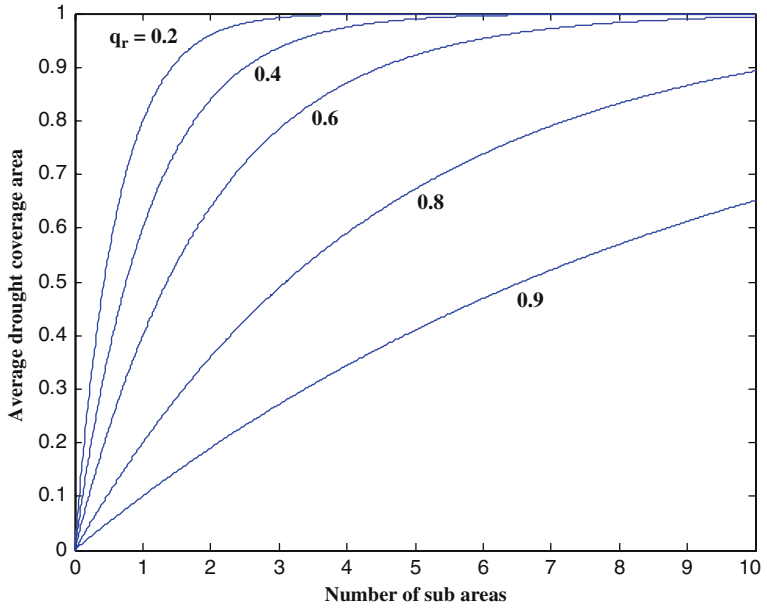

Fig. 2.29 Drought percentage areal coverage

Figure 2.29 shows the change of drought-stricken area percentage with the number of deficit sub-areas, **i**, for given deficit probability, q_r.

For regional drought variations in the first time interval (i = 1), from Eq. (2.90), $P^1{}_A = p_r$. On the other hand, for the whole area to be covered by drought, theoretically $i \rightarrow c\ \infty$ and therefore $P^{\infty}{}_A = 1$. It is obvious that the temporal agricultural drought percentage for a region of m sub-areas at any time i, is $p_r \leq P^i{}_A \leq 1$.

As the probability of deficit spell in a region increases, the average drought area attains its maximum value in a relatively shorter time as can be written from Eq. (2.90) as

$$i = \mathrm{Ln}(1 - P^i_A)/\mathrm{Ln}(1 - \rho_r). \tag{2.91}$$

Hence, this expression provides the opportunity to estimate the average time period that is required for a certain percentage of the region to be covered by drought. Figure 2.30 indicates the change of i with p_r, which is the surplus probability.

Furthermore, in practical applications the probability of deficit can be approximated empirically as 1/m or preferably as 1/(m+1). The substitution of these conditions into Eq. (2.91) gives

$$i = \mathrm{Ln}(1 - P^i_A)/[\mathrm{Ln}(m/(m+1)]. \tag{2.92}$$

This expression confirms that regional drought durations are affected mainly by its size rather than its shape, as was claimed by Tase and Yevjevich (1978).

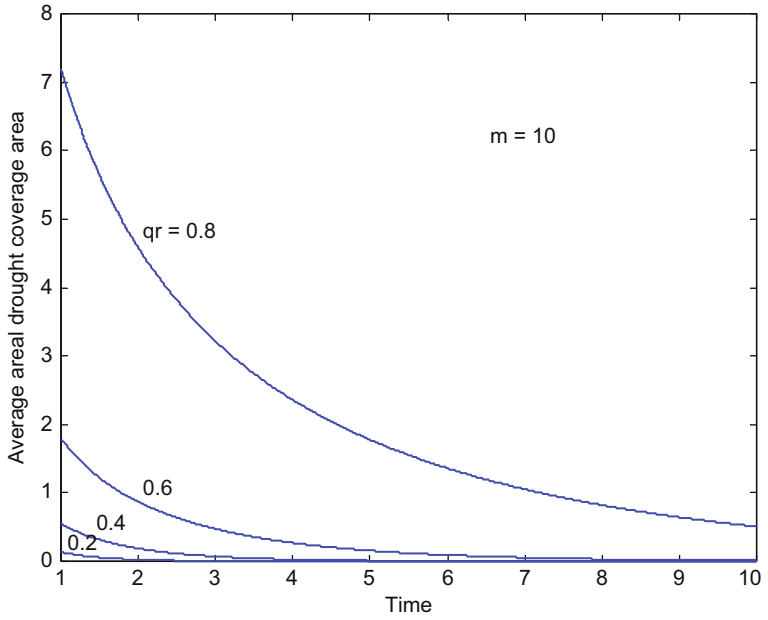

Fig. 2.30 Drought time change by p_r

The next significant regional drought parameter is the variance, which is a measure of drought variability. In general, the smaller the variance the smaller is the areal drought coverage percentage. The variance of the regional persistence model can be found from Eqs. (2.76) and (2.79) after some algebra as

$$V_i\,(A_d) = m\left(1 - q_r^t\right)\, q_r^t. \tag{2.93}$$

Similarly, it is better in practice to standardize this variance by dividing both sides by the total area, m, which gives percentage variance, $P_V{}^{i,T}$ in the case of i sub-area coverage after T time duration,

$$P_V{}^{i,T} = (1 - q_r^i)q_r^T. \tag{2.94}$$

Furthermore, consideration of Eq. (2.90) together with this last expression yields the relationship between percentages of average and variance drought coverage as

$$P_V{}^{i,T} = P_A^i q_r^T. \tag{2.95}$$

Figure 2.31 shows the change of regional drought variance percentage with i deficit affected number of sub-areas at different times for a given deficit probability, $q_r = 0.7$.

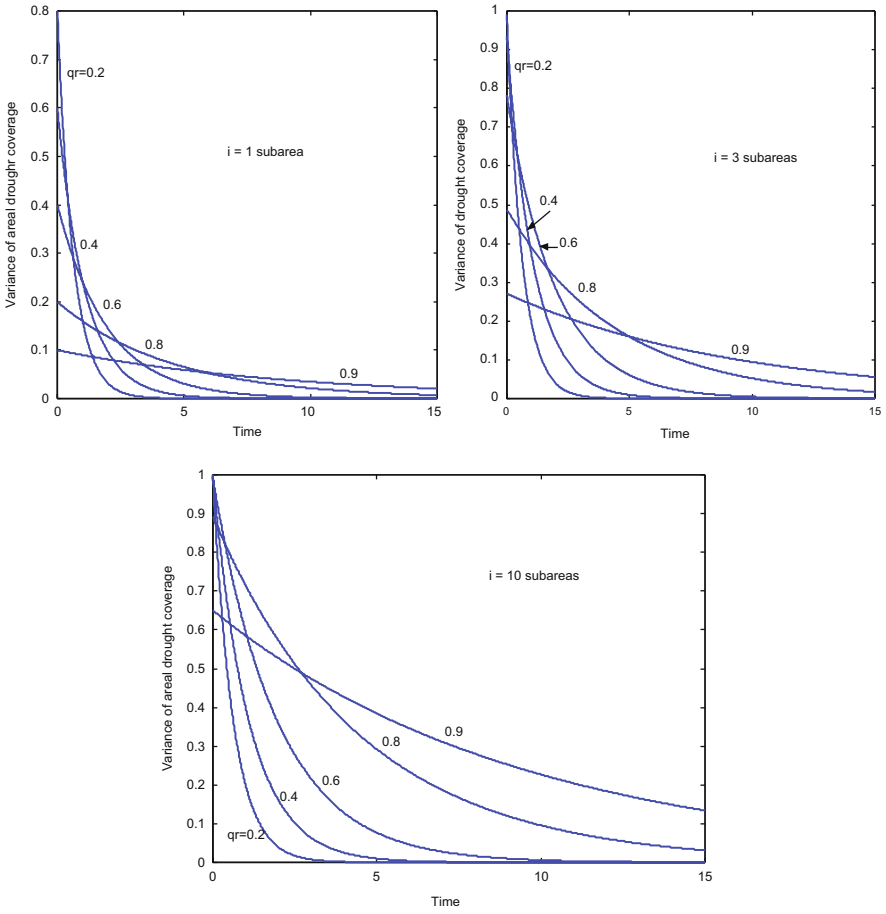

Fig. 2.31 Areal drought variance percentage variation

Another application of spatio-temporal agricultural drought occurrence is possible by considering spatial deficit probability, q_r, and temporal surplus probability, p_t. It is rather cumbersome to find a concise expression for the expectation of this case at all times. However, for the first time interval,

$$E_1\left(A_d\right) = m\left(1 - q_r\right)\left(1 - p_t\right), \tag{2.96}$$

which exposes explicitly the contribution of the regional and temporal dry spell effects on the average areal drought. Figure 2.32 shows drought spatial and temporal average variations for the given probabilities.

Finally, from the variance of the drought area coverage by simple spatio-temporal model considerations, it is possible to derive for the first time interval that

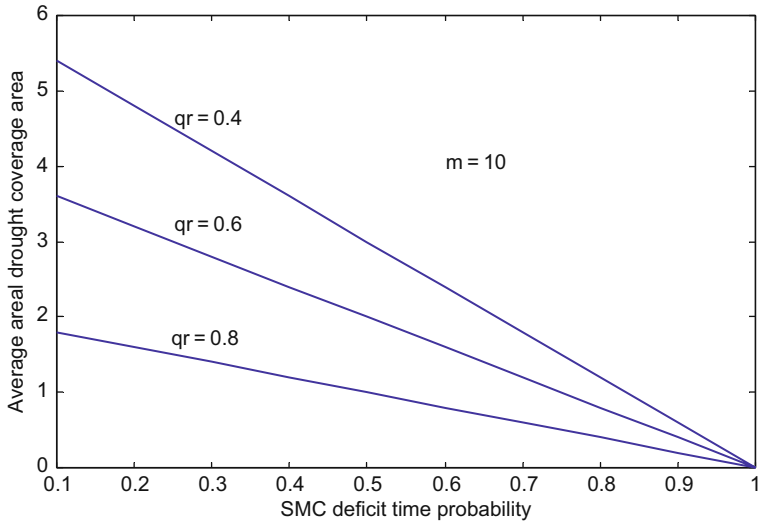

Fig. 2.32 Average areal drought coverage by considering spatio-temporal variations during the first time interval

Fig. 2.33 Average variance of drought area for various basic probability values

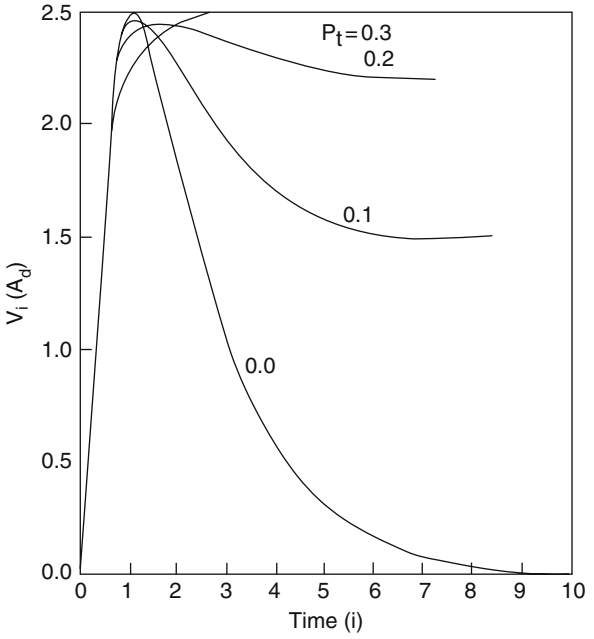

$$V_1(A_d) = E_1(A_d)\ (q_r + p_t p_r)\,. \tag{2.97}$$

The numerical solution of this expression is given for various combinations of p_r and p_t in Fig. 2.33.

As a result the pdfs of regional and temporal agricultural droughts are derived for independent dry and wet spell occurrences. Two basically different probabilistic models are proposed for regional drought modeling. Regional drought parameter variations are assessed graphically. The following conclusions are valid for regional and temporal drought occurrences:

1) Drought occurrences are dependent on the regional and temporal dry and wet spell probabilities, as well as size of the region considered.
2) Drought area distribution within a region without considering temporal probabilities becomes negatively skewed as its size increases. Initially, it can be approximated by a normal distribution. For multi-seasonal model the same distribution has an approximate normal pdf, provided that continuous drought duration is not considered. Otherwise, it is positively skewed.
3) Drought probabilities over a region are more affected by its size.

References

Akin, J. E., 1971. Calculation of areal depth of precipitation. J. Hydrol. 12, 363–376.

Bayraktar, H., Turalioglu, F. S., and Şen, Z., 2005. The estimation of average areal precipitation by percentage weighting polygon method in Southeastern Anatolia Region, Turkey. Atmos. Res. 73, 149–160.

Box, G. E. P., and Jenkins, G. M., 1976. Time Series Analysis, Control and Forecasting. Holden Day, San Francisco.

Bras, R. L., and Rodriguez-Iturbe, I., 1985. Random Functions and Hydrology. Addison-Wesley Publishing Co., Reading, MA, 599 pp.

Bruce, J. P., and Clark, R. H., 1966. Hydrometeorology. Pergamon Press, New York, 319 pp.

Chow, V. T., 1964. Handbook of Applied Hydrology. McGraw-Hill, New York.

Chu, P. S., and Karz, R.W., 1985. A time-domain approach. Mon. Wea. Rev. 113, 1876–1888.

Cramer, H., 1946. Mathematical Methods of Statistics. Princeton University Press, New Jersey, p. 213.

Davis, A., 2002. Statistics Data Analysis Geology. John Wiley and Sons, London, 638 pp.

Dirichlet, G. L., 1850. Über die Reduktion der positiven quadratischen Formen mit drei unbestimmten ganzen Zahlen. Journal für die Reine und Angewandte Mathematik 40, 209–227.

Feller, W., 1967. An Introduction to Probability Theory and its Application. John Wiley and Sons, New York, 509 pp.

Fisher, R. A., 1912. On an absolute criterion for filtering frequency curves. Messenger Math. 41, 155.

Gauss, K. F., 1809. Theory of the motion of the heavenly bodies about the sun in conic section. Dover, New York (1993).

Hevesi, J. A., Istok, J. D., and Flint, A. I., 1992. Precipitation estimation in mountainous terrain using multi-variate geostatistics, Part I: Structural analysis. J. Appl. Meteorol. 31, 661–676.

Huff, F. A., and Neill, J. C., 1957. Areal representativeness of point rainfall. Trans. Amer. Geophys. Union 38(3), 341–351.

Jackson, I. J., 1972. Mean daily rainfall intensity and number of rainy days over Tanzania. Geogr. Ann. A. 54, 369–375.
Kedem, B., Chiu. L. S., and Karni, Z., 1990. An analysis of the threshold method for measuring area-average rainfall. J. App. Meteor. 29, 3–20.
Kendall, M. G., 1954. Note on the bias in the estimation of autocorrelation. Biometrika 42, 403–404.
Koch, S., and Link, R. F., 1971. Statistical Analysis of Geological Data. Dover Publications, New York, 375 pp.
Kolmogorov, A. N., 1941. Interpolation and extrapolation von stationaren zufalligen folgen. Bull. Acad. Sci. USSR, Ser. Math. 5, 3–14.
Quenouille, M. H., 1956. Notes on bias in estimation. Biometrika 43, 353–360.
Schubert, S. D., Saurez, M. J., and Schemm, J. K., 1992. Persistence and predictability in a perfect model: J. Atmos. Sci. 49(5), 256–269.
Şen, Z., 1974. Small sample properties of stationary stochastic processe4s and Hurst phenomenon in hydrology. Unpublished Ph. D. Thesis, Imperial College of Science and Technology, University of London, 256 pp.
Şen, Z., 1980. Regional drought and flood frequency analysis: theoretical considerations. J. Hydrol. 46, 265–279.
Şen, Z., 1998a. Small sample estimation of the variance of time-averages in climatic time series. Int. J. Climatol. 18, 1725–1732.
Şen, Z., 1998b. Average areal precipitation by percentage weighted polygon method. ASCE J. Hydrol. Eng. 3(1), 69–76.
Şen, Z., 2002. İstatistik Veri İşleme Yöntemleri (Hidroloji ve Meteoroloji) (Statistical Data Treatment Methods – Hydrology and Meteorology). Su Vakfı yayınları, 243 sayfa (in Turkish).
Şen, Z., 2008. Kuraklik Afet ve Modern Modelleme Yontemleri (Drought Disaster and Modern Modeling Methods). Turkish Water Foundation (in Turkish).
Stout, G. E., 1960. Studies of severe rainstorms in Illinois. J. Hydraul. Div. Proc. ASCE, HY4, 129–146.
Summer, G., 1988. Precipitation Process and Analysis. John Wiley and Sons, New York, 455 pp.
Tabios, G. O. III, and Salas, J. D., 1985. A comparative analysis of techniques for spatial interpolation of precipitation. Water Resour. Bull. 21, 365–380.
Tase, N., 1976. Area-deficit-intensity characteristics of droughts. Hydrology Paper 87, Colorado State University, Fort Collins.
Tase, N., and Yevjevich, Y., 1978. Effects of size and shape of a region on drought coverage. Hydrol. Sci. Bull. 23(2), 203–213.
Thiessen, A. H., 1912. Precipitation averages for large areas. Mon. Wea. Rev. 39, 1082–1084.
Voronoi, G., 1907. Nouvelles applications des paramètres continus à la théorie des formes quadratiques. Journal für die Reine und Angewandte Mathematik 133, 97–178.
Wiesner, C. J., 1970. Hydrometeorology. Chapman and Hall Ltd., London, 232 pp.
Wiener, N., 1942. The extrapolation, interpolation and smoothing of stationary time series. OSRD 370, Report to the Services 19, Research Project DIC-6037, MIT.
Wiener, N., 1949. The Extrapolation, Interpolation and Smoothing of Stationary Time Series. John Wiley & Sons, Inc., New York.
Wilson, J. W., and Atwater, M. A., 1972. Storm rainfall variability over Connecticut. J. Geophys. Res. 77(21), 3950–3956.
Zadeh, L. A., 1965. Fuzzy sets. Information Control 8, 338–353.
Zadeh, L.A., 1973. Outline of a new approach to the analysis of complex systems and decision processes. IEEE Trans. Syst. Man. Cybern. 3, 28–44.

Chapter 3
Classical Spatial Variation Models

Abstract Men have tried to model spatial behavior of the natural phenomena since a long time, with initiative simple models such as the weighting functions, which are supposed to represent regional dependence structure of the phenomenon concerned. Unfortunately, commonly employed weighting functions are not actually data-dependent and hence they are applicable invariably in each spatial prediction, which is not convenient since each spatial phenomenon will have its own spatial dependence function. Spatial data distribution can be uniform, randomly uniform, homogeneous, isotropic, clustering, etc., which should be tested by a convenient test as described in the text. Besides statistically it is also possible to depict the spatial variation through trend surface fit methods by using least squares technique. In this chapter, finally, adaptive least squares techniques is suggested in the form of Kalman filter for spatial estimation.

Keywords Cluster sampling · Data group · Geometric weights · Kalman filter · Nearest neighbor · Random field · Spatial pattern · Trend surface · Uniformity test

3.1 General

The spatial nature of earth sciences phenomena expelled the researchers to explore spatial statistical procedures whereas the classical statistics remained at the service as usual. In general, any phenomenon with spatial variations is referred to as the ReV by Matheron (1963). ReVs fall between the random fields where the spatial variations have independence and deterministic variability depending on the spatial correlation value. The most significant methodologies of the spatial analysis is Kriging, which is discussed in Chapter 5, but prior to their development earth scientists were using different empirical and geometrical rational approaches in assessing ReVs. Hence, in this chapter these rather preliminary and simple but effective methods will be discussed with their drawbacks. The trend surface analysis is an offshoot of statistical regression; kriging is related to time series analysis, and contouring is an extension of interpolation procedures.

Z. Şen, *Spatial Modeling Principles in Earth Sciences*,
DOI 10.1007/978-1-4020-9672-3_3,

3.2 Spatio-Temporal Characteristics

Our minds are preconditioned on the Euclidean geometry and, consequently, ordinary human beings are bound to think in 3D space as length, width, and depth in addition to the time as the fourth dimension. Hence, all the scientific formulations including differential equations and others include space and time variability. Earth, environmental, and atmospheric variables vary along these four dimensions. If their changes along the time are not considered, then it is frozen in time; and therefore, a steady situation remains along the time axis, but ReV in concern has variations in the space. A good example for such a change can be considered as geological events, which do not change appreciably during human lifetime. For instance, iron content of a rock mass varies rather randomly from a point to another within the rock mass and hence spatial variation is considered. Another example is the measurement of rainfall amounts at many irregularly located meteorological stations spread over an area, i.e., simultaneous measurement of rainfall amounts; again the time is kept constant and the spatial variations are sought.

On the other hand, there are time variations that are referred to as temporal variations in the natural phenomenon. For such a variation, it suffices to measure the event at a given location, which is the case in any meteorology station or in groundwater wells. Depending on the time evolution of the event whether it is continuous or not, time series records can be obtained. A time series is the systematic measurement of any natural event along the time axis at regular time intervals. Depending on this time interval, time series is called as hourly, daily, weekly, monthly, or yearly time series.

Contrary to time variations, it is not possible to consider space series where the records are kept at regular distances, except in very specific cases. For example, if water samples along a river are taken at every 1 km, then the measurements provide a distance series in regularity sense. In fact, distance series are very limited as if there are no such data sequences in practical studies. On the other hand, depending on the interest of event, they appear as time series data but they are not time series due to irregularity or randomness in the time intervals between successive occurrences of the same event. Flood and drought occurrences in hydrology correspond to such cases. One cannot know the duration of floods or droughts. Likewise, in meteorology the precipitation occurrence or any dangerous levels of air pollutants concentrations do not have time series characteristics.

Any natural event evolves in the four-dimensional human visualization domain and consequently its records should involve the characteristics of both time and space variability. Record with this property is said to have spatio-temporal variation. It is the main purpose of this chapter to present the classical methodologies for spatial data treatment regional estimations and interpretations, based on simple but effective methodologies.

3.3 Spatial Pattern Search

Human is biased toward regular pattern geometries, appearances, and presentation rather than irregular or random features. Although at the first instance he/she can distinguish visually between the regular and the irregular patterns in space, he/she may not know their quantitative assessment methodologies at the time. For instances, everyday the pattern of clouds is different than previous days and the most regular ones are either overcast situation or cloudless patterns. However, in between, there are millions of different irregular patterns that cannot be distinguished simply from each other in fine scales. It is, therefore, necessary to sample such situations at a set of irregular measurement sites and then use quantitative methodologies for the identification of a set of parameters or a spatial map for each case, which can then be compared and classified into different categories.

Usually the pattern is invisible, such as oil, gold, and groundwater resources, sub-surface geological features, but based on the sampling and thereafter the data treatment with objective methodologies as well as personal expertise and intuition, the general spatial features may be depicted in the form of maps.

The worth of data in earth sciences and geology is very high since most of the interpretations and decisions are based on their qualitative and quantitative information contents. This information is hidden in representative field samples, which are analyzed for the extraction of numerical or descriptive characteristics, which are referred to as data. Data collection in earth sciences is difficult, expensive, and requires special care for accurately representing the geological phenomenon. After all, various parameters necessary for the description and modeling of the geological event, such as bearing capacity, fracture frequency, aperture, orientation, effective strength, porosity, hydraulic conductivity, chemical contents, etc., are hidden within each sample, but they represent a specific point in space and time. Hence, it is possible to attach temporal and three spatial reference systems with data, as shown in Fig. 3.1.

In geological sciences and applications, the concerned phenomenon can be examined and assessed through the collection of field data and accordingly meaningful solutions can be proposed. It is, therefore, necessary to make the best use of available data from different points. Geological data are collected either directly in the field or field samples are transferred to laboratories in order to make necessary analyses and measurements. For instance, in hydrogeology domain, among field measurements are the groundwater table elevations, pH, and total dissolved solution (TDS) readings whereas some of the laboratory measurements are chemical elements in parts per million (ppm). There are also office calculations that yield hydrogeological data such as hydraulic conductivity, transmissivity, and storage coefficients. In the mean time, many other data sources from soil surveys, topographic measurements, geological prospection, remote sensing evaluations, and others may also support data for further investigation. The common property of these measurements and calculations of laboratory analysis is that they include uncertainty

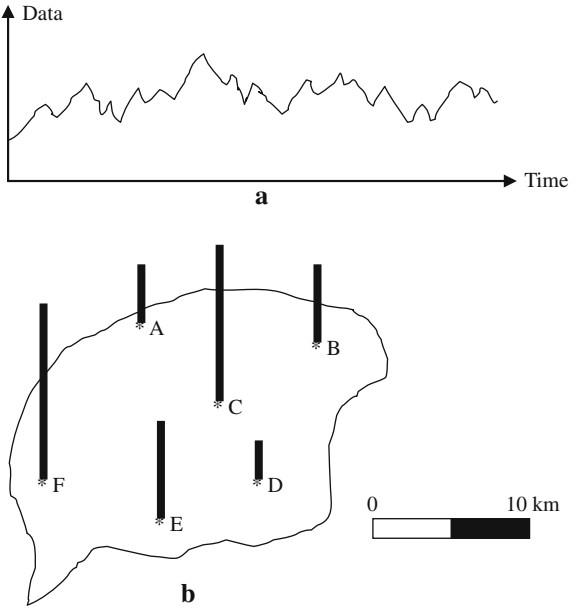

Fig. 3.1 Data variation by (**a**) time, (**b**) space

attached at a particular time and sampling point. Hence, the first question is how to deal with rather uncertainly (randomly) varying data? At times the data are random, sometimes chaotic, and still in other cases irregular or very regular. These changes can be categorized into two broad classes as systematic and unsystematic. Systematic data yield mathematically depictable variations with time, space, or both. For instance, as the depth increases so does the temperature and this is an example for systematic variation. Especially, if there is only one type of geological formation, then systematic variation becomes more pronounced. Otherwise, on the basis of rather systematic variation on the average, there are unsystematic deviations, which might be irregular or random. Systematic and unsystematic data components are shown in Fig. 3.2.

In many studies systematic changes are referred to as the deterministic components, which are due to systematic natural (geography, astronomy, climatology) factors that are explainable, and unsystematic variations are unexplainable or random parts that need special treatment.

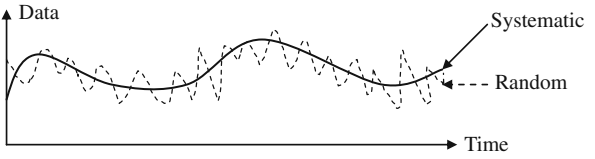

Fig. 3.2 Systematic and unsystematic components

3.4 Spatial Data Analysis Needs

It is obvious that the spatial patterns or arrangements of individual sampling locations in any study area have different patterns. The problem is to visualize qualitatively and quantitatively the change of an ReV over these points and then over the area. Appreciation of some differences between the set records of concerned variable at a set of measurement stations is the first step prior to any formal model application. It helps in the final modeling stage if the variation feature of the ReV variable is deduced first with simple but effective methods. In order to achieve such a preliminary work, the following steps become helpful:

1. Data Collection: Since the sampling locations are considered on a plane, their locations can be described by abscissas, X, and ordinates, Y. This procedure is referred to finding the easting and northing from the longitudes and latitudes. Although it is not possible to meet always in the practical studies, it is preferable that the spatial distribution of sampling sites should be rather evenly distributed over the study area, and if possible constitutes points of a regular grid. The first descriptive exposition of sampling sites may be their location distribution, but without its relationship to the ReV it does not mean much in spatial analysis. The sampling locations may already be fixed for researchers, such as the existing well locations (water or oil), meteorology stations, urban areas. If the distribution of a variable Z with respect to easting and northing is given as in Table 3.1, then its frequency distribution can be calculated for various classes and presented in Fig. 3.3.

It is obvious from this figure that as the number of classes increase, the categories change both in class limits and in frequency values.

On the other hand, it is possible to see the scatter of these data as in Fig. 3.4. If ReV is denoted in general as Z, then the points in this scatter diagram can be grouped depending on some criterion as follows with respective symbols.

$$
\begin{array}{cc}
\circ & Z < 189 \\
+ \quad 189 & < Z < 536 \\
* \quad 536 & < Z < 936 \\
x \quad 936 & < Z < 1310 \\
\quad 1310 & < Z < 1632 \\
\diamond & Z > 1632
\end{array}
$$

These symbols help to make two types of interpretations, namely interclass and smaller or less than a given class limits, two mutually exclusive but collectively exhaustive groups. According to the attached symbols, one can deduce the following interpretations:

a) The majority of small ReVs are gathered at high easting but low northing regions. Two exceptional clusters of the same type appear at low easting and northing regions and also in high easting but medium and high northing regions. In short, there are three clusters of small ReVs. Each cluster has its special dependence

Table 3.1 Easting, northing, and ReV

Easting	Northing	ReV (m)	Easting	Northing	ReV (m)
40.78	30.42	31	41.25	29.02	30
40.52	30.3	100	41.73	27.23	232
39.72	40.05	1631	41.10	29.06	114
37.00	35.33	20	40.60	43.08	1,775
41.17	29.04	130	41.40	27.35	46
40.73	31.60	742	37.93	41.95	896
39.62	27.92	120	41.18	29.62	31
40.18	29.07	100	42.03	35.17	32
40.32	27.97	58	40.98	27.48	4
40.15	29.98	539	40.65	29.27	4
38.40	42.12	1578	39.83	34.82	1,298
40.13	26.40	3	38.50	43.5	1,671
41.17	27.8	183	38.75	30.53	1,034
40.55	34.97	776	38.78	35.48	1,053
37.88	40.18	677	37.75	30.55	997
39.58	28.63	639	37.97	32.55	1,032
39.60	27.02	21	37.20	28.35	646
39.92	41.27	1869	41.28	36.33	4
41.67	26.57	51	36.70	30.73	50
39.78	30.57	789	40.92	38.4	38
40.98	28.80	36	41.37	33.77	799
40.20	25.90	72	39.75	37.02	1,285
40.97	29.08	33	39.73	39.5	1,156
40.93	26.40	10	41.17	29.05	56
40.78	29.93	76	39.93	44.03	858
40.90	29.18	28	38.43	38.08	862

feature different than others. The frequency of low ReV occurrences fall within this type of data.

b) The ReV variability with values between 189 and 536 takes place also at high easting and low northing region, with the most concentrated cluster of ReVs less than 189. In fact, these two groups can be assumed as one cluster in larger scale as ReV values less than 536.

c) The ReV values that lie between 536 and 936 are scattered almost all over the sampling area, but they do not fall within the major sampling area where easting is high and northing is low. This group of sampling points has the maximum ReV variability over the region in an independent manner. In other words, although ReVs less than 189 have high regional variability, but at least they are fathered in three clusters.

d) Those ReV values between 536 and 1,310 show a single cluster within the medium easting and northing region, without intermixing with other classes. They show a directional extension along the northeast southwest trend in Fig. 3.4.

e) The high values of ReV more than 1,310 are gathered at medium easting but high northing region of the sampling area.

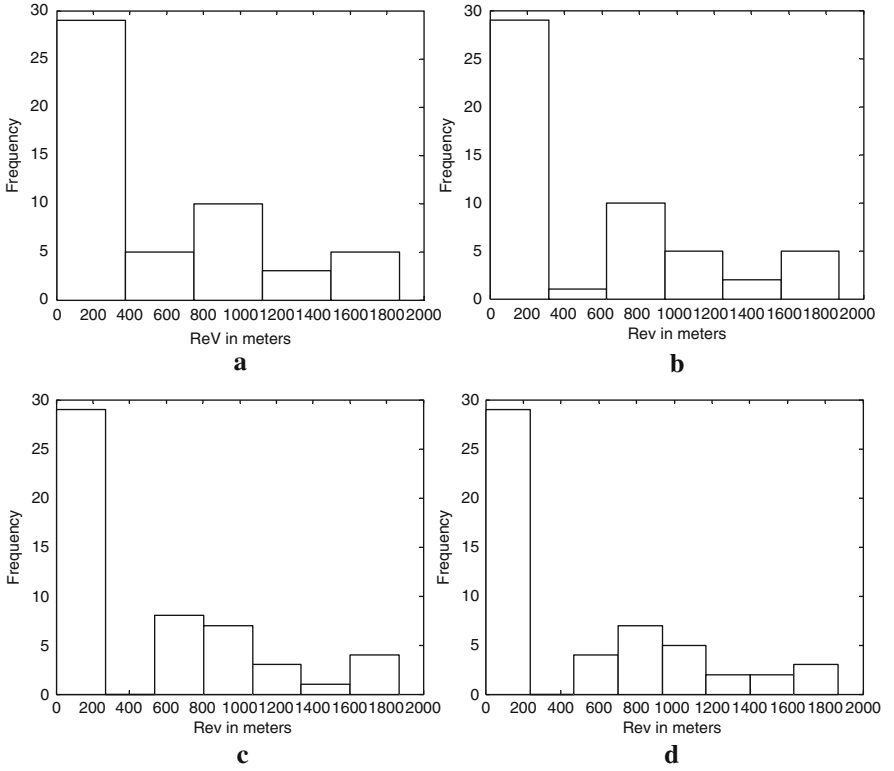

Fig. 3.3 Relative frequency diagram of ReV with (**a**) 5-class; (**b**) 6-class; (**c**) 7-class; (**d**) 8-class

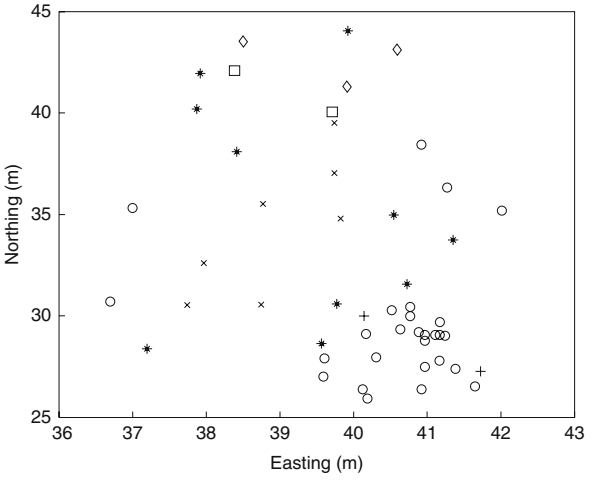

Fig. 3.4 Spatial pattern of each class

f) If the symbols are followed from the smallest to moderate and then to the biggest ReV values in Fig. 3.4, it is clear that there is an increasing trend from low northing sampling locations toward high northing direction. In the middle northing region along the easting direction, there is a hill with low values at low and high easting regions.

The above interpretations of the ReV data scatter based on the sampling locations yield clues that become very useful in actual modeling scheme. So far only linguistic interpretations are deduced and they are the basic ingredients or rules in fuzzy logic system modeling (Zadeh, 1968; Şen, 2004).

It is important to notice from the qualitative information that distinctive features are depicted by considering the differences or dissimilarities between the scatter points and the attached ReV values at each point. The first difference implies the distances between the sampling points and the second is the difference between the ReV values at two sites. Hence, in any quantitative study these two differences should be taken into consideration. These differences are considered independently from each other, but there may be regional dependence between them. For instance, visualization of a trend in step f implies such a regional dependence. As will be explained in Chapter 5, the relationship between the distance of two sampling points and the difference in their ReV values can be depicted by semivariogram (SV) concept.

2. Univariate data description: It is necessary and helpful to explore the uni-, bi-, and multivariate statistical properties of the ReV data irrespective of sampling point locations. The second step in geostatistics (or, for that matter, any statistical analysis) is to describe the data using univariate (and if possible, bivariate or multivariate) descriptive statistics. Among the univariate descriptive statistics are the arithmetic mean, median, mode, standard deviation, skewness, kurtosis, etc.

These parameters can be obtained either from the frequency diagram (as in Fig. 3.3) or through the classical mathematical expression of the parameters (Koch and Link, 1971). Often used parameters are presented in Table 3.2 for the ReV data in Table 3.1.

In spatial analysis one should note that there is only one univariate parameter value for any given ReV variable. As will be explained later in more detail, the

Table 3.2 Univariate statistical parameters

Parameter	Value
Minimum	3
Mode	4
Median	125
Arithmetic mean	506.05
Maximum	1,869
Standard deviation	571.11
Skewness	0.89
Kurtosis	0.41

Table 3.3 Representative ReV values

Easting (m)	Northing (m)	ReV (m)
40.78	30.42	31
40.52	30.3	100
41.17	29.04	130
39.62	27.92	120
40.18	29.07	100
40.32	27.97	58
	Parameters	Value
	Minimum	31
	Mode	100
	Median	100
	Arithmetic average	89.83333
	Maximum	130
	Standard deviation	37.96007
	Skewness	37.96007
	Kurtosis	0.363526

univariate parameter values do not change with direction in the sampling area. Whatever the direction, although, the projection of sampling point sequence and distances will change but the univariate statistical parameters will remain the same. This explains why the univariate parameters cannot be useful in the spatial dependence search directly. The spatial variation can be measured by considering comparatively the properties of at least two ReV values at two distinctive sampling locations,

3. Bivariate data description: This can de achieved by considering at least two sampling points simultaneously by comparing their ReV values. It can be achieved simply by considering either a direction or without any direction. In order to familiarize the reader with each one of these approaches, six ReV values with their easting and northing values are considered from Table 3.1 and presented in Table 3.3. The scatter of sampling points in this case is given in Fig. 3.5.

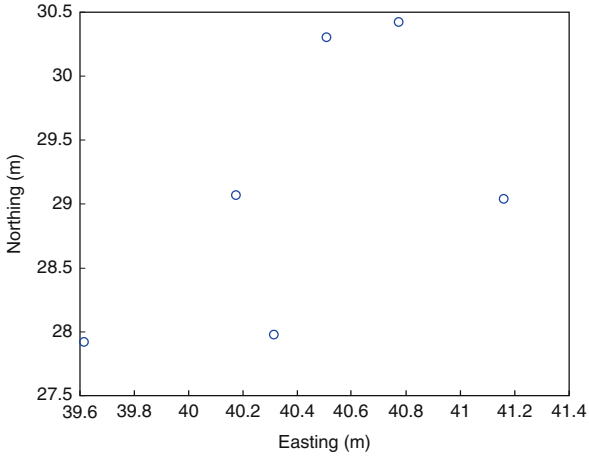

Fig. 3.5 ReV sampling locations

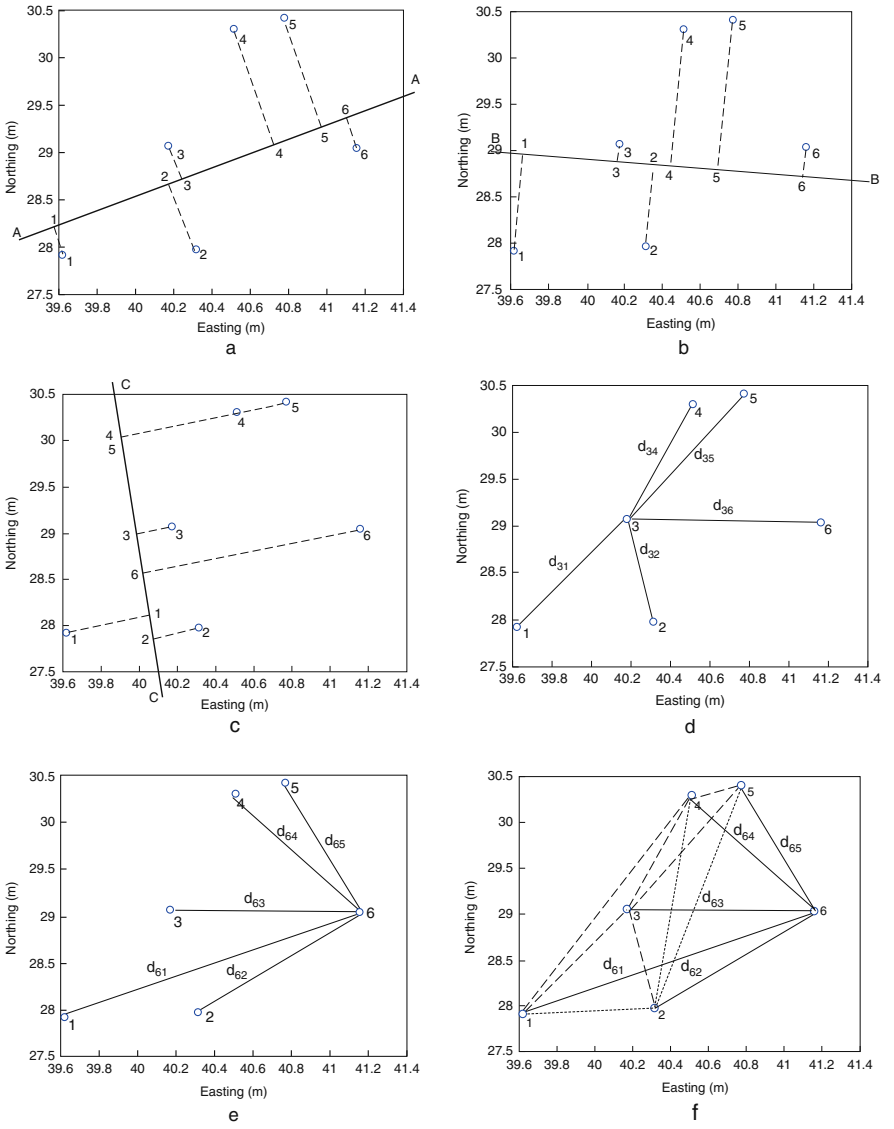

Fig. 3.6 (**a**) A–A direction; (**b**) B–B direction; (**c**) C–C direction; (**d**) Partial directional (Point 3) configuration; (**e**) Partial directional (Point 6) configuration; (**f**) Unidirectional (Global) configuration

On the basis of the data in this table, the spatial relationship between the distance and the ReV values can be thought in three categories, namely punctual, directional, and global assessments.

In the directional case all the sampling points are projected onto desired number of directions and the ReV values are considered not at the sampling points but

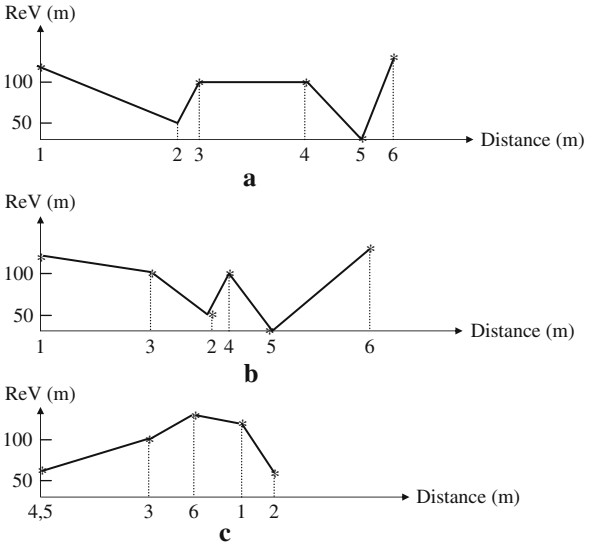

Fig. 3.7 Directional variations (**a**) A–A direction; (**b**) B–B direction; (**c**) C–C direction

at the projection points. In this manner, two-dimensional sampling point scatter is transformed into one-dimensional directional samplings as shown in Fig. 3.6.

A close inspection of these figures indicates that the sequence of sampling points and the distances between two successive points differ from each case. This is the first indication that depending on the sequential properties, the spatial variations show different appearances. The directions correspond to cross sections of three-dimensional ReV along these directions. In order to confirm this situation, Fig. 3.7 presents the variation of ReV values with distance along the direction. It is obvious that although the univariate statistical parameters remain as they are in Table 3.3, whatever the direction, they expose different patterns.

Comparison of these three cross sections shows different patterns. Especially, in section C–C points 4 and 5 fall on the same directional point and in this case the representative ReV value is taken as the average of the two values. The directional graphs show the change of ReV with distance, but the distances among the points are irregular. Had it been that they are regular, then the classical time series analysis could be applied for their statistical analysis. In practice, it is time consuming to rely on such directions and the question is whether there is an easy statistical way to inherent the common features of all the directions and then to express the regional variability by a mathematical formulation, which helps to make ready calculations provided that the spatial data of ReV are available. This can be achieved by SV, or covariogram analysis (Chapter 5).

3.5 Simple Uniformity Test

In the case of sampling point scatter as in Fig. 3.4, it is necessary to decide whether the points in each sub-quadrangle (sub-area) arranged in a manner have more or

less the same uniformity? In the case of uniformity, there is no superiority among sub-areas and each sub-area has the same likelihood of sampling point occurrences. If there are n sampling points over the whole area and the number of sub-areas is k, then the expected average uniform sampling number, U_E, for each sub-area is

$$U_E = \frac{n}{k}. \tag{3.1}$$

This indicates the average number of sampling points per sub-area. However, the actual sampling point count, C_i, (i = 1, 2, . . ., k) in i-th sub-area is different from each other and in general from the uniform sampling number. It is possible to check the uniformity by the Chi-square test as

$$\chi^2 = \sum_{i=1}^{k} \frac{(C_i - U_E)^2}{U_E}. \tag{3.2}$$

The Chi-square distribution has $\nu = k - 2$ degrees of freedom, and one can find from the Chi-square distribution tables in any statistical text book (Benjamin and Cornell, 1970) the critical Chi-square value, χ^2_{cr}, that corresponds to this degree of freedom. If $\chi^2 \leq \chi^2_{cr}$, then the distribution of the points in each sub-area over the whole area is uniform.

Example 3.1
The positions of many earthquake measurement stations are given in Fig. 3.8, and it has been divided into nine equal sub-areas. The question is whether the spatial scatter of station locations is uniformly distributed in the area or not?

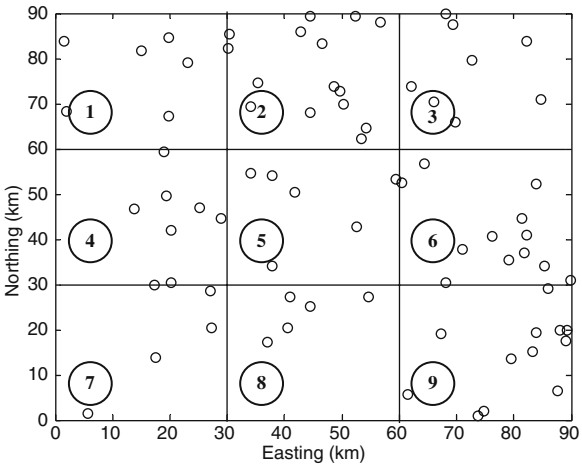

Fig. 3.8 Earthquake station location scatter

Table 3.4 Sub-areal stations

Sub-area No.	Station No.
1	7
2	15
3	8
4	7
5	6
6	12
7	4
8	5
9	12
Total	75

Table 3.4 indicates the number of stations in each sub-area where the station locations on the boundary are considered as belonging to the right and upper sub-areas.

According to Eq. (3.1), the expected average uniform number of stations in each sub-area is 75/9 = 8.33, which can be taken as a round number equal to 8. The application of Eq. (3.4) leads to $\chi^2 = 14$. Since the degree of freedom is $\nu = 9 - 2 = 7$, the critical χ^2_{cr} value at 5% significance level appears as 14.2 (i.e., $\chi^2 \leq \chi^2_{cr}$) and hence the distribution of the points is almost uniform.

3.6 Random Field

If the distribution of sampling points in the study area is not uniform, then one starts to suspect whether they constitute a random field or not? The random field is the collection of many randomly scattered points in an area where there is no spatial correlation between the points. If the points are completely random without any spatial (regional) dependence, then the only way of their spatial treatment is the probability axioms.

Let us consider the whole study area, A, with m sampling locations. If they are random, then the probability of one sampling point occurrence can be expressed as a percentage,

$$\lambda = \frac{m}{A}, \tag{3.3}$$

which lies between 0 and 1 exclusive. Now the total area is considered in terms of very small sub-areas where the number of sub-areas, n, is much larger than the number, m, sampling point (n >> m). This means that m/n goes to zero as the number of sub-areas increase. Each one of the n sub-areas can be considered as a pixel (see Fig. 2.2), which is very small, compared to total area. This makes it possible to consider that each pixel is almost equal to the influence area of one sampling point. It is, therefore, impossible to have two sampling points within each pixel. Hence, the area of influence for each sampling point can be calculated as

$$a = \frac{A}{n}, \tag{3.4}$$

which is the pixel area. Since each sampling point has the occurrence probability of λ per area, then in the influence area the probability of sampling occurrence becomes

$$p_o = \lambda a = \lambda \frac{A}{n}. \tag{3.5}$$

Accordingly, the probability of non-occurrence of the sampling point in a pixel can be obtained simply as

$$p_n = 1 - p_0 = 1 - \lambda \frac{A}{n}. \tag{3.6}$$

If the question is to find k sampling sites in n pixels, then in the remaining n−k pixels there will not be any sampling point. Since the spatial sampling point occurrences and non-occurrences are independent from each other, the production operation of the probability theory gives the probability of k sampling point occurrence according to Binomial pdf as

$$p_k = \binom{n}{k} (p_0)^k (p_n)^{n-k} = \binom{n}{k} \left(\lambda \frac{A}{n}\right)^k \left(1 - \lambda \frac{A}{n}\right)^{n-k}. \tag{3.7}$$

After this line, the remaining is the application of pure mathematical principles; and as n goes to very large numbers (mathematically positive infinity), then Eq. (3.7) takes its new shape as

$$p_k = e^{-\lambda A}[(\lambda A)^k / K!], \tag{3.8}$$

which has the name of Poisson distribution in common statistics. This equation requires only the rate of sampling points, λ (Eq. 3.3), sampling point number, k, and the area of the concerned region. The combined value λA indicates the mean number of stations per quadrant. All these values are practically observable or calculatable, and therefore it is possible to calculate p_k from Eq. (3.8). If for a given confidence interval (90 or 95%) the critical probability value, p_{cr} is found from the Poisson distribution tables in any textbook on statistics (Benjamin and Cornell, 1970) and if $p_k < p_{cr}$, then the sampling points are randomly distributed in the area.

However, in earth sciences the distribution of sampling points is exactly neither random nor uniform.

Example 3.2

It is now time to search for the spatial random character of the same example given in the previous section. As shown in Fig. 3.9 the whole area is divided into $9 \times 9 = 81$ quadrants.

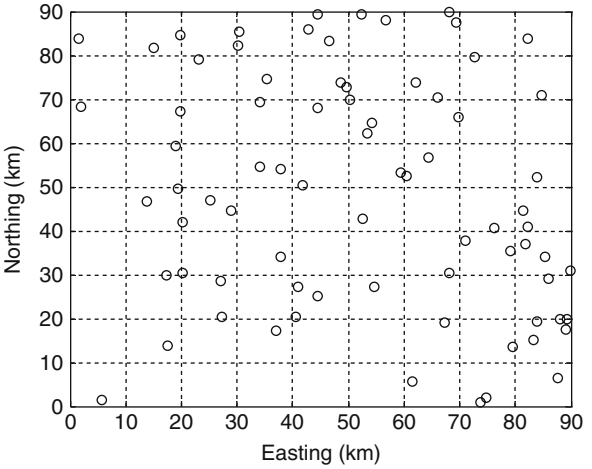

Fig. 3.9 Quadrants and station locations

The mean number of stations in each quadrant is $\lambda A = 75/81 = 0.926$. The first column in Table 3.5 shows the number of quadrants with 1, 2, 3, etc., stations. The probability of occurrence calculations is given in the second column.

According to Eq. (3.2) one can calculate that $\chi^2 = 1.064$. Since there are five categories, the degree of freedom is $\nu = 5 - 2 = 3$. The critical value of χ^2 for $\nu = 3$ and the significance level of 5% is 7.81. The test statistics is less than this critical value and so the hypothesis of randomness is acceptable.

The mean number of stations per quadrant λA and its variance can be estimated as

$$s^2 = \frac{\sum_{i=1}^{T} (r_1 - m/T)^2}{T - 1}, \tag{3.9}$$

where r_i is the number of stations per quadrant and T is the number of quadrantsis. It is well known that in Poisson distribution the arithmetic average is equal to variance, and by using this rule it is possible to make further interpretations. For instance, if

Table 3.5 Applied and theoretical numbers of quadrants

Number of stations	Equation (3.8) calculations	Number of quadrants	
		Theoretical	Actual
0	0.3961	32	31
1	0.3668	30	29
2	0.1698	14	14
3	0.0524	4	6
4	0.0121	1	1
Total	0.9972	81	81

the arithmetic average is greater (smaller) than the variance, the scatter of stations is more uniform (clustered) than random. If the two parameters are equal to each other, the scatter of stations accords with a complete random behavior. However, at this stage it must be kept in mind that some sampling differences occur between these two parameters and in practice it is not possible to have them equal in an exact manner.

3.7 Cluster Sampling

Due to stratification of many earth sciences events the sampling procedure also shows grouping pattern in different non-overlapping clusters (classes) as in Fig. 3.3. In the modeling of cluster sampling there are two stages. First is the modeling of cluster centers and then the second is the modeling of sampling points within each cluster relative to its center. The first is inter-cluster modeling and the second is within cluster modeling. As stated in many publications, the negative exponential distribution can be used to model the occurrence of clustered points in space in a manner equivalent to the use of the Poisson model to represent random field points. The cluster point distribution is modeled according to the Poisson distribution and the points in each cluster by the logarithmic distribution. Hence, the negative exponential distribution function provides the occurrence of k sampling points probability as (Davis, 2002)

$$P_k = \binom{n+k-1}{k} \left(\frac{p_o}{1+p_o}\right)^k \left(\frac{1}{1+p_o}\right)^n, \tag{3.10}$$

where k is the number of sampling points, p_o is the probability of event occurrence at a sampling site, and n is the degree of clustering of the occurrences. If n is large, the clustering is less spelled and the sampling point distribution is close to random field distribution of the points. However, as n approaches to zero the clustering pattern becomes more pronounced over the area. The density of sampling points is

$$\lambda = np_o. \tag{3.11}$$

The following mathematical approximation is considered for solving Eq. (3.10):

$$P_0 = \frac{1}{(1+p_o)^n}, \tag{3.12}$$

and the following recursive formula,

$$P_k = \frac{(n+k-1)\left(\frac{1}{p_o}+p_o\right)}{k} P_{k-1}, \tag{3.13}$$

helps to calculate the subsequent probabilities. The clustering parameter can be calculated as

$$n = \frac{\left(\frac{m}{T}\right)^2}{s^2 - \frac{m}{T}}, \tag{3.14}$$

where s^2 is the variance in the number of occurrences per tract, which is defined as

$$\lambda A = \frac{m}{T},$$

or

$$T = \frac{m}{\lambda A}. \tag{3.15}$$

Likewise, the probability of occurrence can be calculated as

$$p_0 = \frac{\lambda}{n} = \frac{\frac{m}{T}}{n}.$$

Example 3.3
The same example given in the previous section can be adopted for the application of cluster test. It is already calculated that $\lambda A = 0.926$. The variance, s^2, in the number of occurrences per quadrangle (sub-area) is 0.897. With these values at hand, the clustering effect from Eq. (3.14) becomes $n = 27.74$. Hence, from Eq. (3.12) $p_0 = 0.0323$, and it is possible to calculate from Eq. (3.13) the probability that a given quadrant will have 1, 2, 3, etc., stations as shown in Table 3.6.

In order to test the theoretical values with the actual correspondences, it is necessary to apply chi-square test, which yields $\chi^2 = 1.249$. Since there are five categories, the degree of freedom is $\nu = 5 - 2 = 3$. The critical value of χ^2 for $\nu = 3$ and the significance level of 5% is 7.81. The test statistics is less than this critical value and so the hypothesis of randomness is acceptable.

Table 3.6 Negative exponential distribution expected number of quadrants with r stations

		Number of quadrants	
Number of stations	Probability	Theoretical	Actual
1	0.4140	33.5	31
2	0.3593	29.1	29
3	0.1616	13.1	14
4	0.0501	4.0	6
5	0.0120	1.0	1
Total	**1.0020**	**81.0**	**81**

3.8 Nearest Neighbor Analysis

Rather than considering quadrangles in the subdivision of the total area into sub-areas and then to make calculations on the basis of the sampling points within the sub-area, it is preferable to consider the neighbor points next to each other. Logically, if there are n sampling points within a total area, A, then the size of each equal sub-area, a, is simply calculated according to Eq. (3.4). This area is supposed to include two nearest points on the average. It is considered as a square and therefore the side length, L, of the square is the square root of the area,

$$L = \sqrt{a}. \tag{3.16}$$

Hence, the mean distance between two points is

$$\overline{d}_T = \frac{1}{2}L. \tag{3.17}$$

The variance of the average distance between two points can be calculated rationally as

$$\sigma_T^2 = \frac{(4-\pi)}{4\pi n^2}A. \tag{3.18}$$

In the derivations of Eqs. (3.17) and (3.18), the area is assumed without boundary, i.e., very extensive. However, this is not the situation in practice, and therefore these statistical parameters are without areal extent restrictions and hence they provide under-estimations. If the constants are worked and the standard error of estimate is calculated, the result becomes

$$s_{Te} = \frac{0.26136}{\sqrt{\frac{a}{n^2}}}. \tag{3.19}$$

If the number of sampling points is more than six, then the distribution of the average distance between nearest neighbors comply with a normal pdf. The mean and the variance of this pdf are given by Eqs. (3.17) and (3.19), respectively. Hence, for decision the standardized normal pdf value, x, can be obtained as

$$x = \frac{\overline{d} - \overline{d_T}}{s_{Te}}. \tag{3.20}$$

As mentioned earlier the theoretical Eqs. (3.17) and (3.18) are in under-estimations, and therefore a correction factor less than 1 must be imported. Many researchers suggested different adjustments, but the one given by Donnelly (1978) found frequent use. According to his extensive numerical simulation studies, the theoretical mean distance and its variance can be expressed as (Davis, 2002)

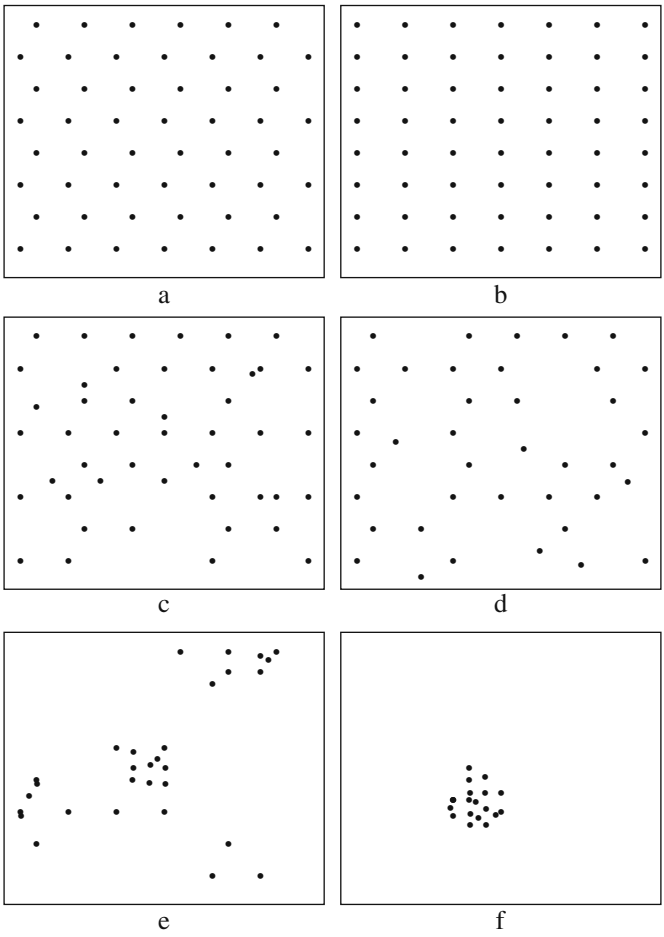

Fig. 3.10 Nearest-neighbor ratio statistics

$$\overline{d_T} \approx \frac{1}{2}\sqrt{\frac{A}{n}} + \left(0.514 + \frac{0.412}{\sqrt{n}}\right)\frac{P}{n}, \tag{3.21}$$

and

$$\sigma_T^2 \approx 0.0070\frac{A}{n^2} + 0.035P\frac{\sqrt{A}}{n^{2.5}}, \tag{3.22}$$

where P is the perimeter of the regular map. The ratio, R_d, of the expected and observed mean nearest-neighbor distances can be used to indicate the spatial pattern as

$$R_d = \frac{\bar{d}}{\bar{d}_T}. \tag{3.23}$$

This ratio approaches to zero where all the sampling points are very close to each other with almost negligible average distance. Another extreme point appears as R_d approaches 1, where the random field scatter of sampling points takes place. When the mean distance to the nearest neighbor is maximized, then R_d takes its maximum value as 2.15. Figure 3.10 indicates the sampling point distribution with different distance ratio indices.

The distance ratio indices for Fig. 3.8a to f are equal to 2.15, 1.95, 1.20, 0.89, 0.31, and 0.11, respectively.

3.9 Search Algorithms

One of the critical differences between various local-fit algorithms for interpolating to a regular grid is the way in which "nearest neighbors" are defined and found. Some may depend on the number of nearest points and others adopt a radius of influence and depend on the points within this area of influence (Chapter 2). Some search techniques (such as the optimum interpolation technique) may be superior to others in certain situations, especially concerning the data points arrangement. There are a variety of search procedures that may be selected by the user. The simplest method finds the n nearest neighboring data points in a Euclidean distance sense, regardless of their irregular distribution around the estimation node, which is fast and satisfactory if the observations are distributed in a comparatively uniform manner, but provides poor estimates if the data are closely spaced along widely separated traverses.

One of the objections to a simple nearest neighbor search is that all the nearest points may lie, for instance, in a narrow wedge on one side of the grid node (Fig. 3.11). Hence, the estimation is essentially unconstrained, except in one direction. It is possible to avoid such a situation by restricting the search in some way, which ensures that the points are equitably distributed about the estimation point.

The simplest method introduces a measure of radial search as a quadrant. Some minimum number of points must be taken from each of the four quadrants around the estimation point. An elaboration on the quadrant search is an octant search, which introduces a further constraint on the radial distribution of the points used in the estimation procedure. A specified number of control points must be found in each of the 45° segments surrounding the estimation point. These constrained search procedures require finding and testing more neighboring points than in a simple search, which increases time consumption. It is also possible to consider all points within a radius R of the estimation point. Estimates made using the other search procedures are based on a fixed number of points collected at variable distances from the grid node. This search algorithm uses a variable number of points within a fixed distance of the estimation point.

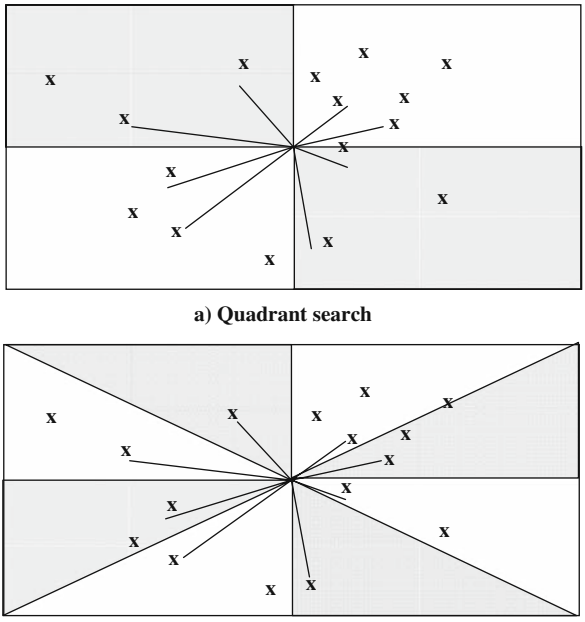

Fig. 3.11 Regular directional nearest point systems, (**a**) Quadrant; (**b**) Octant

Any constraints on the search for the nearest points, such as a quadrant or octant requirement, will obviously expand the size of the neighborhood around the estimation point. This occurs because some nearby control points are likely to be passed over in favor of more distant points, in order to satisfy the requirement that only a few points may be taken from a single sector. Unfortunately, the autocorrelation of a surface decreases with increasing distance, so more remote points are less closely related to the estimation point. This means the estimate may be poorer than if a simple nearest neighbor search procedure is used.

3.9.1 Geometric Weighting Functions

Operational objective analysis procedures are suggested for interpolating in a practical way the information from unevenly distributed observations to a uniformly distributed set of grid points.

The earliest studies were by Gilchrist and Cressman (1954), who reduced the domain of polynomial fitting to small areas surrounding each node with a parabola. Bergthorsson and Döös (1955) proposed the basis of successive correction methods, which did not rely only on interpretation to obtain grid point values but also a preliminary guess field is initially specified at the grid points. Cressman (1959) developed a number of further correction versions based on reported data falling within a specified distance R from each grid point. The value of R is decreased with successive scans and the resulting field of the latest scan is taken as the new approximation.

Barnes (1964) summarized the development of a convergent weighted-averaging analysis scheme, which can be used to obtain any desired amount of detail in the analysis of a set of randomly spaced data. The scheme is based on the supposition that the two-dimensional distribution of an atmospheric variable can be represented by the summation of an infinite number of independent waves, i.e., Fourier integral representation. A comparison of existing objective methods up to 1979 for sparse data is provided by Goodin et al.(1979). Their study indicated that fitting a second-degree polynomial to each subregion triangular in the plane, with each data point weighted according to its distance from the subregion, provides a compromise between accuracy and computational cost. Koch et al. (1983) presented an extension of the Barnes method, which is designed for an interactive computer scheme. Such a scheme allows real-time assessment both of the quality of the resulting analyses and of the impact of satellite-derived data upon various meteorological data sets. Both Cressman and Barnes methods include power parameter and radius of influence values, which are rather subjectively determined in the current meteorological practice.

In any optimum analysis technique, the main idea is that the estimation at any point is considered as a weighted average of the measured values at irregular sites. Hence, if there are $i = 1, 2, \ldots, n$ measurement sites with records Z_i, then the estimated site solar irradiation, Z_C, can be calculated according to Eq. (2.27), which is most commonly used in different disciplines because of its explicit expression as the weighted average. Weighting functions proposed by Cressman (1959), Gandin (1963), and Barnes (1964) also appear as sole functions of the distances between the sites only. Unfortunately, none of the weighting functions are event-dependent, but they are suggested on the basis of the logical and geometrical conceptualizations of site configuration. Various geometrical weighting functions are shown in Fig. 3.12.

The weighting functions that are prepared on a rational and logical basis without consideration of regional data have the following major drawbacks.

(a) They do not take into consideration the natural variability of the regional variability features. For instance, in meteorology, Cressman (1959) weightings are given as

$$W(r_{i,E}) = \begin{cases} \frac{R^2 - r_{i,E}^2}{R^2 + r_{i,E}^2} & \text{for } r_{i,E} \leq R \\ 0 & \text{for } r_{i,E} \geq R \end{cases}, \tag{3.24}$$

where $W(r_{i,E})$ corresponds to W_i in Eq. (2.27); $d_{i,E}$ is the distance between estimation point and other points; R is the radius of influence, which is determined subjectively by personal experience.

(b) Although weighting functions are considered universally applicable all over the world, they may show unreliable variability for small areas. For instance, within the same study area, neighboring sites may have quite different weighting functions.

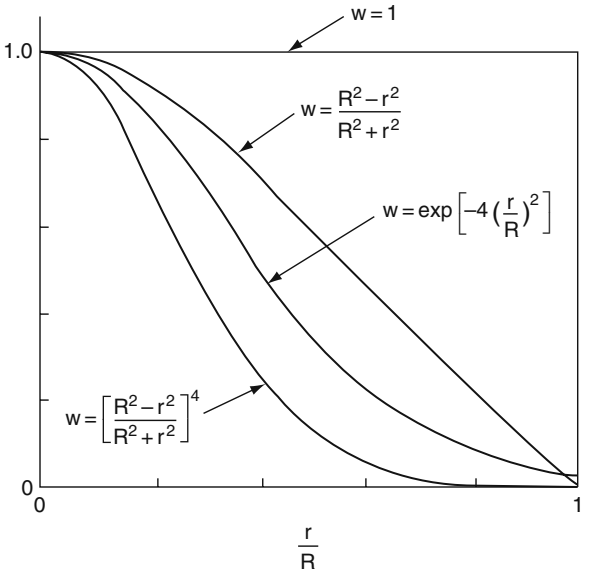

Fig. 3.12 Weighting functions

(c) Geometric weighting functions cannot reflect the morphology, i.e., the regional variability of the phenomenon. They can only be considered as practical first approximation tools.

A generalized form of the Cressman model with an extra exponent parameter α is suggested as

$$W(r_{i,E}) = \begin{cases} \left(\frac{R^2 - r_{i,E}^2}{R^2 + r_{i,E}^2}\right)^{\alpha} & \text{for } r_{i,E} \le R \\ 0 & \text{for } r_{i,E} \ge R \end{cases}. \tag{3.25}$$

The inclusion of α has alleviated the aforesaid drawbacks to some extent, but its determination still presents difficulties in practical applications. Another form of geometrical weighting function was proposed by Sasaki (1960) and Barnes (1964) as

$$W(r_{i,E}) = \exp\left[-4\left(\frac{r_{i,E}}{R}\right)^2\right]. \tag{3.26}$$

In reality, it is expected that weighting functions should reflect the spatial dependence behavior of the phenomenon. To this end, regional covariance and SV functions are among the early alternatives for the weighting functions that take into account the spatial correlation of the phenomenon considered. The former method requires a set of assumptions such as the Gaussian distribution of the regionalized

variable. The latter technique, semivariogram (SV), does not always yield a clear pattern of regional correlation structure (Şen, 1989).

3.10 Trend Surface Analysis

The main purpose of trend surface analysis is to summarize data that are numerous to grasp readily by eye from the list of numbers. A spatial trend is a systematic change usually in a geographical (longitude and latitude) direction in the ReV. The trend surface analysis is also called a "global interpolator" because it uses all data. Most interpolators (called "local interpolators") use only a sample of points to estimate the value at each grid node location. It fits the entire surface with a polynomial equation by the ordinary least squares method. Once trend surfaces were the only basic tool as maps for communication in earth sciences. In trend analysis, the statistical model coefficients are estimated and the equation is presented as a contour map. Trend surface presentation in the form of contour maps is the same as the preparation of topographic maps, where the spatial dependence is not considered explicitly. The mathematical model of the trend surface is ready in the form of polynomial equation, which relates the geographic variables x and y to the ReV, z as

$$z = a_0 + a_1 x + a_2 y + a_3 x^2 + a_4 xy + a_5 y^2, \tag{3.27}$$

where a_i's are the model coefficients to be estimated from the available data recorded at a set of geographical points within the study area. Although there are many statistical models, this model is appropriate for a smooth concave and convex surface. The locations of local maximum and minimum can be obtained from Eq. (3.27) by taking the partial derivative with respect to x and y, which yields

$$\frac{\partial z}{\partial x} = a_1 + 2a_3 x + a_4 y,$$

and

$$\frac{\partial z}{\partial y} = a_2 + a_4 y + 2a_5 y.$$

When these derivatives are set equal to zero, the solution for the extreme points become

$$x_e = \frac{a_2 a_4 - 2 a_1 a_5}{4 a_3 a_5 - a_4^2},$$

and

$$y_e = \frac{a_1 a_4 - 2 a_2 a_3}{4 a_3 a_5 - a_4^2}.$$

Different interpretations can be made of an extreme case depending on the analysis. Among the possibilities are that the extreme point may be a structural high, low, or inflection point.

In any trend surface analysis the only limit on the number of coefficients is that one cannot have more than the number of sample points. It is good for approximating the general form of the surface. Estimates of individual values are not very good (including at sample points). The interpolated surface will always have the same value as the sample value where there are sample points, and assigns each point to be interpolated the same value as the nearest sample point. It gives a stair-step shape to the surface discontinuities.

Trend surface analysis is a popular numerical technique in trying to explore the three-dimensional features of any phenomena based on the geographical coordinates; but due to a set of restrictive assumptions they cannot be regarded as successful at the time. Hence, it is frequently misused and, consequently, the conclusions based on such uses may also be in great error. Majority of problems arise from the measurement site distribution, lack of real data fit, extensive computational requirements, and at times inappropriate applications. In general, trend surface fitting methodologies are multivariate statistical model fitting to a set of regional measurement data with restrictive assumptions. A uniform density of data points is important in many types of analysis, including trend surface methods.

Trend analysis separates the ReV into two complementary components, namely regional nature of deterministic variations and local fluctuations around the regional component. The regional and local components are dependent on the scale of the ReV. In any trend analysis there are three variables.

1) The basic variables are the geographical coordinates, which give the exact locations of the sampling points in the study area. For trend analysis the longitude and latitude are converted to easting and northing values with respect to a common reference point. In trend analysis the choice of the reference point does not make any difference in further calculations.
2) The trend component is the regional representation of the event in rather deterministic manner, which has the form

$$\hat{z} = a_0 + a_1 x + a_2 y + a_3 x^2 + a_4 xy + a_5 y^2, \tag{3.28}$$

where x and y are some function or combination of the geographical coordinates of the sample locations. This expression yields the trend component as at the i-th location of the ReV. Although there are non-linear terms, this equation is called linear because the terms are added together.
3) The trend coefficients are chosen such that the squared deviations of measurements from the trend surface are minimized. The sum of the squares from the trend surface is equivalent to the variance of the ReV. The multiple linear regressions are also defined similarly, and therefore the trend analysis is similar to the multivariate analysis in the classical statistics.

3.10.1 Trend Model Parameter Estimations

It is possible to obtain the coefficient estimations in Eq. (3.27) through the application of regression methodology with the criterion of least squares analysis. This is a very formal way of deriving the coefficient estimation expressions in terms of the data values. However, in this book a more practical expression is obtained by successive independent variable term multiplication and average taking procedure. The procedure says the following steps.

1) Consider the main Eq. (3.27) and then take the arithmetic average of both sides, which leads to

$$\overline{z} = a_0 + a_1\overline{x} + a_2\overline{y} + a_3\overline{x^2} + a_4\overline{xy} + a_5\overline{y^2}. \tag{3.29}$$

This is the first estimation expression where all the arithmetic averages can be obtained from an available data set. Since there are six coefficients as unknowns, it is necessary to obtain five more expressions.

2) Multiply both sides of the main equation by the first term variable on the right-hand side and then take the arithmetic averages. This procedure yields finally,

$$\overline{zx} = a_0\overline{x} + a_1\overline{x^2} + a_2\overline{yx} + a_3\overline{x^3} + a_4\overline{x^2y} + a_5\overline{xy^2}. \tag{3.30}$$

3) Apply the same procedure as in the previous step, but this time multiplying both sides by the second independent variable, i.e., y, which gives

$$\overline{zy} = a_0\overline{y} + a_1\overline{xy} + a_2\overline{y^2x} + a_3\overline{yx^2} + a_4\overline{xy^2} + a_5\overline{y^3}. \tag{3.31}$$

4) Multiply both sides by x^2 and then take the arithmetic average of both sides, which leads to

$$\overline{zx^2} = a_0\,\overline{x^2} + a_1\overline{x^3} + a_2\overline{x^2\,y} + a_3\overline{x^4} + a_4\overline{x^3y} + a_5\overline{x^2\,y^2}. \tag{3.32}$$

5) This time the independent variable is xy and accordingly its use under the light of aforementioned procedure results in

$$\overline{xyz} = a_0\,\overline{xy} + a_1\overline{x^2y} + a_2\overline{x\,y^2} + a_3\overline{x^3y} + a_4\overline{x^2y^2} + a_5\overline{xy^3}. \tag{3.33}$$

Finally, considering the last independent term variable as y^2, the same rule yields the following expression

$$\overline{y^2z} = a_0\,\overline{y^2} + a_1\overline{y^2x} + a_2\overline{y^3} + a_3\overline{y^2x^2} + a_4\overline{xy^3} + a_5\overline{y^4}. \tag{3.34}$$

Hence, the necessary equations are obtained for the trend surface model coefficients estimation. In matrix notation these equations can be written explicitly as

$$\begin{bmatrix} a_0 \\ a_1 \\ a_2 \\ a_3 \\ a_4 \\ a_5 \end{bmatrix} = \begin{bmatrix} 1 & \overline{x} & \overline{y} & \overline{x^2} & \overline{xy} & \overline{y^2} \\ \overline{x} & \overline{x^2} & \overline{xy} & \overline{x^3} & \overline{x^2y} & \overline{xy^2} \\ \overline{y} & \overline{xy} & \overline{y^2} & \overline{x^2y} & \overline{xy^2} & \overline{y^3} \\ \overline{x^2} & \overline{x^3} & \overline{x^2y} & \overline{x^4} & \overline{x^3y} & \overline{x^2y^2} \\ \overline{xy} & \overline{x^2y} & \overline{xy^2} & \overline{x^3y} & \overline{x^2y^2} & \overline{xy^3} \\ \overline{y^2} & \overline{xy^2} & \overline{y^3} & \overline{x^2y^2} & \overline{xy^3} & \overline{y^4} \end{bmatrix}^{-1} \begin{bmatrix} \overline{z} \\ \overline{xz} \\ \overline{yz} \\ \overline{x^2z} \\ \overline{xyz} \\ \overline{y^2z} \end{bmatrix}.$$

The right-hand side of this last expression includes various averages that are calculable from a given set of data, and therefore the parameter estimation is possible after the inverse of square matrix. This matrix is symmetrical around the main diagonal. It is also possible to construct the titles of calculation table by considering these averages as in Table 3.7 the following table titles.

Table 3.7 Trend surface calculation table

x	y	z	x^2	xz	xy	yz	y^2	x^3	x^2y	x^2z	xyz	y^2z	xy^2	y^3	x^4	x^3y	x^2y^2	xy^3	y^4

The arithmetic average of each column gives the elements of each matrix on the right-hand side of Eqs. (3.31, 3.32, 3.33, 3.34, 3.35, 3.36, and 3.37).

Example 3.4

A set of earthquake records are given for some part of Turkey, and the magnitude is required to be related to easting (x) and northing (y) coordinates for the prediction of Richter magnitude. The first three columns of Table 3.8 give the easting, northing, and earthquake magnitude values, respectively. For the sake of argument, simple linear trend surface equation is adopted as

$$z = a + bx + cy, \tag{3.35}$$

where a, b, and c are the trend surface parameters. According to the steps given above, the rest of the table is prepared accordingly.

There are three unknowns and it is necessary to obtain three equations in the light of practical trend surface calculations. By considering the last row of averages from Table 3.8, one can write the necessary equations simply as

$$\begin{aligned} 6.38 &= a + 39.12b + 33.30c \\ 249.64 &= 39.12a + 1533.62b + 1306.02c \\ 211.97 &= 33.30a + 1306.02b + 1150.11c. \end{aligned}$$

The simultaneous solution of these equations yields $a = 5.63$, $b = 0.0314$, and $c = -0.0143$, and hence the final linear trend surface expression is given as

$$z = 5.56 + 0.0314x - 0.0143y.$$

Table 3.8 Earthquake data and trend calculations

Number	x	y	z	xz	X^2	xy	yz	y^2
1	40.3	38.4	5.1	205.53	1624.09	1547.52	195.84	1474.56
2	38	27	6	228	1444	1026	162	729
3	39	39	6.3	245.7	1521	1521	245.7	1521
4	40.5	42.7	6.2	251.1	1640.25	1729.35	264.74	1823.29
5	38	26.5	6	228	1444	1007	159	702.25
6	40.18	38.1	6.75	271.215	1614.432	1530.858	257.175	1451.61
7	42.5	26.4	5.9	250.75	1806.25	1122	155.76	696.96
8	41	34	6.2	254.2	1681	1394	210.8	1156
9	36	30	6.25	225	1296	1080	187.5	900
10	40.65	27.2	7.75	315.0375	1652.423	1105.68	210.8	739.84
11	40.6	27.1	6.4	259.84	1648.36	1100.26	173.44	734.41
12	40.1	26.8	6.9	276.69	1608.01	1074.68	184.92	718.24
13	38	30	6.9	262.2	1444	1140	207	900
14	40.27	36.38	7.1	285.917	1621.673	1465.023	258.298	1323.504
15	39.26	26.71	7	274.82	1541.348	1048.635	186.97	713.4241
16	35.5	34	5.8	205.9	1260.25	1207	197.2	1156
17	39.7	42.8	5.3	210.41	1576.09	1699.16	226.84	1831.84
18	39.96	41.94	6.8	271.728	1596.802	1675.922	285.192	1758.964
19	38.55	30.78	5.9	227.445	1486.103	1186.569	181.602	947.4084
20	41.33	43.41	6	247.98	1708.169	1794.135	260.46	1884.428
21	38	30.5	5.9	224.2	1444	1159	179.95	930.25
22	37.03	29.43	6.1	225.883	1371.221	1089.793	179.523	866.1249
23	35.84	29.5	7	250.88	1284.506	1057.28	206.5	870.25
24	36.54	27.33	7.3	266.742	1335.172	998.6382	199.509	746.9289
25	40.94	43.88	6	245.64	1676.084	1796.447	263.28	1925.454
26	38.1	27.1	6.5	247.65	1451.61	1032.51	176.15	734.41
27	40.5	26.5	6.1	247.05	1640.25	1073.25	161.65	702.25
28	40.2	37.9	6.1	245.22	1616.04	1523.58	231.19	1436.41
29	37.98	44.48	7.6	288.648	1442.48	1689.35	338.048	1978.47
Averages	**39.12172**	**33.30483**	**6.384483**	**249.6336**	**1533.642**	**1306.022**	**211.9668**	**1150.113**

3.11 Multisite Kalman Filter Methodology

Trend surface analysis depends on continuous and regular mathematical surfaces, which does not consider individual features in any site separately, but globally fits the model to the available spatial data at fixed time. It is necessary to repeat the same procedure for any subsequent time interval independently from the previous step. It is, therefore, necessary to adopt a spatial model, which digests the spatial data at a given time and then updated the model output with the new recordings at the same locations in the region. It is possible to achieve such a task through Kalman Filter (KF) procedure. KF is an optimal state estimation process applied to a dynamic system that involves random perturbations. The atmosphere can be regarded as an uncertain dynamical system (Kalman, 1960; Dee, 1991). More precisely, KF gives a linear, equitable, and minimum error variance recursive algorithm to optimally estimate the unknown state of a dynamic system from the noisy data taken at continuous

or discrete real-time intervals. KF supplies a measure of accuracy of an analysis in the form of its error covariance (Kalman and Bucy, 1961). Therefore, it allows the impact of different observation sets to be compared.

KF is the most general approach to statistical estimation and prediction. It has been shown by Harrison and Stevens (1975) that all forecasting methods are special cases of KF. This filter can deal with changes in the model, parameters, and variances. The difficulty with KF is that many technical questions have not yet been answered satisfactorily. The approach itself has grown out of engineering practices. Consequently, many statisticians and operation researchers know little about it, or find it difficult to understand, because it is most often described in state space notation. Furthermore, many practical difficulties still exist as the initial estimates for parameters, variances, covariance, and transition matrix. As shown in Fig. 3.13, the discrete KF is an iterative procedure containing several elements, which are described in the next sections.

The filter is supplied with initial information, including the prior estimate of initial parameters, which is based on all the knowledge about the process, and the error covariance associated with it, and these are used to calculate a Kalman gain. The error between the parameter estimation and the measured data is determined and multiplied by Kalman gain to update the parameter estimate and estimation error. The updated error and parameters are used as inputs to a model, in order to predict the projected error and parameters at the next time instance. The first derivation of the KF recursive equations is the "filter" equation. The equations used in the discrete KF are given in detail by Brown and Hwang (1992). Latif (1999) has performed multisite KF development and application for Turkish precipitation in detail.

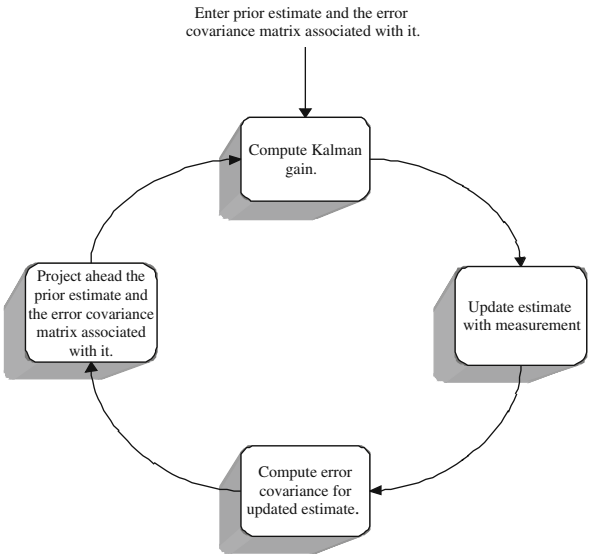

Fig. 3.13 KF iterative procedure

The objective of this section is to investigate and develop a KF model approach to multisite precipitation modeling, and prediction in addition to the assessment of associated errors. In order to have an online prediction operation, it is desirable to be able to deal with a multitude of rainfall events. The precipitation predictor should not be fixed with time and space, but should adapt itself to the evolving meteorological conditions. Any stochastic model is associated with various uncertainties. KF consists of combining two independent estimates to form a weighted estimate or prediction. One estimate can be a prior prediction or an estimate based on prior knowledge, and the other a prediction based on new information (new data). The purpose of KF is to combine these two pieces of information to obtain an improved estimate.

3.11.1 One-Dimensional Kalman Filter

Suppose that there is a random variable, X_k, whose values should be estimated at a set of certain times t_0, t_1, t_2, ... ,t_n and that X_{k-1} satisfies the following dynamic system equation,

$$X_k = \varphi X_{k-1} + W_{k-1}. \tag{3.36}$$

In this expression, ϕ is a known parameter relating X_k to X_{k-1}, and W_{k-1} is a pure independent random number with zero mean $\overline{W}_{k-1} = 0$ and the variance equals to Q. Let the measurement, Z_k, at time k is given as

$$Z_k = H_k X_k + V_k, \tag{3.37}$$

where V_k is another white noisy with zero mean and variance, R, and H is the measurement parameter.

In order to improve the prior estimate $\hat{X}_{k/k-1}$, the noisy measurement at time k, Z_k is used as

$$\hat{X}_{k/k} = \hat{X}_{k/k-1} + K_k(Z_k - H_k\hat{X}_{k/k-1}), \tag{3.38}$$

where $\hat{X}_{k/k}$ is the updated estimate and K_k is the Kalman gain. Notice that $(Z_k - H_k\hat{X}_{k/k-1})$ is just the error in estimating Z_k. For deciding on the value of K, the variance of the error be computed as

$$\begin{aligned} E\left[(X_k - \hat{X}_{k/k})^2\right] &= E\left[\left(X_k - \hat{X}_{k/k-1} - K_k(Z_k - H_k\hat{X}_{k/k-1})\right)^2\right] \\ &= E\left[(1 - K_kH_k)(X_k - \hat{X}_{k/k-1}) + K_kV_k\right]^2 \\ &= P_{k/k-1}(1 - K_kH_k)^2 + RK_k^2, \end{aligned} \tag{3.39}$$

where the cross-product terms drop out because V_k is assumed to be uncorrelated with X_k and $\hat{X}_{k/k-1}$. So, the variance of updated estimation error is given by

$$P_{k/k} = P_{k/k-1}(1 - K_k H_k)^2 + R K_k^2. \tag{3.40}$$

If it is necessary to minimize the estimation error, then minimization of $P_{k/k}$ is required by differentiating $P_{k/k}$ with respect to K_k and setting the derivatives equal to zero. A little algebra shows that the optimal K_k is obtained as

$$K = HP_{k/k-1}\left[P_{k/k-1}(K_k)^2 + R\right]^{-1}. \tag{3.41}$$

In these calculations X_k is a column matrix with many components. Then Eqs. (3.35, 3.36, 3.37, 3.38, 3.39, 3.40 and 3.41) become matrix equations, and the simplicity as well as the intuitive logic of the KF become obscured. The covariance matrices for W_{k-1} and V_k vectors are given by

$$E\left[W_k W_i^T\right] = \begin{Bmatrix} Q_k, & i = k \\ 0, & i \neq k \end{Bmatrix},$$

$$E\left[V_k V_i^T\right] = \begin{Bmatrix} R_k, & i = k \\ 0, & i \neq k \end{Bmatrix},$$

$$E\left[W_k V_i^T\right] = 0, \qquad \text{for all k and i.,}$$

where Subscript T denotes transpose of the vector.

These equations fall into two groups, time and measurement update equations. The time update equations are responsible for projecting forward (in time) the current state and error covariance estimates to obtain the a priori estimates for the next time step. The measurement update equations are responsible for incorporating a new measurement into the a priori estimate to obtain an improved estimate. The time update equations can also be thought of as predictor equations, while the measurement update equations can be thought of as corrector equations. Indeed, the final estimation algorithm resembles that of a predictor algorithm for solving numerical problems, as shown in Fig. 3.14.

The specific equations for the time updates are as follows:

$$\hat{X}_{k+1/k} = \Phi_{k+1\,k}\hat{X}_{k/k}, \tag{3.42}$$

and

$$P_{k+1/k} = \Phi_{k+1\,k} P_{k/k} \Phi_{k+1\,k}^T + Q_k. \tag{3.43}$$

On the other hand, the measurement update (corrector) equations are as follows:

$$K_k = P_{k/k-1} H_k^T (H_k P_{k/k-1} H_k^T + R_k)^{-1}, \tag{3.44}$$

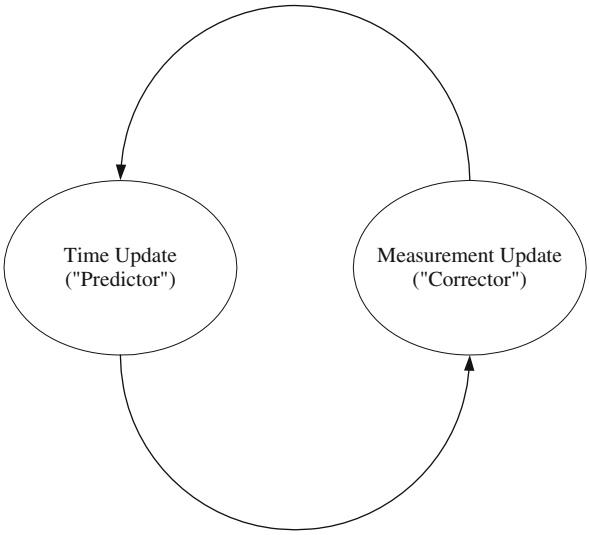

Fig. 3.14 The ongoing discrete KF cycle

$$\hat{X}_{k/k} = \hat{X}_{k/k-1} + K_k(Z_k - H_k\hat{X}_{k/k-1}), \tag{3.45}$$

and

$$P_{k/k} = P_{k/k-1} - K_k H_k P_{k/k-1}. \tag{3.46}$$

It is possible to summarize KF estimation execution steps under the light of previous derivations as follows:

1) Enter prior estimate $\hat{X}_{k/k-1}$, which is based on all our knowledge about the process prior to time t_{k-1}, and also suggest the error covariance matrix associated with it $P_{k/k-1}$.
2) Compute the Kalman gain as $K_k = P_{k/k-1}H_k^T(H_kP_{k/k-1}H_k^T + R_k)^{-1}$.
3) Update the estimate with measurement Z_k as $\hat{X}_{k/k} = \hat{X}_{k/k-1} + K_k(Z_k - H_k\hat{X}_{k/k-1})$.
4) Compute error covariance for updated estimate as $P_{k/k} = P_{k/k-1} - K_kH_kP_{k/k-1}$.
5) Project ahead the updated estimate $\hat{X}_{k/k}$ and the error covariance matrix associated with it $P_{k/k}$, to use it as a prior estimation for the next time step $\hat{X}_{k+1/k} = \Phi_{k+1\,k}\hat{X}_{k/k}$ and finally $P_{k+1/k} = \Phi_{k+1\,k}P_{k/k}\Phi_{k+1\,k}^T + Q_k$.

Once the loop is entered as shown in Fig. 3.12, then it can be continued as much as necessary. Initially, when the model parameters are only rough estimates, the gain matrix ensures that the measurement data are highly influential in estimating the state parameters. Then, as confidence in the accuracy of the parameters grows with each iteration, the gain matrix values decrease, causing the influence of the measurement data in updating the parameters and associated error to reduce.

3.11.2 Kalman Filter Application

To investigate and develop a KF model approach to multisite precipitation modeling, 30-year records (1956–1985) of annual rainfall for the 52 stations are used. As shown in Fig. 3.15 these stations are distributed over an area approximately covering all of Turkey, with more concentration in the northwestern part.

The study area lies between latitudes 36°: 70′ N and 42°: 03′ N and longitude 25°: 90′ E and 44°: 03′ E, extended over an area of about 780,576 square kilometers. The geographic locations (latitude, longitude, and elevation in meter above mean sea level) of precipitation stations are represented in Table 3.9.

Precipitation is characterized by variability in space and time. In addition, there are many factors affecting the magnitude and distribution of precipitation, elevation of station above mean sea level, various air mass movement, moisture, temperature, pressure, and topography. The magnitude and distribution of precipitation vary from place to place and from time to time, even in small areas. The application of multisite KF model as developed in this chapter approach to multisite precipitation modeling, which illustrates some interesting points in the annual precipitation pattern.

Figure 3.16 provides the observed and estimated annual rainfall values at Adapazarı from 1956 to 1984.

It is to be noticed from this figure that the observed and estimated values follow each other closely, which indicates that KF provides an efficient method for modeling of annual rainfall. Some statistical parameters of annual observed and estimated rainfall values during the time period (1956–1985) are summarized in Table 3.10.

From another point of view, Fig. 3.16 provides the observed and estimated annual rainfall values at 52 selected stations in Turkey for 1985. From Fig. 3.17 and Table 3.10, again as noticed before, in the case of one station (Adapazarı), the observed and estimated values follow each other closely, which indicates that KF provides an efficient method for modeling of annual rainfall in both time and space dimension.

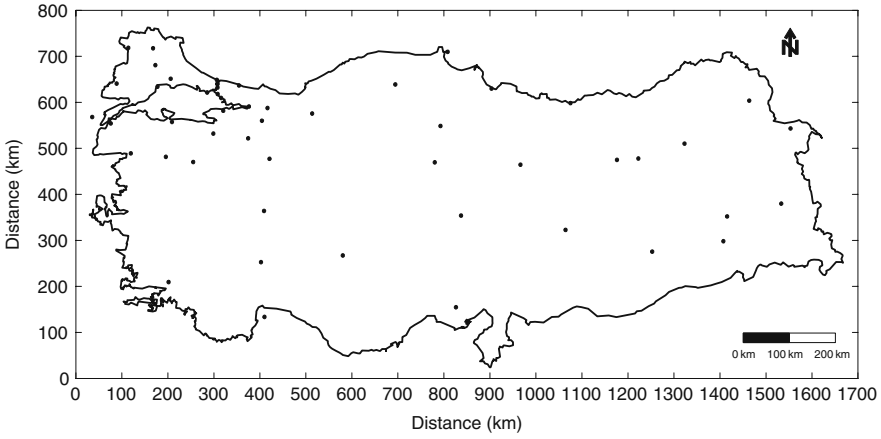

Fig. 3.15 Distribution of rainfall stations over Turkey

Table 3.9 Station locations and elevation above mean sea level

No.	Station No.	Station name	Latitude (N)	Longitude (E)	Elevation (m)
01	068	Adapazarı	40°:78′	30°:42′	31
02	662	Ali Fuat Paşa – Adapazarı	40°:52′	30°:30′	100
03	102	Ağrı	39°:72′	40°:05′	1,631
04	350	Adana	37°:00′	35°:33′	20
05	620	Bahçeköy – İstanbul	41°:17′	29°:05′	130
06	070	Bolu	40°:73′	31°:60′	742
07	150	Balıkesir	39°:62′	27°:92′	120
08	116	Bursa	40°:18′	29°:07′	100
09	115	Bandırma – Balıksir	40°:32′	27°:97′	58
10	122	Bilecık	40°:15′	29°:98′	539
11	164	Bitlis	38°:40′	42°:12′	1,578
12	112	Çanakkale	40°:13′	26°:40′	3
13	054	Çorlu – Tekirdağ	41°:17′	27°:80′	183
14	084	Çorum	40°:55′	34°:97′	776
15	280	Diyarbakır	37°:88′	40°:18′	677
16	651	Dursun bey – Balıkesir	39°:58′	28°:63′	639
17	653	Edremit – Balıkesir	39°:60′	27°:02′	21
18	096	Erzurum	39°:92′	41°:27′	1,869
19	050	Edirne	41°:67′	26°:57′	51
20	124	Eskişehir	39°:78′	30°:57′	789
21	058	Florya – İstanbul	40°:98′	28°:80′	36
22	673	Gökçeada – Çanakkale	40°:20′	25°:90′	72
23	062	Göztepe – İstanbul	40°:97′	29°:08′	33
24	674	İpsala – Edirne	40°:93′	26°:40′	10
25	010	İzmit	40°:78′	29°:93′	76
26	063	Kartal – İstanbul	40°:90′	29°:18′	28
27	059	Kumköy – İstanbul	41°:25′	29°:02′	30
28	601	Kırklareli	41°:73′	27°:23′	232
29	011	Kandilli	41°:10′	29°:06′	114
30	098	Kars	40°:60′	43°:08′	1,775
31	052	Luleburgaz – Kirklareli	41°:40′	27°:35′	46
32	210	Siirt	37°:93′	41°:95′	896
33	020	Şile – İstanbul	41°:18′	29°:62′	31
34	026	Sinop	42°:03′	35°:17′	32
35	056	Tekirdağ	40°:98′	27°:48′	4
36	118	Yalova – İstanbul	40°:65′	29°:27′	4
37	132	Yozgat	39°:83′	34°:82′	1,298
38	170	Van	38°:50′	43°:50′	1,671
39	190	Afyon	38°:75′	30°:53′	1,034
40	195	Kayseri – Erkilet	38°:78′	35°:48′	1,053
41	240	Isparta	37°:75′	30°:55′	997
42	244	Konya	37°:97′	32°:55′	1,032
43	292	Muğla	37°:20′	28°:35′	646
44	030	Samsun	41°:28′	36°:33′	4
45	300	Antalya	36°:70′	30°:73′	50
46	034	Giresun	40°:92′	38°:40′	38
47	074	Kastamonu	41°:37′	33°:77′	799
48	090	Sivas	39°:75′	37°:02′	1,285
49	092	Erzincan	39°:73′	39°:50′	1,156
50	061	Sarıyer – İstanbul	41°:17′	29°:05′	56
51	100	Iğdır	39°:93′	44°:03′	858
52	200	Malatya – Erhav	38°:43′	38°:08′	0862

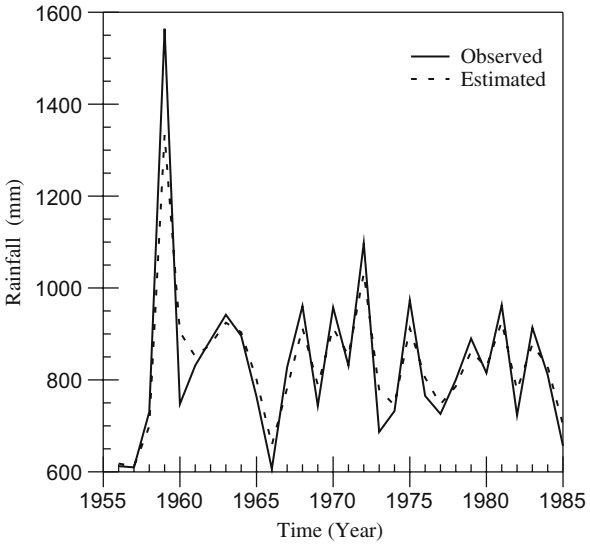

Fig. 3.16 Observed and estimated annual rainfall values at Adapazarı from 1956 to 1984

Contour maps of observed and estimated annual rainfall for 1956–1985 and percentage errors of estimated annual rainfall are presented in Figs. 3.18 and 3.19, respectively. In Fig. 3.18, dashed lines indicate the estimated annual average precipitation contours.

According to the areal values of observed and estimated annual rainfalls, the multisite KF method has a slight tendency toward under-estimation. Standard deviation of estimated value is smaller than that of observed one (Fig. 3.20). Its mean is less variable and, therefore, more smoothed than the observed values.

Furthermore, Fig. 3.17 proves that the estimated values of annual rainfall at most of the sites in the study area are close to the observed values, especially in the part where more stations are available such as in the northwestern part of Turkey. The percentage error of estimated values vary from –6 in station number 52 (underestimation) to 6 in station number 49 (overestimation), with overall average about 0.121%.

The magnitude and distribution of precipitation vary from place to place and from time to time even in small areas. Describing and predicting the precipitation variability in space and/or time are the fundamental requirements for a wide variety of human activities and water project designs. In this chapter, a KF technique has been developed for the prediction of annual precipitation amounts at a multiple site. In this manner, the precipitation amount at any year and stations is predicted by considering all the available stations interrelationships.

Once a model has been selected, then KF processing requires specification of initial state vector, error covariance matrix associated with this initial state vector, system noise covariance, measurement noise covariance, state transition matrix, and connection matrix. Most of this information should be based on

Table 3.10 Statistics parameters of observed and estimated annual rainfall values (1956–1985)

No.	Station name	Mean (mm)		St. Dev. (mm)		Minimum (mm)		Maximum (mm)		Range (mm)		Skewness	
		Obs.	*Est.*	*Obs.*	*Est.*	*Obs.*	*Est.*	*Obs.*	*Est.*	*Obs.*	*Est.*	*Obs.*	*Est.*
1	Adapazarı	835.5	834.6	183.4	135.3	606.3	611.7	1,564	1,332	957.7	720.3	2.18615	1.50665
2	Ali Fuat Paşa – Adapazarı	660.6	661	107.7	85.1	484.9	519.1	922.5	851.1	437.6	332	0.36170	0.13996
3	Ağrı	506.7	504.7	91.9	66.6	352	389.1	693.1	612.7	341.1	223.6	0.13271	−0.0978
4	Adana	690.4	688.7	221.3	184.4	319.4	360	1,265	1,149	945.6	789	0.86862	0.66023
5	Bahçeköy – İstanbul	1,287	1,284	478.6	354.7	848.1	866.2	2,698	2,325	1,850	1,459	1.73873	1.56783
6	Bolu	549.2	549.2	83.3	59.3	377.4	429.1	716.8	659.7	339.4	230.6	0.14283	0.16372
7	Balıkesir	606.7	606.1	163.6	126.3	362.6	385.6	1,192	1,036	829.4	650.4	1.59256	1.25458
8	Bursa	680.6	680.1	109.1	82.7	447.8	521.1	871	835	423.2	313.9	0.16262	−0.0062
9	Bandırma – Balıkesir	719	718.9	149.3	115	456.2	494.7	1,086	988.2	629.8	493.5	0.71735	0.55033
10	Bilecik	445.1	444.5	75.4	57.5	320.6	332.8	624.7	563.1	304.1	230.3	0.62528	0.39746
11	Bitlis	1,164	1,160	287.5	235.8	564.5	734.2	1,866	1,738	1,301	1,004	0.27270	0.51462
12	Çanakkale	636.6	640.4	139.9	108.9	414.8	459.8	977.7	868.5	562.9	408.7	0.64583	0.45769
13	Çorlu – Tekirdağ	570.6	571.1	104.1	81.5	431.2	456.4	801.3	759.9	370.1	303.5	0.58876	0.64617
14	Çorum	432.1	430.7	79.7	59.1	285.5	296.8	606.7	542.9	321.2	246.1	−0.05457	−0.2570
15	Diyarbakır	490	489	134.5	99.3	146.3	276	748.8	671	602.5	395	−0.10185	0.24572
16	Dursun bey – Balıkesir	779.1	782.2	171.6	130.6	479.3	575	1,199	1,079	719.7	504	0.36409	0.15470
17	Edremit – Balikesir	696.2	697.2	144.1	111.6	512.9	548.4	1,175	1,061	662.1	512.6	1.36238	1.2798
18	Erzurum	410.1	409.8	85.3	61.3	291.1	308.1	638.5	551.8	347.4	243.7	0.92707	0.49036
19	Edirne	593.2	594.4	102.2	72.1	430.5	496.6	863.6	792.2	433.1	295.6	0.85735	0.87714
20	Eskişehir	393.1	391.8	94.8	51.7	215.8	220.1	524	486.8	326.2	266.7	−0.18598	−0.9474
21	Florya – Istanbul	656.4	655.5	117.3	89.3	500.8	540	1,026	942.6	525.2	402.6	1.02088	1.07883
22	Gökçeada – Çanakkale	792.5	796.4	212.2	162.8	483	543.8	1,451	1,235	968	691.2	1.28517	0.92635
23	Göztepe – Istanbul	698.7	696.7	127.4	98.3	538.8	559	1,047	990.9	508.2	431.9	0.87054	0.94386
24	İpsala – Edirne	612.5	616.3	98.7	77.5	386.5	434.7	808.9	763.9	422.4	329.2	0.15228	0.11054
25	İzmit	766.6	764.9	150.2	119.9	554.9	557.2	1,088	1,012	533.1	454.8	0.37969	0.12170
26	Kartal – İstanbul	651.1	649.5	118.5	90.9	475.6	496.9	871.9	832.4	396.3	335.5	0.16123	0.05385
27	Kumköy – İstanbul	796.1	793.2	185.8	143.7	519.5	581.9	1,278	1,145	758.5	563.1	1.02989	0.88983

Table 3.10 (continued)

No.	Station name	Mean (mm)		St. Dev. (mm)		Minimum (mm)		Maximum (mm)		Range (mm)		Skewness	
		Obs.	*Est.*	*Obs.*	*Est.*	*Obs.*	*Est.*	*Obs.*	*Est.*	*Obs.*	*Est.*	*Obs.*	*Est.*
28	Kirklareli	589.4	592.5	133.9	97.5	371.5	417.5	1,000	876.9	628.5	459.4	1.17951	0.99290
29	Kandilli	827.7	825.5	148.7	117.5	600.5	631.5	1,230	1,143	629.5	511.5	0.54675	0.42092
30	Kars	470.5	472.2	106.1	78.2	298.5	361.7	718.8	661.1	420.3	299.4	0.75373	0.81958
31	Luleburgaz – Kırklareli	652.3	655.4	182.2	138.8	399.7	437.4	1,360	1,159	960.3	721.6	2.00788	1.57797
32	Siirt	684.5	682.4	183.4	141.5	420.8	474.5	1,229	1,060	808.2	585.5	1.02095	0.91065
33	Şile – İstanbul	800.8	796.2	251.5	211.6	454.6	491.5	1,697	1,537	1,242	1,045	1.74568	1.66792
34	Sinop	640.2	639.7	134.2	109.6	414.7	455.2	990.4	917.1	575.7	461.9	0.83072	0.77820
35	Tekirdağ	604.2	606.6	192.6	141.2	405.2	434.8	1,464	1,192	1,059	757.2	3.1807	2.50102
36	Yalova – İstanbul	770.4	769.2	266.9	202.7	473.2	484.7	1,959	1,617	1,486	1,132	3.216	2.60607
37	Yozgat	565.8	562.6	109.2	86	391	412.9	858.2	771.3	467.2	358.4	0.72179	0.44662
38	Van	377.9	377.9	62.7	47.6	267.9	292.5	486	461.1	218.1	168.6	−0.1035	0.04482
39	Afyon	408.6	407.7	89.5	69	239	259.3	618	576.6	379	317.3	0.14329	−0.0192
40	Kayseri – Erkilet	364.8	365.2	60	45.3	263	278.6	535	475.3	272	196.7	0.75670	0.2949
41	Isparta	557.6	557.8	160	122.7	332	371.4	968	891.5	636	520.1	0.70164	0.85167
42	Konya	326.1	325	77.6	63.7	193	225	545	483.7	352	258.7	0.95732	0.66484
43	Muğla	1,165	1,164	298.3	229.3	658	767.4	1,805	1,672	1,147	904.6	0.53785	0.44423
44	Samsun	693.7	694.2	129.4	103.2	442.2	503.5	1,011	955	568.8	451.5	0.45975	0.72549
45	Antalya	1,074	1,072	293.4	228.3	554	608.7	1,914	1,747	1,360	1,138	0.29616	0.28473
46	Giresun	1,240	1,244	153.2	125.5	1,057	1,090	1,679	1,668	622	578	1.17704	1.63857
47	Kastamonu	457.6	455	82.2	67.3	308	312.1	617	574.9	309	262.8	0.17054	−0.1840
48	Sivas	411.8	410.1	79.2	56.4	286	298.8	575	519.8	289	221	0.03905	0.09282
49	Erzincan	368.8	367.6	71.7	56.8	257	277.9	563	504.1	306	226.2	0.86580	0.62331
50	Sarıyer – İstanbul	796.6	794.3	150.8	130.6	574.9	597.8	1,171	1,102	596.1	504.2	0.91685	0.72847
51	Iğdır	251.9	253.2	77.3	55.5	114.5	154.9	501.2	422.9	386.7	268	1.0145	1.00863
52	Malatya – Erhav	402.7	403.1	100	72.1	248	292.1	593	533.9	345	241.8	0.42067	0.33824

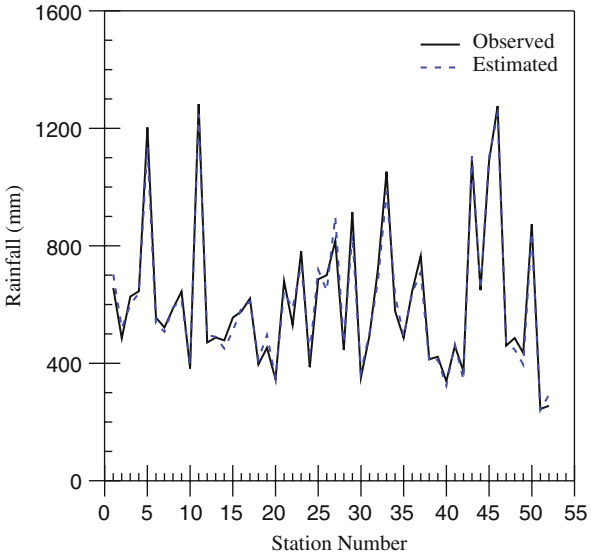

Fig. 3.17 Observed and estimated annual rainfall values at selected stations in Turkey for 1985

physical understanding and on all the previous knowledge about the process prior to t_{k-1}. If little historical information is available to specify the above matrices, then KF may be started with very little objective information and adapted as the data become available. However, the less the initial information, greater diagonal elements should be selected in the covariance matrices. In this manner, the algorithm will have flexibility to adjust itself to sensible values in a relatively short space of time.

The average amount of rainfall values at the selected stations are used as the elements of initial state vector. Sufficiently great diagonal elements of error covariance matrix are needed with initial state vector provided in the initial moment. Then, the prediction error covariance steadily decreases with time and arrives at a stable value after some steps, indicating the efficiency of the prediction algorithm.

After the initial-state descriptions are read as first step, then the Kalman gain matrix for the one-step prediction can be computed, with necessary assumptions, as the connection matrix is unity, i.e., all stations are reporting their observations. The diagonal elements of measurement noise covariance matrix is taken smaller than those of the system covariance matrix, because the observed values are relatively noise-free compared with the errors which result from the system.

Initially, when the model parameters are only rough estimates, with little objective information, the Kalman gain matrix ensures that the measurement data are highly influential in estimating the state parameters. Then, as confidence in the accuracy of the parameters grows with each iteration, the gain matrix values decrease, causing the influence of the measurement data in updating the parameters and associated error.

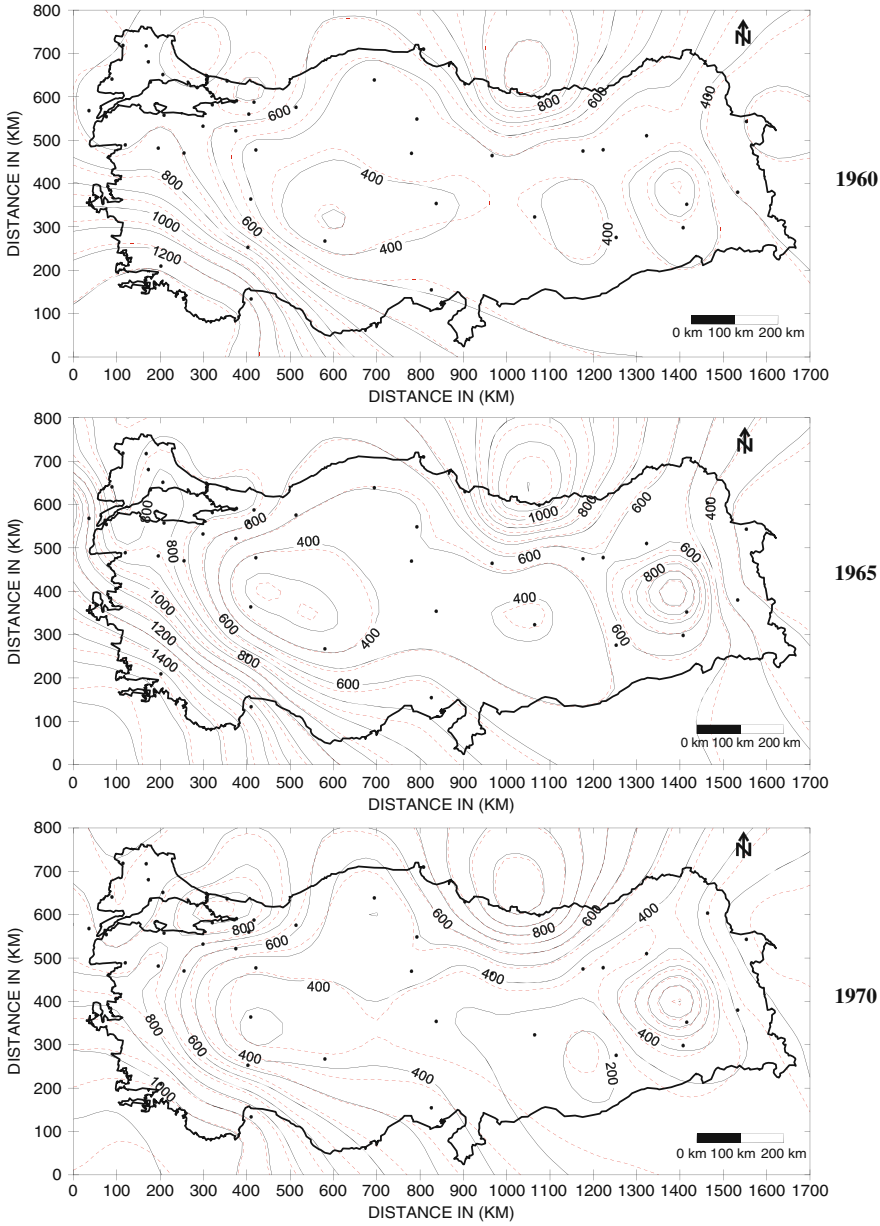

Fig. 3.18 Contour map of observed and estimated annual precipitation 1960–1985

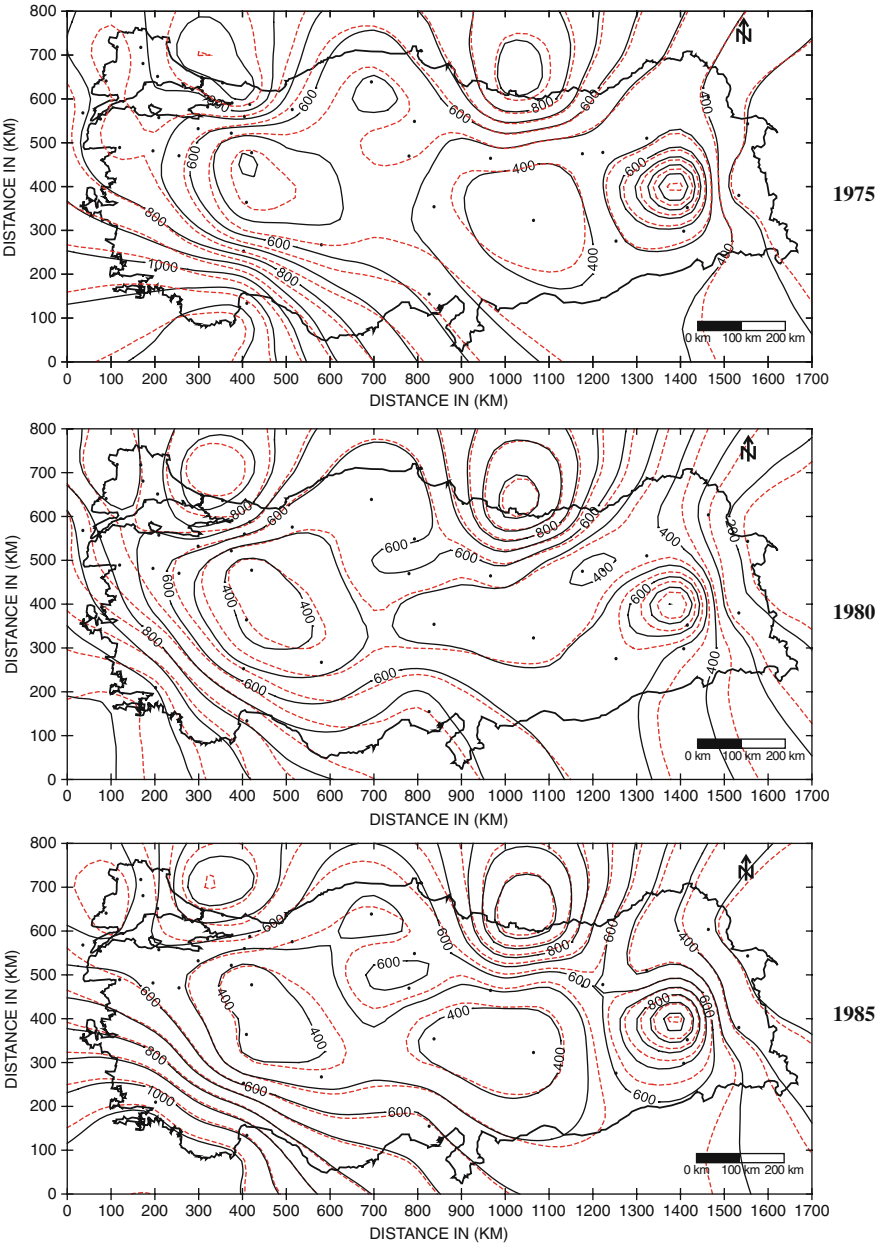

Fig. 3.18 (continued)

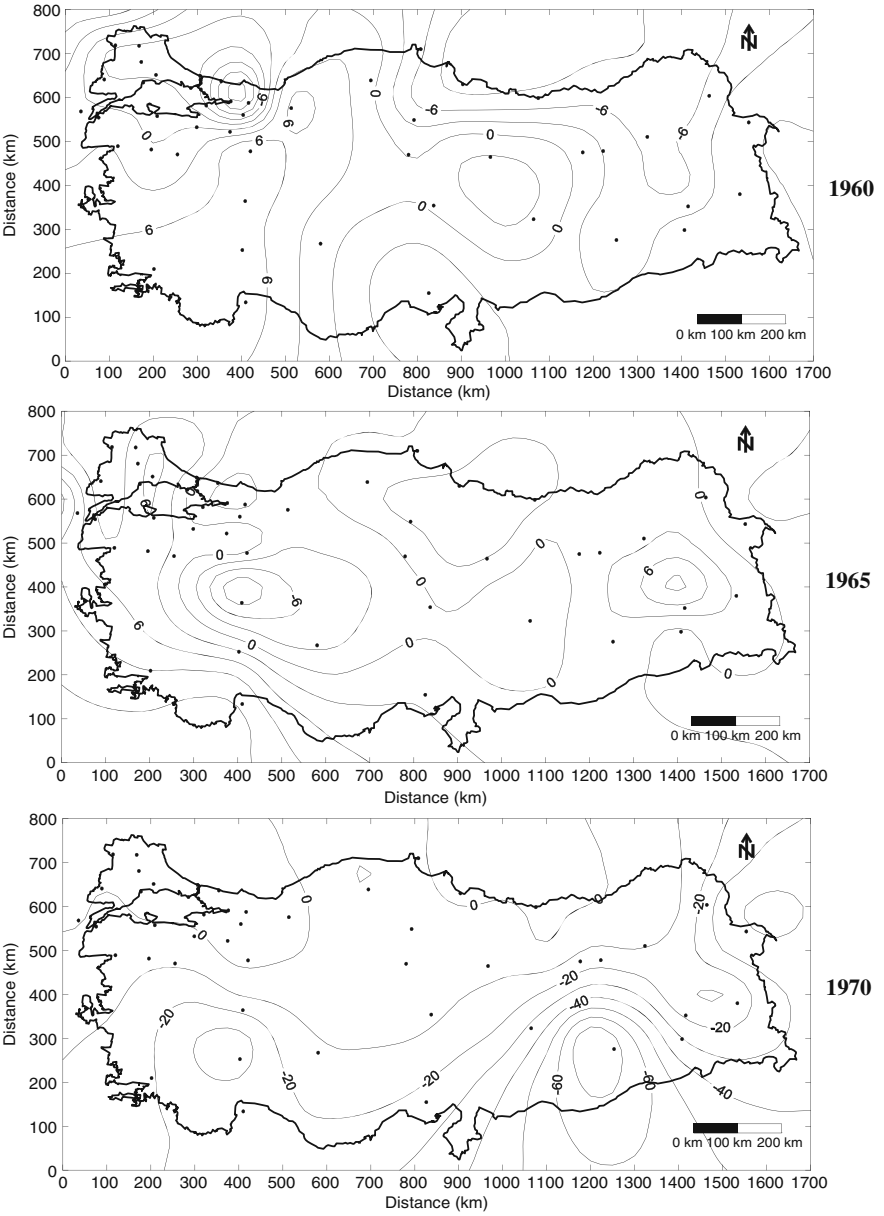

Fig. 3.19 Contour map of percentage error of estimated annual rainfall 1960–1985

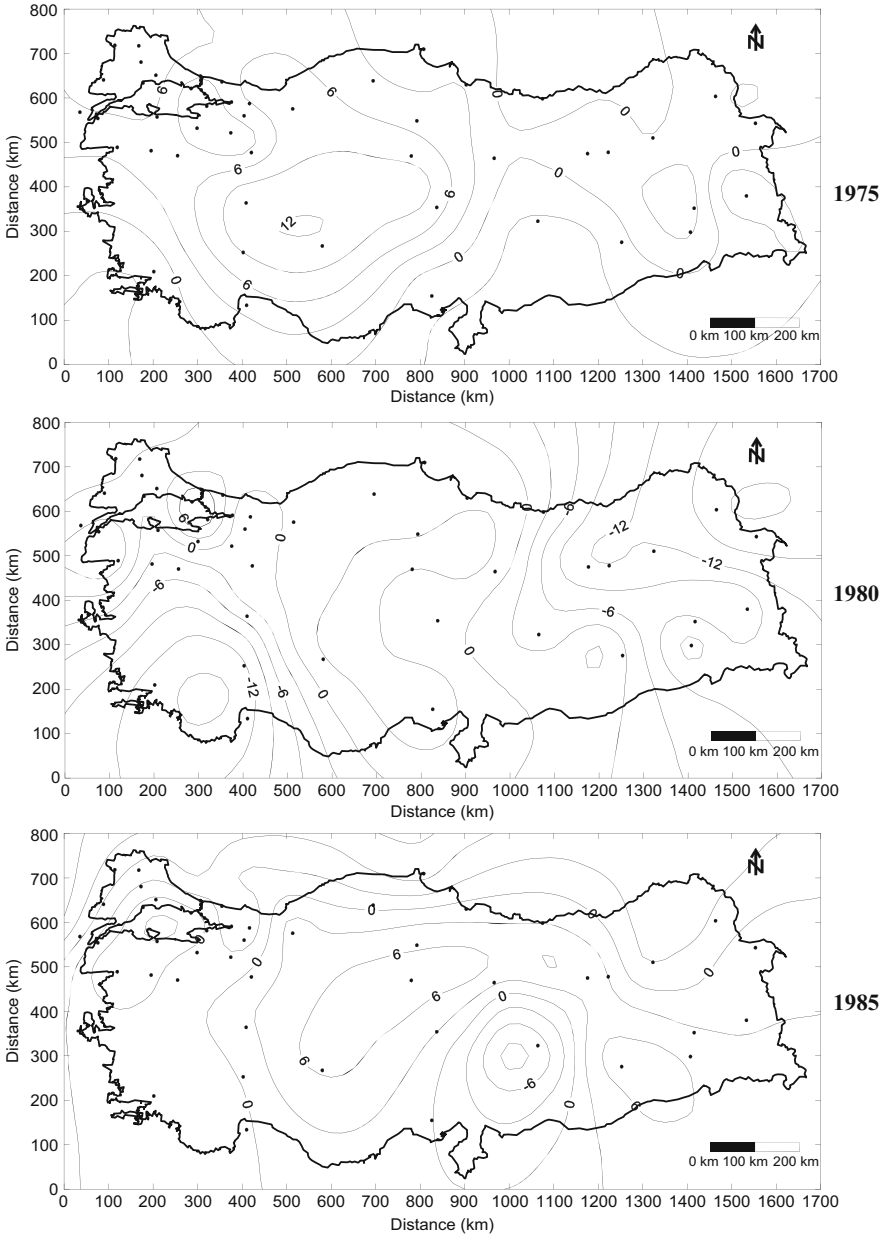

Fig. 3.19 (continued)

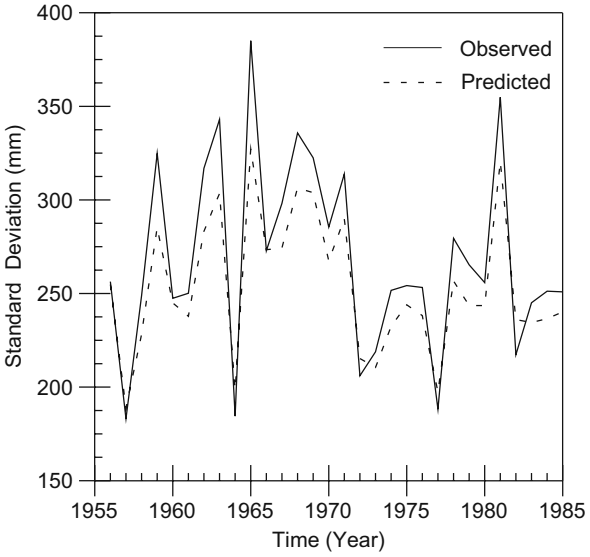

Fig. 3.20 Standard deviation of observed and estimated areal rainfall values for 1956–1985

With the assumption of an initial estimate, the measurement is used to improve the initial estimate by a linear blending of the noisy measurement and the prior estimate. The covariance matrix associated with the updated estimate is computed by using the error covariance matrix associated with initial state vector, connection and Kalman gain matrices.

The updated estimates can be projected ahead via the transition matrix, where the contribution of system error can be ignored, because it has zero mean. However, the estimate of transition matrix may be difficult, but the system is quite robust to the transition matrix values, and that they can, therefore, be set to fixed values. They have a minimal effect on the results. However, for simplicity transition matrix is assumed to be unity.

Projecting ahead the error covariance matrix, where the updated error covariance matrix can be computed, and for the system noise covariance matrix, one can use his/her judgment to select appropriate values. He/she can then examine the actual operation of the filter and adjust these values online if the situation changes at a later time. Similar to the covariance of initial values, KF is started with large diagonal elements in the system noise covariance matrix.

The projected ahead estimation and the error covariance matrix are used as initial estimation for the next time step. Once the multisite KF loop is entered, then it can be continued as much as necessary.

It is to be noticed that for one station the observed and estimated values follow each other closely, which indicates that KF provides an efficient method for modeling of annual rainfall. The observed and estimated annual rainfall values at 52 selected stations in Turkey, for 1985, follow each other closely, which indicates that

KF provides an efficient method for modeling of annual rainfall in both time and space dimensions.

The estimated values of annual rainfall at most of the sites in the study area are close to the observed values, specially in the part where more stations are available, such as in the northwestern part of Turkey. The percentage error of estimated values vary from –6 (underestimation) to 6 (overestimation), with overall average about 0.121%.

References

Barnes, S. L., 1964. A technique for maximizing details in numerical weather map analysis. J. Appl. Meteor. 3, 396–409.

Benjamin, J. R., and Cornell, C. A., 1970. Probability Statistics and Decision Making in Civil Engineering. McGraw-Hill Book Inc., New York.

Bergthorsson, P., and Döös, B. R., 1955. Numerical weather map analysis. Tellus 7, 329–340.

Brown, R. G., and Hwang Y. C., 1992. Introduction to Random Signals and Applied Kalman Filtering (Second edition). John Wiley & Sons, New York.

Cressman, G. P., 1959. An operational objective analysis system. Mon. Wea. Rev. 87, 367–374.

Davis, A., 2002. Statistics Data Analysis Geology. John Wiley and Sons, New York, 638 pp.

Dee, D. P., 1991. Simplification of Kalman filter for meteorological data assimilation. Q. J. R. Meteorol. Soc. 117, 365–384.

Donnelly, K. P., 1978. Simulations to determine the variance and edge effect of total nearest neighbor distance. In: Hodder, I. (Ed.), Simulation Studies in Archaeology. Cambridge University Press, Cambridge, UK, pp. 91–95.

Gandin, L. S., 1963. Objective Analysis of Meteorological Fields. Hydromet Press, Leningrad, 242 pp.

Gilchrist, B., and Cressman, G. P., 1954. An experiment in objective analysis. Tellus 6, 309–318.

Goodin, W. R., McRea, G. J., and Seinfeld, J. H., 1979. A comparison of interpolation methods for sparse data: application to wind and concentration fields. J. Appl. Meteor. 18, 761–771.

Harrison, P. J., and Stevens, C. F., 1975. Bayesian forecasting. University of Warwick, Working Paper No. 13.

Kalman, R. E., 1960. A new approach to linear filtering and prediction problems. Trans ASME, Ser. D, J. Basic Eng. 82, 35–45.

Kalman, R. E., and Bucy, R., 1961. New result in linear filtering and prediction theory. Trans ASME, Ser. D, J. Basic Eng. 83, 95–108.

Koch, S., and Link, R. F., 1971. Statistical Analysis of Geological Data. Dover Publications, New York, 375 pp.

Koch, S. E., DesJardins, M., and Kocin, P. J., 1983. An iterative Barnes objective map analysis scheme for use with satellite and conventional data. J. Appl. Meteor. 22, 1487–1503.

Latif, A. M., 1999. A Kalman filter approach to multisite precipitation modeling in meteorology. Unpublished Ph.D. thesis, Istanbul Technical University, 125 pp.

Matheron, G., 1963. Principles of geostatistics. Econ. Geol. 58, 1246–1266.

Matheron, G., 1965. Les Variables Regionalisees et leur Estimation. Masson, Paris, 306 pp.

Sasaki, Y., 1960. An objective analysis for determining initial conditions for the primitive equations. Tech. Rep. 60-16T.

Şen, Z., 1989. Cumulative semivariogram models of regionalized variables. Math. Geol. 21, 891–903.

Şen, Z., 2004. Fuzzy Logic and System Models in Water Sciences. Turkish Water Foundation Publication, Istanbul, Turkey, 315 pp.

Zadeh, L. A., 1968. Fuzzy algorithms. Inform. Control 12, 94–102.

Chapter 4
Spatial Dependence Measures

Abstract Rather than geometrical weighting functions as in Chapter 2, it is preferable to obtain spatial dependence function from a set of measurements points. Prior to such a functional derivation, it is necessary to examine the isotropy and homogeneity of the spatial data directionally and the point-wise features of the regionalized variable (ReV). The basics of semivariogram (SV), with its different components such as sill, nugget, and radius of influence, are presented in descriptive and application manners. Similar to SV cumulative SV (CSV) and point CSV (PCSV), concepts are explained with applications to groundwater quality data. It is emphasized that PCS helps to depict the spatial behavior features around any sampling point by taking into consideration the contribution from the surrounding measurement points. It is shown that for each location of measurement it is possible to obtain the radius of influence, if necessary along any direction, and their regional contour maps provide the radius of influence at non-measurement locations. Once the radius of influence is known, then it is possible to depict which nearby measurement locations should be taken into consideration in the calculation of unknown data value. The validity of any method can be decided on the basis of cross-validation error minimization. A new concept of spatial dependence function (SDF) is developed without the need that regional data have normal (Gaussian) probability distribution. The application of SDF is presented for earthquake and precipitation data from Turkey.

Keywords Cumulative semivariogram · Homogeneity · Isotropy · Nugget · Point cumulative semivariogram · Range · Spatial correlation · Sample semivariogram · Sill · Spatial dependence function

4.1 General

Uncertainty within earth sciences data and geologic maps is rarely analyzed or discussed. This is undoubtedly due, in part, to the difficulty of analyzing large sets of paper files. The increasing use of computers for storing, retrieving, and serving large data sets has made it easier to systematically analyze these data and preparation of maps and models from them.

Z. Şen, *Spatial Modeling Principles in Earth Sciences*,
DOI 10.1007/978-1-4020-9672-3_4,

General error theory can be a useful method for characterizing the uncertainty within spatial data. For most data, errors can be due to inaccuracies in record keeping, description, identification of behavior and location, generalization, and correlation. While analysis by error theory can be employed to evaluate the uncertainty within the data used in mapping, other methods can be used to more fully evaluate the uncertainty within specific maps. As already mentioned in Chapter 2, the area of influence method was developed to use three map characteristics (longitude, latitude, elevation) for estimating uncertainty within the maps of earth sciences. This method uses the spatial distribution of data points, the probability of mis-identification of the targeted unit, and the size of the targeted geologic feature to calculate the probability that additional, unidentified targets can exist. Insight gained from the use of error theory and the area of influence methods can be used to describe the uncertainty included in spatial maps.

Earth scientists need maps based even on few samples for extensive decisions in executing certain projects. It is, therefore, necessary for him/her to be able to visualize the subject through limited amount of data preliminarily, which can then be expanded to more effective directions with the coming of additional data. Although there is ready software for mapping if the user is not familiar with some basic principles of the methodology implemented, then the conclusions may be at bias at the minimum. At the early stages of any study, maps are needed for efficient spatial relationships without any involved mathematical formulations. In general, maps relate three variables (triplets as mentioned in Chapter 2), most of the time two are the longitude and latitude or geographical coordinates of the sample points and therefore they show the spatial variability of a single variable. However, in this chapter imaginary maps of three different earth science variables are also presented for better logical arguments, interpretations, and conclusions. Maps help to perceive large-scale spatial relationships easily on a small piece of paper.

Maps are based on the point data measurements, the distances between the points, and the density of points. Since most natural phenomenon is of continuous type, maps are representations of finite number of measurement sites and their continuous surface expressions. Hence, the more and better scattered the measurement points within the study area the better is the map representation of the natural phenomenon. The most common ones are the topographic maps with continuous contour lines of elevations, which are derived from a set of discrete location surveys. In the drawing of maps not only the measurements but also the artistic talent and skills of the expert are also taken into consideration. Hence, in many early maps subjective biases have entered the domain of mapping, but recently more objective mapping methodologies are developed and the objectivity is more enhanced.

The reliability of contour maps is directly dependent on the total density of the sampling points as well as on their uniform distribution (Chapter 3). However, in practice the uniformity of the sampling points is seldom encountered and the maps are prepared by avoiding this point. For instance, numerical, statistical, or probabilistic versions of weather prediction methods are based on the data available from irregularly distributed sites within synoptic regions. The very success of such

prediction methods significantly depends on the production of regularly gridded data at nodes of a mesh laid over the region concerned. Hence, in any spatial prediction study the following two steps are important:

1) that measured data at practically convenient but irregular sites must be transferred to regularly selected grid points, and then,
2) the use of these grid point estimates in a convenient modeling scheme through digital computers.

4.2 Isotropy, Anisotropy, and Homogeneity

In operational regional interpolation systems, many simplifying assumptions are made about the nature of the correlation, and it is represented by an analytic function of the distance. This assumption implies that the ReV is statistically homogeneous and isotropic. Gustafsson (1981) has defined the statistical homogeneity properties and isotropy of meteorological fields in reference to the covariance. A ReV is homogeneous and second-order stationary, if the covariance is independent of a translation of the two positions. This means that the covariance depends only on the difference between the positional vectors, i.e., distance. Homogeneity in reference to the covariance implies that the variance is constant. A ReV is isotropic in reference to the covariance, if the covariance is independent of a rotation in the field around the center point on the line between two positions.

For any practical application of the spatial modeling, it is necessary to construct a model for the spatial correlation to be used in the scheme. To simplify the construction of these correlation models, it is an advantage if the homogeneity and isotropy conditions are fulfilled. Much work has gone into proper choice of correlation functions of ReV. One simplifying assumption is that the correlations are assumed to be isotropic and homogeneous, which make them dependent only on distance as stated by Thiebaux and Pedder (1987) and Daley (1991). For instance, the real atmosphere is anything but homogeneous and isotropic, and hence it is assumed that the deviation from the first guess (climatologic mean) field are homogeneous and isotropic. These assumptions are made in most, if not all, interpolation analysis schemes (Bergman, 1979; Lorenc, 1981; Rutherford, 1976; Schlatter, 1975). Also homogeneity and isotropy were assumed by Gandin (1963), Eddy (1964) and Kruger (1969a,b) for most meteorological fields.

Natural phenomena physical processes have preferred orientations. For example, at the mouth of a river the coarse material settles out fastest, while the finer material takes longer to settle. Thus, the closer one is to the shoreline the coarser the sediments while the further from the shoreline the finer the sediments. When interpolating at a point, an observation 100 m away, but in a direction parallel to the shoreline, is more likely to be similar to the value at the interpolation point than is an equidistant observation in a direction perpendicular to the shoreline. Anisotropy takes these trends in the data into account during the gridding process.

Usually, points closer to the grid node are given more weight than points farther from the grid node. If, as in the example above, the points in one direction have more similarity than the points in another direction, it is advantageous to give points in a specific direction more weight in determining the value of a grid node. The relative weighting is defined by the anisotropy ratio. The underlying physical process producing the data as well as the sample spacing of the data are important in the decision of whether or not to reset the default anisotropy settings.

Anisotropy is also useful when data sets have fundamentally different units along different dimensions. For example, consider plotting a flood profile along a river. The x coordinates are locations, measured in km along the river channel. The t coordinates are time, measured in days. The Z(x, t) values are river depth as a function of location and time. Clearly in this case, the x and t coordinates would not be plotted on a common scale, because one is distance and the other is time (Fig. 4.1). One unit of x does not equal one unit of t. While the resulting map can be displayed with changes in scaling, it may be necessary to apply anisotropy as well.

Another example of anisotropy might be employed for an isotherm map (equal temperature lines, contour map) of average daily temperature over a region. Although the X and Y coordinates (as Easting, say X and Northing, say Y) are measured using the same units, the temperature tends to be very similar. Along north–south lines (Y lines) the temperature tends to change more quickly (getting colder as one heads towards the north) (see Fig. 4.2). In this case, in gridding the data, it would be advantageous to give more weights to data along the east–west axis than along the north–south axis. When interpolating a grid node, observations that lie in an east–west direction are given greater weight than observations lying an equivalent distance in the north–south direction.

In the most general case, anisotropy can be visualized as an ellipse. The ellipse is specified by the lengths of its two orthogonal axes (major and minor) and by an orientation angle, θ. The orientation angle is defined as the counter clockwise angle between the positive X and, for instance, minor axis (see Fig. 4.3). Since the ellipse is defined in this manner, an ellipse can be defined with more than one set of parameters.

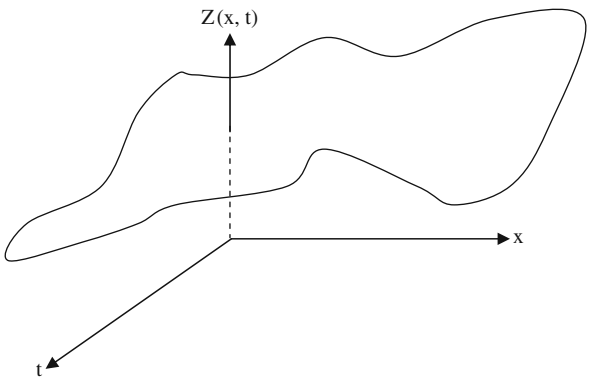

Fig. 4.1 Spatio-temporal depth variations

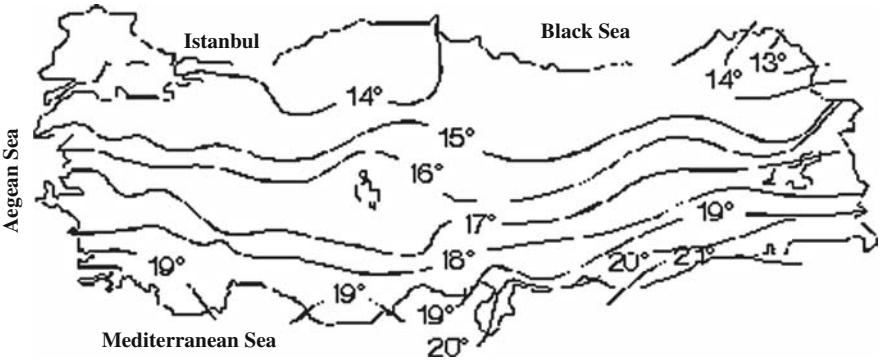

Fig. 4.2 Average annual temperature of Turkey

For most of the gridding methods, the relative lengths of the axes are more important than the actual length of the axes. The relative lengths are expressed as a ratio in the anisotropy group. The ratio is defined as major axis divided by minor axis. If it is equal to 1, then the ellipse takes the form of a circle. The angle is the counter clockwise angle between the positive X axes and minor axis. The small picture in the anisotropy group displays a graphic of the ellipse to help describe the ellipse. An anisotropy ratio less than 2 is considered mild, while an anisotropy ratio greater than 4 is considered severe. Typically, when the anisotropy ratio is greater than 3, its effect is clearly visible on grid-based maps. The angle is the preferred orientation (direction) of the major axis in degrees.

An example where an anisotropy ratio is appropriate is an oceanographic survey to determine water temperature at varying depths. Assume the data are collected every 1,000 m along a survey line, and temperatures are taken every 10 m in depth at each sample location. With this type of data set in mind, consider the problem of creating a grid file. When computing the weights to assign to the data points, closer data points get greater weights than points farther away. A temperature at 10 m in

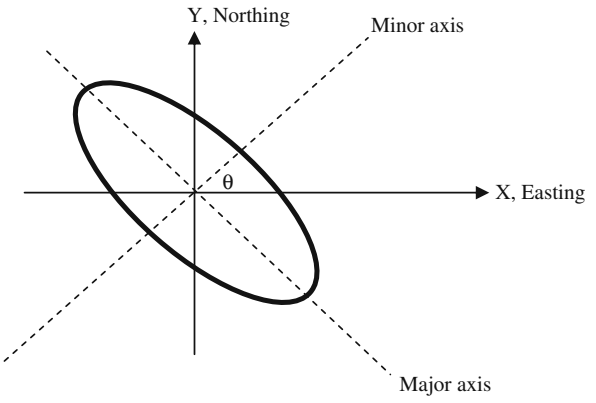

Fig. 4.3 Anisotropy ratio and angle

depth at one location is similar to a sample at 10 m in depth at another location, although the sample locations are 1,000s of meters apart. Temperatures might vary greatly with depth, but not as much between sample locations.

4.3 Spatial Dependence Function

The first step is referred to as the objective analysis and the second one is the spatial modeling phase. For sure, a sound objective analysis is the primary prerequisite of successful modeling. For instance, meteorologists strive for effective interpolation in order to enhance their mesoscale analysis and forecasts. Objective analysis studies of meteorological variables started with the work by Panofsky (1949). He attempted to produce contour lines of upper-wind movements by fitting third-order polynomials and employing least squares method to the observations at irregular sites. The least squares method leads to predicted field variables, which depend strongly on the distribution of data points when a suitable polynomial is fitted to full grid. Optimum analysis procedures are introduced to meteorology by Eliassen (1954) and Gandin (1963). These techniques employ historical data about the structure of the atmosphere to determine the weights to be applied to the observations. Here, the implied assumption is that the observations are spatially correlated. Consequently, observations that are close to each other are highly correlated; hence, as the observations get farther apart the spatial dependence decreases. It is a logical consequence to expect regional dependence function as in Fig. 4.4, assuming that at zero distance the dependence is equal to 1 and then onward there is a continuous decrease or decreasing fluctuations depending on the ReV behavior.

In this figure there are three spatial dependence functions (SDFs) as A, B, and C. Logically, A and B indicate rather homogeneous and isotropic regional behavior of ReV whereas C has local differences at various distances. However, all of them decrease down to zero SDF value. The distance between the origin and the point where the SDF is almost equal to zero shows the radius of influence as R_1 or R_2. Provided that the ReV behavior is isotropic (independent of direction), the radius of area can be calculated as a circle around each station, with radius equal to the radius of influence. These are subjective and expert views about the spatial dependence structure of any ReV. Their objective counterparts can be obtained from a

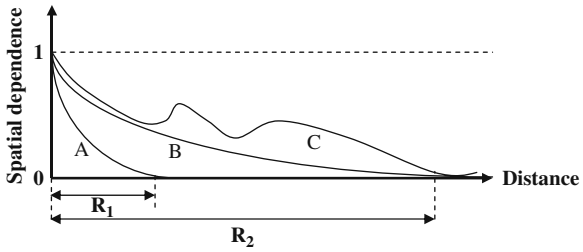

Fig. 4.4 Spatial dependence functions

set of spatial data as will be explained later in this chapter. The spatial predictions are then made by considering a spatial model with a domain equal to the radius of area. For instance, Gilchrist and Cressman (1954) reduced the domain of polynomial fitting to small areas surrounding each node with a parabola. Bergthorsson and Döös (1955) proposed the basis of successive correction methods, which did not rely only on interpretation to obtain grid point values but also a preliminary guess field is initially specified at the grid points (Chapter 5). Cressman (1959) developed a number of further correction versions based on reported data falling within a specified distance R from each grid point. The value of R is decreased with successive scans (1,500, 750, 500 km, etc.) and the resulting field of the latest scan is taken as the new approximation. Barnes (1964) summarized the development of a convergent weighted-averaging analysis scheme, which can be used to obtain any desired amount of detail in the analysis of a set of randomly spaced data. The scheme is based on the supposition that the two-dimensional distribution of a ReV can be represented by the summation of an infinite number of independent waves, i.e., Fourier integral representation. A comparison of existing objective methods up to 1979 for sparse data is provided by Goodin et al. (1979). Their study indicated that fitting a second-degree polynomial to each sub-region triangular in the plane with each data point weighted according to its distance from the sub-region provides a compromise between accuracy and computational cost. Koch et al. (1983) presented an extension of the Barnes method, which is designed for an interactive computer scheme. Such a scheme allows real-time assessment both of the quality of the resulting analyses and of the impact of satellite-derived data upon various earth sciences data sets. However, all of the aforementioned objective methods have the following common drawbacks.

1) They are rather mechanical without any physical foundation, but rely on the regional configuration of irregular sites. Any change in site configuration leads to different results although the same ReV is sampled.
2) They do not take into consideration the spatial covariance or correlation structure within the ReV concerned.
3) They have constant radius of influence without any directional variations.

Hence, spatial anisotropy of observed fields is ignored. Although some anisotropic distance function formulations have been proposed by Inman (1970) and Shenfield and Bayer (1974), all of them are developed with no explicit quantitative reference to the anisotropy of observed field structure of the ReV.

According to Thiebaux and Pedder's (1987) assessment of the work done by Bergthorsson and Döös, "the most obvious disadvantage of simple inverse distance-weighing schemes is that they fail to take into account the spatial distribution of observations relative to each other." Two observations at equidistant from a grid point are given the same weight regardless of relative values at measurement sites. This may lead to large operational biases in grid point data when some observations are much closer together than others within the area of influence.

Especially after 1980s, many researchers are concentrated on the spatial covariance and correlation structures of the ReVs. Lorenc (1981) has developed a

methodology whereby, first of all, the grid points in a sub-region are analyzed simultaneously using the same set of observations and then sub-areas are combined to produce the whole study area analysis. Some papers are concerned with the determination of unknown parameters of the other covariance functions or SDFs, which provide required weightings for ReV data assimilation. Along this line, the idea proposed by Bratseth (1986) depends on the interpretation of the ReV covariances into the objective analysis. His analysis caused a recent resurgence of the successive correction method in which the optimal analysis solution is approached. His method uses the correlation function for the forecast errors to derive weights that are reduced in regions of higher data density. Later, Sashegyi et al. (1993) employed his methodology for the numerical analysis of the data collected during the Genesis of Atlantic Lows Experiment, (GALE). Practical conclusions of Bratseth's approach have been reported by Franke (1988) and Seaman (1988).

On the other hand, Buzzi et al. (1991) described a simple and economic method for reducing the errors that can result from the irregular distribution of data points during an objective analysis. They have demonstrated that a simple iterative method for correcting the analysis generated by an isotropic distance-weighting scheme applied to a heterogeneous spatial distribution of observations cannot improve analysis accuracy, but also results in an actual frequency response that approximates closely the theoretical response of the predicted weight-generating function. They have shown that in the case of heterogeneous spatial sampling, a Barnes analysis could produce an unrealistic interpolation of the sampled field even when this is reasonably well resolved by error-free observations. Iteration of a single correction algorithm led to the method of successive correction (Daley, 1991). The method of successive correction has been applied as a means to tune adaptively the a posteriori weights. Objective analysis schemes are practical attempts to minimize the variance estimation (Thiebaux and Pedder, 1987).

Pedder (1993) provided a suitable formation for successive correction scheme based on a multiple iteration using a constant influence scale that provides more effective approach to estimate ReVs from scattered observations than the more conventional Barnes method which usually involves varying the influence scale between the iterations. Recently, Dee (1995) has presented a simple scheme for online estimation of covariance parameters in statistical data assimilation systems. The basis of the methodology is a maximum-likelihood approach in which estimates are obtained through a single batch of simultaneous observations. Simple and adaptive Kalman filtering techniques are used for explicit calculation of forecast error covariance (Chapter 3). However, the computational cost of the scheme is rather high.

Field measurements of ReVs such as ore grades, chemical constitutions in ground water, fracture spacing, porosity, permeability, aquifer thickness, dip and strike of a structure are dependent on the relative positions of measurement points within the study area. Measurements of a given variable at a set of points provide some insight into the spatial variability. This variability determines the ReV behavior as well as its predictability. In general, the larger the variability, the more heterogeneous is the ReV environment and as a result the number of measurements required to model, simulate, estimate, and predict the ReV is expected to be large. Large variability implies also that the degree of dependence might be rather small even

for data whose locations are close to each other. A logical interpretation of such a situation may be that either the region was subjected to natural phenomena, such as tectonics, volcanism, deposition, erosion, recharge, climate change, or later to some other human activities as pollution, ground water abstraction, mining, etc.

However, many types of ReVs are known to be spatially related in that the closer their positions, the greater is their dependence. For instance, spatial dependence is especially pronounced in hydrogeological data due to groundwater flow as a result of the hydrological cycle, which homogenizes the distribution of chemical constituents within the heterogeneous mineral distribution in geological formations.

The factors of ReVs are sampled at irregular measurement points within an area at regular or irregular time intervals. No doubt, these factors show continuous variations with respect to other variables such as temperature, distance. Furthermore, temporal and spatial ReV evolutions are controlled by temporal and spatial correlation structures within the ReV itself. As long as the factors are sampled at regular time intervals, the whole theory of time series is sufficient in their temporal modeling, simulation, and prediction. The problem is with their spatial constructions and the transfer of information available at irregular sites to regular grid nodes or to any desired point. Provided that the structure of spatial dependence of the ReV concerned is depicted effectively, then any future study such as the numerical predictions based on these sites will be successful. In order to achieve such a task it is necessary and sufficient to derive the change of spatial correlation for the ReV data with distance.

In order to quantify the degree of variability within spatial data, variance techniques can be used in addition to classical autocorrelation methods (Box and Jenkins, 1976). However, these methods are not helpful directly to account for the spatial dependence or for the variability in terms of sample positions. The drawbacks are due to either non-normal (asymmetric) distribution of data and/or irregularity of sampling positions. However, the semivariogram (SV) technique, developed by Matheron (1963, 1971) and used by many researchers (Clark, 1979; Cooley, 1979; David, 1977; Myers et al., 1982; Journel, 1985; Aboufirassi and Marino, 1984; Hoeksema and Kitandis, 1984; Carr et al., 1985) in diverse fields such as geology, mining, hydrology, earthquake prediction, groundwater, can be used to characterize spatial variability and hence the SDF. The SV is a prerequisite for best linear unbiased prediction of ReVs through the use of Kriging techniques (Krige, 1982; Journel and Huijbregts, 1978; David, 1977).

4.4 Spatial Correlation Function

By definition, SCF, ρ_{ij} between i and j, takes values between -1 and $+1$ and can be calculated from available historical data as

$$\rho_{ij} = \frac{\overline{(Z_i^o - \overline{Z}_i)(Z_j^o - \overline{Z}_j)}}{\sqrt{\overline{(Z_i^o - \overline{Z}_i)^2}\,\overline{(Z_j^o - \overline{Z}_j)^2}}}, \tag{4.1}$$

where over bars indicate time averages over a long sequence of past observations, Z_i^o and Z_j^o represent observed precipitation amounts at these stations, and finally, $\overline{Z}i$ and $\overline{Z}j$ are the climatological mean of precipitations. Furthermore, ρ_{ij} is thought as attached with the horizontal distance $D_{i,j}$ between stations i and j. Consequently, if there are n stations, then there will be $m = n(n-1)/2$ pairs of distances and the corresponding correlation coefficients. Their plot results in a scatter diagram that indicates the SCF pattern for the regional rainfall amounts considered as a random field. Figure 4.5 presents such scatter diagrams of empirical SCFs concerning monthly rainfall amounts (Şen and Habib, 2001). At a first glance, it is obvious from this figure that there are great scatters at any given distance in the correlation coefficients, and unfortunately, one cannot easily identify a functional trend. The scatter can be averaged out by computing mean correlation coefficient over relatively short distance intervals (Thiebaux and Pedder, 1987). The following significant points can be deduced from these SCFs.

1) Each monthly average SCF shows a monotonically decreasing trend.
2) Due to averaging procedure within the first 15 km interval, it may appear in Figs. 4.5 and 4.6 that the correlation coefficient at lag zero is not equal to +1 as expected. Monthly average SCFs for the data considered are given in Fig. 4.6. Herein, averaging is taken over successive 30 km intervals. This discrepancy is entirely due to the averaging scheme rather than a physical reality. Hence, this is not a physically plausible result but unavoidable consequence of the averaging procedure.
3) The more the averaging correlation coefficient within the first 30 km the more strongly related spatial correlation appears between the measurement sites.

4.4.1 Correlation Coefficient Drawback

Although the cross-correlation function definition can give a direct indication of the dependence of variations from the mean at any two sites, it suffers from the following drawbacks.

1) Auto-correlation and cross-correlation formulations require symmetrical (normal, Gaussian) pdf of data for reliable calculations. It is well established in literature that most of the earth sciences data pdfs accord rarely with normal (Gaussian) pdf but a Weibull, Gamma or logarithmic pdfs, which are all skewed (Benjamin and Cornell, 1970; Şen, 2002).
2) Since the cross-correlation (as the auto-correlation) is valid for symmetrically distributed ReVs (and random variables, RVs), the available data must be transformed into normal pdf prior to application of these methods.
3) In the spatial calculation of the cross-correlation, it is necessary to have a sequence of measurements with time at each site, which is not the case in many earth sciences problems where there are only one measurement at each site.

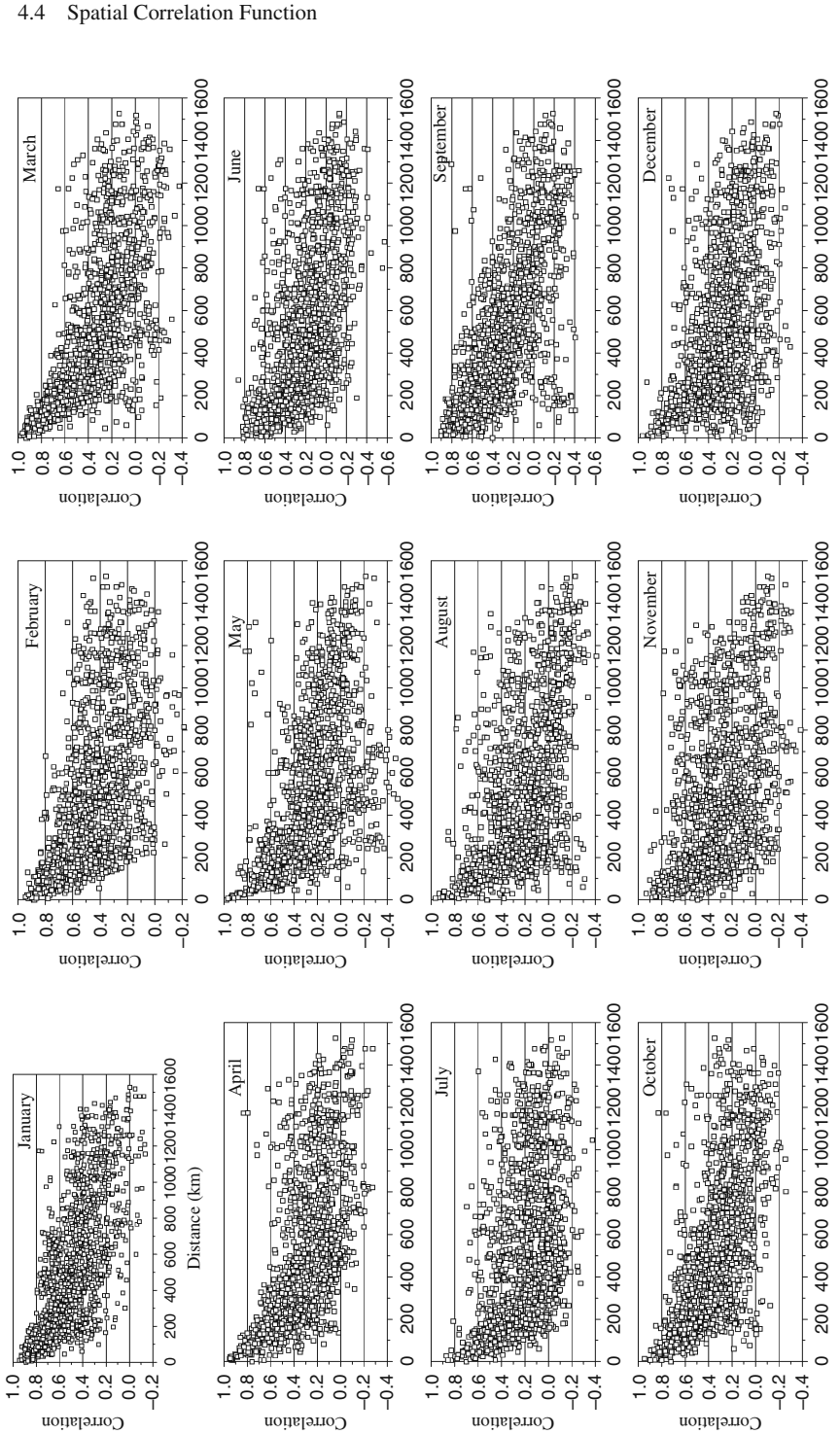

Fig. 4.5 Empirical spatial correlation functions

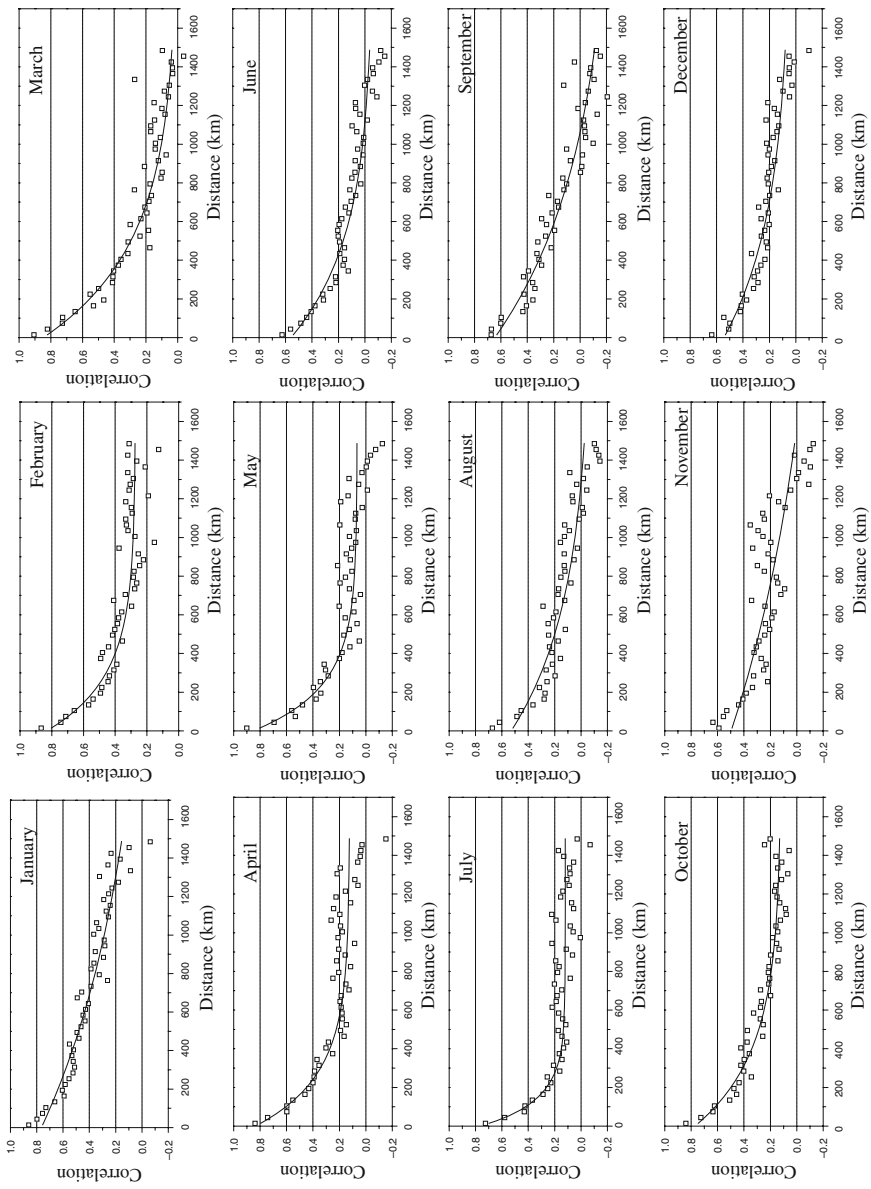

Fig. 4.6 Average and theoretical spatial correlation coefficient

4) The correlation function measures the variation around the arithmetic average values of the measurements at individual sites. However, in the spatial variability calculations, a measure of relative variability between two sites is necessary.
5) Especially for the last two points, the SV (Matheron, 1963) or cumulative SV (CSV) (Şen, 1989) concepts are developed and their modifications as the point CSV (PCSV) are presented and used for the regional assessment of earth sciences data.

For instance, Barros and Estevan (1983) presented a method for evaluating wind power potential from a 3-month long wind record at a site and data from a regional network of wind systems. Their key assumption was that "wind speed has some degree of spatial correlation," which is a logical conclusion, but they failed to present an effective method for the objective calculation of the spatial variability, except by employing cross- and auto-correlation techniques. Their statement does not provide an objective measure of spatial correlation. Skibin (1984) raised the following questions.

1) What is "a reasonable spatial correlation?" Are the correlation coefficients between the weekly averages of wind speed a good measure of it? Answers to these questions are necessary by any objective method. For instance, PCSV technique can be employed for this purpose.
2) Do the weekly averages represent the actual ones?
3) How applicable to the siting of wind generators the results obtained by the use of spatial correlation coefficients?

In deciding about the effectiveness of the wind speed measurement at a site around its vicinity, the topographic and climatic conditions must be taken into consideration. The smaller the area of influence the more homogeneous orographic, weather, and climatologic features are and, consequently, the simplest is the model. However, large areas more than 1,000 km in radius around any site may contain different climates with different through and ridges, high and low pressure areas with varying intensities. Furthermore, in heterogeneous regions with varying surface properties (such as land–sea–lake–river interfaces) and variable roughness parameters, the local wind profile and wind potential can be affected significantly. The wind energy potential and the groundwater availability are highly sensitive to height variations of hills, valleys, and plains (Şen, 1995). The reasons for wind speed variations are not only of orographical origin but also of different flow regimes (i.e., anabatic–catabatic influences compared with hill top conditions, upwind compared with leeside sites, flow separation effects). All these effects will lose their influence further away from the siting point. It can be expected that smaller distance from the site corresponds to a larger correlation. Here, again it is obvious that the spatial dependence decreases with distance as in Fig. 4.5 (correlation property). Barros and Estevan (1983) noticed that a small region had higher correlation coefficients between the sites. On the contrary, the spatial independence increases with the distance (SV property).

Barchet and Davis (1983) have stated that better estimates are obtained when the radius of influence is about 200 km from the site. However, this information is

region-dependent and there is a need to develop an objective technique whereby the radius of influence can be estimated from a given set of sites.

4.5 Semivariogram Regional Dependence Measure

The regional correlation coefficient calculation requires a set of assumptions, which are not taken into consideration in practical applications (Şen, 2008). First of all, calculation of spatial correlation coefficient requires time series records at each site. This is not possible in many earth sciences studies such as in ore grading, soil properties, hydrogeological parameters. Rather than a time series availability at each site, there is only one record, say ore grade record at a set of sites, and therefore it is not possible to calculate spatial correlation function. However, the only way to depict the spatial correlation from a set of single records at a set of locations is through the SV methodology.

4.5.1 SV Philosophy

The very basic definition of the SV says that it is the half squared-difference variation of the ReV by distance. ReV theory does not use the autocorrelation, but instead uses a related property called the SV to express the degree of relationship between measurement points in a region. The SV is defined simply as half-square (variance) of the differences between all possible point pairs spaced a constant distance, d, apart. The SV at a distance $d = 0$ should be zero, because there are no differences (variance) between points that are compared to themselves. The magnitude of the SV between points depends on the distance between the points. The smaller the distance the smaller is the SV, and at larger distances SV value is larger. The SV is a practical measure of average spatial changes. The underlying principle is that, on the average, two observations closer together are more similar than two observations farther apart. This is a general statement where the directional changes are not considered. The plot of the SV values as a function of distance from a point is referred to as an SV. However, as points are compared to increasingly distant points, the SV increases.

The simplest and most common form of ReV is a triplet, and therefore it is illuminating first to consider the surface in 3D and then according to the SV definition it is possible to infer its shape intuitively by mental experiment.

1) Continuously deterministic uniform spatial data: If the ReV is a deterministic horizontal surface of homogeneous, isotropic, and uniform data as in Fig. 4.7, then the average half-difference square of such data is zero at every distance as in Fig. 4.8.
2) Discontinuously deterministic partially uniform spatial data: The continuity in Fig. 4.7 is disrupted by a discontinuous feature (cliff, fault, facies change, boundary, etc.) as in Fig. 4.9.

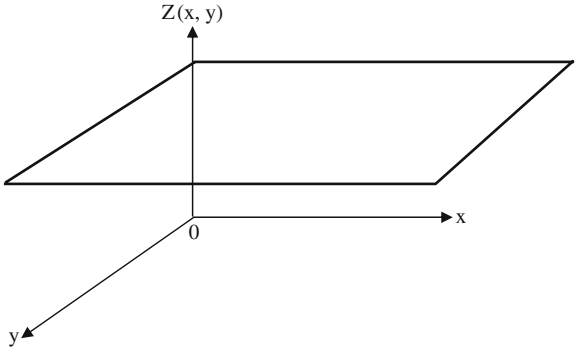

Fig. 4.7 Homogeneous, isotropic, and uniform ReV

Fig. 4.8 Perfectly homogeneous and isotropic ReV SV

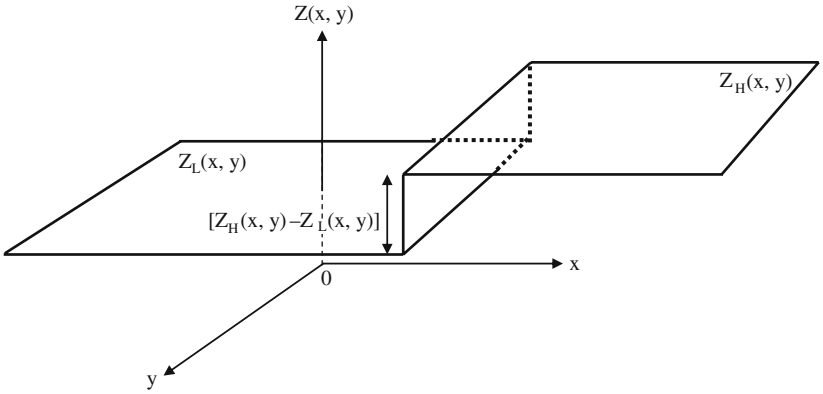

Fig. 4.9 Discontinuous surface

The average square-difference at various distances leads to an SV with a discontinuity at the origin (see Fig. 4.10), the amount of which is equal to the square-difference between higher, $Z_H(x, y)$, and lower, $Z_L(x, y)$, data values as

$$\gamma\,(d) = [Z_H(x,y) - Z_L(x,y)]^2. \tag{4.2}$$

The resulting SV is expected to take the shape as in Fig. 4.10, where there is a non-zero value at the origin. Such a jump at the origin indicates discontinuity

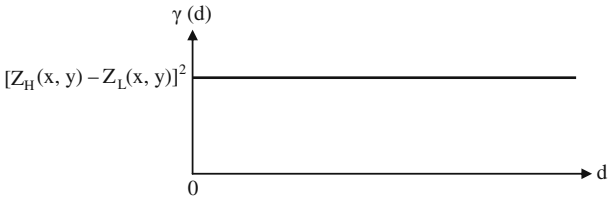

Fig. 4.10 Completely random ReV SV

Fig. 4.11 Continuous linear trend

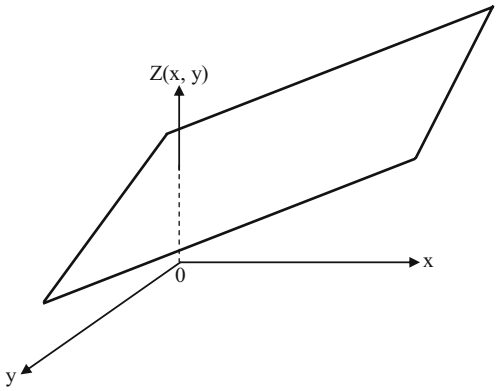

embeddings in the spatial event and it is referred to as "sill" in geostatistics literature.

3) Continuously deterministic spatially linear trend data: If the ReV is a linear surface along the X axis as in Fig. 4.11, then the SV along the X axis by definition has a quadratic form without any decrease (Fig. 4.12).
   This SV does not have any horizontal portion and at large distances the slope increases in an extreme manner.
4) Discontinuously deterministic spatially linear trend data: If the trend surface in Fig. 4.11 has a discontinuity (Fig. 4.13), then the SV shape appears as in Fig. 4.14, where there is a jump at the origin, which is referred to as nugget effect in SV terminology.

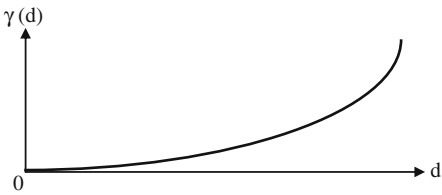

Fig. 4.12 Linear trend surface SV in X direction

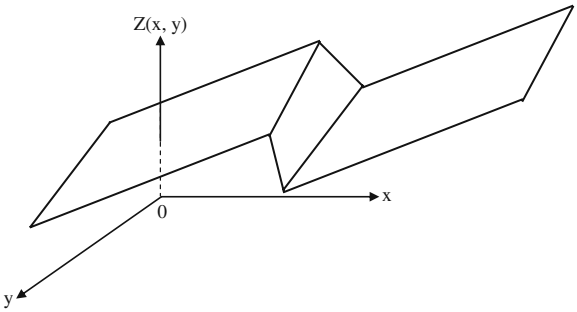

Fig. 4.13 Discontinuous trend surface

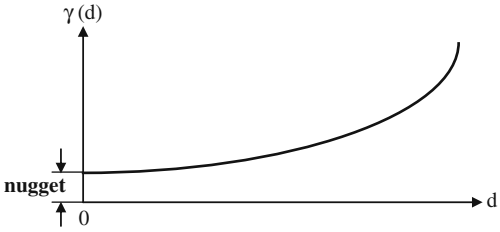

Fig. 4.14 Discontinuous trend surface SV in X direction

5) Completely independent spatial data: If the ReV is completely random with no spatial correlation as in Fig. 4.15, then the SV will be equal to the variance, σ^2, of the ReV at all distances as in Fig. 4.16. A decision can be made about the continuity (or discontinuity) and smoothness of the ReV by visual inspection from the sample SV. If at small distances the sample SV does not indicate passage from the origin (nugget effect), then the ReV includes discontinuities, where there is no regional dependence in the ReV at all. Its SV appears as a horizontal straight line similar to SV in Fig. 4.10.

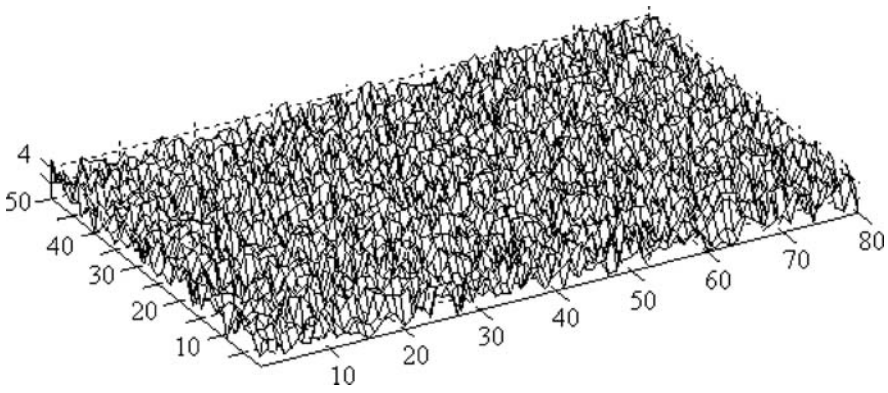

Fig. 4.15 Independent spatial data

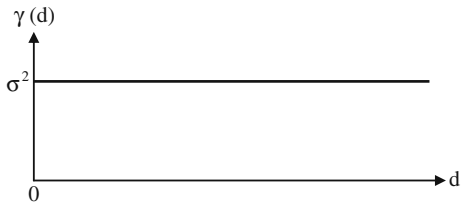

Fig. 4.16 Completely random ReV SV

The SV in this spatial random event case is equivalent to the expectation of Eq. (4.2), which after expansion and expectation E(.) operation application on both sides leads to

$$\mathrm{E}\left[\gamma\ (\mathrm{d})\right] = \mathrm{e}\left[\mathrm{Z}_{\mathrm{H}}^{2}(\mathrm{x},\mathrm{y})\right] - 2\mathrm{E}[\mathrm{Z}_{\mathrm{H}}(\mathrm{x},\mathrm{y})\mathrm{Z}_{\mathrm{L}}(\mathrm{x},\mathrm{y})] + \mathrm{e}\left[\mathrm{Z}_{\mathrm{L}}^{2}(\mathrm{x},\mathrm{y})\right].$$

Since the ReV is assumed as spatially independent with zero mean (expectation), the second term of this expression is equal to zero and the other terms are equal to the variance, σ^2, of the spatial event. Finally, this last expression yields $\mathrm{E}\left[\gamma\ (\mathrm{d})\right] = 2\sigma^2$. In order to have the SV expectation equal to the variance in practical applications, it is defined as the half-square difference instead of squared-difference as in Eq. (4.2). Consequently, the SV of an independent ReV appears as having a sill value similar to Fig. 4.10, but this time the sill value is equal to the spatial variance of the ReV.

4.5.2 SV Definition

The SV is the basic geostatistical tool for visualizing, interpreting, modeling, and exploiting the regional dependence in an ReV. It is well known that even though the measurement sites are irregularly distributed, one can find central statistical parameters such as mean, median, mode, variance, skewness, but they do not yield any detailed information about the phenomenon concerned. The greater the variance the greater is the variability, but unfortunately this is a global interpretation without detailed useful information. The structural variability in any phenomenon within an area can best be measured by comparing the relative change between two sites. For instance, if any two sites, distant d apart, have measured concentration values Zi and Zi+d, then the relative variability can simply be written as $(Z_i - Z_{i+d})$. However, similar to Taylor (1915) theory concerning turbulence, the squared-difference, $(Z_i - Z_{i+d})^2$, represents this relative change in the best possible way. This squared-difference has appeared first in the Russian literature as the "structure function" of ReV. It subsumes the assumption that the smaller the distance, d, the smaller will be the structure function. Large variability implies that the degree of dependence among earth sciences records might be rather small even for sites close to each other.

In order to quantify the degree of spatial variability, variance and correlation techniques have been frequently used in the literature. However, these methods cannot account correctly for the spatial dependence due to either non-normal pdfs and/or irregularity of sampling positions.

The classical SV technique has been proposed by Matheron (1963) to eliminate the aforementioned drawbacks. Mathematically, it is defined as a version of Eq. (4.28) by considering all of the available sites within the study area as (Matheron, 1963; Clark, 1979)

$$\gamma(d) = \frac{1}{2n_d} \sum_{k=1}^{n_d} (Z_i - Z_{i+d})^2, \tag{4.3}$$

where k is the counter of the distance, which can be expanded by considering the regional arithmetic average, $\overline{Z}$, of the ReV as follows:

$$\begin{aligned}\gamma(d) &= \frac{1}{2} \sum_{k=1}^{n_d} \left[(Z_i - \overline{Z}) - (Z_{i+d} - \overline{Z}) \right]^2 \\ &= \left[(Z_i - \overline{Z})^2 - 2(Z_i - \overline{Z})(Z_{i+d} - \overline{Z}) + (Z_{i+d} - \overline{Z})^2 \right].\end{aligned}$$

The elegancy of this formulation is that the ReV pdf is not important in obtaining the SV, and furthermore, it is effective for regular data points. It is to be recalled, herein, that the classical variogram, autocorrelation, and autorun techniques (Şen, 1978) all require equally spaced data values. Due to the irregularly spaced point sources, the use of classical techniques is highly questionable, except that these techniques might provide biased approximate results only. The SV technique, although suitable for irregularly spaced data, has practical difficulties as summarized by Şen (1989). Among such difficulties is the grouping of distance data into classes of equal or variable lengths for SV construction, but the result appears in an inconsistent pattern and does not have a non-decreasing form as expected in theory. As the name implies a SV, $\gamma(d)$, is a measure of spatial dependence of an ReV.

Due to independence any cross-multiplication of Z_i and Z_j will be equal to zero on the average, and hence this is equivalent to regional variance, σ^2, as explained in the previous section. Figure 4.16 shows this mental experiment SV as a horizontal straight line. Hence, at every distance the SV is dominated by sill value only. Expert reasoning of SV models in the previous figures help to elaborate some fundamental and further points as follows.

1) If the ReV is continuous without any discontinuity, then the SV should start from the origin, which means that at zero distance SV is also zero (Figs. 4.8 and 4.12).
2) If there is any discontinuity within the ReV, then at zero distance a non-zero value of the SV appears as in Figs. 4.10, 4.14, and 4.16.
3) If there is an extensive spatial dependence, then the SV has increasing values at large distances (Figs. 4.12 and 4.14).

4) When the spatial dependence is not existent, then the SV has a constant non-zero value equal to the regional variance of the ReV at all distances as in Fig. 4.16.
5) Under the light of all what have been explained so far, it is logically and rationally obvious that in the case of spatial dependence structure in ReV the SV should start from zero at zero distance and then will reach the regional variance value as a constant at large distances. The SV increases as the distance increases until at a certain distance away from a point it equals the variance around the average value of the ReV, and will therefore no longer increase, causing a flat (stabilization) region to occur on the SV, which is called as a sill (Fig. 4.17). The horizontal stabilization level of sample SV is referred to as its sill. The distance at which the horizontal SV portion starts is named as the range, R, radius of influence or dependence length after which there is no spatial (regional) dependence between data points. Only within this range, locations are related to each other and hence all measurement locations in this region are the nearest neighbors that must be considered in the estimation process. This implies that the ReV has a limited areal extend over which the spatial dependence decreases or independence increases in the SV sense as in Fig. 4.17.
   The classical SV is used to quantify and model spatial correlations. It reflects the idea that closer points have more regional dependence than distant points. In general, spatial prediction is a methodology that imbeds the spatial dependence in the model structure.
6) At some distance, called the range, the SV will become approximately equal to the variance of the ReV itself (see Fig. 4.17). This is the greatest distance over which the value at a point on the surface is related to the value at another point. The range defines the maximum neighborhood over which control points should be selected to estimate a grid node, to take advantage of the statistical correlation among the observations. In the circumstance where the grid node and the observations are spaced so that all distances exceed the range, Kriging produces the same estimate as classical statistics, which is equal to the mean value.
7) However, most often natural data may have preferred orientations and as a result ReV values may change more along the same distance in one direction than another (Fig. 4.3). Hence, in addition to distance, the SV becomes a function of direction (Fig. 4.18).

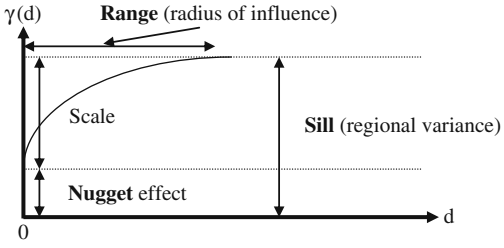

Fig. 4.17 Classical global SV and elements

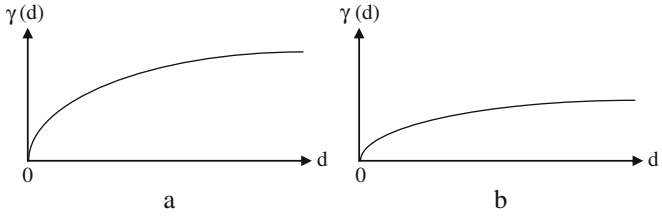

Fig. 4.18 Classical directional SV (**a**) major axis, (**b**) minor axis

It is possible to view the general of SV as a three-dimensional function as the change of SV value, $\gamma(\theta,d)$, with respect to direction, θ, and separation distance, d. Of course, θ and d are the independent variables. In general, specification of any SV requires the following information:

a) Sill (regional variance)
b) Range, (radius of influence)
c) Nugget, (zero distance jump)
d) Directional values of these parameters.

The last point is helpful for the identification of regional isotropy or anisotropy. For the Kriging application the convenient composition of these parameters must be identified through a theoretical SV. Whether a given sample SV is stationary or not can be decided from its behavior at large distances. If the large distance portion of the SV approaches a horizontal line, then it is stationary, which means intuitively that there are rather small fluctuations with almost the same variance at every corner of the region.

If the SV is generated from paired points selected just based on distance (with no directional component), then it is called isotropic (iso means the same; tropic refers to direction) or omni-directional. In this case, the lag-distance measure is a scalar and the SV represents the average of all pairs of data without regard to their orientation or direction. A standardized SV is created by dividing each SV value by the overall sample variance, which allows SVs from different data sets on the same entity for facilitating mutual comparison.

On the other hand, SVs from points that are paired based on direction and distance are called anisotropic (meaning not isotropic). In this case, the lag measure is a vector. The SVs in this case are calculated for data that are in a particular direction as explained in Section 4.3. The regularity and continuity of the ReV of a natural phenomenon are represented by the behavior of SV near the origin. In SV models with sill (Fig. 4.17), the horizontal distance between the origin and the end of SV reflects the zone where the spatial dependence and the influence of one value on the other occur, and beyond this distance the ReVs Z(x) and Z(x+d) are independent from each other. Furthermore, SVs, which increase at least as rapidly as d^2 for large distances d indicate the presence of drift (trend), i.e., non-stationary mathematical expectation. Plot of SV graphs for different directions gives valuable

information about continuity and homogeneity. If SV depends on distance d only, it is said to be isotropic; but if it depends on distance as well as direction, it is said to be anisotropic. A properly fitted theoretical SV model allows linear estimation calculations that reflect the spatial extent and orientation of spatial dependence in the ReV to be mapped. Details on these points can be found in standard text books on geostatistics (Davis, 1986; Clark, 1979).

There are also indicator SVs, which are calculated from data that have been transformed to a binary form (1 or 0), indicating the presence or absence of some variable, or values that are above some threshold. In the calculation of sample SVs the following rules of thumb must be considered.

1) Each distance lag (d) class must be represented by at least 30–50 pairs of points.
2) The SV should only be plotted out to about half the width of the sampling space in any direction.

Characterizing spatial correlation across the site through experimental SV can often be the most time-consuming step in a geostatistical analysis. This is particularly true if the data are heterogeneous or limited in number. Without a rationale for identifying the major direction of anisotropy, the following steps might be useful in narrowing the focus of the exercise.

1) Begin with an omni-directional SV with a bandwidth large enough to encompass all data points on the site. In practice, maximum lag distance can be taken as 1/3 of the maximum distance between the data points.
2) Select the number of lags and lag distances sufficient to span a significant portion of the entire site, and choose the lag tolerance to be very close in value to the lag distance itself.
3) Calculate the SV. In most cases, data become less correlated as the distance between them increases. Under these circumstances, the SV values should produce a monotonic increasing function, which approaches a maximal value called the sill. In practice, this may not be the case with SV values that may begin high or jump around as distance increases.
4) Adjust the number of lags and lag tolerances until, generally, a monotonic increasing trend is seen in the SV values. If this cannot be achieved, it may be that a geostatistical approach is not viable or that more complicated trends are occurring than can be modeled. If a visual inspection of the data or knowledge about the dispersion of contamination indicates a direction of correlation, it may be more appropriate to first test this direction.
5) Assuming the omni-directional SV is reasonable, add another direction to the plot with a smaller tolerance. You may have to adjust the bandwidth and angle tolerance to produce a reasonable SV plot.
6) If the second direction rises slower to the sill or rises to a lower sill, then this is the major direction of anisotropy.
7) If neither direction produces significantly lower spatial correlation, it may be reasonable to assume an isotropic correlation structure.

8) Add a cone structure with direction equal to the major direction plus 90°, and model the SV results in this direction.
9) If the data are isotropic, choose the omni-directional SV as the major direction.

4.5.3 SV Limitations

The SV model mathematically specifies the spatial variability of the data set and after its identification the spatial interpolation weights, which are applied to data points during the grid node calculations, are direct functions of the Kriging model (Chapter 5). In order to determine the estimation value all measurements within the SV range are assigned weights depending on the distance of neighboring point using the SV. These weights and measurements are then used to calculate the estimation value through Kriging modeling. Useful and definite discussions on the practicalities and limitations of the classical SV have been given by Şen (1989) as follows.

1) The classical SV, $\gamma(d)$, for any distance, d, is defined as the half-squared-difference of two measurements separated by this distance. As d varies from zero to the maximum possible distance within the study area, the relationship of the half-square-difference to the separation distance emerges as a theoretical function, which is called the SV. The sample SV is an estimate of this theoretical function calculated from a finite number, n, of samples. The sample SV can be estimated reliably for small distances when the distribution of sampling points within the region is regular. As the distance increases, the number of data pairs for calculation of SV decreases, which implies less reliable estimation at large distances.
2) In various disciplines of the earth sciences, the sampling positions are irregularly distributed in the region, and therefore, an unbiased estimate of SV is not possible. Some distances occur more frequently than others, and accordingly their SV estimates are more reliable than others. Hence, a heterogeneous reliability dominates the sample SV. Consequently, the sample SV may have ups and downs even at small distances. Such a situation gives rise to inconsistencies and/or experimental fluctuations with the classical SV models, which are, by definition, non-decreasing functions, i.e., a continuous increase with distance is their main property. In order to give a consistent form to the sample SV, different researchers have used different subjective procedures.
    a) Journel and Huijbregts (1978) advised grouping of data into distance classes of equal length in order to construct a sample SV. However, the grouping of data pairs into classes causes a smoothing of the sample SV relative to the underlying theoretical SV. If a number of distances fall within a certain class, then the average of half-squared-differences within this class is taken as the representative half-squared-difference for the mid-class point. The effect of outliers is partially damped, but not completely smoothed out by the averaging operation.

b) To reduce the variability in the sample SV, Myers et al. (1982) grouped the observed distances between samples into variable length classes. The class size is determined such that a constant number of sample pairs fall in each class. The mean values of distances and half-squared-differences are used for the classes as a representative point of sample SV. Even this procedure resulted in an inconsistent pattern of sample SV (Myers et al., 1982), for some choices of the number, m, of pairs falling within each class. However, it was observed by Myers et al. that choosing m = 1,000 gave a discernible shape. The choice of constant number of pairs is subjective and, in addition, the averaging procedures smooth out the variability within the experimental SV. As a result, the sample SV provides a distorted view of the variable in that it does not provide, for instance, higher-frequency (short wave length) variations. However, such short-wavelength variations, if they exist, are so small that they can be safely ignored.

The above procedures have two basic common properties, namely predetermination of a constant number of pairs or distinctive class lengths and the arithmetic averaging procedure for half-squared-differences as well as the distances. The former needs a decision, which in most cases is subjective, whereas the latter can lead to unrepresentative SV values. In classical statistics, only in the case of symmetrically distributed data the mean value is the best estimation, otherwise the median becomes superior. Moreover, the mean value is sensitive to outliers. The following points are important in the interpretation of any sample SV.

1) The SV has the lowest value at the smallest lag distances (d) and increases with distance, leveling off at the sill, which is equivalent to the overall regional variance of the available sample data. It is the total vertical scale of the SV (Nugget effect + sum of all component scales). However, linear, logarithmic, and power SVs do not have a sill.
2) The range is the average distance (lag) within which the samples remain spatially dependent, and it corresponds to the distance at which the SV values level off. Some SV models do not have a length parameter; e.g., the linear model has a slope instead.
3) The nugget is the SV value at which the model appears to intercept the ordinate. It quantifies the sampling and assaying errors and the short-scale variability (i.e., spatial variation that occurs at distance closer than the sample spacing). It represents two often co-occurring sources of variability.
   a) All unaccounted for spatial variability at distances smaller than the smallest sampling distance.
   b) Experimental error is often referred to as human nugget. According to Liebhold et al. (1993), interpretations made from SVs depend on the size of the nugget because the difference between the nugget and the sill (if there is one) represents the proportion of the total sample variance that can be modeled as spatial variability.

4.6 Sample SV

In practice, one is unlikely to get SVs that look like the one shown in Fig. 4.17. Instead, patterns such as those in Fig. 4.19 are more common.

Important practical information in the interpretation and application of any sample SV is to consider only about d/3 of the horizontal distance axis values from the origin as reliable.

A digression is taken in this book as for the calculation of sample SVs. Instead of easting- and northing-based SVs, it is also possible to construct SVs based on triple variables. In the following different triple values are assessed for the SV shapes and interpretations. For instance, in Fig. 4.20 the chloride change with respect to calcium and sodium are shown in 3D and various sample SVs along different directions are presented in Fig. 4.21.

This figure indicates that the change of chloride data with respective independent variables (magnesium and calcium) are of clumped type without leveling effect. It is possible to consider Fig. 4.20 as having two parts, namely an almost linear trend and fluctuations (drift) around it. In such a case a neighborhood definition and weights assignments become impossible. Therefore, the ReV is divided into two parts, the residual and the drift. The drift is the weighted average of points within the neighborhood around the estimation value. The residual is the difference between the ReV and the drift.

The residual is a stationary ReV in itself and hence allows construction of an SV. However, once again the problem of not being able to define a neighborhood arises. Therefore, an arbitrary neighborhood is chosen from which a drift can be calculated. The calculation includes the points within the assumed neighborhood

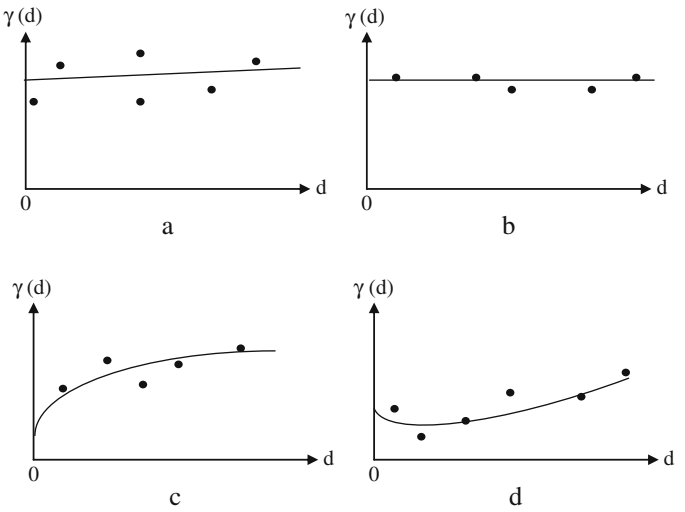

Fig. 4.19 Common forms of sample SVs (**a**) random; (**b**) uniform; (**c**) clumped with leveling; (**d**) clumped without leveling

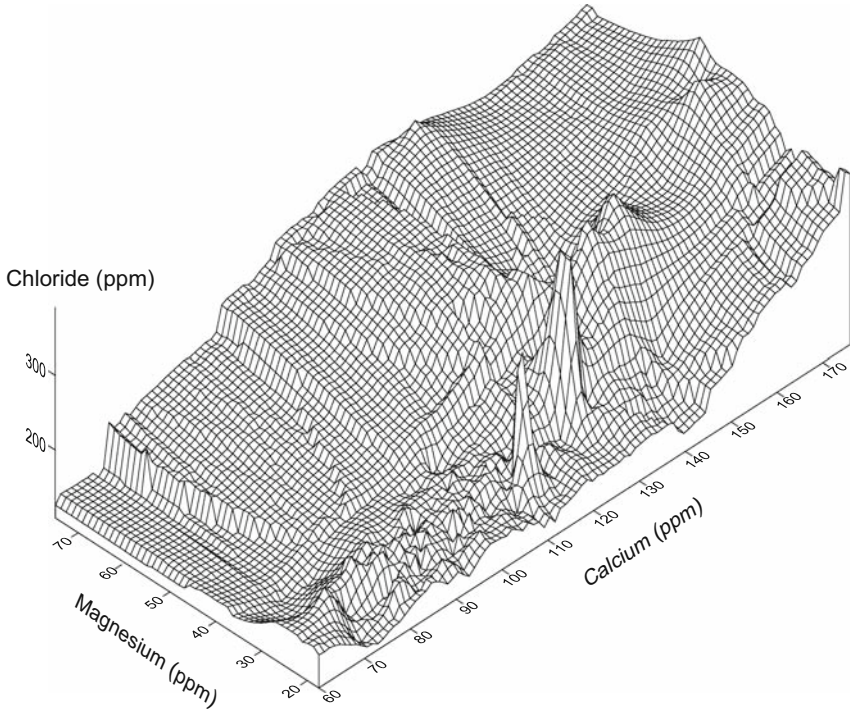

Fig. 4.20 Triple surface of chloride

and a corresponding coefficient for each point, which will be explained in more detail in the Kriging section. The only variable left in the calculation is the SV; however, no SVs exist from which to obtain the SV. Therefore, a reasonable SV is assumed and compared to the resultant residual SV. If the two are the same, then the assumptions made about the neighborhood and SV are correct, and regional estimation can be made. If they differ, then another SV must be used until they become the same. It is possible to identify from an SV the optimum distance after which regional dependence is zero or constant. By definition, the SV is half the variance of the difference between all possible points at a constant distance apart. The existence of underlying trend implies the expectation of sample SV similar to ideal case as in Fig. 4.12.

Zero and 30° directional SV in Fig. 4.21 a and b have such a trend, whereas other directional sample SVs along 60° and 90° have more or less random type, provided that only d/3 of the distance axis variables (0–15) are considered.

It is obvious that practically there is no nugget effect in these sample SVs, which is rather obvious from Fig. 4.20 where the trend surface does not have discontinuity as in Fig. 4.12. Similarly, 3D representation of bicarbonate variation with calcium and magnesium is presented in Fig. 4.22, with a global (without different directions) sample SV in Fig. 4.23.

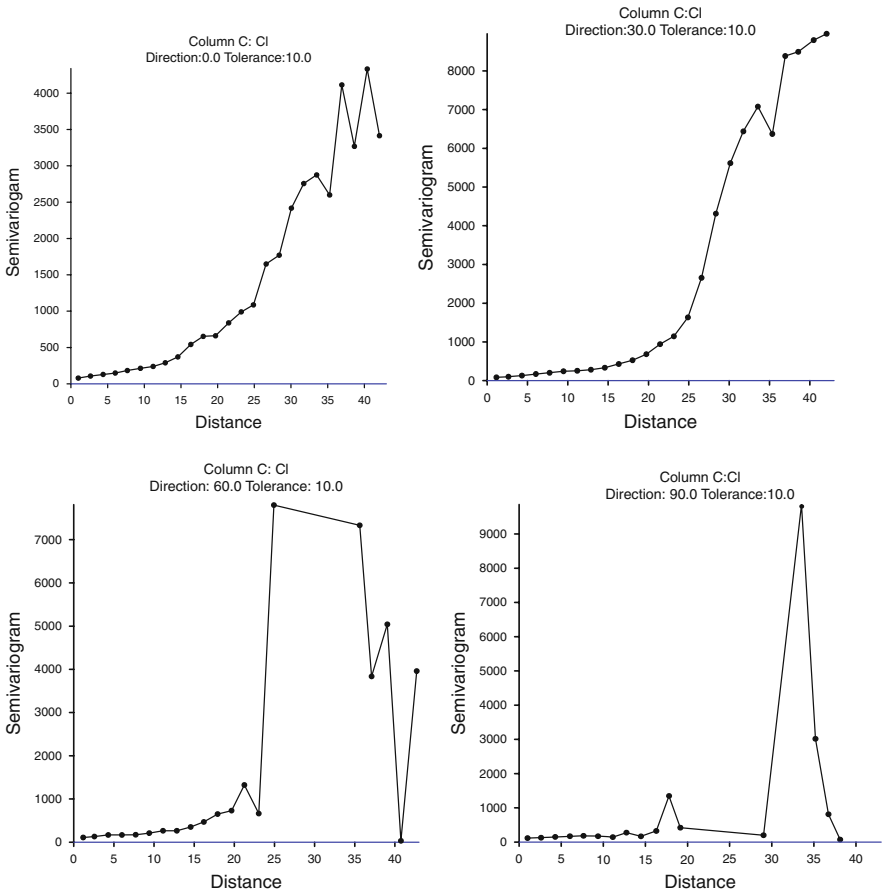

Fig. 4.21 Chloride sample SVs

Visual inspection of Fig. 4.22 indicates that a trend surface is embedded in the ReV. This trend surface is almost horizontal with a very small angle, and accordingly its global sample SV in Fig. 4.23 has almost horizontal sector within d/3.

Total dissolved solids (TDS) measurement is an indicator of the water quality variation with respect to calcium and magnesium, and its variation is presented in Fig. 4.24 with corresponding global SV in Fig. 4.25.

4.7 Theoretical SV

Useful discussion on the computation of the SV in one or two dimensions has been given by Clark (1979) and Hohn (1988). The SV as computed from the data will tend to be rather lumpy and the more irregular the data less regular it will appear. Whatever the extend of lumpiness, the graph of γ (d) may often be linked to one or

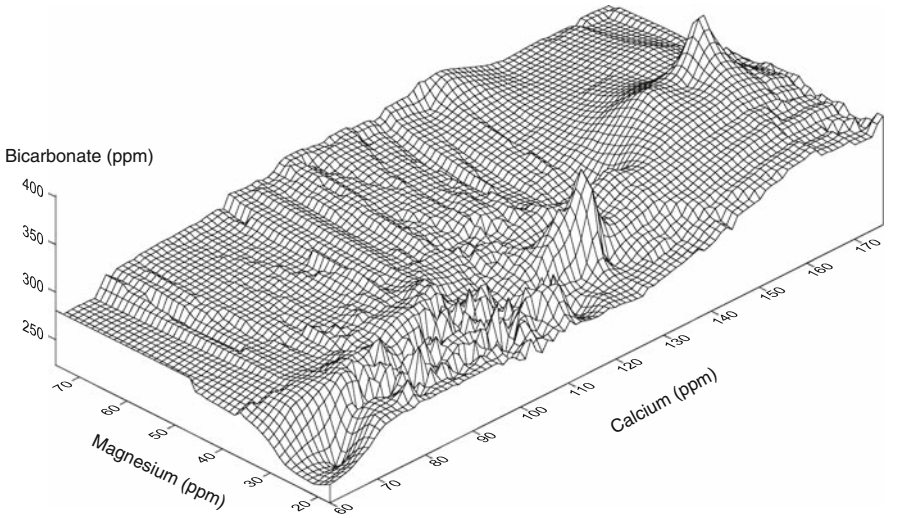

Fig. 4.22 Triple surface of chloride

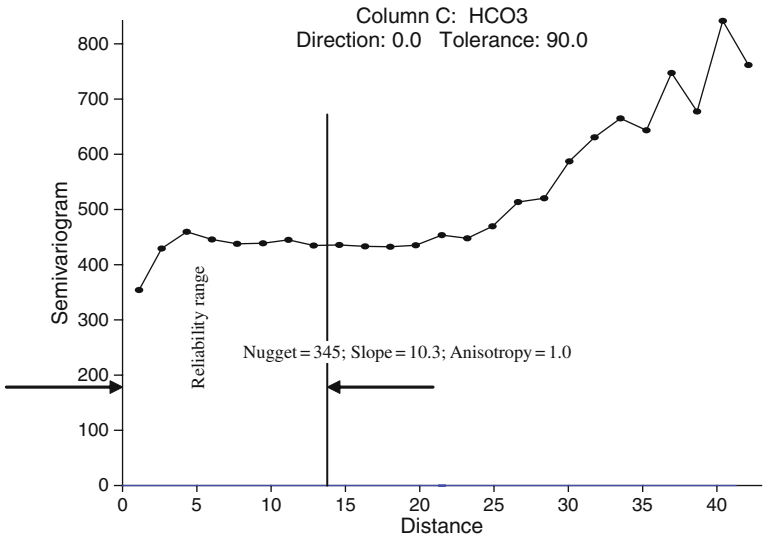

Fig. 4.23 Bicarbonate sample SV

other of a small number of theoretical (ideal) and simple curves that relate γ (d) to d, which are referred to as the theoretical SVs. These theoretical curves are models of SV that have been defined on theoretical and sample basis. The fitting of the theoretical SV curve from a set of functions to the experimentally available one derived from real data has been developed into the art of "structural analysis" discussed in detail by a number of researchers (Journel and Huijbregts, 1978; Myers et al., 1982; Hohn, 1988). The main theoretical SV types are linear, spherical, exponential, Gaussian, or cubic types as will be explained later in detail. These

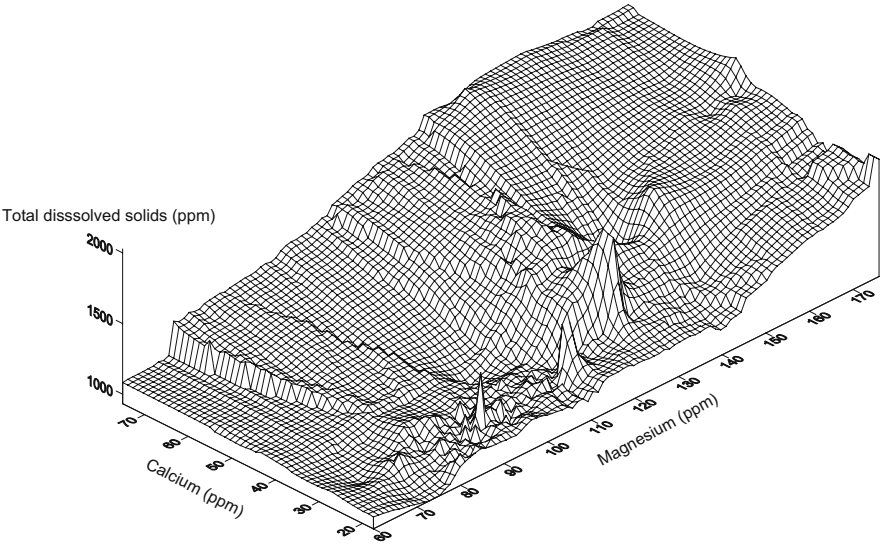

Fig. 4.24 Triple surface of total dissolved solids

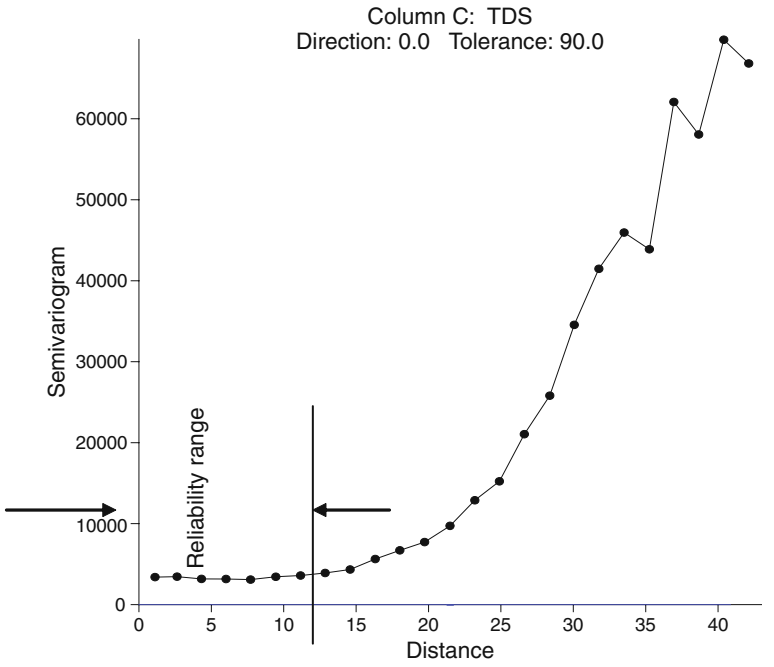

Fig. 4.25 Total dissolved solids SV

functions express rather well qualitatively the characteristics of ReV and act as a quantified summary of the structural information, which is then channeled into the estimation procedures of the natural (geologic, hydrologic, meteorological, atmospheric, etc.) phenomena.

In order to apply Kriging modeling to an ReV, the first step is to obtain sample SV from the available data and then to match this sample SV to a theoretically suitable mathematical function. It describes the relationship between the difference of values and distance with a mathematical function. Several different types of functions can be used, each with a different form to the distance function. In addition to its shape or form, the SV model is described by three parameters, namely nugget, sill, and range. Nugget shows how much variance is observed at a distance of zero. It shows up because there may be variation at distances shorter than the sample spacing or because there are errors in the measurements. It corresponds to discontinuity feature existence in the ReV. The sill shows how much variation is observed when the SV levels off at large distances. Most SVs become constant at large distances, provided that the ReV has spatial dependence without any systematic trend component. Once it is far enough away, there is no relationship in the ReV between the distances of two points. The range shows how far one has to cover distance before the SV levels off to the sill. At distances less than the range an ReV will be said to be spatially dependent and beyond the range distance the ReV has no effect and there is no spatial dependence. Finally, if the directional SVs are very different, one may need to specify an anisotropy parameter. For instance, the N-S SV may be different from the E-W SV (there is a different range, sill, nugget value, and rather different shape).

The development of an appropriate SV model for a data set requires the understanding and application of advanced statistical concepts and tools, which is the science of SV modeling. In addition, the development of an appropriate SV model for a data set requires knowledge of the tricks, traps, pitfalls, and approximations inherent in fitting a theoretical SV model to real world data, which is the art of SV modeling. Skill with the science and art are both necessary for success.

The development of an appropriate SV model requires numerous correct decisions. These decisions can only be properly addressed with an intimate knowledge of the data at hand, and a competent understanding of the data genesis (i.e., the underlying processes from which the data are drawn).

Several SV models have been developed to describe the various underlying spatial patterns in data. Examples of isotropic models including spherical, exponential, linear, power, and Gaussian models are used as input in the Kriging ReV estimation process (Chapter 5).

4.7.1 Simple Nugget SV

This corresponds to a random field with no regional dependence structure at all. In such a case the ReV is represented by its variance, σ^2, only. Its mathematical form is given as

$$\gamma(d) = \begin{cases} \sigma^2 & \text{for} \quad d > 1 \\ 0 & \text{for} \quad d = 0 \end{cases}. \tag{4.4}$$

The random field that this SV represents is not continuous (Fig. 4.15). No matter what the distance is (small or large), each ReV is completely independent and different from others. In this case the spatial analysis methodology is the probability principles only (Fig. 4.16). The special case of this nugget SV occurs when there is not any spatial variability but a uniform ReV value at each point (see Figs. 4.7 and 4.8). The mathematical model is then $\gamma(d) = 0$ for all d values.

4.7.2 Linear SV

If the ReV does not have any discontinuity, then its simplest model is given as,

$$\gamma\ (d) = \beta d, \tag{4.5}$$

where β is the only model parameter with its meaning of the slope of the straight line (see Fig. 4.26).

A more general form of theoretical linear SV is the mixture of nugget and the linear SVs. It postulates a linear relationship between the cumulative half-squared-difference and the distance as

$$\gamma_c(d) = \alpha + \beta d. \tag{4.6}$$

in which α corresponds to nugget effect and β is the slope of the theoretical SV as in Fig. 4.27.

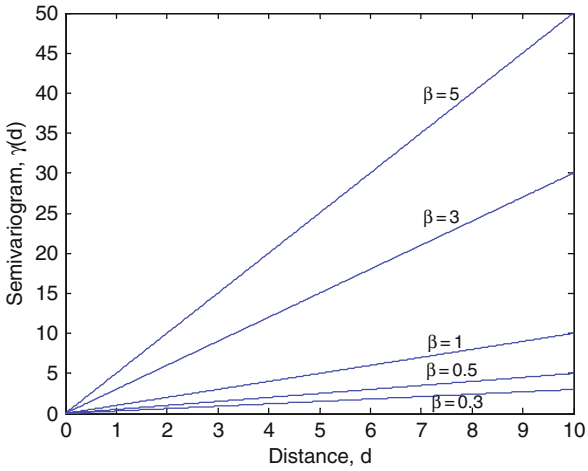

Fig. 4.26 Linear SV model

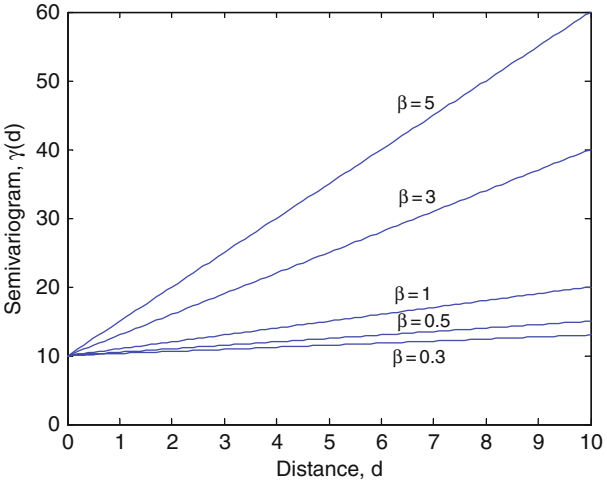

Fig. 4.27 General linear SV

The unknowns α and β can be solved from a sample SV either by substitution of two most characteristic points that should be preserved in the theoretical SV or through a least squares regression line fitting. The first approach is rather subjective but may represent expert in a better way. On the other hand, according to theory, the expected value of the sample variance is the average value of the SV between all possible pairs of sample locations, which yields one equation (Barnes, 1991). The second equation is generated by equating the experimental SV for nearest neighbors to the modeled SV. Thus, it is possible to write

$$\gamma_s\ (d) = \alpha + \beta \bar{d},$$

$$\gamma_n\ (d) = \alpha + \beta \bar{d}_n,$$

where $\bar{d}_n$= average distance to the nearest neighbor, $\bar{d}$ = average inter-sample separation distance, $\gamma_n(d)$ = one-half the averaged squared-difference between nearest neighbors, and $\gamma_s(d)$ = sample variance. By solving the two equations for the two unknown parameters, and checking for unreasonable values, one can get the final formulae used in the Kriging technology:

$$\alpha = \max\left[\frac{\bar{d}\gamma_n\,(d) - \bar{d}_n\gamma_s\,(d)}{\bar{d} - \bar{d}_n}, 0\right],$$

and

$$\beta = \max\left[\frac{\gamma_s\,(d) - \gamma_n\,(d)}{\bar{d} - \bar{d}_n}, 0\right].$$

4.7.3 Exponential SV

The mathematical expression of theoretical exponential SV model is given as (Cressie, 1993)

$$\gamma\,(\mathrm{d}) = \alpha\,\left(1 - \mathrm{e}^{-\beta \mathrm{d}}\right), \tag{4.7}$$

where the two model parameters are $\alpha > 0$ and $\beta > 0$. This model is used commonly in hydrological studies. Figure 4.28 shows exponential models with different variance values and $\beta = 1$. It does not have a nugget value and hence represents continuous ReVs, which are stationary, because at large distances exponential SV approaches a horizontal asymptote.

4.7.4 Gaussian SV

Its general expression is given in the following mathematical form (Pannatier, 1996):

$$\gamma\,(\mathrm{d}) = \alpha\,\left(1 - \mathrm{e}^{-\beta \mathrm{d}^2}\right), \tag{4.8}$$

where $\alpha > 0$ and $\beta > 0$ are the two parameters and according to their values it takes different forms. Figure 4.29 shows a set of Gaussian SV with different α values and $\beta = 1$. Since at large distances there is a horizontal portion, the representative ReV is also stationary.

At small distances the Gaussian model appears as proportional to d^2, which implies that the ReV is smooth enough to be differentiable, i.e., the slope of SV tends to a well-defined limit as the distance between the two points.

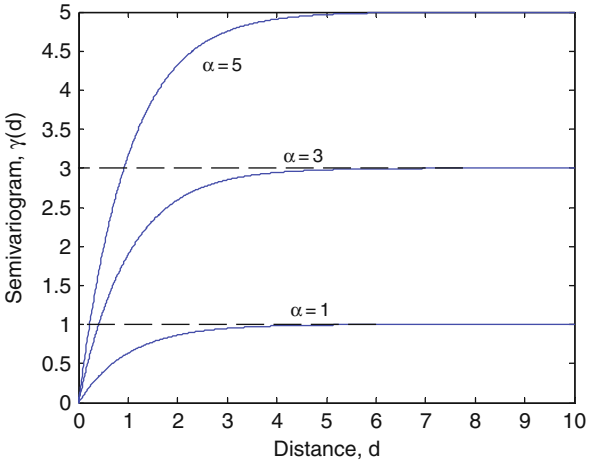

Fig. 4.28 Exponential SV model

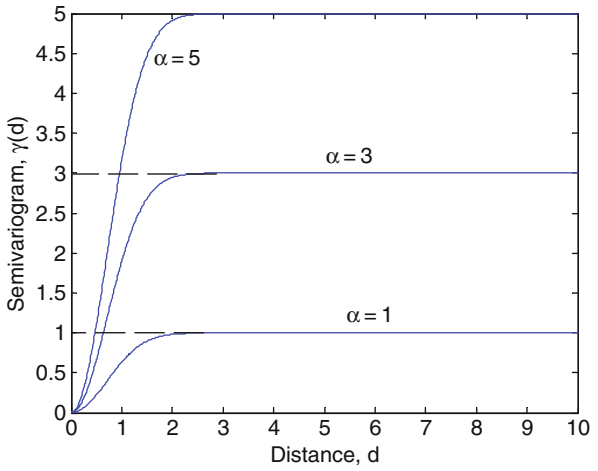

Fig. 4.29 Gaussian SV model

4.7.5 Quadratic SV

Its mathematical expression is given by Alfaro (1980) as

$$\gamma\ (\mathrm{d}) = \begin{cases} \alpha \mathrm{d}\,(2-\mathrm{d}) & \mathrm{d} < 1 \\ \alpha & \mathrm{d} \geq 1 \end{cases}, \tag{4.9}$$

where the single model parameter $\alpha > 0$. Its shape is given in Fig. 4.30 for different α values. As it increases the sill value decreases, which means that the fluctuations become smaller. It represents stationary ReVs with non-differentiable properties.

4.7.6 Rational Quadratic SV

Cressie (1993) provided this SV for use with the following expression:

$$\gamma\ (\mathrm{d}) = \alpha \left(\frac{\mathrm{d}^2}{1+\mathrm{d}^2} \right), \tag{4.10}$$

where $\alpha > 0$ is the model parameter. It has similar behavior to Gaussian model at small distances, which implies that the ReV is differentiable and rather continuous. Increase in α parameter value causes increase in the sill level, which further shows that the fluctuations in the ReV from its average level become bigger (see Fig. 4.31).

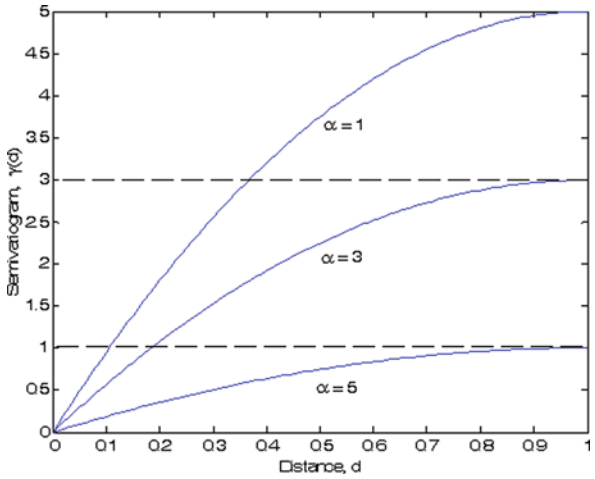

Fig. 4.30 Quadratic SV model

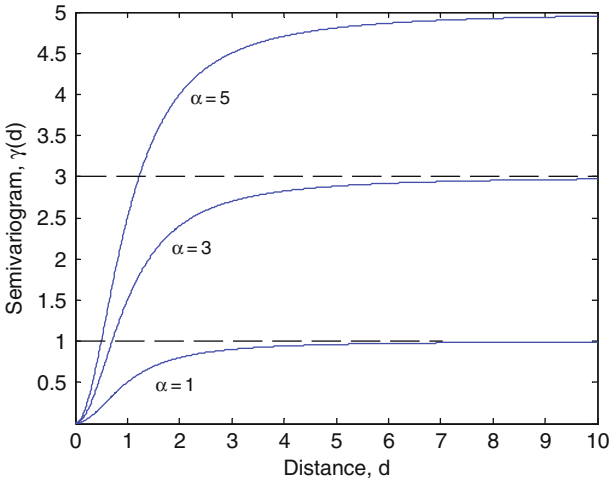

Fig. 4.31 Rational quadratic SV model

4.7.7 Power SV

Its general form is presented by Pannatier (1996) as

$$\gamma\,(d) = \alpha\left|d^{m}\right|, \tag{4.11}$$

where $\alpha > 0$ and $0 < m < 2$ are the model parameters. Convex and concave forms result, respectively, for $0 < m < 1$, and $1 < m < 2$ as in Fig. 4.32. Besides, it reduces

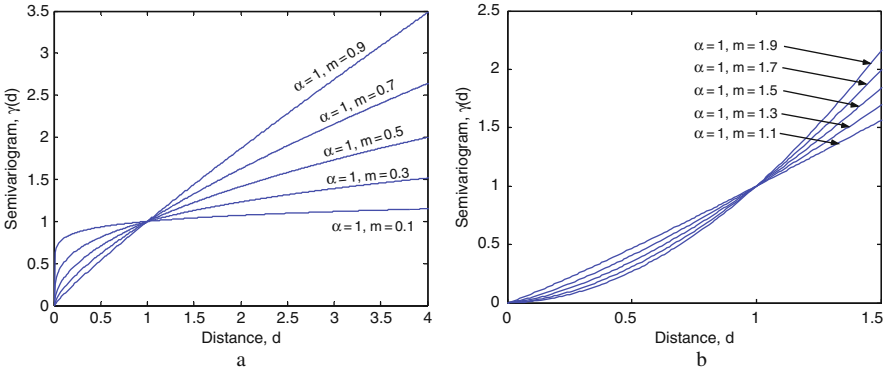

Fig. 4.32 Power SV model, (**a**) concave, (**b**) convex

to a linear model (Eq. 4.5) for m =1. Depending on whether m > 1 (m < 1), the SV represents a differentiable (non-differentiable) ReVs. Additionally, none of the theoretical SVs approach to a sill value, and therefore the represented ReV does not have stationary property. These SVs describe the same appearance of realizations at every scale, and therefore they are referred to as self-similar ReVs. This is because they appear as a straight line on a double-logarithmic paper with different slopes.

The main difference of this model from the others is that it has a non-zero value for zero distance, i.e., it has a nugget effect. The forms of different cumulative SVs resulting from Eq. (4.11) are shown in Fig. 4.32.

4.7.8 Wave (Hole Effect) SV

Cressie (1993) gave the general mathematical expression of this model as

$$\gamma\,(\mathrm{d}) = \alpha\left(1 - \frac{\sin \mathrm{d}}{\mathrm{d}}\right), \tag{4.12}$$

where again $\alpha > 0$ is the model parameter (see Fig. 4.33). This model describes ReVs with excursions above the mean tend to be compensated by excursions below the mean. It exhibits linear behavior at small distances, which implies that the corresponding ReVs are continuous but not differentiable. They are less smooth than the realization of a random field

4.7.9 Spherical SV

Pannatier (1996) presented the general expression as

$$\gamma\,(\mathrm{d}) = \begin{Bmatrix} \alpha \mathrm{d}\left(1.5 - 0.5\mathrm{d}^2\right) & \mathrm{d} < 1 \\ \alpha & \mathrm{d} \geq 1 \end{Bmatrix}, \tag{4.13}$$

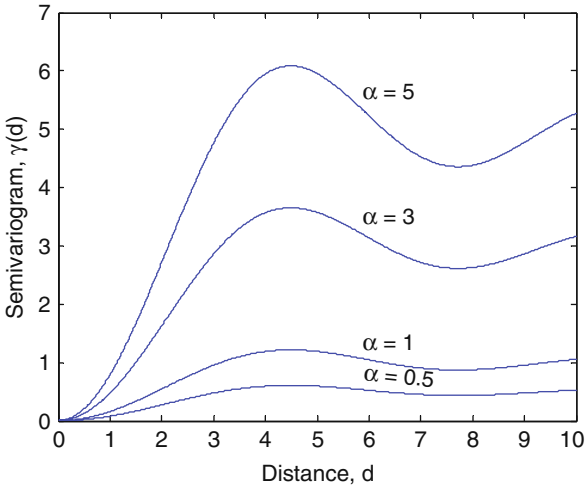

Fig. 4.33 Wave (hole effect) SV model

with model parameter $\alpha > 0$. At small distances it is proportional with distance, and therefore its representative ReV is non-differentiable but continuous. At large distance the existence of horizontal level (sill) implies that the ReV is stationary. Its shapes are presented in Fig. 4.34.

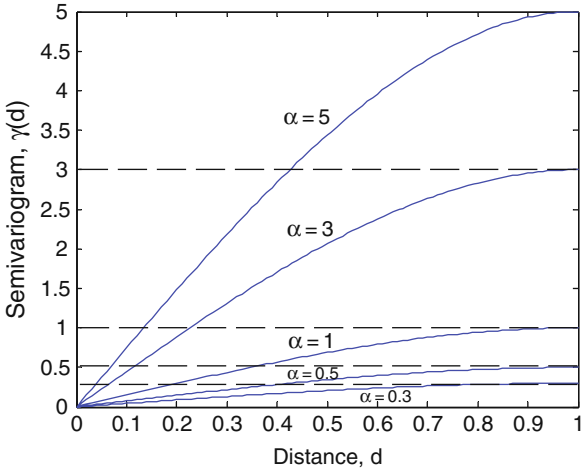

Fig. 4.34 Spherical SV model

4.7.10 Logarithmic SV

It is a single parameter model with mathematical expression as

$$\gamma\,(\mathrm{d}) = \alpha \ln \mathrm{d} \quad \mathrm{d} > 0. \tag{4.14}$$

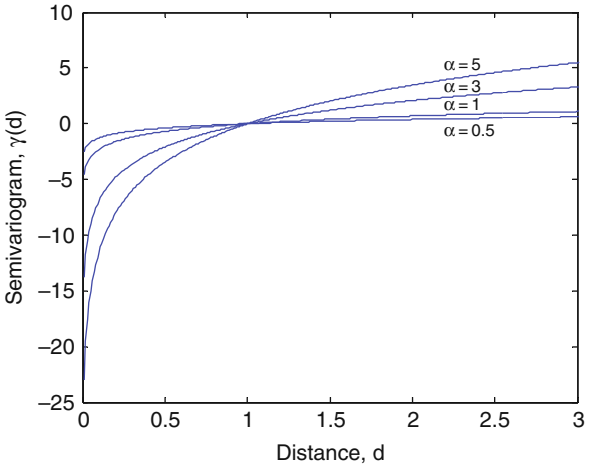

Fig. 4.35 Logarithmic SV model

It appears as a straight line on a semi-logarithmic paper (logarithmic distances) and α represents the slope of this line. Various logarithmic SVs are presented in Fig. 4.35. Since there is no sill, the corresponding ReV is non-stationary. It can be used only for integrals over finite volumes and cannot be used directly with point data values of the ReV (Kitanidis, 1997).

4.8 Cumulative Semivariogram

The CSV method proposed by Şen (1989) as an alternative to the classical SV technique of Matheron (1965) has various advantages over any conventional procedure in depicting the regional variability, and hence spatial dependence structure CSV is defined similarly to the SV, the only difference is that successive cumulative summations are adopted. CSV has all of the advantages claimed for SV; besides, it provides more objective way in deriving theoretical models to the regional dependence behavior of the regionalized variable. Furthermore, standardization of CSV provides a basis in identifying regional stationary stochastic models (Şen, 1992). The CSV is a graph that shows the variation of successive half-squared difference summations with distance. Hence, a non-decreasing CSV function is obtained, which exhibits various significant clues about the regional behavior of the ReV. The CSV provides a measure of spatial dependence. The CSV can be obtained from a given set of ReV data by executing the following steps.

1) Calculate the distance $d_{i,j}$ ($i \neq j = 1, 2, \ldots, m$) between every possible pair of sparse measurement sites. For instance, if the number of sample sites is n, then there are $m = n(n–1)/2$ distance values.

2) For each distance, $d_{i,j}$ calculate the corresponding half-squared differences, $D_{i,j}$, of the ReV data. For instance, if the ReV has values of Z_i and Z_j at two distinct sites at distance $d_{i,j}$ apart, then the half-squared difference is

$$D_{i,j} = \frac{1}{2}\left(Z_i - Z_j\right)^2. \tag{4.15}$$

3) Take the successive summation of the half-squared differences starting from the smallest distance to the largest in order. This procedure will yield a non-decreasing function as

$$\gamma(d_{i,j}) = \sum_{i=1}^{m}\sum_{i=1}^{m} D_{i,j}. \tag{4.16}$$

where $\gamma(d_{i,j})$ represents CSV value at distance $d_{i,j}$.

4) Plot $\gamma(d_{i,j})$ values versus the corresponding distance $d_{i,j}$. The result will appear similar to the representative CSV functions as in Fig. 4.36. The sample CSV functions are free of subjectivity because no a priori selection of distance classes is involved in contrast to the analysis as suggested by Perrie and Toulany (1989) in which the distance axis is divided into subjective intervals, and subsequently averages are taken within individual intervals, which are regarded as the representative value for this interval.

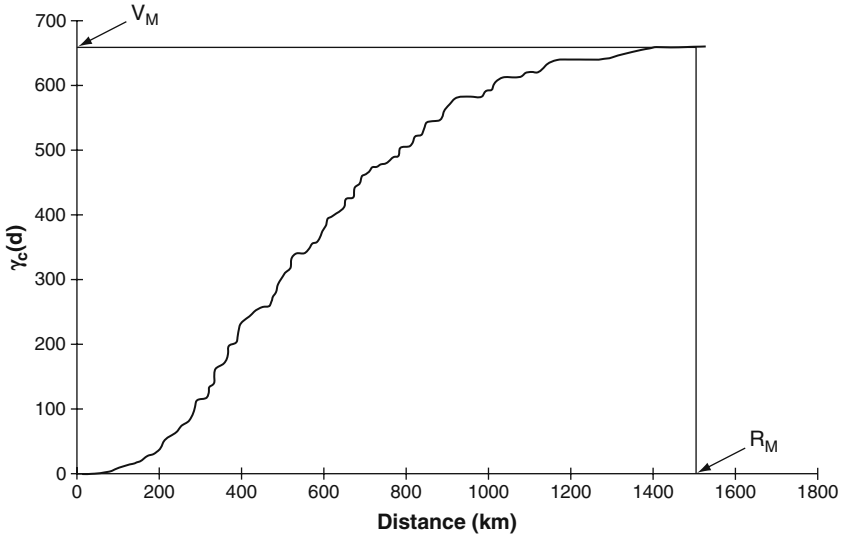

Fig. 4.36 Representative CSV

In his discussion on the practical difficulties of classical SV, Şen (1989) has noticed the reliability of SV estimations at small distances, with regular distribution of sampling points within the region. However, in various disciplines of geological sciences, the sampling positions are irregularly distributed in the region (such as in the earthquake epicenters) where some distances occur more frequently than others; thus, a heterogeneous reliability dominates the sample SV. In order to overcome these shortcomings, he developed CSV technique on the basis of the ReVs theory. This technique possesses all of the objective properties of the classical SVs and, in addition, it helps to identify the hidden and local dependencies within a region. It is defined as the successive summation of half-squared differences, which are ranked according to the ascending order of distances extracted from all possible pairs of sample locations within a region. Mathematically, CSV is expressed as

$$\gamma_c\,(d_k) = \sum_{i=1}^{k} d\left[d^i\right] \quad (k = 1,2,...,m), \tag{4.17}$$

where $\gamma_c\,(d_k)$ is the value of the k-th ordered distance CSV value and superscript i indicates the rank. The procedure of sample CSV calculations as well as its model form and equations have been given by Şen (1989) as in Fig. II.12. These models are counterpart to those of classical SV models, but with different interpretations of the model parameters. The attributes and advantages of CSV can be summarized as follows.

1) The CSV is a non-decreasing function; however, there may be local flat portions, implying constancy of the regionalized variables at certain distance, i.e., the same values have been observed at two locations h apart.
2) The slope of the theoretical CSV at any distance is an indicator of the dependence between pairs of regionalized variables separated by that distance.
3) The sample CSV reflects even smaller dependencies between data pairs, which are not possible to detect with classical SV due to the averaging procedure.
4) The sample CSV is straight forward in applications and free of subjectivity, because there is no need for a priori selection of distance classes. In fact, the real distances are employed in the construction of the sample CSV rather than class mid-point distance.
5) The CSV model may be used for irregularly distributed sample positions within the study region.
6) The underlying model for any regionalized variable can be detected by plotting the cumulative half-squared differences versus distances on arithmetic-semi-logarithmic or double logarithmic. Appearance of sample CSV points on any one of these papers as a straight line confirms the type of model. Such an opportunity is missing in the samples of classical SV.
7) Model parameter estimates are obtained from the slope and intercept values of the straight line.

8) Any classical SV model has a theoretical CSV counterpart, which can be obtained through an integration operation.
9) These characteristics and advantages make the CSV attractive for practical applications.

4.8.1 Sample CSV

The CSV proposed in the previous section is applied to the transmissivity, total dissolved solids, and piezometric level records in the Wasia sandstone aquifer in the eastern part of the Kingdom of Saudi Arabia (Şen, 1989). A complete hydrogeological study of this area has been performed recently by Subyani (1987).

GAMA3 software developed for computing the classical SV by Journel and Huijbregts (1978) has been applied to groundwater variables such as transmissivity, piezometric level, and total dissolved solids from the Wasia sandstone aquifer. The resulting sample SV and sample CSV plots are presented in Figs. 4.37, 4.38, and 4.39. It is clear from these figures that the half-squared-difference points are scattered in such a way that it is not possible to distinguish a clear pattern in the sample SVs, which suffer from fluctuations even at small distances. Comparisons of the sample SVs in these figures with the sample CSVs indicate that the latter are more orderly and have distinctive non-decreasing patterns.

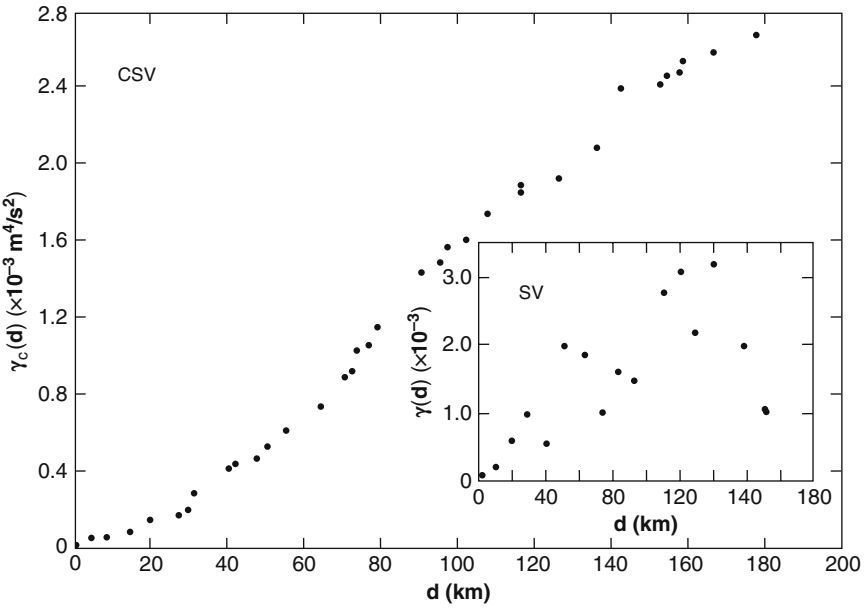

Fig. 4.37 Sample CSV for Wasia sandstone transmissivity

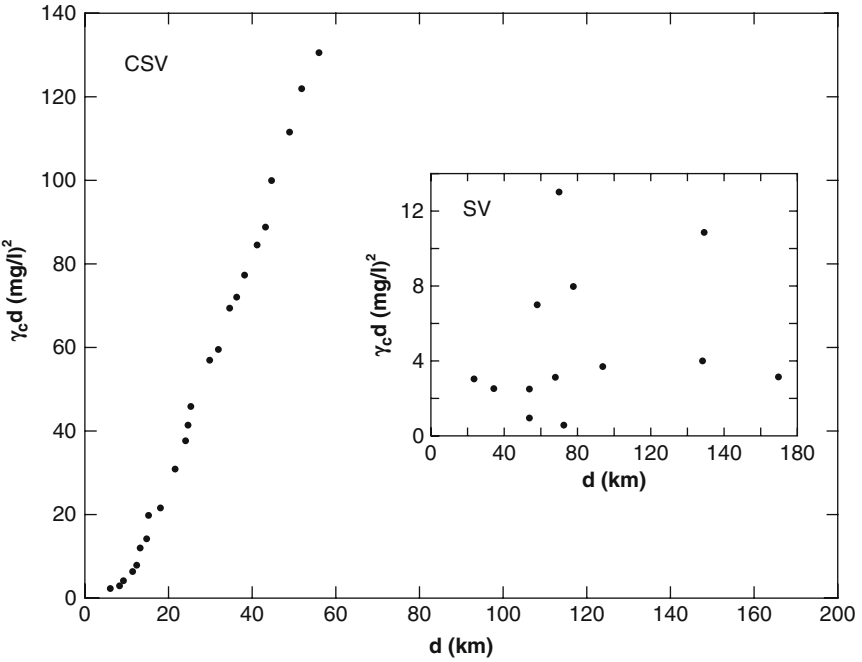

Fig. 4.38 Sample CSV for Wasia sandstone dissolved solids

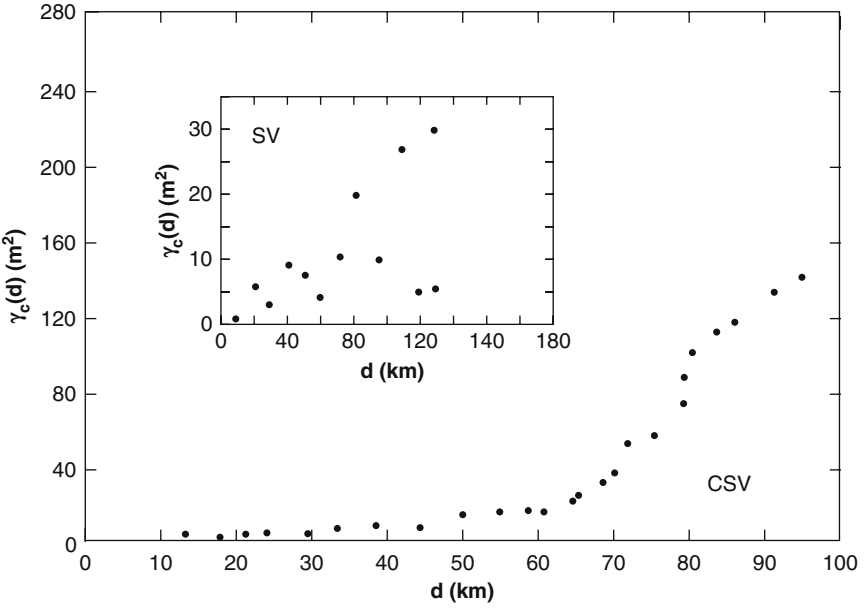

Fig. 4.39 Sample CSV for Wasia sandstone piezometric level

A sample CSV often yields more or less a straight line for large distances, which corresponds to the sill concept in the classical SV. Furthermore, the sample CSV starts as a curve with different curvatures over some distance domain before it becomes almost a straight line. The length of the distance domain over which the sample CSV occurs as a curve is a counterpart of the range in the classical SV. Hence, it is straightforward to determine the range from the sample CSV. The piezometric level sample CSV in Fig. 4.39 shows an initial range portion, which has zero half-squared-differences for about 10 km. Such a portion implies physically that the piezometric level does not change significantly within distances less than 60 km. In fact, the Wasia aquifer has remained free of any tectonic movements, it is extensive, and the recharge is negligible, but it is discharged by local well groups that are situated at large distances from each other (Powers et al., 1966).

4.8.2 Theoretical CSV Models

In order to be able to apply Kriging estimation techniques to an ReV, a functional relationship must be established between the distance and the measure of regional dependence, which, herein, is the CSV. These models must be non-decreasing functions. Although numerous functions have this property, in practice restricting them to a few simple ones is desirable. By considering basic definitions of both the classical and the CSVs, they may be related through an integration as

$$\gamma_c\,(d) = \int_0^d \gamma\,(u)\,du, \tag{4.18}$$

or through differentiation as

$$\gamma\,(d) = \left.\frac{d\gamma_c\,(u)}{du}\right|_{u=d}. \tag{4.19}$$

Therefore, a CSV counterpart may be found for any given classical SV using Eq. (4.18). Furthermore, Eq. (4.19) indicates that the theoretical classical SV value at any distance is equal to the slope of the theoretical CSV at the same distance. In the following, models which have been used previously for SVs by many researchers will be assessed from the CSV point of view.

4.8.2.1 Linear Model

The linear CSV model signifies that the phenomenon has regional independence and it evolves in accords with an independent (white noise) process. Hence, in an objective analysis of such a phenomenon one needs to know only the mean and standard deviation, and consequently the prediction of any grid point value can be withdrawn from an independent process because the radius of influence is equal to zero. This is

the most extreme case, which rarely happens in earth sciences domains. This model postulates a linear relationship between the cumulative half-squared difference and the distance as

$$\gamma_c\,(d) = \alpha + \beta d, \tag{4.20}$$

in which α and β are the model parameters (Fig. 4.40a). The sample CSV of the regionalized variable that abides by this model will appear as a straight line on arithmetic paper.

In fact, α is the intercept on the CSV axis and β is the slope of this straight line. This slope corresponds to the sill value in the classical SV, which represents a pure nugget effect (Şen, 1989). Furthermore, β represents exactly the variance of the underlying random field. Hence, the smaller the slope of the straight line, the smaller the random fluctuation in the ReV. If the slope is equal to zero, theoretically, this indicates a complete deterministic uniform variation in the ReV. The sample CSV scatter diagram and the fitted regression line to pH values measured at 71 sample locations within the Umm Er Radhuma Limestone aquifer in the Eastern Provinces, Saudi Arabia (Fig. 4.41), has the form

$$\gamma_c\,(d) = -0.213 + 1.144d,$$

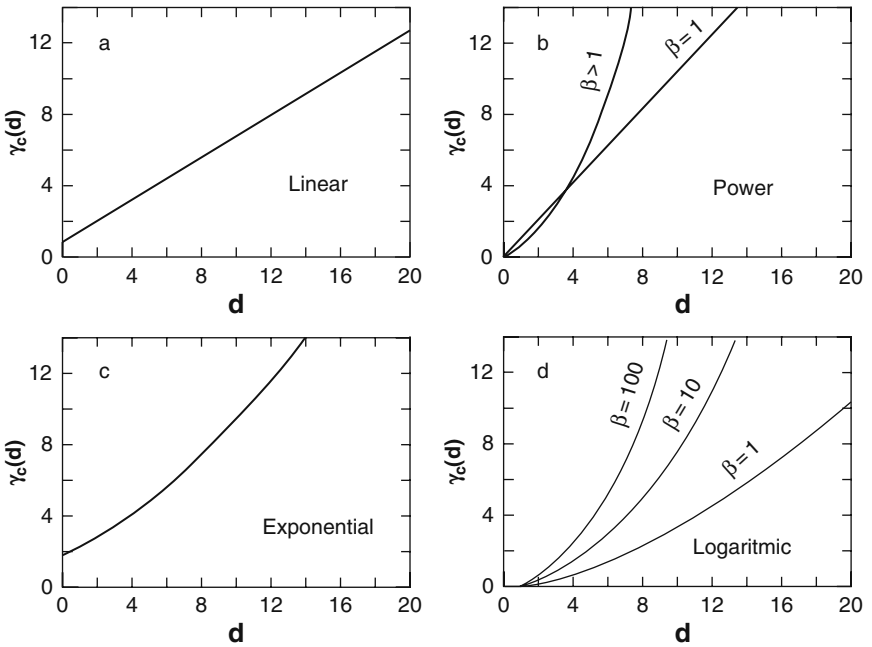

Fig. 4.40 Theoretical CSVs

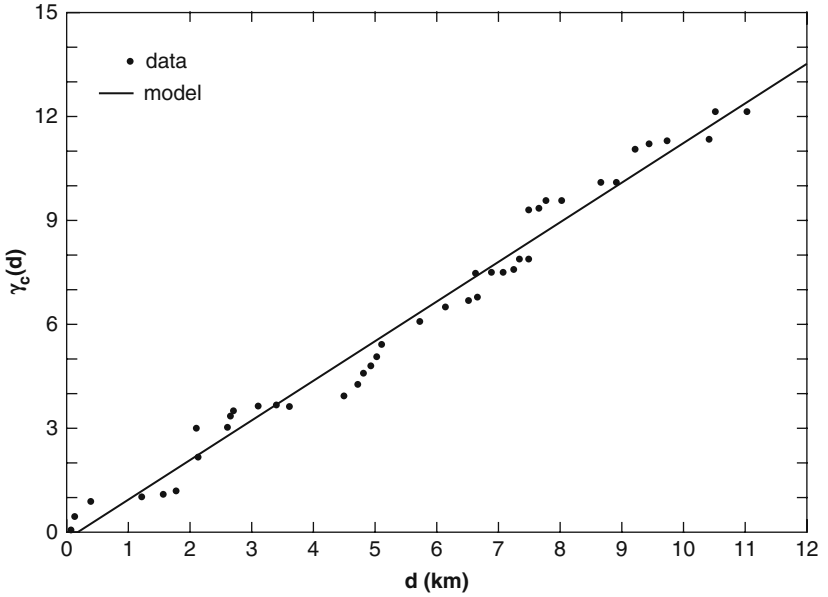

Fig. 4.41 Sample CSV for pH in Umm Er Radhuma aquifer

from which the parameter estimates are $\alpha = -0.213$ and $\beta = 1.144$. The hydrochemical data were presented by Şen and A1-Dakheel (1985) for major anions and cations.

4.8.2.2 Power Model

This is a two-parameter model which yields a set of different shapes for the theoretical CSV (Fig. 4.40b). The mathematical expression for this model is

$$\gamma_c\,(d) = \alpha d^{\beta}, \tag{4.21}$$

in which α is the scale parameter and β is the shape parameter. Because $0 < \beta < 2$ for a theoretical SV from a power family (Journel and Huijbregts, 1978, p. 165), parameter β for the theoretical CSV in Eq. (4.21) is restricted to the range $1 < \beta < 3$. The derivative of Eq. (4.21) yields also a power form for the classical SV. Obviously, use of a double logarithmic paper facilitates parameter estimation. Sulfate concentrations in the Umm Er Radhuma aquifer groundwater show on double logarithmic paper a more or less straight line pattern (Fig. 4.42).
The mathematical expression of this straight line by the regression technique can be found as

$$\log \gamma_c\,(d) = 0.46 + 0.841d,$$

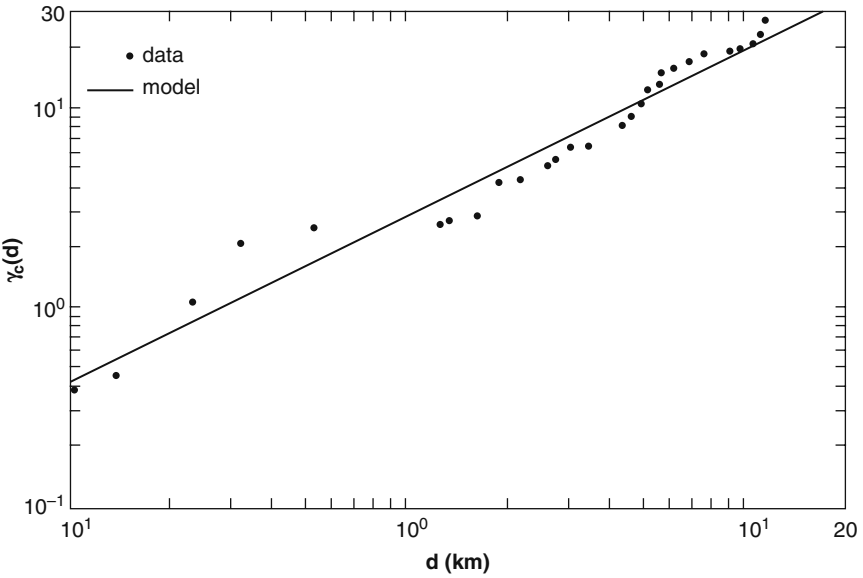

Fig. 4.42 Sample CSV for sulfate in Umm Er Radhuma aquifer

hence, parameter estimates are $\log \alpha = 0.46$ or $\alpha = -2.88$ and $\beta = 0.84$. The original form of this model prior to transformation can be written as $\gamma_c(d) = 2.88d^{0.84}$.

4.8.2.3 Exponential CSV

The general form of this CSV can be written as

$$\gamma_c\,(d) = \alpha e^{\beta d}, \tag{4.22}$$

where α and β are scale and shape parameters, respectively. The main difference of this model from the others is that it has a non-zero value for zero distance, i.e., it has a nugget effect. Forms of different CSVs resulting from Eq. (4.22) are shown (Fig. 4.40c). The sample CSV can be checked for concordance with this model by plotting $\log \gamma_c(d)$ vs. d on semi-logarithmic paper. If the sample points appear as a straight line, the exponential model is the generating mechanism of the regional variability within the regionalized variable. The slope of this line directly yields an estimate of β, whereas the intercept on the $\gamma_c(d)$ axis leads to an estimate of β. This model does not have a unique classical SV, which has appeared in the geostatistical literature. The sample CSV for bicarbonate concentrations in the Umm Er Radhuma aquifer appears as a straight line on semi-logarithmic paper (Fig. 4.43). The appearance of this straight line implies that the convenient model for bicarbonate concentrations for this aquifer is of exponential type. The regression line of this scatter diagram is

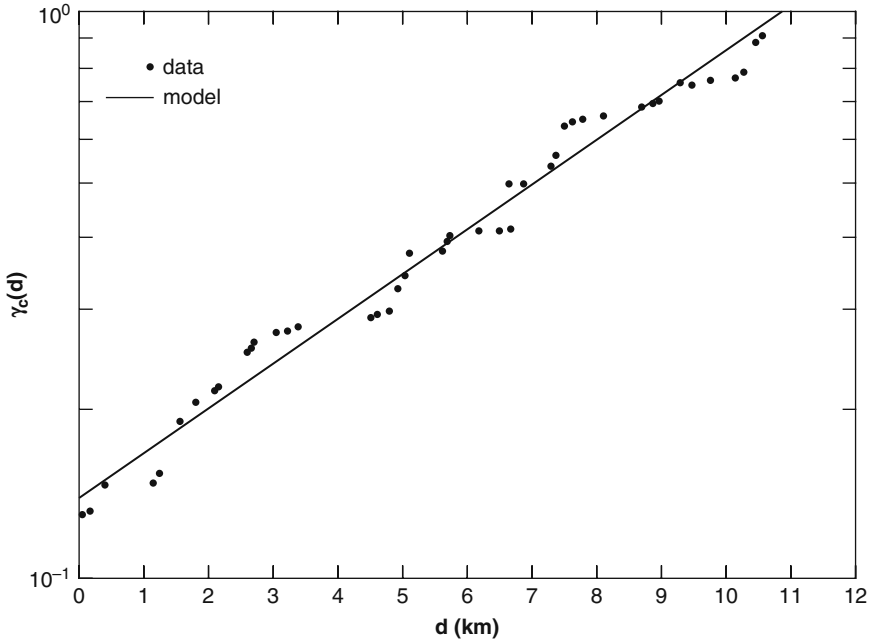

Fig. 4.43 Sample CSV for bicarbonate in Umm Er Radhuma aquifer

$$\log \gamma_c\,(d) = -0.86 + 0.079d,$$

and, correspondingly, the model parameter estimates are $\log\ \gamma_c(d) = -0.86$ or $\alpha = 0.14$ and $\beta = 0.079$. Hence, the original form of the model can be written as $\gamma_c\,(d) = 0.14e^{0.079d}$.

4.8.2.4 Logarithmic CSV

The mathematical expression of this model can be written as

$$\gamma_c\,(d) = \begin{cases} \alpha + \beta \log d & \text{for } d > 1 \\ 0 & \text{for } d < 1 \end{cases}, \tag{4.23}$$

in which α and β are the two model parameters. This model differs from the exponential one in that it has an intercept on the distance axis similar to the sample CSV for piezometric level (Fig. 4.39). Different forms of the logarithmic models are presented (Fig. 4.40d). The model can be depicted from a sample CSV plotted on semi-logarithmic paper as $\gamma_c(d)$ vs. log d. If the sample points appear as a straight line, the validity of the logarithmic model is confirmed. The slope of this straight line is equal to β, and the cumulative half-squared difference corresponding to $d = 1$

yields the estimate of a. Such a model is similar to what is referred to in the classical SV terminology as the De Wijsian model (DeWijs, 1972).

Other models for the CSV can be constructed from classical CSV models through Eq. (4.18). For instance, the exponential model of the classical SV, which is

$$\gamma(d) = \alpha\left[1 - e^{-\beta d}\right], \tag{4.24}$$

corresponds to a CSV model, which is

$$\gamma_c(d) = \alpha\left[d - \frac{1}{\beta}e^{-\beta d}\right], \tag{4.25}$$

in which α and β are model parameters. A close inspection of Eq. (4.25) indicates that for large distances, $(1/\beta)\exp(-\beta d) \approx 0$; consequently, at large distances this model appears as a straight line (on arithmetic paper) whose slope is an estimate of α. In addition, this model has an intercept value, $\gamma_c(0)$, which is equal to α/β. Provided that α is known from the slope at large distances, this ratio yields the estimate of β. These α and β values are the parameters of the classical exponential SV model. This last example shows that the CSV method may help to estimate the parameters of the classical SV by simple graphical procedures.

4.8.2.5 Gaussian CSV

The Gaussian classical SV corresponds to the CSV model,

$$\gamma_c(d) = \alpha\left[d - \sqrt{\frac{2\pi}{\beta}}\phi(d,\beta)\right], \tag{4.26}$$

where $\phi(d, \beta)$ is the area under the normal probability density function (with zero mean and variance $1/\beta$) from 0 to d. Obviously, α can be estimated as the slope of this straight line. That is

$$\phi(d,\beta) = \sqrt{\frac{\beta}{2\pi}}\int_0^d \exp\left(-\frac{d^2\beta}{2}\right)dd. \tag{4.27}$$

Last but not the least, it is also possible to have different types of CSV models along different directions for the same earth sciences phenomenon. In such a situation, there is structural heterogeneity within the phenomenon.

Various theoretical CSV models are fitted to the sample CSV by simple least squares technique. A weighted or generalized least-squares approach would probably be preferable because the sample CSV values are correlated and do not have equal variance. Future researches should be directed toward how to implement

a weighted or generalized least squares approach in particular, what should the weights be, and how strong are the correlations between neighboring CSV values?

4.9 Point Cumulative Semivariogram

The PCSV function is proposed by Şen and Habib (1998) as the CSV calculated for a single point (site). The PCSV identifies the spatial variability of earth sciences ReV around a single site rather than the whole region. It presents the regional effect of all the sites within the study area on a particular site. Consequently, the number of PCSVs is equal to the number of available sites. Each PCSV provides a basis for nearby station variability interpretations, and their mutual comparisons at different sites lead to invaluable information for describing the heterogeneity of the ReV in an area. The treatment of available spatial data at n sites according to the following steps leads to sample PCSV for a particular site.

1) Calculate the arithmetic average, $\overline{Z}$, and standard deviation, Z_s, from the available data. Standardize the data according to the following formulation,

$$z_i = \frac{Z_i - \overline{Z}}{Z_S}. \tag{4.28}$$

2) Calculate the distances between the desired site and the remaining sites. If there are m sites, the number of distances is $n-1$, $d_i (i = 1, 2, \ldots, n-1)$.
3) For each pair calculate the squared differences as $(z_c – z_i)^2$ where z_c and z_i are the ReVs at the concerned and i-th sites, respectively. Consequently, there are (n–1) squared differences.
4) Rank the distances in ascending order and plot distances d_i versus corresponding successive cumulative sums of half-squared differences. Hence, a non-decreasing function is obtained similar to Fig. 4.36, which is named as the sample PCSV for the desired site.

   All these steps imply that the PCSV, $\gamma(d_c)$ for site C can be expressed as

$$\gamma(d_c) = \frac{1}{2} \sum_{i=1}^{n-1} (z_D - z_i)^2. \tag{4.29}$$

5) Application of these steps in turn for each site leads to n sample PCSVs of ReV.

These sample PCSVs are the potential information sources in describing the ReV characteristics around each site. Among these characteristics are the radius of influence, spatial dependence, and structural behavior of the regionalized variable near the site such as the nugget (sudden changes) and sill effects, and heterogeneity as will be explained in the following section.

Example 4.1
The PCSV proposed in the previous section is applied to seismic data from Turkey (Erdik et al., 1985). Conventional probabilistic procedures are used to construct the seismic hazard maps for Turkey. Seismic hazard is defined as the probability occurrence of ground motion due to an earthquake of a particular site capable of causing significant loss of value through damage or destruction at a given site within a definite time period. The PCSV technique is applied to all sites; some of the sample PCSVs are presented in Fig. 4.44, and after grouping, the major sample trends of PCSV appeared as shown in Fig. 4.45. Consideration of these figures individually or comparatively leads to the following significant interpretations, which can be implemented in any future seismic hazard mapping models of Turkey (Şen, 1997).

1) Individual seismic PCSVs have rather different appearance from each other, which indicates that the regional seismic distribution in Turkey is heterogeneous. It is a necessary and sufficient requirement for areal heterogeneity that the sample PCSV should exhibit different patterns within the limits of sampling error at different sites. A first glance through the whole sample PCSVs gave the impression that, in general, there are ten distinctive categories of them within Turkey. These categories are labeled alphabetically from A to J as shown in Fig. 4.45. Each of these categories has different features, which reflect the seismic record behavior around the station concerned. For instance, those sample PCSVs, which are in category F (see Fig. 4.45), have an initial part with convex curvature (at small distances) and then either single or multiple broken straight lines follow at large distances. On the other hand, in category D sample PCSVs do not have any curvature but many broken straight lines and have an intercept on the horizontal distance axis. An abundance of broken straight lines indicates the heterogeneity involved around the station concerned at different distances.

   In category B the sample PCSVs expose single straight line, indicating that there are rather homogeneous areas of influence around these stations.

   The stations within each category can be regarded as homogeneous collectively, and hence it is clear that the whole study area has about ten distinct homogeneity regions of seismic variation. Further useful interpretations about the sample PCSVs can be listed as follows:
2) Some of the sample PCSVs does not pass through the origin. This is tantamount to saying that the seismic occurrences at these sites cannot be considered as regionally smooth processes, but rather the seismic event is under the control of some local and/or regional geological factors. This further implies that in the spatial seismic occurrences, uniform conditions do not prevail but rather complex combination of multitude tectonic events. Last but not the least, if the sample PCSV has an intercept on the vertical axis, it implies the existence of a nugget effect in the regional variability at the site concerned (Fig. 4.45 J).
3) Some of the sample PCSVs have intercepts, R0, on the horizontal (distance) axis (see categories C, F, and I). This means that at distances less than R0 the

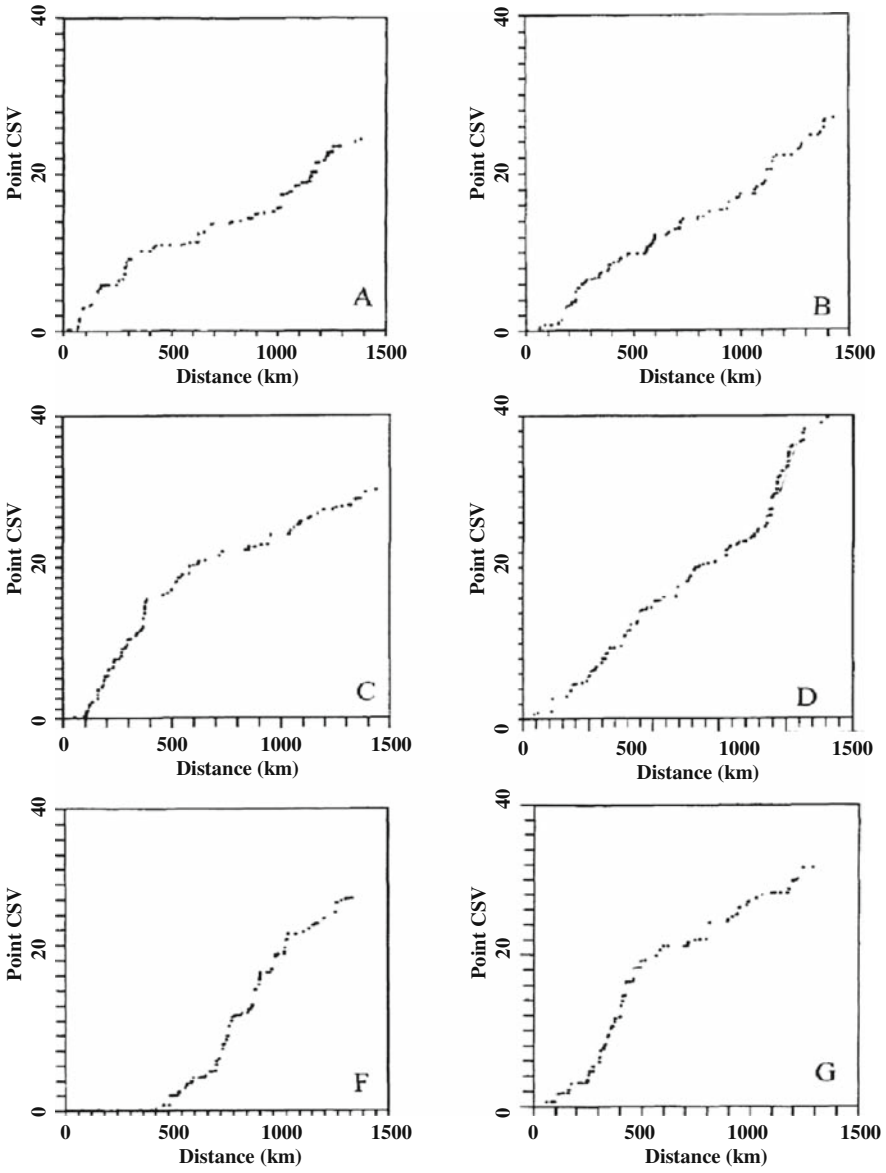

Fig. 4.44 PCSVs of seismic events in Turkey

sample PCSV value is equal to zero, hence from Eq. (4.29) $Z_c \cong Z_i$ implying structural control within the regional seismic event. Furthermore, in general, big seismic values follow big seismic values and small ones follow small seismic values, i.e., there are isolated islands of high or low seismic locations around the site.

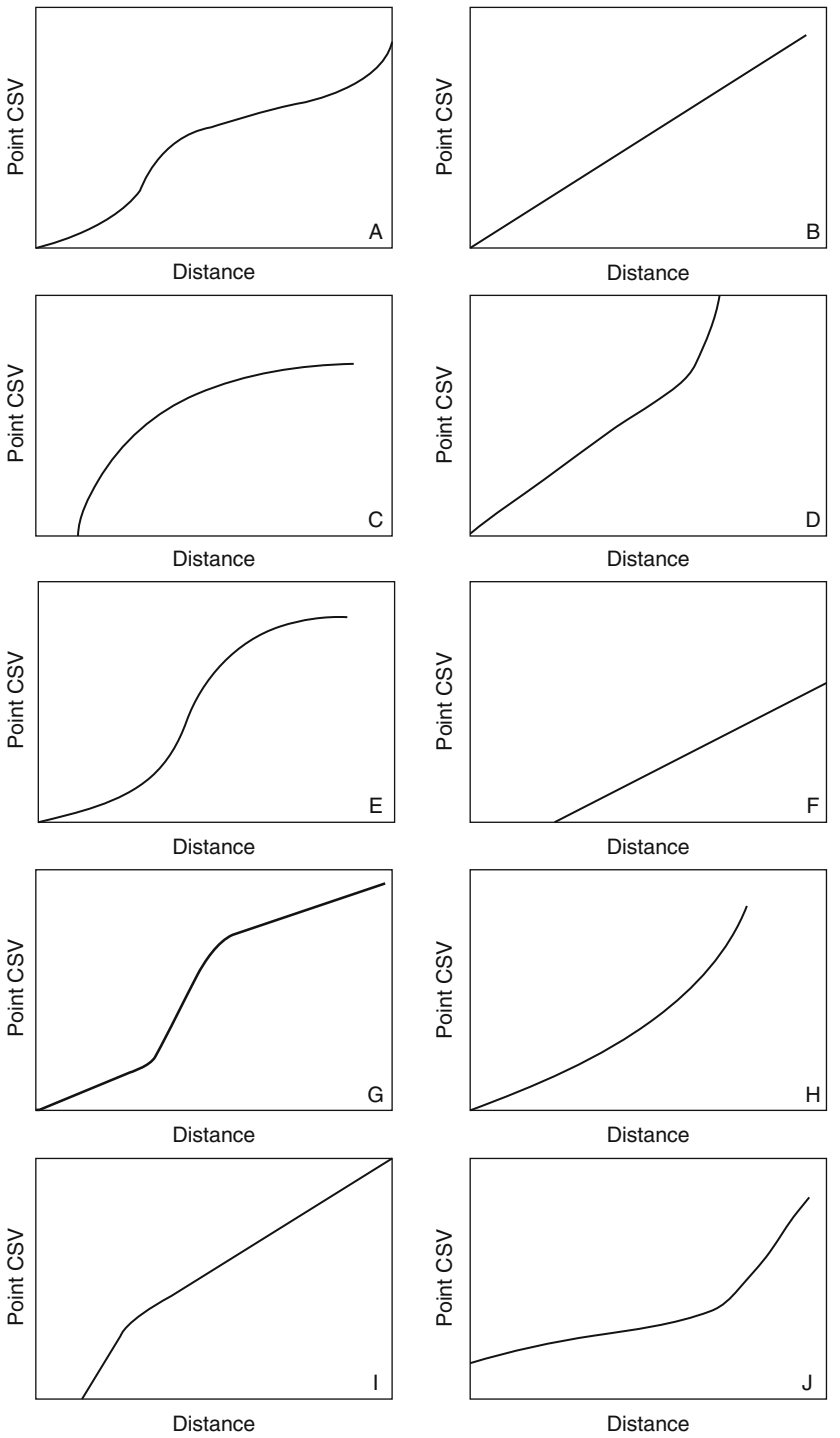

Fig. 4.45 Seismic PCSV categories in Turkey

4) That each sample PCSV fluctuates about a straight line for large distances. The existence of straight line portions in the PCSV implies that seismic activities at large distances are independent from each other. This is equivalent to the regional sill property in the classical SV, but PCSV provides information about the sill at individual sites (see Fig. 4.45 J). These portions correspond to horizontal segments at large distances in classical SV as defined by Matheron (1963). Furthermore, this is the only range where the classical formulations keep their validity.
5) A group of sample PCSVs passes through the origin (see category in Fig. A, B, D, E, G, and H). Such a property on the PCSV diagram implies the continuity of seismic effects from the site outward. Continuity means that there are no nugget effects or discontinuities within the regional seismic variable at the site concerned.
6) Some of the sample PCSVs has "curvature portions" for a moderate range of distances (categories E and G). In fact, such a range corresponds to the distance scale as defined in the turbulent flow by Taylor (1915). After this range, the PCSVs converge to straight lines (Şen, 1989). The initial curvature implies that the seismic at these sites has regional dependencies, which weaken toward the end of curvature distance range, (Şen, 1989). Since curvatures are convex, there are positive regional structural dependence (Şen, 1992). Furthermore, the curvature implies that the seismic has areal structural dependence.
7) In some of the sample PCSVs, there is no curvature part at all (categories B and F). Such a situation is valid in cases where the regional seismic distributions arise predominantly due to the activities of external factors only. Furthermore, there is no structural correlation, i.e., seismic phenomena evolve randomly over the region concerned.
8) As suggested by Şen (1992), the sample CSVs help to identify the underlying generating mechanism of regional phenomenon. Likewise, the sample PCSVs provide clues about the seismicity-generating mechanism around the site concerned. For instance, if the sample PCSV passes through the origin and has straight line portions only, then the regional phenomenon concerned complies with independent (white noise) process with no regional dependence at all. However, when the sample PCSV is in the form of straight line but does not pass through the origin, then a moving average process is the underlying generating mechanism of the regional variability (Şen, 1992). The PCSVs in category F have such a property, and therefore it is possible to conclude that moving average mechanisms are dominant at these sites.
9) In the case of a single straight line following a curved initial portion, the slope of long-distance straight line portion is related to the regional standard deviation of the underlying precipitation generating mechanism.
10) As mentioned above, the PCSV is an indicator of cumulative similarity of the seismic varıatıon at a station with other stations. Practically, if the two PCSV at different sites follow the same pattern within the limits of sampling errors, then they are said to be similar. Such a similarity implies heterogeneity to exist between two sites. They may be partially similar to each other at some distances if the PCSV values at the same distances are close to each other

again within the limits of an acceptable sampling error. In practice, in order to appreciate the distances over which the seismic records measured at different sites are similar to each other, it is helpful to look at the regional map for fixed PCSV levels. Herein, for the sake of discussion two PCSV levels at 10 and 20 are considered for construction of such a regional similarity map. Table 4.1 shows the distances obtained from the PCSV graphs at 10 and 20 PCSV values. Obviously, it is possible to prepare similar maps for any desired study area.

Table 4.1 Similarity measures at fixed level of PCSV

	Fixed PCSV Levels	
Station Number	10	20
1	180	305
2	300	1110
3	440	940
4	405	1295
5	300	1110
6	295	150
7	500	800
8	540	760
9	595	1120
12	370	600
13	180	435
14	280	435
20	470	1310
21	325	520
22	460	1065
23	220	500
24	200	280
30	580	1460
31	250	500
32	400	1070
33	305	880
34	350	1035
40	360	975
41	95	115
42	450	735
43	405	900
50	370	1165
51	220	470
52	430	650
53	280	420
60	115	295
61	300	420
62	320	1025
63	400	1205
70	705	1050
71	210	395
72	300	750

Table 4.1 (continued)

	Fixed PCSV Levels	
Station Number	10	20
73	275	700
80	100	205
81	405	1110
82	620	800
83	215	500
91	200	645
92	200	500
93	320	1135
100	200	280
101	325	580
102	220	620
103	230	680
104	120	195
105	110	290
106	500	645

The relevant similarity maps are shown in Figs. 4.46 and 4.47. For a fixed PCSV level the smaller is the distance the more the seismic activity effect at the site and the smaller is the regional dependence, i.e., the location of the site has relatively intense seismic occurrences than the other sites or the regions. For instance, in Fig. 4.46 the map shows intense seismic occurrences in the eastern part of Turkey, surrounded by the 120 contour line. The next most intensive seismic variations are observed in the central, northeast, and western portions of the country where contour lines of 280 occur. However, the least sensitive locations are in the southern parts, with similarity contours of about 600.

On the other hand, at the higher level of similarity as presented in Fig. 4.47 the study area seems more heterogeneous, but major distinctive regional zones as in Fig. 4.46 remain the same.

Principles of PCSV have been explained and applied to seismic data in Turkey. This type of PCSVs provides detailed information about a regional variable at and near the measurement sites as well as among the sites. The main purpose of the CSV technique is to check the heterogeneity of the regionalized variable. If the empirical point CSVs at different sites have similar patterns within a certain error band such as 5–10%, then the regionalized variable is homogeneous and otherwise heterogeneity exists. The point CS concept brings an additional new concept, which provides an opportunity to make spatial variability interpretations at each site rather than regionally. Interpretations of relevant PCSV at any site provide useful information concerning the smoothness, structural control, regional dependence, continuity, and the radius of influence. The PCSV methodology proposed in this paper is applied to the scattered seismic variation over Turkey. Finally, a similarity map is obtained, which provides a basis for the regional heterogeneity assessments.

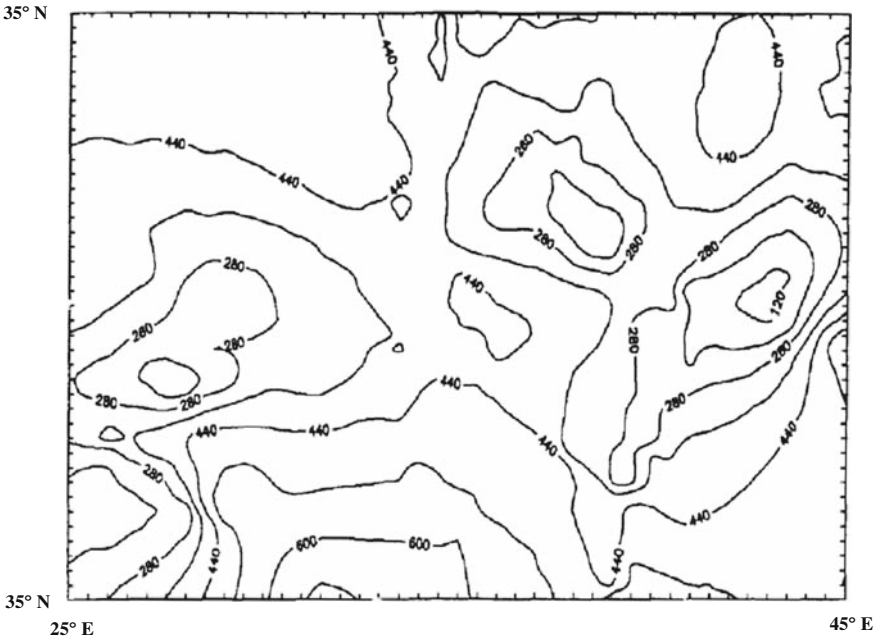

Fig. 4.46 Similarity map at 10 PCSV value

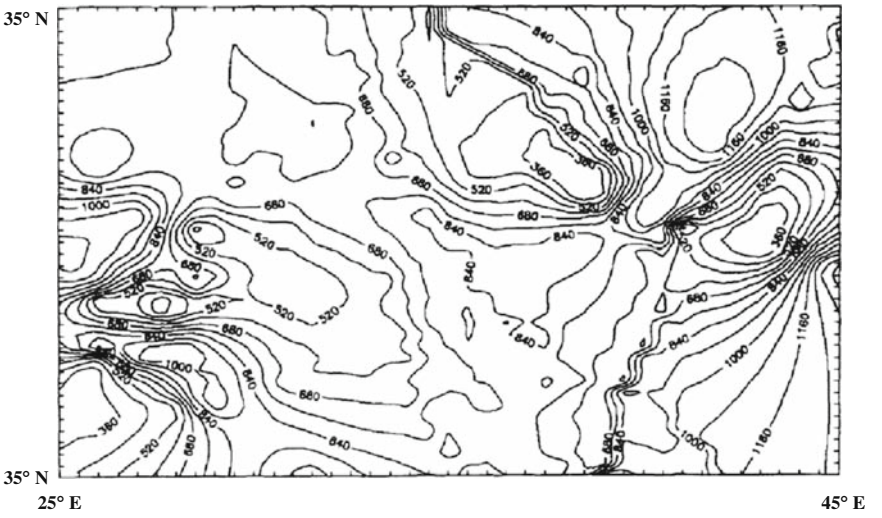

Fig. 4.47 Similarity map at 20 PCSV value

4.10 Spatial Dependence Function

As already mentioned, calculation of a sample CSV (or PCSV) leads to a non-decreasing function with distance. It is said in Section 2.2 that all the classical weighting functions appear as a non-increasing function with distance. It is, therefore, logical to execute the following steps in order to obtain a valid and standard weighting function from the sample CSV similar to the classical weighting functions.

1) Depict on the sample CSV the maximum distance, R_M, and corresponding sample CSV value, V_M. R_M corresponds to the distance between the two farthest station locations in any study area (see Fig. 4.36).
2) Divide all the distances (CSV values) by R_M (by V_M) and the result appears as a scaled form of the sample CSV within limits of 0 and 1 on both axes. This shows the change of dimensionless CSV with dimensionless distance.
3) Subtraction of the dimensionless CSV values from the maximum value of one appears as a non-increasing function of the dimensionless distance as shown in Fig. 4.48, which has similar pattern to all the classical weighting functions as explained in the previous section. This function is referred to as the standard dependence function (SDF).

Example 4.2

In order to explain the experimental CSV and thereof derived SDFs, the monthly rainfall amounts at a set of stations are considered, each with at least 30 years of records in the northwestern part of Turkey (Şen, 1997). Some of the CSVs are presented in Fig. 4.49 with corresponding classical and calculated SDF values in Fig. 4.50.

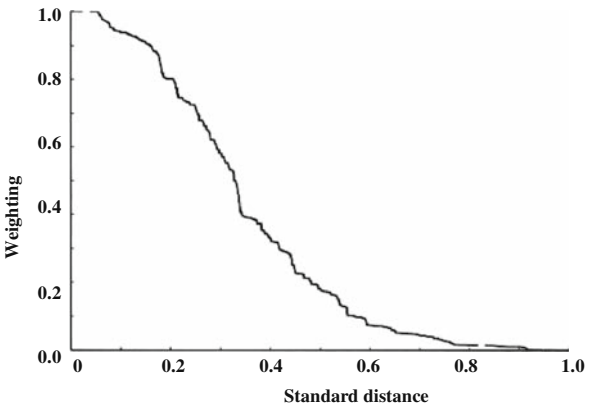

Fig. 4.48 A representative SDF

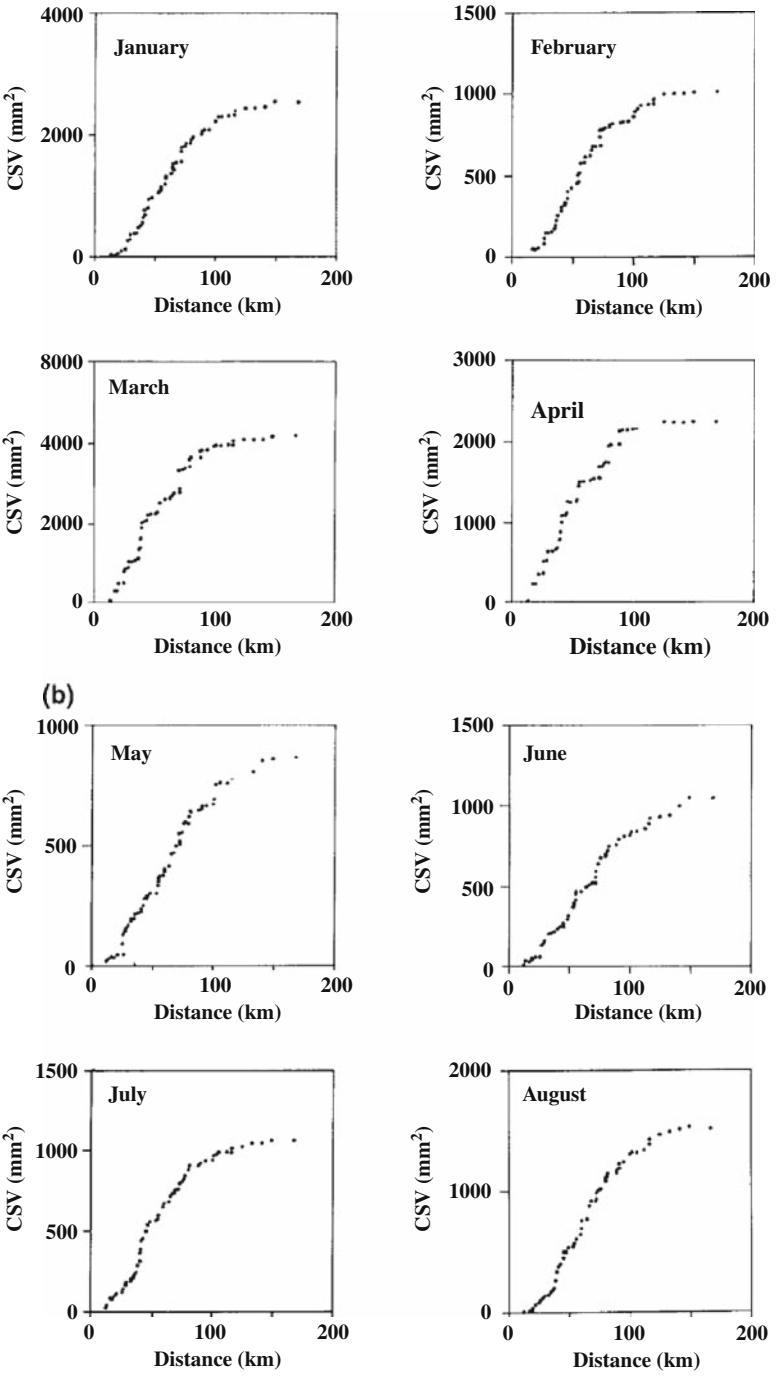

Fig. 4.49 Monthly CSVs

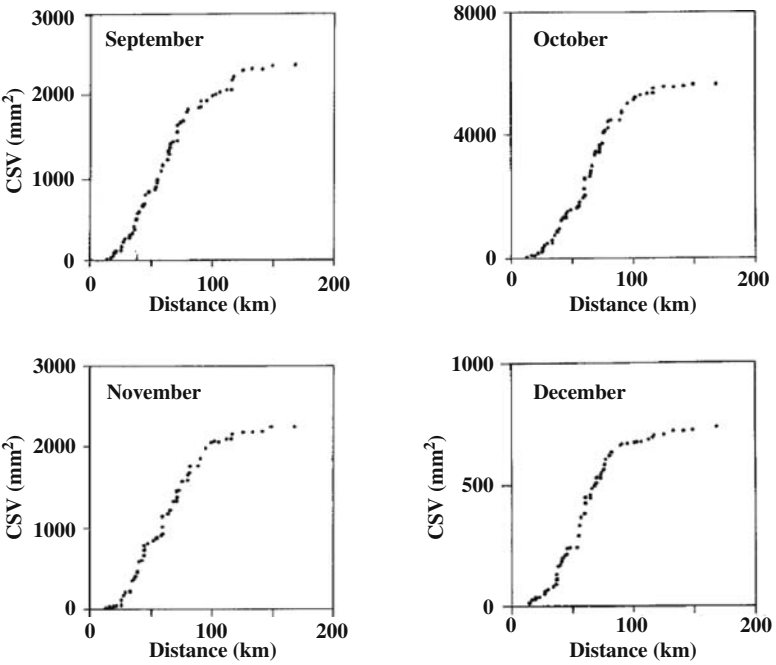

Fig. 4.49 (continued)

It is possible to conclude from Fig. 4.49 that

1) They all reach almost horizontal CSV value at large distances, which mean that after a certain distance there is no regional effect of one station on other stations' rainfall amount. This distance corresponds to R in Eq. (3.24, 3.25, and 3.26).
2) Initially, all the CSV's have an intercept on the horizontal distance axis at about 5 km. This corresponds to almost the smallest distance between the stations.
3) The smallest and the greatest CSV values at large distances occur during July and October, respectively, which are the transition months in this region from the Black Sea to the Mediterranean Sea climate in July and vice versa in October.

On the other hand, Fig. 4.50 includes the geometric weighting functions already given in Fig. 3.31 for the sake of comparison. The following interpretations and conclusions can be drawn from these figures for each month.

1) In January, the experimental CSV weighting function does not conform by any of the classical models. Initially, at small distances it is above all the models and then becomes closer to exponential model, but only up to about 0.30 dimensionless distances, deviating from it thereafter.

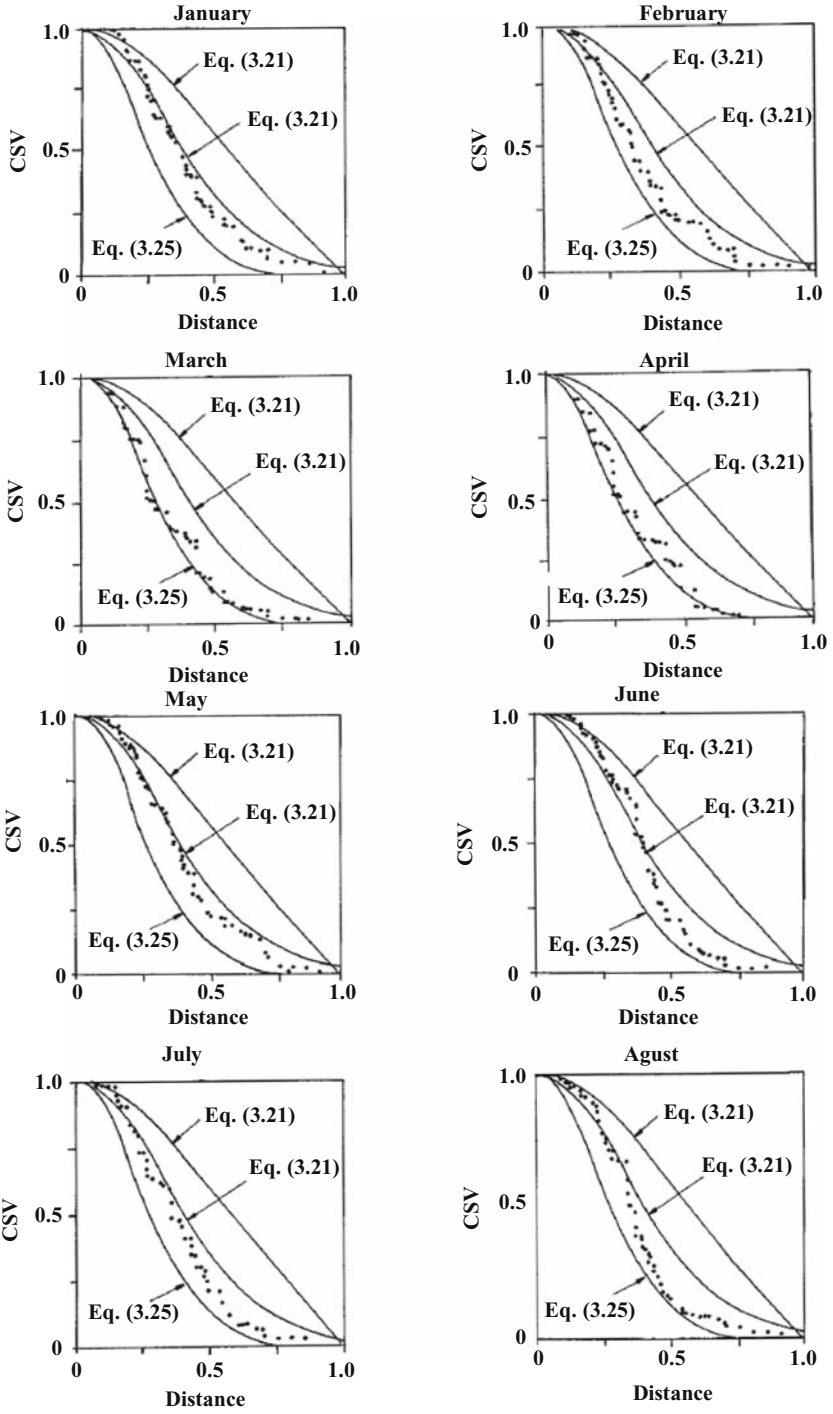

Fig. 4.50 Monthly weighting functions

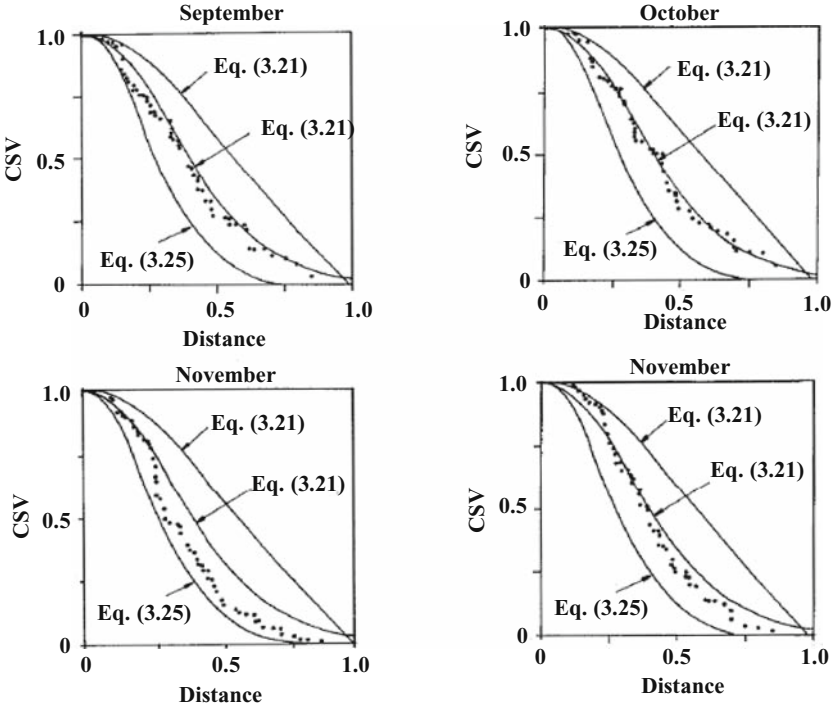

Fig. 4.50 (continued)

2) In February, perhaps initial portion confirms with the exponential model, but later becomes closer to the power model.
3) March experimental CSV follows the power law of the weighting functions at almost every distance.
4) Similar pattern to March repeats itself in April, but in May although initially there is a portion abiding with the power model, then it converts to exponential model. In June, the experimental CSV weighting function comes even closer to the exponential weighting function.
5) During September very small and big distances come closer to the ratio and power models, respectively, but for moderate distance it has an exponential form. So the mixture of three models appears as a hybrid model in representing the regional variability. Such a phenomenon cannot be estimated only by considering one of the classically available models. In the remaining months, similar interpretations are valid.

These discussions indicate that classical geometric weighting models do not have full justification for the whole of the meteorological phenomenon, but they are good first approximations. They cannot be valid for the whole regional variability in any study area.

Example 4.3 For the implementation of the SDF and spatial estimation methodology, the iron (Fe) percentage (%) concentration dataset used by Clark (1979, p. 95, Table 4.5) is adopted. Although there are 50 sampling points, in order to make comparison with fuzzy clustering results by Pham (1997) only 21 sites are given in Table 4.2, because he considered only 21 sampling points from Clark's table. Figure 4.51 shows the locations of the sites within the study area.

It is obvious that there is a rather uniform distribution of these sites in a representative manner over the whole study area.

The CSV is given in Fig. 4.52. The maximum CSV corresponding to 350 m is 4,250, and accordingly the SDF is obtained and the results are presented in Fig. 4.53.

Similar to all the regional estimation procedures, weighted average formulation as in Eq. (2.27) is used together with the weights obtained from SDF in Fig. 4.53.

In order to assess the validity of the proposed weighted average procedure, a cross-validation technique is used. According to this a data value at one site is supposed to be unknown and is removed from the data set. This removed value is then estimated with the remaining set of data and by using the SDF together with Eq. (2.27). This procedure is repeated for all the sites, knowing that a data removed for estimation at its location is put again in the set for the estimation at another location.

Table 4.2 Measured and estimated Fe % concentrations and errors

Sample No. (1)	Measured (2)	Estimate (3)	Relative error (%) (4)
1	35.5	32.85	7.45
2	29.4	32.78	11.51
3	36.8	33.72	8.36
4	33.7	34.15	1.32
5	35.3	33.33	5.58
6	32.5	32.56	0.19
7	30.6	33.88	10.73
8	30.1	33.52	11.37
9	40.1	33.76	15.81
10	31.6	33.84	7.10
11	34.8	33.32	4.24
12	28.6	32.76	14.55
13	41.5	33.48	19.32
14	33.2	33.51	0.92
15	34.3	33.56	2.31
16	31.0	33.82	9.09
17	29.6	32.50	9.78
18	40.4	33.70	16.59
19	28.5	34.08	19.59
20	24.4	34.55	41.62
21	39.5	32.91	16.69
Average	33.40	33.46	11.15

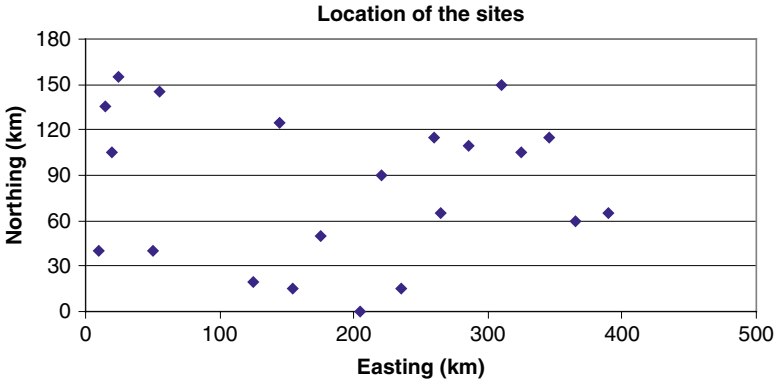

Fig. 4.51 Fe % concentration locations

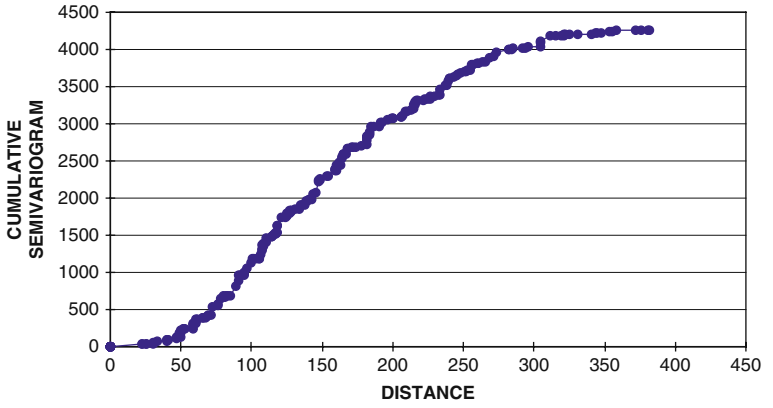

Fig. 4.52 Fe % concentration sample CSV

There are two procedures in the estimation of the site Fe % concentrations. In the first one, all the other sites are considered for their simultaneous contributions, and therefore in the estimation of any site's Fe % concentration, all the distances from this site to others (n−1 sites) are measured from the map in Fig. 4.51. Subsequently, these distances are entered into Fig. 4.53 on the horizontal axis and the corresponding RDF weights are found from the vertical axis for each distance. In this manner, all the sites are treated equally by the same procedure and hence, instead of measured values, their estimations through the SDF and the cross-validation procedure are calculated. Column (3) in Table 4.2 shows estimated Fe % concentrations and their corresponding relative errors are calculated as the ratio of the absolute difference between the measured and the estimated values divided by the measured value multiplied by 100, which is shown in column (4).

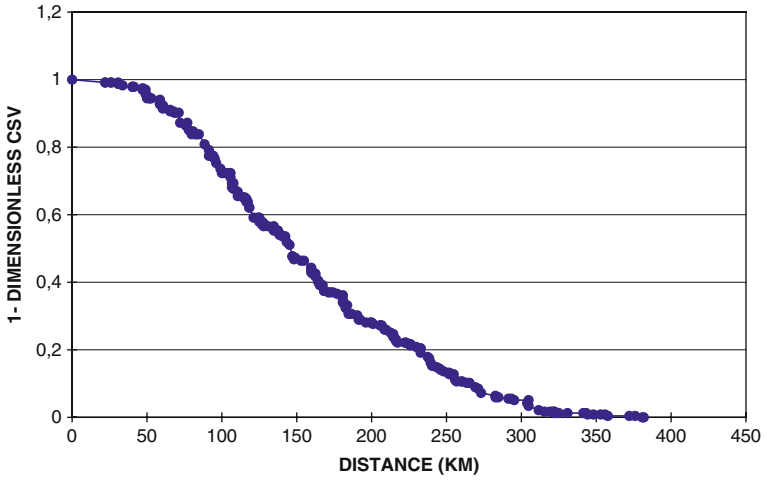

Fig. 4.53 Fe % concentration (**a**) dimensionless CSV, (**b**) SDF

$$\text{Relative error} = 100 * \frac{|\text{measured} - \text{estimated}|}{\text{measured}}.$$

It is obvious that for almost half of the sites, the relative error is more than 10%, which indicates the unsuitability of the so far proposed procedure. For extreme Fe % concentration sites, the relative errors are very high. However, the averages of measured and estimated values are very close together with 2% relative error. On this basis, it may be concluded that the proposed procedure yields reasonable values on the average, but fails to estimate individual site values. This procedure takes into account the contribution of all the sites in the estimation and disregards the concept of the radius of influence.

In order to assess visually, the correspondence between the measured and the estimated values, Fe % concentrations are presented in Fig. 4.54a against the site number sequency along the horizontal axis. Unfortunately, consideration of all the sites in this regional estimation procedure by using Eq. (2.27) and SDF function for weights calculation yields to average estimations, which do not represent the high and low points satisfactorily as obvious from Fig. 4.54a. On the other hand, Table 4.3 shows also the results by the inverse distance square and four fuzzy clustral procedures as suggested by Pham (1997). The comparisons of average relative errors in the last row of this table indicate that the SDF method has the least relative error percentage. It is even better than the five-cluster case, which has been stated as the best solution by Pham (1997).

In order to improve the representativeness of the Fe % concentrations regionalized variable estimations at sites, herein, an adaptive new technique is suggested, which does not only estimate the regional value at a site but also provides the number of the nearest sites that should be considered in the best possible regional estimation.

Table 4.3 Fe % concentration estimations by different techniques

Sample No. (1)	RDF (2)	Inverse square distance (3)	Fuzzy clustering (4)			
			Three	Four	Five	Six
1	32.85	33.44	34.16	34.19	34.83	33.10
2	32.78	31.92	33.28	32.39	31.76	33.20
3	33.72	30.87	34.04	30.50	31.28	31.00
4	34.15	30.77	33.96	33.60	30.23	31.15
5	33.33	36.67	33.11	33.53	35.75	35.23
6	32.56	35.61	33.46	33.11	34.10	34.69
7	33.88	33.24	33.97	33.60	33.00	33.22
8	33.52	35.47	33.63	33.22	33.95	37.46
9	33.76	32.62	33.88	32.83	34.23	34.44
10	33.84	33.24	33.38	33.28	33.12	32.38
11	33.32	36.66	33.84	33.04	34.02	34.29
12	32.76	30.50	33.61	32.19	31.63	31.69
13	33.48	29.85	33.93	33.93	31.32	30.17
14	33.51	34.60	34.11	33.82	30.95	32.20
15	33.51	37.35	33.23	32.96	33.54	34.68
16	33.82	33.24	34.34	33.78	33.78	34.06
17	32.50	34.67	33.05	33.25	38.10	35.17
18	33.70	34.04	34.93	34.37	34.47	35.73
19	34.08	34.12	33.78	33.21	34.68	34.98
20	34.55	32.29	31.87	32.06	32.48	32.13
21	32.91	34.06	33.16	33.18	32.74	31.98
Averages	33.45	33.58	33.65	33.14	33.33	33.49
Average relative errors (%)	11.15	12.66	12.55	12.65	12.01	12.61

Accordingly, the radius of influence is defined as the distance between the estimation site and the far distant site within the adjacent sites that are considered in the regional estimation procedure. The following steps are necessary for the application of this adaptive procedure.

(a) Take any site for cross-validation and apply Eq. (2.27) by considering the nearest site only. Such a selection is redundant and corresponds to the assumption that, if only the nearest site measurement is considered, then the regional estimation will be equal to the same value. This means that in such a calculation the radius of influence is the minimum and equal to the distance between the estimation and the nearest sites.
(b) Consider now two of the nearest sites to the estimation site and apply the RDF weighting method according to Eq. (2.27). Consideration of two sites will increase the radius of influence as the distance between the estimation and the next nearest site and the estimation value will assume weighted value of the two nearest sites. Since the weights and measurements are positive numbers,

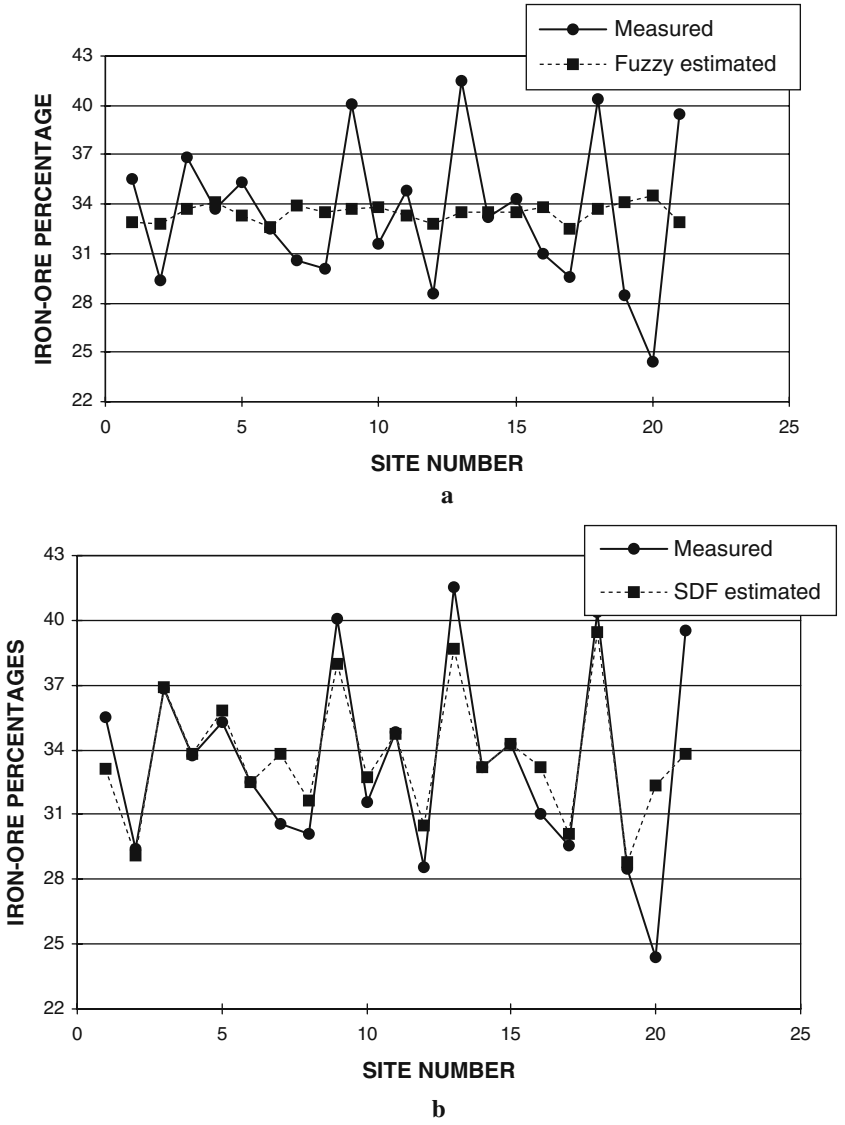

Fig. 4.54 Measured and estimated Fe % concentration, (**a**) whole points, (**b**) adaptive method

the estimated value will be between the measurements at the two nearest sites. There will be a squared estimation error as the square of the difference between measured and estimated values.

(c) Repeat the same procedure now with three nearest stations and calculate the square error likewise. Subsequently, it is possible to continue with 4, 5, . . . , (n−1) nearest sites consequently, and for each case to calculate corresponding

Table 4.4 Detailed calculation steps for site-14 regional estimation

Number of nearest sites (1)	Estimation (2)	Square error (3)
2	31.94	1.58
3	29.46	13.96
4	30.75	6.00
5	32.42	0.60
6	32.21	0.97
7	32.38	0.67
8	32.82	0.14
9	32.59	0.37
10	32.72	0.23
11	33.21	0.00
12	33.12	0.01
13	33.48	0.08
14	33.80	0.36
15	33.69	0.24
16	33.63	0.18
17	33.57	0.13
18	33.55	0.12
19	33.48	0.08
20	33.51	0.09

square error. The first one with the least square error yields the number of nearest sites for the best regional Fe % concentration estimation. The distance of the farthest site in such a situation corresponds to the radius of influence. As an example, herein, only site-14 calculations are presented in detail in Table 4.4. It is obvious that when Eq. (2.27) is applied by considering 11 nearest sites, the estimation error square becomes the least with the radius of influence equal to 127.47 m.

Application of the above adaptive procedure to Fe % concentrations results in the estimation values, number of the nearest sites with the minimum squared error, and the radius of influence, which are presented in Table 4.5. Notice that this table includes the complete list of samples as given by Clark (1979, p. 95, Table 4.5). This table yields the following points:

1) The adaptive estimation procedure gives average iron ore concentration value similar to average measurements with 2.31% error. Hence, similar to all the previous methods, adaptive estimation also gives reasonable average values.
2) Comparison of average relative error in Table 4.4 with average relative errors in Table 4.4 shows clearly that the adaptive method with 4.74% error is the best among all approaches, and the reduction in the relative error implies that deviations from average level are taken into account effectively. Figure 4.49b presents the adaptive estimations together with the measured values for Pham (1997) data

set. If Fig. 4.49a and b are compared, it is then obvious that deviations are better accounted by the adaptive method.

3) The adaptive approach provides the radius of influence for each station as shown in the last column of Table 4.5. The average radius of influence is about 88.5 m with maximum and minimum values of about 223 and 13 m, respectively.

By making use of the radius of influence from Table 4.5, it is possible to construct equal radii regional map as shown in Fig. 4.55.

Table 4.5 Estimations and radius of influence

Easting (1)	Northing (2)	% Fe (3)	Estimation (4)	Relative error (%) (5)	Number of nearest sites (6)	Radius of influence (m) (7)
0	170	34.30	32.15	6.27	3	13.25
10	40	35.50	33.10	6.76	10	199.06
15	135	28.60	30.50	6.64	3	41.23
55	145	29.40	29.10	1.02	2	41.23
125	20	41.50	38.65	6.87	2	58.31
175	50	36.80	36.91	0.30	5	69.46
120	180	33.40	31.52	5.63	6	73.16
160	175	36.00	33.27	7.58	5	97.84
240	184	30.20	31.30	3.64	4	86.17
260	115	33.20	33.21	0.03	11	127.47
235	15	33.70	33.84	0.42	3	69.46
365	60	34.30	34.26	0.12	4	94.34
285	110	35.30	35.83	1.50	3	47.17
345	115	31.00	33.17	7.00	8	127.47
335	170	27.40	28.12	2.63	6	65.13
325	195	33.90	34.75	2.51	6	123.10
350	235	37.60	38.02	1.12	5	73.10
290	230	39.90	41.15	3.13	4	68.17
10	390	27.20	29.12	7.06	3	55.64
85	380	34.20	32.75	4.24	3	112.51
50	270	30.20	31.60	4.64	6	78.32
200	280	30.40	31.06	2.17	4	85.76
400	355	39.90	41.73	4.59	5	67.23
360	335	40.00	42.16	5.40	5	72.15
335	310	40.60	41.18	1.43	4	83.72
5	195	33.90	34.73	2.45	3	198.12
20	105	32.50	32.50	0.00	9	164.50
25	155	29.60	30.14	1.82	3	50.25
50	40	30.60	33.82	10.52	14	222.99
155	15	40.40	39.50	2.23	3	52.50
145	125	30.10	31.63	5.08	3	92.19
130	185	35.30	33.18	6.01	3	187.15
175	185	41.40	39.17	5.39	3	59.37
220	90	28.50	28.82	1.12	2	51.48
205	0	40.10	37.96	5.34	4	82.46
265	65	24.40	32.34	32.54	3	51.48
390	65	31.60	32.73	3.58	2	67.29

Table 4.5 (continued)

Easting (1)	Northing (2)	% Fe (3)	Estimation (4)	Relative error (%) (5)	Number of nearest sites (6)	Radius of influence (m) (7)
325	105	39.50	33.89	14.20	4	60.21
0	170	34.30	32.15	6.27	3	13.25
310	150	34.80	34.77	0.09	4	61.03
385	165	29.90	28.16	5.82	5	97.25
325	220	37.80	36.08	4.55	6	75.34
375	215	29.80	26.18	12.15	5	56.76
200	230	37.40	35.83	4.20	4	82.63
55	375	27.40	28.17	2.81	3	62.75
395	245	36.50	35.08	3.89	5	192.50
165	355	40.80	39.15	4.04	5	55.25
270	285	32.90	34.75	5.62	4	155.50
365	340	40.00	40.80	2.00	5	86.13
330	320	44.10	45.83	3.92	5	69.12
330	290	41.40	37.16	10.24	4	60.73
Averages		34.50	34.42	4.74	5	88.51

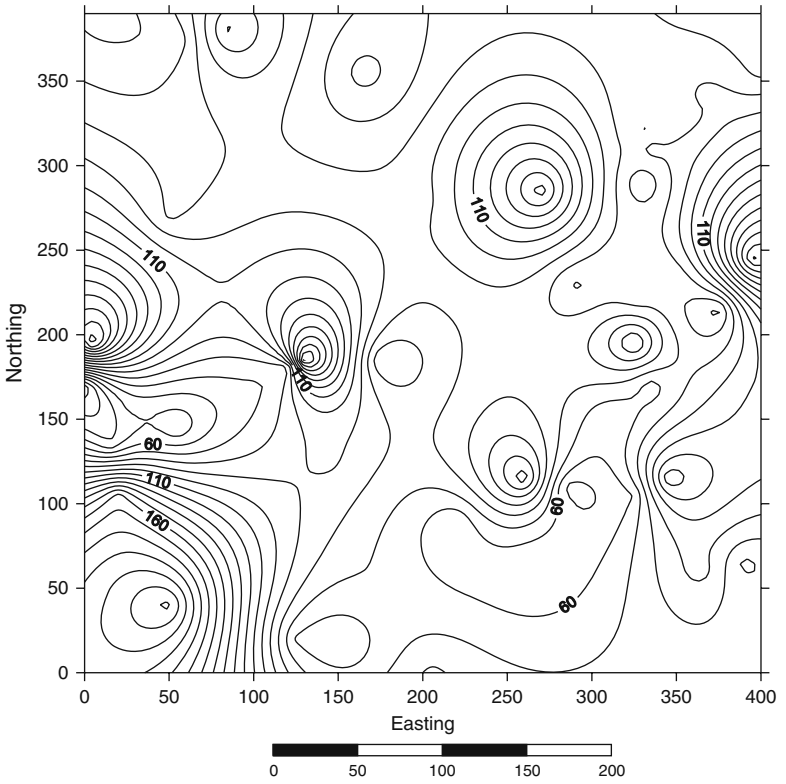

Fig. 4.55 Iron ore radius of influence map (m)

Table 4.6 Regional interpolation

Site No. (1)	Easting (2)	Northing (3)	Radius of influence (m) (4)	Estimation Fe (%) (5)
1	36	136	63	30.02
2	27	90	172	32.71
3	86	116	97	30.13
4	45	29	200	33.81
5	95	47	118	34.88
6	186	23	68	38.49
7	218	58	50	32.63
8	222	129	95	31.77
9	268	98	80	32.35
10	327	134	93	33.47
11	272	43	58	28.99
12	340	40	80	32.30
13	331	65	77	32.78
14	327	87	70	33.08
15	368	96	103	34.37

From this map one can know the relevant radius of influence for any desired point within the study area. Once this radius is determined, then a circle with the center at the prediction point is drawn. The measurement sites within this circle are taken into consideration in the application of Eq. (2.27) for regional estimation through the SDF weights.

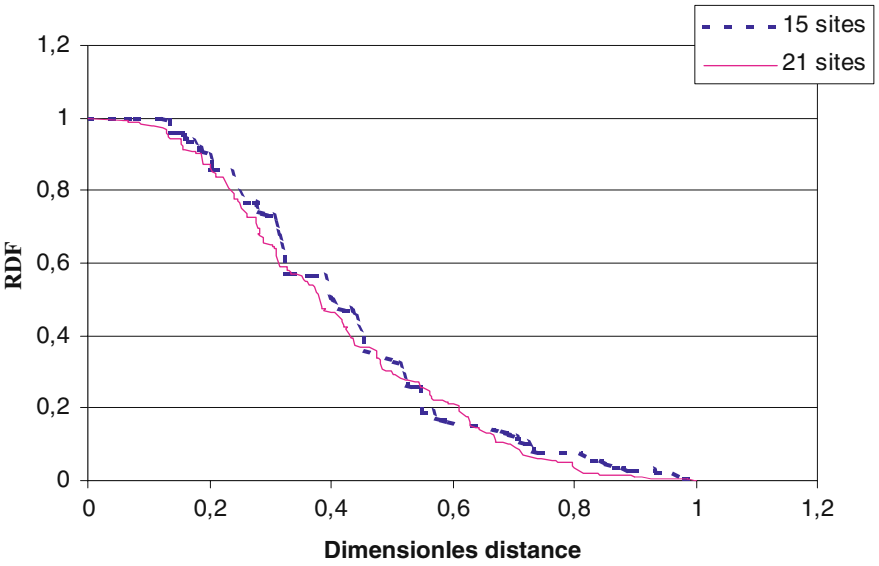

Fig. 4.56 Measured and estimated SDFs

After having completed the cross-validation procedure and the map of the radius of influence, it is now time to present spatial interpolation procedure with RDF usage as follows.

1) Select any number, say 15, of spatially scattered points within the study area as shown in Fig. 4.51. These sites are the locations without measurements. For the sake of argument, they are selected rather arbitrarily with easting and northing coordinates as shown in Table 4.6.
2) Radius of influence of each site is determined from the map in Fig. 4.55 and written in the forth column of Table 4.6.
3) Consideration of the radius of influence for each site defines the number of measurement sites within this radius, which are basis for the Fe% concentration

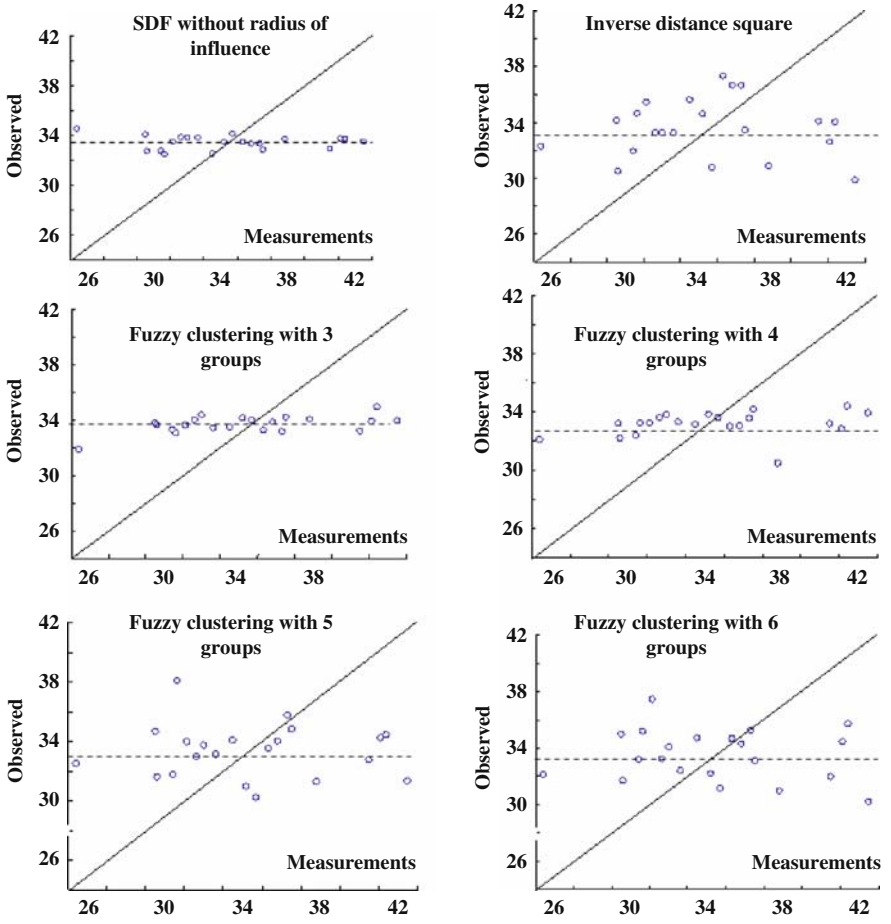

Fig. 4.57 Comparative model verifications

estimation through Eq. (2.27) at this site. Hence, the measurement sites that will be considered in the spatial interpretation of the Fe % concentration at the site are identified.

4) Subsequently, distances between the interpolation site and the effective measurement sites are calculated.
5) The entrance of these distances on the horizontal axis in the SDF (Fig. 4.49b) yields the weights on the vertical axis.
6) Substitution of all the relevant values into Eq. (2.27) provides the Fe % concentration value estimations at each site, which are shown in the last column of Table 4.6.
7) In order to check the reliability of the estimations, the question is now whether these spatial estimations will yield almost the same SDF or not. For this purpose, the SDF calculation steps are applied to data in Table 5.6.
8) Figure 4.56 indicates the resulting SDF for the measured and estimated Fe % concentrations. The maximum relative difference between these two SDFs is less than 5%, which confirms the practical validity of the SDF adaptive estimation procedure methodology as proposed in this paper.

It is now time to compare all the methods with the measured data on a Cartesian coordinate system with the measured values on the horizontal axes and the model outputs on the vertical axes as in Figs. 4.57 and 4.58.

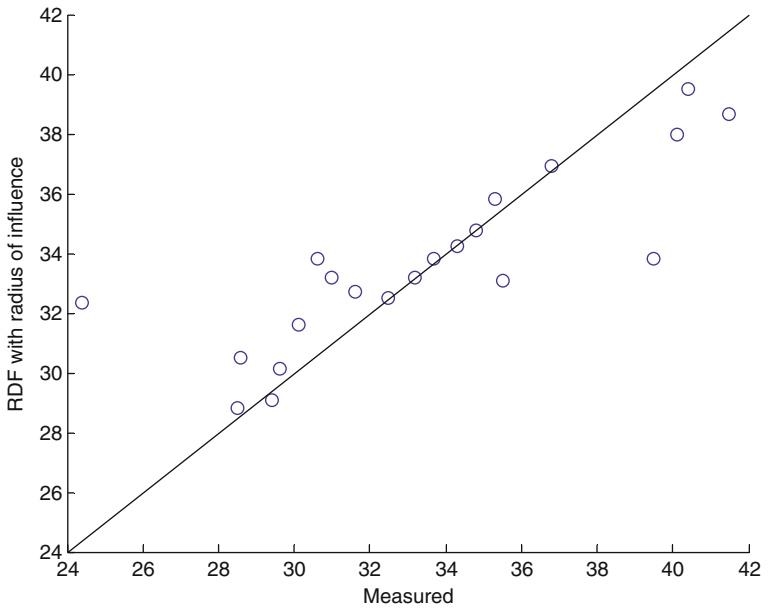

Fig. 4.58 SDF model verification

References

Aboufirassi, M., and Marino, M. A., 1984. A geostatistically based approach to the identification of aquifer transmissivities in Yolo Basin, California. Math. Geol. 16(26), 125–137.

Alfano, M., 1984. Statistical inference of the semivariogram and the quadratic model. In: G. Verly, and others (Eds.), Geostatistics for Natural Resources Characterization. Reidel, Dordrecht, Holland, pp. 45–53.

Barchet, W. R., and Davis, W. E., 1983. Estimating long-term mean winds from short-term wind data. Technical Report Number PNL-4785, Pacific Northwest Lab. Richland, WA (USA), 31 pp.

Barnes, R. J., 1991. The variogram sill and the sample variance. Math. Geol. 23(4), 673–678.

Barnes, S. L., 1964. A technique for maximizing details in numerical weather map analysis. J. Appl. Meteor. 3, 396–409.

Barros, V. R., and Estevan, E. A., 1983. On the evaluation of wind power from short wind records. J. Appl. Meteor. 22, 1116–1123.

Benjamin, J. R., and Cornell, C. A., 1970. Probability Statistics and Decision Making in Civil Engineering. McGraw-Hill Book Inc., New York.

Bergman, K., 1979. Multivariate analysis of temperatures and winds using optimum interpolation. Monthly Weather Rev. 107, 1432–1444.

Bergthorsson, P., and Döös, B. R., 1955. Numerical weather map analysis. Tellus 7, 329–340.

Box, G. E. P., and Jenkins, G. M., 1976. Time Series Analysis, Control and Forecasting. Holden Day, San Francisco.

Bratseth, A. M., 1986. Statistical interpretation by means of successive corrections. Tellus 38A, 438–447.

Buzzi, A., Gomis, D., Pedder, M. A., and Alonsa, S., 1991. A method to reduce the adverse impact that inhomogeneous station distributions have on spatial interpolations. Mon. Wea. Rev. 119, 2465–2491.

Carr, J. R., Bailey, R. E., and Deng, E. D., 1985. Use of indicator variograms for enhanced spatial analysis. Math. Geol. 17(8), 797–812.

Clark, I., 1979. The semivariogram – Part 1. Eng. Min. J. 180(7), 90–94.

Cooley, R. L., 1979. A method of estimating parameters and assessing reliability for models of steady state groundwater flow, 2, Applications of statistical analysis. Water Resour. Res. 15, 603–617.

Cressie, N. A. C., 1993. Statistics for Spatial Data (revised edition). Wiley, New York, 900 pp.

Cressman, G. P., 1959. An operational objective analysis system. Mon. Wea. Rev. 87, 367–374.

Daley, R., 1991. Atmospheric Data Analysis. Cambridge University Press, Cambridge, 475 pp.

David, M., 1977. Geostatistical Ore Reserve Estimation. Elsevier, New York, 340 pp.

Davis, J., 1986. Statistic and data analysis in geology. John Wiley & Sons, Inc., New York, 560 pp.

Dee, D. P., 1995. On-line estimation of error covariance parameters for atmospheric data assimilation. Mon. Wea. Rev. 123, 1128–1145.

DeWijs, H. J., 1972. Method of successive differences applied to mine sampling: Trans. Inst. Min. Metal. Sect. A, Min. Industry 81, 78–81.

Eddy, A., 1964. The objective analysis of horizontal wind divergence fields. Quart. J. Roy. Meteorol. Soc. 90, 424–440.

Eliassen, A., 1954. Provisional report on calculation of spatial covariance and autocorrelation of the pressure field, Report No. 5 (Oslo: Videnskaps-Akademiet Institut for Vaer og Klimaforskning).

Erdik, M., Doyuran, V., Akkaş, N., and Gülkan, P., 1985. A probabilistic assessment of the seismic hazard in Turkey. Tectonophysics 117(3/4), 295–330.

Franke, R., 1988. Statistical interpretation by iteration. Mon. Wea. Rev. 116, 961–963.

Gandin, L. S., 1963. Objective Analysis of Meteorological Fields. Leningrad, Gidromet; Translated from Russian, Jerusalem, Israel Program for Scientific Translations, 1965, 242 pp.

Gilchrist, B., and Cressman, G. P., 1954. An experiment in objective analysis. Tellus 6, 309–318.

Goodin, W. R., McRea, G. J., and Seinfeld, J. H., 1979. A comparison of interpolation methods for sparse data: application to wind and concentration fields. J. Appl. Meteor. 18, 761–771.

Gustafsson, N., 1981. A review of methods for objective analysis. In: L. Bengtsson, M. Ghil, and E. Källén (Eds.), Dynamic Meteorology: Data Assimilation Methods. Springer-Verlag, pp. 17–76.

Hoeksema, R. J., and Kitandis, P. K., 1984. An application of the geostatistical approach to the inverse problem in two dimensional groundwater modeling. Water Resour. Res. 20(7), 1003–1020.

Hohn, M. E., 1988. Geostatistics and Petroleum Geology. Van Nostrand Reinhold, New York, NY.

Inman, R. L., 1970. Operational objective analysis schemes at the National Severe Storms Forecast Center. U.S. National Severe Storms Laboratory Tech. Circular 10, Norman, OK, 50 pp.

Journel, A. G., and Huijbregts, C. I., 1978. Mining geostatistics. Academic Press, London, 710 pp.

Journel, A. G., 1985. The deterministic side of geostatistics. Math. Geol. 17(1), 1–15.

Kitanidis, P. K. 1997. Introduction to Geostatistics: Applications in Hydrogeology. Cambridge University Press, Cambridge, 249 pp.

Koch, S. E., DesJardins, M., and Kocin, P. J. 1983. An iterative Barnes objective map analysis scheme for use with satellite and conventional data. J. Appl. Meteor. 22, 1487–1503.

Krige, D. G., 1982. Geostatistical case studies of the advantages of log-normal, De Wijsian Kriging with mean for a base metal mine and a gold mine. Math. Geol. 14(6), 547–555.

Kruger, H. B., 1969a. General and special approaches to the problem of objective analysis of meteorological variable. Quart. J. Roy. Meteorol. Soc. 95(403), 21–39, January.

Kruger, H. B., 1969b. Objective analysis of pressure height data for the tropics. Monthly Weather Rev. 94(4), 237–257.

Liebhold, A. M., Halverson, J., and Elmes, G., 1993. Quantitative analysis of the invasion of gypsy moth in North America. J. Biogeogr. 19, 513–520.

Lorenc, A. C., 1981. A global three-dimensional multivariate statistical interpolation scheme. Monthly Weather Rev. 109, 701–721.

Matheron, G., 1963. Principles of geostatistics. Econ. Geol. 58, 1246–1266.

Matheron, G., 1965. Les Variables Regionalisees et leur Estimation. Masson, Paris, 306 pp.

Matheron, G., 1971. The theory of regionalized variables and its applications. Ecole de Mines, Fontainbleau, France.

Myers, D. E., Begovich, C. L., Butz, T. R., and Kane, V. E., 1982. Variogram models for regional groundwater geochemical data: Math. Geol. 14(6), 629–644.

Pannatier, Y., 1996. VARIOWIN: Software for Spatial Data Analysis in 2D. Springer-Verlag, New York, NY.

Panofsky, H. A., 1949. Objective weather map analysis. J. Meteor. 6, 386–392.

Pedder, M. A., 1993. Interpolation and filtering of spatial observations using successive correlations and Gaussian filters. Mon. Wea. Rev. 121, 2889–2902.

Perrie, W., and Toulany, B., 1989. Correlations of sea level pressure field for objective analysis. Mon. Wea. Rev. 117, 1965–1974.

Pham, T. D., 1997. Grade estimation using fuzzy-set algorithms. Math. Geol. 29(2), 291–305.

Powers, R. W., Ramirez, L. F., Redmond, C. D., and Elberg, E. L., 1966. Geology of the Arabian Peninsula. Sedimentary Geology of Saudi Arabia. U.S. Geol. Survey, Prof Paper 560-D, 1–47, New York.

Rutherford, I. D., 1976. An operational three-dimensional multivariate statistical objective analysis scheme. Proceedings of the JOC Study Group, Conference on four-dimensional Data Assimilation, Paris, November 17–21,1975. The GARP Programme on Numerical Experimentation, Report No. 11, January 1976.

Sashegyi, K. D., Harms, D. E., Madala, R. V., and Raman, S., 1993. Application of the Bratseth scheme for the analysis of GALE data using a mesoscale model. Mon. Wea. Rev. 121, 2331–2350.

Schlatter, T. W., 1975. Some experiments with a multivariate statistical objective analysis scheme. Monthly Weather Rev. 103, 246–257.

Seaman, R. S., 1988. Some real data tests of the interpolation accuracy of Bratseth's successive correction method. Tellus 40A, 173–176.
Şen, Z., 1978. Autorun analysis of hydrologic time series. J. Hydrol. 36, 7585.
Şen, Z., 1989. Cumulative semivariogram models of regionalized variables. Int. J. Math. Geol. 21(3), 891–903.
Şen, Z., 1992. Standard cumulative semivariograms of stationary stochastic processes and regional correlation: Math. Geol. 24, 417–435.
Şen, Z., 1995. Applied Hydrogeology for Scientists and Engineers. CRC Lewis Publishers, Boca Raton, FL, 496 pp.
Şen, Z., 1997. Objective Analysis by cumulative semivariogram technique and its application in Turkey. J.Appl. Meteorol. 36(12), 1712–1724.
Şen, Z., 2002. İstatistik Veri İşleme Yöntemleri (Hidroloji ve Meteoroloji). Su Vakfı yayınları, 243 sayfa.
Şen, Z., and Habib, Z. Z., 1998. Point cumulative semivariogram of areal precipitation in mountainous regions. J. Hydrol. 205, 81–91.
Şen, Z., and Habib Z., 2001. Monthly spatial rainfall correlation functions and interpretations for Turkey. Hydrol. Sci. J. 46(5), 829–829.
Şen, Z., 2008. Solar Energy Fundamentals and Modeling Techniques. Atmosphere, Environment, Climate Change and Renewable Energy. Springer Verlag, 276 pp.
Shenfield, L., and Bayer, A. E., 1974. The utilization of an urban air pollution model in air management. Proc. 15th Meeting of the Expert Panel on Air Pollution Modeling, NATO Committee on the Challenges to Modern Society, Brussels, Belgium, 35 pp.
Skibin, D., 1984. A simple method for determining the standard deviation of wind direction, J. Atmos. Oceanic Tech., 1, 101–102.
Subyani, A. M., 1987. Hydrogeology of the Wasia aquifer and its geostatistical modeling. Unpublished M.Sc. Thesis, Faculty of Earth Sciences, King Abdulaziz University, 170 pp.
Taylor, G. I., 1915. Eddy motion in the atmosphere. Phil. Trans. Roy. Soc. A 215, 1.
Thiebaux, H. J., and Pedder, M. A., 1987. Spatial Objective Analysis, Academic Press, London, 299 pp.

Chapter 5
Spatial Modeling

Abstract In general, *spatial variability* is concerned with different values for any property, which is measured at a set of irregularly distributed geographic locations in an area. The aim is to construct a regional model on the basis of measurement locations with records and then to use this model for regional estimations at any desired point within the area.

Earth science phenomenon varies both in time and in space; and its sampling is based on measurement stations' configuration. In many practical applications measured data are seldom available at the point of interest, and consequently the only way to transfer the solar irradiation data from the measurement sites to the estimation point is through regional interpolation techniques using powerful models. The spatial variability is measured in the most common way through the recorded solar irradiation time series at individual points. The relative variability between the stations (the difference of simultaneous values between each pair of stations) is treated commonly by spatial autocorrelation function, which is used for inter-station dependence based on a set of restrictions.

Spatial variability is the main feature of regionalized variables, which are very common in physical sciences. In practical applications, the spatial variation rates of the phenomenon concerned is of great significance in fields such as solar engineering, agriculture, remote sensing, and other earth and planetary sciences. A set of measurement stations during a fixed time interval (hour, day, month, etc.) provides records of the regionalized variable at irregular sites, and there are few methodologies to deal with this type of scattered data. There are various difficulties in making spatial estimations originating not only from the regionalized random behavior but also from the irregular site configuration.

Optimum interpolation modeling technique is presented for spatio-temporal prediction of regionalized variable (ReV) with application to precipitation data from Turkey. Kriging method is explained with simple basic concepts and graphics and then various Kriging application methodologies are explained for the spatial data modeling. The distinctions between simple, ordinary, universal, and block Kriging alternatives are presented in detail. Finally, triple diagram mapping methodology for spatial modeling is presented with applications at five different climate locations.

Z. Şen, *Spatial Modeling Principles in Earth Sciences*,
DOI 10.1007/978-1-4020-9672-3_5,

Keywords Spatial estimation · Optimum interpolation · Spatial correlation function · Cross-validation · Geostatistics · Kriging · Intrinsic property · Simple Kriging · Ordinary Kriging · Universal Kriging · Block Kriging · Triple diagram · Regional rainfall pattern

5.1 General

Modeling is a procedure that helps researchers, planners, politicians, and many experts alike to make future predictions in time or spatial estimations in a region. It is an interactive procedure where the natural event records (data), modeler's expert view, and prediction (estimation) stages work parallel at times and places in a serial manner for the best conclusions and numerical result. During a modeling procedure three different worlds are entered in a sequential manner. These are real-world affairs, interpretation in conceptual world, and mathematical formulation stage in symbolic world. The real world can be grasped by visual observations, experiments, and numerical sampling. It is, therefore, very useful to make field trips to the study area and have verbal (linguistic) information directly from the local authorities and settlers about the phenomenon and its ReV behaviors. This very first stage includes verbal and numerical data collection. Verbal information can be in the form of logical premises, which relate the concerned output variable to various input effective factors. The second stage consists of simple assumptions for the simplification of phenomenon investigation, which is very complex especially in the earth sciences. Among such simplifications are the scale of the model, behavior of different input and output variables such as their isotropy, homogeneity, uniformity, geometrical shape (rectangle, cylindrical, circular, etc.), geological or atmospheric setup simplifications. Depending on the type of the problem, it is possible first to try and apply conventional methods such as scatter plots between input and output variables so as to acquire insight about the internal behavior of the phenomenon, basic histograms, simple regressions, which may provide some further illuminations about the internal generating mechanism of the ReV functionality. After such basic and simple information, more representative formulations for the modeling are sought and questioned by updating basic assumptions and simplifications. Once a satisfaction is felt, then the formulation is applied with the data available and then the prediction (estimation) is achieved, which must be checked against the observation values (cross-validation). Whatever is the complexity, suitability, and verifiability of the model, there is always a difference between the model output and the measurements. This is the model error and then the model must be trained according to the desired error level. For instance, if the relative error is not less than desired level, say 5%, then the existing model must be updated either by releasing the basic assumptions or by changing the model formulation structure. Hence, the validation of the model is reiterated according to the previous sequence and this procedure is repeated until the desired level of error or less is reached. This is tantamount to saying that the model is verified with available numerical and verbal information, and finally it

is ready for temporal and/or spatial predictions (estimations) at locations where the data measurements are not available.

The first spatial model is performed by Student (1907), who summed up the number of the particles per unit area instead of the analysis of the spatial positions of particles in a liquid. He divided the 1 mm^2 area of a hemacytometer into 400 equal squares and counted the yeast cells. Later, Fisher (1935) used the spatial analysis in agricultural area. Yates (1938) searched about the influence of spatial correlation at the randomization process, where completely random regionalized variables are considered for modeling purposes.

This chapter is concerned with the spatial prediction of the ReV and two of the most important procedures, namely the optimum interpolation and Kriging models, are presented in detail.

5.2 Spatial Estimation of ReV

The spatial interpolation of earth sciences data aims at estimating the ReV value at a given site based on the nearby observations (measurements) sites (Fig. 5.1). Most often the input variables are longitudes and latitudes (easting and northing) and the ReV is one of the earth sciences variables, i.e., triplicate as mentioned in Chapter 2.

This is a problem of operational earth sciences that is regularly encountered in the spatial estimation procedures. The 2D statistically optimum interpolation models are useful in the analysis and modeling of ReVs, where spatial dependence functions (SDF) are used for depicting the radius of influence in the case of isotropic ReVs or area of influence for anisotropic ReVs variability (Chapters 2 and 4). One of the fundamental, effective, and objective analysis is the transformation of measurements from irregularly distributed sites to regular gridded networks for use in the numerical prediction schemes or mapping methodology through spatial models such as the Kriging methodology, which assigns a spatial estimation value to any point without measurement through a suitable estimation procedure. Hence, in practice, there are twofold purposes in describing the spatial variability in earth science ReVs by objective analysis.

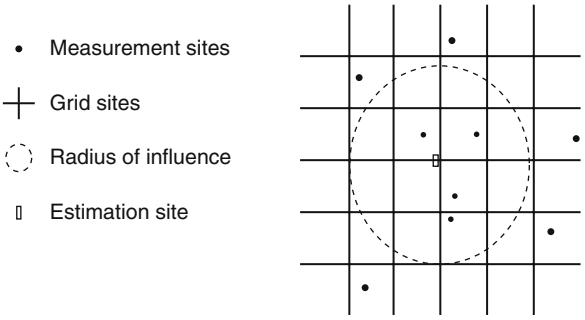

Fig. 5.1 Elements in a spatial estimation

1) A regular grid of nodes serves as the initial data for numerical forecast models or mapping methodologies.
2) Coordinates of a rather great number of iso-line points help to construct equal-value lines (contour lines) such as isohyetal maps.

In any spatial prediction, the problems are with spatial (areal and elevation) modeling and with the transfer of information from available irregular measurement sites to regular grid nodes or to any desired point of interest. In general, ReV at any location bears some relationship to nearby locations. The strength of the relationship normally decreases as the distance between the location increases (Chapter 4, Section 4.10). There are various spatial data modeling techniques for data interpolation from the measurement sites to any desired point as follows (Schlatter, 1988).

1) Surface fitting methods: The first objective analysis method in meteorology was the surface fitting type devised by Panofsky (1949). In this method, the analysis value is represented as a continuous mathematical function, which fits irregularly scattered measurements. Among these methods are the polynomial interpolation (Panofsky, 1949), orthogonal polynomials (Dixon, 1969, 1976); splines (Fritsch, 1971), and finally spectral approaches (Flattery, 1970).
2) Empirical linear interpolations: The value of any variable at a particular location is estimated as a weighted sum of observations. Among such interpolation techniques are the iterative successive correction methods (Cressman, 1959; Barnes, 1964), which are already explained in Chapters 2 and 4.
3) Statistical objective analysis: These are estimation methods at any desired point where spatial correlation (dependence) structure determines the weights applicable to each observation. The major approaches in this category are the optimal interpolation (Gandin, 1963), the covariance models for atmospheric variable (Buell, 1958), adaptive filtering (Kalman, 1960; Şen, 1980, 1983), and recently the CSV method (Şen, 1997).
4) Variational techniques: These include more mathematical abstractions than other methods and two of them are the incorporation of dynamic constraints (Sasaki, 1958) and the fitting models to data at different times (Ledimet and Talagrand, 1986).
5) Geostatistical approaches: These models are based on the classical SV and Kriging techniques (Matheron, 1963; Clark, 1979; Journel and Huijbregts, 1978). Various alternatives of SV are presented by different authors (see Chapter 4),
6) Objective modeling: The analysis of ReV produces the optimum solution in the sense that interpolation error is minimized on the average. This method allows for the extraction of as much useful information as possible from the measurements. The problems associated with optimum interpolation analysis can be summarized as follows.

    a) It requires knowledge of covariance, which is often not known and thus its estimate is necessary from the available data. Establishing such an estimate is often fraught with difficulty as a host of local factors are involved.

b) Essentially, one must determine the priority about which station measurements are significantly correlated with the value at the point of estimation (interpolation), i.e., one must determine a region of influence around the interpolation point as in Fig. 5.1.

5.3 Optimum Interpolation Model

A technique commonly used for meteorological analysis is the "optimal interpolation model" (OIM), which is very similar to Kriging method except that some prior knowledge of climatological (obtained from a 6 or 12 hour numerical forecast) background fields are assumed. Apparently, the optimum interpolation method was suggested first by Eliassen (1954). However, Gandin (1963) developed the method over a number of years and his name is associated with it in the literature. Eddy (1964) was also one of the early developers of this method. Detailed literature review on this subject is given by Şen and Habib (2000).

In any numerical analysis technique the main idea is that estimation at any point is considered as a weighted average of the measured values at irregular sites. Hence, if there are Z_i^o (i = 1, ..., n) observation stations with the number of prediction site k, then the general prediction in the form of weighted average formula becomes similar to Eq. (2.27) as

$$Z_k^a = \frac{\sum_{i=1}^{n} W_i Z_i^o}{\sum_{i=1}^{n} W_i}, \tag{5.1}$$

where Z_k^a is the estimate value and W_i's show the weightings between the i-th site and the grid point k (Fig. 5.1). In the literature, all weighting functions that are proposed by various researchers appear as functions of the distance between the sites only. The major drawbacks of such weighting functions are already presented in Chapter 2.

OIM assumes that analyses of data are represented by first guess data plus corrections, which are linear combinations of differences between the first guess and the observed data. The coefficients of linear combination are determined statistically so as to minimize the expected square error of data. The coefficients of linear combination are expressed by error covariance matrices of observed and forecast data (estimated data), when forecast data are used as "first guess." Thus the covariance matrix has a great influence on the final estimation. It is assumed that measurements are spatially correlated and such correlations are calculated as in Chapter 4 (Figs. 4.5 and 4.6). This implies that measurements are close together in clusters, i.e., highly correlated, and that as they get farther apart they become independent similar to what has been explained in the SV definition in Chapter 4. Although the method presented here is a fully 2D version of optimum interpolation, similar approach is

applicable to 3D or to multivariate problems. In all OIM the following points should be kept in mind.

1) One of the significant advantages in the use of OIM is the ability to estimate a variability at any site from the observations at adjacent sites.
2) The interpolation weights depend on the statistical structure of the ReVs measured as a sequence of time series and not on the individual measurement values at a given time.
3) The expected analysis errors are produced as a function of the distribution and accuracy of the data.
4) It is more expensive computationally than other commonly used methods. The method is computer intensive as the number of computations and amount of computer storage are concerned.
5) The correlation (dependence) models require a long history of first guess field for he accurate determination of empirical coefficients.
6) The statistical error functions are estimates, not exact values.

Furthermore, the basic assumptions that are embedded in any OIM can be summarized as follows.

1) The measurements have a spatial dependence, which implies that as long as they are close together the spatial dependence is high, otherwise they become more independent.
2) There is no dependence (no correlation) between the measurements and the first guess field errors.
3) OIM as described here may be applied to any scalar field when the correlation and error patterns for that field are known.
4) The field to be analyzed is statistically homogeneous and isotropic.

Consider any grid point, k, with n observations, Z_i^o ($i = 1, \ldots, n$) around it, which will be used to calculate the analyzed value, Z_k^a, at this grid point. The main idea is that Z_k^a is determined as the sum of a first guess value, Z_k^g, at grid point k plus a linear combination of the deviations of the observed values from the first guess values ($Z_i^o - Z_i^g$) (see Fig. 5.2). This is to say that

$$Z_k^a = Z_k^g + \sum_{i=1}^{n} W_i (Z_i^o - Z_i^g), \tag{5.2}$$

where n is the number of stations (in other words, it may also be considered as the number of influencing stations). The W_i's are the interpolation weights; as intuitively mentioned above, one would expect the W_i's to be positive and decrease monotonically with increasing distance from the grid point, k.

Assume that the true value, Z_k^T, can be subtracted from both sides of the above equation. Usually, the true value is not known, but some knowledge may be known

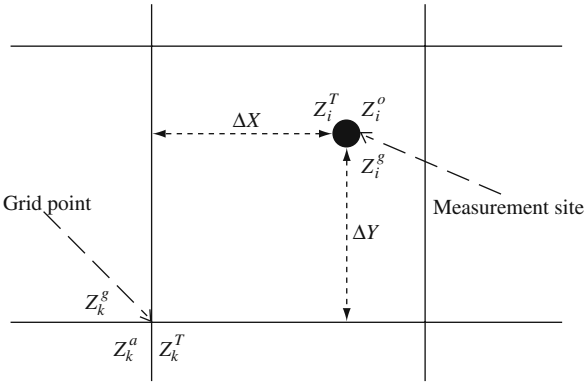

Fig. 5.2 Location of grid point and measurement site

about its statistical parameters, and that will prove useful in the following method. With these considerations, Eq. (5.2) becomes

$$(Z_k^T - Z_k^a) = (Z_k^T - Z_k^g) - \sum_{i=1}^{n} W_i(Z_i^o - Z_i^g). \tag{5.3}$$

The values of the guess fields at each observation location may be determined by using bilinear interpolation. The difference between each observation and corresponding guess values may be computed as

$$Z_i^o - Z_i^g = (Z_i^o - Z_i^T) + (Z_i^T - Z_i^g) = \tilde{Z}_i + \hat{Z}_i, \tag{5.4}$$

where the deviation of the true value Z_i^T from the first guess value at observed station is $\hat{Z}_i$ (guess error at station i); the deviation of true value from the first guess at grid point is $\hat{Z}_k$ (guess error at grid k); and, finally, $\tilde{Z}_i$ denotes the deviation of true value from the observed value at station i (the observational errors at station i), which can be written as

$$\left.\begin{aligned} \hat{Z}_i &= (Z_i^T - Z_i^g) \\ \hat{Z}_k &= (Z_k^T - Z_k^g) \\ \tilde{Z}_i &= (Z_i^o - Z_i^T) \end{aligned}\right\} \tag{5.5}$$

By substituting Eqs. (5.4) and (5.5) into Eq. (5.3), one can obtain

$$(Z_k^T - Z_k^a) = \hat{Z}_k - \sum_{i=1}^{n} W_i(\tilde{Z}_i + \hat{Z}_i). \tag{5.6}$$

Furthermore, the interpolation weights W_i are obtained by condition that the mean square error (MSE) of interpolation is the minimum, which corresponds to the method of least squares. This condition can be expressed as

$$E = \overline{(Z_k^T - Z_k^a)^2} = \text{Minimum}, \tag{5.7}$$

where the over bar denotes an ensemble average in the case of a large grid point number. Insertion of Eq. (5.6) into Eq. (5.7) and evaluation of the square term leads to

$$\begin{aligned} E = &\left\{\overline{\hat{Z}_k - \sum_{i=1}^{n} W_i(\tilde{Z}_i + \hat{Z}_i)}\right\}^2 = \overline{\hat{Z}_k^2} + \sum_{i=1}^{n}\sum_{j=1}^{n} W_i W_j \overline{(\tilde{Z}_i + \hat{Z}_i)(\tilde{Z}_j + \hat{Z}_j)} \\ &-2\sum_{i=1}^{n} W_i \overline{(\hat{Z}_k \tilde{Z}_i + \hat{Z}_k \hat{Z}_i)} \\ &= \overline{\hat{Z}_k^2} + \sum_{i=1}^{n}\sum_{j=1}^{n} W_i W_j (\overline{\tilde{Z}_i \tilde{Z}_j} + \overline{\tilde{Z}_i \hat{Z}_j} + \overline{\hat{Z}_i \tilde{Z}_j} + \overline{\hat{Z}_i \hat{Z}_j}) \\ &-2\sum_{i=1}^{n} W_i (\overline{\hat{Z}_k \tilde{Z}_i} + \overline{\hat{Z}_k \hat{Z}_i}), \end{aligned} \tag{5.8}$$

where $i = 1, \ldots, n$ and $j = 1, \ldots, n$. By assuming that there is no dependence (no correlation) between the observational and the first guess field errors, one can obtain

$$\overline{\tilde{Z}_i \hat{Z}_j} = \overline{\hat{Z}_i \tilde{Z}_j} = \overline{\hat{Z}_k \tilde{Z}_i} = 0. \tag{5.9}$$

Consideration of these equations renders Eq. (5.8) to a simplified form as

$$E = \overline{\hat{Z}_k^2} + \sum_{i=1}^{n}\sum_{j=1}^{n} W_i W_j (\overline{\tilde{Z}_i \tilde{Z}_j} + \overline{\hat{Z}_i \hat{Z}_j}) - 2\sum_{i=1}^{n} W_i \overline{(\hat{Z}_k \hat{Z}_i)}, \tag{5.10}$$

which can be rewritten as follows:

$$E = \gamma_{kk} + \sum_{i=1}^{n}\sum_{j=1}^{n} W_i W_j (\gamma_{ij} + \tilde{\gamma}_{ij}) - 2\sum_{i=1}^{n} W_i \gamma_{ik}. \tag{5.11}$$

The elements in this last expression are defined as

$$\gamma_{kk} = \overline{(Z_k^T - Z_k^g)^2}, \tag{5.12}$$

which represents the variance of the guess error at the grid point k, and

$$\gamma_{ij} = \overline{(Z_i^T - Z_i^g)(Z_j^T - Z_j^g)} \tag{5.13}$$

is the covariance of the guess error at location i and with guess error variance at location j as

$$\gamma_{ki} = \overline{(Z_k^T - Z_k^g)(Z_i^T - Z_i^g)}, \tag{5.14}$$

which is the guess error covariance at the grid point k with the guess error at location i,

$$\tilde{\gamma}_{ij} = \overline{(Z_i^o - Z_i^T)(Z_j^o - Z_j^T)}. \tag{5.15}$$

This is the covariance of the observation error at the location i with the observation error at station j.

The statistical interpolation is a minimum variance estimation procedure and attempts to minimize the expected analysis error variance. The problem is to find the weights W_i that minimize the variance. Hence, differentiating Eq. (5.11) with respect to each of the weightsW_i and equating the result to zero after necessary algebraic manipulations lead succinctly to

$$\sum_{i=1}^{n} W_i(\gamma_{ij} + \tilde{\gamma}_{ij}) = \gamma_{kj}. \tag{5.16}$$

Interpolation of Eq. (5.2) using weights from Eq. (5.16) is called "optimum interpolation." However, these weights are optimal only if the observation and first guess error covariance are correct. On the other hand, if the assumed observation and first guess error covariance are not correct, then Eq. (5.7) is not minimized strictly. In this case, the interpolation weights in Eq. (5.10) are not optimal and it is called statistical interpolation.

Multiplication of Eq. (5.16) by W_j and summation for j =1, . . ., n, leads to

$$\sum_{i=1}^{n}\sum_{j=1}^{n}(\gamma_{ij} + \tilde{\gamma}_{ij})W_iW_j = \sum_{j=1}^{n} W_j\gamma_{kj}. \tag{5.17}$$

Finally, subtraction of this expression from Eq. (5.11) gives the minimum interpolation error as

$$E = \gamma_{kk} - \sum_{i=1}^{n} W_i\gamma_{ik}. \tag{5.18}$$

5.3.1 Data and Application

The region of application is Turkey, with stations as shown in Fig. 5.3. The grid for this analysis is on a polar stereographic projection oriented along the 35E longitude line (Habib, 1999). There are 16 columns and 8 rows in the array, for a total of 128 grid points.

The data employed in this study are the mean monthly precipitation records collected from the statistics published by Turkish State Meteorological Office.

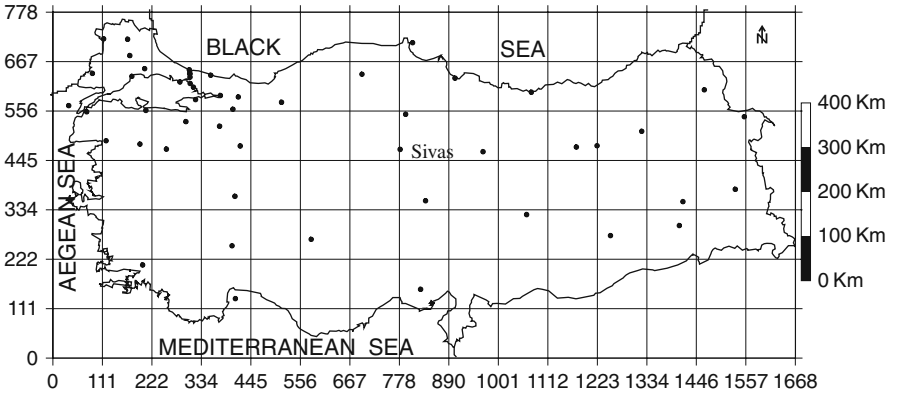

Fig. 5.3 Grid points and measurement sites in Turkey

Fifty-two stations for 30-year period from 1960 to 1990 are selected with monthly rainfall measurements.

The spatial scatter distribution of these measurement sites is given in Fig. 5.4, which shows an irregular pattern. In general, the transfer of information from the measurement sites to grid points is necessary for any type of modeling as numerical solution or mapping the ReVs. Here each site monthly precipitation time series, which may also be monthly average groundwater levels, groundwater quality values (calcium, magnesium, sodium, potassium, sulfate, bicarbonate, chloride, nitrate, total dissolved solids, electric conductivity, etc.) and alike.

In practical applications of the optimum interpolation such as the analysis of rainfall, one uses the climatological mean as the first guess value. Hence, the following expression is considered for the interpolation point value (Habib, 1999).

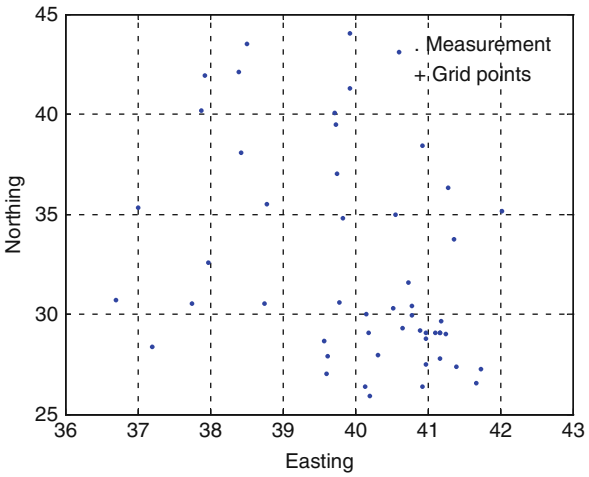

Fig. 5.4 Spatial distributions of the data points

$$Z_k^a = \overline{Z}_k + \sum_{i=1}^{n} W_i(Z_i^o - \overline{Z}_i), \tag{5.19}$$

where $Z^a{}_k$ and $Z^0{}_i$ are the calculated and observed rainfall values corresponding to the arithmetic averages of $\overline{Z}k$ and $\overline{Z}i$, respectively, at interpolation point k and observation stations $i = 1, 2, \ldots, n$, and W_i's are the interpolation weights. In order to calculate these weights, the interpolation formula can be obtained by multiplying both sides of Eq. (5.19) by $(Z^0{}_j - Z_j)$ and taking the expectation leading to

$$\sum_{i=1}^{n} W_i \rho_{ij} = \rho_{kj}, \tag{5.20}$$

where ρ_{ij} is the spatial correlation coefficients between stations i and j, and ρ_{kj} between stations j and k. This equation is valid in the case when $E(Z_k) = E(Z_k{}^a)$, which implies unbiased estimator. In short, interpolation weights, W_i, are dependent on the statistical structure of the spatial correlation function (SCF) of the rainfall records at irregular sites. Once the SCFs are obtained from the available data, then the value of ρ_{kj} can be read from this function depending on the distance between k and j, and, consequently, the only unknowns in Eq. (5.20) are the weights that can be calculated from the set of n linear equations. The correlation functions are presented in the previous chapter (Figs. 4.5 and 4.6). The expected analysis error, ε_{kj}, at grid point k, which results from the introduction by using information at location j, can be expressed as (Habib, 1999)

$$\varepsilon_k = 1 - \sum_{i=1}^{n} W_i \rho_{ki} = 1 - \rho_{kj}. \tag{5.21}$$

Most often in practice, $0 < \rho_{kj} < 1$ and therefore $0 \leq \varepsilon_{kj} \leq 1$. It is obvious that the expected error does not depend directly on the observed values but again on the spatial statistical structure of the rainfall amounts. Under the light of the aforementioned discussion, the following OIM steps are necessary for practical applications.

1) Specify the geographical locations (longitude and latitude) of interpolation points.
2) Specify the estimation locations.
3) Compute a first guess field value (climatologic means, i.e., arithmetic averages) for each station locations.
4) Compute the background error correlations, which correspond to the differences between observed and average values.
5) Find a suitable model for the background error SCF.
6) Select the measurement sites that will influence the interpolation point.
7) Solve the system in Eq. (5.20) and obtain the interpolation weights.

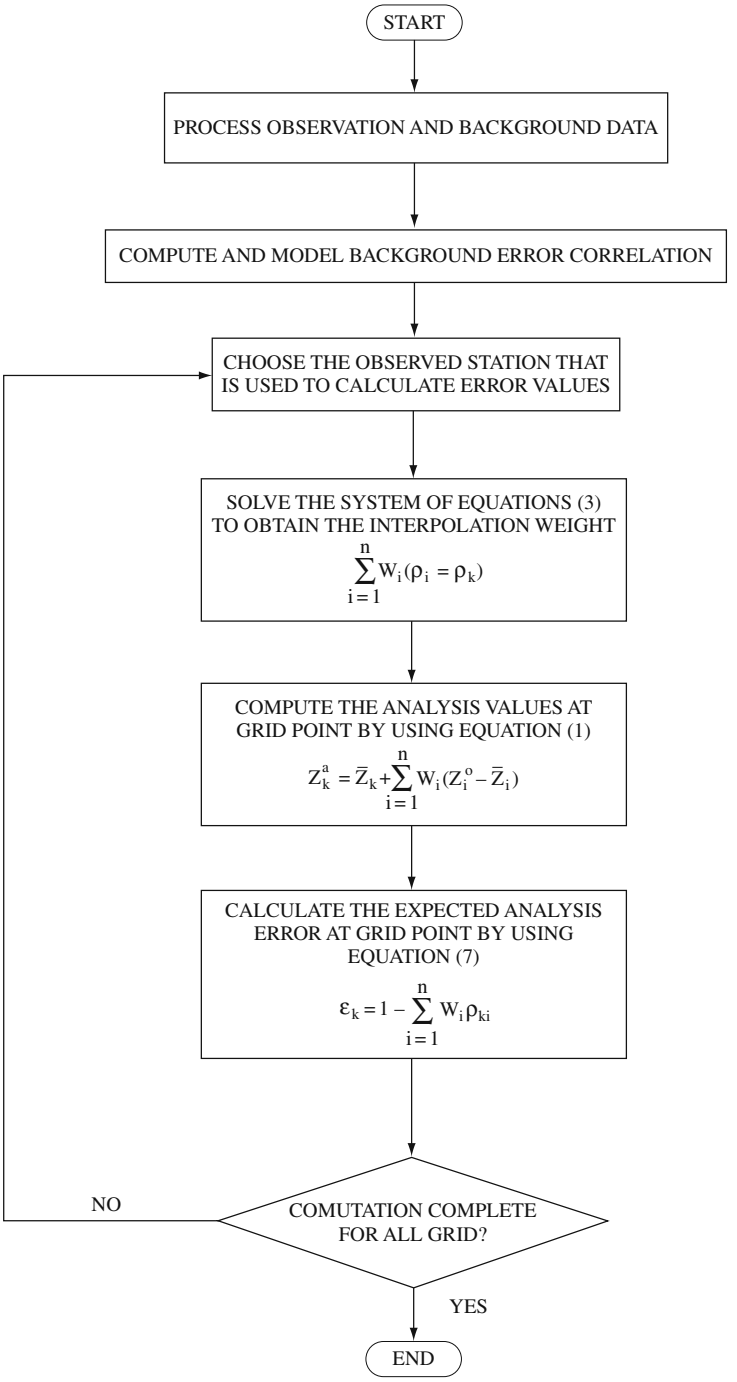

Fig. 5.5 OIM execution steps

8) Compute the interpolation point value by using Eq. (5.19).
9) Calculate the expected analysis error at the interpolation point by using Eq. (5.21).
10) Repeat steps (5) to (8) for all desired interpolation points. Figure 5.5 shows the necessary steps in the execution of a regional modeling procedure according to OIM approach.

5.3.1.1 Spatial Correlation Function

Although there are several models to represent the correlation by continuous functions, the basic modeling form is adapted as "the negative-exponential" for all monthly spatial correlation types. The full correlation array is reduced to distance-interval-averaged values (Fig. 4.6). Hence, most of the heterogeneity is averaged out in the computed lag-correlation and the computation time is greatly reduced. In general, the negative-exponential model has the following mathematical expression,

$$\mathrm{R(d)} = \mathrm{a} + \mathrm{be}^{-\mathrm{d/c}}, \tag{5.22}$$

where R(d) represents the theoretical SCF and d is considered as the distance between i-th and j-th stations; a, b, and c are the model parameters. These parameters are determined by fitting a mathematical function to the array of computed correlation versus corresponding distances between measurement sites. Each one of the monthly average SCF is fitted to this model by employing the ordinary least squares regression approach. The resulting parameter values for each month are presented in Table 5.1, in addition to the overall monthly average parameter values.

All the monthly spatial correlation functions (SCF), say for Sivas station (see Fig. 5.3), are confined between January and July as one can see from Fig. 5.6. It

Table 5.1 Spatial correlation model parameters

Month	*a*	*b*	*C*
January	−0 .15553	0.90883	1352.15221
February	0.27266	0.55969	270.50807
March	0.00000	0.85671	575.8087
April	0.12362	0.71309	255.97296
May	0.06599	0.78690	220.55975
June	−0.06992	0.62878	506.51055
July	0.11930	0.65853	131.18509
August	−0.08718	0.61655	653.76575
September	−0.29293	0.95016	909.51275
October	0.11815	0.65535	370.6699
November	−0.33159	0.82909	1707.53125
December	0.03030	0.51511	636.63236
Average	−0.01650	0.72650	623.2176

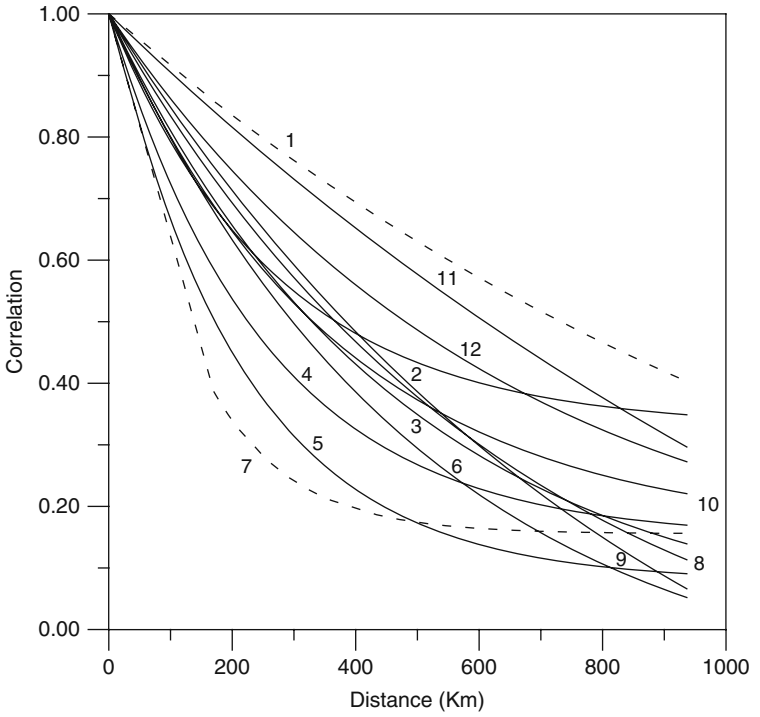

Fig. 5.6 Spatial correlation function of Sivas city for different months

is also clear from this figure that summer months have less SCF values than winter months.

This is due to the fact that in this region cyclonic rainfall types are dominant in winter whereas convectional type of rather local rainfall occurs in summer season. Of course, orographic rainfall effects play more effective role in winter season than summer. However, it is not possible to identify this type of rainfall from the SCFs. In Fig. 5.6 one can note that the maximum continuity appears in winter months. This is due to the fact that in this region frontal rainfall types are dominant in winter whereas conventional type of rather local rainfall occurs in summer season.

At large distances, February has strong persistent SCF, which implies that in this month there are cyclonic rainfall types because they cover large areas. Similar trends are also observed in April and May. On the other hand, comparatively steeper SCFs indicate convectional rainfall types, which appear over rather smaller area during summer months.

It is possible to show the variation of SDF for any measurement station as the center of concentric contour. The extreme and average SCFs are shown for Sivas city as given in Fig. 5.7.

The benefit from these figures is that at any given month of the year and a given correlation level, say 0.050, it is possible to determine the influence area around the

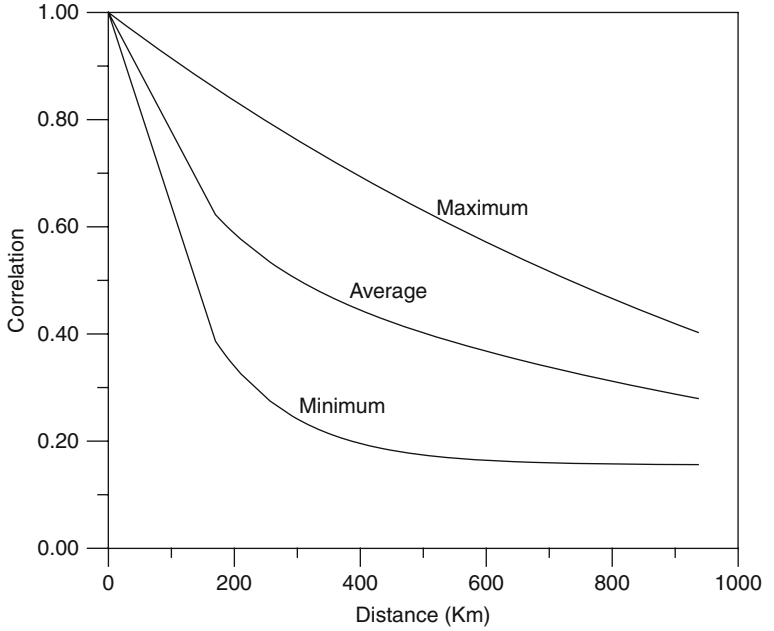

Fig. 5.7 Sivas correlation contour lines

station. On the average, the minimum correlation value for 200 km (other distances have similar interpretations) appears in July and the maximum correlation value is in January. It is also clear from this figure that summer months have less spatial correlation values than winter months. Table 5.2 shows the values of the percentage of the variance of observational error, which has a minimum of 14.32 in March and a maximum of 50.46 in November. Similarly, the correlation of the observed values varies between a minimum of 0.4975 in November and a maximum of 0.8567 in March.

It is possible to find the correlation $\rho(d)$ of the true (first guess) values of the meteorological variables at distance d as

$$\rho(d) = \frac{R(d)}{R(0)}, \tag{5.23}$$

where R(d) and R(0) are the correlations of the observed values at d and at zero distances, respectively. This equation is used to calculate the correlation of the first guess (true) values of the ReVs. The negative-exponential model in Eq. (5.22) at zero distance can be defined as

$$R(0) = a + b, \tag{5.24}$$

Table 5.2 Some pertinent statistics

Month	R (0)	Percentage of σ_e^2
January	0.7533	24.67
February	0.8323	16.76
March	0.8567	14.32
April	0.8367	16.32
May	0.8528	14.71
June	0.5588	44.11
July	0.7775	22.24
August	0.5293	47.06
September	0.6572	34.27
October	0.7735	22.65
November	0.4975	50.25
December	0.5454	45.46
Average	0.7059	29.40

and, finally, by substituting Eqs. (5.22) and (3.24) into Eq. (5.23) it is possible to obtain

$$\rho(d) = \frac{\left(a + be^{-d/c}\right)}{a + b}. \tag{5.25}$$

This expression can be used for the indirect evaluation of the correlation of the first guess (true) values of ReVs by means of extrapolating the correlation of the observed values at zero distance $d = 0$ as shown in Fig. 5.8, or by using Eq. (5.23) or Eq. (5.25) for finding the correlation of the true values.

5.3.1.2 Expected Error

The expected analysis error is a by-product of the OIM analysis procedure as already stated in Eq. (5.18). It is computed at each analysis point and is a function of the amount, quality, and distribution of the data near each point. If no data are present, the expected error remains unchanged from its initial value. The calculation and modeling of errors result in an analysis that is not necessarily optimum (Lorenc, 1981). The expected error is thus a measure of what the analyzer "thinks" the error is (Schlatter and Branstator, 1987).

Figure 5.9 includes maps of the expected error of rainfall calculated from Eq. (5.18) for whole months at Sivas station. It is obvious that there are a number of areas where expected error changes quite rapidly. For instance, there is a bull's-eye feature in all months, which is enclosed by the minimum expected error. There is also a similar area of less circular contours surrounding the region at the north center of the study area.

At the first glance, it is possible to depict that contours are less densely occurring over terrestrial area during September–February winter period. However, the

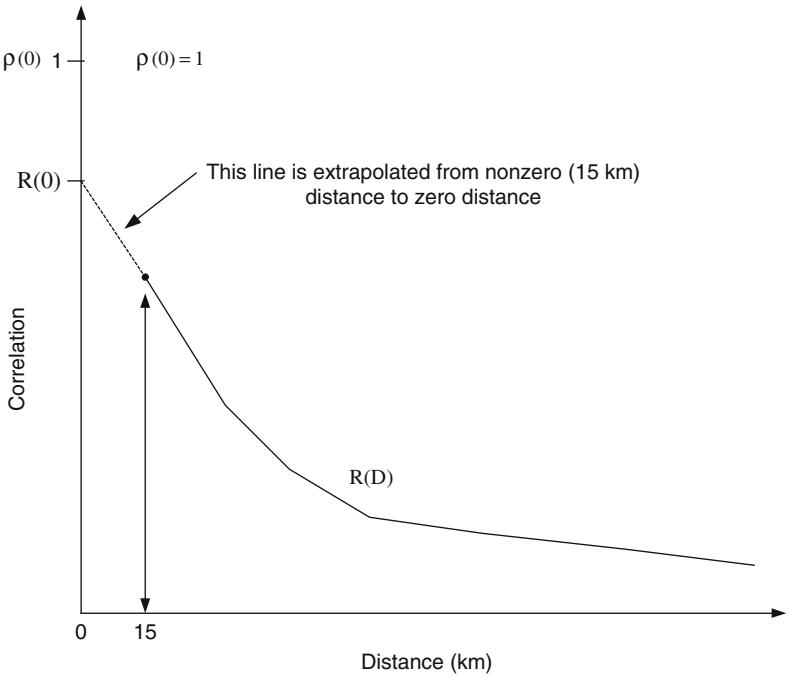

Fig. 5.8 Estimation of zero intercept value

contours are very dense from March to October. The reason for such a digression is due to the fact that the rainfall occurrences are comparatively more sporadic (i.e., regionally random) during March–October duration. This is also because the convective rainfall occurrences appear almost independently from each other. However, areal continuity of winter rainfall is a signature of cyclonic weather movements. Such continuity results in comparatively very small expected error amounts, say for instance in January (Fig. 5.9), where errors vary between 0.05 and 0.15 over the Anatolia within Turkey. On the contrary, in July (Fig. 5.9) error band varies between 0.20 and 0.70. Table 5.3 shows the relation between expected mean square error (MSE) and months.

One can note that the maximum expected error appears in summer months (for example, in July 0.3480), because the rainfall has more discontinuous ReV as explained above. On the other hand, the minimum expected error is in winter months (for example, in January 0.0193), because the rainfall in this season is areally extensive and more continuous.

5.3.1.3 Data Search and Selection Procedure

In order to find the weights W_i, the inversion of the correlation (covariance) matrix must be computed at each grid point. The size of the correlation matrix is directly

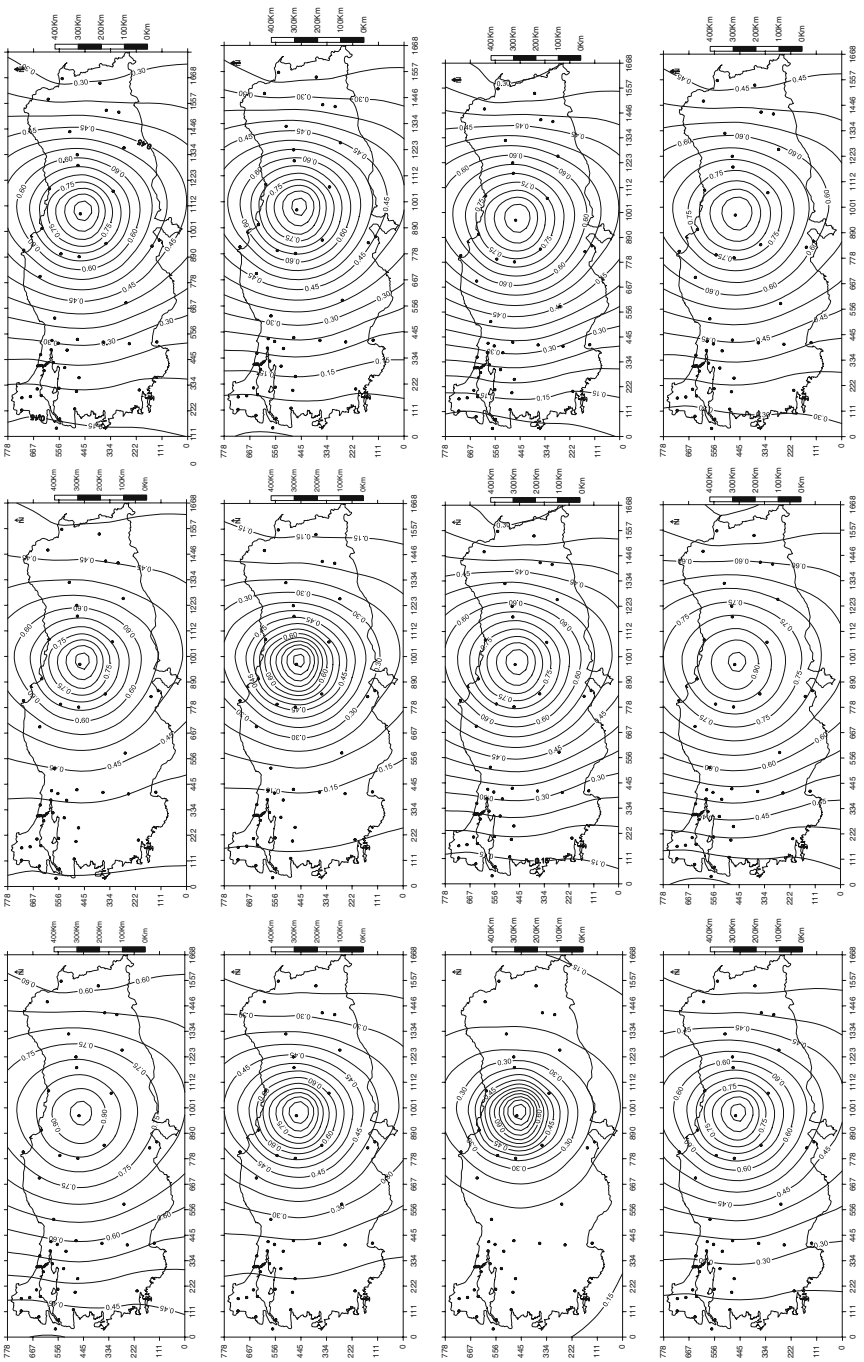

Fig. 5.9 Equal correlation lines between Sivas city and other stations

Table 5.3 Monthly expected errors

Month	MSE
January	0.0193
February	0.0935
March	0.0834
April	0.1700
May	0.2500
June	0.1000
July	0.3480
August	0.1200
September	0.0657
October	0.0994
November	0.0238
December	0.0463
Average	0.1141

related to the number of observations permitted to influence each grid point. The choice of a search strategy that controls the stations which are included in the interpolation procedure is an important consideration in any approach to OIMs.

The most common approach in choosing the stations that contribute to the interpolation is to define a search neighborhood within which all available stations will be used. Herein, a simple search strategy is adapted using all station within a circular search neighborhood with a limited radius of influence.

Meleschko and Prigodich (1964) have shown that the interpolation error reaches a minimum at about six to eight measurements and shows no further improvement with the inclusion of more sites. In order to fix this idea with the data at hand, the change of expected MSE is plotted versus the number of neighboring station for each month. However, it appeared that such graphs are very similar to each other. It is objectively seen from Fig. 5.10 that on the average the number of influencing

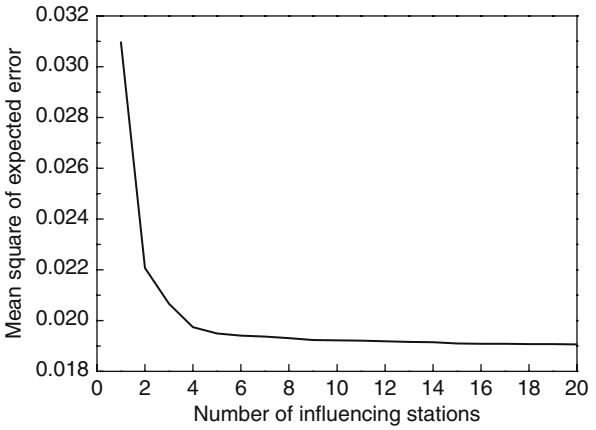

Fig. 5.10 Relationship between the number of influencing stations

stations does not change significantly above four sites. For more station numbers, the expected error mean square remains on almost the same minimum level.

5.3.1.4 Cross-Validation of the Model

The accuracy of OIM is investigated with the help of numerical experiments from the surrounding sites and in comparison to the interpolated values with the measurements, (Gandin, 1965). Similarly, cross-validation techniques allow comparison of estimation and true values using only the information available in the measurements (Isaaks and Srivastava, 1989). In a cross-validation technique, the interpolation method is tested at the measurement site, and the measurement value at a particular station is discarded temporarily from the surrounding sites. Once the estimate is calculated, it is possible to compare it with the measurement value that is initially removed from the station. This procedure is repeated for all available sites, with the comparison of observed, interpolated, and actual values by using simple statistical parameters such as means and standard deviations. The statistical parameters of the comparison between various estimations methods and of the true values are summarized in Table 5.4 for January 1984.

In general, the difference between the average estimate from the OIM and the true average reflects a tendency toward over-estimation or under-estimation. However, in this case the analysis method has a slight tendency toward over-estimation, as seen from Table 5.4. The estimations have less variability than measurements. However, this reduced variability of analysis values is often referred to as smoothing. Therefore, the measurements are less smoothed than the analysis values. A scatter plot of measurements versus estimations provides additional evidence on how well an estimation method has been performed. Figure 5.11 shows the scatter plot of measurements versus estimations for January 1984, which indicates that there is a good relationship between estimations and measurements, especially for less than 200 mm. This is also supported by the root MSE, which is 29.9, and the mean percentage error is -9.07%. Furthermore, the square of the correlation, which is a measure of the variance explained by the model, is equal to 0.76.

In order to see the correspondence matching between measurements and estimations as well as monthly rainfall amounts, the monthly statistical parameter variations are presented in Figs. 5.12 and 5.13. It is seen that on the basis of averages,

Table 5.4 Univariate statistics of optimum interpolation analysis

Parameters	Observation	Estimation
n	52	52
Mean	76.6	74.70
Minimum	5	0
Maximum	361	266.9
Range	356	267
Variance	3407.60	2905.61
Std. dev.	58.37	53.90

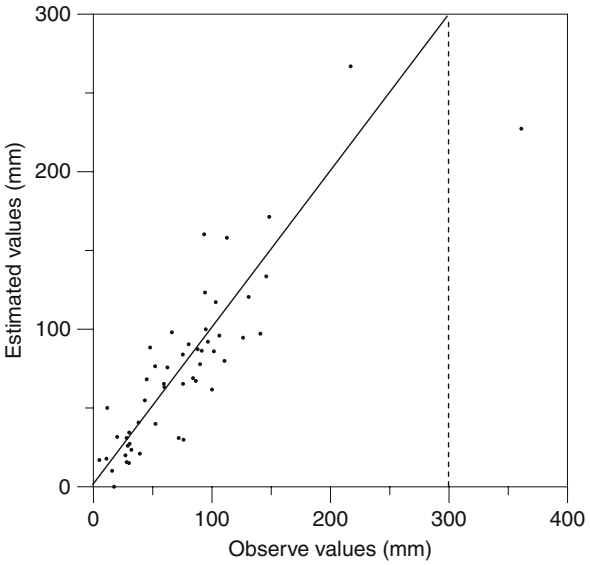

Fig. 5.11 Scatter plot of observed versus estimated values for January 1984

measurements and estimations are very close to each other with less than 1% error. Although there are more discrepancies for monthly standard deviations, generally 2.5% but high errors appear in November and December.

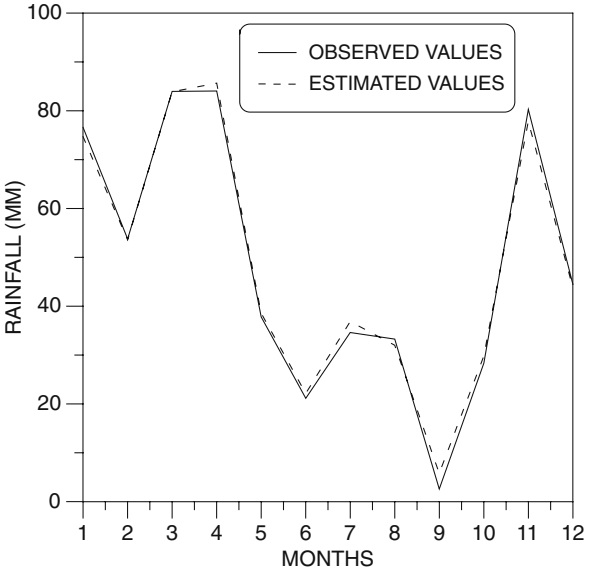

Fig. 5.12 Arithmetic mean of observed and predicted monthly values

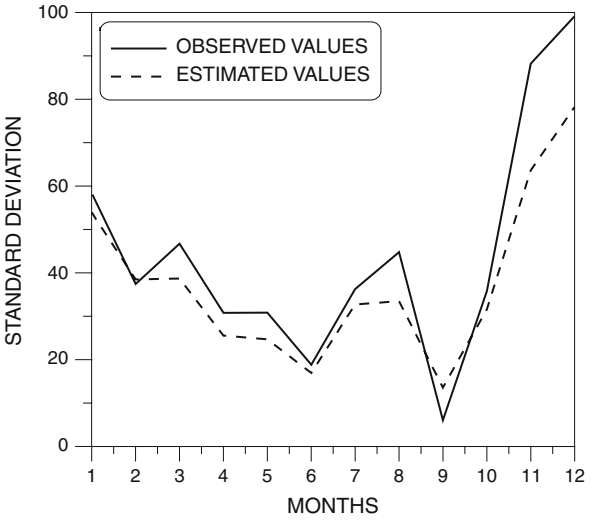

Fig. 5.13 Standard deviation of observed and predicted monthly values

5.4 Geostatistical Analysis

It is a branch of applied statistics with the original purpose of spatial data processing for estimating changes in ReVs. However, the principles have been applied to a variety of areas in geology and other scientific disciplines. A unique aspect of geostatistics is the use of ReVs, which are variables that fall between random and completely deterministic behaviors (Chapter 1). ReVs describe phenomena with geographical distribution (e.g., elevation of ground surface) and exhibits spatial continuity, which is not always possible to sample at every location. Therefore, unknown values must be estimated from the data taken at specific locations. The size, shape, orientation, and spatial arrangement of the sample locations are termed as the support and influences the capability to predict the unknown samples. If any of these characteristics change, then the unknown values also change. The sampling and estimation of ReVs are done so that a pattern of variation in the phenomenon under investigation can be mapped, such as a contour map for a geographical region. In addition to spatial and temporal variation in nature, spatial and temporal dependence or continuity also occurs. Geostatistics include a set of statistical procedures that can be used to analyze and model spatial relationships in nature. The spatial variation is somewhat similar to the time variation in some properties; time observations are dependent and occur in equally spaced time intervals in 1D, whereas the spatial observations are dependent and occur in 2D or 3D and the distance between points are not necessarily equal intervals as they are in time variations. In earth sciences, most of the natural phenomena behave simultaneously in space and time, as soil moisture content, water level, and precipitation data may consist of long time series at various locations. The spatio-temporal variation of the natural phenomena implies a significant amount of

uncertainty. Moreover, this variation is, in general, non-homogeneous in space and non-stationary in time.

Matheron (1963) was the first to use the term "geostatistics," which was defined by him as "the application of the formalism of random function to the reconnaissance and estimation of natural phenomena." The basis of the method is the ReV theory and concepts of this theory can be split into two main successive steps.

1) Establish the theoretical basis for expressing the structural properties of a natural phenomenon in a useful mathematical form as SV or CSV.
2) Provide a particular means for solving various problems of estimation such as the Kriging methodology, which guarantees a solution to the estimation problem (Kriging) and deals with the ReV by using the probabilistic theory of random function.

By now, however, there are a number of excellent books on the subject, including both introductory (Clark, 1979) and advanced aspects (David, 1977; Journel and Huijbregts, 1978). The classical parametric and non-parametric geostatistics are introduced recently for application in the field of earthquake ground motion evaluation (Glass, 1978; Carr and Glass, 1984, 1985; Carr et al., 1985).

Almost all variables encountered in the earth sciences can be regarded as ReVs. For seismic zonation this is an ideal one in describing earthquake ground motions. Each observation of ground motion can be considered simply as a unique realization of an Rev, which adequately represents local random behavior tempered by global attenuation. Furthermore, provided that a valid SV can be developed, Kriging is well suited for the estimation process to result in data regionalization.

5.4.1 Kriging Technique

Geostatistics, which is also referred as ReV, was basically developed for statistical study of the natural phenomena in mining field, including other spatial phenomena in earth sciences (Matheron, 1963; Davis, 1986). The natural phenomena that have spatial distribution vary from one place to another with apparent continuity structure. The first step in geostatistics is to study and determine the spatial structure and dependence from the measurement characteristics of the natural phenomena (Chapter 4). The spatial structure can be established by SV, CSV, or PCSV as convenient. Using the underlining generation structure, it is possible to estimate the characteristics at unsampled locations and extend findings of the regional behavior in natural phenomena through Kriging techniques.

In any geostatistical modeling there are two stages as the estimation of SV (CSV or PCSV) from a given set of regionalized data for the extraction of spatial dependence and then Kriging methodology, which provides estimates for locations where no data are available. The SV is the source of information used in Kriging to achieve optimal weighting functions for mapping. Kriging uses theoretical SV

in calculating estimates at a set of grid nodes. These Kriging estimates are best-linear-unbiased-estimates (BLUE) of the ReV at a set of locations, provided that the surface is stationary and the correct form of the theoretical SV has been determined (Chapter 4).

In many disciplines such as petroleum exploration, mining, groundwater, and water pollution analysis, data are available at a set of predetermined spatial locations (water and oil wells, meteorology stations, etc.). The purpose is to make regional estimation at any location based on the available data at these locations. It is necessary to often have maps based on a regular grid and the estimations are used to produce 2D contour maps or 3D surface plots. In theory, only Kriging method of grid generation can produce better estimates (in the sense of being unbiased and having minimum error). In practice, the effectiveness of the technique depends on the correct specification of several parameters that describe the SV and the model of the drift (regional trend). However, because Kriging is robust, even with a naive selection of parameters it will do no worse than conventional grid estimation procedures (Chapter 2).

The price that must be paid for optimality in estimation is computational complexity compared to the techniques presented in Chapter 3. A large set of simultaneous equations must be solved for every grid node estimated by Kriging. Therefore, computer run times will be significantly longer if a map is produced by Kriging rather than by conventional gridding. Kriging can be computationally very intense but increasingly available in software packages, and it is the best method for many purposes. In addition, an extensive prior study of the data must be made to test for stationarity, determine the form of the SV, set the neighborhood size, and select the proper order of the drift, if it ever exists. These properties are not independent and because the system is underdetermined, trial-and-error experimentation may be necessary to determine the best combination. For this reason, to warrant the additional costs of analysis and processing, Kriging probably should be applied in those instances where the best possible estimates of the surface are essential, the data are of reasonably good quality, and the estimates of the error are needed.

5.4.1.1 Intrinsic Property

Mathematically speaking, let x be a point in space and Z(x) the value of the function at point x. It is usually highly variable and non-continuous, and therefore cannot be estimated directly. Thus the structure with variation will be studied by examining its increment. The basic idea of the theory is to consider the function Z(x) as one realization of random function from the exhaustive ensemble. This is tantamount to assuming a well-defined and unique sequence of numerical values into a realization of random process. Only one realization of that process is available and the problem is to find the characteristics of the ReV in order to make the estimation of unknown points possible. Obviously, it is not rigorously possible to infer the probability law of any random function from its single realization, because it has limited finite number of sample points. Thus, many realizations, $Z_1(x)$, $Z_2(x)$, . . ., $Z_k(x)$ of the ReV are required for identifying the probability law. In order to render the situation into a

practically tractable one, the assumptions of spatial homogeneity and stationarity are needed. An ReV is said to be strictly stationary if any conventional statistical properties of the medium such as the mean, variance, covariance do not change with distance. This assumption is seldom encountered in natural phenomena. Therefore, an ReV is to be first-order stationary when the random variable has the same mean value irrespective of location. However, in the linear geostatistics, it will be enough to assume first of all that the weak or second-order stationarity exists. The second-order stationarity assumption consists of two following conditions.

1) The arithmetic average, m (expected value for any term), value of the ReV is the same all over the area,

$$\mathrm{E}\left[\mathrm{Z}(\mathrm{x})\right] = \mathrm{m} \tag{5.26}$$

or equivalently,

$$\mathrm{E}\left[\mathrm{Z}(\mathrm{x}) - \mathrm{Z}(\mathrm{x}+\mathrm{d})\right] = 0. \tag{5.27}$$

2) The spatial covariance of the ReV is the same all over the field of interest.

$$\mathrm{Cov}\left\{\left[\mathrm{Z}\left(\mathrm{x}\right) - \mathrm{m}\right]\left[\mathrm{Z}\left(\mathrm{x}+\mathrm{d}\right) - \mathrm{m}\right]\right\} = \mathrm{Cov}\left(\mathrm{d}\right), \tag{5.28}$$

where d is the distance separating between two sites at locations x and x + d.

If it is assumed that for every d this spatial covariance is independent of the location, then the second-order stationarity is valid. By holding the full second-order stationarity, the covariance Cov(d) approaches the variance, σ_Z^2 of the random variable as $\mathrm{d} \to 0$,

$$\mathrm{Cov}\left(0\right) = \left\{\left[\mathrm{Z}\left(\mathrm{x}\right) - \mathrm{m}\right]\left[\mathrm{Z}\left(\mathrm{x}\right) - \mathrm{m}\right]\right\} = \mathrm{E}\left\{\left[\mathrm{Z}\left(\mathrm{x}\right) - \mathrm{m}\right]^2\right\} = \mathrm{Var}\left[\mathrm{Z}\left(\mathrm{x}\right)\right] = \sigma_Z^2 .$$

A second-order stationarity is, however, really justifiable, and a weaker assumption may be adopted instead. The mean value, m, is always unknown, and may not be constant, so that the variance and covariance cannot be computed directly. It is, therefore, beneficial to define an alternative statistic, which does not require the mean value. For instance, successive difference as in Eq. (5.27) may be zero, but its square is not essentially zero. Considering these characteristics, a consistent set of assumptions weaker than second-order stationarity have been made and called by Matheron (1963) as the "intrinsic hypothesis," which subsumes the following expressions.

$$\mathrm{Var}\left[\mathrm{Z}(\mathrm{x}) - \mathrm{Z}(\mathrm{x}+\mathrm{d})\right] = \mathrm{E}\left\{\mathrm{Z}\left(\mathrm{x}\right) - \mathrm{Z}\left(\mathrm{x}+\mathrm{d}\right) - \mathrm{E}\left[\mathrm{Z}\left(\mathrm{x}\right) - \mathrm{Z}\left(\mathrm{x}+\mathrm{d}\right)\right]^2\right\}$$

Consideration of Eq. (5.27) leads to

$$\mathrm{Var}\left[\mathrm{Z(x)} - \mathrm{Z(x+d)}\right] = \mathrm{E}\left[\mathrm{Z(x)} - \mathrm{Z(x+d)}\right]^2 = 2\gamma\,(\mathrm{d})\,, \tag{5.29}$$

where $2\gamma\,(\mathrm{d})$ is the variogram and $\gamma\,(\mathrm{d})$ is the SV or half-variogram. It should be noted that second-order stationarity implies the intrinsic hypothesis, but the converse is not true.

In addition, under the hypothesis of second-order-stationarity, the covariance and SV are two equivalent tools that characterize the autocorrelation between two variables Z(x+d) and Z(x) separated by d as

$$\gamma(\mathrm{d}) = \mathrm{Cov}(0) - \mathrm{Cov}(\mathrm{d}). \tag{5.30}$$

The validity of this expression is true especially if the ReV has a Gaussian (normal) pdf. Estimation of the SV is preferable to estimation of the covariance, because the experimental SV does not require a prior estimate of the population mean. Besides, SV calculation requires a set of measurements with no time variation. Under the same condition, the relationship between the model autocovariance, $\rho(\mathrm{d})$ and SV is

$$\gamma\,(\mathrm{d}) = \sigma_Z^2\left[1 - \rho\,(\mathrm{d})\right]. \tag{5.31}$$

5.5 Geostatistical Estimator (Kriging)

After successful matching of theoretical SV model, one can use Kriging to estimate what weights should be applied to each surrounding point to estimate the value of the ReV at an unknown location (e.g., a grid node, see Fig. 5.1). Kriging calculates the weighted average of neighboring values and assigns it to each grid node. Kriging can also calculate the error variance for each estimated value, which means that it is possible to know what the most likely value is at each location and how likely that it is to be the actual value. In its most basic form, Kriging does not work where there is a trend in the field (high values on one end and low on another). Universal Kriging addresses this limitation by first calculating a trend surface, then using Kriging to estimate the values of the difference between the real surface and the trend surface (called residuals). The problem of local estimation appears in finding the best estimator of the mean ReV value over a limited domain. The use of Kriging estimations is advantageous because it is not limited to a simple point estimation of the region magnitude (Delhomme, 1978; Marsily, 1986).

Kriging is the name given to a local estimation technique. Provided that the basic assumptions of no trend and a model for the SV (or CSV) are known or determined in some way from the data, then the Kriging produces always BLUE of the unknown ReV characteristics. In the case of non-stationarity, several non-bias conditions are required and this leads to the technique known "universal Kriging" or unbiased Kriging of order say, n. When groups of variables are correlated, the co-Kriging technique can be used to estimate any ReV (e.g., response spectra) from the data available on all the correlated variables (e.g., peak acceleration, velocity, and displacement in addition to the response spectra). Other classes of estimators are also

used in practice; for instance, non-linear estimator can be built by prior transformation of the data. Disjunctive Kriging (Matheron, 1971), Lognornal Kriging (Krige, 1951), and indicator Kriging (Journel, 1983) are examples of non-linear estimators. All Kriging techniques are based on the simple linear models as

$$Z_E = \lambda_1 x_1 + \lambda_2 x_2 + ... + \lambda_n x_n, \tag{5.32}$$

where Z_E is the estimator of the true value at location E, and λ_i are the weights allocated to each observation such that

$$\sum_{i=1}^{n} \lambda_i = 1. \tag{5.33}$$

The technique minimizes estimation variables by solving a set of Kriging equations, which include covariance between the point or volume to be estimated and the sample points and covariance between each pair of sample points. The weights calculated through solving the system of equations, which depend upon the size and shape of the volume to be estimated, the distance and direction of each sample from the volume to be estimated, the distance between the samples, and the SV or CSV.

The equations and their full derivation as well as attributes and advantages of Kriging can be found in numerous publications such as Matheron (1971), David (1977), Journel and Huijbregts (1978), and Clark (1979). The following points are some of the characteristics and advantages of Kriging technique.

1) If one has a model for the SV (or CSV), he/she can produce the minimum variance using the Kriging technique.
2) If the proper models are used for the SV (or CSV) and the system is set up correctly, then there is always a unique solution to the Kriging system.
3) If one has regular sampling, and hence the same sampling set up at many different positions within the region, it is not necessary to recalculate the Kriging system each time.
4) Kriging is not limited to a single point estimation of the given magnitude Z, but can also be used
    a) to estimate the mean value, $\overline{Z}$, on a given block, e.g., on the mesh of model or a sub-domain of any shape of watershed,
    b) to obtain the estimation variance of magnitude Z, i.e., roughly the confidence interval of this estimation,
    c) to locate the best situation for a new measurement point, e.g., by minimizing the overall uncertainty in the field under consideration.
5) Kriging is advantageous because it considers the following points explicitly.
    a) The number of spatial configuration of observation points within the study region

b) The position of the data points within the region of interest
c) The distance between the data points with respect to the area of interest
d) The spectral continuity of the interpolated variable.

For instance, in an earthquake ground motion study, Kriging can be used for evaluating the earthquake ground motion hazard within the region of interest and for estimating the tripartite earthquake response spectra at a site of interest. It is already stated that potential errors in the data collection may lead to nugget effect (Chapter 4), which becomes evident especially from the sample SV, and its existence causes smoothing operation through the Kriging and less confidence in individual data points versus the overall trend of the data. It has the same unit as the SV. There are two components that give rise to nugget effect, namely variances due to error, σ_e^2, and separation, σ_s^2. The latter variance is a measure of variation that occurs at separation distances of less than the typical nearest neighbor sample spacing. The more the random fluctuation of the same data at a given location, the greater is the error variance and the less is the prediction reliability. Consequently, Kriging tends to smooth the surface, and therefore it is not a perfect estimator.

5.5.1 Kriging Methodologies and Advantages

Once the degree of spatial dependence has been established, then the SV can be used to interpolate values for points not measured through the process of Kriging, which is an interpolation method that uses the sample (empirical, experimental) SV to weight sample points based on their locations in space relative to the point value that is to be estimated. Therefore, a first step in Kriging is to fit a theoretical function to the SV model that describes the theoretical SV. Kriging has many things in common with traditional point-interpolation methods such as inverse distance (or square) weighting, triangulation, polygonization, etc. methodologies, which are explained in Chapter 2. The result of Kriging is an interpolated surface map of ReVs. There are several types of Kriging methodology.

1) Ordinary Kriging: It is similar to multiple linear regression and interpolates values based on point estimates.
2) Indicator Kriging: It is used to estimate indicator variables. Indicator Kriging is simply ordinary Kriging performed on the indicator-transformed data.
3) Punctual Kriging: Both ordinary and indicator Kriging methodologies are forms of punctual Kriging because they are used to estimate values for exact points within the sampling unit. Punctual Kriging is the most common method used in earth sciences. It helps to estimate the value at a point from a set of nearby sample values using Kriging. The kriged estimate for a point will usually be quite similar to the kriged estimate for a relatively small block centered on the point, but the computed Kriging standard deviation will be higher. When a kriged point happens to coincide with a sample location, the kriged estimate will equal the sample value.

4) Block Kriging**:** Its interpolations are based on values in a particular finite area. It is a more accurate and intensive computation that uses point estimates within a block to derive an average estimate for the block.
5) Co-Kriging is a modification of ordinary Kriging that relies on the fact that many phenomena are multivariate and that the primary variable of interest is undersampled. Co-Kriging estimation is done by minimizing the variance of the estimation error using the cross-correlation (dependence) between several variables. Estimates are derived for both the primary and the secondary variables. The co-Kriging technique is a modification of the simpler technique of Kriging. It is used to merge two variables or more. Estimation of co-Kriging contains a primary variable of interest and one or more secondary variables. Improvement in the interpolation of one variable by using other variables is important (David, 1977; Journel and Huijbregts, 1978; Myers et al., 1982). There are two steps in co-Kriging estimation.

    a) Evaluation of the cross-correlation (or co-SVs) between variables to obtain information about continuity and dependencies.
    b) Construction of contour maps for the primary variable.

Seo (1998) used linear co-Kriging to interpret rainfall data from a set of rain gages and radar information. He concludes that the consistency of the improvement by gage-radar estimation makes co-Kriging an attractive tool in rainfall estimation. Martinez (1996) applied co-Kriging to improve the accuracy of evapo-transpiration estimation over a regular grid by including the effects of topography.

Among other spatial estimation techniques, Kriging methodology has the following advantages.

1) It yields BLUE for the ReV modeling in earth sciences.
2) It is best because it minimizes the error variance in the estimate, unbiased because the weights sum to one, linear because it is a simple weighted average.
3) Also uses a weighted average method to calculate the value at unsampled locations (Eq. 2.27).
4) Weights are determined by considering the representative sample and then theoretical SV (or CSV) and the estimation problem are solved by using matrix algebra.

In the application of Kriging algorithm, there are four successive essential steps as follows.

1) When computing the interpolation weights, the algorithm considers the spacing between the point of estimation and the data sites. The algorithm considers also the inter-data spacing, which allows for declustering.
2) When computing the interpolation weights, the algorithm considers the inherent length scale of the data. For example, there are regions where the topography varies much more slowly than some other regions. If two points' elevations at

the same distance are considered in these two different topographies, then in the slowly changing regional elevation case it would be reasonable to assume a linear variation between these two observations, while in the other region such an assumed linear variation would be unrealistic. The algorithm adjusts the interpolation weights accordingly.

3) When computing the interpolation weights, the algorithm considers the inherent trustworthiness of the data. If the data measurements are exceedingly precise and accurate, the interpolated surface goes through each and every observed value. If the data measurements are suspect, the interpolated surface may not go through an observed value, especially if a particular value is in stark disagreement with neighboring observed values. This is an issue of data repeatability.
4) Natural phenomena are created by physical processes, which have often preferred orientations. For example, at the mouth of a river the coarse material settles out fastest, while the finer material takes longer to settle. Thus, the closer one is to the shoreline the coarser the sediments, while the further from the shoreline the finer the sediments. When computing the interpolation weights, the algorithm incorporates this natural anisotropy. When interpolating at a point, an observation 100 m away but in a direction parallel to the shoreline is more likely to be similar to the value at the interpolation point than is an equidistant observation in a direction perpendicular to the shoreline.

The last three items incorporate something about the underlying process from which the observations are taken. The length scale, data repeatability, and anisotropy are not a function of the data locations. These enter into the Kriging algorithm via the SV (or CSV). The length scale is given by the SV range (or slope), the data repeatability is specified by the nugget effect, and the anisotropy is given by the anisotropy (Chapter 4).

5.6 Simple Kriging

This Kriging method has straightforward mathematical derivations based on the following three basic assumptions.

1) The spatial sampling points are representatives of the ReV at a set of given locations with measurement values.
2) The ReV is considered as a second-order random field variable with mean, variance, and SV.
3) The mean of ReV is known, which limits the application of this Kriging modeling alternative severely.

In practical applications there are many cases where the areal mean of the ReV is known and hence direct application of the simple Kriging methodology becomes

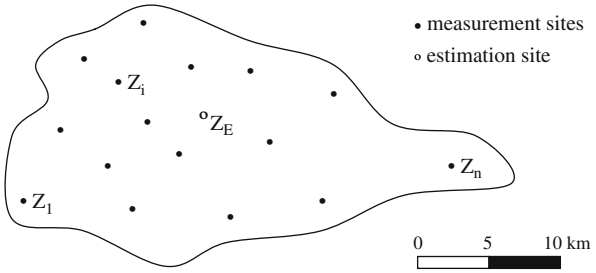

Fig. 5.14 ReV sample sites and estimation site

attractive. Especially, in the case of second-order stationarity (mean and variance constancy) the whole ReV samples can be standardized according to classical statistical standardization formulation and hence the standardized ReV has zero mean and unit variance. Let a set of measurement locations are scattered irregularly over the study area as in Fig. 5.14, where there are n measurement and one estimation sites.

The regional variability of the ReV is recognized by a suitable regional dependence (covariance or SV) function between each pair of the measuring sites. Kriging estimation is considered as the weighted average of the measurement values on the estimation point with distant-dependent weighting values, λ_i. The Kriging estimation, Z_E, is a linear weighted average of the surrounding measurements Z_i ($i = 1, 2, \ldots, n$) as follows.

$$Z_E = \overline{Z} + \sum_{i=1}^{n} \lambda_i \left(Z_i - \overline{Z}\right), \tag{5.34}$$

where $\overline{Z}$ indicates the regional constant mean value of the ReV. If there are n neighboring sites for the estimation calculation, then there will be n^2 elements in the covariance (or SV) matrix, with the variances on the main diagonal. Due to the diagonal symmetry the number of different elements in the matrix is equal to $n(n-1)/2$ as follows.

$$C = \begin{bmatrix} \text{var}(z_1) & \text{cov}(z_1,z_2) & \ldots & \text{cov}(z_1,z_n) \\ \text{cov}(z_2,z_1) & \text{var}(z_2) & \ldots & \text{cov}(z_2,z_n) \\ \cdot & \cdot & \cdots & \cdot \\ \cdot & \cdot & \cdots & \cdot \\ \cdot & \cdot & \cdots & \cdot \\ \text{cov}(z_n,z_1) & \text{cov}(z_n,z_2) & \ldots & \text{var}\,(z_n) \end{bmatrix} \tag{5.35}$$

In this matrix each element is dependent also on the distance difference (relative distance) between the two sites. It is obvious that $\text{Cov}(z_i, z_j) = \text{Cov}(z_j, z_i)$ and furthermore $\text{Cov}(z_i, z_i) = \sigma_i^2$, which is the variance at site i. However, if the

ReV is standardized with constant regional mean, $\overline{Z}$ and variance, σ_Z^2 then Cov(z_i, z_i) = 1 and the covariance corresponds to dependence (correlation) coefficient as $\rho(z_1, z_2) = \text{cov}(z_1, z_2)$. For standardized ReV, Eq. (5.35) takes the following form.

$$\rho = \begin{bmatrix} 1 & \rho(z_1,z_2) & \ldots & \rho(z_1,z_n) \\ \rho(z_2,z_1) & 1 & \ldots & \rho(z_2,z_n) \\ . & . & \ldots & . \\ . & . & \ldots & . \\ . & . & 1 & . \\ \rho(z_n,z_1) & \rho(z_n,z_2) & \ldots & 1 \end{bmatrix} \tag{5.36}$$

This is the regional correlation matrix for ReV. Similar to this matrix one can write also the distance matrix, D, between these n sites, with zero distances along the main diagonal as follows.

$$D = \begin{bmatrix} 0 & \text{dis}(z_1,z_2) & \ldots & \text{dis}(z_1,z_n) \\ \text{dis}(z_2,z_1) & 0 & \ldots & \text{dis}(z_2,z_n) \\ . & . & \ldots & . \\ . & . & \ldots & . \\ . & . & 0 & . \\ \text{dis}(z_n,z_1) & \text{dis}(z_n,z_2) & \ldots & 0 \end{bmatrix} \tag{5.37}$$

This matrix is also symmetrical with respect to the main diagonal. Hence, both the covariance and the distance matrices provide information in the form of, say, upper triangular matrices. The plot of distance matrix values on the horizontal axis versus corresponding regional correlation coefficients from the correlation matrix provides a general shape as in Fig. 5.15, which may be referred to as the regional dependence (correlation) function. Logically, as the distance increases the correlation coefficient between the ReV values decreases, and therefore Fig. 5.15 has a decreasing trend with distance and theoretically this function should be asymptotic to the horizontal axis. Consideration of Eq. (5.31) with unit variance yields the corresponding SVs in the same figure.

The general expression in Eq. (5.34) for the simple Kriging can be rewritten for a standardized ReV as

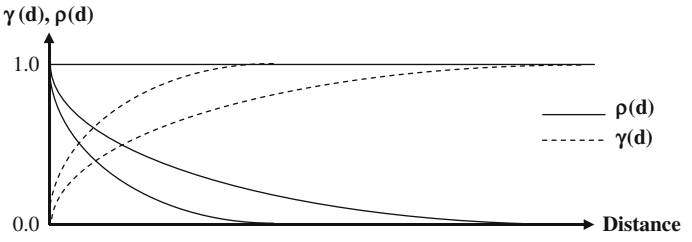

Fig. 5.15 Covariance–distance graph

$$z_E = \sum_{i=1}^{n} \lambda_i z_i. \tag{5.38}$$

Here there are n unknowns and accordingly n equations are necessary for the simultaneous solution. For this purpose, both sides of Eq. (5.38) are multiplied by each measurement ReV variable and then the averages (expectations) are taken. The resultant set of equations becomes

$$\begin{aligned}
&\sum_{i=1}^{n} \lambda_i \rho(z_i, z_1) = \rho(z_E, z_1) \\
&\sum_{i=1}^{n} \lambda_i \rho(z_i, z_2) = \rho(z_E, z_2) \\
&\cdots\cdots\cdots\cdots\cdots\cdots\cdots\cdots \\
&\sum_{i=1}^{n} \lambda_i \rho(z_i, z_k) = \rho(z_E, z_k)
\end{aligned} \tag{5.39}$$

In order to bring this set of simultaneous equations into a matrix form, the following additional succinct vector definitions are necessary. The unknown column vector is

$$\lambda = \begin{bmatrix} \lambda_1 \\ \lambda_2 \\ . \\ . \\ \lambda_n \end{bmatrix} \tag{5.40}$$

Finally, the right-hand side of Eq. (5.39) represents the known part, say, column vector, B, which is defined as

$$B = \begin{bmatrix} \rho(z_E, z_1) \\ \rho(z_E, z_2) \\ . \\ . \\ \rho(z_E, z_n) \end{bmatrix}; \tag{5.41}$$

with these notations at hand, Eq. (5.39) can be written shortly as

$$C\Lambda = B,$$

or the inversion operation gives the solution implicitly as

$$\Lambda = C^{-1}B. \tag{5.42}$$

After the determination of the weighting values, λ_i, from this last expression their substitution into Eq. (5.38) leads to the estimation of the standard ReV, which is then converted to non-standard (original) ReVs as

$$Z_E = \overline{Z} + \sigma_E^2 z_E, \tag{5.43}$$

where z_E is an $(n \times 1)$ matrix of the measured ReV values with zero mean and unit variance.

The simple Kriging procedure can also be applied by considering the relationship between the SV and the covariance function as given in Eq. (5.31). However, the application of this transition between the covariance and the corresponding SV will be reliable only in the case of the normally distributed ReVs. Otherwise, the results obtained from the use of the covariance will be biased. The reader can see the difference by applying the simple Kriging once with the covariance and then with the SV functions of the same set ReV measurements. The simple Kriging is equivalent to multiple regression procedure where the covariance is used for the parameter estimation.

All what has been explained in this section is based on the covariance function for the depiction of spatial dependence. Since there is a relationship between the covariance and the SV functions in the case of standardized ReV according to Eq. (5.31) as $\rho(d) = 1 - \gamma(d)$, then the replacement of the covariance terms in all the equations of this section provides an alternative spatial modeling of ReV based on SV. The variance of the estimation in case of covariance use is

$$\sigma_E^2 = 1 - B' \Lambda. \tag{5.44}$$

When the SV is used for the spatial modeling, the same estimation variance becomes

$$\sigma_E^2 = B' \Lambda. \tag{5.45}$$

The critic of the simple Kriging is that it depends on the statistical property of the covariance (or SV) function preservation in the final estimations. In other words, the spatial estimation is achieved in such a way that the overall spatial dependence function (SDF) of the ReV is preserved throughout the procedure. Unfortunately, neither the cross-validation nor the unbiasedness procedures are applied explicitly in the simple Kriging procedure.

Example 5.1

The earthquake magnitude measurements at five stations are presented in Table 5.5 with the positions in Fig. 5.16. The spatial estimation, Z_E, will be obtained from all the five measurement sites.

The distance matrix between each pair of data is calculated with the following results.

$$D = \begin{bmatrix} 0 & & & & \\ 0.534689 & 0 & & & \\ 0.349005 & 0.326195 & 0 & & \\ 0.664208 & 0.185368 & 0.370756 & 0 & \\ 0.483628 & 1.015764 & 0.772863 & 1.129264 & 0 \end{bmatrix}$$

Table 5.5 Spatial data

ReV	Easting (km)	Northing (km)	Magnitude
Z_1	24.47950	40.40017	1.87
Z_2	24.48400	39.86550	1.92
Z_3	24.68783	40.12017	2.2
Z_4	24.63183	39.75367	2.15
Z_5	24.54383	40.87950	2.07
Z_E	24.59567	40.12667	2.65

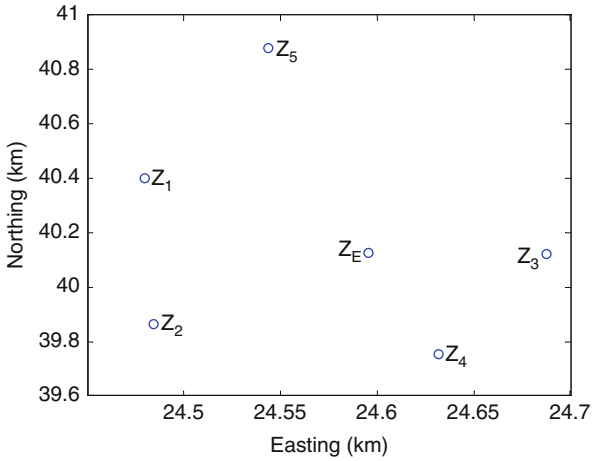

Fig. 5.16 Spatial scatter of data locations

On the other hand, the distances between the estimation site, Z_E, and measurement sites are as follows.

	1	2	3	4	5
E	0.297151	0.284038	0.092392	0.374746	0.754616

Provided that the ReV is standardized, the corresponding half-squared differences (i.e., SV) matrix can be obtained by substituting Eq. (5.31) with $\sigma_Z^2 = 1$ into Eq. (5.36), which leads to

$$\gamma = \begin{bmatrix} 0 & 1-\gamma(z_1,z_2) & \dots & 1-\gamma(z_1,z_n) \\ 1-\gamma(z_2,z_1) & 0 & \dots & 1-\gamma(z_2,z_n) \\ \cdot & \cdot & \cdots & \cdot \\ \cdot & \cdot & \cdots & \cdot \\ \cdot & \cdot & \cdots & \cdot \\ 1-\gamma(z_n,z_1) & 1-\gamma(z_n,z_2) & \dots & 0 \end{bmatrix} \tag{5.46}$$

There are two different ways to calculate the SV values in practical works, either from a given small sample as in Table 5.6 without knowing the basic structure of the sample SV or after defining the structural form of the sample SV from a large number of data, which is preferred to be more than 30 data values. The former approach gives a matrix, which that represents half-squared differences subtraction from 1 according to Eq. (5.46) between the earthquake magnitudes becomes from Table 5.5.

$$\gamma = \begin{bmatrix} 0 & & & \\ 1-0.00125 & 0 & & \\ 1-0.05445 & 1-0.03920 & 0 & \\ 1-0.03920 & 1-0.02645 & 1-0.00125 & 0 \\ 1-0.02000 & 1-0.01125 & 1-0.00845 & 1-0.00320 \end{bmatrix}$$

Likewise, Eq. (4.41) can be written by considering Eq. (5.31) as

$$B = \begin{bmatrix} 1-\gamma(z_E,z_1) \\ 1-\gamma(z_E,z_2) \\ . \\ . \\ 1-\gamma(z_E,z_n) \end{bmatrix} \tag{5.47}$$

It is not possible to estimate the SV values in this vector because the earthquake value at prediction location is not known. Therefore, it is necessary to know the global SV that would depend on many location records, and it is assumed herein that a priory structural analysis had produced the sample SV model as a linear model

$$\gamma(d) = 0.015 + 0.1d.$$

Now one can calculate the SV value from the distances between the estimation point and other surrounding points in Fig. 5.16, which leads to

$$B = \begin{bmatrix} 1-0.0447151 \\ 1-0.0434038 \\ 1-0.0242392 \\ 1-0.0524746 \\ 1-0.0904616 \end{bmatrix}$$

Of course, it is now possible to calculate the matrix in Eq. (5.46) according to the distance matrix above by using large sample SV equation, which leads to

$$\gamma = \begin{bmatrix} 0 & & & \\ 1-0.0684689 & 0 & & \\ 1-0.0499005 & 1-0.0476195 & 0 & \\ 1-0.0814208 & 1-0.0335368 & 1-0.0520756 & 0 \\ 1-0.0633628 & 1-0.1165764 & 1-0.0922863 & 1-0.279264 \end{bmatrix}$$

The final solution can be found by taking inverse of this Γ, which appears as follows.

$$\gamma^{-1} = \begin{bmatrix} -0.7747 & 0.3017 & 0.2867 & 0.2763 & 0.2058 \\ 0.3017 & -0.7773 & 0.2822 & 0.2041 & 0.2866 \\ 0.2867 & 0.2822 & -0.7600 & 0.2391 & 0.2558 \\ 0.2763 & 0.2041 & 0.2391 & -0.9102 & 0.4471 \\ 0.2058 & 0.2866 & 0.2558 & 0.4471 & -0.9829 \end{bmatrix}$$

Hence, application of Eq. (5.42) leads to the final weight values as,

$$\lambda = \begin{bmatrix} 0.2801 \\ 0.2668 \\ 0.2641 \\ 0.2387 \\ 0.2526 \end{bmatrix}$$

It is now possible to calculate the prediction value from Eq. (5.32), which gives $Z_E = 2.65$.

5.7 Ordinary Kriging

This procedure has two assumptions of the simple Kriging, with conflict of the third one, which is assumed to be constant regionally but unknown. Hence, it is not possible to apply the standardization procedure to the ReV measurements because the mean value is unknown. Similar expression to Eq. (5.34) can be written, but with the consideration of unknown regional mean, m, value as

$$Z_E = m + \sum_{i=1}^{n} \lambda_i (Z_i - m) \tag{5.48}$$

Comparison of this with Eq. (5.34) indicates that rather than the standardized ReV variables, non-standardized ReVs are used. If both sides of this last expression is arithmetically averaged, one can then obtain

$$m = m + m \sum_{i=1}^{n} \lambda_i - m = 0,$$

which yields the restrictive condition, as has already been given by Eq. (5.33). Hence, the first rule in the ordinary Kriging is that the summation of all the weights ought to be equal to 1. It indicates that the Kriging weights are independent of the ReV average. This is referred to as the unbiasedness principle in the Kriging literature. It is possible to write Eq. (5.48) as

$$Z_E = m\left(1 - \sum_{i=1}^{n} \lambda_i\right) + \sum_{i=1}^{n} \lambda_i Z_i, \tag{5.49}$$

where the parenthesis in the first term on the right-hand side is equal to zero by definition. Equation (5.33) is as a condition to the main estimation expression in Eq. (5.48), which can be rewritten with the estimation error term, ε_E as

$$(Z_E - m) = \sum_{i=1}^{n} (\lambda_i Z_i - m) + \varepsilon_E.$$

In the following this estimation error variance will be minimized. Let us leave the estimation error as a subject,

$$\varepsilon_E = (Z_E - m) - \sum_{i=1}^{n} (\lambda_i Z_i - m).$$

It is known by definition that the error estimation overall arithmetic average, $\bar{\varepsilon}_E$, is equal to zero. The square of both sides can be obtained as

$$\varepsilon_E^2 = (Z_E - m)^2 - 2\sum_{i=1}^{n} (\lambda_i Z_i - m)(Z_E - m) + \left[\sum_{i=1}^{n} (\lambda_i Z_i - m)\right]^2,$$

or more explicitly

$$\varepsilon_E^2 = (Z_E - m)^2 - 2\sum_{i=1}^{n} (\lambda_i Z_i - m)(Z_E - m) + \sum_{j=1}^{n}\sum_{i=1}^{n} \left(\lambda_j Z_j - m\right)(\lambda_i Z_i - m).$$

If the estimation is made n times, then the average error estimate square (variance) will be obtained as

$$\frac{1}{n}\sum_{l=1}^{n} \left(\varepsilon_E^2\right)_l = \frac{1}{n}\sum_{l=1}^{n} (Z_E - m)^2 - 2\frac{1}{n}\sum_{l=1}^{n}\sum_{i=1}^{n} (\lambda_i Z_i - m)(Z_E - m) + \frac{1}{n}\sum_{l=1}^{n}\sum_{j=1}^{n}\sum_{i=1}^{n} \left(\lambda_j Z_j - m\right)(\lambda_i Z_i - m)$$

or

$$\frac{1}{n}\sum_{l=1}^{n} \left(\varepsilon_E^2\right)_l = \frac{1}{n}\left[\sum_{l=1}^{n} (Z_E - m)^2\right] - 2\sum_{i=1}^{n}\left[\frac{1}{n}\sum_{l=1}^{n} (\lambda_i Z_i - m)_l (X_E - m)_l\right] + \sum_{j=1}^{n}\sum_{i=1}^{n}\left[\frac{1}{n}\sum_{l=1}^{n} \left(\lambda_j Z_j - m\right)((\lambda_i Z_i - m))\right]$$

The first average in the big brackets on the right-hand side is equal to the estimation variance, σ_E^2, the second term average is equivalent to estimation-measurement covariance, Cov (Z_E, Z_i) and the last term is the covariance between two measurements, Cov (Z_i, Z_j). In fact, the average terms based on n values are equivalent to their respective expectations as n goes to infinity theoretically. The last expression can be written with these new covariance values as

$$\overline{\varepsilon_{El}^2} = \sigma_E^2 - 2\sum_{i=1}^{n} \mathrm{Cov}\,(Z_E, Z_i) + \sum_{j=1}^{n}\sum_{i=1}^{n} \mathrm{Cov}\,(Z_i, Z_j). \tag{5.50}$$

This expression must be minimized with the condition in Eq. (5.33) and, therefore, the minimization equation can be written with the Lagrange multiplier, μ, as

$$\overline{\varepsilon_{El}^2} = \sigma_E^2 - 2\sum_{i=1}^{n} \mathrm{Cov}\,(Z_E, Z_i) + \sum_{j=1}^{n}\sum_{i=1}^{n} \mathrm{Cov}\,(Z_i, Z_j) + \mu\sum_{i=1}^{n} \lambda_i. \tag{5.51}$$

This can be written in the matrix and vector form after the definition of the following quantities.

$$C = \begin{bmatrix} \mathrm{cov}(z_1,z_1) & \mathrm{cov}(z_1,z_2) & \dots & \mathrm{cov}(z_1,z_n) & 1 \\ \mathrm{cov}(z_2,z_1) & \mathrm{cov}(z_2,z_2) & \dots & \mathrm{cov}(z_2,z_n) & 1 \\ . & . & \dots & . & . \\ . & . & \dots & . & . \\ . & . & \dots & . & . \\ \mathrm{cov}(z_n,z_1) & \mathrm{cov}(z_n,z_2) & \dots & \mathrm{cov}(z_n,z_n) & 1 \\ 1 & 1 & & 1 & 0 \end{bmatrix}, \tag{5.52}$$

which can be written based on the SV formulation alternatively as

$$\lambda = \begin{bmatrix} \lambda_1 \\ \lambda_2 \\ . \\ . \\ \lambda_n \\ \mu \end{bmatrix}, \tag{5.53}$$

and finally

$$B = \begin{bmatrix} \mathrm{cov}(z_E,z_1) \\ \mathrm{cov}(z_E,z_2) \\ . \\ . \\ \mathrm{cov}(z_E,z_n) \\ 1 \end{bmatrix}. \tag{5.54}$$

The measurement vector that includes n nearest values is given as

$$M = \begin{bmatrix} Z_1 \\ Z_2 \\ . \\ . \\ Z_n \\ 0 \end{bmatrix}. \tag{5.55}$$

With these notations, the first ordinary Kriging weights may be estimated by using either the covariance or SV values from

$$\Lambda = C^{-1}B. \tag{5.56}$$

The ordinary Kriging estimate of the regionalized variable at location E can be obtained as

$$Z_E = M^T\Lambda = M^TC^{-1}B. \tag{5.57}$$

Finally, the ordinary Kriging estimation variance is

$$\sigma_E^2 = B^T\Lambda = B^TC^{-1}B. \tag{5.58}$$

The estimate and estimation error depend on the weights chosen. Ideally, Kriging tries to choose the optimal weights that produce the minimum estimation error. In order to derive the necessary equations for Kriging, extensive calculus use is required, which is not included here; however, information about the derivation can be found in various textbooks, such as by Clark (1979) and Olea (1975). Optimal weights produce unbiased estimates and have a minimum estimation variance, which are obtained by solving a set of simultaneous equations. In the case of SV the corresponding expressions to Eqs. (5.52, 5.53 and 5.54) are

$$\begin{bmatrix} \gamma(z_1,z_1) & \gamma(z_1,z_2) & \dots & \gamma(z_1,z_n) & 1 \\ \gamma(z_2,z_1) & \gamma(z_2,z_2) & \dots & \gamma(z_2,z_n) & 1 \\ . & . & \dots & . & . \\ . & . & \dots & . & . \\ . & . & \dots & . & . \\ \gamma(z_n,z_1) & \gamma(z_n,z_2) & \dots & \gamma(z_n,z_n) & 1 \\ 1 & 1 & & 1 & 0 \end{bmatrix}, \tag{5.59}$$

$$\lambda = \begin{bmatrix} \lambda_1 \\ \lambda_2 \\ . \\ . \\ \lambda_n \\ -\mu \end{bmatrix}, \tag{5.60}$$

$$B = \begin{bmatrix} \gamma(z_E, z_1) \\ \gamma(z_E, z_2) \\ . \\ . \\ \gamma(z_E, z_n) \\ 1 \end{bmatrix}, \tag{5.61}$$

respectively.

Example 5.2
Ordinary Kriging methodology is demonstrated by considering groundwater levels at five sites as given in Table 5.6 with easting, northing, and groundwater level elevation values. The graphical locations are shown in Fig. 5.17.

The distances between each pair are given as in the following matrix.

$$D = \begin{bmatrix} 0 & & & & \\ 3.512834 & 0 & & & \\ 2.236068 & 4.338202 & 0 & & \\ 1.860108 & 2.154066 & 2.19545 & 0 & \\ 1.529706 & 5.035871 & 2.731300 & 3.310589 & 0 \end{bmatrix}$$

Table 5.6 Well coordinates and groundwater levels

Well location	Easting (km)	Northing (km)	Elevation (m)
Z_1	4.2	3.0	89
Z_2	3.7	6.5	75
Z_3	1.8	2.6	98
Z_4	2.9	4.5	81
Z_5	4.3	1.5	105
Z_E	3.2	3.0	91.27

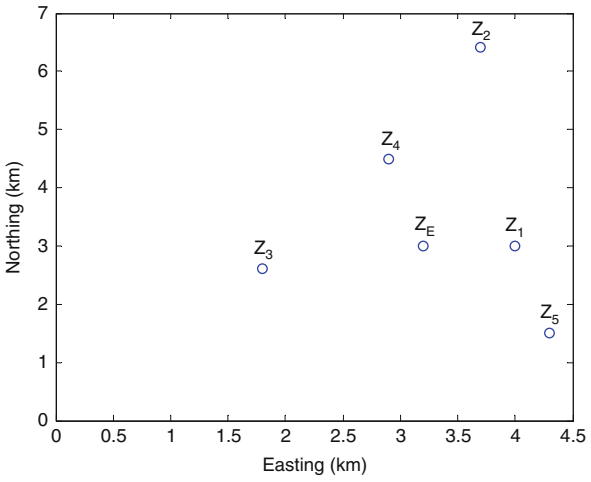

Fig. 5.17 Sample geographical locations

The distances between the estimation point, Z_E, and others are given as,

	1	2	3	4	5
E	0.8	3.535534	1.456022	1.529706	1.860107524

After calculations the half-squared difference matrix appears as follows.

$$\gamma(\mathrm{d}) = \begin{bmatrix} 0 & & & & \\ 332112.5 & 0 & & & \\ 313632.0 & 264.5 & 0 & & \\ 327240.5 & 18.0 & 144.5 & 0 & \\ 308112.5 & 450.0 & 24.5 & 288.0 & 0 \end{bmatrix}$$

For large sample sizes the structure of the SV is determined as a linear function as

$$\gamma(\mathrm{d}) = 0.3 + 3.8\mathrm{d},$$

and accordingly the SV matrix turns out to be as

$$\gamma = \begin{bmatrix} 0 & 13.68 & 8.78 & 7.37 & 6.11 & 1 \\ 13.68 & 0 & 16.78 & 8.47 & 19.93 & 1 \\ 8.78 & 16.78 & 0 & 8.86 & 10.68 & 1 \\ 7.37 & 8.47 & 8.86 & 0 & 12.88 & 1 \\ 6.11 & 19.93 & 10.68 & 12.88 & 0 & 1 \\ 1 & 1 & 1 & 1 & 1 & 0 \end{bmatrix}.$$

The inverse of this matrix becomes

$$\gamma^{-1} = \begin{bmatrix} -0.1489 & 0.0122 & 0.0159 & 0.0465 & 0.0742 & -0.1032 \\ 0.0122 & -0.0603 & -0.0016 & 0.0524 & -0.0027 & 0.4696 \\ 0.0159 & -0.0016 & -0.0788 & 0.0393 & 0.0252 & 0.2699 \\ 0.0465 & 0.0524 & 0.0393 & -0.1317 & -0.0065 & -0.0512 \\ 0.0742 & -0.0027 & 0.0252 & -0.0065 & -0.0902 & 0.4149 \\ -0.1032 & 0.4696 & 0.2699 & -0.0512 & 0.4149 & -10.9519 \end{bmatrix}.$$

Likewise, from Eq. (5.61) realizing the distances between the estimation site and other sites as given above, it is possible o obtain

$$\mathrm{B} = \begin{bmatrix} 3.34 \\ 13.74 \\ 5.83 \\ 6.11 \\ 7.37 \\ 1 \end{bmatrix}.$$

It is possible to find from Eq. (5.56) the lambda values as

$$\lambda = \begin{bmatrix} 0.4916 \\ -0.0275 \\ 0.2676 \\ 0.2004 \\ 0.0679 \\ -0.5255 \end{bmatrix}.$$

One can evaluate the estimation value from Eq. (5.57), which leads to $Z_E = 91.27$ m. The Kriging estimation variance is the weighted sum of the SV for the distance from the points to the estimation location, which can be calculated from Eq. (5.58) leading to $\sigma_E^2 = 4.02\ m^2$. This implies that the standard error of estimation is $\sigma_E = 2.00$ m.

It is possible to make such calculations with estimation and its estimation variance at every point. For this purpose it is useful to make cross-validation by considering each measurement as if it does not exist and Kriging methodology gives the estimation and error variance. Hence one can construct two maps for the Kriging estimates as a best guess of the mapped variable configuration and an error map showing the confidence envelope that surrounds this estimation. All these are based on the measurement and estimation sites configuration and distances between measurements used in the estimation process, and on the degree of spatial continuity of the ReV as expressed by the spatial covariance and preferably SV models.

5.8 Universal Kriging

Unfortunately, the ordinary Kriging cannot be used unless the ReV has a constant mean although it is not known. Because the successive differences conceal the regional mean in the SV calculations. This means that in the case of a systematic variation in the regional average such as abrupt changes (Fig. 4.9), trends (Fig. 4.11), oscillations, the ordinary Kriging assumption of constant mean is violated. It is, therefore, necessary to develop another ReV estimation procedure, which should take into consideration these systematic mean variations. The universal Kriging considers first-order stationary ReV as consisting of two components, namely the regional drift and the residuals. The drift is the long-term average (expectation) value of the ReV within the estimation site neighborhood. It slowly varies and it is the non-stationary component of the local region. On the other hand, the residuals are the differences between the measurements and the corresponding drift values. If the drift is removed from the ReV, then the residuals can be modeled by the ordinary Kriging principles. Hence, in the procedural structure of the universal Kriging there are three steps.

1) Removal of the drift values from the measurements of the ReV.
2) Application of the ordinary Kriging to establish the residuals at non-measurement points
3) Addition of these residual values to the original drift values.

The difference between the trend surface as defined in Chapter 3, Section 3.10, and the drift covers partial local area whereas the trend surface extends over all the ReV variability domain. The underlying drift component can be removed from the original measurements of the concerned ReV through different methodologies. Among these are linear and non-linear trend surface fitting, double-dimensional Fourier analysis, etc. These methodologies depict the drift component, and its subtraction from the original measurements leaves the residuals with almost zero arithmetic average. Under the statistical theory that includes universal Kriging, a single-valued, continuous, mapable property is called an ReV and is considered to consist of two parts, a drift, or expected value, and a residual, or deviation from the drift. The drift may be modeled by a local polynomial function within a neighborhood, which is analogous to a local trend surface. If the drift is removed, the residual surface can be regarded as first-order stationary in a statistical sense. Hence, again the simple or ordinary Kriging models can be used for the residual data set. After the estimation of residuals again, the summation with the convenient drift values, the original ReV can be estimated.

Apart from this rather complicated and piecewise application, it is also possible to develop universal Kriging equations including another condition of drift in the derivations with another Lagrange multiplier. Hence, the original measurements can be used directly in the calculations. For example, similar set of equations can be derived for the universal Kriging to Eqs. (5.57, 5.58, and 5.59) and Eq. (5.53) as

$$C = \begin{bmatrix} \gamma(z_1,z_1) & \lambda(z_1,z_2) & \dots & \gamma(z_1,z_k) & 1 & L_{1,1} & L_{2,1} \\ \gamma(xz_2,z_1) & \gamma(z_2,z_2) & \dots & \gamma(z_2,z_k) & 1 & L_{1,2} & L_{2,2} \\ . & . & \dots & . & . & . & . \\ . & . & \dots & . & . & . & . \\ . & . & \dots & . & . & . & . \\ \gamma(z_k,z_1) & \gamma(z_k,z_2) & \dots & \lambda(z_k,z_k) & 1 & L_{1,1} & L_{2,1} \\ 1 & 1 & \dots & 1 & 0 & 0 & 0 \\ L_{1,1} & L_{1,2} & \dots & L_{1,k} & 0 & 0 & 0 \\ L_{2,1} & L_{2,2} & \dots & L_{21,k} & 0 & 0 & 0 \end{bmatrix} \tag{5.62}$$

$$\lambda = \begin{bmatrix} \lambda_1 \\ \lambda_2 \\ . \\ . \\ \lambda_k \\ \mu_0 \\ \mu_1 \\ \mu_3 \end{bmatrix}, \tag{5.63}$$

and finally

$$B = \begin{bmatrix} \gamma(z_E,z_1) \\ \gamma(z_E,z_2) \\ . \\ . \\ \gamma(z_E,z_k) \\ 1 \\ L_{1,k} \\ L_{2,k} \end{bmatrix}, \tag{5.64}$$

respectively. Herein, z_i represents a vector of the coordinates of point I, while $L_{1,i}$ ($L_{2,i}$) is the scalar value representing the location of this point along coordinate axis horizontal (vertical) or 1 (2), for instance, east–west (north–south) direction. The vector of universal Kriging weight Λ is found by Eq. (5.56), except that W and B are given by Eqs. (5.62) and (5.64). The measurement vector that includes k nearest values is given as

$$M = \begin{bmatrix} Z_1 \\ Z_2 \\ . \\ . \\ Z_k \\ 0 \\ 0 \\ 0 \end{bmatrix}. \tag{5.65}$$

In this vector there are (k + d + 1) elements, where the last d+1 elements that correspond to the Lagrange multipliers are zero.

Universal Kriging is a procedure that can be used to estimate values of a surface at the nodes of a regular grid from irregularly spaced data points. If the surface is second-order stationary, or can be made stationary by some transformation, the spatial autocorrelation will express the degree of dependence between all locations on the surface, and most particularly between observations and grid nodes.

Example 5.3

The problem given in Example 5.2 can be extended for the application of Universal Kriging. By making use of Table 5.6, the numerical form of the coefficients matrix can be obtained similar to the previous example but with additional location values as

$$\gamma = \begin{bmatrix} 0 & 13.68 & 8.78 & 7.37 & 6.11 & 1 & 4.2 & 3.0 \\ 13.68 & 0 & 16.78 & 8.47 & 19.93 & 1 & 3.7 & 6.5 \\ 8.78 & 16.78 & 0 & 8.86 & 10.68 & 1 & 1.8 & 2.6 \\ 7.37 & 8.47 & 8.86 & 0 & 12.88 & 1 & 2.9 & 4.5 \\ 6.11 & 19.93 & 10.68 & 12.88 & 0 & 1 & 4.3 & 1.5 \\ 1 & 1 & 1 & 1 & 1 & 0 & 0 & 0 \\ 4.2 & 3.7 & 1.8 & 2.9 & 4.3 & 0 & 0 & 0 \\ 3.0 & 6.5 & 2.6 & 4.5 & 1.5 & 0 & 0 & 0 \end{bmatrix}.$$

The inverse of this 8×8 matrix can be obtained as

$$\Gamma^{-1} = \begin{bmatrix} -0.1248 & 0.0212 & -0.0192 & 0.0342 & 0.0887 & -0.9626 & 0.2474 & 0.0031 \\ 0.0212 & -0.0328 & -0.0222 & 0.0552 & -0.0184 & -0.5517 & 0.0815 & 0.1934 \\ -0.0192 & -0.0222 & -0.0252 & 0.0559 & 0.0108 & 1.7447 & -0.3575 & -0.0652 \\ 0.0342 & 0.0522 & 0.0559 & -0.1246 & -0.0177 & 0.2611 & -0.1285 & 0.0333 \\ 0.0887 & -0.0184 & 0.0108 & -0.0177 & -0.0634 & 0.5085 & 0.1571 & -0.1646 \\ -0.9626 & -0.5517 & 1.7447 & 0.2611 & 0.5085 & 40.1311 & -8.5379 & -5.6915 \\ 0.2474 & 0.0815 & -0.3575 & -0.1285 & 0.1571 & -8.5379 & 2.5455 & -0.0474 \\ 0.0031 & 0.1934 & -0.0652 & 0.0333 & -0.1646 & -6.6915 & -0.0474 & 1.5258 \end{bmatrix}.$$

On the other hand, the elements of the right-hand side vector in Eq. (5.39) becomes as follows.

$$\mathrm{B} = \begin{bmatrix} 3.34 \\ 13.74 \\ 5.83 \\ 6.11 \\ 7.37 \\ 1 \\ 3.2 \\ 3.0 \end{bmatrix}$$

The universal Kriging weight vector can be found after the necessary algebraic calculations according to Eq. (5.56) as

$$\lambda = \begin{bmatrix} 0.4625 \\ -0.0362 \\ 0.3094 \\ 0.2157 \\ 0.0486 \\ 0.4546 \\ -0.2998 \\ 0.0123 \end{bmatrix}.$$

Finally, after all these calculations the estimation value can be obtained from Eq. (5.57) as $Z_E = 91.34$ m.

One can notice that for the given example there is no major difference between the ordinary and universal Kriging methodologies. Ordinary Kriging, however, in common with other weighted-averaging methods, does not extrapolate well beyond the convex hull of the control points. That is, most estimated values will lie on the slopes of the surface and the highest and lowest points on the surface usually will be defined by estimation (control) points.

5.9 Block Kriging

All above mentioned Kriging methods (simple, ordinary, and universal) can be considered as punctual Kriging methodologies because their estimations are obtained at the support of individual sites. In the block Kriging, however, line, areal, or volume supports are considered and a single estimation value is obtained, which is representative for the whole support. This Kriging procedure also starts to work on a set of ReV measurement values, but its final product is valid for a certain domain in 1, 2, or 3 dimensions according to the type of problem. For instance, in ore grade reserve, pollution concentration, etc. estimations 3D shapes are considered. Rainfall maps and the hydrographs are of 2D.

The early versions of Kriging techniques were all concerned with the block Kriging since the ore reserves and grade degrees were the major concentrations for research in the domain of geology. In fact, the most commonly used block Kriging is similar to the ordinary Kriging with the interpretation of known vector, B, elements, which are taken as the average of the spatial covariance or SV values within the interest of block domain, A. Actually, the elements of vector B_n represent the covariances or SVs between the observations and A, integrated over the domain of 2D or 3D.

The major problem prior to the block Kriging application is the determination of block sizes. Each smaller subarea or sub-volume is represented by the geographical coordinates of its center point, and spatial covariance or SV is determined between an observation, Z_i, and each of the center points within a block. Then all of these covariance or SV is averaged in order to determine the point-to-block spatial covariance, cov(A, Z_i) or SV, $\gamma(A, X_i)$ between block A and observation. If possible, the subdivisions of blocks should be regular and should be the same. It has been suggested by Isaaks and Srivastava (1989) that $4\times4 = 16$ and $4\times4\times4 = 64$ subdivisions are adequate for the area and volume blocks. The fundamentals of block Kriging are presented in a simple manner by Olea (1999). It is commonly the counterpart of ordinary Kriging and a set of normal equations must be solved similar to Eq. (5.59). In this new formulation the spatial dependence function (SDF) either in the form of covariance or SV (or CSV) does not represent the relationship between two points, but they are the averages of the spatial covariance or SV (or CSV) between the point observations, Z_i, and all possible points within an area, A.

Figure 5.18 shows the line and areal blocks and measurement point i. In Fig. 5.18a the line is drawn into four pieces and the distances between the center of each piece and the measurement point I as $d_{1,i}$, $d_{2,i}$, $d_{3,i}$ and $d_{4,i}$. Likewise, in Fig. 5.18b there are 16 sub-areas in a given block with distances $d_{1,i}$, $d_{2,i}$, . . ., $d_{16,i}$.

Since the distances are known, their corresponding SV values can be calculated easily from a given theoretical SV function. The arithmetic averages of the relevant SV values give the representative SV value for line or areal block. Furthermore, now the block is considered as a point with this average SV value, and then accordingly one of the convenient Kriging techniques as mentioned above can be applied suitably.

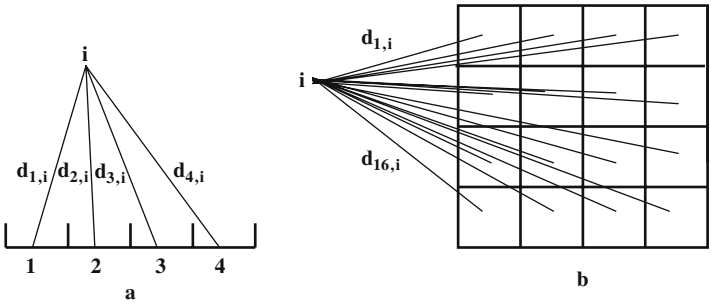

Fig. 5.18 Block pieces (**a**) line, (**b**) area

5.10 Triple Diagram Model

Since gradual (trend) or abrupt (shifts) climatic change questions have gained particular attention in recent years most of the researches on lake level changes are concerned with meteorological factors of temperature and precipitation data. Along this line of research Hubert et al. (1989), Vannitseni and Demaree (1991), and Sneyers (1992) used statistical methods to show that temperature, pressure, and flow series in Africa and Europe have altered several times during the present century. On the other hand, as stated by Slivitzky and Mathier (1993), most of the modelling of levels and flow series on the Great Lakes has assumed stationarity of time series using either Markov or ARIMA (AutoRegressive Moving Average) processes presented by Box and Jenkins (1976). These models may work on lags of one, two, three, or more, but they consider the linear structure in the lake level fluctuations. Since, lake level fluctuations do not have stationarity property, classical models such as Markov and ARIMA processes cannot stimulate lake levels reliably. Multivariate models using monthly lake level variable failed to adequately reproduce the statistical properties and persistence of basin supplies (Loucks, 1989; Iruine and Eberthardt, 1992). On the other hand, spectral analysis of water levels pointed to the possibility of significant trends in lake level hydrological variables (Privalsky, 1990). Almost all these scientific studies relied significantly on the presence of an autocorrelation coefficient as an indicator of long-term persistence in lake level time series. However, many researchers have shown that shifts in average lake level might introduce unrealistic and spurious autocorrelations. This is the main reason why the classical stochastic and statistical models often fail to reproduce the statistical properties. However, Mathier et al. (1992) were able to reproduce adequately the statistical properties of a shifting-mean model. In the following sequel a version of the Kriging methodology is adopted and used for the lake level estimations. For this purpose, the world's largest soda lake, Lake Van on the Anatolian high plateau in eastern Turkey (38.5°N and 43°E) is adopted for application (Fig. 5.19). Lake Van area has very severe winters with frequent temperatures below 0°C. Most of the

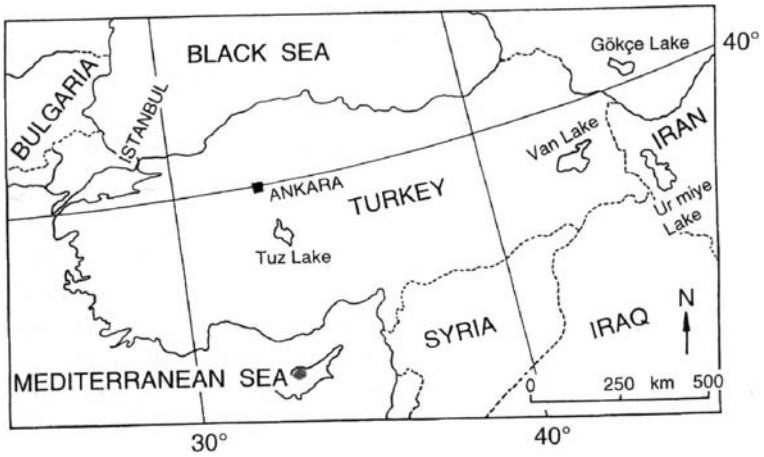

Fig. 5.19 Location map

precipitation falls during winter season in the form of snow and toward the end of spring heavy rainfalls occur. High runoff rates occur in spring during snowmelt, and more than 80% of annual discharge reaches the lake during this period. The summer period (July to September) is warm and dry with average temperatures of 20°C. Diurnal temperature variations are about 20°C.

Human beings can visualize at the maximum three-dimensional variations. The best configuration and interpretation of such variations can be achieved in three-dimensional Cartesian coordinate systems through contour maps. Generally, maps are regarded as the variation of a variable by location variables that are either longitudes and latitudes or eastings and northings (Isaaks and Srivastava, 1989; Cressie, 1993; Kitanidis, 1997). Hence, it is possible to estimate the concerned (mapped) variable value for a given pair of location variables. Since one wants to predict the current lake level from previous records, it is suggested that two previous records replace the two location variables. In this manner, it is possible to map the current values of a variable based on two previous values of the same variable. The first step in any Kriging methodology prior to mapping is to determine the sample SV, which guides for the theoretical model that will be employed in the classical Kriging modelling. For this purpose, the scatter of SV values versus distance is obtained for lag-one, -two, and -three. In order to depict the general trend of the scatter diagram, the distance range is divided into nine intervals, and the average of the SV values that fall within each interval is considered as the representative SV value within the mid-point distance of that interval as suggested by Myers et al. (1982). Different theoretical SV models such as linear, power, spherical, and Gaussian types are tried for the best fit, and at the end the Gaussian SV is seen to have the best match with the sample SV trend (see Fig. 5.20). The Gaussian model is the most suitable in all lags and the properties of fitted Gaussian SV model are presented in Table 5.7.

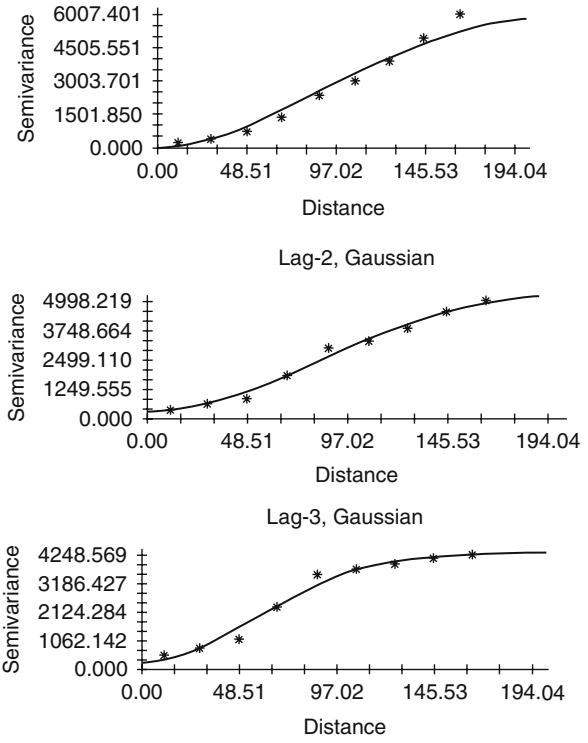

Fig. 5.20 Empirical and theoretical SV for three lags

Such a mapping technique is referred to as triple diagram method (TDM) (Şen, 2008). Such maps are based on three consecutive lake levels. TDMs help to make interpretations in spite of extremely scattered points. Although Davis (1986) has suggested for mapping the application of various simple regional techniques such as inverse distance, inverse distance square, which consider the geometrical configuration of the scatter points only without the use of a third variable; herein, preparation of the TDM is based on classical Kriging technique.

The construction of a TDM requires three variables, two of which are referred to as independent variables (predictors) and they constitute the basic scatter diagram. The third is the dependent variable, which has its measured values attached to each scatter point. The equal value lines are constructed by the Kriging methodology concepts explained in earlier sections of this chapter.

Table 5.7 Theoretical Gaussian SV parameters

Lag	Nugget (cm^2)	Sill (cm^2)	Range (cm)	Correlation coefficient
1	70.0	6,250	213.20	0.977
2	270.0	5,555.0	586.80	0.990
3	250.0	4,327.0	136.0	0.977

Lake Van water level records are used for the implementation of the Kriging methodology so as to obtain triple diagrams that give the common behavior of three variables, which are taken consequently from the historical time series data. The first two variables represent the two past lake levels and third one indicates the present lake levels. Hence, the model has three parts, namely observations (recorded time series) as input, triple diagram as response, and the output as prediction. It is possible to consider lags between the successive data at one, two, three, etc. intervals. Such an approach is very similar to a second-order Markov process, which can be expressed as

$$H_i = \alpha H_{i-1} + \beta H_{i-2} + \varepsilon_i, \tag{5.66}$$

where H_i, H_{i-1}, and H_{i-2} are the three consecutive lake levels; α and β are model parameters; and finally, ε_i is the error term. The application of such a model requires, prior to any prediction procedure, the parameter estimations from the available data. Furthermore, its application is possible under the light of a set of assumptions, which includes linearity, normality (Gaussian distribution of the residuals, i.e., ε_i's), variance constancy, ergodicity, and independence of residuals. The triple diagram replaces Eq. (5.66) without any restriction in the form of map. Such a map presents the appearance of natural relationship between three consecutive time values of the same variable.

In order to apply the triple diagram approach, it is necessary to divide the data into training and testing parts. Herein, the past 24 months (two years) are left for the test (prediction) whereas all other data values are employed for training, which is the TDM as in Fig. 5.21.

Prior to any prediction, it is possible to draw the following interpretations from these figures.

1) In the case of lag-one there is a strong relationship between H_{i-1} and H_{i-2} with increasing contour values of H_i along almost 45° line (see Fig. 5.21a). The small H_i values are concentrated at small H_{i-1} and H_{i-2} values; this implies the clustering of small values of the three consecutive lake levels. Similarly, high lake level values of the three consecutive levels also constitute high values cluster. This means that small values follow small values and high values follow high values, which indicates positive correlations. Local variations in the contour lines appear at either low (high) H_{i-1} or high (low) H_{i-2} values. Consequently, better predictions can be expected within a certain band around the 45° line (Fig. 5.22). It is possible to deduce the following set of logical rules from Fig. 5.21b.

   IF H_{i-1} is low and H_{i-2} is low, THEN H_i is low,
   IF H_{i-1} is medium low and H_{i-2} is medium, THEN H_i is medium,
   IF H_{i-1} is high and H_{i-2} is high, THEN H_i is high.

   These rules can be used for fuzzy logic inference system as suggested by Zadeh (1968).

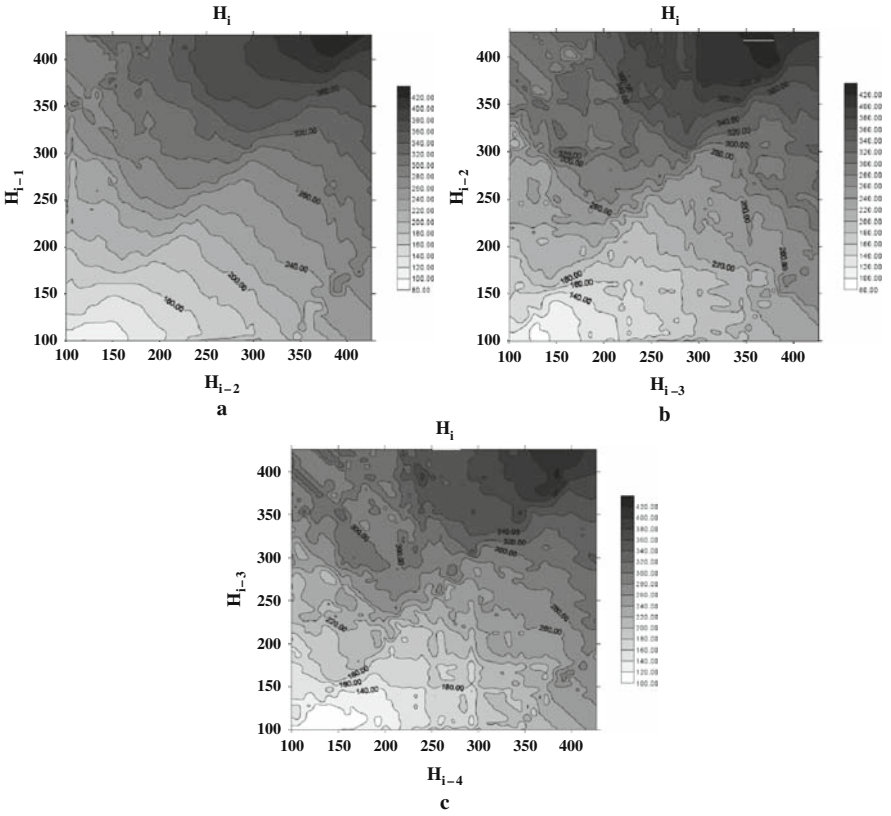

Fig. 5.21 Lake level TDMs (**a**) lag-one, (**b**) lag-two, (**c**) lag-three

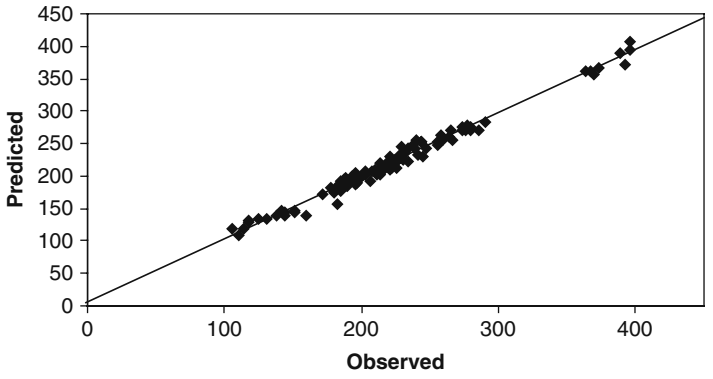

Fig. 5.22 Lag-one model verification

2) In Fig. 5.21b the variations in the contour lines become very distinctive and rather haphazard compared to Fig. 5.21a. This implies that with the increment in the lag value, present time lake level prediction will have more relative error. There is also a distinctive 45° line, but with comparatively narrower band of certainty around it.
3) Finally, at lag-three case (Fig. 5.21c) the contour pattern takes even more haphazard variation. This implies increase in the relative error of predictions.

Şen et al. (1999, 2000) identified suitable models and estimates for lake level fluctuations and their parameters for trend, periodic, and stochastic parts. A second-order Markov model is found suitable for the stochastic part. As explained before, TDM of lake levels can replace the second-order Markov process. In this manner, it is not necessary to use first- and second-order autocorrelation coefficients, in order to take into account more persistence. In order to make predictions for the past 24 months that are not used in the triple diagram constructions in Fig. 5.21, it is necessary to enter H_{i-1} and H_{i-1} for each month on vertical and horizontal axes, respectively. The prediction value of H_i can be either read from this map approximately, or calculated by using Kriging prediction equations. The prediction results are shown in Table 5.8 with corresponding relative error amounts. Individual errors

Table 5.8 Lag-one lake level prediction (cm)

H_{i-2}	H_{i-1}	H_i	Prediction	Relative error (%)
119	112	110	109.32	0.62
107	111	114	118.40	3.72
125	130	125	134.87	7.32
130	125	118	128.43	8.12
125	118	105	118.60	11.47
120	138	142	145.50	2.41
138	142	138	139.53	1.10
142	138	131	134.16	2.35
138	131	117	131.64	11.12
127	141	151	144.08	4.58
141	151	151	146.85	2.75
151	151	144	144.46	0.32
137	140	144	138.76	3.64
140	144	159	140.22	11.81
144	159	182	157.03	13.72
199	202	195	203.62	4.23
202	195	185	191.33	3.31
195	185	177	182.29	2.90
189	193	202	202.01	0.00
193	202	221	209.94	5.00
202	221	245	229.48	6.34
262	254	244	252.90	3.52
254	244	239	243.16	1.71
244	239	241	231.89	3.78
			Average	4.83

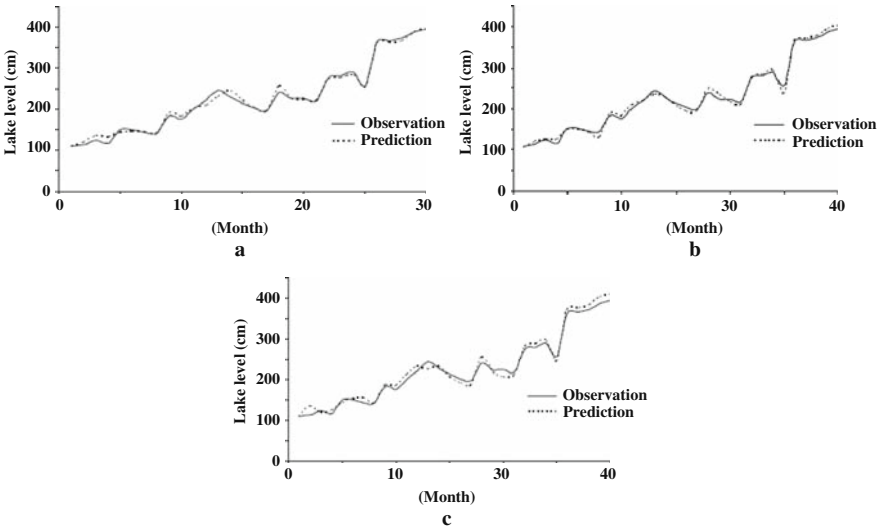

Fig. 5.23 Observed and predicted lake levels (**a**) lag-one, (**b**) lag-two, (**c**) lag-three

are slightly greater than 10%, but the overall prediction relative error percentage is about 4.83%.

Figure 5.23 indicates the observed and predicted H_i values. It is obvious that they follow each other very closely, and on the average observed and predicted lake level series have almost the same statistical parameters.

The triple diagram model depicts even the increasing trend, which is not possible directly with the second-order Markov process. During the prediction procedure there is no special treatment of trend, but even so it is modeled successfully. However, in any stochastic or statistical modeling, it is first necessary to make trend analysis and separate it from the original data. In order to further show the verification of the triple diagram approach for lake level predictions, in Fig. 5.22 the test data are plotted versus the predictions. It is obvious that almost all the points are around 45° line and hence the model is not biased. Predictions are successful at low or high values.

5.11 Regional Rainfall Pattern Description

The mean annual and seasonal rainfall records in the southwest of Saudi Arabia are adapted from the reports published by the Hydrology Division, Ministry of Agriculture and Water in Saudi Arabia, and Al-Jerash (1985). Rainfall records at 63 stations from 1971 to 1990 are selected for the Kriging application (Fig. 5.24). These stations are chosen based on four criteria (Subyani, 2004, 2005).

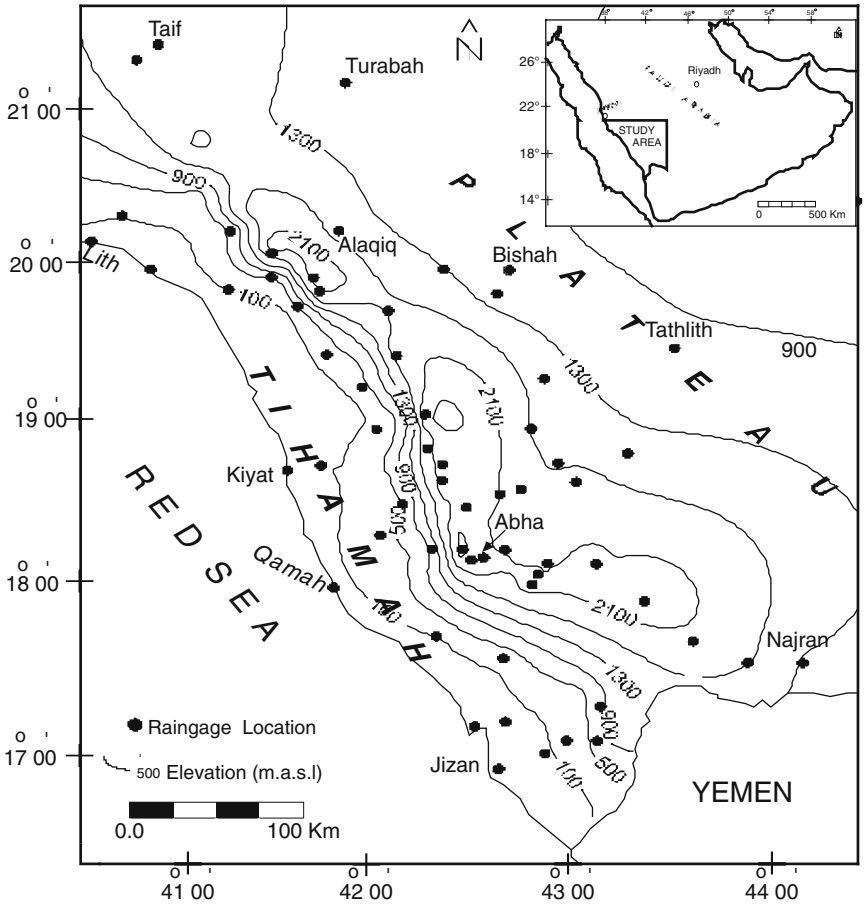

Fig. 5.24 Topographic map in southwest Saudi Arabia

1) They represent the best spatial coverage of the region.
2) They maximize the same monthly rainfall records.
3) They have continuous monthly rainfall.
4) They reflect the wide variety of environments within the study area – literally from coast (Tihamah), mountains, and to leeside of the mountains (desert).

Descriptive statistics for the 63 stations are listed in Table 5.9 for these three regions. All together 25 stations are located within the coast; 24 within mountains; and 14 stations within the leeside.

Problems in the data, such as non-normality, trend, and outliers, should be fixed before developing any kind of model. Normality of the sample data distribution is known to improve the results from Kriging. Transformation is very important to make the data more symmetric, linear, and constant in variance. Since annual

Table 5.9 Dataset grouped into three regions

Region	Number of stations	Winter (mm)	Spring (mm)	Summer (mm)	Fall (mm)	Annual (mm)
Coast (Tihamah)	25	141[a]	199	238	152	684
		13[b]	6	5	3	55
		53.5[c]	51.4	58.6	53.7	217.2
		33.4[d]	51.3	58.2	40.5	160.3
Mountains	24	169	264	148	69	527
		20	80	16	10	150
		78.5	155.3	57.1	30.8	321.8
		47	53.5	35.4	18.8	120.4
Lee Side (Desert)	14	28	99	30	37	150
		7	29	3	3	44
		17.4	64.4	11.9	9.6	103.3
		6.6	17.8	8.22	8.3	27.7

[a] Sample maximum; [b] Sample minimum; [c] Sample mean; [d] Sample standard deviation

and seasonal rainfall data are considered, it is pragmatic to find one transformation, which works reasonably well for all. The Box-Cox transformation is widely used and can be easily managed so that the skewness of transformed data Z(x,t) becomes close to zero (Salas, 1993).

However, rainfall histogram in arid regions, as stated by Hevesi et al. (1992), behaves as lognormal distribution. Hence, the transformation as $Y = \ln Z(x)$ is applied for determining approximately normal annual and seasonal data. It is accepted as normally distributed, if the computed Kolmogorov-Smirnov statistic (D_{max}) is less than the corresponding critical value. The critical value for the 5% level of significance is $D_{0.05} = 0.171$, which is greater than D_{max} of transformed data. Thus the null hypothesis of the transformed data normality cannot be rejected at 0.05 level of significant. Further investigation can be done by visually observing the normal probability plots, and most of the data lie on a straight line for the transformed rainfall values. In addition, the skewness coefficients are reduced close to zero (Subyani, 2005). Table 5.10 shows the statistics and normality test for original and transformed annual and seasonal data.

The back-transformed value, i.e., exp (Y(x)) is biased predictor. However, the unbiased expression for the Kriging estimates Z(x) is given by Aboufirassi and Mariño (1984), Gilbert (1985), and Deutsch and Journel (1992). As

$$Z^*(x) = \exp\left\{Y^*(x) + \sigma_y^2/2\right\}, \tag{5.67}$$

where $Z^*(x)$ is the original data in millimeters; and $Y^*(x)$ is the natural logarithm, and σ_y^2 is the lognormal Kriging variance. The estimation variance is given as

$$\sigma_{Z^*}^2 = \left(Z^*\right)^2 \left[\exp\left(\sigma_y^2\right) - 1\right]. \tag{5.68}$$

These two last expressions are used for constructing the rainfall isohyetals and their variances. Figure 5.25 shows the sample and fitted SV for the natural log of average annual rainfall (LnAAR). An isotropic spherical model with no nugget, but with a sill equal to the sample variance of 0.48, and a range of 110 km, is selected as the best representation of the spatial structure.

Table 5.10 Descriptive statistics and normality test for annual and seasonal data

Season	Mean (mm)	Median (mm)	St. Dev. (mm)	Skewness	CV(%)	K-S (D_m)
Annual	232	178	151	0.8	0.65	0.18
Winter	55.0	41.0	43.1	1.15	0.78	0.20
Spring	94.0	81.0	68.0	0.72	0.72	0.14
Summer	47.6	32.0	47.3	1.84	0.99	0.17
Fall	35.2	21.0	33.2	1.44	0.95	0.19
ln-Annual	5.22	5.18	0.7	−0.7	0.13	0.10
ln-Winter	3.71	3.71	0.79	−0.051	0.21	0.07
ln-Spring	4.21	4.39	0.92	−0.65	0.22	0.11
ln-Summer	3.38	3.46	1.06	−0.24	0.31	0.08
ln-Fall	3.1	3.04	1.02	−0.15	0.33	0.08

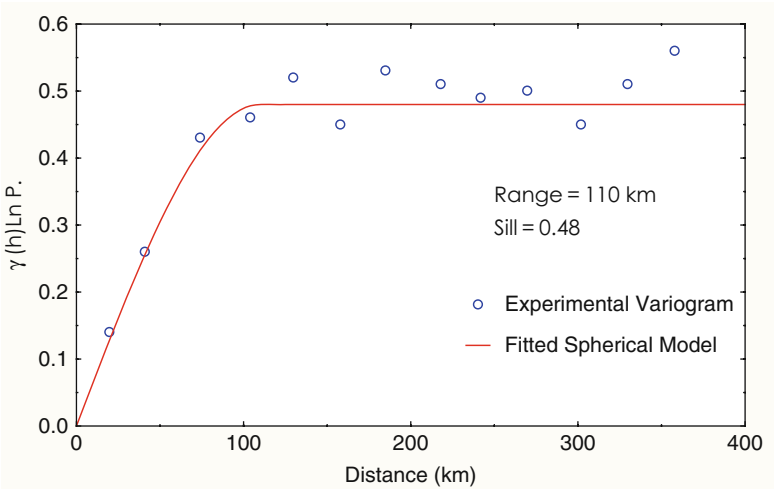

Fig. 5.25 Experimental and fitted SV model for Ln-annual rainfall

Cross-validation is applied to check whether the spherical model is adequate to describe the spatial correlation of the annual rainfall. For diagnostic check, the mean estimation error (MEE) and the root-mean-square errors (RMSE) for LnAAR are 0.067 and 0.94, respectively, which suggest the validity of the spherical model. Similar tests are performed for seasonal values and the results are shown in Table 5.11.

Figure 5.26 presents the sample and theoretical SVs and their parameters for winter, spring, summer, and fall seasons. In winter, the sample SV model is fitted with the small nugget as 0.05. The sill is 0.67 and the practical range of dependency, i.e., radius of influence, is 70 km (Fig. 5.26a).

In spring sample SV behaved as an exponential model with nugget of 0.1. The sill is 0.95 with a practical range of dependency equal to 90 km (Fig. 5.26b). In the summer and fall, the sample SV behaves as a spherical model. The sill for these two seasons is around 1.00, and the ranges of correlation are within 140 km and 110 m, respectively (see Fig. 5.26c and d).

Kriging estimates are computed for the average annual and seasonal rainfall amounts. The sample SV represents the continuity structure quite well. The cross-validation supports selection of models and their parameters. For Kriging estimation and variance, the back-transformed values are applied.

Table 5.11 SV Cross-validation

Season	Model	N	MEE	RMSE
Ln-Annual	Spherical	60	0.067	0.94
Ln-Winter	Exponential	60	0.027	0.84
Ln-Spring	Exponential	61	0.08	0.71
Ln-Summer	Spherical	62	0.07	0.91
Ln-Fall	Spherical	62	0.04	1.08

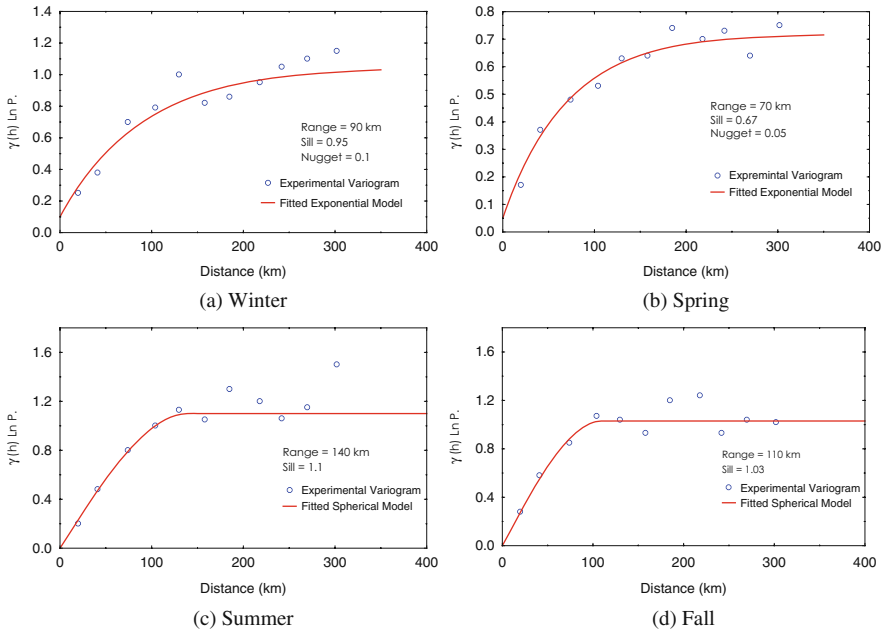

Fig. 5.26 Experimental and fitted SV models for Ln-seasonal rainfall

The kriged isohyets for annual rainfall show a rapid increase in average from the Red Sea shore line up to the mountains and a gradual decrease to the north and east parts of the study area (Fig. 5.27a).

Orographic effects are produced toward the mountain area with the maximum kriged estimate exceeding 350 mm/year. In the east and northeast parts of the study area, Kriging estimates are around 100 mm/year. In the northern part with a moderate elevation reaching more than 1,000 m, Kriging estimates also exceed 100 mm/year. This figure reflects the topographic variation similar to Fig. 5.24 with annual rainfall that generally increases with elevation.

Kriging variances indicate similar behavior to the average annual rainfall estimates. Small values near the clusters of stations in the mountain area (Fig. 5.27b) indicate high estimation accuracy, whereas large values in the north, east, and northeast indicate low estimation accuracy areas owing to the scarcity of sample locations. Generally, high estimation variances appear at areas of lacking data.

In winter (December–February), rainfall is associated most of the time with moist and cold air of northerly Mediterranean origin, which is coupled with the local effects of the Red Sea convergence zone the Scarp mountains as well as orographic rainfall occurrences. Figure 5.28a shows that the Kriging estimates exceed 120 mm in the middle and northern section of the mountainous areas.

However, they do not exceed 30 mm in the south of Tihamah, because there is no Mediterranean or Red Sea effect, and the elevation is not high enough for orographic rainfall occurrence. On the other hand, the southern part of the study area receives less than 100 mm of rainfall due to the absence of monsoons. The Plateau area (east

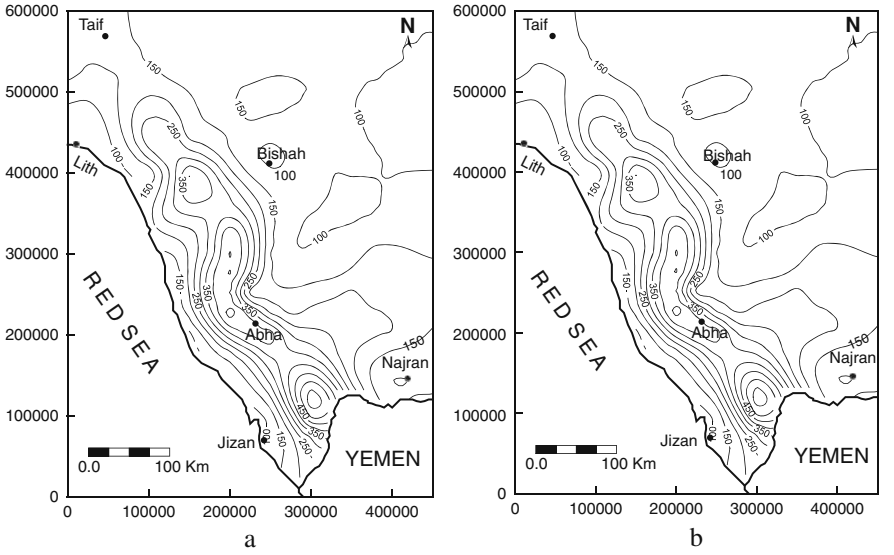

Fig. 5.27 Isohyetal map of Kriging for annual rainfall (mm)

and northeast parts of the study area) receives less than 20 mm, because it is located in the shadow (lee-side) area. Kriging estimation variance map has a similar trend throughout the study area as shown in Fig. 5.28b.

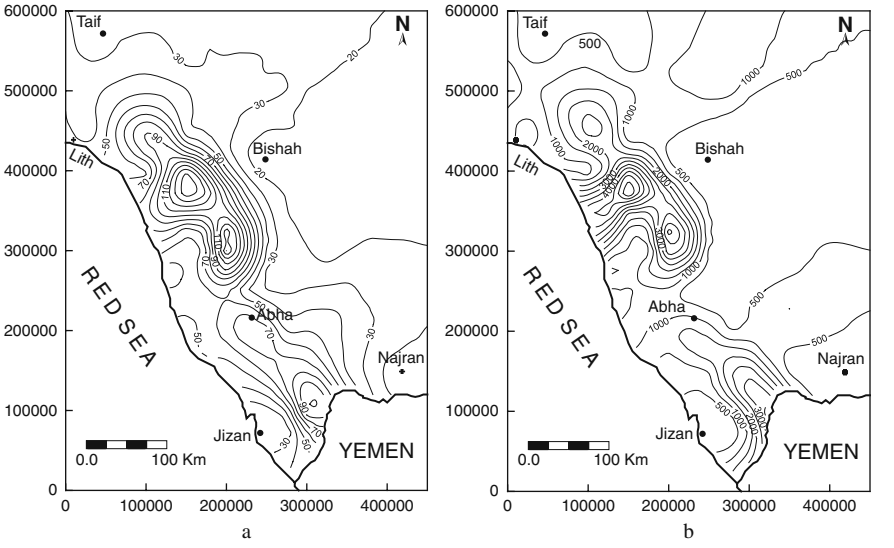

Fig. 5.28 Isohyetal map of Kriging for winter rainfall (mm)

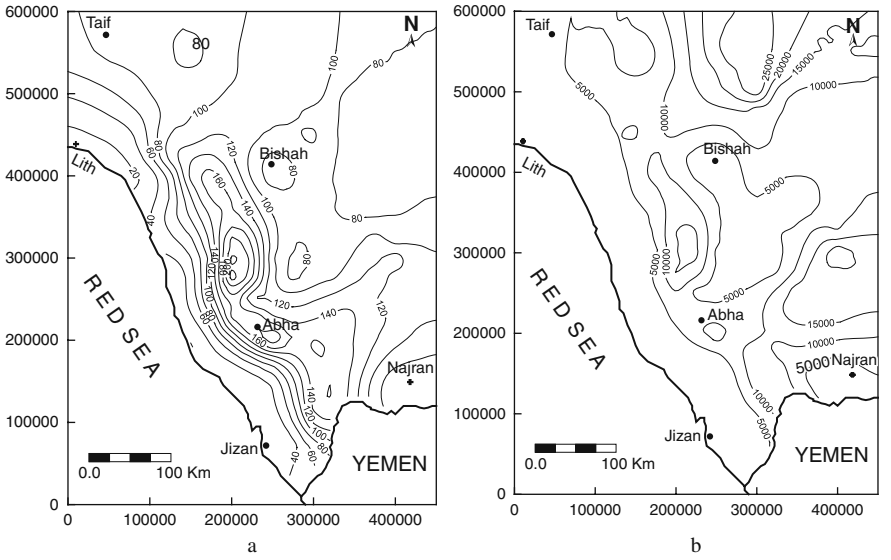

Fig. 5.29 Isohyetal map of Kriging for spring rainfall (mm)

In spring (March–May), the whole region comes under the influence of southeast monsoon air stream flow, the Red Sea convergence zone, and Mediterranean depression, which distribute the rainfall in all regions. The Kriging estimates give more detailed information about the rainfall distribution as shown in Fig. 5.29a.

Rainfall in this figure increases gradually from the Red Sea coast (40 mm) to the mountain where the highest amount of rainfall falls (more than 160 mm) and decreases to the plateau area, which receives about 100 mm. Generally, the southwest region of the Arabian Peninsula receives the highest amount of rainfall during the spring season compared to other seasons. This high amount of rainfall is a result of increasing African–Mediterranean interaction effect, where rainfall occurs orographically in the mountains and southeast monsoon effect where the Plateau and eastern slope receive more rainfall than the Red Sea coast. Kriging variances show an increase in estimation accuracy as shown in Fig. 5.29b.

In summer (June–August), the southwest monsoon flow from the Indian Ocean and the Arabian Sea is the predominant factor, which increases the rainfall along the Scarp mountains and low elevation areas in the south of the study area. Kriging estimates for summer season exceed 120 mm in the mountains and 160 mm in the foothills near the Yemen border at the southwestern corner of the Arabian peninsula (Fig. 5.30a).

Rainfall decreases toward the northern part of the study area due to its distance from the monsoon effect, even though this area has a high elevation. Moreover, the Kriging variances show no change in estimation accuracy in the foothills and mountains, but they cannot be calculated with reliability in the plateau areas due to the paucity of data (see Fig. 5.30b).

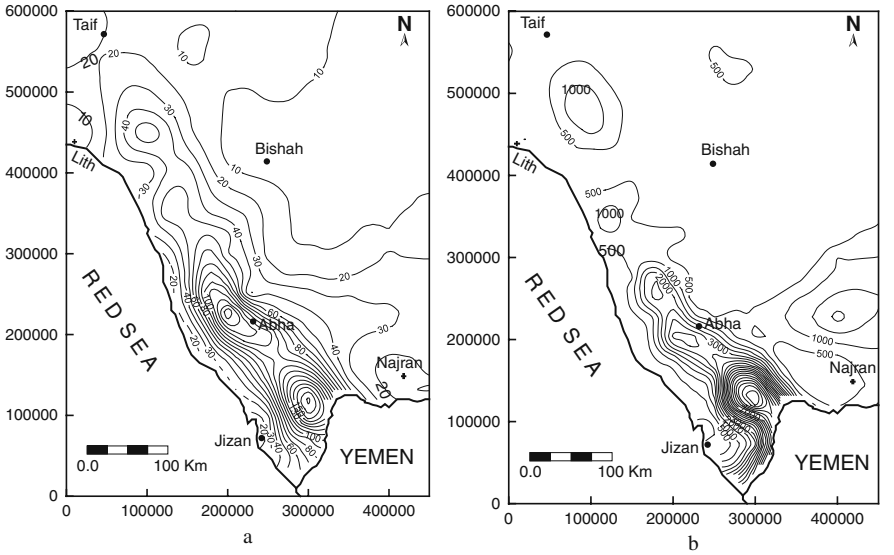

Fig. 5.30 Isohyetal map of Kriging for Summer rainfall (mm)

In fall (September–November), the local diurnal circulation and the southern air stream weakens. In other words, it is a transition period from summer to winter and, in general, the area receives little amount of rainfall. The Kriging estimation in the foothills and the mountains in the southern part of the study area shows that they receive higher amount of rainfall than the northern areas, similarly to the fall monsoon flow effects as shown in Fig. 5.31a. The Kriging variances show an increase in

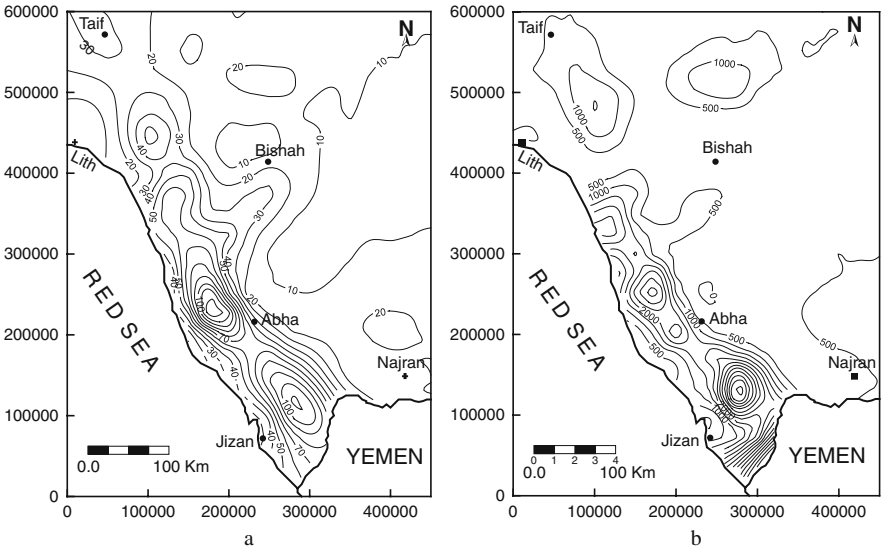

Fig. 5.31 Isohyetal map of Kriging for fall rainfall (mm)

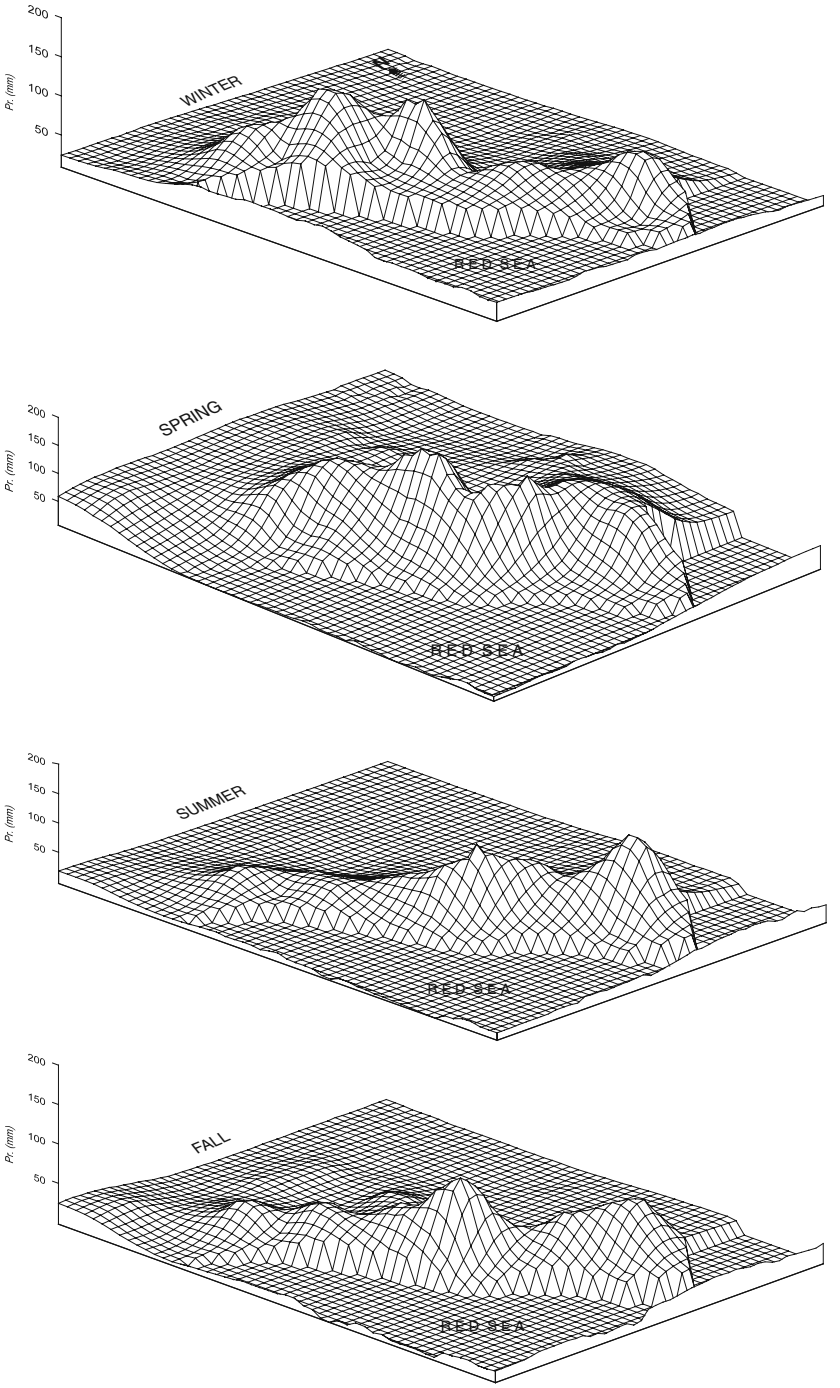

Fig. 5.32 Spatiotemporal Kriging maps for rainfall in southwest Saudi Arabia

estimation accuracy in the northern part of the study area, whereas there is no clear change in the southern part as shown in Fig. 5.31b.

Generally, rainfall is predominant in the northern mountain areas during winter as a result of the Mediterranean effect, and it is widespread in all regions during spring because of the local diurnal circulation effects. Orographic conditions are clear in winter and spring seasons. This orographic factor is also clear for the appearance of the nugget effect in the exponential models in both winter and spring seasons. During summer, rainfall moves toward the south due to the monsoon flow effect, with its southwesterly wind. However, during fall, as a transition season, the area comes under the influence of monsoon as well as the local diurnal circulations. Figure 5.32 illustrates these spatio-seasonal variations of rainfall in the southwest of Saudi Arabia.

The Kriging estimation variances are also investigated concerning the spatial and temporal variation of rainfall in the study area for these four seasons. In space variation, the small value or high estimation accuracy of Kriging variances occurs in the mountainous areas in all seasons. Towards the east, north, and northeast of the study area, there is a consistent increase in variances implying low estimation accuracy. In time variation, Kriging variance increases from winter to fall. These variations in space and time are due to several factors such as

1) Clusters of stations in the mountain areas reflect higher estimation accuracy.
2) Scarcity of stations in north, east, and northeast areas reflects lower estimation accuracy.
3) High variability in summer and fall rainfall gives rise to low accuracy estimation compared with the somewhat lower variability in rainfall during winter and spring seasons.

The description of the rainfall variability in space and/or in time is among the fundamental requirements for a wide variety of human activities and water resources project design, management, and operation. Geostatistical methods are applied to develop new maps for the prediction of rainfall over different seasons. The assigned objectives of this study are to predict the magnitude and variation of the rainfall in space as well as during different time periods. These techniques are applied to rainfall data gathered from meteorological station network covering the southwest region of the Arabian Peninsula. Rainfall in this area is characterized by high variation in spatial and temporal distributions.

References

Aboufirassi, M., and Mariño, M. A., 1984. A geostatistically based approach to the identification of aquifer transmissivities in Yolo Basin, California. Math. Geol. 16(26), 125–137.

Al-Jerash, M., 1985. Climatic subdivisions in Saudi Arabia: an application of principle component analysis, J. Climate 5, 307–323.

Barnes, S. L., 1964. A technique for maximizing details in numerical weather map analysis. J. Appl. Meteor. 3, 396–409.

Box, G. E. P., and Jenkins, G. M., 1976. Time Series Analysis Forecasting and Control. Holden Day, San Francisco, 560 pp.

Buell, C. E., 1958. The correlation between wind and height on a isobaric surface II: summer data. J. Meteorol. 15(12), 502–512.

Carr, J., and Glass, C., 1984. Estimation of earthquake response spectra using Kriging. In: G. Verly et al. (Eds.), Geostatistics for Natural Resources Characterization. Proceedings of the 2nd NATO Advanced Study Institute of Geostatistics for Natural Resources Characterization: Part 2, D. Reidel, Dordrecht, Holland, pp. 745–752.

Carr, J., Bailey, R., and Deng, E., 1985. Use of indicator variogram for an enhanced spatial analysis. J. Math. Geol. 18, 197–213.

Carr, J., and Glass, C., 1985. Treatment of earthquake ground-motion using regionalized variables. J. Math. Geol. 17, 221–241.

Clark, I., 1979. Practical Geostatistics. Applied Science Publishers, London, 281 pp.

Cressie, N. A. C., 1993. Statistics for Spatial Data (revised edition). Wiley, New York, 900 pp.

Cressman, G. P., 1959. An operational objective analysis system. Monthly Weather Rev. 87(10), 367–374.

David, M., 1977. Geostatistical Ore Reserve Estimation. Elsevier Scientific Publishing Company, 364 pp.

Davis, J. C., 1986. Statistics and Data Analysis in Geology. John Wiley & Sons, Inc., New York, 646 pp.

Delhomme, J. P., 1978. Kriging in the hydrosciences. Adv. Resour. 1, 251.

Deutsch, C. V., and Journel, A. G., 1992. GSLIB Geostatistical Software Library and User's Guide. Oxford University Press, New York, TIC: 224174.

Dixon, R., 1969. Orthogonal polynomial as a basis for objective analysis. Meteorological Office, Scientific Paper No. 30, Her Majesty's Stationery Office, London, 20 pp.

Dixon, R., 1976. An objective analysis using orthogonal polynomials. Proceedings of the JOC Study Group Conference on four-dimensional Data Assimilation, Paris, GARP Program on Numerical Experimentation, Report No. 11, pp. 73–85.

Eddy, A., 1964. The objective analysis of horizontal wind divergence fields. Quart. J. Roy. Meteorol. Soc. 90, 424–440.

Eliassen, A., 1954. Provisional report on spatial covariance and autocorrelation of the pressure field. Inst. Weather and Climate Research Academy of Science Oslo Report No. 5.

Fisher, R. A., 1935. The Design of Experiments. Oliver and Boyd, Edinburg.

Flattery, T. W., 1970. Spectral models for global analysis and forecasting, Proceedings of the Sixth AWS Technical Exchange Conference, U. S. Naval Academy, 21–21 September, Air Weather Service Technical Report 242, pp. 42–54.

Fritsch, J. M., 1971. Objective analysis of a two-dimensional data field by the cubic spline technique. Monthly Weather Rev. 99(5), 1122–1143.

Gandin, L. S., 1963. Objective Analysis of Meteorological Fields. Leningrad, Gidromet; Translated from Russian, Jerusalem, Israel Program for Scientific Translations, 1965, 242 pp.

Gandin, L. S., 1965. Objective Analysis, Lectures on Numerical Short-range Weather Prediction, WMO, Regional Training Seminar, pp. 633–677.

Gilbert, S., 1985. Introduction to Applied Mathematics. Wellesley-Cambridge Press, Wellesley, MA 02181.

Glass, C. E., 1978. Application of regionalized variables to micro-zonation. Proc. 2nd Int. Conf. Micro-zonation for Safer Construction 1, 509–512.

Habib, Z., 1999. Optimum interpolation modeling supported by the cumulative semivariogram for spatial-temporal meteorological variables. Unpublished Ph.D. Thesis, Istanbul Technical University, 156 pp.

Hevesi, J. A., Istok, J. D., and Flint, A. L., 1992. Precipitation estimation in mountainous terrain using multivariate geostatistics, Part I. Structural analysis. J. App. Met. 31, 661–676.

Hubert, P., Carbomnel, J. D., and Chaouche, A., 1989. Segmentation des series hydrometeoraloques: application a des series de precipitation et de debits de L'Afrique de L'ouest. J. Hydrol. 110, 349–367.

Iruine, K. N., and Eberthardt, A. K., 1992. Multiplicative seasonal ARIMA models for lake Erie and Lake Ontario water levels. Water Res. Bull. 28(3), 385–396.
Isaaks, E. H., and Srivastava, R. M., 1989. An Introduction to Applied Geostatistics. Oxford University Press, Oxford, 561 pp.
Journel, A. G., and Huijbregts, C. I., 1978. Mining Geostatistics. Academic Press, London, 710 pp.
Journel, A. G., 1983. Non-parametric estimation of spatial distribution. Math. Geol. 15(13), 445–468.
Kalman, R. E., 1960. A new Approach to linear filtering and prediction problem. J. Basic Eng. Series D 82(1), 35–45.
Kitanidis, P. K. 1997. Introduction to Geostatistics: Applications in Hydrogeology. Cambridge University Press, Cambridge, 249 pp.
Krige, D. G., 1951. A statistical approach to some basic mine evaluation problems on the Witwateround. J. Chimic. Min. Soc. South-Africa 52, 119–139.
Ledimet, F., and Talagrand, O., 1986. Variational algorithms for analysis and assimilation of meteorological observation: theoretical aspects. Tellus 38A(2), 97–110.
Lorenc, A. C., 1981. A global three-dimensional multivariate statistical interpolation scheme. Monthly Weather Rev. 109, 701–721.
Loucks, F. D., 1989. Modeling the Great Lakes hydrologic-hydraulic system. Ph D Thesis, University of Wisconsin, Madison.
Marsily, G. D., 1986. Quantitative Hydrogeology, Groundwater Hydrology for Engineers. Academic Press, New York.
Martinez, C. A., 1996. Multivariate geostatistical analysis of evapo-transpiration and precipitation in mountainous terrain. J. Hydrol. 174, 19–35.
Matheron, G., 1963. Principles of geostatistics. Econ. Geol. 58, 1246–1266.
Matheron, G., 1971. The theory of regionalized variables and its applications. Ecole de Mines. Fontainbleau, France.
Mathier, L., Fagherazzi, L., Rasson, J. C., and Bobee, B., 1992. Great Lakes net basin supply simulation by a stochastic approach. INRS-Eau Rapp Scient (fique 362, INRS-Fau, Sainte-Foy), 95 pp.
Meleschko, V. P., and Prigodich, A. E., 1964. Objective analysis of humidity and temperature. Trudy Sympoziuma Pochislenyum Melodam Prognoza Pagody, Gidrometeoizdat, Moscow, U.S.S.R.
Myers, D. E., Begovich, C. L., Butz, T. R., and Kane, V. E., 1982. Variogram models for regional groundwater chemical data. Math. Geol. 14, 629–644.
Olea, R. A., 1975. Optimum mapping techniques using regionalized variable theory: series on spatial analysis no. 3. Lawrence, Kansas, Kansas Geological Survey, 137 pp.
Olea, R. A., 1999. Geostatistics for Engineers and Earth Scientists. Kluwer Academic Publishers, Boston, MA, 303 pp.
Panofsky, H. A., 1949. Objective weather map analysis. J. Meteorol. 6, 386–392.
Privalsky, V., 1990. Statistical analysis and predictability of Lake Erie water level variations. In: H. C. Hurtmann and M. J. Donalhue (Eds.), Proc Great Lakes Water Level Forecasting and Statistics Symposium. Great Lake Comission, Ann Arbor, Michigan, pp. 255–264.
Salas, M., 1993. Analysis and modeling of hydrologic time series. In: D. A. Maindment (Ed.), Handbook of Hydrology. McGraw-Hill, New York, pp. 19.1–19.72.
Sasaki, Y., 1958. An objective analysis based on variational method. J. Meteorol. Soc. Japan 36(3), 77–88.
Schlatter, T. W., and Branstator, G. W., 1987. Experiments with a three-dimensional statistical objective analysis scheme using FGGE data. Monthly Weather Rev. 115, 272–296.
Schlatter, T. W., 1988. Past and present trends in the objective analysis of meteorological data for now-casting and numerical forecasting. Eight Conference on Numerical Weather Prediction, American Meteorological Society, pp. j9–j25.
Seo, D. J., 1998. Real-time estimation of rainfall fields using radar rainfall and rain gage data. J. Hydrol. 208(1–2), 37–52.
Şen, Z., 1980. Adaptive Fourier analysis of periodic-stochastic hydrologic series. J. Hydrol. 46, 239–249.

Şen, Z., 1983. Predictive hydrologic models in hydrology. Nordic Hydrol. 14, 19–32.
Şen, Z., 1997. Objective analysis of cumulative semivariogram technique and its application in Turkey. J. Appl. Meteorol. 36, 1712–1720.
Şen, Z., Kadıoğlu, M., and Batur, E., 1999. Cluster regression model and level fluctuation features of Van Lake, Turkey. Ann. Geophysicae, 17, 273–279.
Şen, Z., and Habib, Z., 2000. Spatial precipitation assessment with elevation by using point cumulative semivariogram technique. Water Resour. Management 14, 311–325.
Şen, Z., Kadıoğlu, M., and Batur, E., 2000. Stochastic modeling of the Van Lake monthly fluctuations in Turkey. Theor. Appl. Climatol. 65, 99–110.
Şen, Z., 2008. Wadi Hydrology. CRC Lewis Publishers, Boca Raton, 386 pp.
Slivitzky, M., and Mathier, L., 1993. Climatic changes during the 20th century on the Laurentian Great Lakes and their impacts on hydrologic regime. NATO Advanced Study Institute, Deauaille, France.
Sneyers, R., 1992. On the use of statistical analysis for the objective determination of climate change. Meteorol Z. 1, 247–256.
Student, 1907. On the error of counting with a hemacytometer. Biometrika 5, 351–360.
Subyani, A. M., 2004. Geostatistical study of annual and seasonal mean rainfall patterns in southwest Saudi Arabia. Hydrol. Sci. J. 49(5), 803–817.
Subyani, A. M., 2005. Hydrochemical identification and salinity problem of groundwater in Wadi Yalamlam basin, Western Saudi Arabia. J. Arid Environ. 60(1), 53–66.
Vannitseni, S., and Demaree, G., 1991. Detection et modelisation des secheresses an Sahel-proposition d'une nouvelle methodologie. Hydra! Continent 6(2), 155–171.
Yates, F., 1938. The comparative advantages of systematic and randomized arrangements in the design of agricultural and biological experiments. Biometrika 30, 444–466.
Zadeh, L. A., 1968. Probability measures of fuzzy events. Oikos. 23, 421–427.

Chapter 6
Spatial Simulation

Abstract Earth sciences phenomena are heterogeneous, anisotropic, non-uniform, random, especially in their spatial behaviors, and their exhaustive sampling is not possible and the only scientific way for the regional and global assessment of these phenomena is through suitable mathematical modeling techniques. The main purpose is to deduce from limited and small samples the general characteristics and finally the generating mechanism of the phenomenon. Development in computer sciences enhanced time-consuming simulation studies, which developed into a feasible and practical tool to reveal non-linear and non-equilibrium evolution of an earth sciences phenomenon based on the fundamental laws governing the nature. Nonlinearity and causality of a natural phenomenon are demonstrated to be consistently explained by simulations based on fundamental laws. Simulation methodology is timely born with practically usable starts of digital computers during 1950s. Simulation studies are essential because the existing analytical methods are not sufficiently powerful to prove the validity of the fundamental laws for naturally occurring phenomena, but simulation could do this effectively. Spatial pattern simulations in one-, two-, and three-dimensional space are explained through autoregressive models, which are based on the spatial correlation function. Rock masses are fractured into different sizes and they are intact from each other due to fracturing. Different simulation techniques are presented for dependent (persistent) and independent fracture patterns, which are exemplified in the field by scanline measurements. Along this line, Rock Quality Designation (RQD) quantification is furnished through various simulation models and final products are presented in terms of various charts that can be used in practical applications. Porous medium is very significant for water, oil, and gas storages, and therefore its spatial behavior is significant for effective assessments, planning, operation, and management. Autorun spatial modeling technique is developed and applied for the simulation of porous medium. Finally, the application of the cumulative semivariogram technique is presented for intact length simulation in rock masses.

Keywords Autoregressive models · Autorun · Simulation · Fracture network · Rock quality designation · Intact length · Persistence · Markov process · ARIMA process · Multi-directional simulation

Z. Şen, *Spatial Modeling Principles in Earth Sciences*,
DOI 10.1007/978-1-4020-9672-3_6,

6.1 General

Spatial simulation models of geological phenomenon such as ore grades, groundwater level elevations, porosity, chemical compositions of different lithological units, fracture spacing are bound to be increasingly important, due to their ability to model the underlying generating mechanism of these phenomena. The first approximations in quantifying the geological phenomena were rather deterministic and they did not take into account any factor of chance in their descriptions. In fact, the variability in these phenomena was known to geologists for many decades, but due to the deterministic training the solutions sought were also deterministic. For instance, at most the arithmetical average of the data concerned is calculated and then this value is treated as the best estimator of the phenomena. This way of calculation gave rise to over-estimations, which consequently made the geologists aware of the fact that the variability within the data should definitely be taken into consideration (Krige, 1951). This awareness led geologists to consider the frequency distribution functions of any spatial variable. Hence, a new trend of statistical methods in analyzing the geological data was started (Krumbein, 1970; Agterberg, 1975). It is a mere application of the statistical methods to process geologic data.

Later, it was recognized that, in addition to variability inherent in the data, the interdependence either within the data themselves or with other variables is very important due to the continuity of spatial variables. In order to account for the dependence either the correlation techniques (Matern, 1960; Switzer, 1965) or the SVs are employed (Matheron, 1965).

As a consequence of the aforementioned developments, the geologists started to think about a convenient model to simulate the spatial variables so as to be able to control them in the case of any change as well as in assessing the risks associated with the data. Of course, developments of digital computers had a great impact on this trend since without computers any simulation study is very tedious, needs great patience, and is rather time-consuming, i.e., not practical.

Although simulation studies in other branches of science like engineering and economics have started long time ago, the simulation of geological phenomena is postponed. This is due to the fact that in other disciplines simulation is needed only along one axis, for instance, time axis. Therefore, the simulation of one dimensional variable is extensively available in the literature (Box and Jenkins, 1970).

General simulation models are possible for the generation of anisotropic as well as isotropic synthetic patterns in 1D, 2D, or 3D, which have significance for the purpose of modeling geologic properties such as ore grades, reservoir porosity, mineral distribution, fracture spacing, aperture, orientation. General procedures for such simulations by the autoregressive processes (including Markov processes) are given for the model parameters estimation and synthetic pattern generation. The model works on the square net basis and generates sequential pattern, first along any desired direction for 1D simulation and then 2D patterns are constructed with reference to two orthogonal 1D sequences. Applications to synthetic 2D pattern are shown for isotropic cases with different model parameters. The extension of model to 3D space is readily available.

Because any geologic phenomenon occurs in space, in general, it has to be simulated in 3D space. The first of spatial simulation models was proposed by Cliff and Ord (1973), who took into consideration an overall spatial correlation coefficient, a set of physical constants, and a random component all within a linear model concept. Later, Journel (1974) proposed a turning-band method whereby 2D or 3D geological variables are projected onto equally spaced lines and then 1D simulation along these lines is transformed into 3D variables. On the other hand, Sharp and Aroian (1985) have presented herringbone method of simulation for 2D and 3D geological variables. However, as explained by Şen (1989a) there are some practical problems with their model.

6.2 3D Autoregressive Model

The general form of the simulation model for 3D is similar to autoregressive models (Markov processes), which can be given as

$$x_{i,j,k} = \alpha x_{i-1,j,k} + \beta x_{i,j-1,k} + \gamma x_{i,j,k-1} + \varepsilon_{i,j,k,} \tag{6.1}$$

where $x_{i,j,k}$ is the spatial variable at a point with coordinates i, j, and k with respect to a reference point as in Fig. 6.1.

Herein, α, β, and γ are the model parameters and $\varepsilon_{i,j,k,}$ is a random component with zero mean and variance, $\sigma_\varepsilon{}^2$, and it is independent from $x_{i-1,j,k}$, $x_{i,j-1,k}$, and $x_{i,j,k-1}$. This model has four parameters, namely α, β, γ, and $\sigma_\varepsilon{}^2$, to be determined from an available set of data. In Eq. (6.1) the geologic variable, $x_{i,j,k}$ is a standard variable with zero mean and unit variance. This does not cause any loss of generality in simulation studies, since after the simulation of standard variables the final form of them can be found as

$$X_{i,j,k} = \mu_{i,j,k} + \sigma_{i,j,k} x_{i,j,k}, \tag{6.2}$$

in which $X_{i,j,k}$ is the spatial variable at position (i, j, k) with mean, $\mu_{i,j,k}$, and standard deviation, $\sigma_{i,j,k}$. Standardization procedure renders the original variable into

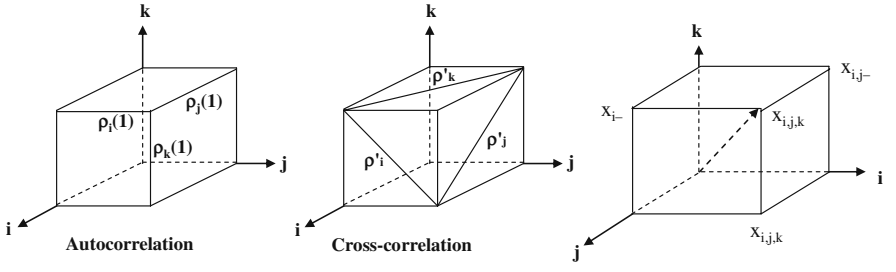

Fig. 6.1 3D space

a second-order stationary variable (Şen, 1979b). Any simulation model has three major stages in arriving at its final goal. These are

1) Given a set of observations $x_{i,j,k}$ (i, j, k = 1, 2, …, n) how to express model parameters as functions of data? This is referred to as parameters estimation stage.
2) How to check the validity of model for given data? This is the identification stage, which is achieved by calculating the residuals as

$$\varepsilon_{i,j,k} = x_{i,j,k} - \alpha x_{i-1,j,k} - \beta x_{i,j-1,k} - \gamma x_{i,j,k-1}. \tag{6.3}$$

   If the model is valid, then the sequence of $\varepsilon_{i,j,k}$ should have an independent (completely independent) structure. This stage is referred to as the diagnostic checking for model suitability.
3) Usage of the suitable model to generate equally likely synthetic sets of data that are statistically indistinguishable from the original data, i.e., they should have the same distribution functions and average statistical parameters. This corresponds to the simulation of the underlying geological phenomenon. In real-time estimations, this is equivalent to prediction stage.

6.2.1 Parameters Estimation

The model parameters must be estimated from available data such that the simulated variables yield statistically indistinguishable parameters in the long run. One of the basic requirements in any simulation is to derive meaningful relationships between the model and the statistical parameters of the available data. The number of model parameters should be equal to the number of statistical parameters and accordingly Eq. (6.1) allows the preservation of four statistical parameters. The expectations (arithmetic averages) provide obsolete information because of the standardization procedure as $E(x_{i,j,k}) = E(x_{i-1,j,k}) = E(x_{i,j-1,k}) = E(x_{i,j,k-1}) = 0$, and $E(\varepsilon_{i,j,k}) = 0$. Further low-order statistical parameters are the spatial variance and three lag-one autocorrelation coefficient each along i, j, and k axes. For the variance, the multiplication of both sides in Eq. (6.1) by $x_{i,j,k}$ and then taking expectations leads to

$$E\left(x_{i,j,k}^2\right) = \alpha E\left(x_{i-1,j,k}x_{i,j,k}\right) + \beta E\left(x_{i,j-1,k}x_{i,j,k}\right) + \gamma E\left(x_{i,j,k-1}x_{i,j,k}\right) + E\left(\varepsilon_{i,j,k}x_{i,j,k}\right), \tag{6.4}$$

where $E\left(x_{i,j,k}^2\right) = 1$, $E(x_{i-1,j,k}x_{i,j,k}) = \rho_i(1)$, $E(x_{i,j-1,k}x_{i,j,k}) = \rho_j(1)$ and $E(x_{i,j,k-1}x_{i,j,k}) = \rho_k(1)$. Because $\varepsilon_{i,j,k}$ is dependent on $x_{i,j,k}$ only, one can write $E(\varepsilon_{i,j,k}x_{i,j,k}) = E(\varepsilon_{i,j,k})^2 = \sigma_\varepsilon{}^2$, the substitution of these last expressions into Eq. (6.4) yields

$$\alpha\rho_i(1) + \beta\rho_j(1) + \gamma\rho_k(1) + \sigma_\varepsilon^2 = 1, \tag{6.5}$$

in which $\rho_i(1)$, $\rho_j(1)$, and $\rho_k(1)$ are the lag-one autocorrelation coefficients along the i, j, and k axes, respectively. It is obvious that Eq. (6.4) reduces to Sharp and Aroian (1985) simulation expression if $\alpha = \beta = \gamma = \phi''$ and with their notations $\rho_i(1) = \rho_{100}$, $\rho_j(1) = \rho_{010}$, $\rho_k(1) = \rho_{001}$ and $\sigma_\varepsilon{}^2 = \sigma_a{}^2$. Multiplication of both sides in Eq. (6.1) by $x_{i-1,j,k}$, $x_{i,j-1,k}$, and $x_{i,j,k-1}$, respectively, and taking expectations leads to three additional equations as

$$\rho_i(1) = \alpha + \beta\rho_k' + \gamma\rho_j', \tag{6.6}$$

$$\rho_j(1) = \alpha\rho_k' + \beta + \gamma\rho_i', \tag{6.7}$$

$$\rho_k(1) = \alpha\rho_j' + \beta\rho_i' + \gamma, \tag{6.8}$$

in which $E(x_{i-1,j,k}x_{i,j-1,k}) = \rho_k{}'$, $E(x_{i-1,j,k}x_{i,j,k-1}) = \rho_j{}'$, and $E(x_{i,j,k-1}x_{i,j-1,k}) = \rho_i{}'$, where $\rho_k{}'$, $\rho_j{}'$, and $\rho_i{}'$ indicate the lag-one cross-correlation coefficients on the $k = j = i =$ constant planes, respectively. Furthermore, because $\varepsilon_{i,j,k}$ is independent of $x_{i-i,j,k}$, $x_{i,j-1,k}$, and $x_{i,j,k-1}$. Hence, $E(\varepsilon_{i,j,k}x_{i-1,j,k}) = 0$, $E(\varepsilon_{i,j,k}x_{i,j-1,k}) = 0$, and $E(\varepsilon_{i,j,k}x_{i,j,k-1}) = 0$. A sketch has been presented in Fig. 6.2 to show the auto- and cross-correlations.

The four unknown model parameters can be obtained as a result of simultaneous solution of Eqs. (6.5, 6.7, and 6.8). It is possible to arrange these equations in matrix form explicitly as

$$\begin{bmatrix} \rho_i(1) & \rho_j(1) & \rho_k(1) & 1 \\ 1 & \rho_k' & \rho_j' & 0 \\ \rho_k' & 1 & \rho_i' & 0 \\ \rho_j' & \rho_i' & 1 & 0 \end{bmatrix} \begin{bmatrix} \alpha \\ \beta \\ \lambda \\ o_\varepsilon^2 \end{bmatrix} = \begin{bmatrix} 1 \\ \rho_i(1) \\ \rho_j(1) \\ \rho_k(1) \end{bmatrix}, \tag{6.9}$$

or implicitly as

$$AX = C, \tag{6.10}$$

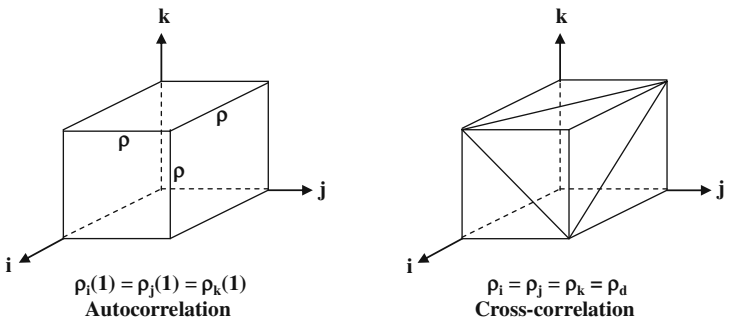

Fig. 6.2 Auto- and cross-correlation representations in anisotropy model

where A is a (4×4) matrix of coefficients with its elements estimated from a given set of data, hence it is known and dependent on the available data only; X is the unknowns vector and includes the model parameters only; and, finally C is the vector of lag-one autocorrelations. The solution of Eq. (6.8) requires matrix inversion of A, after which the solution can be written as

$$X = A^{-1}C. \tag{6.11}$$

It is necessary that A be a positive semi-definite matrix. Alternatively, a point worth to notice is that Eqs. (6.6, 6.7, and 6.8) include three unknowns (α, β, and γ) and after their simultaneous solution the substitution of these model parameters into Eq. (6.5) yields $\sigma_\varepsilon{}^2$. The matrix notation of these three equations is

$$\begin{bmatrix} 1 & \rho_k & \rho_k \\ \rho'_k & 1 & \rho'_i \\ \rho'_j & \rho'_i & 1 \end{bmatrix} \begin{bmatrix} \alpha \\ \beta \\ \gamma \end{bmatrix} = \begin{bmatrix} \rho_i\,(1) \\ \rho_j\,(1) \\ \rho_k\,(1) \end{bmatrix}, \tag{6.12}$$

in which the coefficient matrix is symmetric and positive semi-definite. Application of Cramer's rule leads to the following results:

$$\alpha = \frac{\rho_i(1) + (\rho'_k\rho'_i - \rho'_j)\rho_k(1) + (\rho'_j\rho'_i - \rho'_k)\rho_j(1) - \rho'^2_j\rho_i(1)}{1 - (\rho'^2_i + \rho'^2_j + \rho'^2_k) + 2\rho'_i\rho'_j\rho'_k}, \tag{6.13}$$

$$\beta = \frac{\rho_j(1) + (\rho'_i\rho'_j - \rho'_k)\rho_i(1) + (\rho'_j\rho'_k - \rho'_i)\rho_k(1) - \rho'^2_j\rho_j(1)}{1 - (\rho'^2_i + \rho'^2_j + \rho'^2_k) + 2\rho'_i\rho'_j\rho_{k'}}, \tag{6.14}$$

and

$$\gamma = \frac{\rho_k(1) + (\rho'_j\rho_{k'} - \rho'_i)\rho_j(1) + (\rho'_k\rho'_i - \rho'_j)\rho_i(1) - \rho'^2_k\rho_k(1)}{1 - (\rho'^2_i + \rho'^2_j + \rho'^2_k) + 2\rho'_i\rho'_j\rho'_k}, \tag{6.15}$$

It is clear from Eqs. (6.13, 6.14, and 6.15) that the model parameters (α, β, and γ) are functions of the correlation structure of the geological phenomenon concerned. There are three autocorrelation and three cross-correlation coefficients to be estimated from the data. Hence, the total number of statistical parameters including the average value and the variance to be extracted from the data is equal to eight, provided that the geological phenomenon considered is homogeneous.

6.2.2 2D Uniform Model Parameters

In a homogeneous geologic phenomenon the mean and standard deviation values of the samples are independent of spatial variations. Such a phenomenon is said to be second-order stationary. In addition, if it is also isotropic, then the autocorrelations

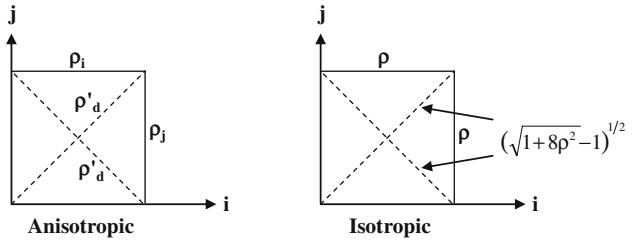

Fig. 6.3 Auto- and cross-correlation representations in isotropic model

and cross-correlations are equal to each other among themselves. This is tantamount to saying that $\rho_i(1) = \rho_j(1) = \rho_k(1) = \rho$ and $\rho_i' = \rho_j' = \rho_k' = \rho_d$ where ρ and ρ_d are isotropic serial and diagonal correlation coefficients. In other words, these correlations do not depend on axial directions as shown in Fig. 6.3. Furthermore, in an isotropic medium the autocorrelations along any direction is dependent only on the variability along this direction. Hence, the dimensions of cubic blocks in spatial simulation become significant. For the sake of simplicity with no loss of generality, herein, the dimensions are assumed as units. Hence, the isotropic autocorrelation, ρ, in Fig. 6.3 should be interpreted as the correlation between the adjacent corner values of the phenomenon on a square mesh.

In 2D simulation this value will reduce into a square unit as shown in Fig. 6.4.

Fig. 6.4 2D isotropic model parameter

The model parameter estimations are found from Eqs. (6.13) and (6.14) by substituting the isotropic medium auto- and cross correlations, i.e., $\rho_k{}' = \rho_k(1) = 0$, $\rho_i 1 = \rho_j(1) = \rho$ and $\rho_i{}' = \rho_j{}' = \rho_d$,

$$\alpha = \frac{\rho}{1 + \rho_d}, \tag{6.16}$$

and β has value identical to α. With this the 2D model mathematical expression becomes

$$x_{i,j} = \alpha(x_{i-1,j} + x_{i,j-1}) + \varepsilon_{i,j}. \tag{6.17}$$

The main problem in a 2D isotropic simulation is to satisfy the equality of cross-diagonal correlations. This has been treated by Şen (1989b) and with the current notations the diagonal correlation coefficient should have the following form

$$\rho_d = \frac{.1 + 8\rho^2 - 1}{2}. \tag{6.18}$$

The variance of the independent random variable, $\varepsilon_{i,j}$, can be found from Eq. (6.9) with necessary substitutions as

$$\sigma_\varepsilon^2 = 1.0 - \frac{2\rho^2}{(1 + \rho_d)}. \tag{6.19}$$

Different interpretations of Eqs. (6.16) and (6.18)−(6.19) indicate already known facts in the simulation literature as follows.

1) If the diagonal correlation is unity ($\rho_d = 1$), then Eqs. (6.16) and (6.19) reduce to the 1D case for which $\alpha = \rho$ and $\sigma_\varepsilon{}^2 = 1 - \rho^2$. These correspond to the properties of lag-one Markov process.
2) For zero autocorrelation ($\rho = 0$), it is possible to see that $\alpha = \beta = 0$; $\rho_d = 0$ and $\sigma_\varepsilon{}^2 = 1$. These properties imply independent random variable with zero mean and unit variance.

For the square net with dimensions (n×n), the generation procedure requires first the generation of n normally distributed independent random variables $\varepsilon_{1,j}$ (j = 1, 2, …, n) with zero mean and variance equal to $(1 - \rho^2)$. Subsequently, these variables are converted into an auto-correlated row sequence by means of the first-order Markov process as

$$x_{1,j} = \alpha x_{1,j-1} + \varepsilon_{1,j} (j = 1, 2, \ldots, n). \tag{6.20}$$

The first column sequence is also generated in the same way except that the initial (n–1) normally distributed independent variables with zero mean and variance equal

to $(1-\rho^2)$ are generated. It is important that the first row value, $\varepsilon_{1,1}$, is used as the initial value for column Markov model, which is expressed as

$$x_{i,1} = \alpha x_{i-1,1} + \varepsilon_{i,1} (i = 2, 3, \ldots, n), \tag{6.21}$$

in which $x_{1,1}$ is taken equal to $\varepsilon_{1,1}$. Then the remainder rows (or columns) are generated through the use of 2D model as

$$x_{i,j} = \alpha(x_{i-1,j} + x_{i,j-1}) + \varepsilon_{i,j} (i, j = 2, 3, \ldots, n). \tag{6.22}$$

Prior to the generation of related 2D isotropic variables, it is necessary to generate an array of $(n-1)\times(n-1)$ independent normal variables, $\varepsilon_{i,k}$, (i, j = 2, 3, . . ., n) with zero mean but variance σ_ε^2 given in Eq. (6.19). These independent variables are converted into autoregressive variables through Eq. (6.22) by taking into consideration the two previously generated 1D sequences. The simulation in 2D can be completed either row by row- or column-wise.

The generation procedure is applied with different autocorrelation coefficients and the sample plots are presented in Fig. 6.5. The points in these figures indicate generated variables that have values greater than the mean value, which is taken as zero. Correspondingly, blanks are the locations of variables less than the mean value. The visual inspection of these figures indicates that they are isotropic, which means to say that there is no preferential direction or stratification along any direction.

6.2.3 Extension to 3D

The simulation procedure extension into 3D space is achieved by the execution of the following three stages.

1) 1D variables are generated along orthogonal i, j, and k directions according to lag-one Markov process. The most important point at this stage is that these three orthogonal direction sequences have a common original random variable which is $\varepsilon_{1,1,1}$.
2) Three layers are generated from the three unidirectional sequences in the previous stage according to the 2D generation scheme through similar equations to Eq. (6.22).
3) 3D isotropic simulation model parameters can be found from Eqs. (6.13) to (6.15), by considering that $\rho_i(1) = \rho_j(1) = \rho_k(1) = \rho$ and $\rho_i' = \rho_j' = \rho_k' = \rho_d$, which leads to the same value of model parameters $\alpha=\beta=\gamma$ as

$$\alpha = \frac{\rho(\rho_d - 1)}{2\rho_d' - \rho_d - 1}. \tag{6.23}$$

Hence, the 3D isotropic simulation model takes the form

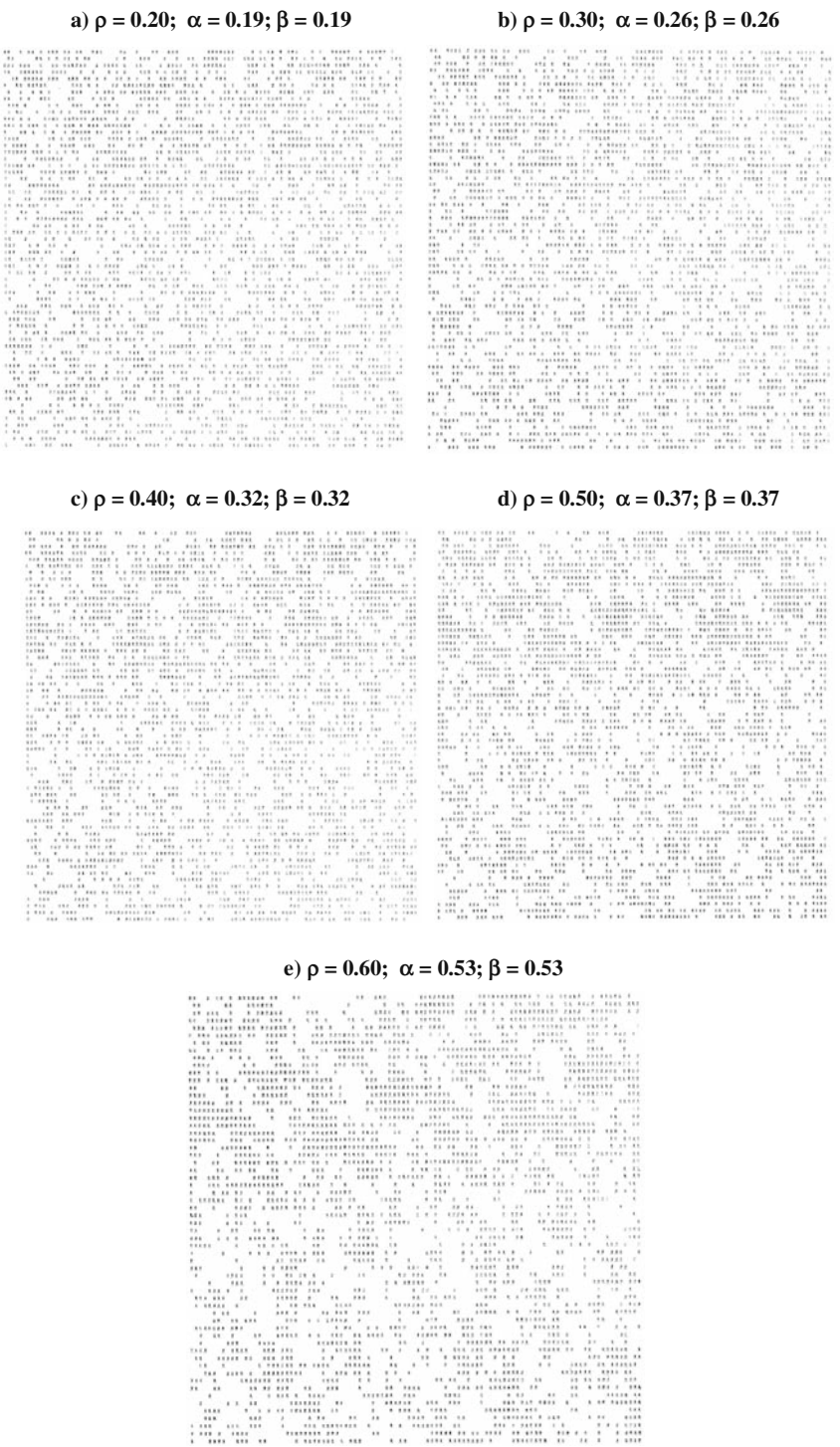

Fig. 6.5 Two-dimensional isotropic pattern for (**a**) $\rho = 0.1$; (**b**) $\rho = 0.2$; (**c**) $\rho = 0.3$; (**d**) $\rho = 0.4$; (**e**) $\rho = 0.5$

$$x_{i,j,k} = \alpha(x_{i-1,j,k} + x_{i,j-1,k} + x_{i,j,k-1}) + \varepsilon_{i,j,k}. \tag{6.24}$$

The substitution of the parameters into Eq. (6.5) leads after some algebra to the variance of 3D independent variables as

$$\sigma_{\varepsilon}^2 = 1 - \frac{3\rho^2(\rho_d - 1)}{2\rho_d^2 - \rho_d - 1}. \tag{6.25}$$

Hence, to complete 3D simulation first normal independent array (n–1)×(n–1) is generated with zero mean and variance $\sigma_\varepsilon{}^2$ as given in Eq. (6.25). These variables are combined together with the layer auto-correlated variables in the previous stage through Eq. (6.24) parallel to any one of the (i, j), (i, k) and (j, k) layer, and the procedure is repeated likewise until the desired domain is covered.

6.3 Rock Quality Designation Simulation

A number of workers have devised various approaches that attempt to standardize and quantify descriptions of rock masses, which are dissected by sets of discontinuities. The very first work was due to Terzaghi (1946), who was mainly concerned with the rock defects and loads on tunnel supports. Later, Deere (1964), Coates (1964), Barton et al. (1974), Bieniawski (1974), Goodman (1976), Şen and Kazi (1984), Şen (1984, 1990a), Ege (1987), and many others proposed either statistical or empirical or analytical methodologies or modifications of existing ones in order to describe the discontinuities quantitatively. All of the aforementioned studies sought average values for discontinuities and their probabilistic descriptions were not mentioned at all. It is the main purpose of this section to seek the pdf for some of the basic rock quality descriptions.

6.3.1 Independent Intact Lengths

Three important geometric properties of discontinuities that are of common interest to engineering geologists are their density (spacing frequency), size (trace length area), and orientation (strike dip direction cosines). The measure that is adopted herein is the spacing between two successive discontinuities, which is referred to as intact length. The intact lengths along any scanline may be measured by the separation of the intersections of discontinuities with sample lines in different directions on the same rock outcrop as shown schematically in Fig. 6.6.

Although there exist several descriptions of rock masses proposed by International Society for Rock Mechanics (1978), the discontinuity spacing, i.e., intact lengths, deserves special attention and detailed study for effective assessment of rock quality. A simple mean for indicating the rock quality is proposed by Deere (1964) as rock quality designation, (RQD). It is, in fact, the ratio of total intact

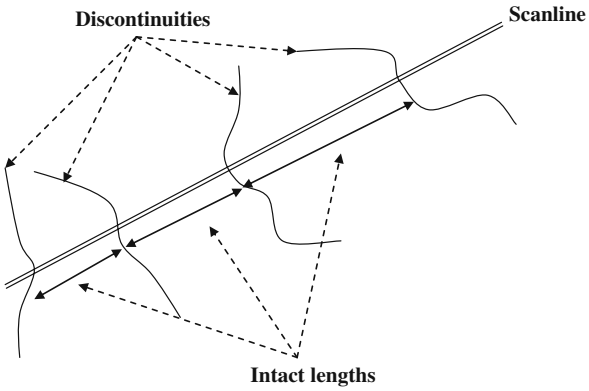

Fig. 6.6 Scanline survey of discontinuities

lengths, each of which is greater than a pre-designated threshold value to the total length of scanline. Due to its relative simplicity, RQD has been used extensively in the rock classification for engineering purposes. Directly RQD or its slight modifications have been employed in a variety of engineering applications. For instance, Piteau (1970) has used RQD for rock slope stability, Barton et al. (1974) in the design of tunnel support, Louis and Pernot (1972) in dam foundations analysis of permeability, and Cording and Mahar (1978) in underground chamber design in rocks, Bieniawski (1974) and Kulhawy (1978) in estimating the strength of rock materials.

Most of the researchers so far in the literature have concentrated in the scanline measurement evaluations analytically (Hudson and Priest, 1979; Priest and Hudson, 1976, 1981; Şen and Kazi, 1984; Şen, 1984; Kazi and Şen, 1985) or empirically (Cruden, 1977; Wallis and King, 1980; or simulation on digital computers by Goodman and Smith, 1980) and Şen (1990b). In order to alleviate some drawbacks in RQD, Şen (1990a) has proposed the concept of rock quality percentage (RQP) and rock quality risk (RQR).

Although the quality of rock based on these measurements can be done by visual inspection, any quantitative method is always better in unifying different opinions about the same rock mass. Therefore, the method of RQD was adopted by Deere (1964, 1968) and was expressed as

$$\mathrm{RQD} = \frac{100}{\mathrm{L}} \sum_{\mathrm{i}=1}^{\mathrm{n}} \mathrm{L_i}, \tag{6.26}$$

where the summation term includes all intact lengths L_i ($i = 1, 2, \ldots, n$) of sound rock between discontinuities that are 0.1 m (0.3 ft) or more apart and L is the total length of the scanline considered. It is obvious from the definition of RQD that its values range between 0 and 100. Furthermore, Deere classified any rock based on the RQD value as in Table 6.1.

Table 6.1 RQD classification

RQD value	Classification
RQD < 25	Very poor
25 < RQD < 50	Poor
50 < RQD < 75	Fair
75 < RQD < 90	Good
90 < RQD < 100	Excellent

Initial analytical expressions for RQD based on negative exponentially distributed intact lengths are presented by Priest and Hudson (1976) for very long scanline. The effects of finite length scanline on RQD value are described by Şen and Kazi (1984). Further analytical studies are presented by Şen (1984) for different intact probability distributions, such as uniform normal lognormal and gamma pdfs. However to the authors' knowledge no work has appeared on RQD simulation based on the pdfs.

Although a relatively uncomplicated and fast procedure, RQD has limited applications in quantifying rock mass quality. This drawback is due to the following disadvantages.

1) It does not reveal anything about the intact length properties, which are shorter than 0.1 m.
2) Two or more scanline measurements with intact lengths (i.e., equally spaced discontinuities) longer than 0.1 m would have all RQD of 100%.
3) It provides directional rock qualities, but fails to give a global quality description for the whole rock mass. For instance, RQDs of 67% and 92% along the north–south and west–east directions, respectively, describe the same rock mass as fair and excellent quality. Hence a dilemma arises as to the global RQD.
4) As already noticed by Şen (1990a), RQD does not provide answers to questions such as in what percentages does each rock quality (excellent good fair poor and very poor) occur within the same rock mass? Or what is the probability (risk) that the RQD value will be less than any given RQD value?

The only way to avoid these problems is to obtain the pdf of RQD itself on the basis of given intact length pdf. Such a task is very difficult by analytical means, and therefore Monte Carlo simulation technique is adopted in this chapter for reaching to the desired goal.

The value of RQD along any scanline is calculated from Eq. (6.26) for the intact lengths, which are longer than a certain threshold value t. In any rock mass the intact lengths x are random variables, which have a certain pdf. In addition, the number n of fractures is also an integer-valued random variable. Consequently, in a statistical context RQD can be regarded as the random summation of random variables that are truncated at the threshold value. The pdf of intact lengths can be obtained empirically in the field from intact length measurements along very long scanline. However, determining the pdf of the RQD requires many scanlines with different

directions and at different places, which is quite tedious and not practical. Therefore, the question arises how to determine the RQD distribution function from the basic pdf of the intact lengths. It has been already shown by Şen (1990a) that an analytical derivation of the RQD distribution function is almost impossible, and therefore the only way to obtain it is by numerical methods using Monte Carlo techniques.

Simulation of stochastic variables is rather similar to the numerical solution methods in mathematics. That is to say provided that the underlying properties of a phenomenon are known, then simulation gives a way of reaching the desired goal numerically. The desired goal here is the RQD distribution. For such a simulation study, the following steps must be considered.

1) Determine the underlying pdfs of the intact lengths within a rock mass. In previous studies, this pdf has been taken to be either negative exponential or lognormal pdf, which have the mathematical forms

$$f(x) = \lambda e^{-\lambda x} \qquad (0 \le x \le \infty), \tag{6.27}$$

and

$$f(x) = \frac{1}{x\sqrt{2\pi}\sigma_{Lnx}} \exp\left\{-\frac{1}{2}\left[\frac{1}{\sigma_{Lnx}} Ln\left(\frac{x}{\overline{m}_x}\right)\right]\right\} \quad (0 < x < \infty), \tag{6.28}$$

respectively, where λ is the average number of discontinuities, $\overline{m}_x$ is the mean of the intact lengths, and σ_{Lnx} is the standard deviation of logarithmic intact lengths. Equation (6.27) has been used in most evaluations of RQD. The logarithmic distribution has not been used as often. The latter has more flexibility in representing the intact lengths, because it takes into account the standard deviation of intact lengths independently of their mean value.

In the simulation study herein, first uniformly distributed random variables u with a range from 0 to 1 are generated and then they are transformed into negative exponentially distributed intact lengths with parameter λ by

$$s = -\frac{2.3}{\lambda} \log u = -\frac{1}{\lambda} Ln\, u. \tag{6.29}$$

However, for the logarithmic distributions first the uniformly distributed pairs of variables (u_1 and u_2) are transformed into a normally distributed random variable pairs (s_1 and s_2) with a procedure already presented by Hammersely and Handscomb (1964) as

$$s_1 = \sqrt{-2 \log u_1} \cos(2\pi u_2). \tag{6.30}$$

$$s_{21} = \sqrt{-2 \log u_1}\, s11\, (2\pi u_2) \tag{6.31}$$

Herein, u_1 and u_2 are uniformly distributed random variables within the range of 0 to 1. The values of s are then transformed into logarithmically distributed intact lengths x using

$$x = e^{-x}, \tag{6.32}$$

in which s represents s_1 or s_2. In this study 1,000,000 identically distributed intact lengths were generated separately with negative exponential or lognormal pdfs.

2) These intact lengths are classified into two groups depending on whether they are greater or smaller than a threshold value t. In the RQD definition as given by Eq. (6.26), the summation of xs over the scanline length is calculated. The scanline length is in fact equal to the summation of the whole intact lengths, provided that it starts and stops at discontinuity.
3) The RQDs for a set of pre-determined numbers are identified.
4) The relative and cumulative frequency distribution functions for RQD values from (3) are calculated.

The cumulative pdf of RQD values resulting from negative exponentially distributed intact lengths with a set of average fracture number were presented in Fig. 6.7 for five different threshold values.

On the same figure, classification of RQD values is also shown. There is a similarity between the grain size distribution of granular rocks and these graphs which show the rock quality distribution of the fractured hard rocks. Field experiences show that any fractured rock is heterogeneous and accordingly more than one type of rock quality exists within the same rock mass. The percentages of these different qualities can be found quantitatively from Fig. 6.7. Inspection of this figure leads to the following significant conclusions.

1) The smaller the average number of discontinuities, the smaller is the range, which indicates the uniformity of the rock quality. For instance, invariably whatever the threshold value the rock has an excellent quality when the average number of discontinuities is equal to unity.
2) As the average number of discontinuities increases, the rock becomes heterogeneous. For instance, in Fig. 6.7 when the threshold value is 0.05, the curve that represents 20 average intact lengths has three different qualities, namely excellent, good, and fair portions. It is clear from the same curve that the majority of values are in the "good" quality zone whereas other qualities are less likely to occur.
3) An increase in the average number of discontinuities leads to deteriorating rock qualities as shown in Fig. 6.8.
4) As the threshold value decreases, the rock quality increases (see Fig. 6.8). On the other hand, for a given threshold value the deterioration rate in the rock quality is higher at small discontinuity numbers. For instance, at 0.20 truncation level the reduction in the rock quality is almost 12% between discontinuity numbers 2 and 4 whereas 3% from 18 to 20.

In addition, the pdfs of RQD for a set of discontinuity numbers and different threshold values are presented in Fig. 6.9 as negative exponentially distributed intact lengths.

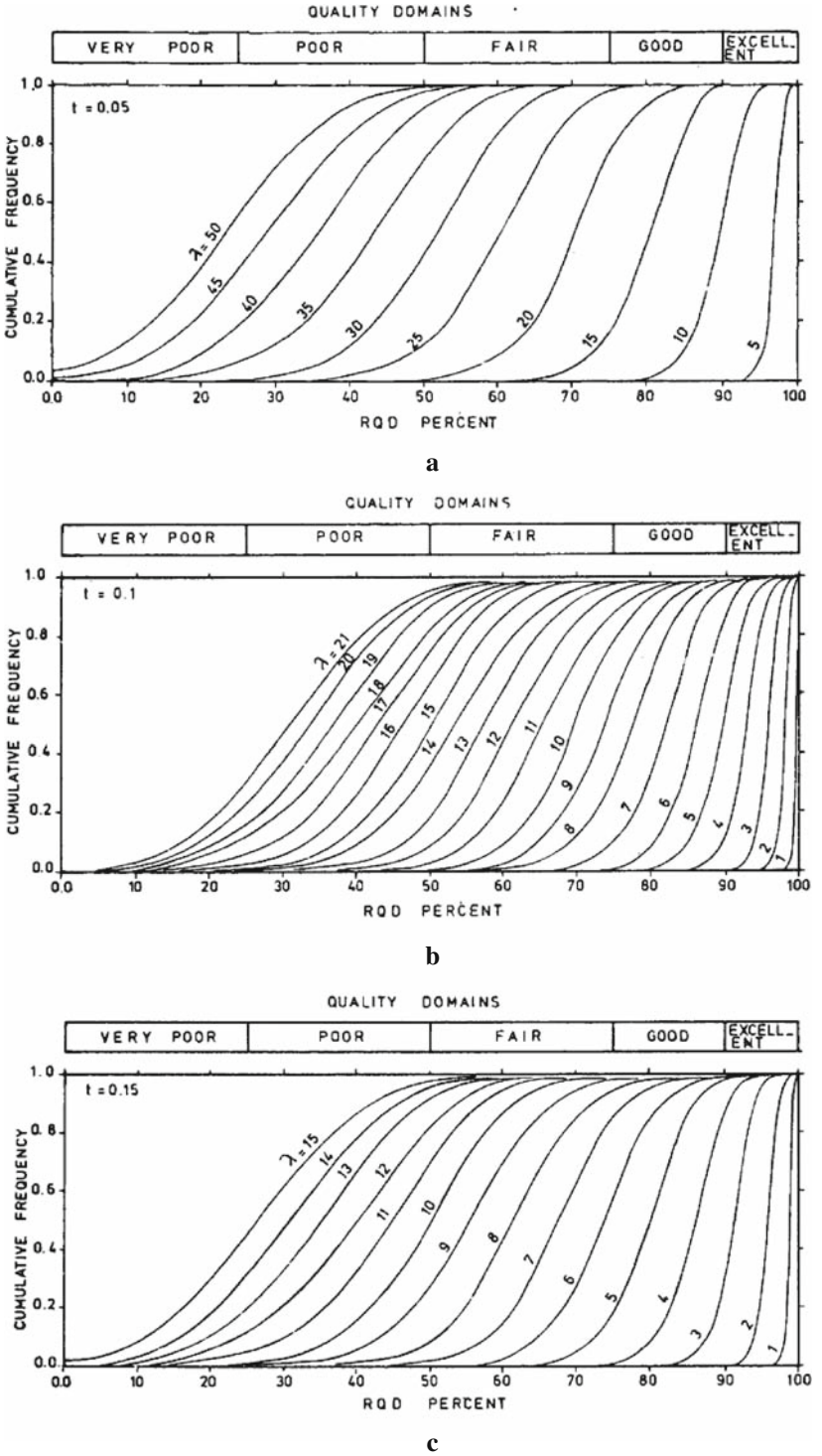

Fig. 6.7 RQD chart for negative exponential pdf with (**a**) $t = 0.05$; (**b**) $t = 0.15$; (**c**) $t = 0.20$

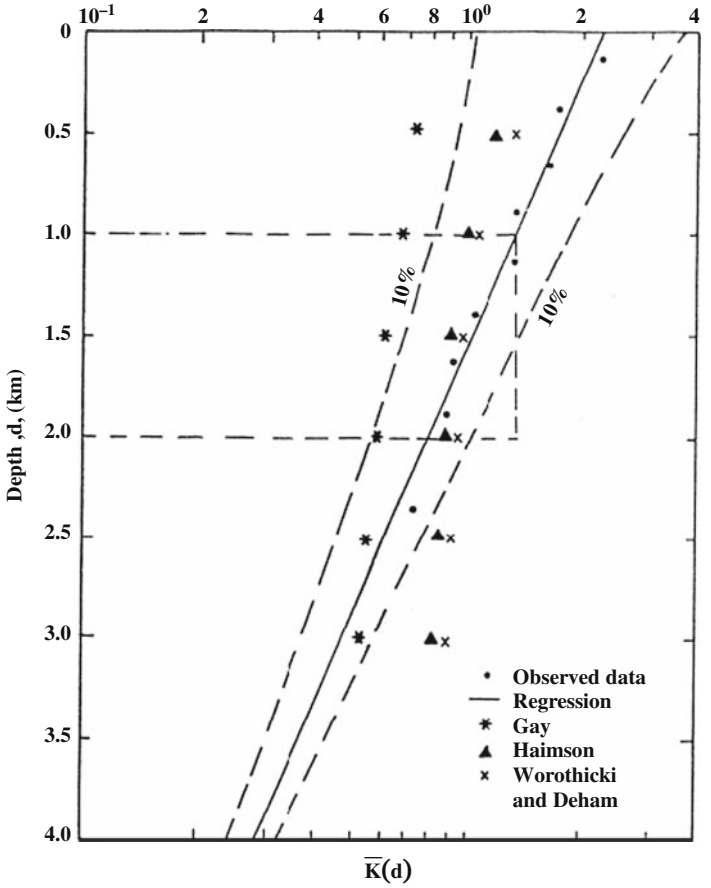

Fig. 6.8 RQD threshold value discontinuity number chart (negative exponential pdf)

One of the most striking properties of these pdfs is that irrespective of the discontinuity number and threshold value, they are invariably symmetric. The positions of the maximum points on any one of these curves along the RQD axis shows the most likely rock quality within the rock mass.

Due to the aforementioned symmetry, the average RQD value coincides with the most likely rock quality value. This point indicates that the average RQD value is equal to the maximum likelihood estimation of the averages resulting from these pdfs. This value corresponds with the classical RQD value as defined by Deere. Besides the mean mode and the median values of the RQD are equal to each other. This last statement suggests that the pdf of RQD within a rock mass can be approximated by a normal distribution as

$$f(r) = \frac{1}{\sqrt{2\pi}\sigma} \exp\left[-\frac{1}{2}\left(\frac{r-\mu}{\sigma}\right)^2\right], \tag{6.33}$$

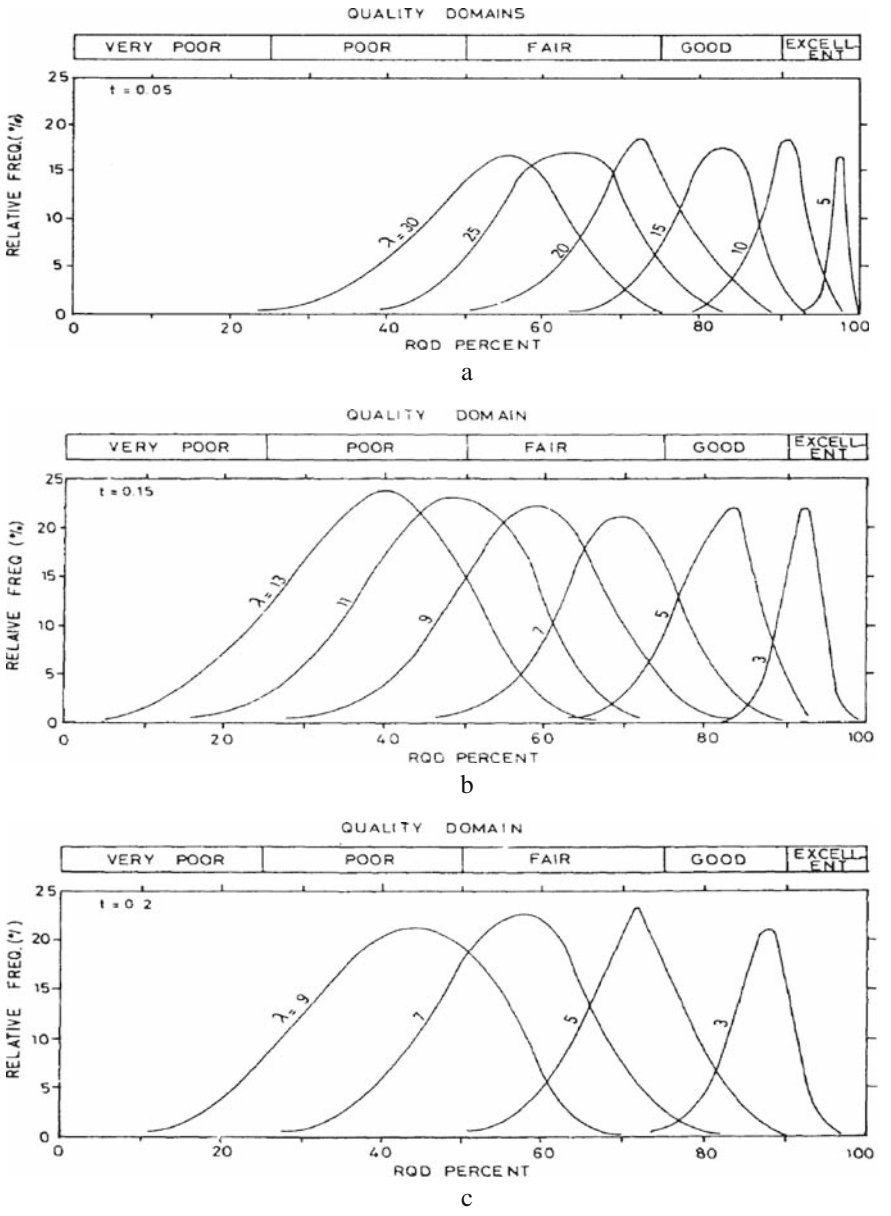

Fig. 6.9 RQD negative exponential pdfs with (**a**) $t = 0.05$; (**b**) $t = 0.15$; (**c**) $t = 0.20$

in which r is a dummy variable representing RQD; μ and σ are the population mean and standard deviation of RQD, respectively. For the negative exponential distribution, Şen and Kazi (1984) have shown already that the RQD has the same mean and standard deviation value, which are expressible as

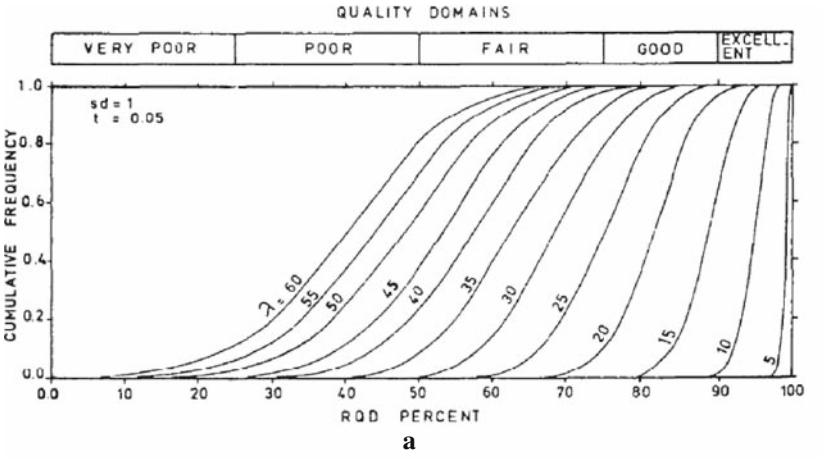

a

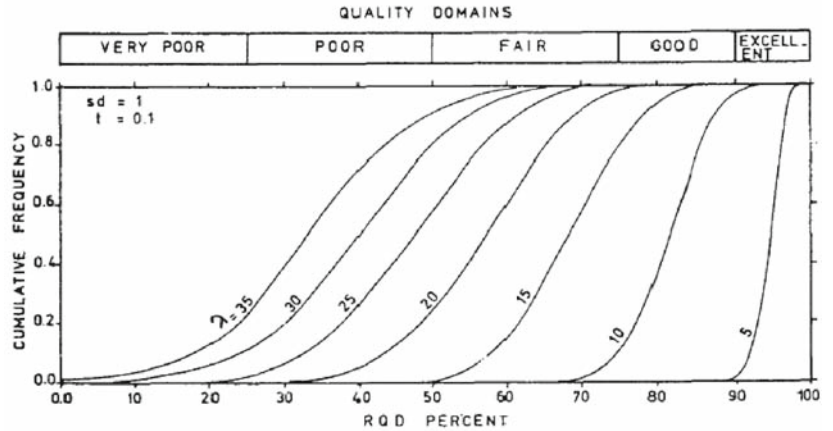

b

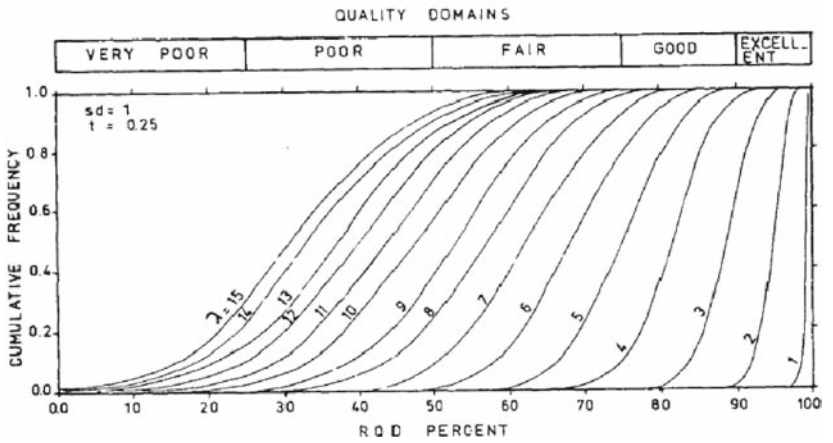

c

Fig. 6.10 RQD description cart for Log-normal PDF (**a**) ($t = 0.05$, $m = 0.0$, $s = 1.0$); (**b**) ($t = 0.15$, $m = 0.0$, $s = 1.0$); (**c**) ($t = 0.25$, $m = 0.0$, $s = 1.0$)

$$\mu = \sigma = 100\,(1 + \lambda t)\ e^{-\lambda t}. \tag{6.34}$$

Finally, the cumulative pdf of RQD for the underlying intact length distribution as the lognormal pdf are given in Fig. 6.10.

All of the conclusions for the negative exponential pdfs are equally valid for these curves. In addition, comparisons of various graphs in Fig. 6.10 indicate different standard deviations, and an increase in the intact length standard deviation improves the rock quality designation. In other words, the less uniform the fracture spacing the stronger the rock mass. The following significant conclusions can be drawn from this study.

1) Any rock mass might have different rock qualities at the same time in different directions.
2) Rock quality deteriorates with increase of the average number of discontinuities for any intact length distribution, but an increase in the standard deviation of log-normal pdf of intact lengths leads to improvements in the rock quality designations.
3) The pdfs of RQD are unimodal in any case, but symmetrical for the negative exponentially distributed intact lengths.
4) Any dominant type of rock quality has almost the same maximum frequency, confined within 0.20–0.25 for threshold levels more than or equal to 0.10 m.

6.3.2 Dependent Intact Lengths

All of the aforementioned studies have a common point in that they give an RQD estimation without consideration of the intact length correlation. However, it is a fact that even on the same outcrop of the rock, there might be correlated intact lengths along scanline taken at various orientations (Eissa and Şen, 1990). Although RQD calculations, according to Deere's (1964) definition directly from the scanline measurements, implicitly account for the intact length correlation, unfortunately, the analytical formulations do account for this correlation neither implicitly nor explicitly. Accordingly, for correlated intact lengths the existing analytical results are in error. It is obvious then that the comparison of analytical and empirical RQD estimations is possible accurately only for the cases of independent intact lengths. Otherwise, such a comparison is meaningless.

An important factor in the analysis of rock quality assessments from discontinuity measurements along a scanline is the correlation of the intact lengths. The autorun model and first-order autorun coefficient are proposed as a method of objectively quantifying the intact length correlation structure and discontinuity occurrences within a rock mass (Şen, 1978, 1984).

Any straight line through the rock mass encounters random number of discontinuities. An intact length is defined as the length of scanline or drill-core between two successive discontinuities. In general, if there are n+1 discontinuity, the number

of intact lengths is n provided that the start and end of the scanline are at discontinuities. A first step in rock mass classification is to consider two types of intact lengths, namely those whose lengths are greater than a pre-designate threshold value or otherwise (Eq. 6.26).

For the sake of convenience, alternative intact lengths will be grouped into two sets as elements a_i, (i = 1, 2, . . ., k) in set A and b_j (j = 1, 2, . . ., l) in set B, where k and l are the number of intact lengths in each set. It is obvious that k+l = n, which is the total number of intact lengths. Furthermore, in an alternate sequence either k = l–1 or l = k–1; however, practically one may assume with no loss of generality that k = l = n/2. In short, the intact lengths along a scanline will be an alternative combination of elements from two sets, namely A = $\{a_1, a_2, \ldots, a_k\}$ and B = $\{b_1, b_2, \ldots, b_l\}$ as shown in Fig. 6.11a. In such a combination, the correlation structure of sequence $a_l, b_l, a_2, b_2, \ldots, a_{n/2}, b_{n/2}$ (see Fig. 6.11b) is utmost important in addition to various statistical descriptions of intact lengths.

Besides, it may well be that the intact lengths in set A have different PDF than B. However, this point lies outside the scope of this chapter. Of course, the assumption of uncorrelated intact lengths simplifies the analytical derivation of RQD but at a sacrifice of precision. Due to such an assumption, there is no term representing the correlation of intact lengths in any RQD formulations that are available so far in the literature. The major elements that effect the RQD calculations are in detail as follows:

1) The number of discontinuities: As mentioned earlier, practically, half of this number will be attached to intact lengths of set A and the second half to set B.
2) Intact length PDF: It has been assumed in the majority of RQD studies as negative exponential type (Priest and Hudson, 1976, 1981). However, the log-normal (Roulean and Gale, 1985) or uniform and gamma pdfs (Şen, 1984) are also employed to a certain extend.

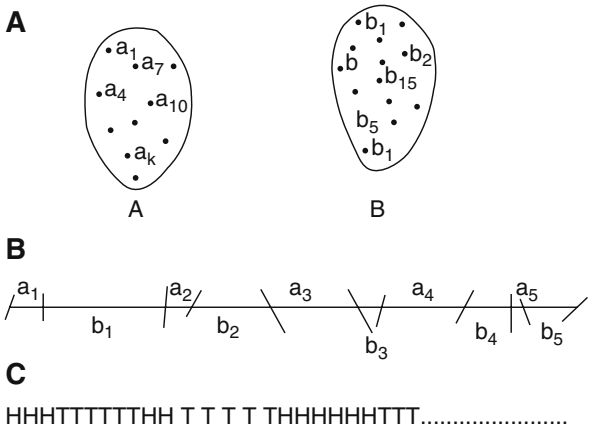

Fig. 6.11 Alternative intact length concepts

3) Correlation structure: Any significant correlation effects not only the discontinuity occurrences but also the intact lengths. This element is ignored invariably in any of the previous RQD studies in the literature. However, only some indirect procedures have been proposed for accounting the intact length correlation (Higgs, 1984; Şen, 1991).
4) Threshold value: It is a fixed value as 0.1 m or 4 inches, below which the intact lengths are not considered in the RQD calculations.

The first two elements are stochastic variables and in nature they are both serially and crossly correlated. Hence, the probabilistic laws of these stochastic parts lead to meaningful analytical expressions for RQD only after the consideration of correlation structure. For instance, logically any increase in the correlation will imply the occurrence of longer intact lengths along a scanline than the case where the intact lengths are independent. It also implies that the number of discontinuities decreases with increasing correlation. Hence, in general, the existence of relatively longer intact lengths, (or lesser number of discontinuities) along a scanline implies improvement in its quality. Consequently, the key in the analytical RQD formulation for correlated intact lengths is the expression of correlation by an objective measure, which is adopted herein conveniently as the autorun coefficient.

6.3.2.1 Correlation Measurement

The main question is whether the intact lengths along any direction are serially correlated or not? As was mentioned above, different authors have shown that the intact lengths are distributed according to various distributions among which the normal pdf has the least significant role. On the contrary, the classical correlation techniques, (auto- and cross-correlation) are valid for normally distributed variables only. Although by suitable transformations intact lengths may be rendered into normally distributed variables, such a transformation distorts the original genuine correlation function to a greater extent (Şen, 1978, 1979a). However, the autorun analysis is robust to any pdf or transformation and yields unbiased as well as consistent estimates of correlation. In general, lag-k autorun coefficient is defined by Şen (1978) as

$$r_k = \frac{2n_k}{n-k}, \tag{6.35}$$

in which n_k is the number of overlapping successive the same type of events lag k-apart; n is the number of unit intact lengths. From the definition, it is obvious that $0 < r_k < 1$. In the case of purely independent observations, whatever the underlying pdf Eq. (6.41) becomes equal to 0.5. Therefore, 0.5 shows the fact that the two observations separated by lag-k are independent from each other. On the other hand, if the observations are perfectly correlated, then $r_k = 1.0$.

The autorun coefficient application is very suitable for binary type of data; therefore, prior to its application the variable concerned such as the intact length must

be rendered into a binary form. For such a purpose the analogy suggested by Priest and Hudson (1976) as an unbiased coin tossing sequence of heads and tails will be adopted herein for alternating intact lengths, where a head represents a unit length of intact rock of type A and a tail represents a unit length of type B. With such an analogy, the scanline in Fig. 6.11b can be considered as a sequence of heads and tails (see Fig. 6.11c). The following significant points emerge in such an analogy:

1) The succession of uninterrupted sequence of heads(tails) represent intact lengths of type A(B).
2) Each appearance of alternate successive events, i.e., head–tail or tail–head succession corresponds to a discontinuity. It is obvious that two successive head–head or tail–tail events represent two units from overall intact lengths. These explanations indicate the suitability of lag-one autorun coefficient, r, in quantifying the intact length correlation structure.
3) The percentages of heads(tails) along a scanline is equal to the probability of type A(B) intact length. Let these probabilities be denoted by p and q, respectively, then obviously $p + q = 1$. In terms of total length, $L_A(L_B)$ for set A(B) intact lengths, the probability can be expressed as $p = L_A/L(q = L_B/L)$.

Assuming uncorrelated intact lengths, Priest and Hudson (1976) have presented the analytical formulation of expected RQD as

$$E\,(RQD) = 100\,(1 + \lambda t)\ e^{-\lambda t}, \tag{6.36}$$

in which λ is the average number of discontinuities. The discontinuities are also assumed to have Poisson PDF with λ as its sole parameter. Equation (6.36) should be used only after the confirmation that the intact lengths are independent.

For instance, a scanline composed of 18, 4, 5, 3 cm intact lengths can be represented on the basis of 1 cm as an intact unit length by analogy to coin tossing as

HHHHHHHHHHHHHHHHHHHHTTTTHHHHHTTT

In such a sequence the probability of an intact length unit of type A (or H) is $p = 23/30 = 0.77$ and the probability of type B (or T) is $q = 7/30 = 0.23$, with $p + q = 1$. These probability values do not tell us whether the intact lengths are independent or not. However, the first autorun coefficient becomes $r = 19/29 = 0.66$; and since it is bigger than 0.5, there is a positive correlation between intact lengths. This implies, in general, that long intact lengths follow long intact lengths and short ones follow short intact lengths.

6.3.2.2 RQD Formulation and Discussion

Mathematical modeling of a scanline can be achieved by considering either the occurrence of discontinuity numbers or intact lengths, both of which are interdependent random variables. Modeling only one of them is sufficient because it implies the properties of the other. For instance, whatever the PDF, there is only one unique relationship between the expected intact length, E(x), and the expected number of discontinuities, E(n) along any scanline as

$$E(n) = \frac{L}{E(x)}, \tag{6.37}$$

in which L is the scanline length. On the other hand, RQD as appears in Eq. (6.26) is equivalent to the summation of random number of random variables; and first by taking the expectations of both sides and then by considering Eq. (6.37), one can write

$$E(RQD) = \frac{100}{L}E(n)E(x^*) = 100\frac{E(x^*)}{E(x)}, \tag{6.38}$$

in which $E(x^*)$ is the expectation of intact lengths greater than a threshold value, t. Due to the fact that $E(x^*) < E(x)$, the ratio of expectations in the expression always assumes a value between 0 and 100. The expectations on the right-hand side of Eq. (6.38) can be found provided that the PDF of random variables concerned are known.

It can be shown similar to autorun modeling (Şen, 1985) that the pdfs of k successive heads and tails are of geometric distribution types as

$$P(n_h = k) = (1 - r_1)r_1^{k-1}, \tag{6.39}$$

and

$$P(n_t = k) = \frac{p}{q}(1 - r_1)\left[1 - \frac{p}{q}(1 - r_1)\right]^{k-1}, \tag{6.40}$$

respectively, where n_h is the number of uninterrupted successive heads and n_t successive tails. It is worthy to notice that for $r = p$ these equations give the independent intact length case as available in the literature (Priest and Hudson, 1976). Furthermore, expectations of intact lengths in sets A and B can be obtained from Eqs. (6.39) and (6.40), respectively, as

$$E(n_h) = \frac{1}{1 - r_1}, \tag{6.41}$$

and

$$E(n_t) = \frac{q}{p(1 - r_1)}. \tag{6.42}$$

As mentioned above the number of set A intact lengths is one less or more than set B intact lengths. In other words, practically they may be assumed as equals, and therefore each type of intact length has its probability of occurrence equal to 0.5. With this information, the overall expectation of intact lengths, E(x), without distinction between sets A and B can be seen to be $E(x) = 0.5E(n_h) + 0.5E(n_t)$, which yields by consideration of Eqs. (6.41) and (6.42) to

$$E(x) = \frac{1}{2p(1 - r_1)} \tag{6.43}$$

or from Eq. (6.37) one can find the expected number of discontinuities as

$$E(n) = 2Lp(1 - r_1). \tag{6.44}$$

In order to verify the validity of this expression, extensive computer simulations have been carried out through the Monte Carlo techniques and the results are shown in Fig. 6.12. It is obvious that a very good agreement has been observed between the simulation and the analytical formulation.

Finally, the average number of discontinuities, $\lambda_{r_1} = E(x)/L$, per unit length becomes

$$\lambda_{r_1} = 2p(1 - r_1), \tag{6.45}$$

where the Subscript signifies the correlatedness of the intact lengths. The probability P(k) of k discontinuity occurrences along a scanline of length x at an average rate of λ_{r_1} becomes, according to the Poisson process,

$$P(k) = e^{-2xp(1-r_1)} \frac{[2xp(1 - r_1)]^{k-1}}{k\acute{y}}. \tag{6.46}$$

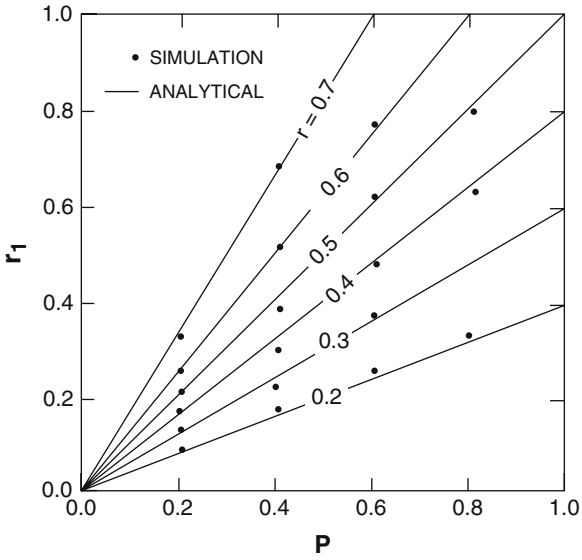

Fig. 6.12 Average number of discontinuity versus scanline length for different autorun coefficients

Since the interest lies in the discontinuity spacing pdf, by considering the distance, d, from one discontinuity to the following, one can write that $P(d < x) = 1 - P(k = 0)$, and hence substitution of Eq. (6.45) leads to cumulative PDF as

$$P(d \leq x) = 1 - e^{-2xp(1-r_1)}.$$

By taking its derivative with respect to x the pdf, f(x), of intact lengths can be derived as

$$f(x) = 2p(1 - r_1)e^{-2xp(1-r_1)}.$$

Subsequently, the expectation of intact lengths that are more than t can be found according to

$$E(x^*) = \int_t^\infty xf\,(x)dx,$$

which leads after the substitution of Eq. (6.46) to

$$E(x^*) = \frac{1 + 2p(1 - r_1)t}{2p(1 - r_1)} e^{-2p(1-r_1)t}. \tag{6.47}$$

Finally, the substitution of Eqs. (6.43) and (6.47) into Eq. (6.38) leads to

$$E(RQD) = 100\left[1 + 2p(1 - r_1)t\right] e^{-2p(1-r_1)t}. \tag{6.48}$$

For independent intact lengths, $r_1 = 0.5$ and the occurrences of unit intact lengths comply with the Binomial distribution, which leads to geometric intact length distribution with $E(x) = 1/p$ or $\lambda = p = 0.5$, and therefore Eq. (6.48) becomes identical to what was suggested by Priest and Hudson (1976) as in Eq. (6.41). Under the light of aforementioned discussions, one can rewrite Eq. (6.48) as

$$E(RQD) = 100\ [1 + \lambda(1 - r_1)t]\, e^{-2\lambda(1-r_1)t}. \tag{6.49}$$

The validity of this formula is checked with extensive Monte Carlo simulation technique by using autorun model for generating correlated intact lengths as proposed by Şen (1985). First of all, estimates of average intact lengths of sets A and B are calculated as

$$n_A = \frac{1}{m_A} \sum_{i=1}^{k} (n_A)_i, \tag{6.50}$$

and

$$n_B = \frac{1}{m_B} \sum_{i=1}^{1} (n_B)_i, \tag{6.51}$$

respectively. Herein, m_A and m_B are the number of intact lengths; $(n_A)_i$ and $(n_B)_i$ are i-th intact length in sets A and B, respectively. The geometric pdf parameter, which is the first-order autorun coefficient, can be estimated from Eq. (5.41) as

$$r_A = (n_A - 1) / n_A. \tag{6.52}$$

Similarly, the geometric pdf parameter, r_B, for set B intact lengths turns out to be

$$r_B = (n_B - 1) / n_B. \tag{6.53}$$

Hence, it is possible to generate geometrically distributed and integer-valued alternate lengths, y, with parameters r_A and r_B, respectively, on a digital computer through

$$y = 1 + \log(\varepsilon) / \log(r_1), \tag{6.54}$$

in which ε is the uniformly distributed random variable between 0 and 1 and r_1 is the geometric distribution parameter, which assumes either the value of r_A or r_B as required. The simulation results are presented in Fig. 6.13 together with the analytical solutions and they show a very good agreement.

The following significant points can be drawn from this figure:

1) The formulation provided by Priest and Hudson (1976) for E(RQD) yields underestimated results if the intact lengths are positively correlated, which is the case in most of the natural rocks as will be presented in the application section of this section.
2) Increase in the correlation structure gives rise to increase in the E(RQD) values.
3) Relatively better RQD values are obtained for the same number of discontinuities but correlated intact lengths.
4) The difference between the dependent and the independent intact length RQD values is relatively less significant at small λ values than big λs. In fact, at 5% relative error level the correlated intact lengths do not lead to significantly different RQD values, provided that $\lambda < 3$ and 10% error level when $\lambda < 10$. In Fig. 5.3 upper and lower confidence limits at 5 and 10% significance levels are shown around the Priest and Hudson independent intact length solution. It is obvious that for small average number of discontinuities their solution gives confident RQD estimates even though the intact lengths are dependent. However, for big average number of discontinuities the significance of intact length correlation becomes very pronounced in the RQD estimations.

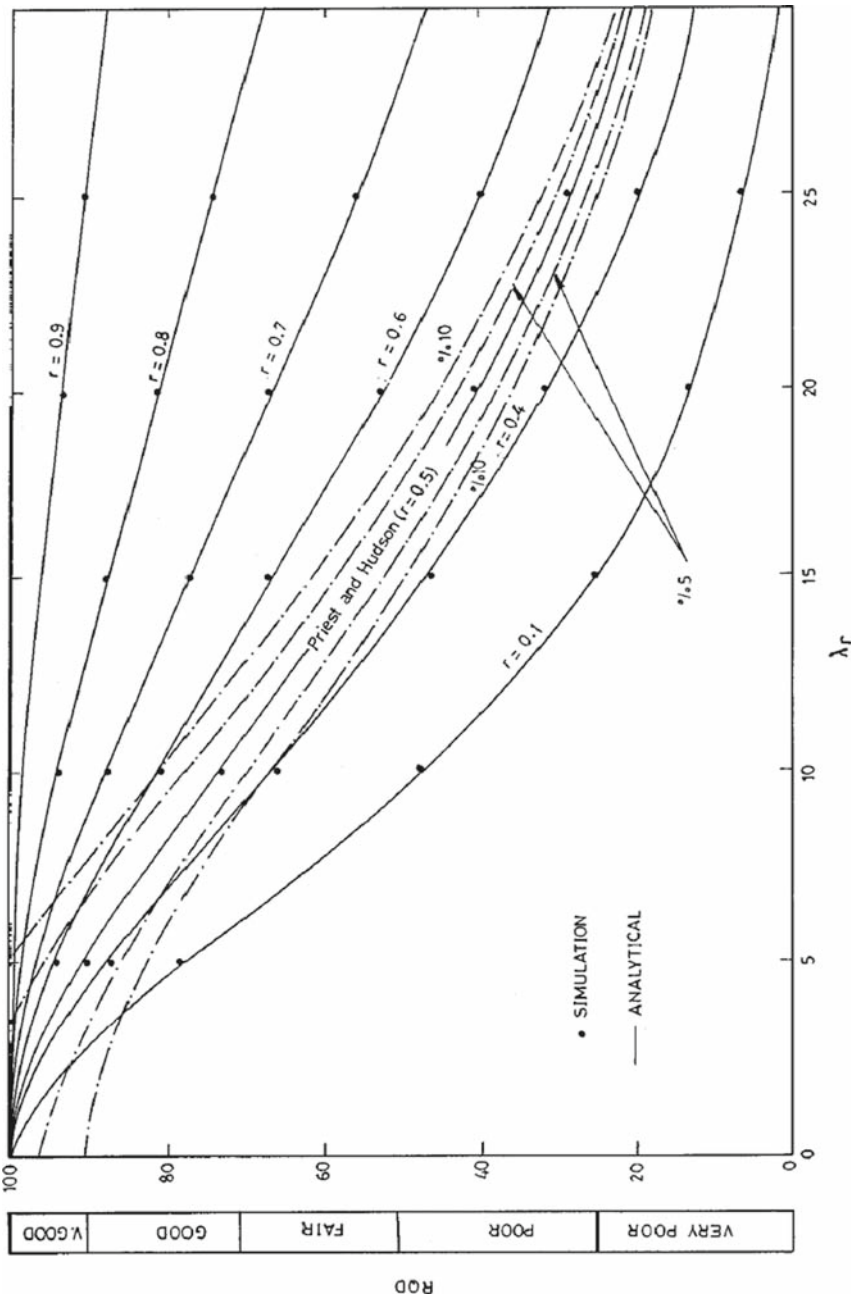

Fig. 6.13 RQD – average number of discontinuity – autorun coefficient chart

6.3.2.3 Applications

The applications of the methodology developed herein are carried out for the field data from various parts of the world. The first field data are recorded along the exposed outcrop surfaces of granitic rocks in the western part of the Kingdom of Saudi Arabia. Extensive geological field survey by Otaibi (1990) showed that the area consists of one rock unit, which is granite of light pink color on fresh surface and dark brown on weathered surface, medium to coarse grained and equi-granular. This area was selected since it has a good combination of well-exposed bedrock and relatively simple fracture pattern. Three sets of fracture orientations can be seen distinctively in this area. Each one of the fracture set is measured by the scanline perpendicular to the fracture traces. The fracture measurements are carried out at three sites. These sites are selected such that they give rather random characterization of the fracture geometry, i.e., they are quite independent from each other. In order to be able to apply the methodology developed herein, the relevant values are calculated and presented in Table 6.2.

It is obvious that the use of independent intact length RQD formulation does not yield significant deviations from the dependent intact length case. This is due to two major reasons. First of all, since the average number of discontinuities is all less than 3, and therefore, as already explained in the previous section, even if the intact lengths are strongly correlated there will not be practically significant difference, i.e., the relative error will be less than 5%. In addition to this major reason, the autorun coefficients are rather close to 0.5, which also confirms the approximation in the results of E(RQD) calculations either by the use of Eqs. (6.36) or (6.47).

The second set of data for the implementation of the methodology are extracted from a previous study by Ryckes (1984) on modes of failure and stability of rock slopes in Tytherington quarry, which is located halfway between Thurnbury and Tytherington for about 16 km north of Bristol in the county of Avon, England. The Paleozoic rocks of the lower coal series in the area are affected by many movements in the past, which led to faults, folds, and unconformities, each of which led to different pattern of intact lengths. Due to these different mechanisms, it is not possible

Table 6.2 Intact length characteristics (Saudi Arabia)

Site	Scanline	λ (1/m)	p	q	r_1	E(ROD)		Error (%)
						Equation (5.3)	Equation (5.16)	
	x	1.56	0.52	0.48	0.51	98	98	0.0
1	y	2.56	0.54	0.46	0.51	97	97	0.0
	z	1.04	0.62	0.38	0.63	99	99	0.0
	x	2.75	0.53	0.47	0.51	97	97	0.0
2	y	1.83	0.59	0.41	0.57	98	99	1.0
	z	1.98	0.63	0.37	0.61	98	99	1.0
	x	1.78	0.48	0.52	0.47	98	98	0.0
3	y	1.80	0.54	0.46	0.52	98	99	1.0
	z	1.56	0.57	0.63	0.55	99	99	0.0

Table 6.3 Intact length characteristics (England)

Scanline	λ (1/m)	p	q	r_1	E(RQD)		Error (%)
					Equation (5.3)	Equation (5.16)	
SL1	6.46	0.46	0.54	0.40	86	81	6
SL2	10.01	0.57	0.43	0.48	74	72	3
SL3	6.52	0.50	0.50	0.43	86	83	4

to expect that these intact lengths have independent correlation structure. In order to depict the regional discontinuity pattern in this area, three scanlines were set up at different directions. The bedding plane orientation is almost horizontal for the first scanline, which will be referred to SL1. The second scanline SL2 has a direction of 20° toward southwest whereas the third, SL3, has an intermediate inclination to the former. The necessary parameters as well as the E(RQD) calculations are presented in Table 6.3.

The major difference between Tables 6.2 and 6.3 is that the average discontinuity numbers of scanlines in Table 6.2 are far bigger than Saudi Arabian measurements; however, the autorun coefficients in Table 6.3 are invariably less than 0.5, indicating that there are negatively correlated intact lengths. Consequently, Priest and Hudson formulation (Eq. 5.3) gives overestimation.

6.4 RQD and Correlated Intact Length Simulation

Generally, in open rock mechanics literature persistence implies the areal extent or size of a discontinuity within a plane (Brown, 1981). It can be quantified crudely by observing the discontinuity trace lengths on the surface of exposures. However, the type of persistance herein is related to the sequential occurrences of intact lengths, which may constitute obvious clusters. Within the contest of this chapter, persistence can be defined as the tendency of short intact lengths to follow short intact lengths and long intact lengths to follow long intact lengths. As Priest and Hudson (1976) say, a high frequency of low spacing values occurs within clusters and a low frequency of high spacing values occur between clusters.

The simple ways of expressing persistance in a sequence of observations is through either the classical serial correlation coefficient or the autorun function (Şen, 1978). Although the former requires the measurements to be normally distributed, the latter is robust and applicable in any distribution case. However, for normally distributed intact lengths both give exactly the same result. In fact, in such a situation the autorun coefficient r is convertible to the correlation coefficient ρ by $\rho = \sin\pi(r - 0.5)$. As a consequence, only for the normally distributed intact lengths one can use interchangeably the autorun and autocorrelation terminologies.

In the following sequel, the intact length persistence is quantified with the help of autorun coefficient r_k for lag-k defined as in Eq. (6.35). In order to apply this formulation to a scanline, the following steps must be executed on any scanline as presented in Fig. 6.14:

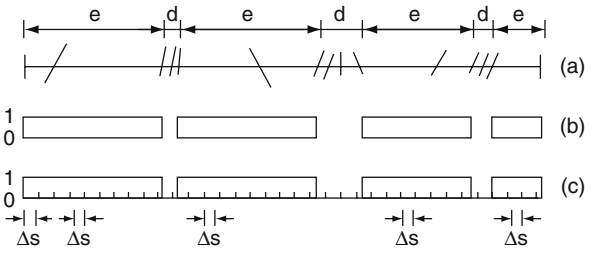

Fig. 6.14 Scanline and models (**a**) effective; (**b**) defective; (**c**) model interval

1) By considering the threshold value equal to 0.1 m (or 4 in) as proposed by Deere (1964), the effective intact lengths are assigned uniform value of +1 and defective lengths as 0 (see Fig. 6.14b). In fact, the resulting modified scanline has zone of square waves, which are separated by zero valued intervals.
2) Divide the scanline into fixed length of finite intervals Δs as shown in Fig. 6.14c where the intervals of fixed lengths are adopted as +1 cm, which is convenient for any practical purpose. The number of such intervals along the scanline is denoted by n.

   The ratio of numbers n within the effective intervals along the scanline to the total interval number n is equivalent to the estimate of RQD, i.e., RQD = 100 (n_1/n).
3) Find the number n of overlapping pairs of 1 and estimate r from Eq. (3.36) for different lags from a sequence of $r_1, r_2, r_3, r_4, \ldots$

The plot of autorun coefficient versus lag value gives rise to graphs that represent the persistance existing in the original intact sequence. A very significant result at this point is that if practically all of the autorun are equal to zero, then the intact lengths originate from an independent random process and hence the calculation of RQD as defined by Deere is reliable, otherwise persistance appears implying clusters in intact lengths and unreliability in RQD calculations.

The applications of the abovementioned persistance procedure to actual data are achieved with considering field measurements from South England near Bristol (Ryckes, 1984) and measurements from the western province of Saudi Arabia collected by authors.

The Paloezoic rocks of the lower coal series in the area are affected by various earth movements in the past, which led to faults folds and unconformaties. The location of intact length measurement sites are on the axis of a syncline, which inclines toward the south. The bedding planes orientation is almost horizontal for the first scanline (SL1). The second scanline (SL2) has a direction of 20^o toward southwest and the third scanline (SL3) has an intermediate inclination to the former. Further detailed information on these scanline measurements can be found in Ryckes (1984). The fourth scanline (SL4) was an illustrative example adopted from Brady and Brown (1985). However, the fifth scanline (SL5) is a representative scanline measurement in crystalline dioritic rocks in southwest of Saudi Arabia.

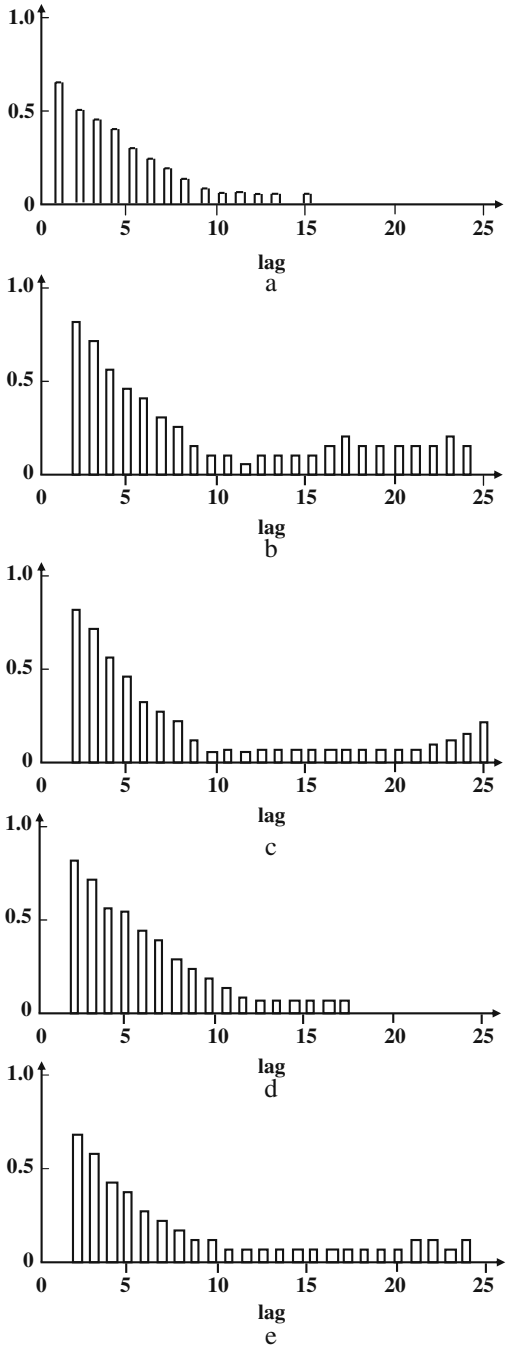

Fig. 6.15 Autorun function for (**a**) SL1; (**b**) SL2; (**c**) SL3; (**d**) SL4; (**e**) SL5

Three scanline measurements from England lead to the autorun functions as shown in Fig. 6.15, and for the illustrative example and the Saudi Arabia scanline measurements autorun functions are given in Fig. 6.15d and e.

A common property in all these figures is that the first autorun coefficient has the greatest value among other lags, and there appears an exponential or power type of decrease with increasing lag value. It is clear that the classical RQD calculations without considering persistance, i.e., assuming that $r_k = 0$ for all lag-k are erroneous and should be rectified accordingly. Logically, the same RQD value may correspond to different persistance levels or vice versa.

The RQD and persistance values for different scanlines considered herein are shown in Table 6.4

Table 6.4 Scanline rock qualities

Scanline	RQD (%)	Quality	Persistence	Quality
SL1	88	Very good	0.68	Fair
SL2	74	Fair	0.82	Very good
SL3	86	Very good	0.73	Fair
SL4	89	Very good	0.78	Very good
SL5	86	Very good	0.70	Fair

A striking conflict appears from this table; so far, the rock qualities on RQD and persistance basis are concerned. For the fourth scanline although the same quality conclusion is arrived, other scanlines are in conflict to some extent. Hence a dilenma arises as to which one is to be chosen for decision-making. The view taken in this research is that persistance-based qualities should be preferred over the RQD-based descriptions since the former takes into consideration not only the mean and variance of intact lengths but also their correlation structure, i.e., clustering effects.

6.4.1 Proposed Models of Persistance

Provided that the autorun functions are available, the question arises as to what type of dependent process represents best the intact length occurrences within a rock mass. A straight forward answer to this question can be given, provided that the autocorrelation structures of different theoretical stochastic processes are known beforehand. For this purpose three stochastic processes will be described herein, namely the independent random process, the lag-one Markov process, and the autoregressive integrated moving average process ARIMA (1, 1).

6.4.1.1 The Independent Process

It does not have any autorun function, i.e., all of the autocorrelation coefficients at each lag except lagzero are equal to zero as shown in Fig. 6.16a. It is the easiest and simplest stochastic process employed in representing natural phenomenon.

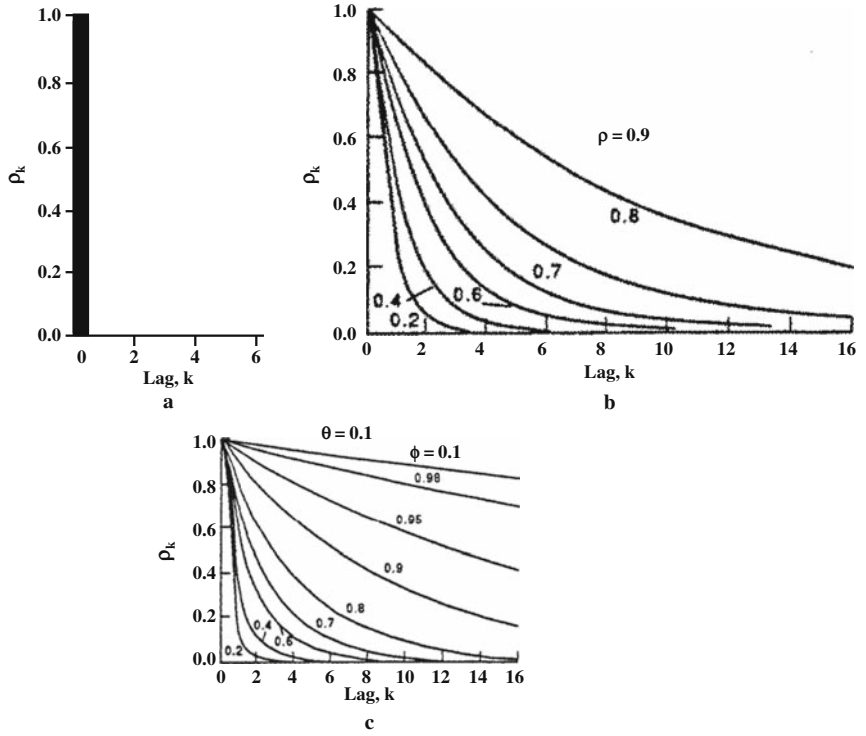

Fig. 6.16 Autocorrelation structure of different processes (**a**) independent process; (**b**) Markov process; and (**c**) ARIMA(1, 1) process

Two parameters, namely the mean and standard deviation, are enough to describe the phenomenon completely. In fact, all of the RQD, RQR, RQP, etc., have been based on the understanding that the phenomenon has an independent structure (Şen, 1990a). Since there has been so many studies in the past concerning this process, its repetition is avoided herein.

6.4.1.2 First-Order Markov Process

In general, geologic variables possess dependent structure, especially when they are at close intervals from each other. The simplest way of representing any dependence is through autoregressive processes such as the lagone Markov process (Şen, 1974). The mathematical form of this process can be written as

$$l_i = \mu + (l_{i-1} - \mu) + \sigma\sqrt{1 - \rho^2}\varepsilon_i, \tag{6.55}$$

in which μ, σ, and ρ are the mean, standard deviation, and first-order serial correlation coefficient, respectively, of intact lengths l_i and, finally, ε_i is a normal random shock with zero mean and unit variance. The autocorrelation structure of this process is given as

$$\begin{aligned} \rho_0 &= 1 \\ \rho_i &= \rho^i, \end{aligned} \tag{6.56}$$

which has been presented for different ρ values in Fig. 6.16b.

6.4.1.3 ARIMA (1, 1) Process

It is used in order to represent more persistently dependent processes, which are noticed during intact length analysis in this study. These processs were prepared first by Box and Jenkins (1970) with the following expression,

$$l_t = \mu + \phi\ (l_{i-1} - \mu) + \varepsilon_i - \theta\varepsilon_{i-1}, \tag{6.57}$$

in which ϕ and θ are model parameters and ε_i is again normal random process with zero mean and unit variance. The autocorrelation structure of this model is given as

$$\begin{aligned} \rho_0 &= 1 \\ \rho_1 &= \frac{(1 - \phi\theta)\,(\phi - \theta)}{\left(1 + \theta^2 - 1\phi\theta\right)} \\ \rho_k &= \phi\rho^{k-1}\ (\text{for}\, k \geq 2)\,, \end{aligned} \tag{6.58}$$

which is drawn for same set of parameters in Fig. 6.16c. Comparisons of graphs in Fig. 6.16 indicate that only ARIMA (1, 1) processes lead to significantly more persistant correlations at large lags than other processes.

6.4.2 Simulation of Intact Lengths

The purpose of this section is to derive the relationship between the RQD and the first-order autorun correlation coefficient as a representative of persistance. As already mentioned above, since the autorun functions in Fig. 6.15 indicate persistance structure in the intact length occurrences, they cannot be represented by classical processes such as the negative exponential distribution, which is based on the assumption that the intact lengths are generated from an independent process. This implies autocorrelation structure as in Fig. 6.16a. It is obvious from Fig. 6.15 that all of the scanlines considered in this study have autorun functions with significant persistances. In order to be able to simulate these persistant patterns, the intact lengths are considered to be normally distributed so that the autorun functions can be considered as equivalents to the autocorrelation functions, which are necessary ingradients for simulation by use of the Markov and ARIMA(1, 1) processes.

Hence the first step in the simulation is to find the best stochastic model that fits the experimental autocorrelation functions. Therefore, the experimental autocorrelation funct ions that are already given in Fig. 6.15 are compared with a set of theoretical autocorrelation structures as obtained from Eqs. (6.50) and (6.57) for Markov and ARIMA(1, 1) models, respectively, by considering different parameter sets. In fact, the identification of model parameters such as ρ, ϕ, and θ are made

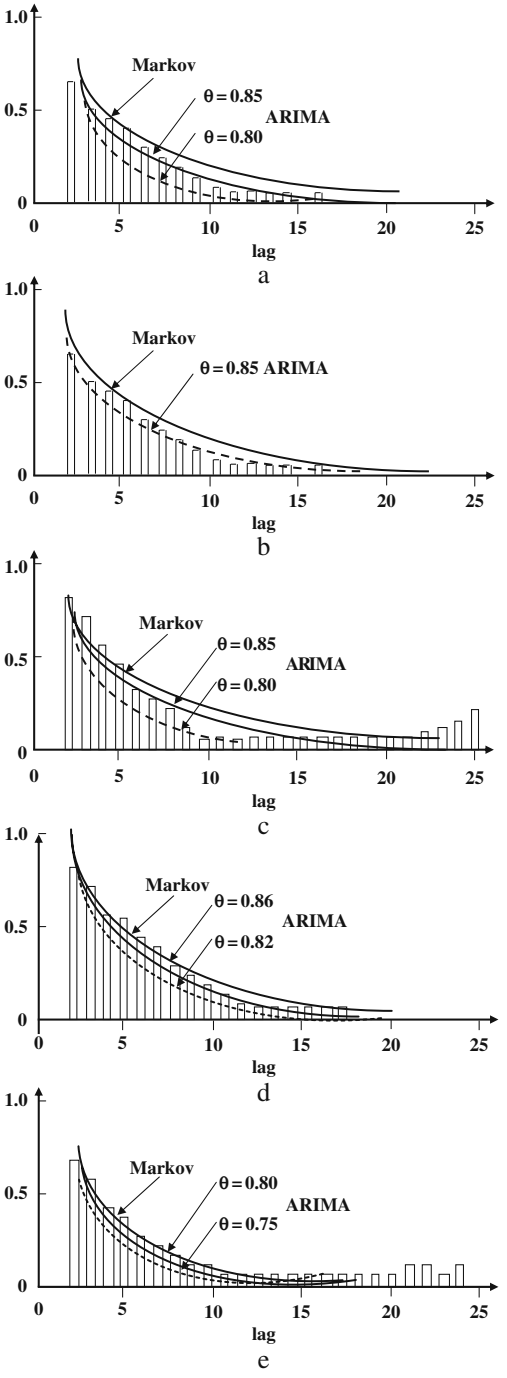

Fig. 6.17 Experimental and theoretical autocorrelation function for (**a**) SL1; (**b**) SL2; (**c**) SL3; (**d**) SL4; (**e**) SL5

by visual comparison of experimental and theoritical autocorrelation functions as presented in Fig. 6.17.

It is obvious that for the Markov process there appears to be only one theoretical autocorrelation function based on the first-order autocorrelation coefficient whereas ARIMA(1, 1) process has different functions for the same correlation coefficient depending on the values of ϕ and θ. In deciding on the best fit only the first onethird of the experimental autocorrelat ion must be considered as reliable. On this basis, it appeared that only SL2 had a very good match with the Markov process and the others accord by the ARIMA(1, 1) process but with different set of parameters. Table 6.5 exhibits the model types and parameter values for each scanline.

It is obvious from this table that the least persistant scanline on the basis of autocorrelation function is SL2. However, positive ϕ–1 values for the other scanlines indicate that the rock quality is comparatively better than SL1.

After the availability of the model parameters from Table 6.5 it is possible to generate synthetic scanlines by using the appropriate model on digital computers. The benefit from such a simulation is to gain detailed insight into the possibilities of the fracture distribution within the rock mass. In fact, simulation results in as many scanlines as required, which are statistically indistinguishable from each other.

This is tantamount to saying that along each synthetic scanline the occurrence of intact lengths will be definitely different, but in the long run they will have the same statistical parameters such as the mean and variance as well as the same autocorrelation structure. In order to explore the relationship between the persistance and the RQD, the following set of different simulations are undertaken.

1. Irrespective of the scanlines considered in this chapter, first of all the relationship between the RQD and the persistance parameters (ρ, ϕ, and θ) are sought for standard intact lengths, i.e., the mean and variance of intact lengths are assumed to be zero and one, respectively. Hence, the generated synthetic scanlines are not affected by any other parameter except the persistance. However, these relationships are obtained for different treshold values as 0.05, 0.10, and 0.15 m. The resulting standard curves for the Markov process are presented in Fig. 6.18.

2. It is obvious that in the Markov process case the RQD is proportionally related to the persistance (in this case ρ), but the relationship is non-linear. RQD is not sensitive to changes in ρ for small ρ-values, for instance, in the case of threshold

Table 6.5 Models and parameters

		Parameters				
Scanline No.	Model	ρ	ϕ	θ	μ	σ
SL1	ARIMA(1,1)	0.68	0.85	0.333	13.77	14.78
SL2	MARKOV	0.82	–	–	9.98	10.13
SL3	ARIMA(1,1)	0.73	0.80	0.152	15.33	14.05
SL4	ARIMA(1,1)	0.78	0.82	0.103	19.78	17.34
SL5	ARIMA(1,1)	0.70	0.80	0.200	14.38	9.49

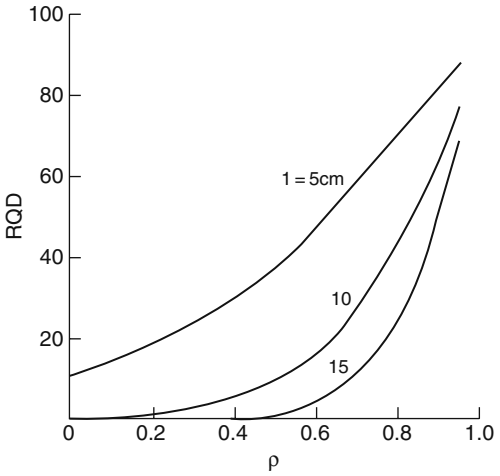

Fig. 6.18 RQD–persistence relation (Markov process)

0.10 m when $\rho < 0.5$. However, for $\rho > 0.5$ the sensitivity increases enormously and therefore the classical RQD calculations may not be reliable, especially when $0.5 < \rho < 1.0$, provided that the underlying generating mechanism of intact lengths is of Markov type. On the other hand, Fig. 5.9 also indicates that the rock quality improves if a low threshold value such as 0.05 m is adopted for the basic RQD definition. On the other hand, the comparison of three curves in the same figure shows that the rock quality improvement from threshold value 0.15 to 0.10 m is less than the transition from 0.10 to 0.05 m.

The same type of simulation, but for the ARIMA(1, 1) model, leads to standard RQD–persistance relationship as in Figs. 6.19 and 6.20, which present only two samples from an infinite number of such relationships.

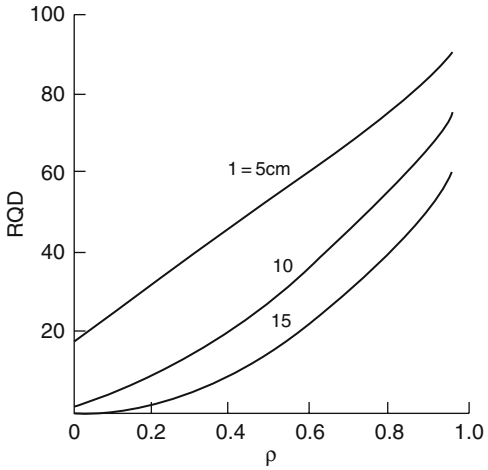

Fig. 6.19 RQD–persistence relation (ARIMA process $\phi = 0.9$)

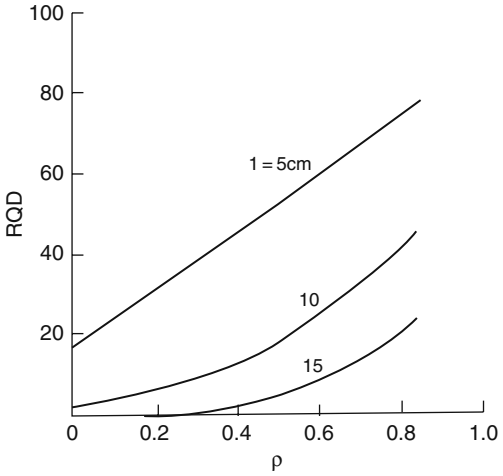

Fig. 6.20 RQD–persistence relation (ARIMA process $\phi = 0.7$)

First comparison of Figs. 6.19 and 6.20 with Fig. 6.18 shows that the ARIMA (1, 1) process implies better rock quality for the same threshold value. This is indeed the logically expected result from the previous discussions. On the other hand, the sensitivity of RQD to persistence parameter changes decreased significantly for $\rho > 0.5$, but increased for $\rho < 0.5$. In other words, the curvature of the curves is very small compared with the Markov process to the extent that even in same cases with such threshold values of 0.05 m the RQD–persistance relationship appears as a straight line. Furthermore, comparison of Fig. 6.19 with Fig. 6.20 indicates that increase in the ϕ value means improvement in in the rock quality, which is due to the fact that large ϕ-values imply longer intact lengths.

3. In order to see the effects of genuine parameters, i.e., mean and variance of the scanlines, a second set of simulation with the same models are performed on digital computers. Some of the representative results for SL1, SL2, and SL3 are presented in Fig. 6.21. A general conclusion from these figures is that the mean and standard deviation of the intact lengths are not sufficient in calculating RQD values. For instance, consideration of Fig. 6.21 leads to the conclusion that the least RQD value as almost 20 will appear, provided that the intact lengths along SL1 occur independently ($\rho = 0$). However, in addition to these two basic parameters, the value of ϕ plays a dominant role by causing increment in the RQD value. Similar statements are valid for other scanlines. Besides, comparison of Fig. 6.21 with Figs. 6.19 and 6.20 shows that as the mean and standard deviation values increase, the sensitivity of persistance parameter decreases. It is therefore plausible to conclude that the longer and less variable become the intact lengths the more reliable will be the classical RQD calculations by Deere's original definition.

The main theme of this study was to emphasize that in practical studies the RQD calculations are not reliable without the consideration of intact lengths correlation structure. It is a well-known fact that the classical RQD evaluations are based on the

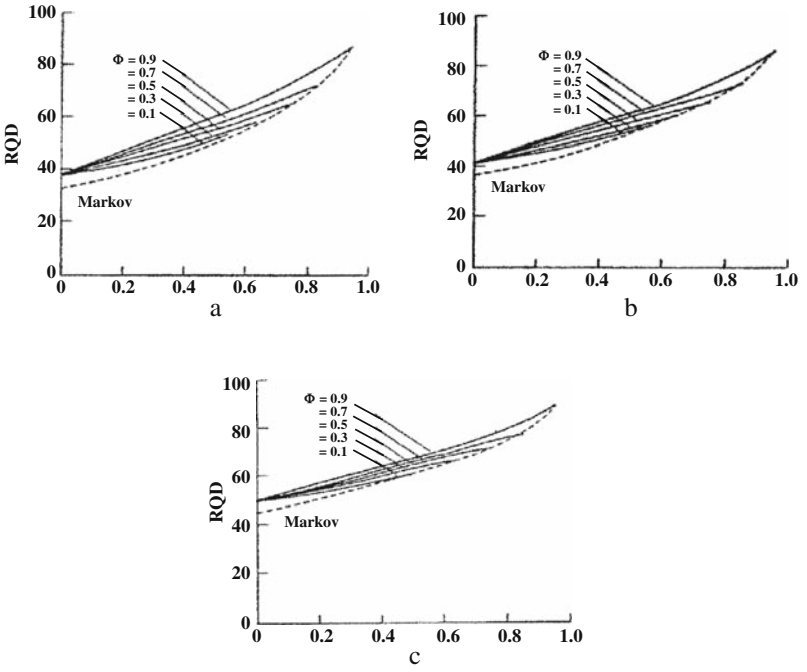

Fig. 6.21 RQD–persistence relation for (**a**) SL1; (**b**) SL2; (**c**) SL3

mean value percentage of the intact lengths that are greater than a threshold value only. However, under the light of the simulation study performed in this chapter, the following important points are worth to notice.

1) The persistance structure of intact lengths gives rise to additional rock quality increments.
2) There exists a proportional relationship between the RQD and the persistance parameter, which is adopted as the first-order autocorrelation coefficient in this study.
3) İt is possible to identify the underlying generating mechanism of the intact lengths by comparing the experimental and theoritical autocorrelation functions of stochastic processes, such as the Markov or ARIMA(1, 1) processes.

6.5 Autorun Simulation of Porous Material

Any porous medium will have either a solid or a void at each point in space. Quantitatively, solid point is represented by –1 and a void point by +1. Figure 6.22 indicates voids as white squares and solids as black patches, and such a spatial distribution of digitized numbers is a bivariate random field or ReV.

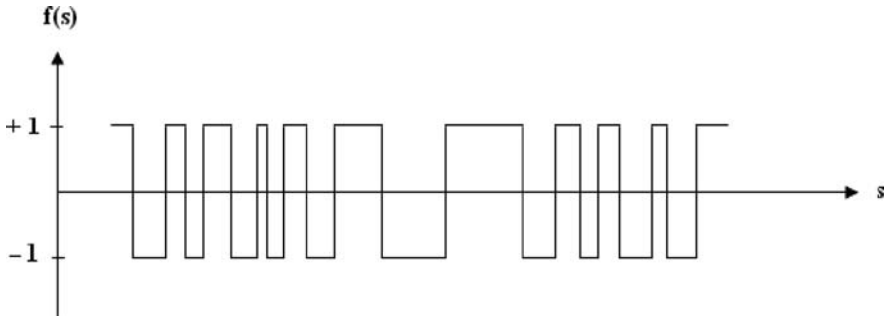

Fig. 6.22 Schematic representation of a line characteristic function

Hence, ReV function, $\xi(x)$, is a two-valued random variable in space as (Şen, 1990b)

$$\xi(x) = \begin{cases} +1 & \text{if} \quad x \in A \\ -1 & \text{if} \quad x \in A^c \end{cases}, \tag{6.59}$$

where $\in$ means "belongs to" A and A^c are the sets of voids and solids, respectively, within a porous medium bulk volume, V. These two sets are mutually exclusive and complementary, so it follows that

$$A \cup A^c = V \tag{6.60}$$

and

$$A \cap A^c = \Phi, \tag{6.61}$$

where $\cup$ and $\cap$ are union and intersection of sets, respectively, and Φ is the empty set. The expression "random function of coordinate" must be understood in the sense that at each point of the 3D space, the value $\xi(x)$ is a random variable, and consequently it cannot be predicted exactly. The values of $\xi(x)$ are subject to a certain pdf. If the pdf is invariant with respect to a shift of the system of points, then the ReV and corresponding porous medium are homogeneous. The same ReV is statistically homogeneous and isotropic when the pdfs are invariant with respect to an arbitrary rotation of the system points (such as a solid body) and to a mirror reflection of the system with respect to an arbitrary plane passing through the origin of the coordinate system. In other words, the statistical moments depend upon the configuration of the grain–void system for which they are formed, but not upon the position of the system in space. In practical terms, the porous medium is isotropic if the properties of any point are the same in all directions from that point. The medium is of heterogeneous composition if its nature or properties of isotropy or anisotropy vary from one point to another in the medium. If the porous medium is statistically homogeneous and isotropic, then the moments do not depend on any preferred direction within the medium.

6.5.1 Line Characteristic Function of Porous Medium

Any internal property of porous medium can be quantified by an arbitrary sampling line, which passes through a rock in any direction. Each point on this line corresponds to either a void or a solid and the sample line characteristic function, f(s), can be defined similarly Eq. (6.59) as

$$f(s) = \begin{cases} +1 & \text{if} \quad s \in A \\ -1 & \text{if} \quad s \in A^c \end{cases}, \tag{6.62}$$

where s is the distance along the sampling line from any arbitrary origin. The graphical representation of f(s) forms a square wave as it passes alternately from void to grain (Fig. 6.22). This function represents one of the possible realizations of the ensemble of the porous medium. It reflects the size distribution of solids and voids, their orientation, and packing within the sandstone. In practice, f(s) may be determined by preparing a high-contrast photographic image of a thin section whose pores have been filled with epoxy.

In order to treat f(s) with classical time-series techniques, such as autocovariance, spectral, autorun analysis, and so forth, it must be defined as random variable set at n points equally spaced Δs apart along the sampling line. Hence, $n\Delta s$ is equal to the sampling line length. The ordered set of f(s) values at $' = 1, 2, \ldots, \infty$, is called a stochastic process. If the pdf is the same for all I, the stochastic process is said to be weakly stationary. In addition, strict stationarity implies that all of the possible joint pdfs are functions of the distance between pairs. However, in practice, strictly stationary processes are not usually encountered. Non-stationarities in sedimentary rock units may arise from the presence of distinctive layering or gradual grading. In general, sedimentary units are considered as stochastically stationary if the pattern of variation in a property is similar in each sampled area of a bed.

6.5.2 Autorun Analysis of Sandstone

The autorun function is especially capable of investigating the sequential properties of random series when only two distinct values exist. Due to its distribution-free behavior, computational simplicity, and robustness to various transformations, it is more flexible than the classical autocorrelation function (Şen, 1978). In general, the autorun function is defined for discrete processes as a conditional probability

$$r(k\Delta s) = P\left[f(k\Delta s) > m / f(\Delta s) > m\right], \tag{6.63}$$

where k is referred to as the lag and m as the truncation level, taken in most cases as the median value. From the definition, it is obvious that values of the autorun function vary between 0 and +1 for any lag-k. Let p be the probability of +1 in a characteristic function (see Eq. 6.62) of infinite length. For a line characteristic function the truncation level can be taken as any value between +1 and –1, exclusively.

For independent processes all of the autorun values at different lags are equal to p. However, for any process the following autorun function properties are valid:

$$\left.\begin{array}{l} r(0) = +1 \\ 0 < r(k\Delta s) < +1 \\ r(\infty) = p \end{array}\right\}. \tag{6.64}$$

The small sample estimate of the lag-k autorun coefficient from finite length characteristic functions can be obtained similar to Eq. (6.35) as

$$r(k\Delta s) = \frac{2n_k}{n-k}, \tag{6.65}$$

where n_k shows the number of overlapping successive +1 pairs at a distance of $k\Delta s$ apart and n is the number of equally spaced points in the porous medium line characteristic function. In the case of independent process $r(k\Delta s) = p$ for any lag (see Fig. 6.23). If $1 \geq r(k\Delta s) > p$, then on the average the points lag-k apart fall on void space; otherwise, when $p > r(k\Delta s) \geq p$, they fall on grain space.

The former situation indicates positive dependence and sometimes is referred to as persistence. It implies physically that grain points and void points follow void points. Şen (1978) has shown the analytical relationship between the autorun and the autocorrelation coefficients for $p = 0.5$ as

$$r(k\Delta s) = \frac{1}{2} + \frac{1}{\pi} \arcsin \rho_{k\Delta s}, \tag{6.66}$$

where $\rho_{k\Delta s}$ is the lag-k autocorrelation coefficient. Assuming a first-order Markov process where $\rho_{k\Delta s} = \rho_{\Delta s}^{k}$, this last expression gives autorun functions as shown in Fig. 6.24. It is obvious that for this case $0 \leq \rho_{k\Delta s} \leq +1$ corresponds to $0.5 \leq \rho_{k\Delta s} \leq +1$. Figure 6.24a–d represents persistence, and the autorun function converges 0.5 asymptotically. These continuous decreases indicate the stationary nature of the underlying sample characteristic function. On the other hand, negative dependence is characterized by autorun functions. In Fig. 6.24, r_k implies $r(k\Delta s)$ and $r(\Delta s)$.

The autorun coefficient is robust and is not dependent on any particular distribution function. Furthermore, it is very convenient for binary random variables. The physical interpretation of the auto-covariance function may be difficult or impossible to make (Jenkins and Watt, 1968). Contrarily, the autorun function has physical meaning as conditional probabilities and is usually simple to interpret. The

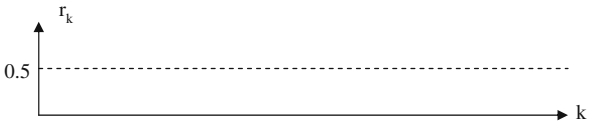

Fig. 6.23 Autorun function of an independent process [$r(k\Delta s) = 0.5$, $p = 0.5$]

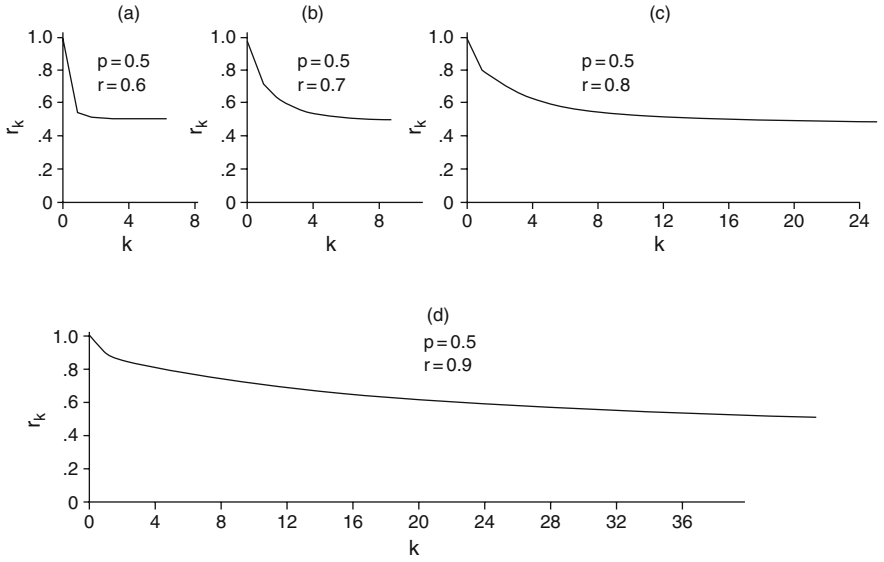

Fig. 6.24 Autorun function of the dependent process for different r(kΔs) values and p = 0.5

asymptotic value of the autorun function corresponds to the porosity of the porous medium. However, in practice autorun coefficients for relatively large lags estimated from Eq. (6.65) yield the approximate porosity.

Another very important physical parameter that is directly related to the autorun function is the specific surface, σ. The specific surface is defined as the ratio of the total surface, S′, of solids (or voids) to the bulk volume of the porous medium concerned. Hence, generally

$$\sigma = \frac{S'}{V.} \tag{6.67}$$

Knowledge of the specific surface is important in cases of adsorption of materials from the fluid flowing through the porous medium. It is also important in the design of sand and gravel filter columns. In hydrogeology it is related to the specific retention of water in sandstone. The finer the grains, the greater will be the specific retention and specific surface.

The random variable, $\eta(x)$, identifying this surface, can be obtained from the basic ReV as

$$\eta(x) = \lim_{\Delta s \to 0} \xi(x)\,\xi(x + \Delta s) = \begin{cases} +1 & \text{for} \quad x \in S^c \\ -1 & \text{for} \quad x \in S \end{cases}, \tag{6.68}$$

where S is the set of points in the porous medium resting on the grain surface and S^c is the complementary set including the remaining points. Hence, –1 is important in

the definition of grain surface. In fact, points on S physically correspond to "crossings" from a grain to a void or vice versa, that is, grain boundaries. Along any sampling line, these crossings occur as random points after each square wave. In the statistical literature these points are referred to as the zero crossing (Mood, 1940). The total number of such crossings in a continuous sequence has been given originally by Rice (1945). An approximate but practical calculation to total cross numbers, T, in any discrete process has been given by Şen (1980) in terms of the first-order autorun coefficient (k = 1), as

$$T = 2n\,[1 - r\,(\Delta s)]\,p. \tag{6.69}$$

Here T represents the points of solid surface along any sampling line, provided that the porous medium is isotropic and homogeneous. Hence, the estimate of specific surface $\hat{\sigma}$ along such a line can be determined after dividing Eq. (6.69) by the length of this line $n\Delta s$

$$\hat{\sigma} = 2\,\frac{1 - r\,(\Delta s)}{\Delta s}p,$$

or more conveniently

$$\hat{\sigma} = 2\,\frac{r\,(0) - r\,(\Delta s)}{\Delta s}p. \tag{6.70}$$

It is important to notice at this stage that the ration in Eq. (6.60) is the slope of the autorun function at the origin. A similar relationship has been obtained with the autocorrelation function slope at the origin by Watson (1955). The population (asymptotic) value of the specific surface can be found from Eq. (6.70) as $\Delta s \to 0$, which leads to

$$\sigma = -2r'\,(0)\,p, \tag{6.71}$$

where $r'(0)$ is the derivative (slope) of the autorun function at the origin. For independent processes, $r'\,(0) = -\infty$ and for completely dependent processes $r'\,(0) = 0$. It is therefore expected theoretically that the specific surface is isotropic and homogeneous materials may take any positive value. Since processes in earth sciences fall between the two aforementioned extremes, their specific surface values fall between zero and infinity. It has been shown by Cramer (1938) that the specific surface of sandstones varies in the range of 150–320 cm^{-1}. The finer the sandstone, the greater the number of crossings on any sampling line, and therefore the slope of the autorun function will be greater, leading to greater specific surfaces. It thus becomes very obvious that fine materials will exhibit much greater specific surface than will coarse materials. Some fine materials contain an enormous grain surface area per unit volume. The generalization of Eq. (6.71) for any preferred direction, say α, within the anisotropic porous medium is possible after dividing it by the surface area of the sphere with unit radius. Hence, Eq. (6.71) becomes

$$\sigma = -\frac{1}{2\pi}\int r'_{\alpha}(0)\, p_{\alpha} d\alpha, \tag{6.72}$$

where $r'_{\alpha}(0)$ and p_{α} are the derivatives of the autorun function at the origin and the porosity along this preferred sampling line, respectively. The numerical calculation of Eq. (6.72) can be achieved by taking various thin sections on different directions.

6.5.3 Autorun Modeling of Porous Media

Since the porous medium has been regarded as a realization of a stochastic process, it is necessary to develop a model for generating pore structure that is more representative than those based deterministically on assemblages of spheres or tubes. However, the spherical beads and capillary tube models are assumed for analytical purposes in solving for fluid flow on the scale of a few pores. Therefore, they are not convenient for generating the stochastic characteristics of the porous medium. A simulation model of the grain-void size distribution can be achieved through the autorun technique. Although such a model does not give, on the average, new information about the medium, it helps to generate all of the possible line characteristics function realizations of the medium. The first simulation model in this direction has been proposed by Roach (1968) for independent processes.

However, in general, the porous medium composition of voids and solids has dependent structure. This is tantamount to having clusters of voids and/or solids; that is, as a general tendency voids follow voids and solids follow solids. The first autorun coefficient, $r(\Delta s)$, provides a criterion to decide whether the porous medium composition has dependent composition; that is, occurrence of any void or solid does not affect others. However, $r(\Delta s)$ is significantly different from the porosity, then dependence and, therefore, clustering exists. When $r(\Delta s) > p$ a positive dependence exists, which means physically that the clustering of voids is predominant. On the contrary, for $r(\Delta s) < p$ clustering of solids is effective.

The probabilities of having at least two successive voids is $r(\Delta s)$, of having three successive voids $r^2(\Delta s)$, and in general having at least j successive voids is

$$P(n_v \geq j) = [r(\Delta s)]^{j-1}. \tag{6.73}$$

It has been shown by Feller (1967) that

$$P(n_v = j) = P(n_v \geq j) - P(n_v \geq j+1). \tag{6.74}$$

Hence, substitution of Eqs. (6.73) and (6.74) yields the probability of having j uninterrupted successive voids on an infinite sampling line as

$$P(n_v = j) = [1 - r(\Delta s)]\,[r(\Delta s)]^{j-1}. \tag{6.75}$$

It indicates that void lengths are geometrically distributed with parameter $r(\Delta s)$. The expectation of void length in an infinite characteristic function can be found from Eq. (6.75) as

$$E(n_v) = \frac{1}{1 - r(\Delta s)}. \tag{6.76}$$

For independent processes, $p = r(\Delta s)$; this equation gives $E(n_\upsilon) = 1/(1 - p)$, which has been presented by Feller (1967). The purpose of a simulation model is to generate statistically indistinguishable synthetic characteristic functions from the observed line characteristic function. In other words, on the average, statistical parameters such as the mean and variance must be preserved in the synthetic characteristic functions. It is possible to generate geometrically distributed void lengths, υ, with parameter $r(\Delta s)$ as

$$v = 1 + \frac{\log \xi}{\log r(\Delta s)}, \tag{6.77}$$

where υ is an integer-valued random variable and ξ is a uniformly distributed random variable between 0 and +1. The solid lengths, g, can be generated similarly to Eq. (6. 77) as

$$g = 1 + \frac{\log \xi}{\log r_g(\Delta s)}, \tag{6.78}$$

where $r_g(\Delta s)$ is the first autorun coefficient calculated from the line characteristics after its multiplication by -1.

Since the void and solid lengths occur alternatively on a sampling line, the initial length can either be selected randomly or according to the final length type on the observed sampling line, and then void and solid lengths are arranged in sequence. However, whichever way is adopted does not make any difference in the final product.

The aforementioned modeling technique for the porous media based on the autorun model has been implemented on a digital computer for parameters $p = 0.5$; $r(\Delta s) = r_g(\Delta s) = 0.5$, 0.7, and 0.9. Very long sequences of synthetic line characteristic functions (10,000 points) have been generated, but three samples with length of 125 points each are presented in Figs. 6.25a, 6.26a, and 6.27a, together with their sample autorun functions in Figs. 6.25b, 6.26b, and 6.27b, respectively. Figure 6.25a represents the independent structure of void-solid occurrences resulting from the autorun model, whereas Figs. 6.26a and 6.27a are samples of dependent structure.

It is clear that on the average the lengths of voids or grains are shorter in Fig. 6.25a than in others; in addition Fig. 6.25a is richer in the number of crossings than others. As the autorun coefficient increases, these lengths as well as the number of crossings increase. Line characteristic functions in Figs. 6.25a, 6.26a, and

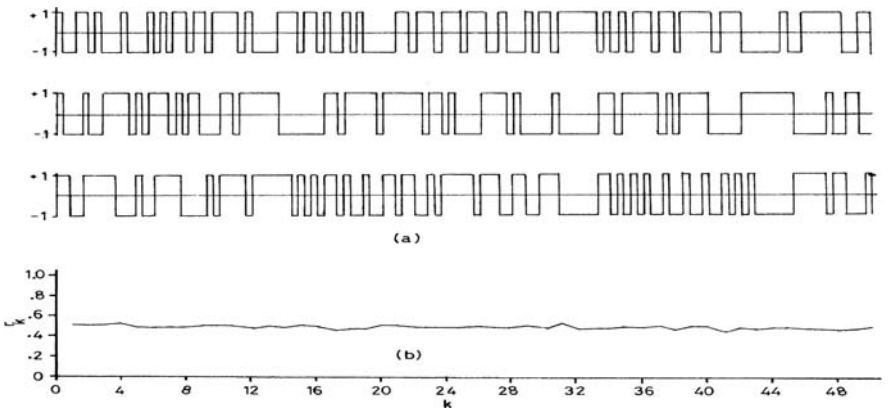

Fig. 6.25 Synthetic line characteristic function [r(kΔs) = 0.5, p = 0.5]

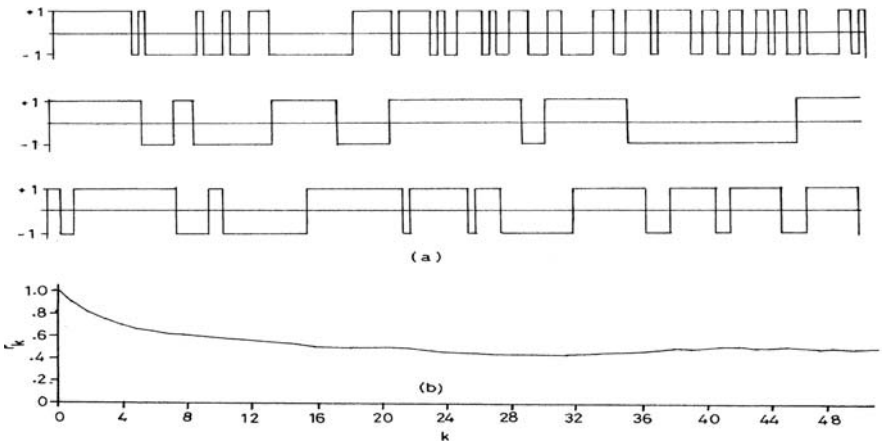

Fig. 6.26 Synthetic line characteristic function [r(kΔs) = 0.7, p = 0.5]

6.27a are the possible realizations of fine, medium, and coarse-grained sandstones, respectively.

On the other hand, generalization of the stochastic model proposed by Roach (1968) for finite sampling lines can be achieved by the autorun coefficient so as to cover dependent porous medium configuration. For this purpose, the following conditional probabilities of the combinations of two successive events at equally spaced points along a sampling line can be written as

$$\begin{aligned} &P(v/v) = r(\Delta s), \\ &P(g/v) = 1 - r(\Delta s), \\ &P(g/g) = 1 - \tfrac{p}{1-p}[1 - r(\Delta s)], \\ &P(v/g) = \tfrac{p}{1-p}[1 - r(\Delta s)]. \end{aligned} \tag{6.79}$$

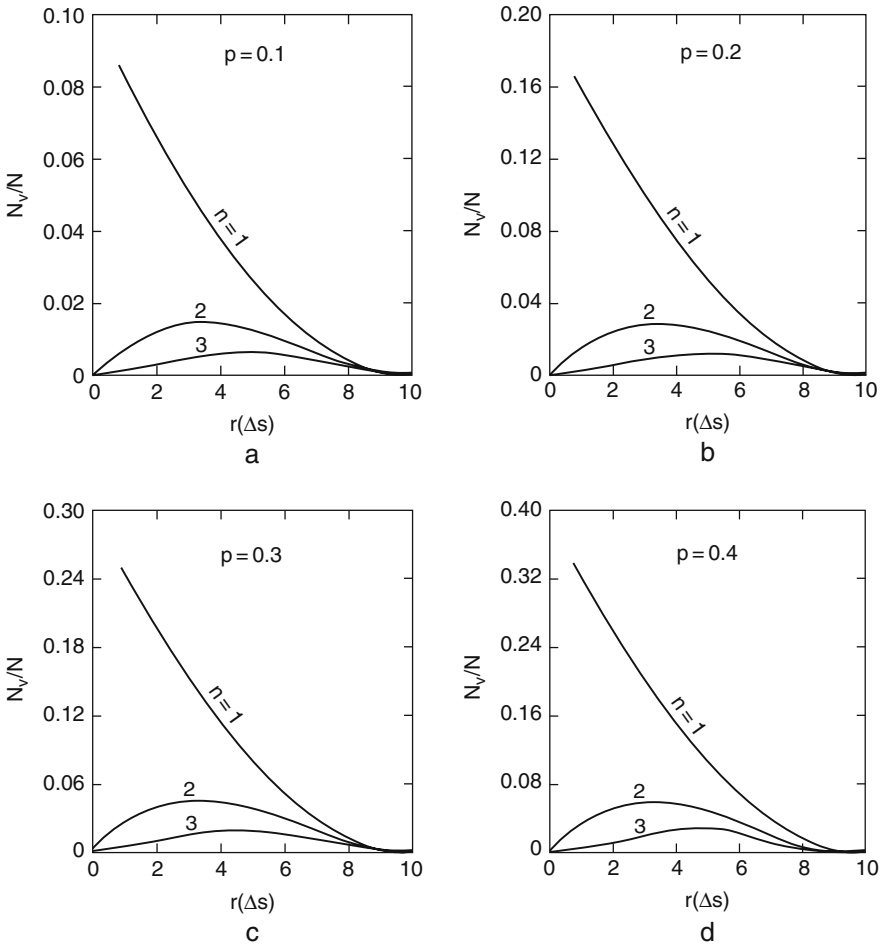

Fig. 6.27 (**a–d**) Number of voids on a line characteristic function

On the average, the probability P(υ) that a point lies in a void space is equal to p, whereas the probability P(g) that a point is within a solid space is q = 1 − p. The void-solid sequence probability is given in Eq. (6.79) as P(υ/g), which defines a crossing point in the line characteristic function. The probability that a solid is followed by a void, P(g, υ), is equal to P(g)P(υ/g) and explicitly

$$P(g,\nu) = p\,[1 - r(\Delta s)]\,.$$

However, the probability P(g, υ, g) of having void length equal to 1Δs can be obtained as P(g, υ)P(g/υ), or as

$$P(g,\nu,g) = p\,[1 - r(\Delta s)]^2\,. \tag{6.80}$$

Similarly, in general, the probability of having the void length equal to $n\Delta s$ becomes

$$P(g,v,v,v,v\ldots,v,g) = p[1 - r(\Delta s)]^{n-1}[1 - r(\Delta s)]^2. \tag{6.81}$$

The number of voids, N_v, of length $n\Delta s$ in a set of N equally spaced points along the sampling line can be obtained as

$$N_v = Np[1 - r(\Delta s)]^{n-1}[1 - r(\Delta s)]^2. \tag{6.82}$$

For the independent process, $r(\Delta s) = p$, and then Eq. (6.82) yields the same result as originally proposed by Roach (1968). Furthermore, a similar expression for the solid can be found as

$$N_g = N(1 - p)\left[1 - r_g(\Delta s)\right]^{n-1}\left[1 - r_g(\Delta s)\right]^2. \tag{6.83}$$

Figure 6.28 shows the change in the number of voids per unit length, N_v/N with the autorun coefficient for given void length of $1\Delta s$, $2\Delta s$, and $3\Delta s$ at different porosities, $p = 0.1$, 0.2, 0.3, and 0.4. It is obvious that the number of voids with length $1\Delta s$ decreases continuously with the increase of the autorun coefficient. However, such a relationship is not valid for other void lengths, because the number of voids with lengths other than $1\Delta s$ has maximum values for autorun coefficients other than zero. For instance, this maximum occurs at about $r(\Delta s) = 0.3$ for $p = 0.3$. Furthermore, whatever the porous medium parameters are in the long run, the number of voids of any length will be more than the voids with smaller lengths. It can be concluded from Fig. 6.28 that the difference between the numbers of voids per unit length for

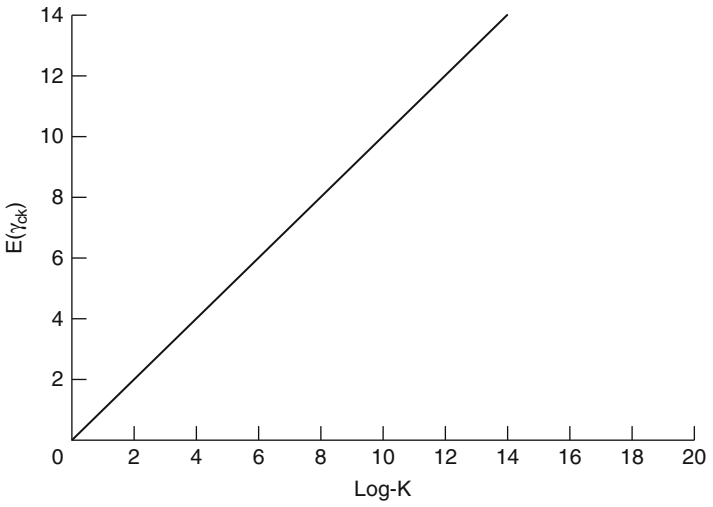

Fig. 6.28 Theoretical standard CSV model of independent intact lengths

voids of length $1\Delta s$ and others is relatively larger at low autorun coefficients. For a line characteristic function with N = 10,000 points, p = 0.3, and $r(\Delta s) = 0.2$, the number of voids for void lengths of $1\Delta s$, $2\Delta s$, and $3\Delta s$ are 1920, 384, and 77, whereas with $r(\Delta s) = 0.8$ they are 120, 96, and 77, respectively.

6.6 CSV Technique for Identification of Intact Length Correlation Structure

Different rock quality description indices that are presented into the rock mechanics literature, which are based on intact lengths, assume that the occurrences of discontinuities and, accordingly, intact lengths are independent from each other. Unfortunately, the validity of such an assumption is questionable, and therefore the final equations for rock quality assessments need to be validated prior to their use.

Otherwise, the results can be regarded only as initial approximations, which might be rough estimations of the rock quality. It is rather obvious that due to different geological phenomena the rock discontinuities appear in local cluster forms, which shows that the intact lengths cannot be considered as independent from each other. In order to check whether the intact lengths along a scanline are independent or dependent from each other, herein, the CSV method has been presented in detail. The basic concept of standard CSV is presented and so simplified that in the case of independent intact length occurrences its variation with the total intact length appears as a straight line, which passes from the origin. Any systematic deviation from straight line implies that the intact length are dependent, and therefore classical rock quality description index must not be used and instead measures that take into account the correlation of intact lengths must be preferred in rock quality studies. Besides, theoretical CSV models are developed for the independent, Markov, and ARIMA(1, 1) processes. These models provide a general guide in the identification of intact length correlation structure as well as the numerical value of such a correlation.

The application of the methodology developed, herein, is presented for scanline measurements at Tytherington quarry in England. The Markovian type of correlation structure is identified for all of the scanlines from this quarry.

Mechanical and/or hydraulic behavior of jointed rock masses require an accurate representation of joint geometry including intact and trace lengths, orientation, intensity, etc. The spacing between two successive joints along an arbitrary sampling line, namely scanline, is referred to as the intact length. Most of the mechanical behavior as well as the quality classification of jointed rock masses are directly related to the intact length occurrences along different directions. According to Terzaghi (1965), the intact lengths along the mean pole direction can be regarded as the true spacing, whereas along any other directions they can be expressed as a function of the true spacing and the angle between the sampling and the mean pole directions. In case of several joint sets, within the same rock mass, it is rather

difficult to measure true spacing for an individual set. In practice, however, scanline measurements include intact lengths between joints belonging to different sets.

Many investigators have examined empirical joint spacing distributions based on measured intact lengths, and generally two different types of theoretical distribution functions were proposed, namely lognormal (Steffen, 1975; Bridges, 1975; Barton, 1977; Şen and Kazi, 1984) and negative exponential distribution (Call et al., 1976; Priest and Hudson, 1976; Einestein and Baecher, 1983; Wallis and King, 1980). Besides, Gamma distribution of intact lengths has been proposed by Şen (1984). However, it seems that the negative exponential distribution appears to be the most frequently used one due to its simplicity. In order to decide whether the intact lengths fit the negative exponential or lognormal distribution, most often the conclusions are based on visual comparison, but Baecher et al. (1977) have used goodness-of-fit tests in the decision-making about the best distribution. For such a test the primary requisite is the histogram of intact lengths. However, any test of goodness-of-fit ignores the internal structure in the intact lengths occurrence along a scanline, i.e., the intact length occurrences are assumed to have a complete random behavior without any dependence on each other. We cannot really assume that nature is nice enough to present us with independent identically distributed intact lengths. In nature the creation of fractures depend on many interactive phenomenanon such as pressure, temperature, volcanic activity, earthquakes. As a consequence, prior to any assessment of intact lengths with the classical techniques, one should confirm their random occurrences. All of the aforementioned studies imply that the intact lengths occur randomly, which might not be the case in actual situations and subsequently overestimations result in the evaluations. Hence, a key question in the intact length evaluation is whether they have an independent structure or not? Provided that the independence is verified, then the use of classical techniques leads to reliable answers. Otherwise, new techniques should be devised so as to take into consideration the dependence structure of intact lengths. This point has been observed first by Higgs (1984), who suggested an empirical technique called "the profile area method" by which the dependence structure within the intact length measurements series is taken into consideration indirectly but in an effective way. Later, Şen (1990b) provided analytical formulation for the profile area method, which showed explicitly that the rock quality measures are not only functions of simple statistical parameters such as the mean and variance values but additionally the serial correlation coefficient. The classical techniques appear as a special case of the analytical formulations when the serial correlation coefficient is practically equal to zero. On the other hand, Eissa and Şen (1990) made an extensive computer simulation by using Monte Carlo techniques so as to generate serially dependent intact lengths according to a very simple Markov model. The calculations of RQD for different serial correlation coefficients indicated that increase in correlation coefficient results in increase in rock quality.

However, neither the empirical method (Higgs, 1984) nor the simulation technique (Eissa and Şen, 1990) is suitable for practical purposes. It is, therefore, suggested herein the use of CSV concept as suggested by Şen (1989a) in evaluating the intact length occurrences and accordingly the rock quality classification. The

CSV technique provides graphs that give additional interpretations in intact length occurrences, and especially in their regional behaviors.

6.6.1 Intact Length CSV

Intact length measurements in the field are dependent on the relative positions of the scanline within the study area. The variability of intact lengths along a scanline leads to the concept of regional variability of intact length with the change in scanline orientation. This variability determines the regional behavior as well as the predictability of the intact lengths on the basis of which the rock quality appreciations can be assessed. Large variability implies that the degree of dependence of intact length on each other might be rather small even for scanlines close to each other. Such a variability may be a product of either one of the active geological phenomenon such as tectonic, volcanic, depositional, erosion, recharge activities.

In order to quantify the degree of variability of regional changes, variance techniques have been used already (Higgs, 1984). On the other hand, Eissa and Şen (1990) and Şen (1991) have employed autocorrelation methods in the intact length assessment. However, these methods cannot account for the regional dependence due to either non-normal distribution and/or irregularity of sampling positions (Şen, 1978).

The SV method has been proposed by Matheron (1963) to get rid of the aforementioned drawbacks. Its elegancy is that the regionalized variable PDF is not important in obtaining the SV, and furthermore it is effective for irregular data positions. It is to be recalled herein that the classical variogram, autocorrelation, and autorun techniques all require equally spaced data values. However, the discontinuities along a scanline are irregularly spaced, and therefore use of classical techniques is highly questionable, except that these techniques provide approximate results only. Although the SV technique is suitable for irregularly spaced data, it has practical difficulties as summarized by Şen (1989a). Among such difficulties is the grouping of distance data into classes of equal or variable lengths for SV construction, but resulting SV results in an inconsistent pattern and does not have a non decreasing form.

However, adaptation of CSV gives with the same data always a non-decreasing pattern without grouping of distances, but rather their arrangement in ascending order. By this arrangement each one of the distances is considered individually in the regional variability of the intact lengths. In general, CSV, $\gamma_s(d_k)$ is defined as a successive summation of squared-differences as

$$\gamma_c(d_k) = \sum_{i=1}^{k} d\left(d^i\right) = \frac{1}{2}\sum_{i=1}^{k}(Z_i - Z_{i-1})^2, \tag{6.84}$$

in which $d(d^i)$ indicates the half-squared difference at i-th order in an ordered intact length arrangements where superscript i indicates the rank; Z_i is the intact length corresponding to rank i.

6.6.2 Theoretical CSV Model

Equation (5.1) in its present form is useful to obtain experimental CSV from a given set of intact lengths, which will be performed in the application. However, the interpretation of these CSVs require a set of relevant theoretical models for their comparison. It is possible to derive theoretical models, provided that the underlying generating mechanism of the intact lengths is known or assumed. To start with, let us take the expectation on both sides in Eq. (6.84), leading to (after the expansion of parenthesis term on the right-hand side)

$$E\left[\gamma_c\left(h_k\right)\right] = \frac{1}{2}\left[E\left(Z_i^2\right) - 2E\left(Z_i Z_{i-1}\right) + E\left(Z_{i-1}^2\right)\right]. \tag{6.85}$$

Let us assume that the intact lengths are second -order stationary, which implies that $E(Z_i{}^2) = E(Z^2{}_{i-1}) = \sigma^2$ and $E(Z_i Z_{i-1}) = \text{cov}(Z_i Z_{i-1}) + \sigma^2$ where $\text{cov}(Z_i, Z_{i-1})$ indicates the covariance between Z_i and Z_{i-1} and finally σ^2 is the variance of intact lengths. It is to be noted that second-order stationary implies that the statistical parameters are independent from i, i.e., from rank. Consideration of these conditions and the substitution of the relevant values into Eq. (6.2)lead to

$$E\left[\gamma_c\left(h_k\right)\right] = \sigma^2\left[k - \sum_{i=1}^{k} \frac{\text{cov}\left(Z_i, Z_{i-1}\right)}{\sigma^2}\right], \tag{6.86}$$

or since from statistical time series analysis (Box and Jenkins, 1970) the ratio term in the parenthesis is defined as the lag-k autocorrelation function, ρ_i, then Eq. (6.86) can be rewritten succinctly as

$$E\left[\gamma_c\left(k_k\right)\right] = \sigma^2\left(k - \sum_{i=1}^{k} \rho_i\right), \tag{6.87}$$

in which ρ_i represents the correlation within the intact length sequence and this expression is a general formulation of the theoretical CSV. The following specific models of CSV can be derived from the available stochastic processes in the literature as employed by Eissa and Şen (1990).

1. Independent model CSV: This is the most widely used assumption in the rock quality assessments that have appeared in the literature (Priest and Hudson, 1976; Hudson and Priest, 1979; Şen 1984, 1990b). The uncorrelatedness of intact lengths implies $\rho = 0$, and consequently the simplest model of all emerges as

$$E\left[\gamma_c\left(k_k\right)\right] = k\sigma^2, \tag{6.88}$$

which means that in the CSV model of such intact length occurrences, the variance plays the dominant role only. The graphical representation of independent CSV model appears as a straight line that passes through the origin as shown in Fig. 6.29. The slope of this straight line gives the variance of intact lengths.

As the variance value becomes smaller and smaller, the independent process CSV becomes closer to the horizontal axis, which represents the distances. For instance, in the case of equal intact lengths along a scanline, the variance becomes zero and hence the horizontal axis represents the CSV. Otherwise, for large variances the CSV model becomes closer to the vertical axis, indicating significant and random differences between successive intact lengths.

2. Markov model CSV: When the intact lengths are serially dependent and the correlation coefficient decreases according to a power law with the increase of lag, then the generating mechanism of them is Markov process, which has the autocorrelation structure as $\rho_0 = 1$, but $\rho_i = \rho_1{}^i$ (i =1, 2, ...), where ρ_i is the lag-one correlation coefficient, which may assume any value between −1 and +1. For this model the CVS model becomes

$$E\left[\gamma_c\left(k_k\right)\right] = k\left(1 - \rho_1 \frac{1 - \rho_1^k}{1 - \rho_1}\right)\sigma^2, \tag{6.89}$$

which reduces to Eq. (6.87) for $\rho_1 = 0$. Positive ρ_1 value means that, the average, long intact lengths follow long intact lengths and short intact lengths follow short intact lengths. On the other hand, negative ρ_1 implies that long intact lengths follow

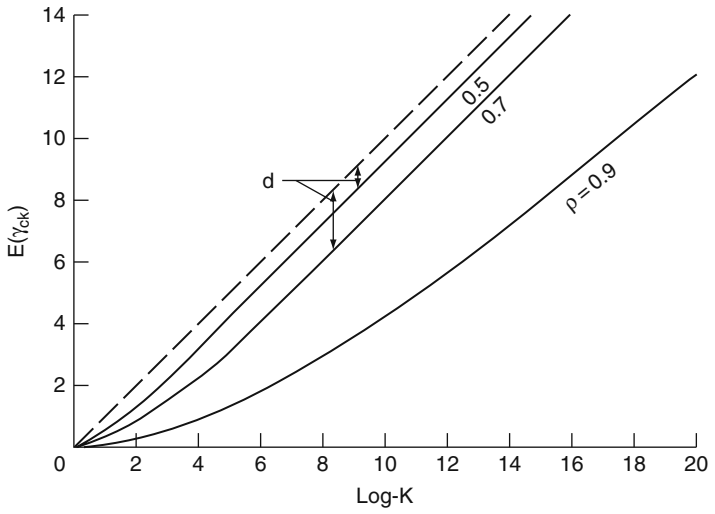

Fig. 6.29 Theoretical standard CSV model for Markovian intact lengths

short intact lengths or vice versa. Equation (6.84) has power form for small k values but becomes straight line for large k-values as

$$E\left[\gamma_c\left(k_k\right)\right] = k\left(1 - \frac{\rho_1}{1-\rho_1}\right)\sigma^2. \tag{6.90}$$

Division of both sides by σ^2 gives rise to the definition of standard CVS, $E\left[\gamma_c\left(k_k\right)\right]/\sigma^2$ as

$$\Gamma\left(k\right) = k\left(1 - \frac{\rho_1}{1-\rho_1}\right). \tag{6.91}$$

The graphical representation of $\Gamma(k)$ is given in Fig. 6.30.

3. ARIMA model CSV: These models have been proposed by Box and Jenkins (1970) and applied to the intact length simulation by Eissa and Şen (1990). The autocorrelation structure of this model is given as

$$\begin{aligned}
&\rho_0 = 1,\\
&\rho_1 = \frac{(1-\phi\theta)(\phi-\theta)}{1+\theta^2-2\phi\theta},\\
&\rho_i = \phi\rho_1^{i-1},
\end{aligned}$$

for $i > 2$. ARIMA model represents intact lengths, which are more persistent than the Markov model case. The substitution of autocorrelation structure into Eq. (6.87) yields, after necessary algebraic manipulation,

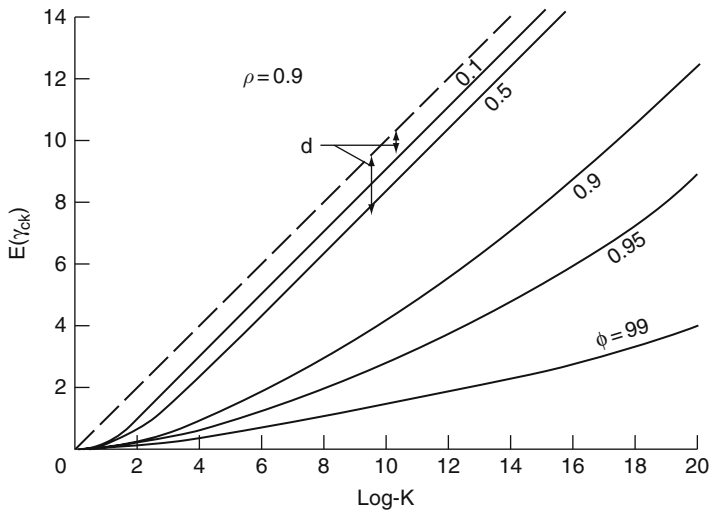

Fig. 6.30 Theoretical standard CSV model for ARIMA intact lengths

$$E\left[\gamma_c\left(k_k\right)\right] = \left(k - \rho_1 \frac{1-\phi^k}{1-\phi}\right)\sigma^2, \tag{6.92}$$

where ϕ is the model parameter representing extra persistence on the Markov model. The standard CSV model is

$$\Gamma(k) = k - \rho_1 \frac{1-\phi^k}{1-\phi}, \tag{6.93}$$

which provides power type of curves for small k values; but as k becomes bigger and bigger, it asymptotically approaches to a straight line portion that can be expressed as

$$\Gamma(k) = k - \frac{k\rho_1}{1-\phi}. \tag{6.94}$$

The graphical representation of ARIMA (1, 1) model standard CSVs are presented in Fig. 6.31.

The comparison of this figure with the Markovian standard CSVs in Fig. 6.30 indicates that in the case of ARIMA (1, 1) model the attendance of CSV to a straight line appears at bigger distances. It is obvious that ARIMA model CVS reduces to Markov and independent model cases for $\phi = \rho_1$ and $\rho_1 = 0$, respectively. Equation (6.94) helps to identify the correlation structure of intact lengths. In order to find the correlation coefficient, it is sufficient to take the derivative of Eq. (6.94) with respect to k, which leads to

$$\Delta\gamma_c = \frac{d\Gamma(k)}{dk} = 1 - \frac{\rho_1}{1-\phi}, \tag{6.95}$$

in which $\Delta\gamma_c$ indicates the slope of standard CSV at large distance. For independent process case $\rho_1 = 0$ and hence $\Delta\gamma_c = 1$.

This is the case where the RQD formulations in terms of the average discontinuity number as given by Priest and Hudson (1976) or Şen (1984) for different distributions is valid. Otherwise, deviations from the straight line that passes through the origin on a standard CSV plot indicates invalidity of all these formulations since the intact lengths are correlated.

If the correlation structure is of Markovian type, i.e., $\phi = \rho_1$, then Eq. (6.95) can be rearranged for the first-order (lag-one) autocorrelation coefficient estimation as

$$\rho = \frac{1-\Delta\gamma_c}{2-\Delta\gamma_c}. \tag{6.96}$$

Example 6.1

The field data for the implementation of the methodology developed herein are extracted from a previous study by Ryckes (1984) on modes of failure and the stability of rock slopes. The scanline measurements are carried out at the Tytherington

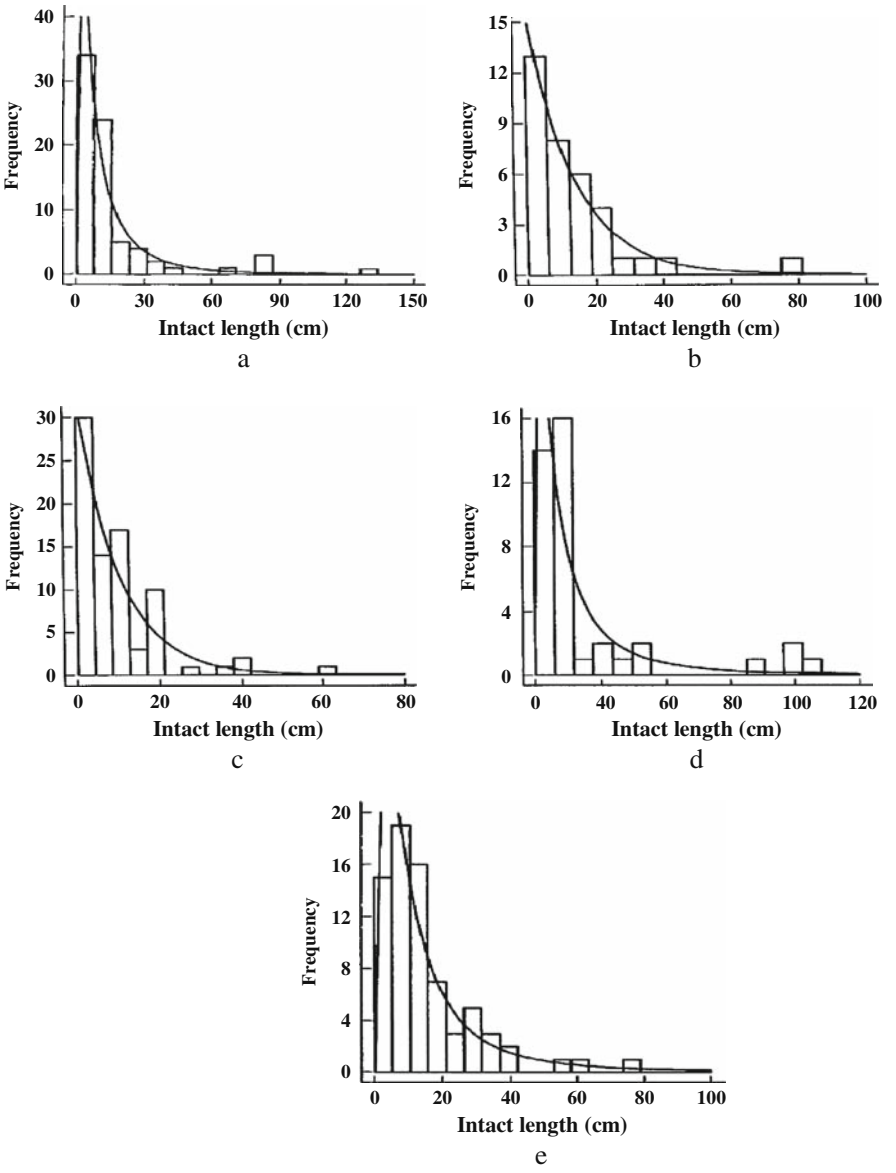

Fig. 6.31 Sample and theoretical pdfs for intact lengths along (**a**) SL1; (**b**) SL11; (**c**) SL12; (**d**) SL2; (**e**) SL3

quarry, which is located halfway between Thurnbury and Tytherington about 16 km north of Bristol in the county of Avon. The Paleozoic rocks of the lower coal series in the area are affected by many movements in the past, which led to faults, folds, and unconformities, each of which led to different pattern of discontinuity spacing,

Table 6.6 Scanline data characteristics

Parameter	SL1	SL11	SL12	SL2	SL3
Length (m)	13.30	4.82	6.19	7.80	11.19
Intact length number	75	35	40	79	73
Average	15.48	13.78	15.48	10.00	15.33
Median	8.00	10.00	7.50	7.00	11.00
SD	219.5	14.87	22.18	10.14	14.05
RQD (%)	84.5	88	79.5	74	86.7
Distribution	Log-normal (Fig. 6.4)	Exponential (Fig. 6.5)	Log-normal (Fig. 6.6)	Exponential (Fig. 6.7)	Log-normal (Fig. 6.8)
χ^2-square	0.260	0.350	7.880	9.046	2.34

i.e., intact length distributions. Due to these different mechanisms it is not possible to expect that the intact length sequence along any scanline in this area has independent correlation structure. In order to depict the regional discontinuity pattern in this area, three scanlines were set up at different directions. The bedding plane orientation is almost horizontal for the first scanline, which will be referred herein as SL1. The second scanline, SL2, has a direction of 20° toward southwest whereas the third scanline, SL3, has an intermediate inclination to the former. All of the scanlines were set up horizontally as two joint sets were recognized to be vertical. The geometrical and statistical summaries of these three scanlines are presented in Table 6.6. Due to its heterogeneous structure the first scanline will be examined in two subsets, which will be referred to as SL11 and SL12.

The frequency distribution functions for scanlines are shown in Fig. 6.32.

The theoretical pdfs have been fitted to the experimental counterparts by using χ^2 tests. For five different scanlines, two types of intact length distributions, namely negative exponential and logarithmic normal, emerge as representative. This difference in the intact length distribution indicates very clearly that their occurrence within the rock mass is heterogeneous, i.e., direction dependent, and consequently even from this observation one can qualitatively conclude that intact lengths have dependent structure. However, classical statistical tests, such as the one used for distribution function identification, do not give any clue about the correlation structure of intact lengths.

Eissa and Şen (1990) suggested the use of correlation function technique in intact length structure exploration. However, correlation techniques are valid only for the normally distributed intact lengths (Şen, 1978). As shown above, none of the intact lengths at Tytherington quarry are distributed normally and consequently the use of correlation techniques is not meaningful. However, the non-normal intact lengths, especially log-normally distributed ones, can be transformed into normal distribution easily, but the transformation of negative exponential distribution exposes great difficulties. Nevertheless, even if the transformation is possible, the transformed intact lengths will not reflect genuine properties of original lengths.

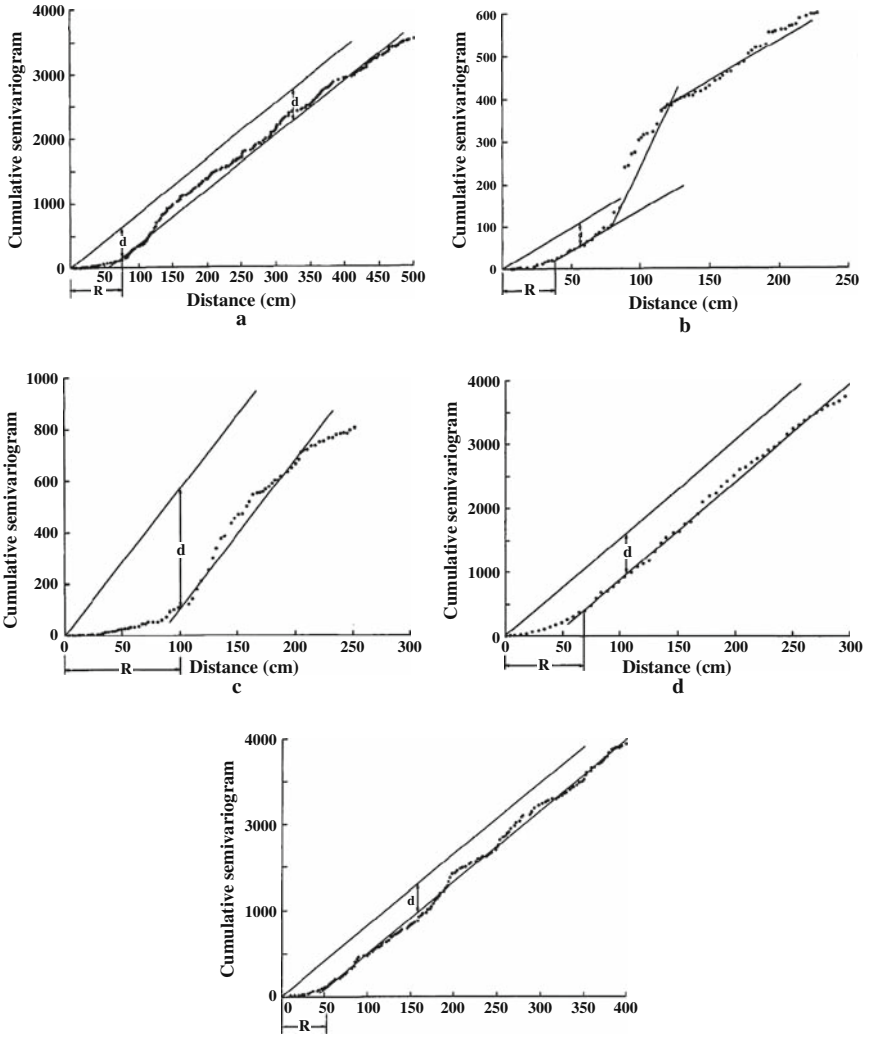

Fig. 6.32 Sample standard CSV of (**a**) SL1; (**b**) SL11; (**c**) SL12; (**d**) SL2; (**e**) SL3

As mentioned in the previous section, the CSVs are robust and valid for any pdf. In fact, the central limit theorem of classical statistics states that whatever the underlying probability distribution of a random variable, its successive summations or averages will have normal distribution. The experimental CSVs for each one of the scanlines considered in this study are presented in Fig. 6.33. At a first glance one can observe the following significant points.

1) None of the CSVs appear as a straight line passing through the origin. This is tantamount to saying that the intact length occurrences along any scanline cannot be considered as independent processes, but they all emerge from dependent

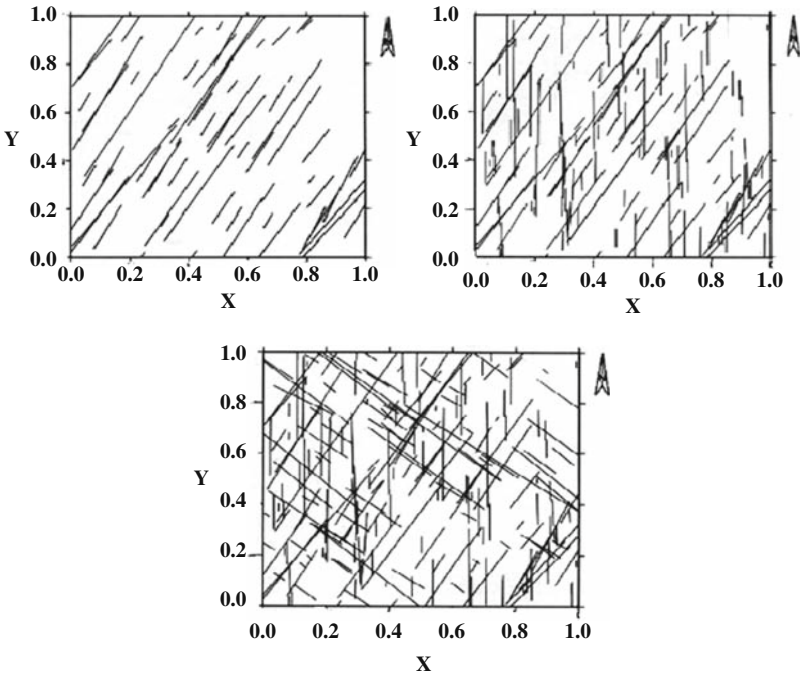

Fig. 6.33 (**a**) A fracture set with 30° orientation from the north; (**b**) Two fractures sets with 0 and 30° orientation from the north; (**c**) Three fractures sets with 0, 30, and 130° orientation from the north

processes. This further implies that in the creature of discontinuities within the rock mass, uniform conditions did not prevail, but rather a complex combination of multitude geological events such as tectonics, cooling, volcanic activities took place jointly.

2) The initial portions of each experimental CSVs shifts toward the distance axis. Such a shift implies the existence of positive correlation between successive intact lengths. It further implies that, in general, big intact lengths follow big intact lengths and small intact lengths follow small intact lengths. Otherwise, if negative correlation should prevail in the occurrence of intact lengths, then the initial CSV portion would shift toward the vertical axis.
3) Each experimental CSV becomes to fluctuate about a straight line for large distance values. As stated before, the existence of such a straight line as a portion in the CSV implies that over the distance range of this straight line portion the intact lengths are independent from each other. This is the only range where the classical rock quality designation formulations keep their validity. Local deviations from the straight line indicate the hidden or minor dependencies in the intact length evaluation.
4) Over an initial distance range, R, the experimental CSV appears as a curve. This range is defined quantitatively as the distance between the original point and the

abscissa of the initial point of the late straight line portion, as mentioned in step (3). It is worth mentioning, herein, that as long as the threshold value necessary in rock quality designation (RQD) calculation is greater than this range value, then the calculation is theoretically sound and valid. Otherwise, threshold values less than this range value will give RQD values, which are unreliable. Hence, CSV provides a criterion for checking the validity of classical RQD values based on 0.1 m (4 inches). Such a valuable criterion cannot be obtained with the correlation techniques. These techniques are valid only for the distance domain over which the CSV appears as a straight line.

5) Existence of straight line at large distances identifies the underlying generating mechanism of the intact lengths as a Markov process. It is already mentioned in the previous section that if the curvature continues even at reduced rates at large distances, then the ARIMA(1, 1) process becomes effective. It is observed that whole the scanlines considered in this chapter have the Markovian nature of dependence, i.e., correlation.
6) The slope of the large distance straight line portion is related to the standard deviation of the underlying intact lengths. It is possible to consider this slope as the population standard deviation of the intact lengths.
7) The vertical distance between the late distance straight line and the one drawn parallel to it passing through the origin reflects the magnitude of correlation coefficient of the intact lengths. Obviously, the smaller this distance the smaller will be the intact length correlation. Under the light of the above mentioned points, the relevant numerical values concerning the initial range, R, vertical distance, d, slope, $\Delta\gamma_c$ of final straight line, and the correlation coefficient estimation from Eq. (5.13) are summarized in Table 6.7.

It is obvious from this table that the correlation coefficient along each scanline has more or less the same magnitude, and therefore the intact lengths dependence may be regarded as regionally isotropic. It implies that only one type of model, which is already identified as Markovian type, can be used in intact length description. The use of this model in intact length generation is outside of this chapter's scope. Last but not the least, the following particular points for each scanline can be inferred from the CSV graphs comparison from Fig. 6.33.

1) The CSVs of SL1, SL2, and SL3 have the similar pattern in that they are composed of initial curvature portion and large distance straight line. However, local deviations around this straight line are rather more persistent in the case of SL1

Table 6.7 CSV parameters

Parameter	SL1	SL11	SL12	SL2	SL3
Range, R(m)	0.74	0.37	1.00	0.68	0.52
Vertical distance, d(m^2)	475.0	54.0	465.0	650.0	325.0
Slope, Δy_c(m)	8.26	2.00	5.70	15.38	8.06
Correlation coefficient, ρ	0.495	0.497	0.493	0.460	0.489

than others. This indicates that the intact lengths along SL1 have same secondary internal structure. In order to discover this structure SL1 is divided into two mutually exclusive portions, namely SL11 and Sl12.

2) The CSVs for SL11 and SL12 in Fig. 6.33b and c are distinctively different than others. They exhibit not a single straight line but two successive straight lines. This implies that along the SL1 direction there is another secondary geological event, which plays a role in the occurrence of discontinuities along this scanline. A reliable explanation on this point can be arrived only after a detailed geological study of the quarry considered.

One of the most recent and significant question about the intact lengths is whether they have independent or dependent occurrences along a given scanline? In the past, without consideration of such a question all of the rock quality classifications derived from the intact length properties were based on the assumption that the intact lengths are identically and independently distributed. The difficulty was due to the lack of a reliable technique in quantifying the correlation structure of intact lengths. However, in this chapter standard CSV are proposed as a practical tool in measuring the intact length correlations. The CSV calculations are straightforward, without any difficulty or ambiguity. The CSV graphs show the change of half squared-differences between intact lengths with ordered distance. The intact lengths are independent only when the standard CSV variation with distance appears as a straight line that passes through the origin. Otherwise, they are dependent and according to the dependence structure standard CSV graphs take different shapes. However, they have some common property such as that at small distances they appear as curves whereas at big distance again straight lines dominate, but their extensions do not pass through the origin. The slope of the straight line portions on standard CSV plot gives opportunity in calculating the intact length correlation coefficient. For instance, if this slope is close to unity, then and only then the intact lengths can be assumed as independent and consequently theoretical RQD relationships with the average number of discontinuities are reliably used in any rock evaluation project. The application of methodology developed in this chapter has been performed for the field data obtained at Tytherington quarry in England.

6.7 Multidirectional RQD Simulation

A simple fracture network model is proposed based on the negative exponential pdf of the discontinuities in all directions. In the fracture-generating procedure, the midpoint coordinates of each fracture is generated by a uniform pdf; the fracture directions are simulated by normal pdfs and the fracture lengths are derived from a log-normal pdf. Three different sets of fractures are presented on a planar surface with different random seeds. The main purpose of this chapter is to asses the rock quality designation, (RQD), on the basis of one, two, and three directional fracture sets. All previous studies up to date theoretically or practically were confined to one direction only. A graphical procedure is presented for depicting the population

estimate of the average number of discontinuities along a scanline. The substitution of this estimate into the relevant RQD equation provides the rock quality estimation in a better representative manner than the classical estimates.

Fracture network models are useful tools for understanding the geotechnical and geohydrological behaviors of rock masses. These networks can be constructed by adopting a model for the fracture geometry (position, direction, trace length, aperture, roughness, etc.), estimating the statistical distribution of the appropriate geometric parameters through field measurements and then generating realizations of statistically indistinguishable networks. Once the geometry of a particular realization is specified, then either flow through the network or the geotechnical properties can be studied. For example, one might benefit from such a procedure in the study of average fracture lengths in various directions, extreme values of apertures or traces, average permeability of fracture network under various boundary conditions, etc. Last but not least, fracture network models might be a part of a larger study of hydrologic response to a perturbation such as the construction of an underground opening containing nuclear waste.

Simple simulation studies were initiated by Goodman and Smith (1980) for unidirectional discontinuity spacing, with the purpose of obtaining an experimental relationship between the RQD and the average number of discontinuities. On the other hand, Baczynski (1980) has proposed a zonal concept for spatial distribution of fractures in rock masses. However, many fracture network studies have been undertaken especially for the water flow through interconnected fractures. Among such studies are the equivalent porous medium permeability in network of discontinuous fractures by Long (1983), the groundwater flow through fractures by Rouleau (1984), mass transport in fractured media by Smith and Schwartz (1984). Recently, extensive computer simulation studies were performed by Şen (1984, 1990b) and Eissa and Şen (1990) in assessing the rock quality classifications. To the best of author's knowledge so far all of the fracture simulation studies in the geomechanics domain are performed unidirectionally for RQD.

6.7.1 Fracture Network Model

In general, the dimensions, orientation, trace lengths, apertures, and other geomechanical properties of each fracture are randomly distributed in nature. Therefore, their replications through Monte Carlo simulations lead to realizations of a possible portion of the fractured medium with the same statistical properties as the observed ones. Once a representative simulation model is developed, it is then possible to obtain the geomechanical properties of the fracture network in detail. Herein, the main geomechanical property is the directional RQD. In order to achieve such a goal in this chapter, the discontinuity network properties are assumed and defined by the following characteristics.

1) The discontinuities within a fracture network are assumed to occur randomly with their midpoint coordinates, obeying the uniform pdf within a unit frame of 1×1. It is possible to enlarge such a basic frame by suitable horizontal and

vertical scales in order to obtain desired frame dimensions. The distribution of discontinuity midpoint location in the frame obeys a 2D Poisson process.

2) Throughout this study the discontinuities are assumed to be planar and of finite trace lengths so that intersection by any arbitrary plane gives rise to a group of linear traces. These traces can be represented by an average length and a measure of variability in terms of standard deviation. In this study, the trace lengths are assumed to originate from a lognormal pdf. Besides, this trace length distribution is independent of the intersection plane orientation.
3) The discontinuity orientations for each set are assumed to have a normal pdf with an average orientation from the north direction, in addition to a reasonable variation expressed by the standard deviation. The occurrences of different directions within each set are independent from each other.

The plausible values of each one of the pdfs mentioned above can be estimated from field studies by examining either borehole cores or exposed rock faces. However, reliable measurements of trace lengths can be obtained from extensive rock faces only. Parameter estimations for the pdfs in describing discontinuities should be determined from both linear and areal measurements. Priest and Hudson (1981) and Hudson and Priest (1983) have presented brief explanations of the scanline measurements, i.e., linear measurements, which provide information about the frequency of discontinuity occurrences along a scanline as well as variability of intact lengths and aperture sizes to a certain extent. However, areal measurements provide significant supplementary information about the discontinuity directions, trace lengths, and midpoints.

6.7.2 RQD Analysis

In its simplest form the RQD is defined as the percentage of intact length summation, S, that is greater than a threshold value such as 0.1 m (4 in) along a scanline length, L, as

$$\mathrm{RQD} = 100\,\frac{\mathrm{S}}{\mathrm{L}}. \tag{6.97}$$

The rock mass is classification is already given in Table 6.1. The practical difficulties in using Eq. (6.97) are as follows

1) It gives a single sample value of RQD along one direction. The practical difficulty may arise in trying to get a different scanline direction so as to assess the possible heterogeneities within the rock mass. For instance, along a highway cut or tunnel excavation, only longitudinal scanlines can be measured for RQD calculations. Lateral scanlines are possible only in large diameter tunnels and large highway cuts. Therefore, it is necessary to set up a fracture network model from the available scanline measurements; and then by using this model many scanlines in a multitude of desired directions can be taken synthetically.

2) Most often in nature, either due to narrow rock surface exposure, or weathering or geomorphologic features, it may not be possible to make measurements along rather long scanlines. This gives rise to another source of error or bias in the RQD calculations according to Eq. (5.1) (Sen and Kazi, 1984). However, a well-defined representative fracture network model provides unlimited opportunities in making scanline measurements as long as desired.
3) The RQD calculations from Eq. (6.97) do not give any insight into the intact length distribution. As mentioned by Şen (1984) different distributions provide different formulations of the RQD calculation. However, in a fracture network model, as developed in this chapter, the intact length distributions are known; and therefore, one can make more accurate RQD estimations.
4) In a scanline measurement, different sets of fractures are measured irrespective of their individual probability distribution functions. Therefore, it is not possible to assess the effect of each set separately from others. However, in a fracture network model such assessments can be made rather easily and the contribution of each fracture set on the RQD value can be quantified individually.
5) Along the scanline adopted in the field, there may occur only intact lengths that are all greater (or smaller) than the threshold value. In such a situation, Eq. (6.97) leads to the rock mass as either excellent (or very poor). In order to account completely for all of the possible intact lengths, the population distribution of fractures at every direction should be known. Such a task can be achieved easily once the fracture network model is established for the rock mass.

Because of the aforementioned points it is worth to investigate the RQD value behavior within a rock mass based on a specific intact length distribution, which is adopted herein as the negative exponential distribution.

The negative exponential distribution function, f(x) of intact lengths can be expressed through Eq. (6.27), with λ as the average number of discontinuity, i.e., fractures, say along one direction. Priest and Hudson (1981) derived the expected RQD value based on this distribution as in Eq. (6.34) with the threshold value, t. Difference between Eqs. (6.97) and (6.27) is such that the former gives only sample estimate of RQD whereas the latter provides population estimation. Of course, in any study the latter type of estimation must be preferred, but its calculation is rather difficult. Theoretically, very long scanline measurements might yield approximately the population RQD value with the use of Eq. (6.97). However, practical difficulties such as small rock surface exposures make such an approximation almost impossible. Besides, the short scanline estimates lead to biased estimations, i.e., underestimation of the RQD value even if many scanlines were available (Şen and Kazi, 1984). Therefore, in the RQD analysis, as proposed herein a new technique of its estimation by using Eq. (6.27) is suggested. The field measurements will not be processed as usually done by Eq. (6.97), but rather by Eq. (6.27).

To this end, let us consider the cumulative probability distribution of the intact lengths by taking integration of Eq. (6.27) from 0 to any x value. After necessary calculations this leads to

$$F(x) = 1 - e^{-\lambda x}, \tag{6.98}$$

where F(x) is the cumulative probability, which is a non-decreasing function of the intact length, x. It assumes any value in the range 0–1. However, in order to bring this equation into a more practical form, first of all the probability, P(x), of an intact length to be greater than a given length x is considered as $P(x) = 1\ F(x)$ and then natural logarithms of both sides in Eq. (6.98) is leading to

$$\ln P(x) = \ln [1 - F(x)] = -\lambda x. \tag{6.99}$$

By taking the differentiation of both sides in this expression, it is possible to obtain $d\ln P(x) = -\lambda dx$ hence, finally,

$$\frac{dx}{d\ln P(x)} = -\frac{1}{\lambda}. \tag{6.100}$$

This equation shows a linear relationship between ln P(x) and x and the slope of straight line is equal to $1/\lambda$. Consequently, the following points can be advised for a practicing geologist in order to find the λ value.

1) Find the probability, P(x), of each intact length measurement.
2) Plot on a semi logarithmic chapter intact lengths versus the probabilities on the logarithmic axis.
3) Fit a straight line through the scatter of field points.
4) Calculate the slope value of the straight line. This slope value is, in fact, equal to $1/\lambda$.
5) Substitute the λ value into Eq. (6.34) and find the population RQD value, μ.

The only practical difficulty in this procedure is encountered in step (1) for calculating the cumulative probability. However, there appears to be two distinctive approaches. One is the usual way of constructing a histogram for the intact lengths, and then transforming it into a cumulative PDF. However, this application raises practical difficulties, especially when the number of intact lengths is small, which is almost the case in any field survey. Another way of obtaining the cumulative probability is an empirical approach, which is based on the rank, m, of any intact length within a set of available data with size n. Hence, the cumulative probability can be expressed as

$$P(x) = \frac{m}{n+1}. \tag{6.101}$$

This empirical approach is used very often in the practical studies, and it does not give any difficulty in the applications. The RQD analysis based on this empirical law, together with the generated intact lengths, is given in the following section.

6.7.3 RQD Simulation Results

The simulation studies in this chapter are based upon a computer program that has been developed to generate in two dimensions a random network of discontinuity pattern. Three different orientations are adopted for the fracture orientation, each of which is assumed to be normally distributed about a given value. Table 5.1 shows the relevant parameters taken for the simulation of fractures in this chapter. However, in any future study, they may be changed according to the field conditions.

This program can typically handle up to any number of sets, each containing any desired number of discontinuities. The program finds the beginning and ending points' coordinates of any trace. The results of this program appear as a numerical representation of a 2D discontinuity network. Such a network is one of the example samples of random discontinuity geometry generated according to the input data shown in Table 6.8.

The sample area size in these generations is considered as 1×1. However, its transformation into any desired size is possible by the multiplication with any desired scale. Some sample realization of generated discontinuity sets are shown in Fig. 6.34 in detail as individual and combined fracture sets.

It is important to notice in the individual sets, i.e., Fig. 6.34a, that some fracture traces intersect with the general frame of the area. These fractures are referred to as censored trace lengths. The generation scheme gives their total trace lengths, but in practice they are never known. On the other hand, some short length traces appear entirely within the sample area. Consideration of the whole set on one sample area, as in Fig. 6.34c, makes the picture rather complex as it is the case in nature.

In order to assess the effect of different fracture sets individually or collectively on the RQD calculations, the sample area is overlain with scanlines in the east–west direction at different levels between 0 and 1. Of course, it is possible to take a scanline at any level, but the discussion here will concentrate on five different levels, which are at 0.1, 0.3, 0.5, 0.7, and 0.9. The computer program lays these scanlines, at these levels, on the sample area of a generated fracture network; subsequently, it finds individually and collectively the intact lengths along them, ordering them in an ascending order, and attaches to each intact length an order to be used in Eq. (6.101). The results are presented on semi-logarithmic chapter as shown in Fig. 6.34.

A visual inspection of these figures indicate that there appear wide ranges of data scatter; and with the consideration of more than one set of fracture, the

Table 6.8 Input data for fracture network generation

		Set 1		Set 2		Set 3	
Property	Distribution	Mean	Variance	Mean	Variance	Mean	Variance
Orientation	Normal	30*	9	130*	9	0*	4
Trace length (m)	Log-Normal	0.2	0.05	0.18	0.04	0.16	0.04
Intact lengths (m)	Negative Exponential	.013	2×10^{-4}	.013	2×10^{-4}	.013	2×10^{-4}
Location	Poisson	0.5	0.5	0.5	0.5	0.5	0.5

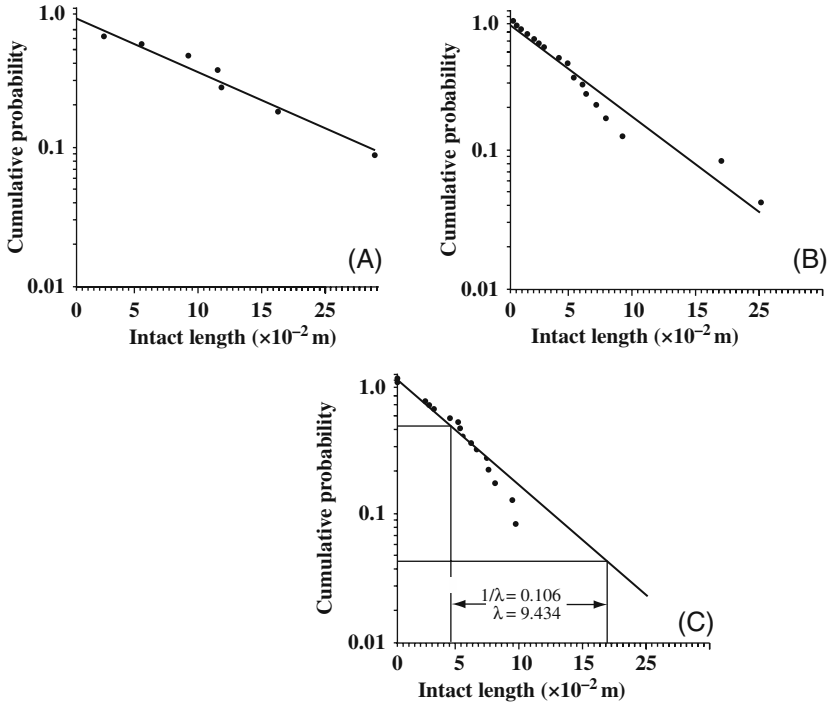

Fig. 6.34 Cumulative probability plots of intact lengths at the 0.1 level. (**A**) single set at 30°; (**B**) two sets at 0 and 30°; (**C**) three sets at 0, 30 and 130°

scatter becomes less. The best straight lines are fitted through the scatter of points; their slopes are found by considering a full cycle on the logarithmic axis. The corresponding length on the horizontal axis is equal to the slope, i.e., 1/λ parameter. This slope calculation procedure is presented in Fig. 64C. The results are summarized in Table 6.9.

Table 6.9 Slope and RQD values for $t = 0.1$ m

	Level	One Set	Two Sets	Three Sets
0.1	Slope	0.267	0.120	0.106
	RQD %	94.5	79.8	75.6
0.3	Slope	0.214	0.135	0.128
	RQD %	92.0	83.0	81.0
0.5	Slope	0.227	0.117	0.079
	RQD %	92.7	79.0	63.9
0.7	Slope	0.212	0.122	0.050
	RQD %	91.8	80.0	40.6
0.9	Slope	0.188	0.092	0.076
	RQD %	90.0	70.4	62.0
Average	RQD %	92.2	78.4	64.6

As is obvious from Table 6.4, the best rock quality is obtained when only one fracture set is considered. As expected, an increase in the number of fracture sets can cause a decrease in the RQD value. There appears a practically significant difference between the RQD values based on the single set of fracture and those on two or three fracture sets. The rock quality is of an excellent type when one set of fractures is considered; whereas the quality deteriorates and becomes very good and fair for two and three fracture sets, respectively. The last row in Table 6.4 gives average RQD values for all the scanlines considered in this study. It is obvious from the comparison of these values that when two sets are considered, the RQD deterioration relative to one set is almost 15%, whereas for three sets consideration is almost 30%.

References

Agterberg, F., 1975. New problems at the interface between geostatistics and geology. Geostat. 75, 403–421.

Baczynski, N. R. P., 1980. Zonal concept for spatial distribution of fractures in rock. In Proceedings of the Thrid Australian and New Zealand Conference on Geomechanics. Wellington, New Zealand, pp. 29–33.

Baecher, G. B., Lanney, N. A., and Einstein, H. H., 1977. Statistical description of rock properties and sampling. 18th U.S. Symposium on Rock Mechanics, Keystone, Colorado, pp. 5C1-1–5C1-8.

Barton, C. M., 1977. Geotechnical analysis of rock structure and fabric in C.S.A. Mine, Cobar, New South Wales. Applied Geomechanics, Technical Paper 24, CSIRO, Australia.

Barton, N., Lien, F., and Lunde, J., 1974. Engineering classification of rock masses for the design of tunnel support. Rock Mech. 6(4), 189–236.

Bieniawski, Z. T., 1974. Geomechanic classification of rock masses and its application in tunneling. Proceedings of the 3rd International Congress on Rock Mechanics, Denver, Colorado, September 1974, Vol. 2A, pp. 27–32.

Box, G. E. P., and Jenkins, G. M., 1970. Time Series Analysis, Forecasting and Control. Holden Day, San Francisco, 475 pp.

Brady, B. H. G., and Brown, E. T., 1985. Rock Mechanics for Underground Mining. Allen-Unwin Press, London.

Bridges, M. C., 1975. Presentation of fracture data for rock mechanics. Second Australia New Zealand Conference on Geomechanics, Brisborne, Australia, pp. 144–148.

Brown, E. T., 1981. Rock Characterization Testing and Monitoring. Pergamon Press, London, 221 pp.

Call, R. B., Savely, J., and Nicholas, D. E., 1976. Estimation of joint set characteristics from surface mapping data 17th U.S. Symposium on Rock Mechanics, pp. 2B21–2B29.

Cliff, A. D., and Ord, J. K., 1973. Spatial Autocorrelation. Pion, London.

Coates, D. F., 1964. Classification of rocks for rock mechanics. Int. J. Rock Mech. Min. Sci. Geomech. Abst. 1(3), 421–429.

Cording, E. J., and Mahar, J. W., 1978. Index properties and observations for design of chambers in rock. Eng. Geol. 12, 113–142.

Cramer, H., 1938. Random Variables and Probability Distribution Mixtures of alcohols, acids and amines. J. Chem. Phys. 6, 847.

Cruden, D. M., 1977. Describing the size of discontinuities. Int. J. Rock Mech. Min. Sci. Geomech. Abstr. 14, 133–137.

Deere, D. U., 1964. Technical description of rock cores for engineering purposes. Rock Mech. Eng. Geol. 7(7), 16–22.

Deere, D. U., 1968. Geologic considerations. In: K. G. Stagg and O. C. Zienkiewicz (Eds.), Rock Mechanics in Engineering Practice. John Wiley and Sons, New York, pp. 4–20.

Ege, J. R., 1987. Core index. A numerical corelogging procedure for estimating rock quality. US Geol. Surv. 954, 1–15.

Einestein, H. H., and Baecher, G. B., 1983. Probabilistic and statistical methods in engineering geology, specific methods and examples. Part I: Exploration. Rock Mech. Rock Eng. 16, 39–72.

Eissa, E. A., and Şen, Z., 1990. Intact length persistance in relation to rock quality designation. Int. J. Rock Mech. Min. Sci. Geomech. Abstr. 28, 411–419.

Feller, W., 1967. An Introduction to Probability Theory and its Application. John Wiley and Sons, New York, 509 pp.

Goodman, R. E., 1976. Method of Geological Engineering in Discontinuous Rocks. West, San Francisco, CA.

Goodman, R. E., and Smith, H. R., 1980. RQD and fracture spacing. J. Geotech. Eng. Division, ASCE 106(GT2), 191–193.

Hammersely, J. M., and Handscomb, D. C., 1964. Monte Carlo Methods. Methuen and Co. Ltd., London, 178 pp.

Higgs, N. B., 1984. The profile-area and fracture frequency methods: two quantitative procedures for evaluating fracture spacing in drill core. Bull. Assoc. Eng. Geol. 21(3), 377–386.

Hudson, J. A., and Priest, S. D., 1979. Discontinuities and rock mass geometry. Int. J. Rock Mech. Min. Sci. Geomech. Abstr. 16, 339–362.

Hudson, J. A., and Priest, S. D., 1983. Discontinuity frequency in rock mass. Int J Rock Mech, Mining Sci Geomech Abstracts. 20(2), 73–89.

International Society for Rock Mechanics, 1978. Standardization of laboratory and field tests. Suggested methods for the quantitative description of discontinuities in rock masses. Int. J. Rock Mech. Min. Sci. Geomech. Abstr. 15, 319–368.

Jenkins, G. M., and Watt, D. G., 1968. Spectral Analysis and Its Applications. HoldenDay, 523 pp.

Journel, A. G., 1974. Simulation conditionelle de gisements miniers-theorie et pratique: These de Doctor Ingenieur, Universite de Noncy.

Kazi, A., and Şen, Z., 1985. Volumetric RQD; An index of rock quality. Proceedings of the International Symposium on Fundamentals of Rock Joints, Bjorkliden, pp. 99–102.

Krige, D. G., 1951. A statistical approach to some basic mine valuation problems on the Witwatersrand. J. Chem. Metall. Min. Soc. South Africa 52, 119–139.

Krumbein, W. C., 1970. Geological models in transition to geostatistics. Geostatistics. Plenum Press, New York, pp. 143–161.

Kulhawy, F. H., 1978. Geomechanical model for rock foundation settlement. J. Geotech. Eng. Division, ASCE 104(GT2), Proc Paper 13547, 211–228.

Long, J. C. S., 1983. Investigation of equivalent porous medium permeability in networks of discontinuity fractures. Unpublished Ph. D. Thesis, University of California, Berkeley, CA.

Louis, C., and Pernot, M., 1972. Three-dimensional investigation of flow conditions of Grand Maison Dam Site. Proceedings of Symposium International Society of Rock Mechanics, Percolation through Fissured Rocks.

Matern, B., 1960. Spatial variation. Medd Statons Skogsforsknings institut, 144 pp.

Matheron, G., 1963. Principles of geostatistics. Econ. Geol. 58, 1246–1266.

Matheron, G., 1965. Les variables regionalises et leur estimation. Masson et Cie., Paris, 306 pp.

Mood, A. M., 1940. The distribution theory of runs. Ann. Math. Stat. 11, 427–432.

Otaibi, A., 1990. Geotechnical investigation and engineering geological maps of Al-Nagabah area. Unpublished Thesis, Faculty of Earth Sciences, King Abdulaziz University, Jeddah.

Piteau, D. R., 1970. Analysis of the genesis and characteristics of jointing in the Nchanga Open pit for the purpose of ultimately assessing the slope stability. Report, Nchanga Consolidated Copper Mines Ltd.

Priest, S. D., and Hudson, J., 1976. Discontinuity spacing in rock. Int. J. Rock Mech. Min. Sci. Geomech. Abstr. 13, 135–148.

Priest, S. D., and Hudson, J. A., 1981. Estimation of discontinuity spacing and trace length using scanline surveys. Int. Rock Mech. Min. Sci. Geomech. Abstr. 18(3), 183–197.

Rice, S. O., 1945. Mathematical analysis of random noise. Bell. Sys. Tech. J. 24, 46–156.
Roach, S. A., 1968. The Theory of Random Clumping. Methuen, London.
Rouleau, A., 1984. Statistical characterization and numerical simulation of a fracture system – Application to groundwater in the Stsipe Granite. Unpublished Ph. D. Thesis, University of Waterloo, Ontario, Canada.
Roulean, A., and Gale, J. E., 1985. Statistical characterization of the fracture system in the Stripa Granite, Sweden. Int. J. Rock Mech. Min. Sci. Geomech. Abstr. 22(6), 353–367.
Ryckes, K. D., 1984. A routine method to evaluate the modes of failure and the stability of rock slopes. Unpublished Thesis, Imperial College of Science, Technology and Medicine, 246 pp.
Şen, Z., 1974. Small sample properties of stationary stochastic models and the Hurst phenomenon in Hydrology. Unpublished Ph.D. Thesis, Imperial College of Science and Technology, University of London, 286 pp.
Şen, Z., 1978. Autorun analysis of hydrologic time series. J. Hydrol. 36, 75–85.
Şen, Z., 1979a. Application of autorun test to hydrologic data. J. Hydrol. 42, 1–7.
Şen, Z., 1979b. Effect of periodic parameters on the autocorrelation structure of hydrologic series. Water Resour. Res. 15(6), 1639–1642.
Şen, Z., 1980. Statistical analysis of hydrologic critical droughts. J. Hydraul. Div. ASCE, Proc. Pap. 14134, 106(HY1), 99–115.
Şen, Z., 1984. RQD models and fracture spacing. J. Geotech. Eng. Amer. Soc. Civ. Eng. 110(2), 203–216.
Şen, Z., and Kazi, A., 1984. Discontinuity spacing and RQD estimates from finite length scanlines. Int. J. Rock Mech. Min. Sci. Geomech. Abstr. 21(4), 203–212.
Şen, Z., 1985. Autorun model for synthetic flow generation. J. Hydrol. 81, 157–170.
Şen, Z., 1989a. Cumulative semivariogram models of regionalized variables. Int. J. Math. Geol. 21(3), 891–903.
Şen, Z., 1989b. Comment on "The generation of multi-dimensional autoregressive series by herringbone method". Math. Geol. 21(2), 267–268.
Şen, Z., 1990a. RQP RQR and fracture spacing: Technical note. Int. J. Rock Mech. Min. Sci. Geomech. Abstr. 22, 135–137.
Şen, Z., 1990b. Spatial simulation of geologic variables. J. Math. Geol. 22(2), 175–188.
Şen, Z., 1991. The profile-area method for statistical evaluation of rock mass quality. Bull. Assoc. Eng. Geol. XXVIII, 351–357.
Sharp, W. E., and Aroian, L. A., 1985. The generation of multidimensional autoregressive series by herringbone method. Math. Geol. 17, 67–79.
Smith, L., and Schwartz, F. W., 1984. An application of the influence of fracture geometry on mass transport in fracture media. Water Resources Res. 20(9), 1241–1252.
Steffen, O., 1975. Recent developments in the interpretation of data from joint surveys in rock masses. Sixth Regional Conference for Africa on Soil Mechanics and Foundations, II, pp. 17–26.
Switzer, P., 1965. A random set process with a Markovian property. Ann. Math. Stat. 36, 1859–1863.
Terzaghi, K. C., 1946. Introduction to tunnel geology: Rock defects and loads on tunnel supports. In: Protor, R. V., and White, T. L., Rock Tunnelling with Steel Supports: The Commercial Shearing and Sampling Co., Youngs Town, Ohio, pp. 15–99.
Terzaghi, R. D., 1965. Sources of error in joint surveys. Geotechnique15, 237–304.
Wallis, P. F., and King, M. S., 1980. Discontinuity spacing in a crystalline rock. Int. J. Rock Mech. Min. Sci. Geomech. Abstr. 17, 63–66.
Watson, 1955. Serial correlation in regression analysis I. Biometrika, 42, 327–341.

Index